

Pipe Design for Improved Particle Distribution and Improved Wear



By

Benjamin Raylor, BEng(Hons), MSc, CEng, MIMechE, MRAeS, MIMarE

This thesis submitted in partial fulfilment of the requirements of the University of Nottingham for the degree of Doctor of Philosophy.

June 1998



Acknowledgements

Firstly I would like to thank Dr. N.J. Miles for providing the finances for the doctorate and Dr. T.F. Jones for providing technical supervision, interlaced with humour. General technical assistance was provided by Chandu Shah, Dr. M.R. Stokes, Shaun Whitehead and Dr. D. Brown. Technical assistance was also given by technicians of the Faculty of Engineering, with a special thanks to William Scully.

The *Institution of Mechanical Engineers* generously provided me with the Clayton award and reduced subscriptions while studying at the University of Nottingham. Thanks also to the *Royal Aeronautical Society* and the *Institute of Marine Engineers* who provided reduced subscriptions and support.

Finally thanks to my parents and sister, Susan, who have kept me sane through this trial of scholarship.

Declaration

The work submitted was carried out by the candidate himself and due acknowledgement has been made for any assistance and information gained from other sources by the use of references.

This work has not been accepted for any other degree and is not currently being submitted in candidature for any other degree.

A handwritten signature in black ink, appearing to read 'B. Raylor', written in a cursive style.

Benjamin Raylor

Abstract

This thesis describes the use of swirl-inducing pipes in water and water/mixture flows, with a particular emphasis on production of swirl before a bend.

The author takes ideas for imparting swirling action to particle laden liquids which have occurred in one form or another throughout the 20th Century. The aim of the project was to reduce wear and produce better particle distribution throughout a bend. In the present investigation two methods were used in the examination of swirl-inducing pipes, namely experimental and numerical. The experimental method made use of a *Swirly-flo* pipe, which is normally found in marine boilers and is used to improve heat exchanger efficiency. The *Swirly-flo* was then placed onto an experimental test rig, which was specifically designed to provide insight into the use of swirl-inducing pipes. The numerical method came from a commercial Computational Fluid Dynamics (C.F.D.) package which allowed the author to examine various shapes for pipes and provided information on the flow fields in a swirl-inducing pipe.

From the experimental results it was shown that swirling the flow before a bend produced less pressure drop across the bend than non-swirling flow. However, the *Swirly-flo* pipe produced a greater pressure loss across its length than the standard pipe. By swirling the particles before the bend the particles were more evenly distributed throughout the bend, which has the potential to remove the characteristic wear zones. Computational Fluid Dynamics was used to investigate various *Swirly-flo* designs. These studies indicated that the optimum pitch to diameter ratio was shown to be 8 for a constant pitch *Swirly-flo* pipe, which was consistent with previous work.

Contents

List of Figures	1
Nomenclature	8
Typeface Note	13
1.0 Introduction	14
1.1 Aims of Thesis	14
1.2 An Overview of Thesis	15
2.0 Literature Survey, Background and Theory	17
2.1 Introduction	17
2.2 The use of Helical Sections in Pipes	17
2.3 Marine <i>Swirly-flo</i> Pipes	23
2.4 Theory	27
2.4.1 Factors Influencing Suspension Rheology	27
2.4.2 Particle Shape	27
2.4.3 Particle Size	27
2.4.4 Particle Concentration	28
2.4.5 Suspension of Particles	29
2.4.6 Pipe Characteristics	32
2.4.7 Swirling of Fluids in a Straight Horizontal Pipe	33
2.4.8 Losses at Bends for Liquids Only	34
2.4.9 The Pump	36
2.4.10 Wear in Pipes	37

3.0	Design and Commissioning of the Test Rig	40
3.1	Design Criteria	40
3.2	Summary of Design Method	41
3.3	The Wooden Frame	42
3.4	Pipe Selection	43
3.5	The Design and Manufacture of the De-aerator	45
3.6	Sala Pump	46
3.7	Speed Control	46
3.8	Electrical Power Meter	48
3.9	Pressure Transducers and Data Logger	51
3.10	Volumetric and Mass Flow	52
3.11	General Commissioning of the Test Rig	53
3.12	Problems in Commissioning	54
3.13	Calibration of Pressure Transducers	54
3.14	Experimental Arrangements	55
3.15	Bead Characteristics	57
3.16	Pump Characteristics	59
4.0	Experimental Work	61
4.1	Water Tests	61
4.2	Determining the Optimum <i>Swirly-flo</i> Pipe Before a Bend	63
4.3	Water/Particle Mixture Tests	65
4.3.1	Concentrations for a Given Loading	65
4.4	Determining the Optimum Orientation of the Long <i>Swirly-flo</i> Pipe	65

4.5	The Effects of the Long <i>Swirly-flo</i> Pipe on Various Concentrations of Beads at Varying Flow Rates	68
4.7	Discussion of Experimental Results	72
4.8	The Experimental Set-up	72
4.9	Results of Experiments	73
5.0	Optimal Design for Swirl in Swirl-Inducing Pipes	81
5.1	Introduction to the <i>Calculus of Variations</i>	82
5.2	Determination of the Geodesic on a Surface of a Cylinder of Revolution	84
5.3	The Brachistochrone Problem Inside a Cylinder of Revolution	87
6.0	Computational Fluid Dynamics	98
6.1	Turbulence	98
6.2	The Equations that Govern Viscous Fluid Motion	100
6.3	The Reynolds Averaged Navier-Stokes Equations	102
6.4	Turbulence Transport Models	105
6.4.1	Zero Equation Models	107
6.4.2	One Equation Models	107
6.4.3	Two Equations Models	107
6.4.4	Algebraic Stress Models	108
6.4.5	Large Eddy Simulation	108
6.4.6	Reynolds Stress Models	109
6.5	The Solution Algorithm	113
6.5.1	The Integral Approach to Finite Volume	113
6.5.2	The S.I.M.P.L.E. Algorithm	114
6.5.3	Interpolation Scheme	116

6.5.4	Boundary Conditions	117
6.5.5	The use of Wall Functions in the Solution	117
6.5.6	Mesh Used	119
6.5.7	The Co-location of Variables	120
7.0	Computational Fluid Dynamics Results	121
7.1	Introduction	121
7.2	Examination of Grid Independence	122
7.3	Experimental Runs	123
7.4	Examination of Colour Plots	138
7.4.1	0.1 Metre Standard Swirly-flo Pipe	138
7.4.2	0.2 Metre Standard Swirly-flo Pipe	139
7.4.3	0.3 Metre Standard Swirly-flo Pipe	139
7.4.4	0.4 Metre Standard Swirly-flo Pipe	139
7.4.5	0.5 Metre Standard Swirly-flo Pipe	140
7.4.6	0.6 Metre Standard Swirly-flo Pipe	140
7.4.7	0.7 Metre Standard Swirly-flo Pipe	141
7.4.8	0.8 Metre Standard Swirly-flo Pipe	141
7.4.9	0.9 Metre Standard Swirly-flo Pipe	141
7.4.10	1.0 Metre Standard Swirly-flo Pipe	142
7.4.11	0.2 Metre Brachistochrone With End Taper	142
7.4.12	0.3 Metre Brachistochrone With End Taper	142
7.4.13	0.4 Metre Brachistochrone With End Taper	143
7.4.14	0.5 Metre Brachistochrone With End Taper	143

7.4.15	0.4 Metre Standard Swirly-flo Pipe Without End Taper	144
7.4.16	0.4 Metre Brachistochrone Pipe Without End Taper	144
7.5	Introduction to the CFD Results	145
7.6	Accuracy of the C.F.D. Results	145
7.6.1	Verification and Validation	145
7.6.2	Comparison of CFD Results with the Nearest Available Data	146
7.6.3	Grid Independence	147
7.7	Discussion of Graphical Results	148
7.8	Comparison between the Standard and Brachistochrone	149
7.9	Discussion of Colour Plots	152
8.0	Conclusions and Recommendations	155
8.1	Conclusions	155
8.2	Recommendations	156
9.0	References	159
Appendix A	Density and viscosity relationships with changing temperature	
Appendix B	FORTTRAN codes for the grid generation of the Swirly-flo and brachistochrone pipes, with and without tapers	
Appendix C	C.F.D. colour plots	
Appendix D	The experimental pressure results with graphs	

List of Figures

Figure 2.1	Gordons' Patent (1899)	19
Figure 2.2	Robinson's Patent For a Continuous Helical Rib (1923)	19
Figure 2.3	Yuille's Patent for a Dredger Pipe Line (1928)	19
Figure 2.4a	Longitudinal view of the <i>Swirly-flo</i> pipe	23
Figure 2.4b	Axial view of <i>Swirly-flo</i> pipe	23
Figure 2.5	Pipes that are tagged	24
Figure 2.6	Rotating Die	25
Figure 2.7	Draw Bench	25
Figure 2.8	Finished <i>Swirly-flo</i> pipes	26
Figure 2.9	Patterns of Particles in Slurry Flow [Redrawn from Chien, (1993) Jones (1997)]	30
Figure 2.10	Schematic Classification of Transition Velocities in terms of Pressure Gradient for a Constant Volume Fraction of Solids (after Jones (1997))	31
Figure 2.11	High Wear Areas on a Bend (copied from Zenz and Othmer, (1960))	39
Figure 3.1	Lower section	42

Figure 3.2	Upper Section	43
Figure 3.3	Unsatisfactory Bends	45
Figure 3.4	De-aerator	46
Figure 3.5	Heenan Inverter	47
Figure 3.6	Sala Pump Viewed From Above, With The Lid Modification	47
Figure 3.7	Fluke Power Meter	49
Figure 3.8	Wiring Diagram for the Power Meter	49
Figure 3.9	Passive Current Clamp and Voltage Leads in situ	50
Figure 3.10	Pressure Transducer before the Rising Main	52
Figure 3.11	Spring Balance with Header Tank	53
Figure 3.12	Standard Schematic Set-up	55
Figure 3.13	<i>Swirly-flo</i> Schematic Set-up	56
Figure 3.14	Long <i>Swirly-flo</i> in-situ	56
Figure 3.15	Screen Sizes of Plastic Beads for Water/Particle Mixtures Tests	57
Figure 3.16	Float and Sink Data for a Sample of Beads	58
Figure 3.17	Electrical Input Power versus Fluid Output Power	59

Figure 3.18	Pump Efficiency Curve for Water-only	60
Figure 3.19	Fluid Power Delivered against Volumetric Flow Rate	60
Figure 4.1	Water-only Friction Factor for Straight Sections (taking account of pipe joints)	61
Figure 4.2	Water-only Pressure Gradient against Volumetric Flow Rate in the Lower Horizontal Section	62
Figure 4.3	Water-only Pressure Gradient against Volumetric Flow Rate in the Rising Main Section	62
Figure 4.4	Water-only Pressure Gradient against Volumetric Flow Rate in the Upper Horizontal Section	63
Figure 4.5	Pressure Drop Across the Bend for Different Sections of <i>Swirly-flo</i> Pipe	64
Figure 4.6	Optimum Position of the Long <i>Swirly-flo</i> Pipe	66
Figure 4.7	Entrance Positions on the Long <i>Swirly-flo</i> Pipe	67
Figure 4.8	Bolt-hole Positions with Corresponding Settling Surfaces	67
Figure 4.9	Pressure Drop Characteristics With and Without the Long <i>Swirly-flo</i> Pipe	68
Figure 4.10	6.1 % concentration v/v with a flow a volumetric flow rate of 1.7 l/s without swirl	69
Figure 4.11	6.1 % concentration v/v with a flow a volumetric flow rate of 1.7 l/s with swirl	69

Figure 4.12	(P3-P4) Pressure Drop with and without a Long <i>Swirly-flo</i> Pipe	70
Figure 4.13	Schematic Cross-Section of the <i>Swirly-flo</i> Pipe	74
Figure 4.14	Flow Field of a Sudden Contraction (copied from Gerhart and Gross, 1985)	75
Figure 4.15	Flow Field of a Sudden Expansion (copied from Gerhart and Gross, 1985)	75
Figure 4.16	Secondary flow and Separation at a Bend (copied from Gerhart and Gross, 1985)	76
Figure 4.17	Particle Distribution without <i>Swirly-flo</i> before the Bend (adapted from Zenz and Othmer, 1960)	79
Figure 4.18	8.0 % concentration v/v with a flow rate of 2.7 l/s without swirl	79
Figure 4.19	Expected Particle Distribution with <i>Swirly-flo</i> before the Bend (adapted from Zenz and Othmer, 1960)	80
Figure 4.20	8.0 % concentration v/v with a flow rate of 2.7 l/s with swirl	80
Figure 5.1	Cylindrical Co-ordinates	84
Figure 5.2	The Brachistochrone Curve and Regular Helix for a Cylinder of 0.7 m	97
Figure 6.1	Arbitrary Control Volume	100

Figure 6.2	Arbitrary Control Volume	114
Figure 6.3	Illustration of Swirly-flo Grid	119
Figure 7.1	Illustration of the Geometry of the Lobes	124
Figure 7.2	Pressure Drop against Axial Distance for Standard Swirly-flo Pipes with constant I (30) and J (25) Cell Numbers	127
Figure 7.3	Pressure Drop against Axial Distance for All Standard Swirly-flo Pipes	127
Figure 7.4	Average w-Velocity against Axial Distance for Standard Swirly-flo Pipes with constant I (30) and J (25) Cell Numbers	128
Figure 7.5	Average w-Velocity against Axial Distance for All Standard Swirly-flo Pipes	129
Figure 7.6	Pressure Drop against w-Velocity for Standard Swirly-flo Pipes with constant I (30) and J (25) Cell Numbers	130
Figure 7.7	Pressure Drop against w-Velocity for All Standard Swirly-flo Pipes	130
Figure 7.8	w-Velocity against Axial distance for 0.5m Standard (Geodesic) Swirly-flo Pipe and 0.5m Brachistochrone	131
Figure 7.9	Pressure Drop Against Axial Distance for the 0.5m Standard (Geodesic) Swirly-flo pipe and the 0.5m Brachistochrone	131
Figure 7.10	Pressure Drop Against w-Velocity for the 0.5m Standard (Geodesic) Swirly-flo pipe and the 0.5m Brachistochrone	132

Figure 7.11	w-Velocity against Axial distance for 0.4m Standard Swirly-flo (Geodesic) Pipe and 0.4m Brachistochrone	132
Figure 7.12	Pressure Drop Against Axial Distance for the 0.4m Standard (Geodesic) Swirly-flo pipe and the 0.4m Brachistochrone	133
Figure 7.13	Pressure Drop Against w-Velocity for the 0.4m Standard (Geodesic) Swirly-flo pipe and the 0.4m Brachistochrone	133
Figure 7.14	w-Velocity against Axial distance for 0.3m Standard (Geodesic) Swirly-flo Pipe and 0.3m Brachistochrone	134
Figure 7.15	Pressure Drop Against Axial Distance for the 0.3m Standard (Geodesic) Swirly-flo pipe and the 0.3m Brachistochrone	134
Figure 7.16	Pressure Drop Against w-Velocity for the 0.3m Standard (Geodesic) Swirly-flo pipe and the 0.3m Brachistochrone	135
Figure 7.17	w-Velocity against Axial distance for 0.2m Standard Swirly-flo Pipe and 0.2m Brachistochrone	135
Figure 7.18	Pressure Drop Against Axial Distance for the 0.2m Standard (Geodesic) Swirly-flo pipe and the 0.2m Brachistochrone	136
Figure 7.19	Pressure Drop Against w-Velocity for the 0.2m Standard (Geodesic) Swirly-flo pipe and the 0.2m Brachistochrone	136
Figure 7.20	Average w-Velocity against Axial Distance for 0.4m Standard pipe and 0.4m Brachistochrone, without Tapered Ends	137
Figure 7.21	Pressure Drop against Average w-Velocity for 0.4m Standard pipe and 0.4m Brachistochrone, Without Tapered Ends	137

Figure 7.22	Pressure Drop against Axial Distance for 0.4m Standard pipe and 0.4m Brachistochrone, Without Tapered Ends	138
Figure 7.23	The Brachistochrone Curve and Regular Helix for a Cylinder of 0.7 m	149
Figure 7.24	Typical w-Velocity against Radius (copied from Kreith and Sonju, 1965)	150
Figure 7.25	The Average profile of the w-velocity at the Exit of the 0.5 m Standard Swirly-flo pipe	150
Figure 7.26	Pressure Drop against w-Velocity for 0.4m Standard pipe (Extrapolated) and 0.4m Brachistochrone, Without End Tapers	151
Figure 8.1	Ribs or Swirl Inducing Mechanism as an Integral Part of the Bend	158

NOMENCLATURE

a	arbitrary acceleration	m/s^2
$C_{1\varepsilon}$	empirical constant	
$C_{2\varepsilon}$	empirical constant	
C_1	empirical constant	
C_2	empirical constant	
C_v	concentration by volume	
$C_{v \max}$	maximum concentration by volume	
D	diameter pipe	m
E_t	total energy per unit volume	J/m^3
f	force per unit mass	N/kg
f	friction factor	
E	Flux vector	
G	degree of swirl ($W_{\text{mo}}/U_{\text{mo}}$)	
g	acceleration due to gravity	m/s^2
K	turbulent kinetic energy	J
K	static pressure loss co-efficient	
K_b	static pressure loss co-efficient for the bend	
K_c	static pressure loss co-efficient for the curvature	
K_d	static pressure loss co-efficient accounting for the re-establishment of fully developed flow downstream of the bend	
L_d	downstream tangent length	m
L_u	upstream tangent-pipe length	m

P	pitch	revolutions/m
p	pressure	Pa
P^*	estimated value of pressure	Pa
$P^\#$	pressure correction	Pa
Q	source term column vector	
Q	general volumetric flow rate	m^3
Q_{pump}	volumetric flow rate of pump	m^3
q	heat transfer per unit volume	J/m^3
r	radius in Cartesians co-ordinates	m
R	mean bend radius	m
Re	Reynolds number	
\underline{S}	surface vector	
t	time	s
u	general velocity	m/s
u_p	velocity of the fluid at point p near the wall	m/s
U	column vector of conservative variables	
U_{mo}	the maximum axial velocity	m/s
u^1	velocity in x-direction	m/s
u^*	estimated value of the velocity in x-direction	m/s
v^1	velocity in y-direction	m/s
v^*	estimated value of the velocity in y-direction	m/s
V	mean flow velocity	m/s

V	fluid velocity	m/s
V_0	velocity at station 0 in pump	m/s
V_1	velocity at station 1 in the pump	m/s
V_{M1}	the velocity at and above which the mixture flows in a symmetric suspension pattern	m/s
V_{M2}	the velocity at which and above which (up to V_{M1}) which the mixture flows in a asymmetric suspension pattern	m/s
V_{M3}	the velocity at which and above which (up to V_{M2}), a moving bed of particles exists on the bottom of the pipe	m/s
V_{M4}	the velocity at which and above which (up to V_{M3}), a bed exists, the lower part of which is stationary	m/s
w^1	velocity in z-direction	m/s
w^*	estimated value of the velocity in z-direction	m/s
W_{mo}	the maximum tangential velocity of a swirling flow	m/s
W_{pump}	power from the pump	m/s
Z_0	reference height on the Sala pump	m
Z_1	vertical distance of station 1 from Z_0	m
z	axial distance cylindrical Cartesian co-ordinates	m

Greek Letters

ΔH_{pump}	total head change produced by the pump	m
ΔP_{bend}	pressure loss across a bend	Pa
δ_{ij}	Kronecker delta	
Δn_p	distance from point p to the wall	m

ε	dissipation rate of turbulent kinetic energy	J/s
ε	effective roughness height	m
k	von Karman constant	
η	efficiency	
ρ	density	kg/ m ³
f	conserved quantity	
θ	turning angle of a pipe bend	degrees
ϕ	angular distance in Cartesian co-ordinates	
ϕ_1	Reynolds number correction	
ϕ_2	downstream correction factor	
ϕ_5	bend angle correction factor	
ν_t	local (turbulent) eddy viscosity (dynamic)	Pa s
μ_t	local (turbulent) eddy viscosity (kinematic)	m ² /s
μ	viscosity (dynamic)	Pa s
μ_{eff}	effective viscosity (= $\mu_t + \mu$)	Pa s
μ	viscosity (kinematic)	m ² /s
μ_l	viscosity (dynamic) of liquid	Pa s
μ_m	viscosity (dynamic) of mixture	Pa s
τ_w	wall shear stress	N/m ²
Ω_j	control volume	m ³
σ_ε	empirical constant	

Subscripts

i,j,k direction specifiers

x,y,z direction specifiers

Superscripts

- time averaged or ensemble average

' Reynolds fluctuation specifier

Mathematical symbols

<> ensemble average

Typeface Note

Swirly-flo a physical pipe manufactured by Durham Tube (A division of Senior Thermal Engineering Limited)

Swirly-flo a computational grid created by the author of similar profile to that of the *Swirly-flo* pipe.

1.0 Introduction

This thesis describes a three-year investigation into conventional and unconventional pipe design in the transportation of water and particle/water mixtures. The water and particle mixtures were examined as they flowed through a right-angled bend. The bend was also examined visually for wear and particle distribution.

In 1993, at British Coal Corporation, Jones proposed a new approach to the problem of settling particles in which a pipe-section could be given a helical profile to promote suspension of particles at relatively low velocities (Jones, 1997). The proposal was supported by the European Coal and Steel Community, but the Technical Services and Research Executive of British Coal was closed down soon afterwards. Fortunately, the E.C.S.C. agreed to continue to support the project at the University of Nottingham. The project described in this thesis started soon afterwards under the direction of Dr. N. J. Miles and supervision from Dr. T.F. Jones.

1.1 Aims of Thesis

The aims of thesis are to examine the effects of a swirl-inducing pipe before a bend, highlighting the flow characteristics under varying slurry concentrations, and determine the optimum swirl-inducing pipe before the bend by using Computational Fluid Dynamics (C.F.D.).

1.2 An Overview of the Thesis

The use of helical designs of pipes to stimulate slurry suspension, and improve the characteristics of slurry transport, originated in dredging. The first patent on record with helical ribs was Gordons' (1899). Using similar methods to stimulate the suspension of particles in a carrier fluid other patents were registered in the earlier part of this century. The first scientific study was carried out by Howard (1939,1941) who examined rifling in pipes and produced full scale tests on the Mississippi River in United States of America. The results of these tests proved satisfactory. Further examination of the effect of helical ribs in pipes was done by the late Professor Wolfe of the University of Toronto, Canada and he concluded that helical ribs inside a pipe reduced the tendency of particles to settle out onto the bottom of the pipe. Another Canadian, Charles (1971,1976) showed that internal ribs produced a good suspension of particles. An optimum pitch to diameter ratio was determined and the height of the ribs were investigated. The final Canadians to contribute to this work were Schriek *et al.*, (1971) who provided a useful summary of the majority of previous work and again highlighted the optimum pitch/diameter ratio.

The thesis provides concise information about the characteristics of particulate transport, in chapter 2, in which the major flow parameters, such as: particle size, particle shape and concentration are discussed. This was then followed by a summary of the wear processes present in particulate transport.

Chapter 3 provides information about the rig assembly and the problems encountered in the manufacture and commissioning of the test facility. The examination of the water and particle flow took place in transparent pipes throughout the test rig. The mass flow rate and volumetric flow rate were monitored. The flows were recorded on a video camera for future use. The flow was induced within the test rig by a centrifugal pump. A de-aerator extracted the air from the fluid, before reaching the test sections, thereby producing a two phase mixture. The chapter also describes the characteristics of the beads, in terms of size and mass.

The experimental tests were then conducted with over 300 detailed runs, in which each one lasted just under an hour. During these runs the pump was modified so that the flow rate of water and solids around the rig was more steady than before. In these runs the efficiency of the pump was determined, with and without the pump modification.

A fundamental investigation was then carried out into the optimum geometry of a swirl inducing pipe, using the *Calculus of Variations*, in conjunction with Computational Fluid Dynamics (C.F.D.). In the *Calculus of Variations* the trajectory of a single particle was examined, whilst only the water phase was examined using Computational Fluid Dynamics (C.F.D), due to the high computational time and financial costs of modelling two-phase flow. This provided the author with knowledge of the internal flow characteristics of a swirl inducing pipe

Results of various swirl inducing pipes is presented in Chapter 7. The circumferential velocity was examined at the exit of the swirl-inducing pipe since this would be the major component that would provide upward motion for any particles within the pipe. Pressure losses were also examined since they would be a critical factor in any industrial application.

The conclusions and recommendations are presented in Chapter 8. The main recommendations involve the improvement of the test rig, with the aid of more pressure transducers and a new datalogger. The *Swirly-flo* pipe could also be improved to reduce the pressure losses at the entrance and exit of the pipe.

2.0 Literature Survey, Background and Theory

2.1 Introduction

This chapter gives the background to the use of innovative pipe geometries to keep moving particles in suspension in pipes and the rheology of particle suspensions, critical velocities of settling slurries and fluid friction in straight pipes and bends. The earliest source came from United States of America patents in the early part of this century, and episodic groups of references could be found in a variety of journals throughout the 20th century. A manufacturing source of swirl-inducing pipes was also found and technical details of that process are presented.

2.2 The Use of Helical Sections in Pipes

The use of helical ribs goes back as far 1899, when H.M. and H.A. Gordon (1899) obtained a United States of America Patent (an extract of which appears in Figure 2.1). The object of the Gordons' invention was to stop the settling of particles in a pipe or conduit. This was done by placing ribs in the pipe or conduit, which caused the flow of the carrying liquid to be diverted so that the flow was from one side of the pipe over the bottom and up the other side. This caused the sediment to be deposited at the top of the pipe and, therefore, kept in suspension. The ribs did not form a continuous helix, but were placed sequentially along the pipe, so as to produce alternately opposite currents of the liquid beyond the ribs. No optimum spacing was specified in the patent for the ribs; neither was the angle of the ribs in the pipes optimised. Engineering judgement was used to obtain the correct angle for a given flow.

Arthur E. Robinson (1923) obtained a patent for an improvement in delivery pipes to hydraulic machines for dredging of earth, clay, sand and gravel. The main purpose of this invention was to reduce the high likelihood, common with

hydraulic dredging, of the spoils becoming lodged in the delivery pipe. This lodging of the spoils was known to cause an increase in power consumption and sometimes led to a complete blockage of the pipeline. These effects were ameliorated by the use of “rifling” in the pipe, similar to that found in a rifle bore. The ribs were arranged in a continuous helix, as illustrated in Figure 2.2. Robinson (1923) suggested three helix threads, but the number of helices was dependent to some extent on judgement, the type of slurry and the available power. The ribs could be discontinuous in nature, that is to say some pipe sections were without ribs, while others had ribs. This was very similar to the Gordons’ idea in that the particles were kept in suspension by changing the flow patterns in the pipe.

Nathaniel A. Yuille (1928) produced another patent with suction dredging as the primary application. The object of this invention was to stop the settling of slurries. The method utilised ribbed pipes placed at sequential intervals along the pipe length, as illustrated in Figure 2.3. This spacing was not optimised for the best suspension of particles, or any other way. The alternating sections were more economical than continuous-helix pipes and reduced the friction-losses of the flow, which in turn caused a reduction of pump power consumption. The pitch of the helix changed along the pipe so that material being pumped through would not become wedged between the spirals but would tend to free itself as the space widened out.

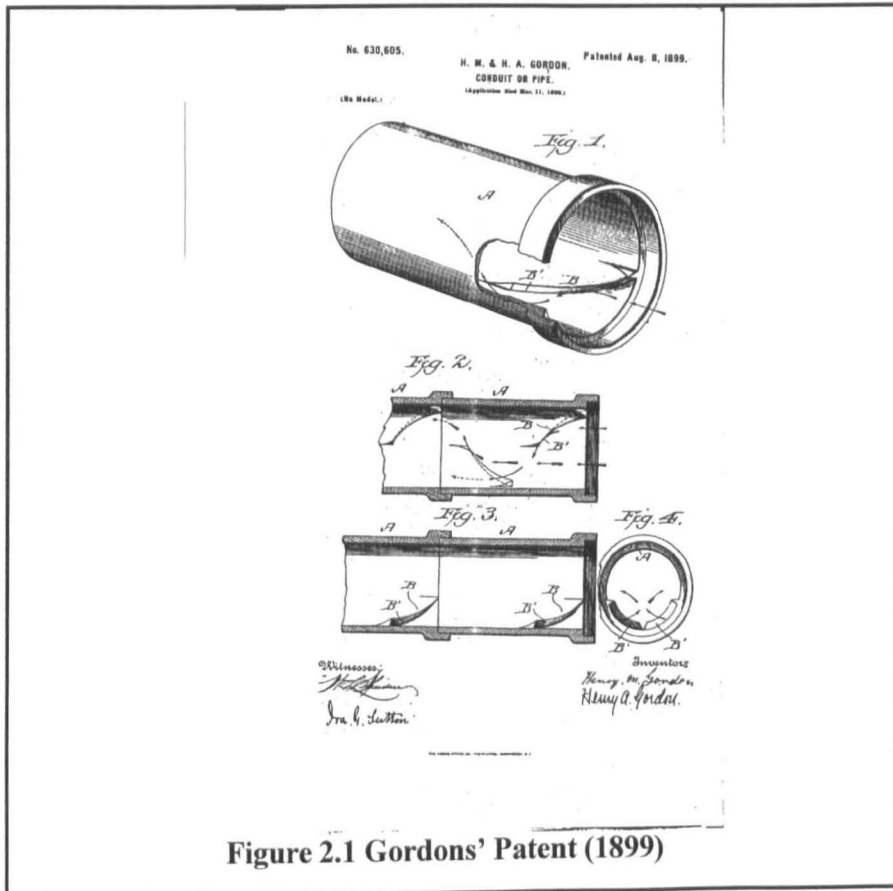


Figure 2.1 Gordons' Patent (1899)

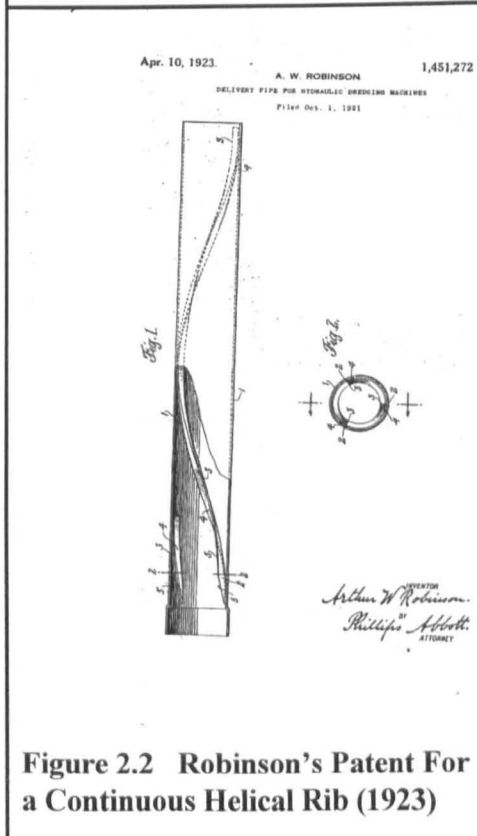


Figure 2.2 Robinson's Patent For a Continuous Helical Rib (1923)

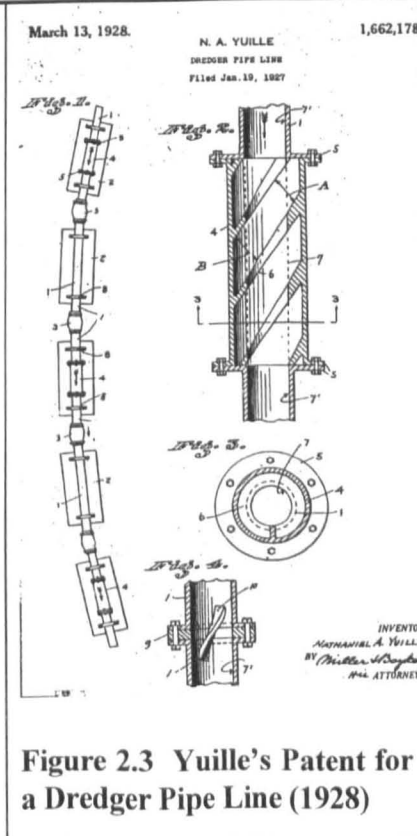


Figure 2.3 Yuille's Patent for a Dredger Pipe Line (1928)

Howard (1939, 1941), who used ribbed pipes in connection with dredging carried out a very thorough examination of rifled pipes. He used 2 inch and 4 inch nominal bore pipes and 24 different configurations of rifles or ribs. The solids consisted of either gravel or clay, ranging in size from 0.0001 mm to 2.5 mm. Howard reached the conclusion that rifling would increase the efficiency of a dredge line when transporting clay or gravel. This was verified by full scale tests on the Mississippi river over a period of two years. In this period the throughput capacity of coarse sand and gravel by dredging was increased by 45%.

In 1966 D. Brian Long presented his undergraduate thesis to the University of Toronto, Canada in "The transportation of solids in helically-ribbed pipes". The University of Nottingham library were unable to obtain this reference but in the following year, S.E.Wolfe (1967), the Professor of Mining Engineering at the University of Toronto published an accessible paper on the use of helically-ribbed pipes in the pumping of slurries. In this paper the following major points were made:

- 1) the flow could be stopped and restarted without any difficulty,
- 2) the low minimum velocities required to keep the solids moving resulted in a much lower pump power consumption and hence a cost reduction,
- 3) the wear in the pipe sections was reduced, due to the lower flow velocities,
- 4) the optimum angle for the helical profile inside the pipe appeared to be 45 degrees to the horizontal.

The helix inside the pipe provided a circumferential flow around the internal wall, causing the sediment on the bottom of the pipe to be returned into mainstream flow. The tendency for the sediment to settle could not be prevented, but the helical ribs inside the pipe reduced this tendency.

Charles *et al.*, (1971) examined the “flow of ‘settling’ slurries in tubes with Internal Spiral Ribs”, in which sand/water slurries were examined with and without ribbed pipes in horizontal sections of varying pitch/diameter ratios. With one rib only, the optimum pitch/diameter was estimated at 5. The flow velocities ranged from 0.5 ft/s to 8 ft/s, whilst the concentrations by volume ranged from 5% to 18%. Two sizes of sand were used, namely 48-65 mesh and 28-35 mesh. The authors also examined the flow of air through ribbed pipe, and in doing so, obtained velocity profiles for a single helically ribbed pipe. The rib had a square profile (1/4 inch x 1/4 inch) in a pipe of diameter 2 inches.

The main conclusions drawn from this work were:

- 1) the velocity distribution of air flowing in a pipe with a helix rib of a pitch to diameter ratio of 3, showed that the helical rib produced turbulence and formed a large rotational motion around the axis of the pipe,
- 2) the solid/liquid flows at high average mixture velocities produced high pressure gradients due to the presence of an internal spiral rib, the opposite was true for low mixture velocities where the pressure gradient was better than a standard smooth pipe,
- 4) the addition of air as a third phase caused an increase in the pressure gradients and therefore was not useful in counteracting the settling tendency of solid particles.

No optimisation of the number of ribs was carried out, nor investigation of rib dimensions in relation to the pipe.

In 1976 Charles and Singh (1976), investigated the effect of the rib height in relation to the diameter of the pipe. In doing so, the authors altered Charles' original pitch/diameter optimum from 5 to 8. The width of the rib was still 1/4", (~ 6mm) whilst the height varied. Therefore, the main conclusion of this study was that the optimum pitch/diameter ratio was 8, with the rib height in the range 10-15% of the pipe diameter.

Schriek *et al.*, (1974) provided a summary of previous work on the use of ribbed pipes, in which he states that Chamberlain (1955 and 1957) did some work on pumping 0.2 mm and 0.65 mm sand through a 12" corrugated pipe. He concluded "under some conditions it is possible to convey sediment at a given rate with minimum horsepower by means of a pipe containing artificial roughness". Schriek *et al.*, (1974) also provided an insight into Chu's M.Sc thesis (Chu,1969), in which Chu concluded that a pitch/diameter of about 5 was the optimum. However, Schriek *et al.*, (1974) concluded that the optimum was nearer 8, but there was a pitch/diameter range from 5 to 11 through which there was no significant change from the optimum. The paper provided no optimum on rib shape or size and recommended that more work was requested on helically ribbed pipes.

Weisman *et al.*, (1994) examined two phase flow patterns and pressure drops in single and double helix pipes with regard to liquid-vapour transport in industrial boilers. The swirling effect of the helical ribs forced the liquid phase to the tube wall while the vapour flowed down the centre of the tube. Weisman and co-workers gained "very little information on the conditions under which the desired swirling flow is obtained."

2.3 Marine *Swirly-flo* pipes

Swirly-flo boiler tubes are used on low pressure water tube boilers for the efficient exchange of heat from the combustion or exhaust gases to the boiler water or steam. According to Milton (1961), “*the swirl given to the gases passing through such tubes ensures a more intimate contact between them and the tube walls and the heat transfer is on that account largely increased.*” A *Swirly-flo* boiler tube of the correct diameter was donated to this project by North Sea Ferries (Van Loo, 1996). A photograph of a *Swirly-flo* tube is presented in Figures 2.4a and 2.4b.

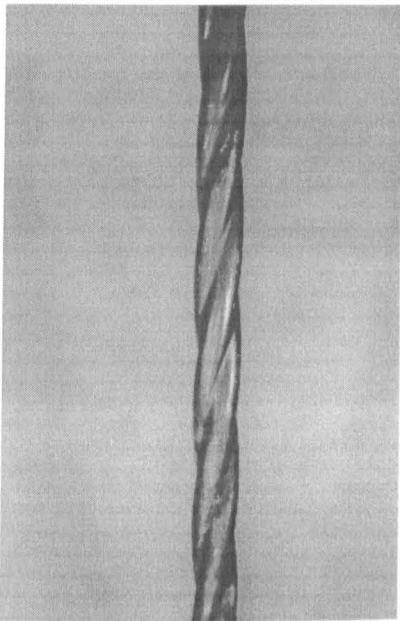


Figure 2.4a Longitudinal view of the *Swirly-flo* pipe

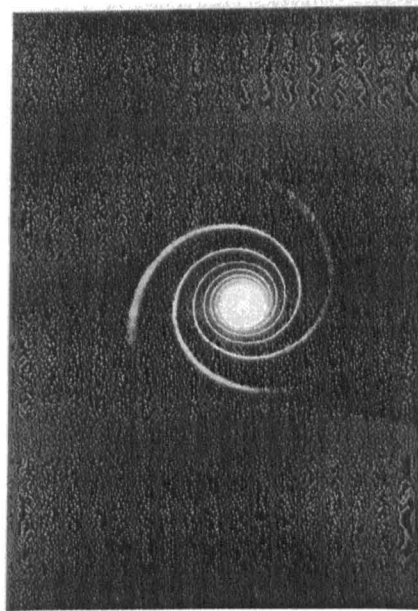


Figure 2.4b Axial view of the *Swirly-flo* pipe

The *Swirly-flo* pipes are manufactured by Durham Tube (A division of Senior Thermal Engineering Limited), Middleton St.George, Darlington under licence to Senior Thermal Engineering Ltd., Wakefield, England.

Manufacture of a *Swirly-flo* pipe starts with a normal straight pipe, which is then *tagged*, that is to say that one end of the pipe is compressed into a smaller diameter, as shown in Figure 2.5. The pipe is then normalised to a

temperature of 900 °C. After this the pipe enters the *wet process*, in which the pipes enter baths of sulphuric acid, water and zinc phosphate. The process of producing the *Swirly-flo* pipe is carried out by cold drawing, through a rotating die. The die and the draw bench are illustrated in Figures 2.6 and 2.7, respectively. The pipe may or may not be heat treated again after this process. The pipes produced by this method are illustrated in Figure 2.8, and the pipes had a pitch/diameter ratio of 8.6, close to the optimum specified by Schriek *et al.*,(1974).

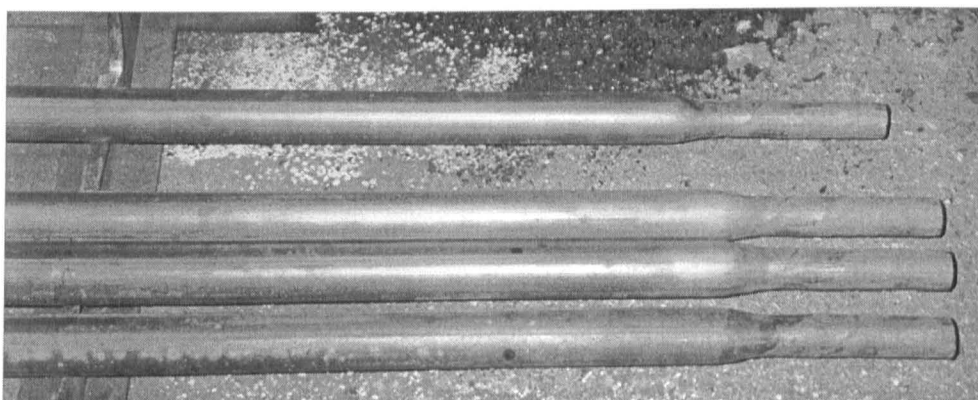


Figure 2.5 Pipes that are tagged

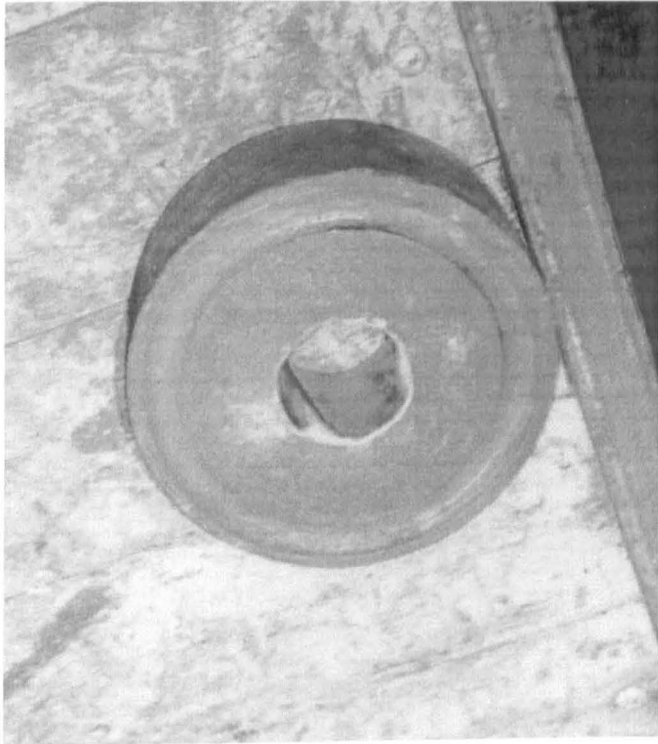


Figure 2.6 Rotating Die

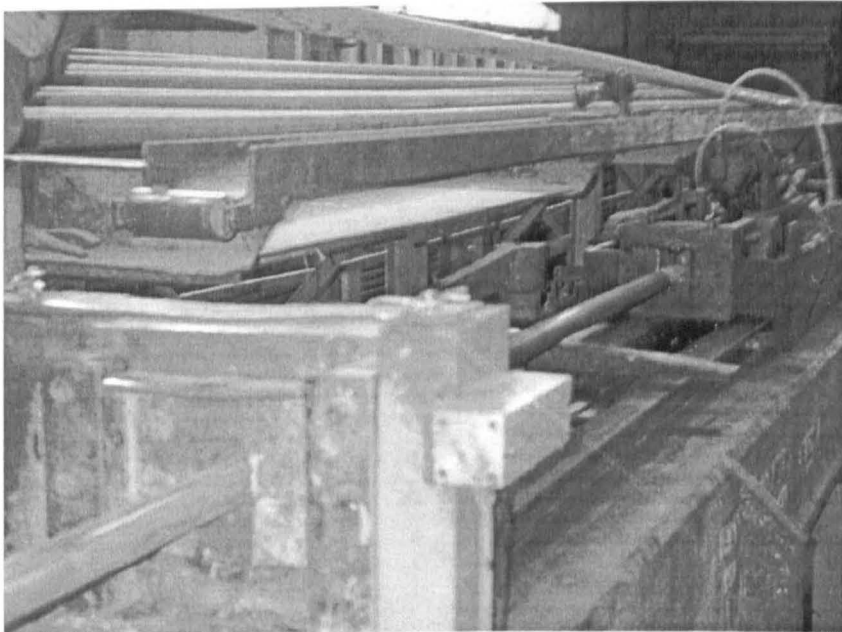


Figure 2.7 Draw Bench

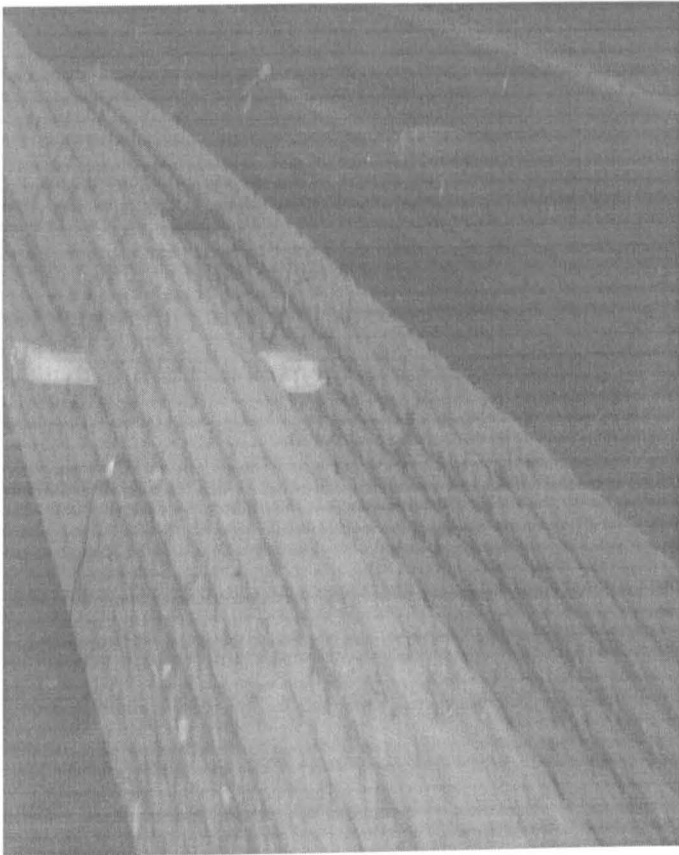


Figure 2.8 Finished *Swirly-flo* pipes

2.4 Theory

2.4.1 Factors Influencing Suspension Rheology

Rheology of a suspension can be Newtonian or non-Newtonian depending on the characteristics of the suspension. The main parameters which govern this are those of the solids and the suspending medium. Particle size and shape, and concentration are the principal factors that affect the viscosity of the suspension.

2.4.2 Particle Shape

Einstein (1906) developed the first theoretical model concerning spheres in a dilute slurry. This model was then furthered by Jeffery (1922), showing that the change in the shape of an ellipsoid in a dilute slurry produces a change in the viscosity of that slurry. According to Shook and Roco (1991), Happel and Brenner (1965) also showed that the viscosity increases as the shape departs from spherical.

Ming-Jau Yin, J.K. Beddow, and A.F. Vetten (1983) from the University of Iowa conducted an experiment on five different particle shapes with the same sphericity. The major conclusions of this paper are listed below:

- 1) the shape of particle does affect the behaviour of the slurry,
- 2) the sphericity is not a unique and adequate shape descriptor.

2.4.3 Particle Size

As a general rule flows of particles that are large, with a low concentration by volume, are often Newtonian in nature (Shook and Roco, 1991). This Newtonian nature was also proposed by Wasp (1977) for suspensions of large symmetrically shaped particles, 50 micrometres or larger. In the Newtonian range, the viscosity is a function of solids

volume concentration. Suspensions of smaller particles or of asymmetrically shaped particles possess non-Newtonian rheology.

2.4.4 Particle Concentration

For dilute suspensions, that is less than 1% by volume of solids, Einstein (1906) developed a formula from theoretical analysis to determine the viscosity as shown below.

$$\frac{\mu_m}{\mu_f} = 1 + 2.5C_v \quad (2.1)$$

This equation only applies to laminar flow, and to particles which are spherical in shape. The equation applies to particles which are large compared to the molecular dimensions and to situations where there are no particle interactions. Guth and Simha (1936) extended Einstein's analysis to concentrations of 20% with a 10% accuracy (Shook and Roco, 1991). The formula for this is shown below.

$$\mu_m = \mu_f(1 + 2.5C_v + 14.1C_v^2) \quad (2.2)$$

Many expressions have been proposed for the viscosity of more concentrated slurries, but none has been wholly successful. Thomas (1965) proposed an empirical equation (2.3) and indicates that it fits the data reasonably well over the entire range.

$$\mu_m = \mu_f[1.0 + 2.5C_v + 10.05C_v^2 + 0.00273 \exp(16.6C_v)] \quad (2.3)$$

The most complete analysis of highly concentrated flows was carried out by Frankel and Acrivos, (1966), in which the relative viscosity depends on the ratio of the concentration to the maximum concentration rather than the concentration itself. (See equation (2.4)) According to the authors this model agreed exceedingly well with the limited data that was available.

$$\mu_m = 1.125 \mu_l \left[\frac{\left[\frac{C_v}{C_{vmax}} \right]^{1/3}}{\left[1 - \frac{C_{vmax}}{C_v} \right]} \right] \quad (2.4)$$

*2.4.5 Suspension of Particles

The major concern in slurry flows is the accurate determination of the lowest velocity at which the suspension system can prevail. Unfortunately several identifiable states of suspension and partial settling have been observed and this means that there is no practical definition of a single "lowest critical velocity" which will apply for all circumstances. Thomas (1965) defined a "minimum transport velocity" as the velocity at which a layer of stationary or sliding particles appear at the lower surface of the pipe. Durand (1953) used a "limit deposit velocity" which he identified by the appearance of "a deposit regime" in the pipe. Graf *et al.* (1970) preferred to identify a "critical deposit velocity" which they defined as the velocity at which the solid particles settled out of suspension and formed a stationary bed.

Chien (1993) illustrated suspension/settling features which occur at increasing slurry flows and this has been incorporated with the key transition velocities of Govier and Aziz (1972). Figure 2.9 shows a reduced set of settling patterns redrawn from Chien's paper (Jones, 1997). Note the difficulty in making precise divisions between suspension regimes and particularly between asymmetric and symmetric suspensions (the V_{MI} transition).

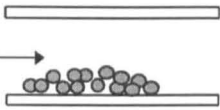
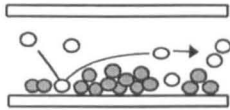
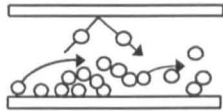
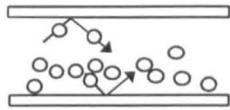
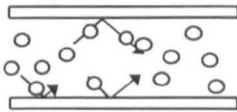
		Velocity, after Govier and Aziz (1972)
	(I) build-up of a stationary bed of particles at the bottom of the pipe	V_{M4}
	(II) <i>saltation</i> over a <u>stationary</u> bed of particles	$\leq V_{M3}$
	(III) <i>dune-like motion</i> as a result of saltation over a <u>moving</u> bed of particles	$V_{M3}-V_{M2}$
	(IV) <i>asymmetric suspension</i>	$V_{M2}-V_{M1}$
	(V) <i>symmetric suspension</i>	$\geq V_{M1}$
● settled particle	○ moving particle	

Figure 2.9 Patterns of Particles in Slurry Flow [Redrawn from Chien, (1993) by Jones (1997)]

The transition velocities in Figure 2.9 are defined in Table 2.1, taking into account the observation that with mixtures of sizes the transitions are less precise than otherwise. Notice that size-sorting effects can be expected to smooth the transitions to V_{M3} and V_{M4} .

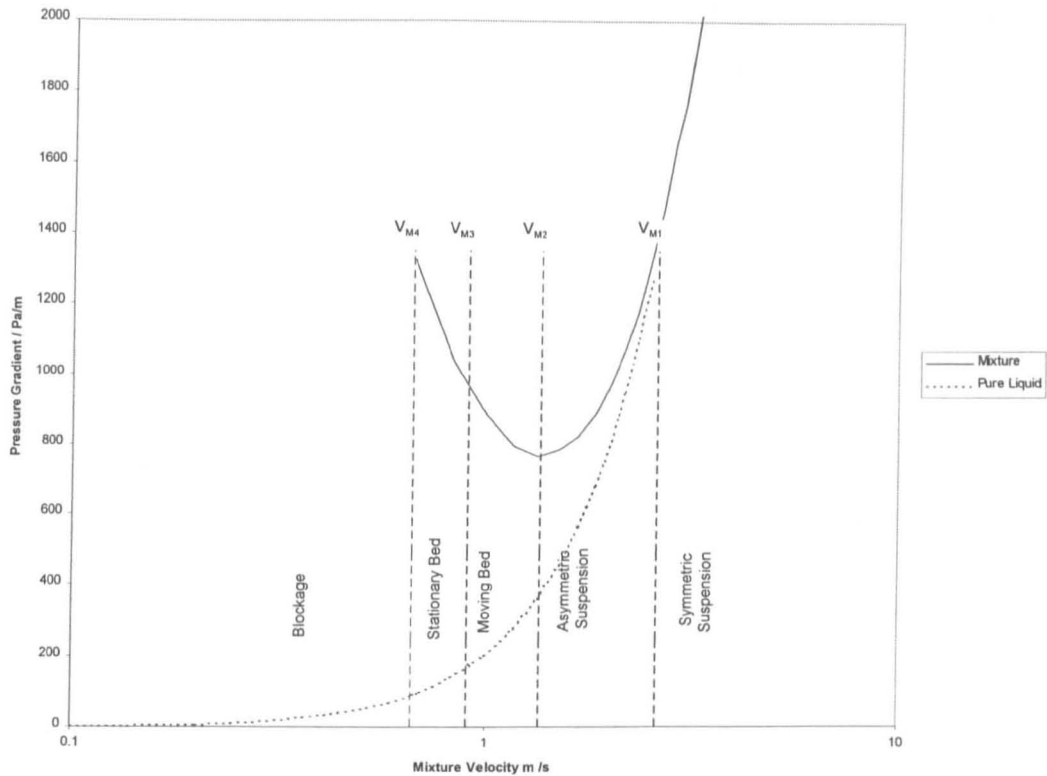


Figure 2.10 Schematic Classification of Transition Velocities in terms of Pressure Gradient for a Constant Volume Fraction of Solids (after Jones (1997))

V_{M1}	the velocity at and above which the mixture flows in the <i>symmetric</i> suspension pattern;
V_{M2}	the velocity at and above which (up to V_{M1}), the mixture flows in the <i>asymmetric</i> suspension; the velocity below which the solids form a deposit on the bottom of the pipe;
V_{M3}	the velocity at and above which (up to V_{M2}), a moving bed of particles exists on the bottom of the pipe; the velocity at which, with <u>mixed-size particles</u> , some particles move by <i>saltation</i> and some are in suspension; the velocity below which the part of the bed in contact with the pipe-wall becomes stationary;
V_{M4}	the velocity at and above which (up to V_{M3}) a bed exists, the lower part of which is <i>stationary</i> and in which the particles in the upper part move by saltation; the velocity at which, with <u>mixed-size particles</u> , some particles are in suspension; the velocity below which <i>blockage</i> occurs.

Simple correlations exist for the transition velocity V_{M1} and V_{M2} but no direct methods are known for V_{M3} and V_{M4} . Fortunately the latter two velocities are of less interest in this thesis.

Historical work on transition velocities was carried out by Hazen and Hardy (1906) who discussed the complementary work on the settling of sand suspensions by Blatch (1906). Blatch concluded that for each value of concentration there was a velocity at which the pressure gradient in the pipe was a minimum, and that this velocity represented a transition between flow with a stationary bed and suspended flow (later this would be termed the V_{M2} velocity). The precise distinction between symmetric suspension and asymmetric suspension, which defines V_{M1} in table 2.1, is difficult to establish in practice.

At low speeds Blatch observed that the greater part of the sand was dragged along the bottom of the pipe and practically clear water occupied the upper half of the pipe. This then caused a very high pressure loss. These high pressure losses are more prominent in gas/solid flow mixtures (Govier and Aziz, 1972). As the flow was then gradually increased the pressure drop decreased when the particles of sand entered into suspension. Then at higher velocities, the loss due to the sand was small since it was suspended. This is reflected in Figure 2.10.

2.4.6 Pipe Characteristics

Correlations for pressure losses in pipes, bends and other flow elements are related to the Reynolds Number, which is defined as:

$$Re = \frac{\rho V D}{\mu} \quad (2.5)$$

where ρ = fluid density kg/m³

V = mean flow velocity m/s

μ = dynamic viscosity of fluid Ns/m²

and D = diameter of pipe m

In defining the Reynolds Number, the various properties of the fluid have to be determined, namely, μ , the dynamic viscosity and ρ , the fluid density. The viscosity of

water varies considerably over normal ambient temperature ranges, as does density to a lesser extent. These variations are accounted for in Appendix A.

For steady, turbulent, incompressible flow in pipes the Darcy-Weisbach equation (Gerhart and Gross, 1985) gives a method of determining the pressure losses due to fluid friction in terms of a dimensionless variable termed the *Friction Factor* (f) ...

$$\Delta P = f \times \frac{\Delta L}{D} \times \frac{\rho V^2}{2} \quad (2.6)$$

Friction factor depends on relative roughness (ϵ/D) and Reynolds Number (Re) and can be determined from the Colebrook (1938) equation, which is...

$$\frac{1}{\sqrt{f}} = -0.86 \ln \left(\frac{\epsilon/D}{3.7} + \frac{2.51}{Re\sqrt{f}} \right) \quad (2.7)$$

The equation can quickly be solved using an iterative procedure, such as the Newton-Raphson method.

2.4.7 Swirling of Fluids in a Straight Horizontal Pipe

Swirling flow through a pipe is a highly complex turbulent flow, even when there is only one phase present, as for example, water. All the investigations into swirling flow, analytical or experimental, have considered only one phase flow, that of the fluid. Talbot (1954) examined laminar swirling flow and in 1961 Sibulkin (1961) produced a summary of the work prior to 1960. Kreith and Sonju (1965) investigated the decay of swirl using a linearised theory for Reynolds numbers in the range of 10000 to 100000. It was observed that turbulent swirl decayed to about 10-20% of its initial intensity in a distance of about 50 pipe diameters and that decay was more rapid for lower Reynolds numbers. Kitoh (1991) is the most modern paper on the turbulent swirling flow in a straight pipe, and examines the proposition that the swirl intensity (non-dimensional angular flux) decays exponentially with pipe length. He found that the decay coefficients were not constant as conventionally assumed, but depended on the swirl intensity. Major flow characteristics were discussed, and, importantly, Kitoh pointed out that the turbulent viscosity model did not work well in this situation and this is why the Reynolds Stress Model is used in modelling the flow through the swirl-inducing pipes, see Chapter 6.

2.4.8 Losses at Bends For Liquids Only

It is customary to express pressure losses in bends as follows ...

$$\Delta P_{bend} = K \times \frac{\rho V^2}{2} \quad (2.8)$$

where ...

ΔP_{bend} = the static pressure drop around the bend

ρ = the fluid density

V = fluid velocity

and K = static pressure-loss coefficient

Single values of K for bends are quoted in various sources (for example (Gerhart and Gross, 1985)), but for accurate work these values cannot be assumed. K is in fact a strong function of Reynolds Number and R/D , the ratio of bend radius to pipe diameter.

Pressure losses are due to four main factors:

1. dynamic pressure losses given by an equation of the form of (2.8),
2. upstream frictional losses due to the length of tangent pipe leading to the bend,
3. downstream frictional losses due to the length of tangent pipe downstream of the bend,
4. gravitational pressure losses due to the vertical distance between pressure-measurement stations.

Combining these terms ...

$$\Delta P = K \times \frac{1}{2} \rho V^2 + \frac{1}{2} \rho V^2 \times f \times \frac{L_u + L_d}{D} + \rho g \Delta z \quad (2.9)$$

ΔP = pressure drop between pressure stations upstream and downstream of the bend,

K = gross pressure-loss coefficient dependent upon the geometry of the bend, pipe roughness and Reynolds number, Re ,

($K=K_b+K_c+K_d$, where K_b is the term for the bend length, K_c is the term representing pressure losses due to the bend *curvature*, and K_d is a term

accounting for the *re-establishment* of fully developed straight-pipe flow in the downstream tangent),

$f =$ friction factor which may be obtained as a function of Re and roughness, ε/D ,

$\varepsilon =$ effective roughness height (for glass and plastic ε is often assumed to be zero or, alternatively, a nominal value between 8×10^{-6} and 2×10^{-5} is chosen (ESDU, 1995),

$L_u =$ upstream tangent-pipe length

$L_d =$ downstream tangent-pipe length

$\rho g \Delta z =$ gravitational pressure drop due to the vertical distance, Δz , between transducers.

Following the method given in (ESDU, 1995)

$$K_b = 0.07 \times \theta \times (R/D) \times f/4 \quad (2.10)$$

where $\theta =$ turning angle of the bend in degrees (= 90 for tests described here)

$$K_c = \frac{\theta}{90} \left(\frac{R}{D} \right)^{\frac{1}{2}} \left[0.03 + 1.3 \left(\frac{\varepsilon}{D} \right)^{\frac{1}{2}} \right] \quad (2.11)$$

and, for $R/D \geq 1$

$$K_d = 0.2 \times (R/D)^{-1.2} \times \phi_1 \times \phi_2 \times \phi_3 \quad (2.12)$$

where

$$\phi_1 = \text{Reynolds number correction} = \left(1 + \frac{10^4}{Re} \right) \quad (2.13)$$

$$\phi_2 = \text{downstream correction factor} = \left(1 - e^{-0.1L_d/D} + \frac{3(e^{-L_d/D})}{(R/D)^2} \right) e^{-\left\{ \frac{1}{(L_d/D)+1} \right\}^{2R/D}} \quad (2.14)$$

$$\phi_3 = \text{bend angle correction factor} = 1.04 - \left[(110 - \theta)^2 / 10^4 \right] \quad (2.15)$$

For $\theta=90$, $\phi_s = 1$.

$$K=K_b+K_c+K_d \quad (2.16)$$

2.4.9 The Pump

The experimental rig for this thesis utilised a pump with integral sump (header tank) and is completely described in Chapter 3. This section describes briefly the equations which govern the pressures and power output from that pump.

Pumping power is the product of the head loss and volumetric flow rate. The head loss from the pump can be derived by using the Bernoulli equation of fluid mechanics.

The increase in total head which the pump provides is given as:

$$\Delta H_{pump} = \left(\frac{V_1^2}{2g} + \frac{P_1}{\rho g} + z_1 \right) - \left(\frac{V_0^2}{2g} + \frac{P_0}{\rho g} + z_0 \right)$$

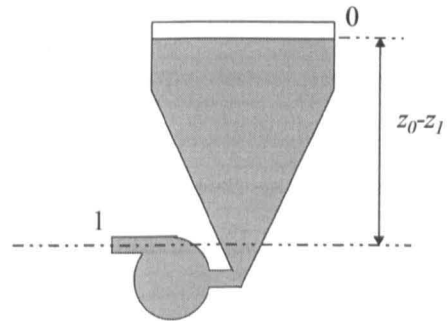
$$\begin{aligned} \text{pumping power} &= \text{press. loss} \times \text{vol. flow rate} \\ &= \Delta H_{pump} \times \rho \times g \times Q_{pump} \end{aligned}$$

where ΔH_{pump} = total head change,

ρ = the effective density of the medium,

Q_{pump} = the delivery flow rate of the pump,

and other variables are defined in the diagram.



Assuming that the velocity at station 0 is zero and the pressure at station 0 is atmospheric, the power produced becomes ...

$$\dot{W}_{PUMP} = \left[P_{1\text{ GAUGE}} + \frac{\rho \times \left\{ Q_{pump} / (\pi d^2 / 4) \right\}^2}{2} + \rho g \Delta z \right] \times Q_{pump} \quad (2.17)$$

This is less than the power consumed by the pump because dead-load and static friction forces must be overcome before any fluid can be pumped. If the output power of the pump is determined and the electrical power consumed by the pump is measured, by the Fluke power meter, and the efficiency of the pump can be evaluated as follows.

$$\eta = \left[\frac{\text{Power out}}{\text{Power in}} \right] \quad (2.18)$$

2.4.10 Wear in Pipes

Industries spend millions of pounds a year to repair erosion damage caused by solid particle impingement. Solid particle erosion affects a large number of industries including the oil and gas, aerospace, automotive and electrical power generation industries. Erosion results in facility downtime, loss of income and high repair costs. In order to reduce these losses a fuller understanding is required of the physical processes involved and factors that influence erosion. These factors include particle properties such as size, shape, density, hardness, and concentration. The properties of the pipe also have an effect, such as elastic modulus, yield stress, and toughness. The interaction of particles and carrier fluid also provides variables that affect the rate of erosion such as particle speed, impingement angle, particle rotation and the type of carrier fluid. (Rybicki and Shadely, 1992)

The following erosion terminology is found to be quite useful in referring to erosion behaviour. “*Normal impingement*” refers to those situations where solid particle impacts the target material at an impingement angle of 90 degrees. “*Oblique impingement*” refers to all impact angles less than 90 degrees. Normal impingement involves velocities which are normal to the surface of the target material, while oblique impingement involves velocity components that are normal and tangential to the surface of the target material. “*Erosion ratio*” is the ratio of the mass of the target material removed or eroded to the mass of impinging particles required to remove that material.

Over the past 40 years, a number of papers have been written with regard to erosion. A large number of possible mechanisms have been presented. A number of models have been developed to predict erosion rates when the values of certain parameters are known.

In 1958, a significant contribution to characterising erosion was made by Finnie (1958). Finnie developed a solid particle erosion model based on a mechanism of material removal resembling that of a cutting or micro-machining process. Finnie performed the tests on a glass target using spherical cast iron particles with a diameter of 600 micrometres. At small angles of impingement, the predictions of the model compared well with experimental data. However, at angles close to the normal, Finnie's model predicts no erosion, which is the contrary to the experimental evidence. Finnie improved his model using empirical correction factors to take account of this fact.

Bitter (1963) theorised that a second component of erosion exists and derived a solid particle erosion model based on this theory. Using the Hertzian contact stress equations of Timoshenko and Goodier (1987), Bitter developed a two part model consisting of components of erosion termed "deformation wear" and "cutting wear." Deformation wear results from repeated impacts that cause cracks to occur which spread away from the initial deformation. Cutting wear results when "particles impact a body at an acute angle, scratching out some of the material from the surface." (Bitter, 1963a) Cutting wear is more complex due to the presence of velocity components normal and tangential to the surface.

Bitter's model provides a good correlation between the theoretical model and the experimental results involving aluminium and copper target materials. However, some of the values for yield stress of the target materials were unrealistically high. Subsequent work by Neilson and Gilchrist (1968) simplified Bitter's equations.

Bitter's model introduced the concept that more than one mechanism of erosion exists. These components can occur simultaneously, yet have differing effects on the material. Quite a few authors have adopted this approach, and many mechanisms of erosion have been suggested, such as surface cracking, subsurface cracking, low-cycle fatigue and target melting. Rybicki and Shadely (1992) give a comprehensive discussion of these mechanisms.

In bends there are certain areas where the wear is higher than the rest of the bend, commonly known as *wear spots*. These areas are illustrated in Figure 2.11, which is based on an illustration found in Zenz and Othmer's book (Zenz and Othmer, 1960). The first region of high wear is when the bend has almost fully turned from the horizontal to vertical. On the outside wall of the pipe, particles begin to circulate against the wall (Region 1, in Figure 2.11). Region 2 shows that as the flow traverses around the bend some of the particles ricochet from the outside of the bend and move to a common impact area on the inside of the bend.

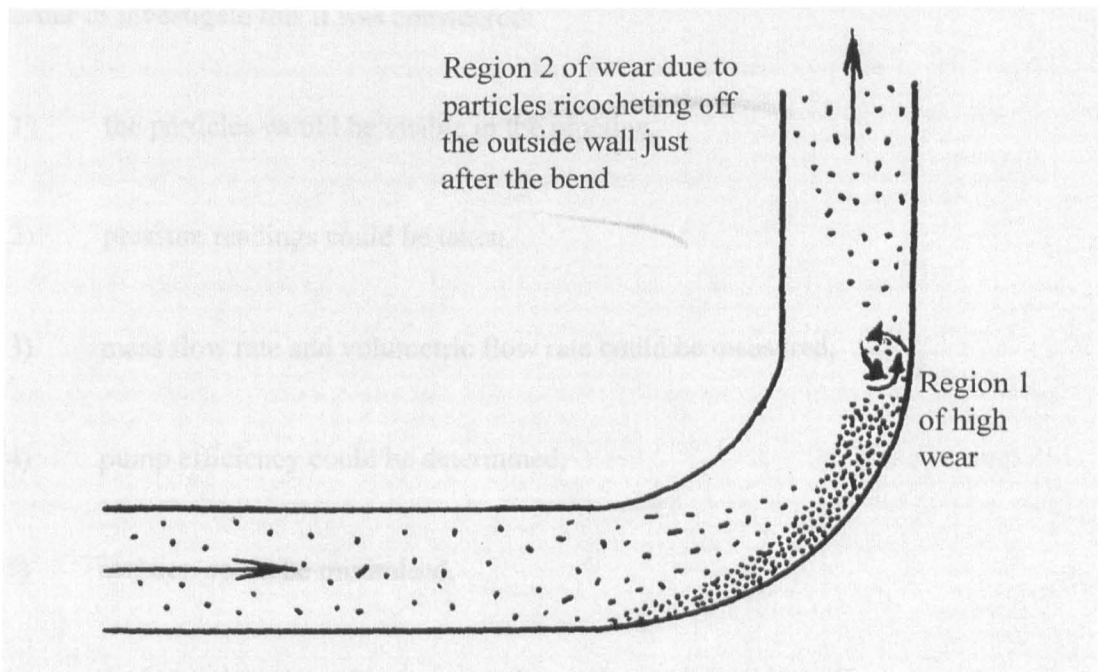


Figure 2.11 High Wear Areas on a Bend (copied from Zenz and Othmer, (1960))

3.0 Design and Commissioning of the Test Rig

3.1 Design Criteria

A rig was designed to study the flow of water/beads mixture in a 50mm bore pipe with and without experimental pipe sections. The most important position for such a section was considered to be before the bend because it was felt that the swirl-inducing pipe would reduce the pressure loss and wear around the bend. No references could be found for previous experimental work with this configuration. In order to investigate this it was considered:

- 1) the particles would be visible in the pipeline,
- 2) pressure readings could be taken,
- 3) mass flow rate and volumetric flow rate could be measured,
- 4) pump efficiency could be determined,
- 5) aeration could be minimised,
- 6) the inter-changing of straight and bend pipework could be effected easily,
- 7) the pump flow rate could be varied so that a range of different velocities could analysed,
- 8) there was provision for draining the rig,
- 9) beads could be added and taken away from the rig to give a set of mixtures with a range of concentrations,
- 10) the header tank was suitable for the pump suction required.

3.2 Summary of Design Method

The method of design and assembly was undertaken with the foreknowledge that outside companies would be involved in manufacturing the test rig. All fabricated components were individually drafted and were given a specific drawing number.

The assembly of the test rig, which was located in L4 Engineering Laboratory, at the University of Nottingham, was carried out in consultation with the technician staff of the Faculty Woodwork Workshop, and the Departmental engineering technicians. The actual pipe test rig was mounted on vertical boards, themselves mounted on the structure of an existing test facility. Careful planning had to be made to ensure that the boards were correctly placed, so that there would be no excessive bending stresses or other loads on the pipe sections, or the wooden boards. The lower section of the rig was raised above the floor. This necessitated the fabrication of stands for the pump and de-aerator.

The header tank, manufactured at the University, was located at the highest part of the rig to allow water and particles to be mixed together. This was also used for retrieving the beads from the test rig. Water/particle mixture from the header tank were led to the pump through a tough reinforced flexible pipe.

The following paragraphs give details of the major components of the test rig together with the relevant measuring equipment. The problems of assembly and fabrication are discussed at the end of this chapter.

3.3 The Wooden Frame

To allow easy interchange of pipes and bends, it was necessary to have a flexible arrangement. This was achieved by attaching the pipe sections to boards made from Medium Density Fibreboard (M.D.F.). This made it possible to mount the pipes anywhere on the board. Figures 3.1 and 3.2 illustrate the general arrangement of the test rig.

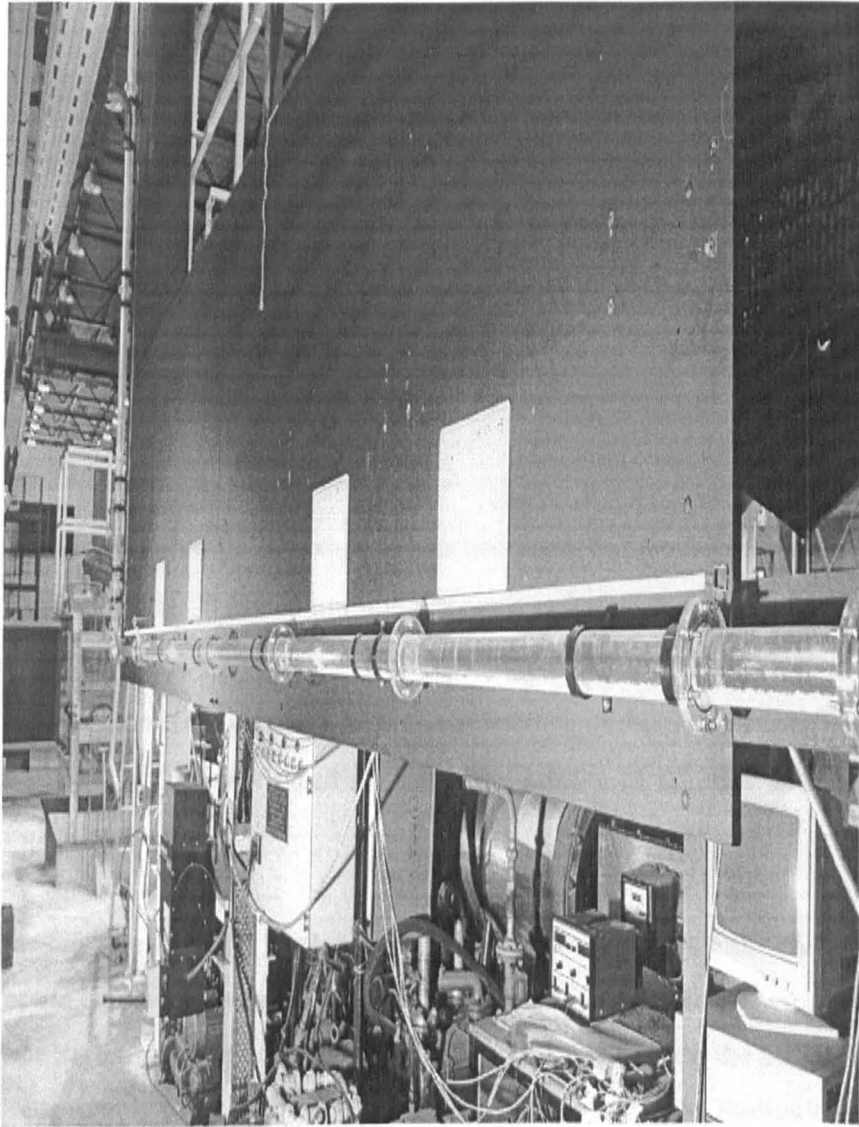


Figure 3.1 Lower section

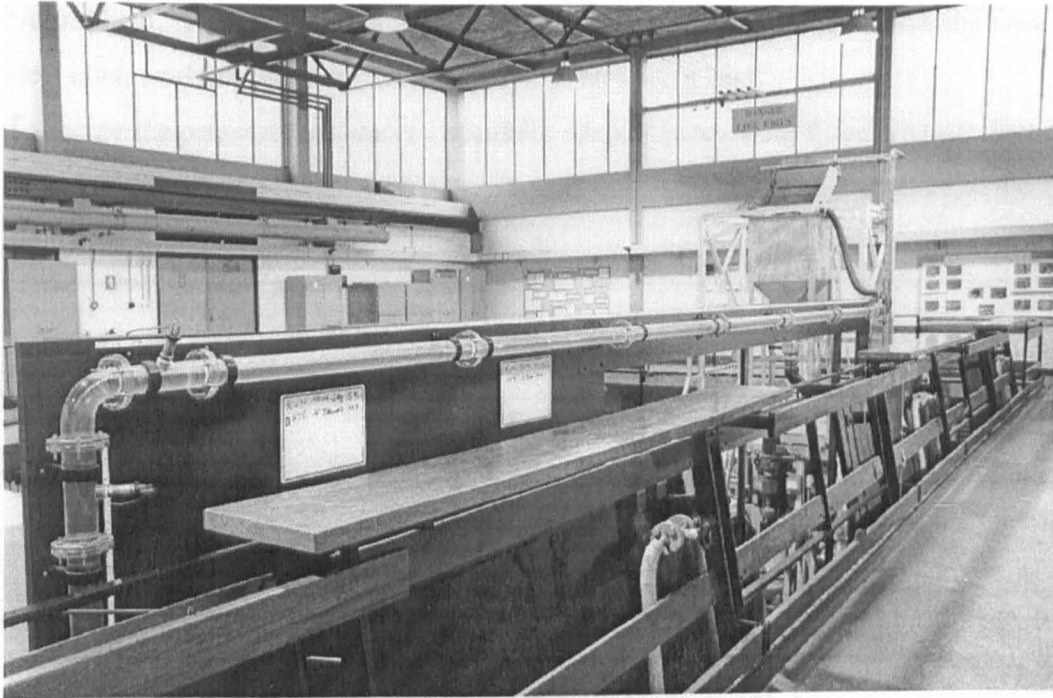


Figure 3.2 Upper Section

3.4 Pipe Selection

To observe the water/particle mixture it was necessary to manufacture the pipe out of a transparent material. After examining alternatives it was decided that *Transpalite*[®] was the best material. (Manufacturing was carried out by Stanley Plastics Ltd., Midhurst, West Sussex, England.) The characteristics of this *Transpalite*[®] are shown in Table 3.1. The pipework had an outside diameter of 65 mm and an internal diameter of 50 mm.

Bent pipework was made by a sub-contractor of Stanley Plastics Ltd. The first attempt at the bends was very poor, as can be seen in Figure 3.3. The circular cross section was severely distorted by the bending process. However, the second attempt proved considerably more successful. All the bends have a mean Radius/Diameter ratio of 0.6. When the manufacturing of the pipes and bends was completed, the pipe work was assembled before delivery, to ensure that all the fittings were satisfactory, and interface flanges were marked for ease of reassembly at the University of

Nottingham. The pipes are joined together by flanges and are secured with stainless steel nuts, washers and bolts; then sealed with an O-ring seal.

To secure the pressure transducers, specially adapted pipes were fitted with a helecoil placed within a boss. This enabled transducers to be screwed in and attached to the pipework.

Table 3.1: Properties of Transpalite® SS			
ASTM Test Procedure	Physical Property	Average Value	ANSI/ASME /PVHO-1 Minimum Specification
D542	Refractive Index	1.49	1.49
D570	Water absorption in 24 hours	0.25 %	0.25 %
D732	Ultimate Shear Strength	79 MPa	55 MPa
D785	Rockwell Hardness	M Scale 108	M Scale 90
D792	Specific Gravity Poisson's Ratio	1.19 0.38	1.19
D696	Coeff of Linear Expansion @ 26 °C	$8.48 \times 10^{-5} / ^\circ\text{C}$	$7.74 \times 10^{-5} / ^\circ\text{C}$
D638	Ultimate Tensile Strength Elongation at Break Modulus of Elasticity	77 MPa 5% 3540 MPa	62 MPa 2% 2758 MPa
D621	Compressive deformation at 275 MPa and 50°C	≤ 0.56 %	≤ 1 %
E398	UV Transmission of a casting batch	≤ 0.08 %	≤ 5%

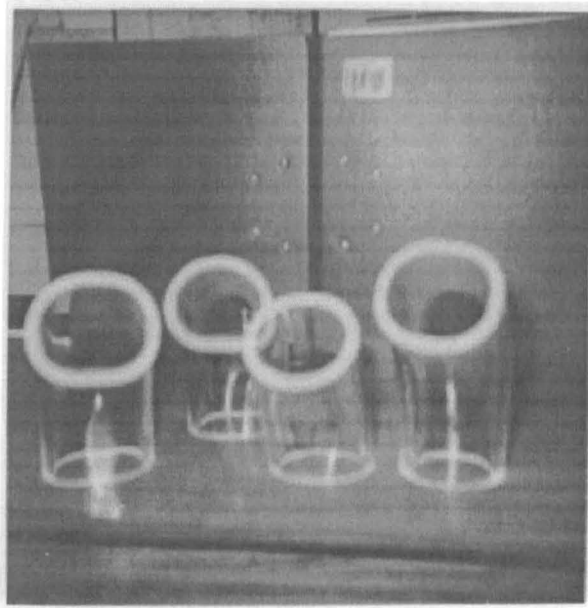


Figure 3.3 Unsatisfactory bends

3.5 The Design and Manufacture of the De-aerator

The de-aerator was manufactured from *Transpalite*[®] by the Faculty Engineering workshop at the University of Nottingham. In the commissioning of the test rig, it was found that the de-aerator did not perform well because it was structurally very weak, giving rise to leaks and was generally of a poor build quality. Following modification of the design and a rebuild the new de-aerator was installed for preliminary tests. The structural integrity was much improved and there were no further leaks. A picture of this de-aerator during a test run is illustrated in Figure 3.4. Flexible couplings were fitted at the entrance and exit of the de-aerator to reduce the vibration from the pump and allow easy installation of the remainder of the pipe system. The flexible coupling links were fixed with stainless steel “jubilee” clips. The de-aerator was fitted with a valve at its base to allow for the drainage of water from the test rig, since this is the lowest point on the rig. From the top of the de-aerator there was a small bore flexible tube, to allow the air released from the water to escape.

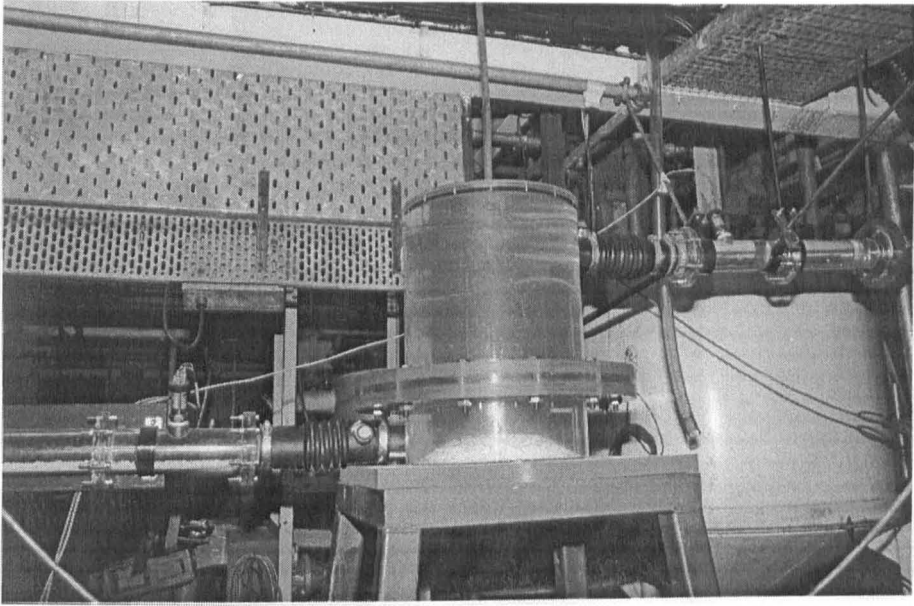


Figure 3.4 De-aerator

3.6 Sala Pump

Due to financial constraints, it was not possible to obtain a pump of the desired specification for the test rig. As a result it was necessary to make modifications to an existing Sala pump and its electrical control. A special electrical junction box was fabricated so that the electrical power could be measured safely. On commissioning of the test rig it was found that the head of water varied in the sump of the pump. It became necessary for an operator to continuously watch and control the head of water in this sump. The problem was overcome by providing a sealed lid for the sump. The Sala pump unit is illustrated in Figure 3.6, which shows the lid modification.

3.7 Speed control

The rotational speed of the pump was controlled by the use of an electrical inverter, which changed the electrical frequency supply to the pump. The inverter is manufactured by Heenan Drives Ltd., Worcester, England. Figure 3.5 shows the inverter used on the test rig.

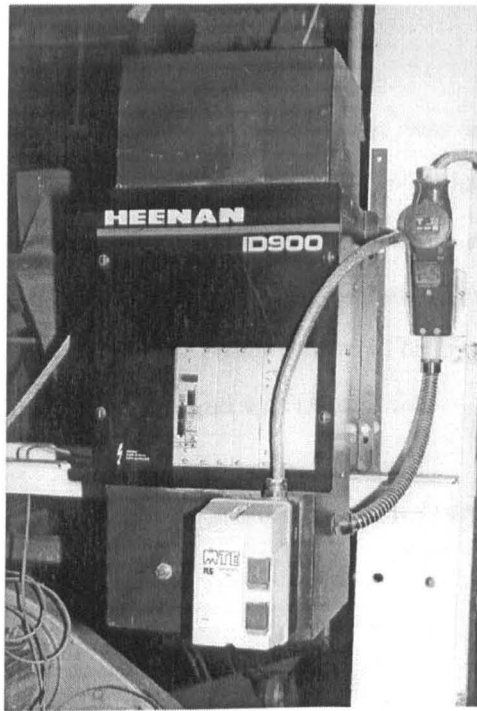


Figure 3.5 Heenan Inverter

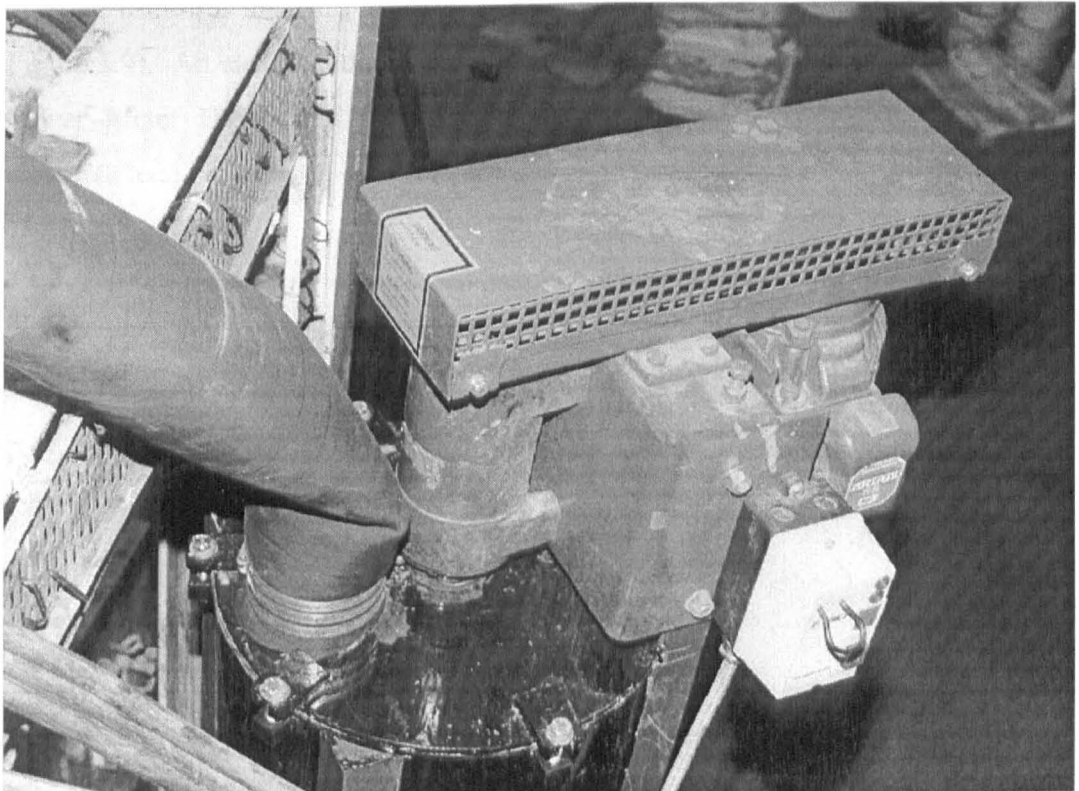


Figure 3.6 Sala Pump Viewed From Above, With The Lid Modification

3.8 Electrical Power Meter

In order to measure the efficiency of the pump it was necessary to obtain the electrical power supplied to the pump. To measure three-phase electrical power, one has to use the “two Watt meter” method for an unbalanced phase load, or variant of this method. The use of a single Watt meter is permissible assuming balanced phase loads which would be the case for the pump motor. The Fluke 39 power meter was utilised for single phase measurement and was chosen for:

- 1) its ability to handle non-sinusoidal waveforms produced from the inverter,
- 2) its ease of use.

The wiring for the connections to the power meter were made safe by the provision of plug-in sockets for the voltage readings across two of the phases and sheathed external cable for the third phase to passively measure the current in one line (see Figure 3.9). An electrical diagram (Figure 3.8) taken from the handbook (Model 39 Power Meter Handbook, 1995) shows the wiring connections for a balanced electrical load. Figure 3.7 illustrates the power meter.

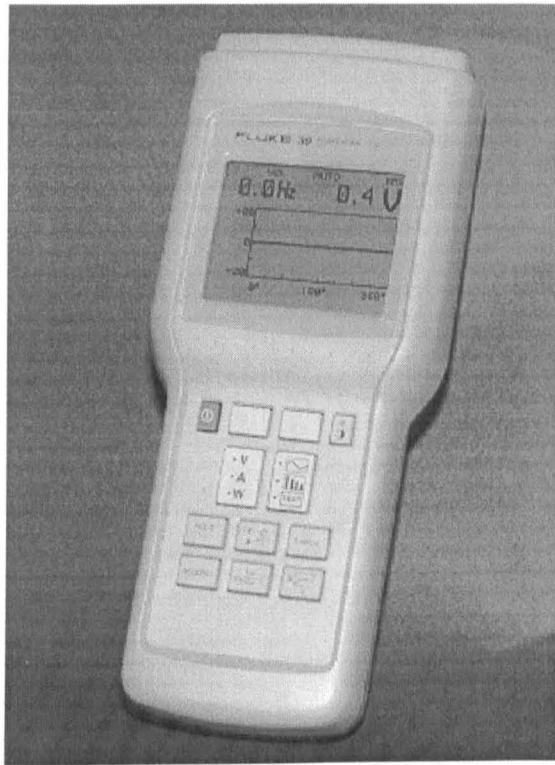


Figure 3.7 Fluke Power Meter

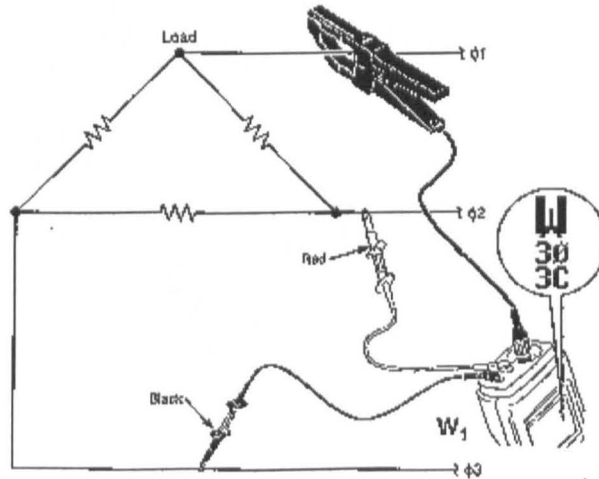


Figure 3.8 Wiring Diagram for the Power Meter

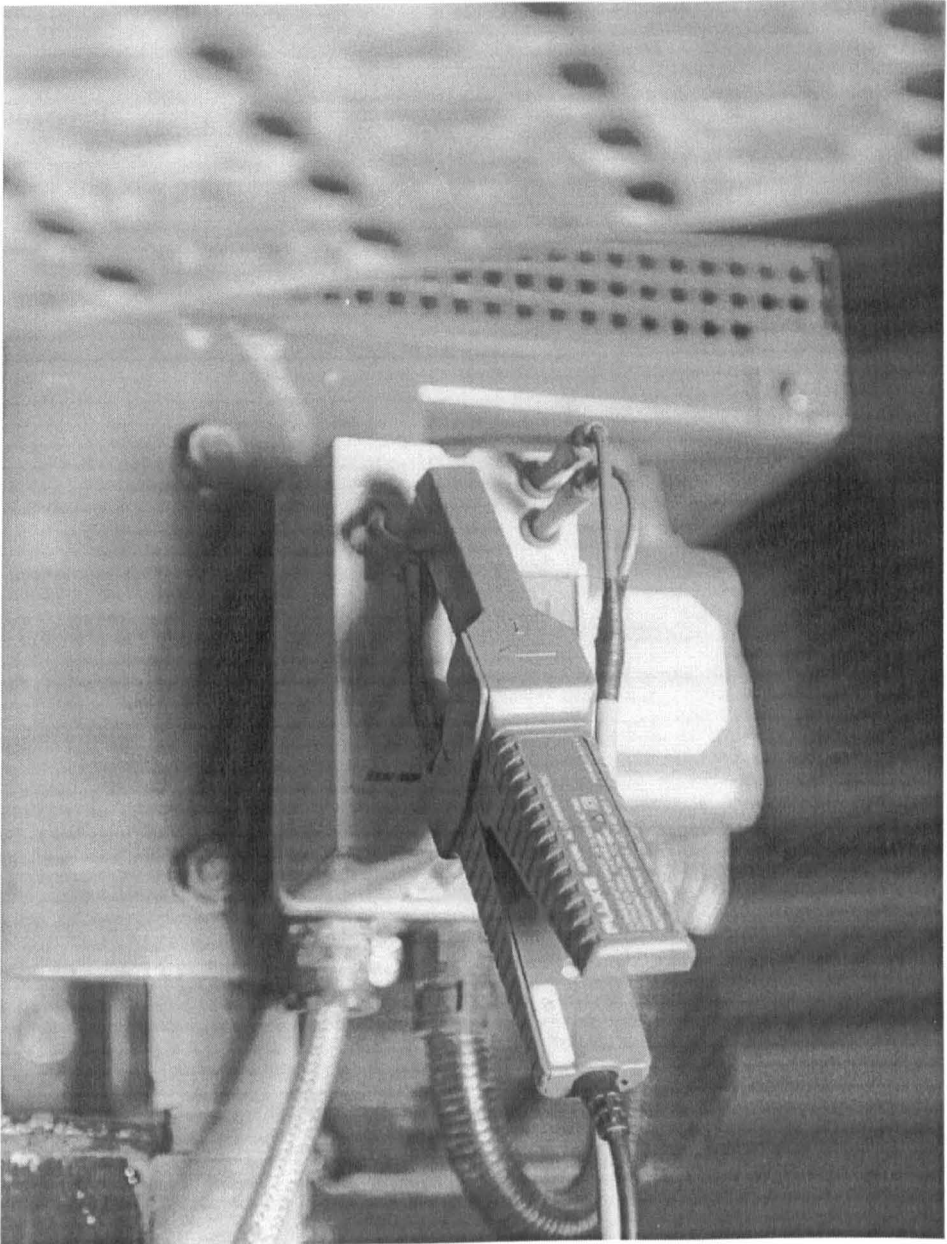


Figure 3.9 Passive Current Clamp and Voltage Leads in situ

3.9 Pressure Transducers and Data Logger

The pressure transducers were chosen for their ability to handle water/particle mixtures and low pressures. The datalogger was selected for ease of installation and reasonable price.

The datalogger had eight channels, one for each of the pressure transducers. The power for the datalogger was from the mains supply which in turn was rectified to 15 Volts direct current. This was connected to a personal computer via a serial port.

The transducers were purchased from Rayleigh Instruments Limited, Essex. A quality certificate for all the transducers was provided by the manufacturer, the details of which are shown below. A picture of a transducer, in situ on the test rig, is shown in Figure 3.10.

Table 3.2 Transducer Properties	
Name: Henschen Type 861 pressure transducer	
Supply voltage	13-32 v DC
Output signal	4-20 mA
Non-linearity and Hysteresis	≤ 0.5 % of final value
Long-term stability	≤ 0.1 % of final value
Long term stability	≤ 0.1 % of final value

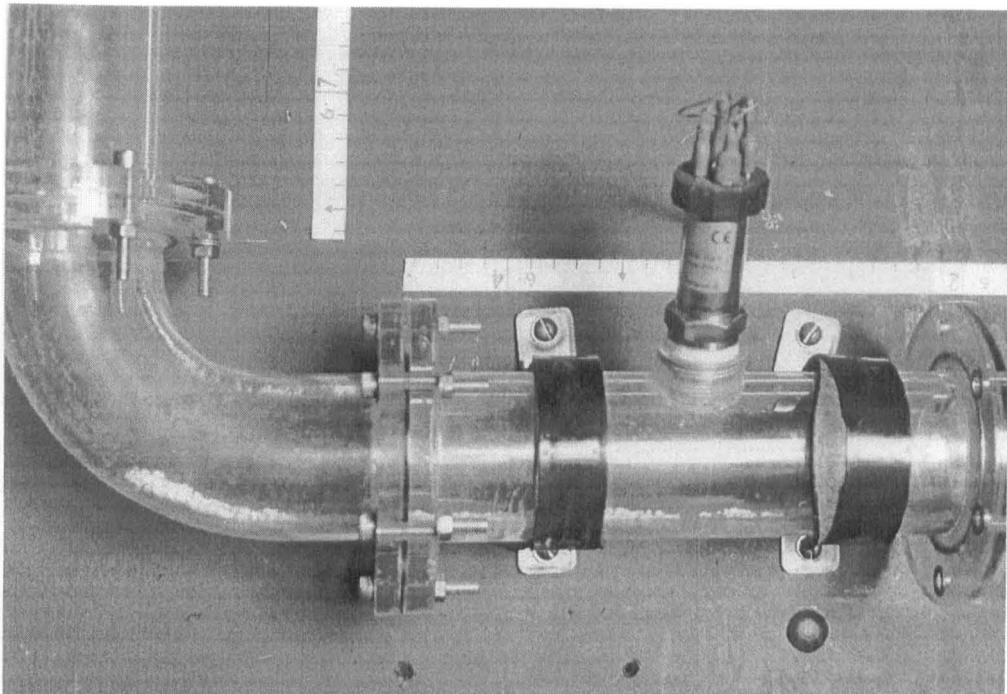


Figure 3.10 Pressure Transducer before the Rising Main

3.10 Volumetric and Mass Flow

Mass and volumetric flow was measured by a calibrated container, spring balance scales and a stop watch. The spring balance was situated above the header tank for the Sala pump. The spring balance was provided with a calibration certificate. Figure 3.11 shows the spring balance above the header tank. The picture illustrates the lifting apparatus, which consisted of two pulley blocks connected to a cantilever beam above the header tank. This use of pulleys provided the operator with a 3:1 mechanical advantage.

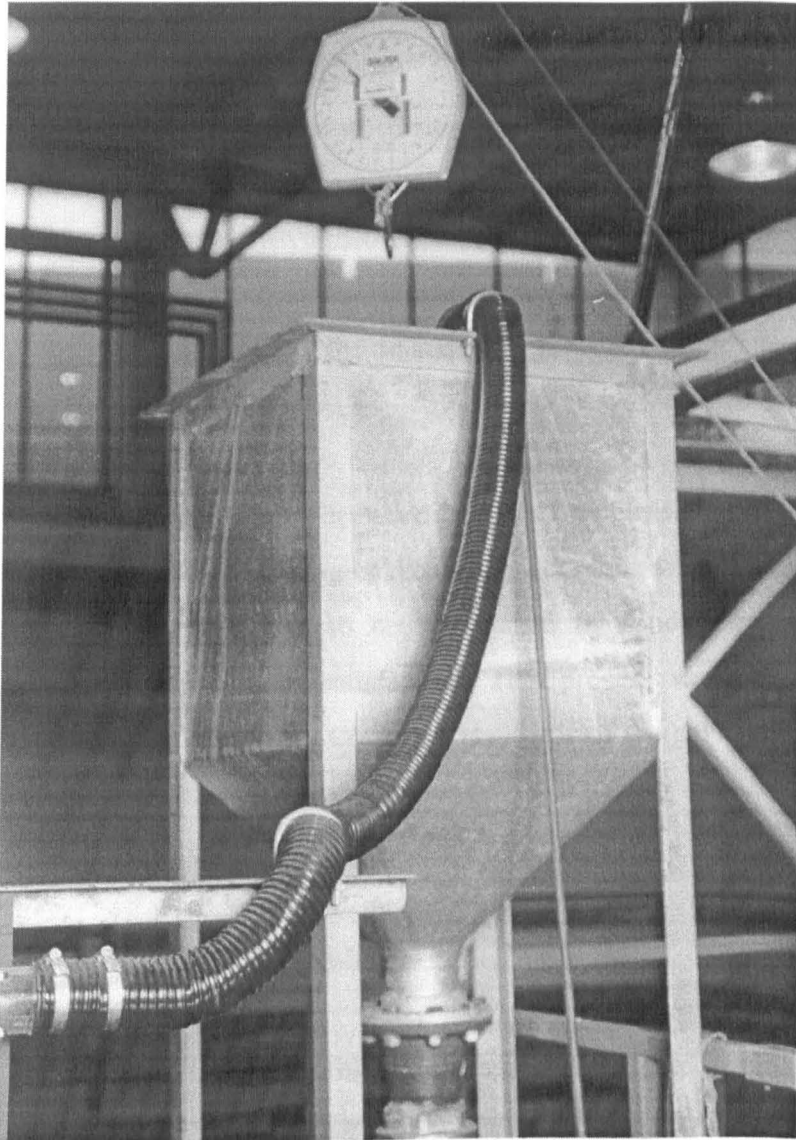


Figure 3.11 Spring Balance with Header Tank

3.11 General Commissioning of Test Rig

The test mixture consisted of mains water and plastic beads which were white in colour. The beads were obtained from Victor Plastics Ltd., Coventry, England, and provided good contrast to the blackboard on which the *Transpalite*[®] pipes were mounted. The characteristics of the beads are outlined later in this chapter.

3.12 Problems in Commissioning

When the rig was constructed the restrictions of beams and columns of the existing structure in the laboratory, caused the pump outlet to be misaligned with the entrance to the de-aerator. This caused asymmetrical forces on the pipe, which then had to be restrained by the use of tie bars. It was then necessary to attach a flexible connection between the outlet pipe and inlet of the de-aerator to prevent “water hammer” in the pipe.

Ideally the header tank should have been constructed of stainless material but was not due to financial constraints. Painting of the steel header tank with Hammerite paint proved unsatisfactory and it had to be refurbished by sand blasting and then galvanising, which proved more satisfactory. This process was carried out by Annometals, Nottingham, England. Corrosion standards of the galvanised steel met BS5466, ISO3768 and DIN 50021 specifications.

3.13 Calibration of Pressure Transducers

The commissioning of the rig involved zeroing the pressure transducers with reference to the datalogger (Signallogger-PC), supplied by Laplace Instruments Ltd. The data obtained from the datalogger was later manipulated using Microsoft® Excel. The transducers measure pressure relative to the atmosphere (gauge).

3.14 Experimental Arrangements

The flow tests were conducted with a standard rig set-up, as illustrated in Figure 3.12. Pressures were logged once a second, and electrical power was sampled using the Fluke Model 39 power meter. Tests were then run at various power settings (approximately equivalent to inverter frequencies varying from 20 Hz to 60 Hz). The pressure reading stations are indicated in Figure 3.12. Where, 1,2,3...8 refer to the pressure reading stations.

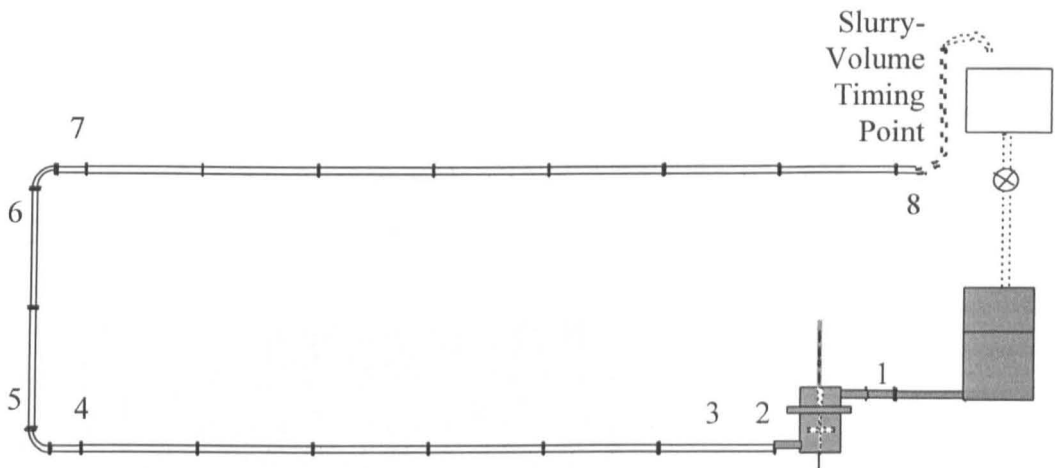


Figure 3.12 Standard Schematic Set-up

The term “standard set-up” refers to all runs that did not use a *Swirly-flo* pipe. When the *Swirly-flo* pipes were used, the position of transducer 3 was changed. This is illustrated in Figure 3.13 and 3.14. Again 1,2,3...8 refer to the pressure reading stations.

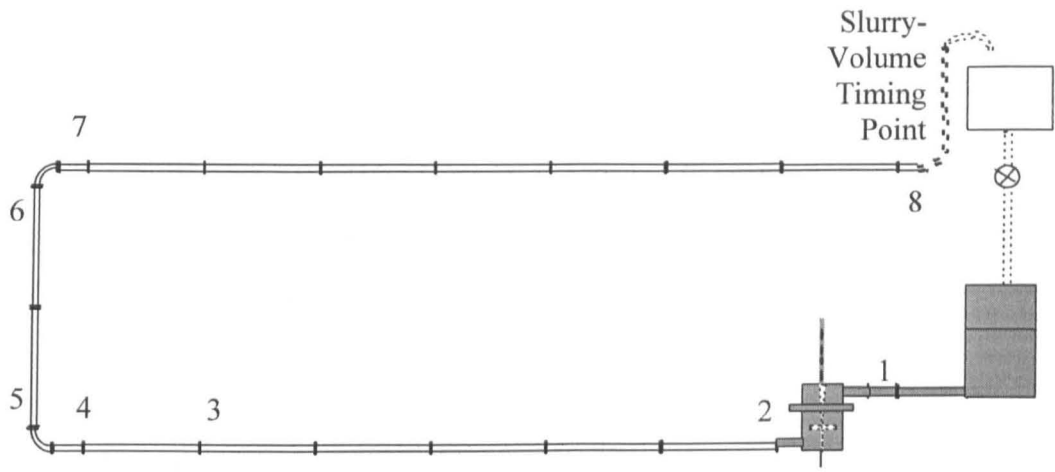


Figure 3.13 *Swirly-flo* Schematic Set-up

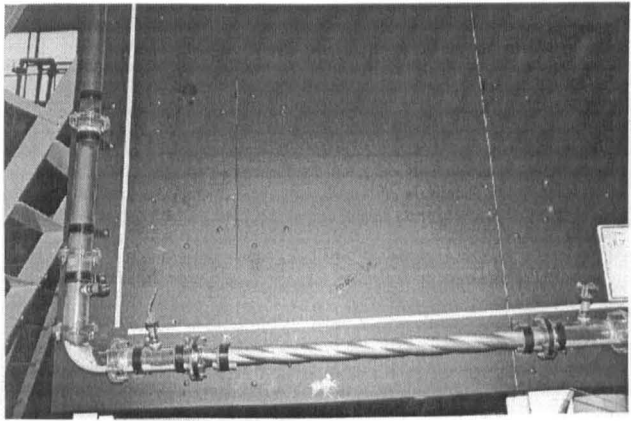


Figure 3.14 Long *Swirly-flo* in-situ

Pressure data was referred to by the station where it was sampled and flow characteristics by the axial length away from the de-aerator flange. For example, the pressure difference across the bend between station 4 and 5 could be variously described as...

$$P_4 - P_5 = \Delta P_{45} = P_{45}$$

3.15 Bead Characteristics

The beads chosen to act as the solid part of the ‘slurry’ were white in colour to provide good contrast with the black backboards. The beads were denser than water with an average specific gravity of 1.46 and were bought from Victor Plastics Ltd., of Coventry, England.

The beads had a roughly cylindrical shape, and their size distribution is shown in Figure 3.15. This gave a median value of 1.75 mm and a calculated mean value of 1.87 mm with a standard deviation of 0.257 mm.

The determination of the density was performed using a float and sink technique, with sodium polytungstate solutions. Table 3.3 shows the results obtained and Figure 3.16 illustrates this graphically. This graph gave a median value of 1.45 relative density, and an average of 1.46, with a standard deviation of 0.005.

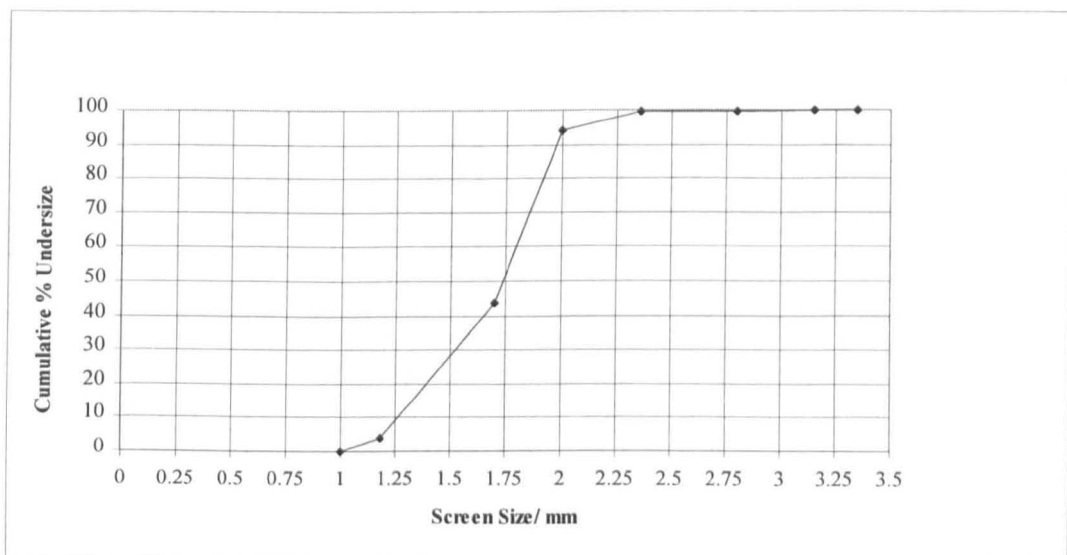


Figure 3.15 Screen Sizes of Plastic Beads for Water/Particle Mixtures Tests

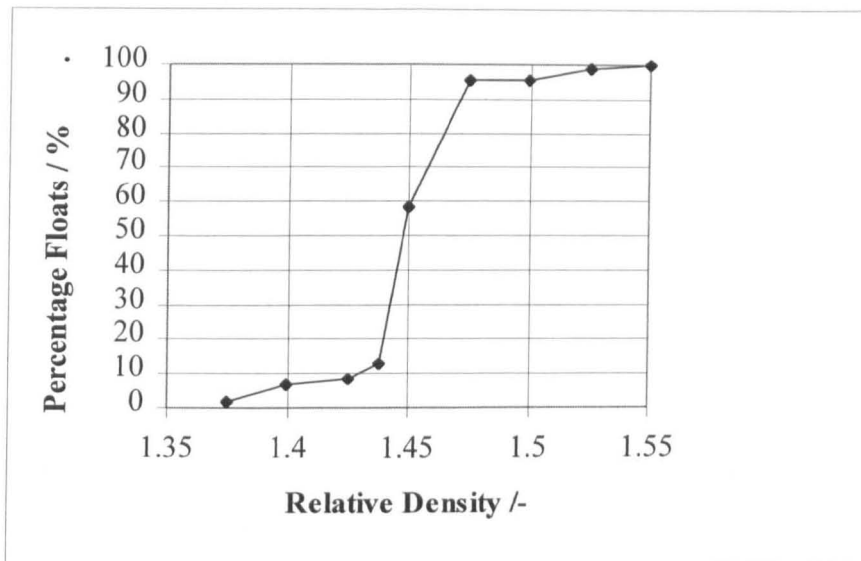


Figure 3.16 Float and Sink Data for a Sample of Beads

Relative Density	Mass (g)	Mass %	Cumulative %
F @ 1.375	23.0	1.4	1.4
1.375 - 1.400	87.0	5.3	6.7
1.400 - 1.425	28.0	1.7	8.5
1.425-1.438	70.2	4.3	12.8
1.438 - 1.450	734.8	45.3	58.1
1.45-1.475	607.7	37.5	95.6
1.475 - 1.500	1.5	0.0	95.7
1.500 - 1.525	50.0	3.0	98.8
S @ 1.525	17.8	1.1	100.0
Total	1620.0	99.6	

Size mm	Mass (g)	Mass %	Cumulative %
less than 1- 1	0	0	0
1 - 1.18	19.1	3.8	3.8
1.18 - 1.7	200.8	40.1	43.9
1.7 - 2	252	50.3	94.3
2 - 2.36	27.3	5.4	99.7
2.36 - 2.8	0	0	99.7
2.8 - 3.15	0.6	0.2	99.9
3.15 - 3.35	0.8	0.2	100
Total	500.5	100	

3.16 Pump Characteristics

The power consumption of the pump with and without the lid modification was examined. The pump was one of the most critical parts of the test rig, and it was necessary to obtain its characteristics before use. This was performed with the standard set-up (Figure 3.13) of the test rig with water.

In Figure 3.17, the two best fit straight lines illustrate how the power delivered to the fluid was increased with the lid modification for the same electrical input power. This was due to the extra head provided by the water in the header tank. This water head stopped a great deal of air entering the water circuit, and provided an increase in efficiency. The electrical power required to start the water moving was less, due to the fact that the resisting head was less.

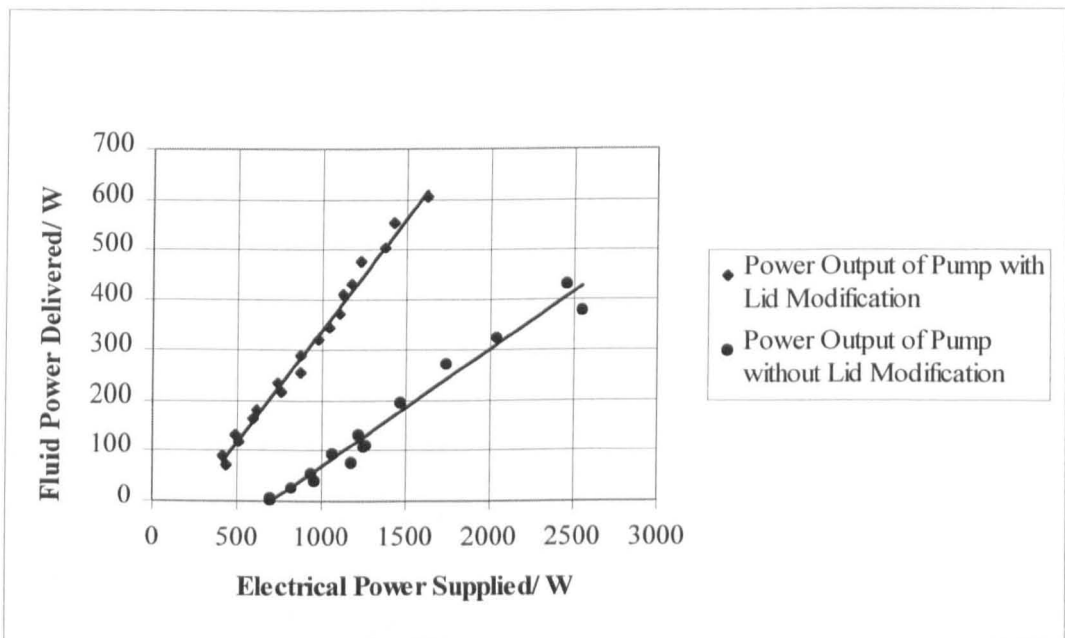


Figure 3.17 Electrical Input Power versus Fluid Output Power

Figure 3.18 illustrates the characteristic efficiency curves for both pump arrangements. After the lid modification it can be seen that the pump efficiency was effectively doubled.

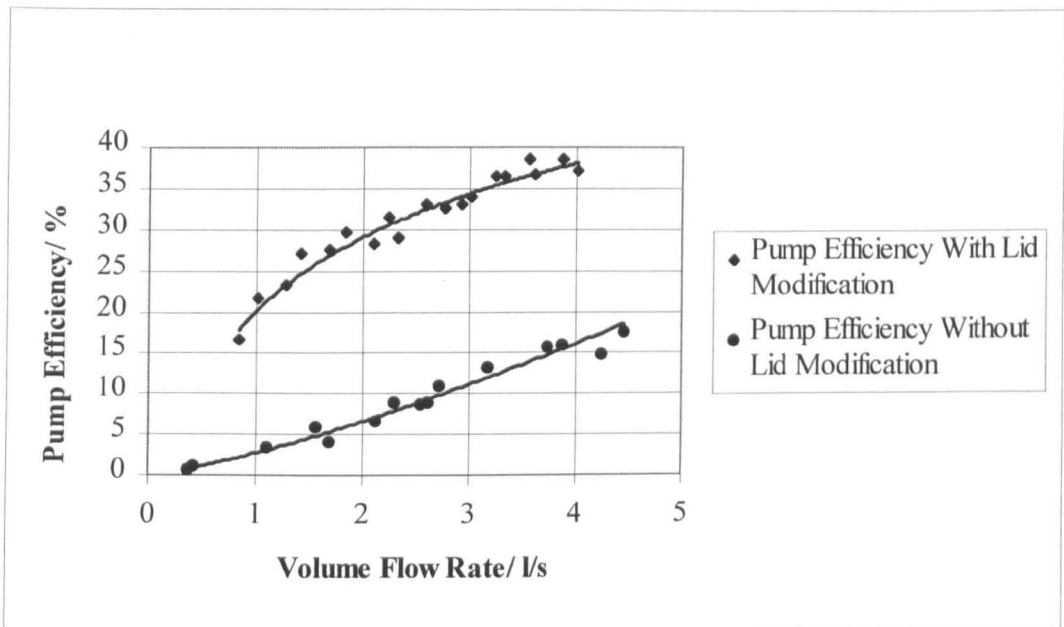


Figure 3.18 Pump Efficiency Curve for Water-only

The final graph for the pump, Figure 3.19, shows the fluid power produced for a given flow rate. The curves are similar, but with the lid modification the power delivered to the fluid for a given flow rate was almost doubled.

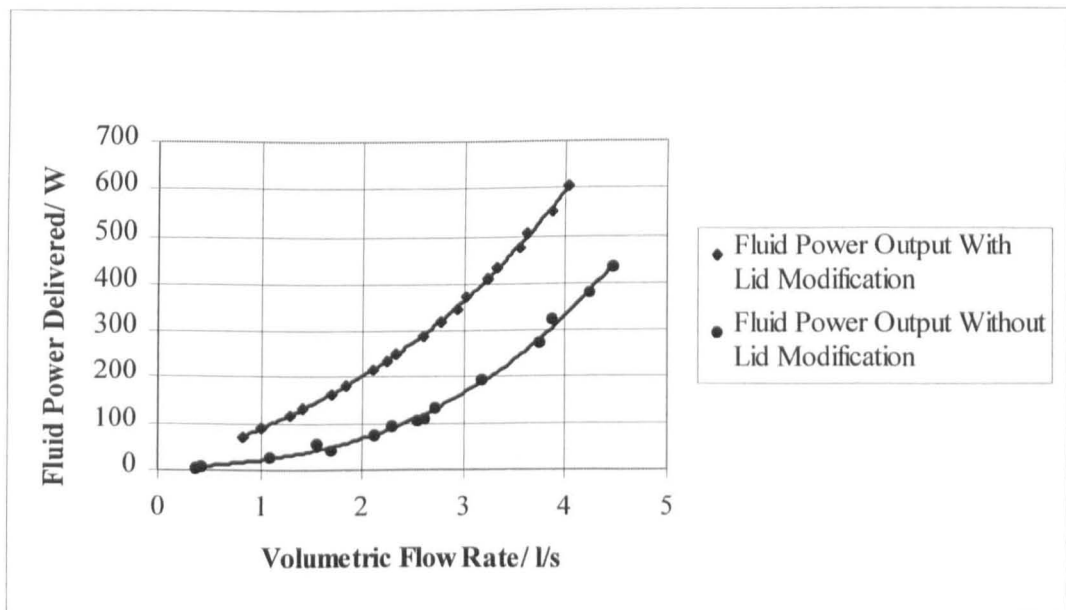


Figure 3.19 Fluid Power Delivered against Volumetric Flow Rate

4.0 Experimental Work

This chapter examines the experiments carried out on the test rig described in chapter

3. The experimental procedure consisted of several parts, namely:

- 1) water tests to produce a benchmark for the water/particle tests,
- 2) conventional pipe set-up before rising main bend with water/particle mixtures,
- 3) long *Swirly-flo* Pipe before the rising main bend with water/particle mixtures.

4.1 Water Tests

Figure 4.1 shows the friction factor against $\rho v^2/2$ for water-only tests. It is known that friction factor varies significantly over large changes in velocity but a starting value of 0.02, obtained from Figure 4.1, was useful for more accurate procedures.

Figure 4.1 also shows that the friction factor was far from constant at low velocities.

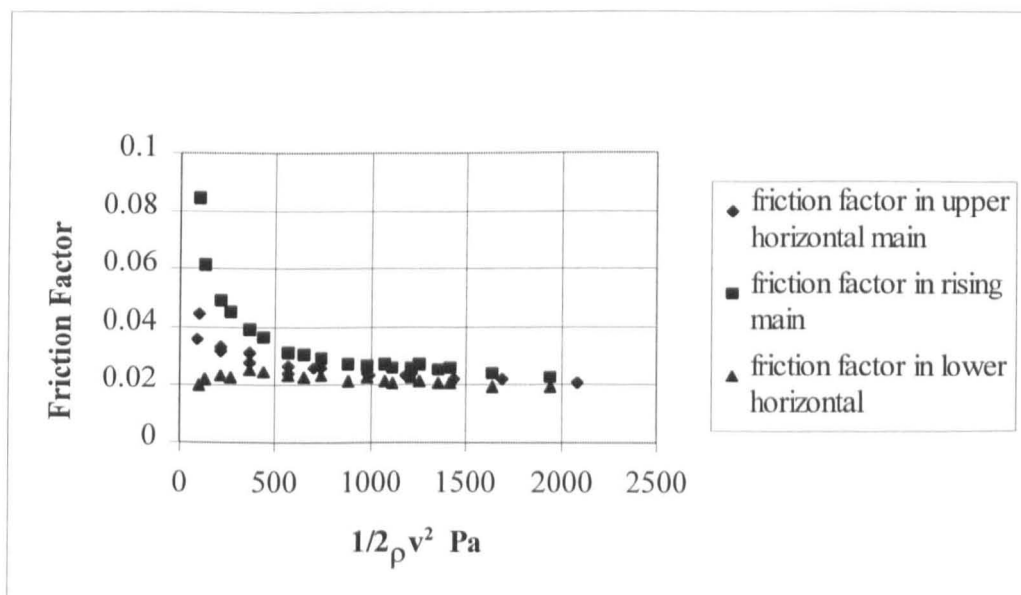


Figure 4.1 Water-only Friction Factor for Straight Sections (taking account of pipe joints)

Neglecting the pressure loss across the joints it was decided to plot the pressure gradient of the lower horizontal, rising main, and upper horizontal sections against volumetric flow rate (Q) and this was compared with the predicted values using the Colebrook equation for friction factor (Colebrook, 1938). Figures 4.2, 4.3 and 4.4 show these results.

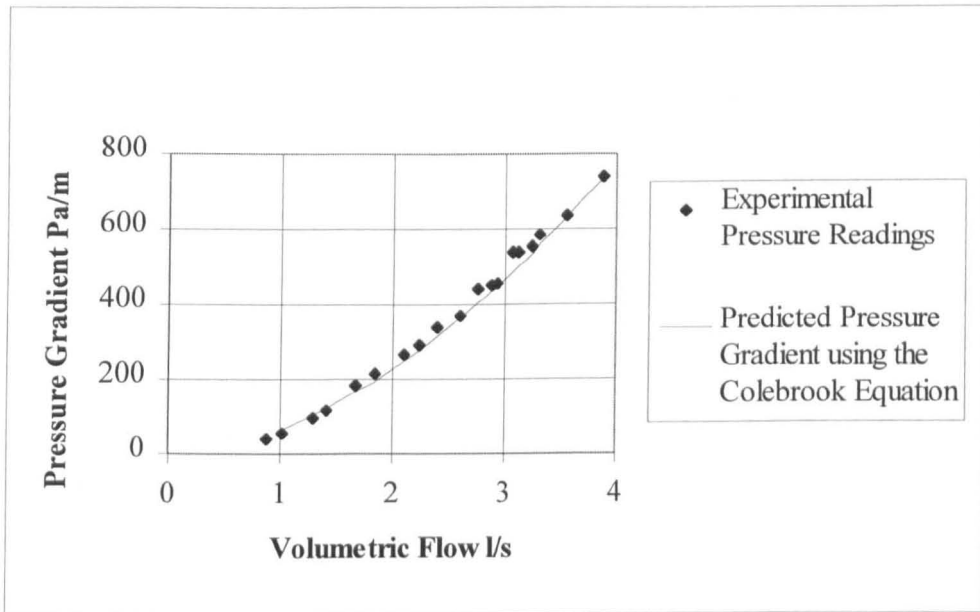


Figure 4.2 Water-only Pressure Gradient against Volumetric Flow Rate in the Lower Horizontal Section

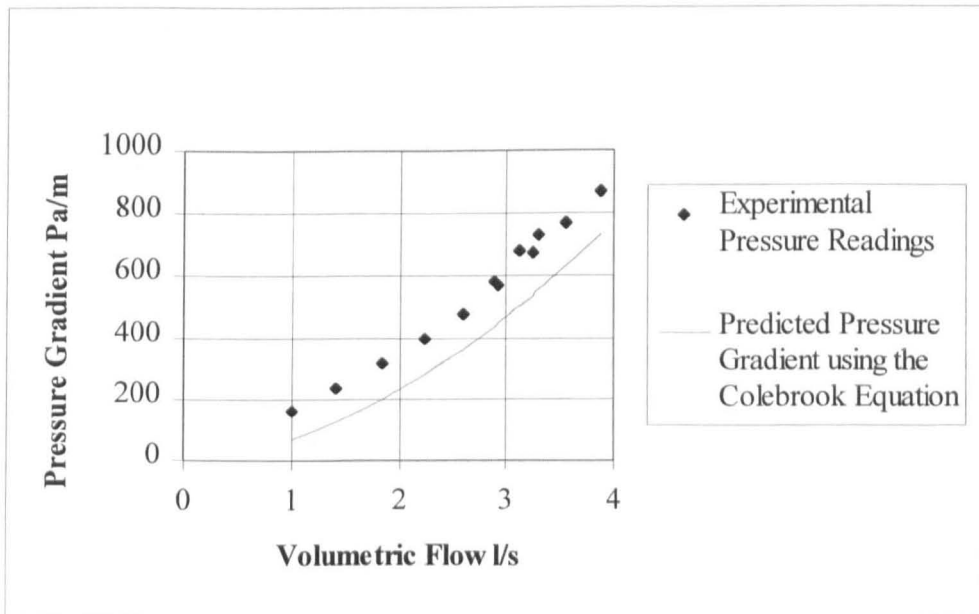


Figure 4.3 Water-only Pressure Gradient against Volumetric Flow Rate in the Rising Main Section

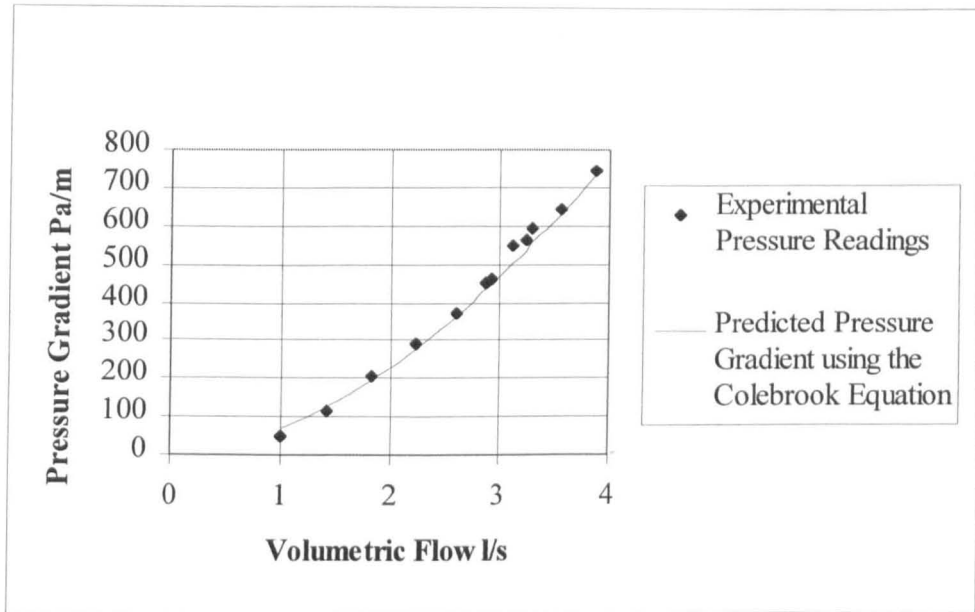


Figure 4.4 Water-only Pressure Gradient against Volumetric Flow Rate in the Upper Horizontal Section

The Colebrook equation provided an excellent benchmark for water, in the upper and lower horizontal sections and was used as the benchmark for water in these sections. It was not satisfactory for the rising main, this was due to the flow not being fully developed at pressure station 5. The Colebrook equation can be only used in fully developed flow.

4.2 Determining the Optimum *Swirly-flo* Pipe Before a Bend

Three lengths of *Swirly-flo* pipe (long, medium and short) were fabricated into rig sections. They were all made from the same pipe stock which had a pitch of one full revolution per 0.43m or 837° per metre. The Long, Medium and Short *Swirly-flo* pipes had lengths of, 1 m, 0.260 m and 0.129 m, respectively.

To determine the most effective *Swirly-flo* pipe section, each section was placed before the bend (between pressure stations 4 and 6) and the pressure effect across the

bend was then measured for various flow rates. This is shown in Figure 4.5. The bend pressure drop was in fact measured between stations 4 and 6 to lessen the effect of flow immediately downstream of the bend.

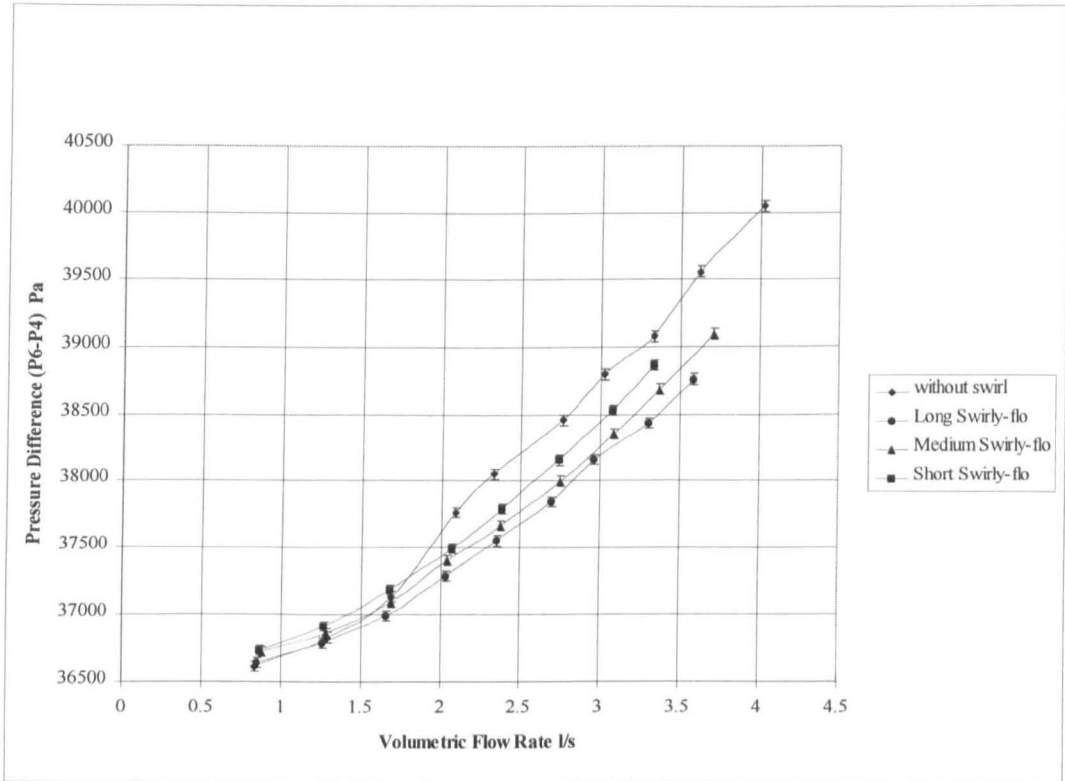


Figure 4.5 Pressure Drop Across the Bend for Different Sections of *Swirly-flo* Pipe

Note that the pressure errors bars represent a pressure error of 0.1%.

4.3 Water/Particle Mixture Tests

4.3.1 Concentrations for a Given Loading

The test runs with solids were partly described by the amount of beads placed into the test rig. As the amounts of beads increased then so did the concentration. Table 4.1 shows the average concentrations taken at the exit of the test rig for a given quantity of beads.

Loading in Kg	Concentration of solids (volume %)
2	6.1
4	8.0
6	9.0
8	10.3

4.4 Determining the Optimum Orientation of the Long *Swirly-flow* Pipe

To determine the optimum position of the pipe, the pipe was rotated through six positions and in each position 2 Kg (concentration 6.1 % v/v) of beads were placed into the rig. Then the pressure drop between stations 4 and 6 were measured for various flow rates. These results produced an optimum position as shown by Figure 4.6.

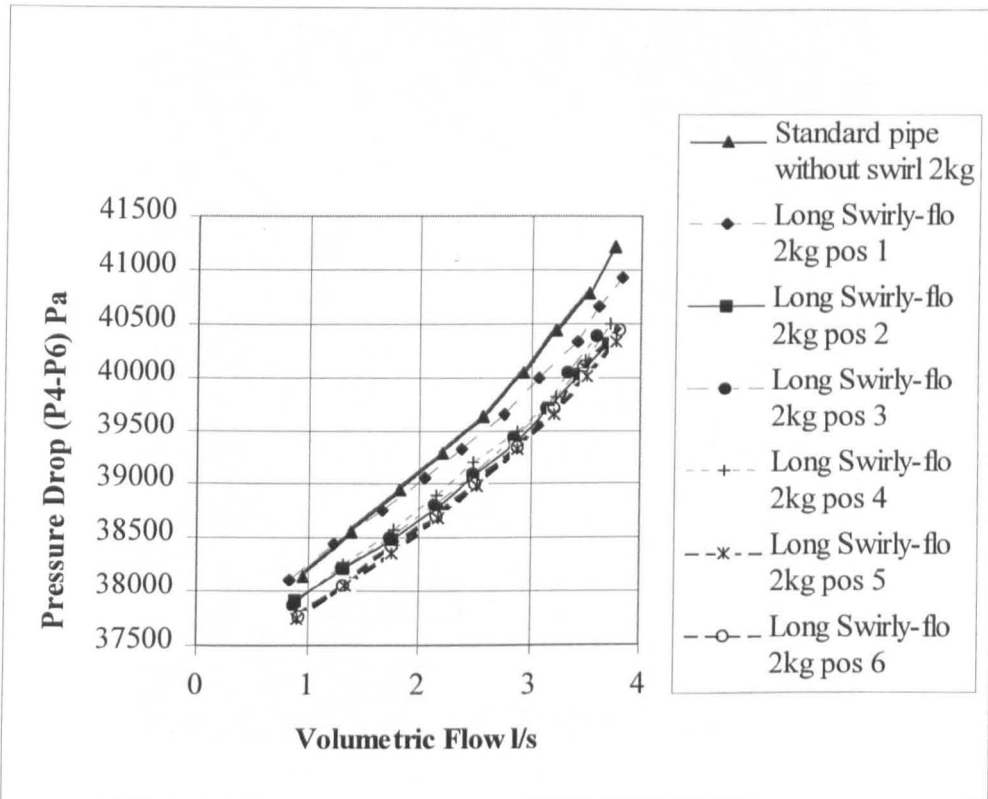


Figure 4.6 Optimum Position of the Long Swirly-flo Pipe

The positions of the *Swirly-flo* pipe were marked with a number from 1 to 6. These numbers referred to the position of the top bolt in the flange, directly opposite any particles settling under gravity. Figure 4.7 shows the various positions at the entrance to the *Swirly-flo* pipe. Figure 4.8 shows an idealised cross-section at the entrance to the *Swirly-flo* pipe, with actual bolt hole positions marked. The corresponding portion of the pipe profile in proximity to any settling particles is shown with an arrow. It can be seen that odd-numbered positions were opposite cusps in the pipe profile, while even-numbered positions were opposite lobes. The cusp opposite position number 5 had been ground during the fitting of the flange.

It appears from Figure 4.6 that the even-numbered bolt positions produced better results, with the exception of position 5 which had the most favourable pressure-drop characteristics of all. This supported the intuitive conclusion that when the lobes at entry were on the bottom of the pipe, lower pressure drops were obtainable, but further detailed investigation would be required.

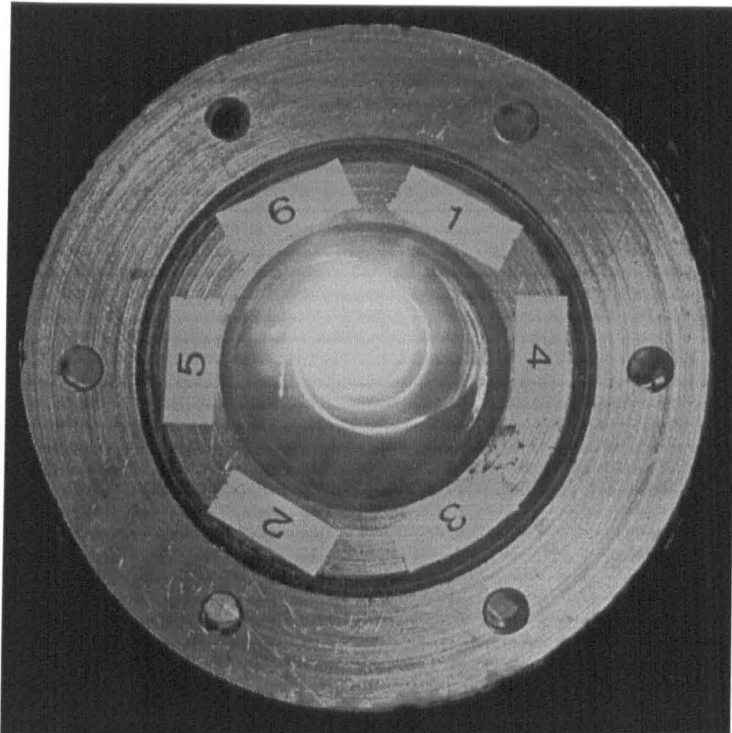


Figure 4.7 Entrance Positions on the Long *Swirly-flo* Pipe

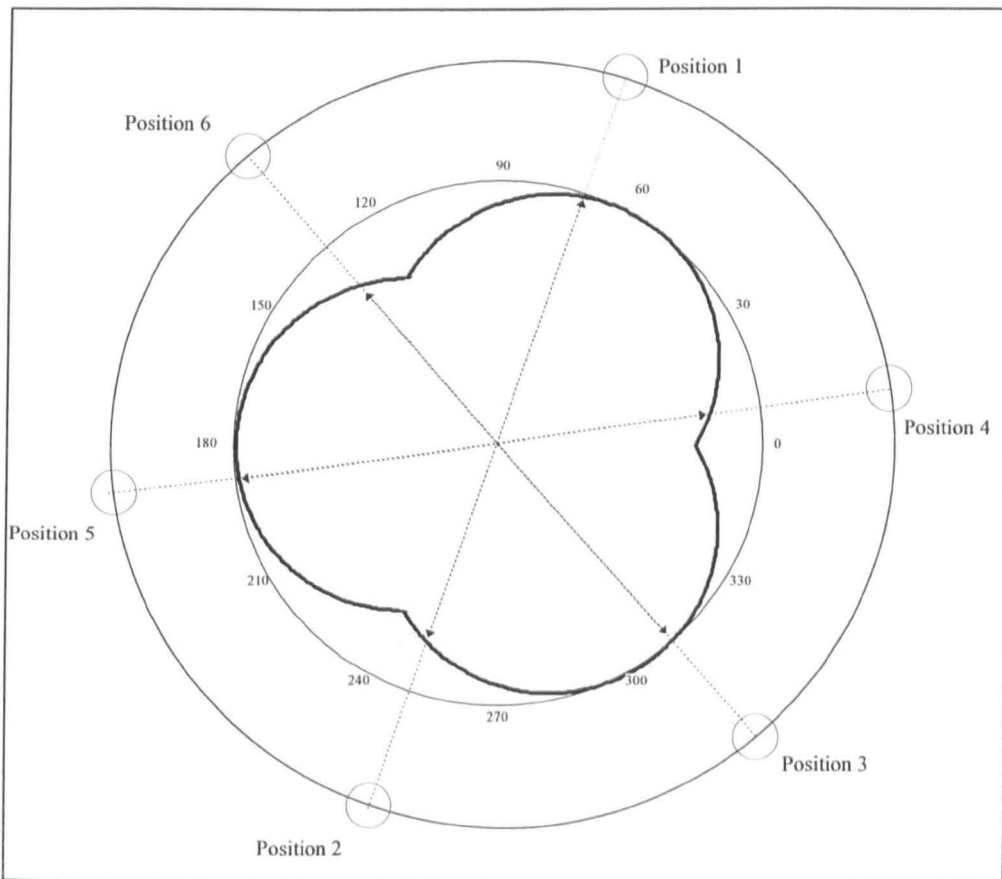


Figure 4.8 Bolt-hole Positions with Corresponding Settling Surfaces

4.5 The Effects of the Long *Swirly-flo* Pipe on Various Concentrations of Beads at Varying Flow Rates

The pressure drop characteristics across the bend (first bend plus the rising main) are shown in Figure 4.9

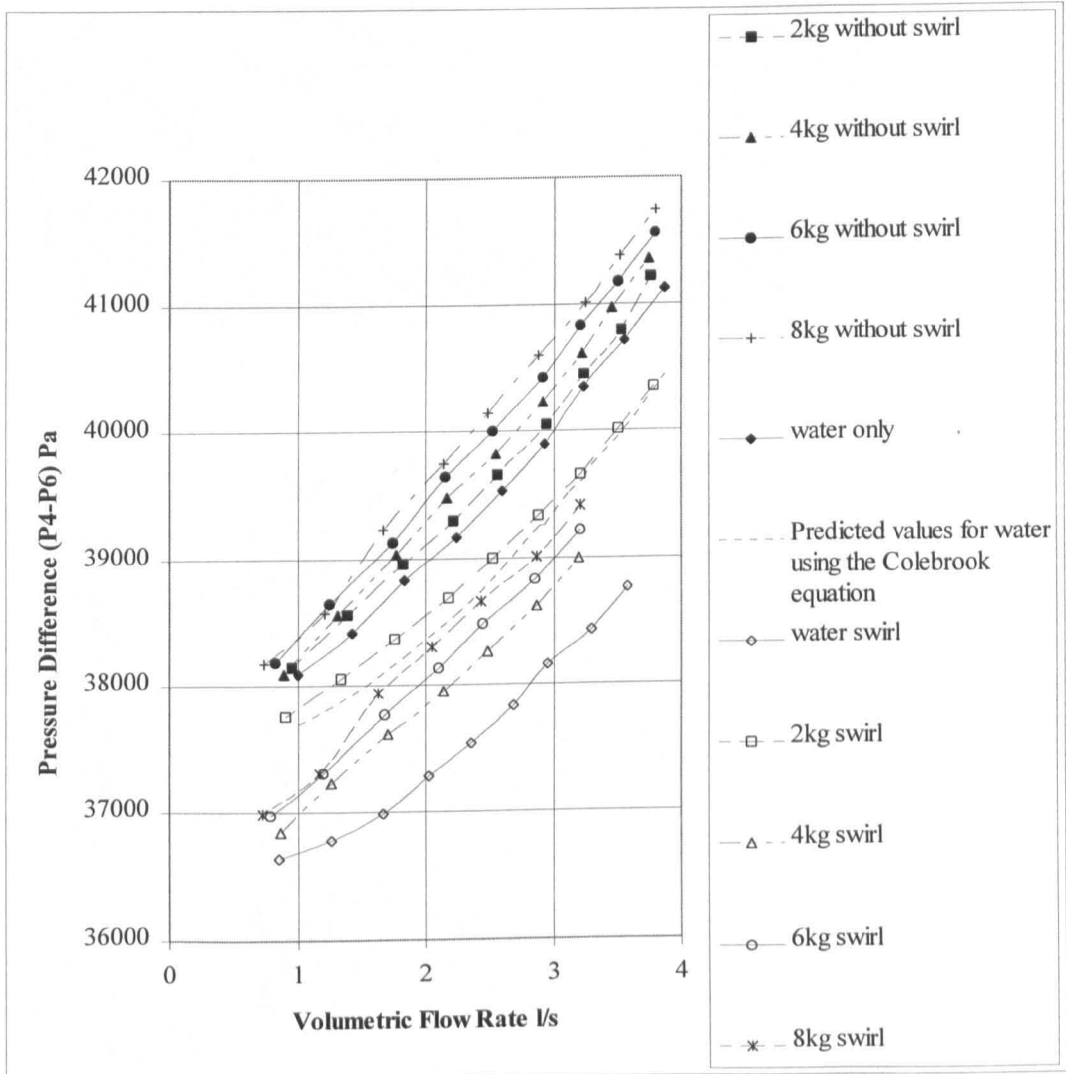


Figure 4.9 Pressure Drop Characteristics With and Without the Long *Swirly-flo* Pipe

The above results show a reduction of pressure loss for all concentrations and water with the use of the *Swirly-flo* pipe. Figures 4.10 and 4.11 illustrate the flow regime with and without swirl.

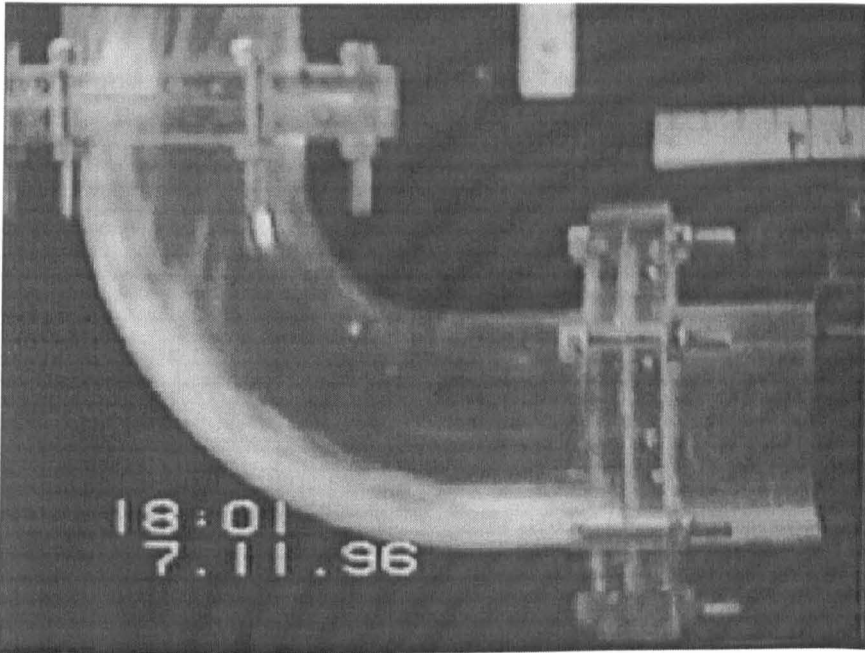


Figure 4.10 6.1 % concentration v/v with a flow a volumetric flow rate of 1.7 l/s without swirl

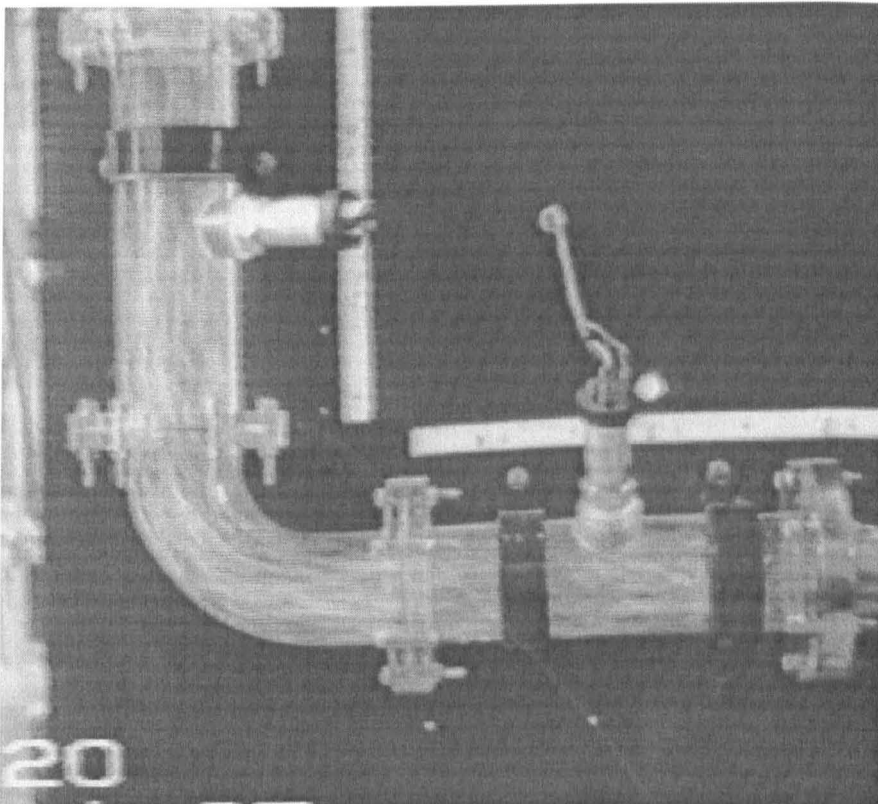


Figure 4.11 6.1 % concentration v/v with a flow a volumetric flow rate of 1.7 l/s with swirl

Figure 4.12 shows the pressure drop across the long *Swirly-flo* pipe before the bend and compares it to the standard pipe at various loadings. These results are also tabulated in Table 4.4, where the pressure drop was taken from station 3 to station 4.

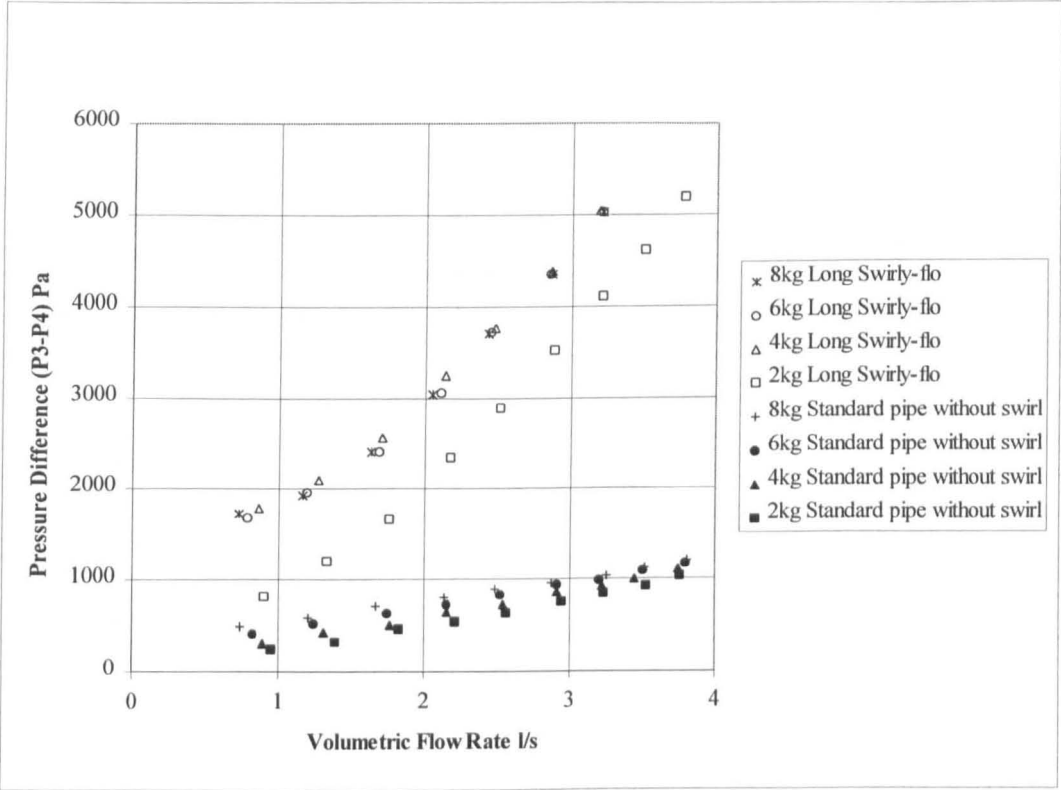


Figure 4.12 (P3-P4) Pressure Drop with and without a Long *Swirly-flo* Pipe

Table 4.2 (P3-P4) Pressure Drop with and without a Long Swirly-flo Pipe

Run	Average flow l/s	normal	Swirly-flo	
		Pressure loss (p3-p6) Pa	Pressure loss (p3-p6) Pa	Nett loss Pa
2kg	0.83	38221	38455	233
2kg	1.23	38703	39107	886
2kg	1.71	39110	39946	1243
2kg	2.06	39566	40756	1646
2kg	2.40	39958	41580	2013
2kg	2.74	40417	42453	2494
2kg	3.05	40899	43291	2874
4kg	0.73	38249	38406	157
4kg	1.16	38796	39147	898
4kg	1.65	39354	40054	1257
4kg	2.05	39769	40990	1636
4kg	2.39	40220	41807	2037
4kg	2.75	40709	42698	2477
4kg	2.97	41177	43330	2620
6kg	0.72	38345	38547	202
6kg	1.14	38800	39178	832
6kg	1.60	39441	40021	1220
6kg	2.06	39885	41071	1630
6kg	2.40	40331	42037	2152
6kg	2.76	40837	42931	2599
6kg	3.03	41500	43697	2860
8kg	0.68	38404	38643	238
8kg	1.12	38917	39182	778
8kg	1.61	39557	40295	1377
8kg	2.05	40032	41332	1775
8kg	2.38	40544	42246	2214
8kg	2.72	41062	43033	2488
8kg	3.06	41556	43956	2894

4.7 Discussion of Experimental Results

The aim of the experimental approach was to monitor key flow characteristics, such as velocity and static pressure, and the flow regimes present. The experimental runs provided a “benchmark” for the *Swirly-flo* pipe, and from this the effects of swirl inducing flow could be observed.

4.8 The Experimental Set-up

On examining the pressure graphs (see Appendix D), there were obviously some fluctuations in the pressure reading and this was especially prominent at low flow rates. The effect was attributed to changes in the level in the header tank which caused a variation in the pressure readings. At high flow rates the effect was reduced. Momentarily, the pump could be drawing more water than was entering the header tank. Other variations could be attributed to the design of the pump which may have produced slight variations in pressure. These variations were most likely to have been masked by the variations in the header tank. For future work there should be a mechanism controlling the height of liquid in the header tank.

The only place where the author could be sure of an accurate determination of the concentration was at the pipe exit above the header tank. By examination of video data and direct observation it was clear that the concentration of solids varied throughout the test rig. Local concentration could not be determined with the required accuracy at crucial points in the test rig, such as, the entrance and exit of the *Swirly-flo* pipe and around the bend. The technique of Shook and Roco (1991) using pressure transducers 5 and 6 to provide an estimation of concentration in the rising main, was tried and discarded due to the fact that the site of the pressure transducer (station 5) after the bend was in a region of flow re-establishment. Concentration is an extremely important parameter in slurry transport, and a more comprehensive survey will be required for future work. This will involve the development of experimental techniques to allow concentration measurement in different parts of the rig circuit.

In the sampling of the mass and volumetric flow rate, three samples were extracted at each flow rate, and an average value taken. This provided consistent results for runs which were repeated several times. In sampling, water and solids were being taken out of the test rig, thus changing the head of water in the header tank. Accordingly an interval of time was allowed between measurement. Time was allowed for the water to rise back to its specific head.

4.9 Results of Experiments

Three lengths of *Swirly-flo* pipe were examined to determine which one produced the greatest effect on the bend in terms of pressure loss. These became known as the long, medium, and short *Swirly-flo* pipes. The results of the pressure drop around the bend showed that at low volumetric flow rates (Figure 4.5) the difference between the long *Swirly-flo* and the medium *Swirly-flo* was marginal but as the speed increased the gap between them became larger. Therefore the long *Swirly-flo* pipe was used in all the further tests.

The long *Swirly-flo* was not specifically designed for the test rig, but due to time constraints and relatively easy supply, it was used. The first long *Swirly-flo* pipe was obtained from North Sea Ferries (Van Loo, 1996) and then cut to the correct length, 1 metre, and flanges were placed on the ends so that it could be fitted to the *Transpalite*[®] pipes. The pitch to diameter ratio (P/D) of this pipe was 8.6, which was very close to the optimum specified by Schriek *et al.*, (1974). The diameter of the *Swirly-flo* pipe was considered to be the maximum core diameter at which an uninterrupted circle could be drawn without the interference from the lobes, an example of this is shown in Figure 4.13. In Figure 4.13 this diameter is considered to be 0.05 m, the same as the *Transpalite*[®] pipes. The actual *Swirly-flo* pipe core diameter was slightly smaller than this.

Before the test runs with beads in the long *Swirly-flo* pipe, the pipe was optimised for position of the flange, which in turn altered the inlet flow regime in the *Swirly-flo* pipe. Each of the six flange holes were marked with a number 1 to 6.

Each number referred to the location of the top bolt. Position 5 showed the most favourable results for the pressure drop around the bend but this was thought to be due to smoothing of the cusp between lobes during the fitting of the flanges. There was evidence that when the lobes were at the bottom of the pipe at entry the most favourable pressure drop results were obtained.

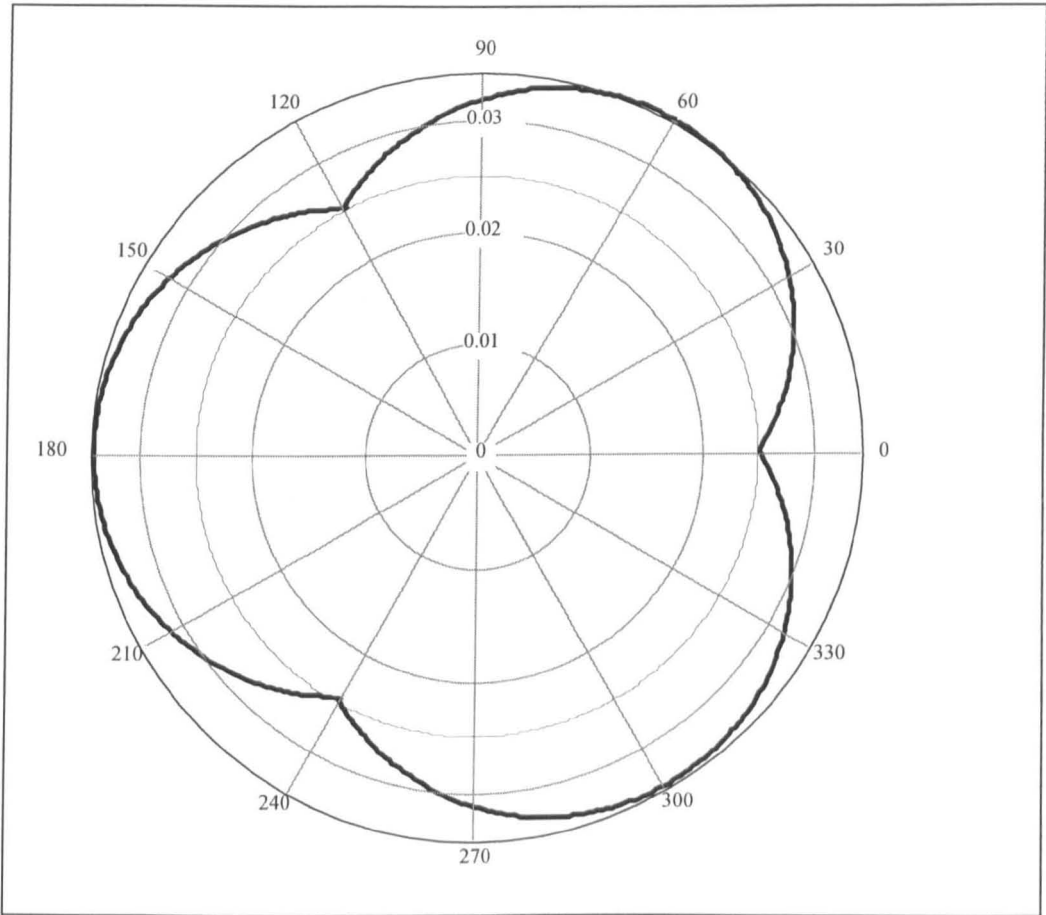


Figure 4.13 Schematic Cross-Section of the Swirly-flo Pipe

For the long Swirly-flo pipe it was not possible to make a smooth entrance and exit. At the inlet the flow had to go through almost a sudden contraction even though the entrance was smoothed out by grinding. Figure 4.14 illustrates the flow characteristics of a sudden contraction which leads to a high pressure loss. The exit of the long Swirly-flo pipe was similar to that of a sudden expansion, as illustrated in Figure 4.15, which also lead to a high pressure loss compared to the rest of the pipework.

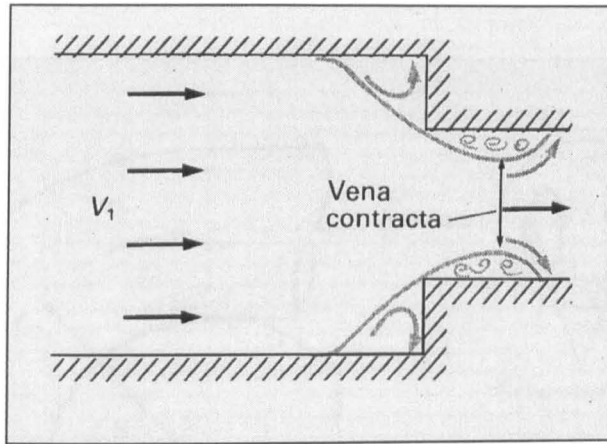


Figure 4.14 Flow Field of a Sudden Contraction (copied from Gerhart and Gross, 1985)

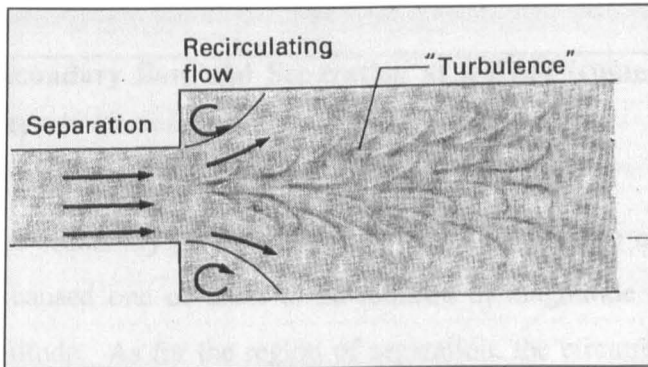


Figure 4.15 Flow Field of a Sudden Expansion (copied from Gerhart and Gross, 1985)

In future the effects of sudden contraction and sudden enlargement at pipe entry and exit to the swirl inducing pipe must be minimised by careful design of entrance and exit ducts. To obtain a benchmark, water was first used with the long *Swirly-flo* pipe before the bend, in the optimum orientation. The swirling of the flow produced a decrease in pressure drop across the bend. This could be explained by the fact that as rotating flow went around the bend it altered the expected separation characteristics of the flow field downstream of the bend. These characteristics are illustrated in Figure 4.16.

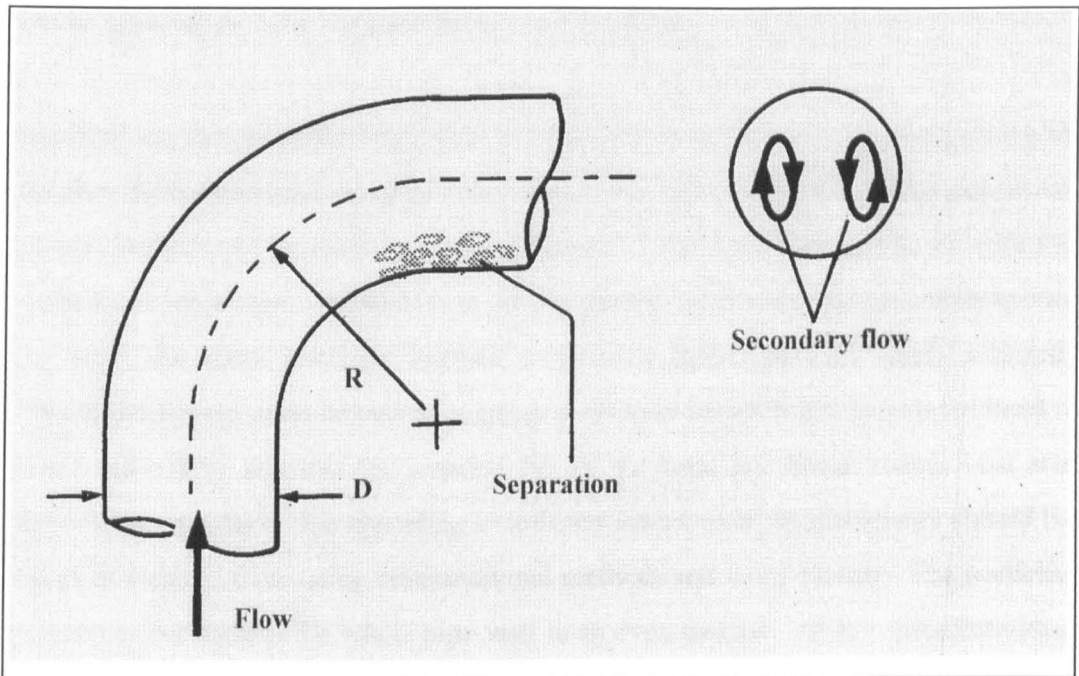


Figure 4.16 Secondary flow and Separation at a Bend (copied from Gerhart and Gross, 1985)

In the case of the secondary flows around the bend the presence of a rotating flow field may have caused one of them to be reduced in magnitude and the other to increase in magnitude. As for the region of separation, the circumferential velocity caused by the long *Swirly-flo* pipe may have reduced the separation in size or removed it altogether. If this was the case it would cause the local axial velocity to decrease in the region and reduce the pressure drop in proportion to the square of velocity.

These effects would have also been present, perhaps to lesser a degree, when pumping beads and water around the test rig. The results indicated that there was an improvement for all concentrations when the long *Swirly-flo* was placed before the bend. However, the 2 kg run with swirl seemed out of sequence with respect to the other runs with swirl, this can be seen in Figure 4.9. The reason for this was unclear. It was believed that the solids may have not been uniformly distributed. In the initial tests the 2 kg run with swirl was showing a pressure drop curve between water with

swirl and the 4 kg with swirl, but when run for a longer time (~1 hr) the results were not so favourable. This requires further investigation.

In observing the solids flowing around the bend it could be seen that the swirling of the flow field caused the beads to rotate around the axis of the pipe, which caused the normal wear zones for particles to be eliminated. This was particularly the case for particles at lower concentrations. As well as producing a lower pressure drop across the bend, the zones normally exposed to wearing action were no longer affected. This could have a great benefit to industry if slurries were swirled before the bend it could effectively increase the working life of the bend and hence reduce cost and down time. To make this appealing to industry actual wear measurements should be taken or inferred from using computational methods and wear models. The particles seemed to rub against the whole pipe wall in an even manner. At low concentrations the flow field was visible as particles were carried with the flow. The flow patterns were observed to execute a roughly helical path.

Figures 4.17, 4.18, 4.19 and 4.20 illustrate the particle flow field with and without a *Swirly-flo* pipe before the bend.

In producing swirl prior to the bend, the pressure drop across the *Swirly-flo* pipe was always larger than the gain in pressure across the bend. This is shown in Table 4.4². This could be explained by the entrance and exit effects previously mentioned, and roughness of the electroplated steel compared to the *Transpalite*[®] pipe. Nevertheless, the removal of the zones of high wear and the lowering of the pressure loss associated with the bend are important effects from the upstream *Swirly-flo* pipe despite the disadvantage of the nett pressure loss. The future optimisation of the design of this pipe holds out the possibility that this disadvantage could be reduced.

The optimisation of the swirl-inducing pipe was one of the prime aims of the project. Experimental results with commercially-available swirl-inducing pipe have highlighted the need for further investigation into the design of a swirl-inducing pipe for this duty. Stated simply, could swirl be improved for minimal pressure loss?

Further experimental work with specially-fabricated pipes would consume considerable time and expense, and would not necessarily produce an optimal design. Mathematical modelling was seen as a first step forward in optimising the design of a swirl-inducing pipe without incurring fabrication costs. This modelling would be based on powerful mathematical techniques to optimise the helical geometry known as the *Calculus of Variations*. Computational Fluid Dynamics (C.F.D.) could then be used to simulate single phase flows through these pipe designs and to provide information about the flows field in swirl-inducing pipe.

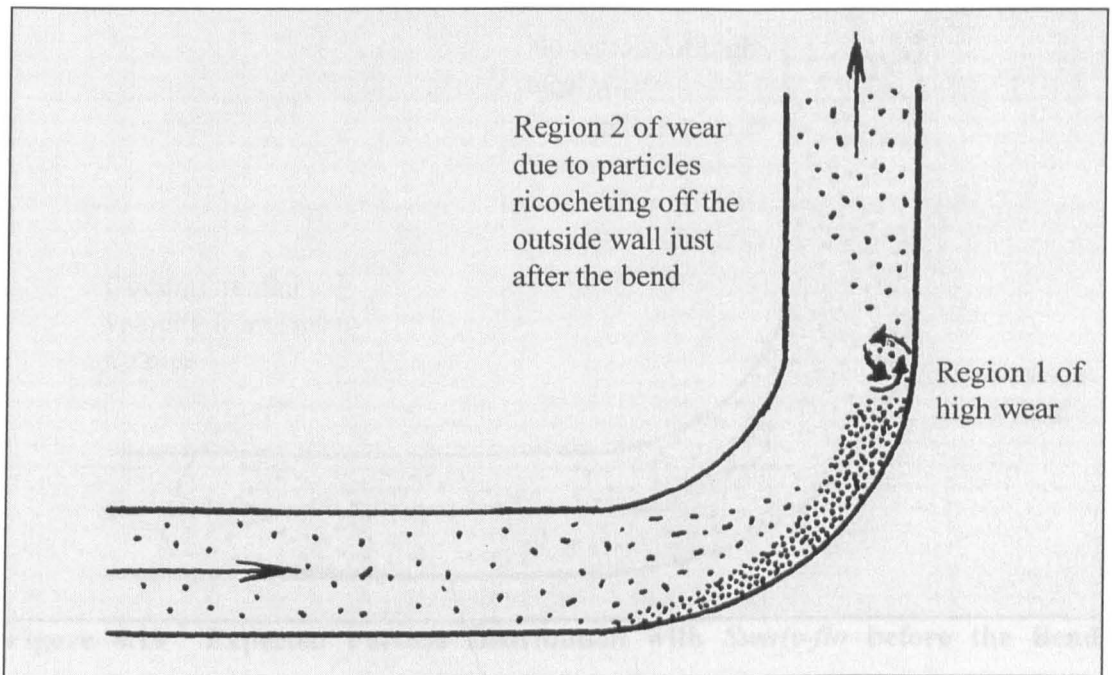


Figure 4.17 Particle Distribution without *Swirly-flo* before the Bend (adapted from Zenz and Othmer, 1960)

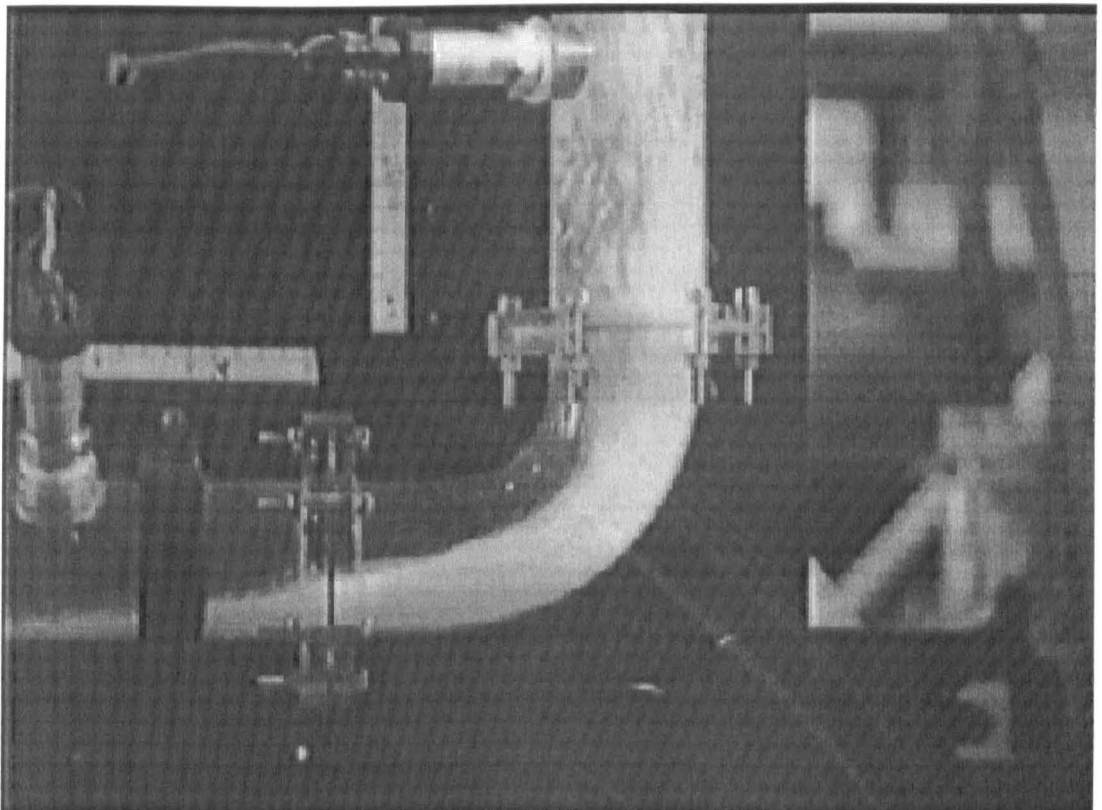


Figure 4.18 8.0 % concentration v/v with a flow rate of 2.7 l/s without swirl

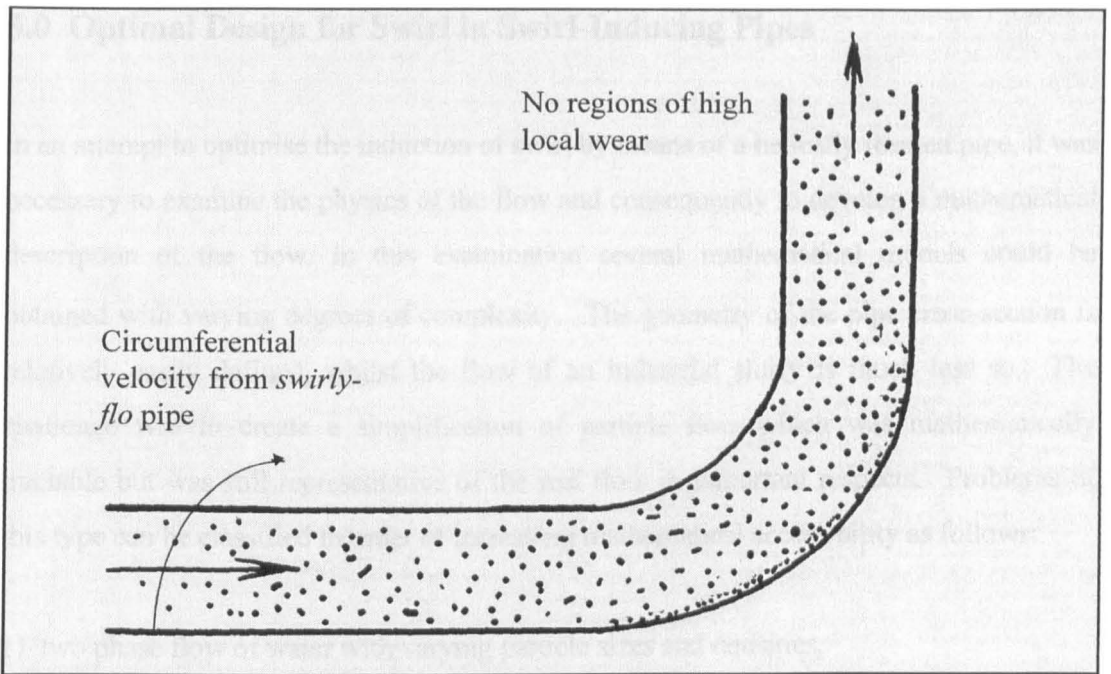


Figure 4.19 Expected Particle Distribution with *Swirly-flo* before the Bend (adapted from Zenz and Othmer, 1960)

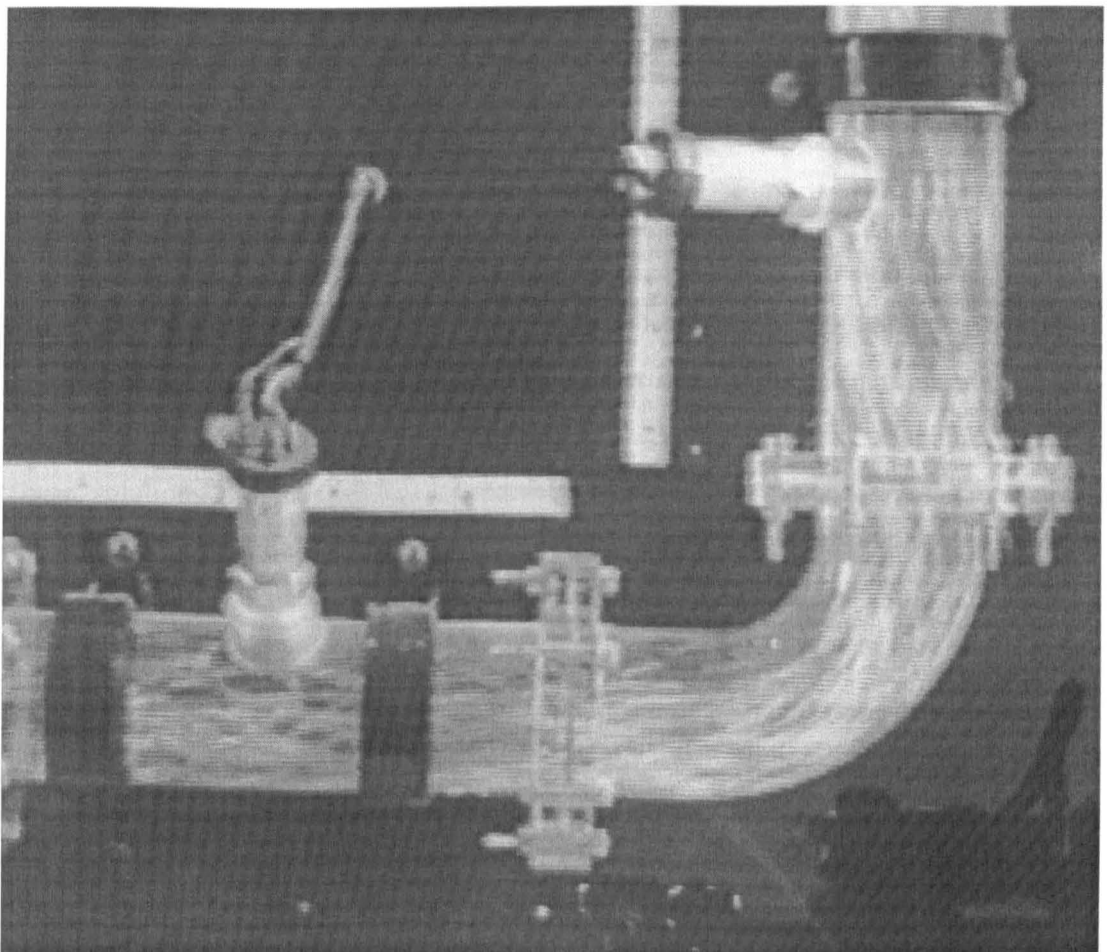


Figure 4.20 8.0 % concentration v/v with a flow rate of 2.7 l/s with swirl

5.0 Optimal Design for Swirl in Swirl-Inducing Pipes

In an attempt to optimise the induction of swirl by means of a helically formed pipe, it was necessary to examine the physics of the flow and consequently to develop a mathematical description of the flow. In this examination several mathematical models could be obtained with varying degrees of complexity. The geometry of the pipe cross-section is relatively easily defined, whilst the flow of an industrial slurry is much less so. The challenge was to create a simplification of particle flow which was mathematically tractable but was still representative of the real flow in important respects. Problems of this type can be classified in order of increasing mathematical accessibility as follows:

- 1) two phase flow of water with varying particle sizes and densities,
- 2) two phase flow of water with single-sized and single-density particles,
- 3) single phase flow,
- 4) a single frictionless particle in a frictionless medium.

In order to solve (1) and (2) a mixture of theoretical and empirical methods are required. Item (3) is computationally possible, and powerful techniques using computational fluid dynamics will be elaborated in chapter 6. The last item, (4), the single particle model, permits an analytical solutions of the trajectory of the particle under constant acceleration. These solutions are independent of particle specifics and properties of the flowing medium. They provide elegant loci for the optimal trajectory of a particle in a cylindrical pipe and, by extension, a first design for the pipe helix.

The flow was simplified to a single particle, with a single path constrained to the inside of a cylinder. With this simplified approach two different criteria for the curve inside the cylinder were looked at, namely:

- 1) the shortest distance (geodesic) between two points inside a cylinder which give one full pitch,
- 2) the shortest time (brachistochrone) between two points in one full pitch.

The above optimisation involves a special type of maximum and minimum problem, which involves the *Calculus of Variations*. Once these geodesic or brachistochrone paths had been established for a given pipe, they were transposed into a computational mesh with 3 lobes, each lobe having the same curve but a different starting point at the beginning of the pipe. The reason for having 3-lobes was two fold: firstly the existence of a 3-lobe pipe in the laboratory and secondly the suggestion by Robinson, (Robinson, 1923) that three could be the optimum. The determination of the flow field was then found by using *Fluent 4.3*.

5.1 Introduction to the *Calculus of Variations*

The first *variational* problem known comes from antiquity, and is known as the problem of Dido (Forray, 1983). Dido, also called Elissa, was the first Queen and founder of Carthage in 814 B.C. (Josephus, *circa 100 A.D.*). On arrival in the region she was given permission, by natives, to settle on land which was not to exceed in size the area which could be covered by an ox-hide. This meant that Dido had to obtain the largest enclosed area with a simply closed curve; this curve was made from ox-hide cut into a narrow thong. By intuition we know this to be a circle, but a mathematical derivation is not obvious. A mathematical solution to this problem is obtainable by the use of the *Calculus of Variations*.

In the 17th century the subject obtained its momentum through the pioneering work of Johann (1667-1748) and Jakob (1654-1705) Bernoulli, two brothers from a family of mathematicians. All the giants of 17th century mathematics made contributions, admittedly by *ad hoc* ingenuity, such as: Newton (1642-1727), Leibniz (1646-1716) and

L'Hopital (1661-1704), (Forray, 1968 and Anderson, J.D., 1991). Finally, Euler (1707-1783), a student of Johann Bernoulli (1667-1748), took up the subject and produced some general methods and in doing so established a firm basis for the *Calculus of Variations*.

The characteristic features of a problem involving the *Calculus of Variations* are given, as follows (Hollingdale, 1989):

- 1) an integral of an expression with an unknown function, for example $y(x)$;
- 2) the necessity to determine the value of this integral which will make it either a maximum or a minimum, subject to the initial conditions.

There are formulae, developed by Euler, that allow one to determine the extremum, although sometimes they are not sufficiently general (Feynman, 1963). In the two cases presented above there is a formula, known as Euler's Equation, which was used to solve the two problems. These two problem will be looked at in the following sections.

5.2 Determination of the Geodesic on a Surface of a Cylinder of Revolution

To make the problem easier cylindrical co-ordinates were used. Figure 5.1 shows the co-ordinate system.

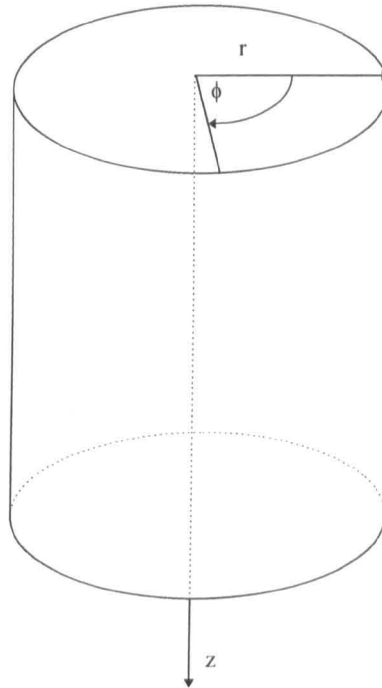


Figure 5.1 Cylindrical Co-ordinates

The first step is to determine the incremental length of arc on the surface, which is...

$$(\delta s)^2 \approx (\delta r)^2 + r^2(\delta\phi)^2 + (\delta z)^2 \quad (5.1)$$

Dividing through by $(\delta z)^2$.

$$(\delta s / \delta z)^2 \approx (\delta r / \delta z)^2 + r^2(\delta\phi / \delta z)^2 + (\delta z / \delta z)^2 \quad (5.2)$$

In the limit $\delta z \rightarrow 0$, equation (5.3) is obtained.

$$\lim_{\delta z \rightarrow 0} (ds/dz)^2 = r^2(d\phi/dz)^2 + 1 \quad (5.3)$$

The elemental length of arc is obtained by transposing (5.3) in terms of ds .

$$ds = \sqrt{r^2(d\phi/dz)^2 + 1} dz \quad (5.4)$$

To obtain the geodesic required the minimum of the following integral (5.5) must be found.

$$\int ds = \int \sqrt{r^2(d\phi/dz)^2 + 1} dz \quad (5.5)$$

To determine the extremum of this integral the *Calculus of Variations* must be used and the formula used is provided by Goldstein's book (Goldstein, 1980), and is commonly called Euler's formula, which is given at equation (5.7) with the notation

$$\frac{df}{dz} = \dot{\phi} \quad (5.6)$$

Euler's Formula

Where, f is the function under integration on the right hand side of equation (5.5).

$$\frac{\partial f}{\partial \phi} - \frac{d}{dz} \left(\frac{\partial f}{\partial \dot{\phi}} \right) = 0 \quad (5.7)$$

$$\frac{\partial f}{\partial \dot{\phi}} = \frac{r^2 \dot{\phi}}{\sqrt{r^2 \dot{\phi}^2 + 1}} \quad (5.8)$$

f has no term in ϕ .

$$\therefore \frac{\partial f}{\partial \phi} = 0 \quad (5.9)$$

Substituting (5.8) and (5.9) into (5.7) gives.

$$\frac{d}{dz} \left(\frac{r^2 \dot{\phi}}{\sqrt{r^2 \dot{\phi}^2 + 1}} \right) = 0 \quad (5.10)$$

Integrating with respect to z ,

$$\frac{r^2 \dot{\phi}}{\sqrt{r^2 \dot{\phi}^2 + 1}} = c \quad (5.11)$$

Re-arranging equation (5.11), gives

$$\dot{\phi} = \frac{c}{\sqrt{r^4 - r^2 c^2}} \quad (5.12)$$

Integrating with respect to z ,

$$\phi = bz + d \quad (5.13)$$

Clearly the term on the right hand side of equation (5.12) is of a constant value.

Therefore, integration of equation (5.12), leads to equation (5.13), where b and d are new constants. This is the equation for a regular helix and is a straight line, in the xy plane. If the cylinder was unwrapped it would produce a straight line in the plane. It is apparent that this is a minimum. The constants, b and d , can be determined for one full revolution over the arbitrary length of pipe. If the helix starts at the origin the constant d equals zero. If one full revolution is required over the length of the cylinder the constant b equals $2\pi/\text{cylinder length}$.

5.3 The Brachistochrone Problem Inside a Cylinder of Revolution

The brachistochrone problem was formulated by Johann Bernoulli (1667-1748) in 1696. (Forray, 1968) The problem involves finding a curve joining two points, say, $A(x_A, y_A)$ and $B(x_B, y_B)$ and where $x_B > x_A$ and $y_B > y_A$. Along this curve a frictionless particle travels from rest under the influence due to gravity. The problem is to determine the curve along which the particle will move from A to B in the least time, commonly known as the curve of quickest descent.

This problem was then modified to be constrained by the wall of cylinder and the acceleration of gravity replaced by an arbitrary acceleration, a . Which represents the axial acceleration given to a stationary particle at the bottom of the pipe. In the course of determining this curve the acceleration term becomes redundant (Forray, 1968). The idea behind this approach is to maximise velocity in the circumferential direction at the exit of the swirl-inducing pipe.

As before, once the curve has been determined it will then be transposed into a computational grid with 3-lobes and then the flow field will be determined by Computational Fluid Dynamics (C.F.D.).

Velocity is given by equation (5.15), which itself is derived from the conservation theorem for energy, equation (5.14).

$$\frac{1}{2}mv^2 = maz \quad (5.14)$$

Which gives v as follows.

$$v = \sqrt{2az} \quad (5.15)$$

Velocity along the curve is given as.

$$v = \frac{ds}{dt} \quad (5.16)$$

By using the chain rule of differential calculus one obtains the following.

$$v = \frac{ds}{dt} = \frac{ds}{dz} \frac{dz}{dt} \quad (5.17)$$

Substituting for ds/dz , gives.

$$v = \frac{ds}{dt} = \sqrt{r^2 (df / dz)^2 + 1} \frac{dz}{dt} \quad (5.18)$$

On simplification this leads to.

$$\sqrt{2az} = \sqrt{r^2 (d\phi / dz)^2 + 1} \frac{dz}{dt} \quad (5.19)$$

Divide through by $\sqrt{2az}$, this gives.

$$1 = \frac{\sqrt{r^2 (d\phi / dz)^2 + 1}}{\sqrt{2az}} \frac{dz}{dt} \quad (5.20)$$

Separating variables and integrating gives equation (5.21) and the problem is to find the minimum of this integral.

$$\int dt = \int \frac{\sqrt{r^2(d\phi/dz)^2 + 1}}{\sqrt{2az}} dz \quad (5.21)$$

Again we resort to equation (5.7) to obtain the extremum:

$$\frac{\partial f}{\partial \phi} - \frac{d}{dz} \left(\frac{\partial f}{\partial \dot{\phi}} \right) = 0 \quad (5.7)$$

This gives the following.

$$\frac{\partial f}{\partial \dot{\phi}} = \frac{1}{\sqrt{z}} \frac{1}{\sqrt{1+r^2(\dot{\phi})^2}} r^2 \dot{\phi} \quad (5.22)$$

$$\frac{\partial f}{\partial \phi} = 0 \quad (5.23)$$

On integration with respect to z , equation (5.24) is obtained.

$$\frac{1}{\sqrt{z}} \frac{1}{\sqrt{1+r^2(\dot{\phi})^2}} r^2 \dot{\phi} - c = 0 \quad (5.24)$$

Now equation (5.24) has to be transposed in terms of $d\phi/dz$.

$$r^2 \dot{\phi} = \sqrt{z} \sqrt{r^2 \dot{\phi}^2 + 1} . c \quad (5.25)$$

$$\frac{1}{\sqrt{z}} \frac{r^2 \dot{\phi}}{\sqrt{r^2 \dot{\phi}^2 + 1}} = c \quad (5.26)$$

$$r^4 \dot{\phi}^2 = z(r^2 \dot{\phi}^2 + 1)c^2 = zc^2 r^2 \dot{\phi}^2 + zc^2 \quad (5.27)$$

$$r^4 \dot{\phi}^2 - zc^2 r^2 \dot{\phi}^2 = \dot{\phi}^2 (r^4 - zc^2 r^2) = zc^2 \quad (5.28)$$

$$\dot{\phi}^2 = \frac{zc^2}{r^4 - zc^2 r^2} = \frac{zc^2}{r^2 (r^2 - zc^2)} = \frac{z^2 c^2}{zr^2 (r^2 - zc^2)} = \frac{z^2 c^2}{r^2 (zr^2 - z^2 c^2)} \quad (5.29)$$

$$\dot{\phi} = \frac{zc}{r\sqrt{zr^2 - z^2 c^2}} \quad (5.30)$$

To obtain ϕ , one has to integrate equation (5.30).

$$\phi = \frac{[-\sqrt{r^2 \frac{z}{c^2} - z^2} + \frac{1}{2} \frac{r^2}{c^2} \arcsin[\frac{2zc^2 - r^2}{r^2}]]}{r} + k \quad (5.31)$$

Initially, the solver software MATHCAD (1994) was used to obtain a rather cumbersome solution for developing the computational grid, see equation (5.31). Subsequently, the integration was carried out by the author who showed that a more elegant form of solution of equation (5.31) exists. This is shown as follows, starting with equation (5.32).

$$\dot{\phi} = \sqrt{\frac{zc^2}{r^2 (r^2 - zc^2)}} \quad (5.32)$$

Let u equal

$$u = \sqrt{zc^2} \quad (5.33)$$

which gives

$$u^2 = zc^2 \quad (5.34)$$

and this gives

$$\frac{dz}{du} = \frac{2u}{c^2} \quad (5.35)$$

leaving

$$dz = \frac{2u \cdot du}{c^2} \quad (5.36)$$

Therefore the integral of equation (5.32) becomes the integral of equation (5.37) in terms of u .

$$\int \frac{\sqrt{u^2}}{\sqrt{r^2(r^2 - u^2)}} \frac{2u \cdot du}{c^2} \quad (5.37)$$

on simplification, equation (5.37) becomes equation (5.38)

$$\int \frac{u2u}{\sqrt{r^2(r^2 - u^2)}} \frac{du}{c^2} \quad (5.38)$$

Taking the constants to the left hand side of the integral sign and extracting the r^2 term out from the denominator, equation (5.39) is obtained.

$$\frac{2}{rc^2} \int \frac{u^2}{\sqrt{(r^2 - u^2)}} du \quad (5.39)$$

Again integration by substitution is used with.

$$u = r \sin \theta \quad (5.40)$$

and,

$$\frac{du}{d\theta} = r \cos \theta \quad (5.41)$$

this then gives.

$$du = r \cos \theta \, d\theta \quad (5.42)$$

Therefore equation (5.39) becomes equation (5.43) in terms of θ .

$$\frac{2}{r c^2} \int \frac{r^2 \sin^2 \theta}{\sqrt{(r^2 - r^2 \sin^2 \theta)}} r \cos \theta \, d\theta \quad (5.43)$$

Since,

$$r \cos \theta = \sqrt{(r^2 - r^2 \sin^2 \theta)} \quad (5.44)$$

equation (5.36) becomes the following.

$$\frac{2}{rc^2} \int \frac{r^2 \sin^2 \theta}{r \cos \theta} r \cos \theta d\theta \quad (5.45)$$

Which then simplifies to equation (5.46).

$$\frac{2r}{c^2} \int \sin^2 \theta d\theta \quad (5.46)$$

Using the standard result equation (5.47) is obtained.

$$\phi = \frac{2r}{c^2} \left(\frac{\theta}{2} - \frac{\sin 2\theta}{4} \right) + k_1 \quad (5.47)$$

This can be re-written as

$$\phi = \frac{2r}{c^2} \left(\frac{\theta}{2} - \frac{2 \sin \theta \cos \theta}{4} \right) + k_1 \quad (5.48)$$

From equation (5.40) it can be determined that,

$$\theta = \sin^{-1} \frac{u}{r} \quad (5.49)$$

On substitution into equation (5.48) the following is obtained.

$$\phi = \frac{2r}{c^2} \left(\frac{\sin^{-1} \frac{u}{r}}{2} - \frac{2 \sin(\sin^{-1} \frac{u}{r}) \cos(\sin^{-1} \frac{u}{r})}{4} \right) + k_1 \quad (5.50)$$

Which leads to equation (5.51)

$$\phi = \frac{r}{c^2} \left(\sin^{-1} \frac{u}{r} - \frac{u}{r} \sqrt{1 - \frac{u^2}{r^2}} \right) + k_1 \quad (5.51)$$

Substituting for u the following is obtained.

$$\phi = \frac{r}{c^2} \left(\sin^{-1} \frac{\sqrt{zc^2}}{r} - \frac{\sqrt{zc^2}}{r} \sqrt{1 - \frac{zc^2}{r^2}} \right) + k_1 \quad (5.52)$$

Applying the boundary conditions to equation (5.52), results in k_1 always being equal to zero and hence simpler than the solution produced by MATHCAD (1994), equation (5.31). Equations (5.31) and (5.52) do look different. However when both are differentiated, one obtains equation (5.32). This illustrates the fact that depending on the method of integration, one may get a different result with a different constant of integration, which is still mathematically correct. The original solution from MATHCAD was used in the development of the computational grid, using a FORTRAN program. It was then necessary to check if the result was a minimum and this would then apply to both methods of integration

To determine whether this result was a minimum the Legendre test was used (Miele, 1965). This states that, f , the integrand used in Euler's equation is mathematically operated on by taking the second derivative with respect to $d\phi/dz$. If this is greater than 0, then the extremum is a minimum.

Legendre Condition

$$f_{\dot{\phi}\dot{\phi}} > 0 \quad (5.53)$$

In this case the Legendre condition for a minimum is satisfied, as the equations that follow illustrate. The first derivative, with respect to $d\phi/dz$, of the integrand in equation (5.21) is given by equation (5.54).

$$\frac{1}{\sqrt{z}} \frac{1}{\sqrt{1+r^2(\dot{\phi})^2}} r^2 \dot{\phi} \quad (5.54)$$

This equation (5.54) has to be differentiated again with respect to $d\phi/dz$. This is shown in equation (5.55) and equation (5.56) is the simplified form of equation (5.55).

$$\frac{1}{\sqrt{z}} \frac{-1}{(1+r^2(\dot{\phi})^2)^{3/2}} r^4 \dot{\phi}^2 + \frac{r^2}{\sqrt{(1+r^2(\dot{\phi})^2)}\sqrt{z}} \quad (5.55)$$

$$\frac{1}{\sqrt{z}} \frac{r^2}{(1+r^2(\dot{\phi})^2)^{3/2}} \quad (5.56)$$

Equation (5.56) is positive for all values of z , and noting that the negative answer of the square root of z , is not physically possible. Hence equation (5.21) gives a minimum.

Using the boundary conditions the constants of integration can be determined, that is c and k , using MATHCAD (1994). According to Byerly (Byerly, 1917) the evaluation of c in similar problems is "a matter of some difficulty", with which the author can fully concur. Table 5.1 shows the constants for given pipe lengths. Each of the pipes has the same boundary conditions, which are, when $z=0$, $\phi=0$ and $z=L$, $\phi=2\pi$.

Length of pipe (m)	c	k
0.1	0.07905694	3.14159286
0.2	0.04748579	8.70767865
0.3	0.03041858	21.220322
0.4	0.02113055	43.975206
0.5	0.01563354	80.3368563
0.6	0.01211902	133.688559
0.7	0.00972947	207.420067
0.8	0.00802452	304.923787
0.9	0.00676061	429.593375
1.0	0.00579432	584.823122
1.1	0.00503665	774.007705

These constants were then entered into a FORTRAN computer program, which can be found in Appendix B, to obtain a computational grid, with 3-lobes having a brachistochrone helix. In Figure 5.2 the difference in path between the regular helix and the brachistochrone is illustrated for a cylinder of 0.7m in length and a diameter of 0.05 m.

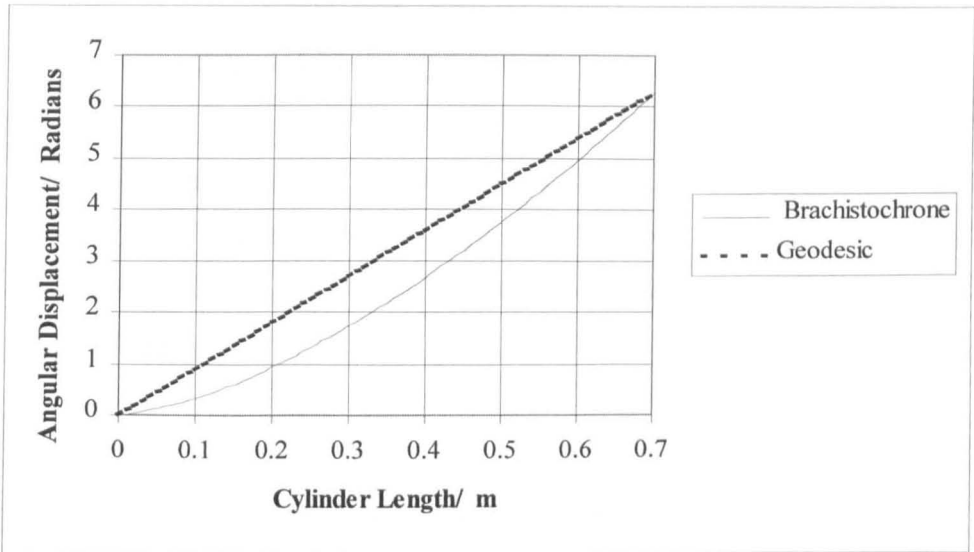


Figure 5.2 The Brachistochrone Curve and Regular Helix for a Cylinder of 0.7 m

6.0 Computational Fluid Dynamics

The aim of using Computational Fluid Dynamics (C.F.D.) is to provide a method of flow visualisation in the *Swirly-flo* pipe, without the need for a specially designed test rig, or pipes. This method also provides a way of optimising the *Swirly-flo* pipes.

Due to the long computational time of running two-phase flow problems in C.F.D., it was decided to just run one phase, that of water. This gave a visualisation of the flow field and an indication of the swirl at the exit of *Swirly-flo* pipes.

This chapter introduces the basic concepts of Computational Fluid Dynamics (C.F.D.), starting with a brief outline of turbulence followed by the equations that govern viscous fluid flow. The solution algorithm of *Fluent 4.3* is then discussed, with generation of the *Swirly-flo* pipe grids.

6.1 Turbulence

From a classical point of view, turbulence is considered as irregular fluid motion in which various quantities such as velocity, pressure and temperature show random variation with time and space co-ordinates, but in such a way that statistically distinct averages can be discerned (Hinze, 1975). Turbulence can also be defined as eddy motion with a wide spectrum of eddy sizes and a corresponding spectrum of fluctuation frequencies. The motion is always rotational, that is the fluid elements have a finite angular velocity. The forms of the largest eddies (low-frequency fluctuation) are usually determined by the boundary conditions, while the forms of the smallest eddies (highest frequency fluctuation) are determined by viscous forces (Rodi, 1980).

Classical theory describes turbulence by its characteristics and not by formal definitions.

The following list, with a brief summary, illustrates the main characteristics of turbulence. (Abbott and Basco, 1989)

1) Irregularity - The flow is so complicated and irregular it is not possible to describe it in a reasonable way.

2) Three-dimensionality - Turbulence is always three-dimensional, even in flows where the flow is predominantly one or two dimensional. Flow fluctuations always have components in all three directions.

3) Diffusivity - The rapid mixing of momentum, heat and mass is a typical feature of turbulent flows.

4) Dissipation - The kinetic energy of turbulent motion is dissipated into heat under the influence of viscosity. The energy source for the turbulence is produced by the mean flow by interaction of the shear stresses and velocity gradients.

Turbulence originates primarily from instabilities in the flow, which generally occur at high Reynolds numbers. Once turbulence is initiated it is not self maintaining and so depends on the flow environment to provide it with energy.

6.2 The Equations that Govern Viscous Fluid Motion

Continuity Equation

$$\frac{\partial \rho}{\partial t} + \nabla \cdot (\rho \mathbf{V}) = 0 \quad (6.1)$$

This equation describes the conservation of mass. The first term represents the rate of change of density at a fixed point in space. The second term describes the convection which represents the rate of mass flux passing out of the control surface (which surrounds an arbitrary control volume) per unit volume.

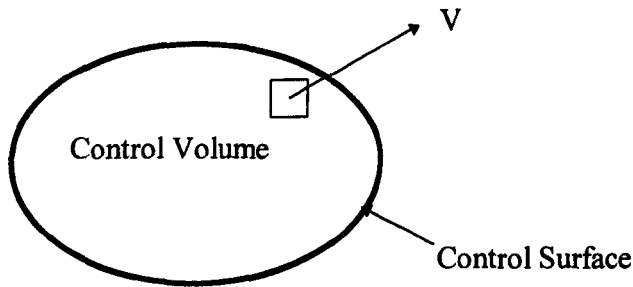


Figure 6.1 Arbitrary Control Volume

Viscous Momentum Equation

$$\frac{\partial(\rho \mathbf{V})}{\partial t} + \nabla \cdot (\rho \mathbf{V} \mathbf{V}) = \rho \mathbf{f} + (-p \delta_{ij} + \tau_{ij}) \quad (6.2)$$

where, τ_{ij} is the viscous stress tensor

$$\tau_{ij} = \mu \left[\left(\frac{\partial u_i}{\partial x_j} + \frac{\partial u_j}{\partial x_i} \right) - \frac{2}{3} \delta_{ij} \mu \frac{\partial u_k}{\partial x_k} \right] \quad (6.3)$$

This equation describes the conservation of momentum. Once again the first term on the left hand side of equation 6.2 represents the rate of change of momentum per unit volume in the control volume. Similarly the second term on the left hand side describes the rate of momentum lost by convection. The first term on the right hand side of the equation represents the so-called body forces. Body forces include gravity and buoyancy. The final term on the right hand side represents the forces due to pressure and viscous stress gradients in the fluid.

Energy Equation

$$\frac{\partial E_t}{\partial t} + \nabla \cdot (E_t V) = \frac{\partial Q}{\partial t} - \nabla q + \rho f \cdot V + \nabla \cdot [(-p \delta_{ij} + \tau_{ij}) \cdot V] \quad (6.4)$$

This equation describes the conservation of total energy. As before the first term on the left hand side of the equation 6.4, represents the rate of change of total energy with time, and the second term the convection of the conserved quantity. The first term on the right hand side represents the rate of heat generation by external sources and the second term represents the rate of heat loss by conduction. The final two terms represent the power associated with the body forces and the pressure and stress gradients, respectively. Where τ_{ij} is the viscous stress tensor and δ_{ij} is the Kronecker delta. The above mentioned equations represent the most comprehensive description of fluid flow, in continuum terms. These equations can be used to solve turbulent flows and this is known as Direct Numerical Simulation (D.N.S.). However, D.N.S. is limited by computational power and large memory requirements. Due to these limits D.N.S. can only be

applied to basic research on standard flows. Flows in complex geometries such as those found in practical devices will generally not use D.N.S. due to the high cost in time and money (Smits, 1992). Since D.N.S. is not a realistic option with present computational facilities, one has to move to the Reynolds-Averaged Navier-Stokes equations (R.A.N.S.).

6.3 The Reynolds Averaged Navier-Stokes Equations

This approach was introduced by Reynolds (Wilcox, 1993), in which the appropriate parameters are decomposed into their mean and fluctuating parts. The Reynolds average of a parameter f is defined as follows and is denoted by \bar{f} .

$$\bar{f} = \frac{1}{\Delta T} \int_{t_0 - \frac{\Delta T}{2}}^{t_0 + \frac{\Delta T}{2}} f dt \quad (6.5)$$

The time period, ΔT , is selected to be large compared with the period of turbulent fluctuations, but small compared to any large scalar transient feature in the flow field. ΔT , is sometimes indicated to approach infinity as a limit, but this should be interpreted as being relative to the characteristic fluctuation period of turbulence.

By definition the Reynolds average of a fluctuating variable is zero (Anderson *et al.*, 1984) that is:

$$\overline{f'} = \frac{1}{\Delta T} \int_{t_0 - \frac{\Delta T}{2}}^{t_0 + \frac{\Delta T}{2}} f' dt = 0 \quad (6.6)$$

The variables that appear in the Navier-Stokes equations can be written as:

$$u = \bar{u} + u'$$

$$v = \bar{v} + v'$$

$$w = \bar{w} + w'$$

The Reynolds-averaged form of the Navier-Stokes equations are derived by replacing the variables with their mean plus the fluctuating components, and then the Reynolds-averaging of the complete equations. For simplicity the Reynolds averaged equations are derived in Cartesian co-ordinates and incompressible form.

Continuity Equation

$$\frac{\partial \bar{u}_j}{\partial x_j} = 0 \quad (6.7)$$

The Reynolds-averaged form of the continuity equation is identical to the original with the turbulent velocity replaced by the mean velocity. The equation is shown using tensor notation, this allows the Reynolds-averaged Navier-Stokes equations to be written on one line.

The Reynolds-averaged form of the momentum equation is similar to the original momentum equation with the turbulent parameters replaced by their mean values. However, additional terms are introduced as a consequence of the Reynolds averaging process. Thus the Reynolds-averaged momentum equations are written as:

Momentum Equations

$$\frac{\partial(\overline{\rho u_i})}{\partial t} + \frac{\partial}{\partial x_j}(\overline{\rho u_i u_j}) = -\frac{\partial \overline{p}}{\partial x_i} + \frac{\partial}{\partial x_j}(\overline{\tau_{ij}} - \overline{\rho u'_i u'_j}) \quad (6.8)$$

$$\overline{\tau_{ij}} = \mu \left(\frac{\partial \overline{u_i}}{\partial x_j} + \frac{\partial \overline{u_j}}{\partial x_i} \right) \quad (6.9)$$

The additional terms in the momentum equation (6.8) are:

$$\overline{\rho u'_i u'_j}$$

These are known as the Reynolds or turbulence stresses, R_{ij} . The Reynolds stress tensor is symmetric and hence has six independent components. These terms represent the transfer of momentum due to turbulent fluctuations. The introduction of these additional unknowns means that the system of equations is no longer closed, that is, there are more unknowns than equations. Therefore, it is necessary for Reynolds-average Navier-Stokes equations to require additional information for the computation of turbulent flows. The resulting problem of finding additional equations or conditions to make up this disparity has come to be called the *closure problem*. To solve this problem requires the introduction of turbulence models.

6.4 Turbulence Transport Models

A transport model is a set of additional equations to Reynolds-averaged Navier-Stokes equations, purporting to express the relations between terms appearing in those equations. The starting point of the *closure* problem is the modelling of the Reynolds stresses in terms of the mean flow quantities. Simple closure models normally use the eddy viscosity hypothesis of Boussinesq (1887). This model considers turbulent eddies as quantities of fluid, which, like molecules, collide and exchange momentum, obeying the kinetic theory of gases. From this Boussinesq suggested the turbulent shearing stresses might be related to the mean rate of strain, a scalar term, μ_t . μ_t is referred to as the turbulence or eddy viscosity (dynamic). This is not a property of the fluid but depends on the local state of turbulence; it is assumed to be a scalar quantity and it may vary significantly from point to point and flow to flow. It must be realised that the available 'transport' models pay no respect to the actual physical modes of turbulence: for example eddies, velocity patterns, and high vorticity regions. Therefore, turbulence models obscure the physical process they purport to represent. Flow visualisation experiments confirm this point (Markatos, 1986) and demonstrate the difficulty of precise definition and modelling. Consequently, it should be of no surprise that the actual physics of turbulence are nowhere to be seen in the 'transport' models; simply because no one can represent them mathematically in the models. It is, however, also true that the engineering community has fortuitously often obtained very useful results by using the 'transport' models; results that would have cost more money and time if done experimentally. Therefore, cautiously exercised and interpreted models can be valuable tools in research and design despite their physical deficiencies. It is customary to classify turbulence models according to the number of transport equations used for turbulence quantities. This is illustrated by table 6.1.

Table 6.1 Classes of turbulence models		
Name	Number turbulent transport equations	Turbulence quantities transported
Zero equation models	0	None
One equation models	1	k, turbulent kinetic energy
Two equation models	2	k, turbulent kinetic energy ϵ, viscous dissipation
Stress/flux models	6	Reynolds stresses
Algebraic stress models	2	k and ϵ to calculate the Reynolds stresses

6.4.1 Zero-Equation Models

The zero-equation model only uses the partial differential equation for the mean flow field and no transport equations for the turbulent quantities. This is also known as the mean field closure (Mellor, 1973). The models of this group relate the turbulence shear stress uniquely to the mean flows at each point. Since this only requires algebraic expressions, they have become very popular (Markatos, 1986). All models in this class use the eddy-viscosity concept of Boussinesq (1877).

6.4.2 One-Equation Models

The one equation model requires the solution of an equation for the turbulent kinetic energy, k , and as a result allows for its transport. The turbulent kinetic energy equation can be derived from the Navier-Stokes equations (Spalding and Launder, 1972). The model requires length scale that is specified algebraically and hence flow dependent. It is difficult to incorporate the length scale empirically for complex flows with separation, streamline curvature or rotation. The one equation model is not very popular since it performs only marginally better than the zero-equation model (Nallasamy, 1987).

6.4.3 Two-Equation Models

The two equation model is one of the most widely used in engineering applications. In the 1970s the Imperial College group, led by Professor Spalding (Spalding and Launder, 1972), experimented with three kinds of two equation models, k - k_l , k - ω , and the k - ϵ model. These three models are closely associated with each other, although they differ in the forms of diffusion and near wall terms employed. However, the k - ϵ model has become the most popular because of the practical advantage that the ϵ -equation requires no extra terms near the walls.

6.4.4 Algebraic Stress Models

These models can be considered as an intermediate between the two-equation models and the Reynolds stress models, they run with a reduced computational effort in comparison to Reynolds stress models.

Algebraic based models are applied between the component of turbulent stress, k the turbulent kinetic energy and ϵ , the dissipation, with coefficients as a function of the mean velocity gradients. This effectively forms an extension of the k - ϵ model. Algebraic models are therefore suitable when the individual transport of the Reynolds stresses is not important.

6.4.5 Large Eddy Simulations

Large eddy simulations involve the integration of the Navier-Stokes Equations in time using the appropriate finite difference or spectral representation, and is therefore free of the closure difficulty. The objective of large eddy simulation is to filter the small eddies from the flow field. This is done in such a way that the continuum equations come to apply only to the resolvable, large-scale eddies. The technique of full simulation is only available for transition flows (Markatos, 1986). Large eddy simulation is still in its infancy and is limited by computer power. Its present disadvantages are as follows: (Markatos, 1986)

- 1) it requires too much computer time and storage,
- 2) realistic models are not available near the walls,
- 3) the use of natural boundaries stretch computer resources to the limit and present synthetic boundaries are questionable.

6.4.6 Reynolds Stress Models

The two-equation models have been used extensively for engineering applications, but the main practical limitation is the assumption of isotropic eddy viscosity. This means that the effects of curvature, rotation and buoyancy have to be modelled separately. To improve on this situation one has to move towards the so-called Reynolds Stress Models (R.S.M.). These models employ transport equations for the individual stresses and are sometimes called second order closure models. Reynolds stress models are extremely computer intensive. However, they are capable of handling rotation and large amounts of curvature, as encountered with a *Swirly-flo* pipe. The two equation models only do this with modification. Naturally, these equations contain terms that need to be modelled in keeping with the postulate of turbulent flows. Such modelling follows the pioneering work of Rotta (1951). The most widely known stress models at the present time are those of: Hanjalic and Launder (1972), Daly and Harlow (1970) and Donaldson (1972). The state of Reynolds stress models as of 1979 has been described by Launder (1979) and the present state as of 1990, by Leschziner (1990).

The Reynolds Stress Model used in *Fluent* (*Fluent*, 1996) is based on the work of Launder (1975). It must be noted that *Fluent 4.3* manual quotes (Launder, 1975) as the source for the constants used in Reynolds Stress Model, when the actual source was Launder (1992). This was where Launder updated the constants used in the Reynolds Stress Model. *Fluent* did not model all the terms, the so-called *wall-echo* or *pressure reflection* were not modelled. These terms re-distribute the normal stresses near the wall and were of a non-trivial value only in this region. The following section will highlight the main points of the turbulence model, since this model was used to solve the flow fields in *Swirly-flo* pipes. It is general practice in literature to call R_{ij} the Reynolds Stress tensor. The exact

transport equation for the transport of R_{ij} is given in equation 6.11, where R_{ij} is given by equation 6.10.

$$R_{ij} = -\frac{\tau_{ij}}{\rho} = \overline{u'_i u'_j} \quad (6.10)$$

$$\frac{DR_{ij}}{Dt} = P_{ij} + D_{ij} - \varepsilon_{ij} + \Pi_{ij} + \Omega_{ij} \quad (6.11)$$

Where, P_{ij} , D_{ij} , ε_{ij} , Π_{ij} , and Ω_{ij} , are the rate of production of R_{ij} , the transport diffusion of R_{ij} , the rate of dissipation of R_{ij} , the transport of R_{ij} due to turbulent pressure-strain interactions and the transport of R_{ij} due to rotation, respectively. Examining each of these term separately we find the following.

Production term

$$P_{ij} = -(R_{im} \frac{\partial U_j}{\partial x_m} + R_{jm} \frac{\partial U_i}{\partial x_m}) \quad (6.12)$$

In general C.F.D. computations with Reynolds stress transport equations retain the production term in its exact form, as shown in equation 6.12.

Diffusion term

$$D_{ij} = \frac{\partial}{\partial x_k} (\frac{\nu_t}{\sigma_k} \frac{\partial R_{ij}}{\partial x_k}) \quad (6.13)$$

The diffusion term is modelled by the assumption that the rate of transport of Reynolds stresses by diffusion is proportional to the gradients of the Reynolds stresses. The majority of commercial C.F.D. packages use the simplest form, as

shown in equation 6.13. The dissipation tensor ε_{ij} is given by equation 6.14. This is based on the hypothesis of local isotropy of Kolmogorov (1941), since most dissipation occurs at the smallest scales. This is set so that it affects the normal Reynolds stresses ($i=j$) only and in equal measure. This is achieved by the use of the Kronecker delta, δ_{ij} . If i equals j then $\delta_{ij} = 1$. If however i does not equal j , then $\delta_{ij} = 0$.

$$\varepsilon_{ij} = \frac{2}{3} \rho \varepsilon \delta_{ij} \quad (6.14)$$

Pressure strain term

$$\Pi_{ij} = -C_1 \frac{\varepsilon}{k} (R_{ij} - \frac{2}{3} k \delta_{ij}) - C_2 (P_{ij} - \frac{2}{3} P \delta_{ij}) \quad (6.15)$$

The pressure-strain terms are the hardest to model in the Reynolds stress model and the most important one to be modelled correctly. The Reynolds stresses are caused by the two major components, namely: pressure fluctuations due to two eddies mixing together and pressure fluctuations due to the interaction of an eddy with a region of flow with a different mean velocity. The overall effect of the pressure-strain term is to redistribute the energy amongst the normal Reynolds stresses, so as to make them isotropic and to reduce the Reynolds shear stress. C_1 and C_2 are constant values of 1.8 and 0.6, respectively.

Rotational term

$$\Omega_{ij} = -2 \omega_k (R_{jm} e_{ikm} + R_{im} e_{jkm}) \quad (6.16)$$

ω_k is the rotation vector and e_{ijk} is the alternating symbol; $e_{ijk} = +1$ if i, j are different and in cyclic order, $e_{ijk} = -1$ if i, j and k are different and in anti-cyclic order and $e_{ijk} = 0$ if any two indices are the same.

Turbulent kinetic energy is needed in the above formula and can be found by adding the three normal stresses together (R_{11}, R_{22}, R_{33}) as shown in equation 6.17.

$$k = \frac{1}{2}(R_{11} + R_{22} + R_{33}) \quad (6.17)$$

The six equations for the Reynolds stress transport are solved along with the model for the scalar dissipation rate, ϵ . The equation for dissipation rate, ϵ , is shown below.

$$\frac{\partial \epsilon}{\partial t} + U_i \frac{\partial \epsilon}{\partial x_i} = \frac{\partial}{\partial x_i} \left(\frac{\nu_i}{\sigma_\epsilon} \frac{\partial \epsilon}{\partial x_i} \right) + C_{1\epsilon} \frac{\epsilon}{k} \nu_i \left(\frac{\partial U_i}{\partial x_j} + \frac{\partial U_j}{\partial x_i} \right) \frac{\partial U_i}{\partial x_j} - C_{2\epsilon} \frac{\epsilon^2}{k} \quad (6.18)$$

The first term on the right hand represents the rate of change of ϵ at fixed point in space. The second term on the right hand side represents the rate of change of ϵ lost by convection (per unit volume) through the control surface, this is sometimes known as the transportation of ϵ . The terms on the right hand side of equation 6.18, moving from left to right are: diffusion of ϵ , generation of ϵ , and destruction of ϵ . $C_{1\epsilon}$, $C_{2\epsilon}$, and σ_ϵ are constants, having the values of 1.44, 1.92 and 1.3, respectively.

Fluent provides additional terms for curvature when cylindrical co-ordinates are used, which was used in this thesis, these terms can be readily found in the *Fluent 4.3* manual. (*Fluent*, 1996)

6.5 The Solution Algorithm

The solution algorithm is based on the finite volume approach. This is the name given to the method by which the integral formulation of the conservation laws are discretized directly into physical space. This approach takes full advantage of an arbitrary computational mesh.

6.5.1 The Integral Approach to Finite Volume

The finite volume approach provides a intuitive association between the physical processes occurring across the bounding surfaces of the control volume and the governing partial differential equations, this is a consequence of the Gauss' Divergence Theorem. The application of this theorem to the conservation laws for a discrete volume is shown in equation (6.19).

$$\frac{\partial}{\partial t} \int_{\Omega} U d\Omega + \int_s \underline{F} \cdot d\underline{S} = \int_{\Omega} Q d\Omega \quad (6.19)$$

Where, Ω_j is the control volume, \underline{S} is the surface vector, \underline{F} is the flux vector and Q the sources (Hirsch, 1988). When the discretized equation associated with U_j is to be defined, Equation (6.19) is replaced by the discrete form:

$$\frac{\partial}{\partial t} (U_j \Omega_j) + \sum_{SIDES} (\underline{F} \cdot \underline{S}) = Q_j \Omega_j \quad (6.20)$$

Where the sum of all the flux terms refers to all the external sides of the control cell Ω_j .

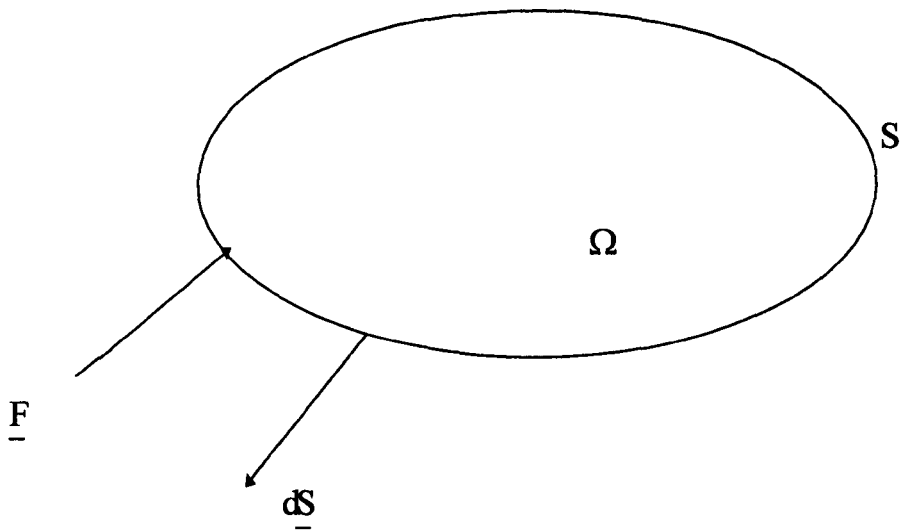


Figure 6.2 Arbitrary Control volume

This is a general formulation of the finite volume method for a selected control volume. The solution of all the relevant quantities is based on the Semi-implicit Method for Pressure-linked Equations, or more commonly known as S.I.M.P.L.E. .

6.5.2 The S.I.M.P.L.E. Algorithm

This method of solution of the incompressible turbulent Navier-Stokes equations is derived from the general strategy outlined by Patanker and Spalding (Patanker and Spalding, 1972). This method comes under the general heading of pressure correction methods. "Pressure correction methods follow the principle of initially solving the momentum equations using a guessed pressure field, in order to obtain an approximate velocity field. The approximate velocity and pressure fields are then corrected such that continuity is satisfied". (Rubini, 1994)

The S.I.M.P.L.E. procedure consists of a set of algebraic equations for velocity components, turbulent kinetic energy, turbulent dissipation, Reynolds stresses and an equation for pressure. The method starts from arbitrary initial conditions (except at the boundaries) and converges to the correct solution after a sequence of iterations.

Each iteration consists the following steps:

- 1) start with estimated P^* , u^* , v^* , and w^* ,
- 2) solve the momentum transport equations using P^* , u^* , v^* , and w^* ,
- 3) solve the pressure correction for $P^\#$, using u^* , v^* , and w^* ,
- 4) update the pressure and the velocity fields using $P^\#$ to obtain u^1 , v^1 , and w^1 ,
- 5) solve the other discretised transport equations, that is the six independent Reynolds stresses and the scalar dissipation rate ϵ ,
- 6) repeat steps 2 to 5 until convergence is reached.

The S.I.M.P.L.E. algorithm has been used to successfully solve a number of incompressible flow problems. In certain cases it is found that the rate of convergence is not satisfactory. This is due to the fact that the pressure correction equation tends to overestimate the value pressure even though the corresponding velocity corrections are reasonable. Due to this fact it may be necessary to alter the pressure correction equation to include an under-relaxation parameter. For the same reason, under-relaxation is employed in the solution of the momentum equations.

The convergence criterion specified that the sum of the normalised residuals must be less than 10^{-4} . This is a measure of the overall conservation of flow properties.

The accuracy of the solution with respect to the computational grid may be considered accurate if alteration in the grid size produces no significant change in the values of dependent variables or fluxes at the points in flow or its boundary which are of interest to the user. Such alteration is obtained by altering the number of grid intervals in all directions of flow.

The number of iterations required for convergence varies substantially depending on the grid system, under-relaxation factors, and inlet turbulent intensity as determined by Zigh (1993). Computations were performed on a the University V.M.S. Alpha and the Rutherford Appleton Laboratory J923 Cray.

6.5.3 Interpolation Scheme

The computer algorithm for the solution of the Navier-Stokes equations stores the computed velocity components and scalar variables at geometric centres of the control volumes defined in the grid. During the solution process it is necessary to compute the values of the variables at the control volume boundaries. Therefore it is necessary to use some form of interpolation technique. This is achieved by using the Power-Law interpolation (P.L.D.S.) based on the work of Patanker (1980). This method uses the Power-Law since it was believed the exact exponential solution would be too costly to compute. An important feature of the Power Law scheme is it can give rise to strong numerical induced diffusion if the flow is skewed relative to the mesh lines of the computational grid in regions of high vorticity or shear. This is due to the fact that the leading truncation error is of order one in the interpolation scheme, which leads to numerical diffusion.

6.5.4 Boundary Conditions

Insertion of correct boundary conditions requires modification of the finite volume formulation near boundary points. Due to the elliptical nature of the conserved equations, boundary conditions must be specified at all boundaries along the domain being considered. The inlet conditions are known beforehand and can be specified at the beginning of the calculation. Conditions at the exit from the region of interest are not known beforehand. The algorithm stipulates that the overall continuity must be satisfied and the flow is fully developed at the exit boundary. Therefore zero gradient boundary conditions are applied at the exit of the region of interest and on an axis of symmetry (with the exception of perpendicular velocity components which must vanish at an axis of symmetry). The boundary conditions led on to the use of wall functions.

6.5.5 The use of Wall Functions in the Solution

Fluid near the wall surface is stationary and turbulent eddies must stop near the wall. In the absence of turbulent (Reynolds) shear stresses the fluid is dominated by viscous shear. This is often known as the laminar sublayer or the linear sublayer. As one moves away from the wall viscous and turbulent effects both become important, so a new law is invoked, which is known as the log law. These formulae for flow near the wall are commonly called the law of the wall (Gerhart and Gross, 1985).

$$\frac{u_p}{u_*} = \frac{l}{\kappa} \ln(E y^+) \quad (6.21)$$

Fluent decides what rule to use by evaluating a dimensionless parameter, y^+ . The dimensionless parameter y^+ is a type of Reynolds number. Depending on the value of y^+ , *Fluent* chooses the log-law (eqn 6.21) if $y^+ > 11.225$ and if $y^+ < 11.225$ then equation (6.22) is used.

Where:

$$u^* = \sqrt{\frac{\tau_w}{\rho}} \quad (6.22)$$

and $y^+ = \rho u^* \Delta n_p / \mu$

κ = von Karman's constant (0.42)

E = empirical constant (9.81)

u_p = velocity of the fluid at point p near the wall

Δn_p = distance from p to the wall

ρ = density of fluid

τ_w = wall shear stress

μ = viscosity (dynamic)

where: $\tau_w = \mu \frac{\Delta v}{\Delta n} \quad (6.23)$

Δv = the velocity parallel to the wall at height Δn

6.5.6 Mesh Used

The mesh used was derived from a *FORTRAN* program that produced a mesh that *Fluent* 4.3 could read. This program allows the user to change the pitch and length of a *Swirly-flo* pipe with ease, and saves time by not having to draw each different *Swirly-flo* pipe on a C.A.D. (Computer Aided Design) machine. The program makes sure that the internal grid moves with twist of the pipe, so that the majority of cells are not skewed to the direction of flow. That is to say that the majority of the axial flow enters each cell perpendicular to the cell wall. This would reduce numerical diffusion, as stated in 6.5.3. The computer programs for producing the grid can be found in Appendix B. An example of a surface grid is illustrated in Figure 6.3.

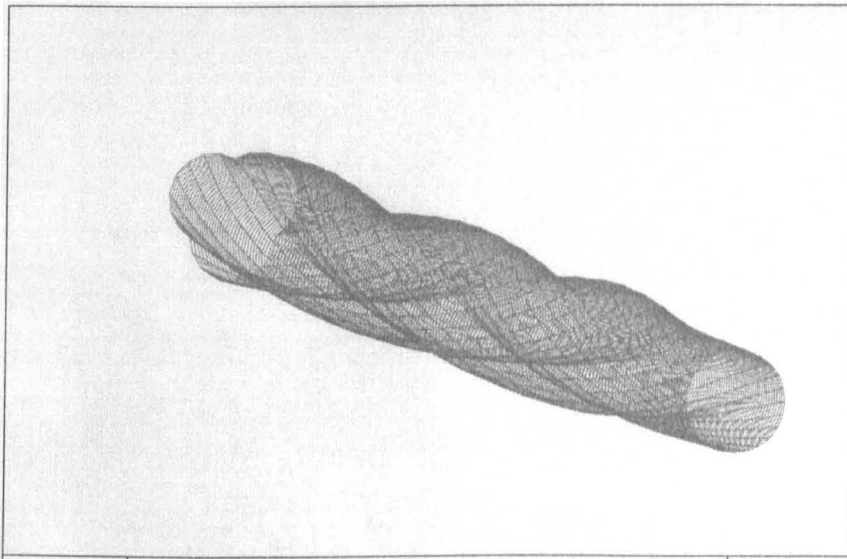


Figure 6.3 Illustration of Swirly-flo Grid

6.5.7 The Co-location of Variables

The co-location of variables means that all variables are stored in the same location on the computational grid. There are two main reasons to use the co-location of variables. The first of these is that it provides a simplification in the computer code. That is, in principle only one routine needs to be developed to solve the general transport equation, since the coefficients for each variable will be very similar (Rubini, 1994).

Secondly, the use of staggered grids when used with a curvilinear grid, limits the choice of co-ordinate transforms that may be used (Rubini, 1994).

7.0 Computational Fluid Dynamics Results

7.1 Introduction

This chapter contains the results obtained from examining pipes, using C.F.D., with constant pitch and those of a non-linear nature, that is those governed by the brachistochrone curve. All computational runs were carried out with a constant set of parameters, unless otherwise stated, and are shown in Table 7.1.

Initial u-Velocity (axial component)	1 m/s
Initial v-Velocity (radial component)	0 m/s
Initial w-Velocity (circumferential component)	0 m/s
Density	1000 Kg/m³
Viscosity (μ)	0.0009 Pa s
Reynolds number	55555
Characteristic Length	0.05 m
Turbulence Intensity [(r.m.s of u')/u_{avg}]$\times 100$) at Entrance of Pipe	10 %

The initial input velocities are all zero, except the axial velocity of 1 m/s. This velocity is constant all the way across the inlet of any swirl-inducing pipe. This represented fully developed turbulent flow at the entrance of the pipe. The viscosity and density represent that of water. Characteristic length was chosen to be the exit diameter of the pipe and the turbulence intensity was set at 10% at the inlet, which is normal for pipe flows (*Fluent*,1996). Before these experimental test runs were carried out it was necessary to show grid independence.

7.2 Examination of Grid Independence

To test for grid independence the shortest constant pitch grid was used, that of 0.1 metre standard Swirly-flo pipe, with a taper. (Appendix C, 1-C). This was used since it could provide the user with an extremely high degree of twist, or a small pitch/diameter ratio (P/D). Testing for grid independence was necessary because it reduced the effect of the grid to an acceptable level in the solution of the equations of viscous turbulent flow.

Table 7.2 Grid Independence Comparison			
	Standard Grid (30x50x40)	Half Standard Grid (15x25x20)	Quarter Standard Grid (8x13x10)
Average w-velocity at exit	0.32	0.38	0.32
Average u-velocity at Exit	1.75	1.72	1.60
Average Turbulent Kinetic Energy/ Unit Mass	0.01	0.01	0.01

Table 7.2 illustrates some important parameters at the exit of a 0.1 standard Swirly-flo pipe. The numbers in the brackets in Table 7.2, refer to the number of cells in a particular direction. For example (30x50x40), refers to 30 cells in the circumferential direction (I), 50 cells in the radial direction (J) and 40 cells in the longitudinal direction (K). The product of these numbers becomes the number of cells in the liquid flow. The grid is based on cylindrical Cartesian co-ordinates. The column labelled "Half Standard Grid" refers to a set of results for which the number of computational cells was halved in the axial, radial and circumferential directions compared to the standard grid. In the quarter standard grid column the number of cells in these directions was reduced to a quarter of the standard grid. It was not possible to double the grid in all three directions due to the computational limits presently available. It is realised that some values can

not be halved and have an integer number, so *Fluent 4.3* determines the most appropriate values.

In looking at the u-velocity and the turbulent kinetic energy terms it can easily be seen that the values seem to approach a consistency at resolution. In respect to the w-velocity the values do not start to converge as readily as the other two, this could be due to the fact that the (15x25x20) grid does not produce quite the same outline perimeter of the pipe due to the odd number of cells in the I and J direction. Therefore, the writer assumed that the w-velocity was already consistent at the coarsest exit.

It was then considered that a satisfactory level of grid insensitivity was achieved, and the cell to length ratios of the standard grid set up would be continued, where possible, throughout any grid.

Since the solution procedure is iterative *Fluent 4.3* uses, as a criterion of convergence, the sum of the normalised residuals being less than 10^{-4} . This is a measure of the overall conservation of flow properties.

7.3 Experimental Runs

The test runs were designed to investigate the effect of the pitch on the production of swirl at the exit of a swirl inducing pipe. All the runs were carried out with the same input parameters (Table 7.1), where possible. Due to the limits of computational time all the test runs consisted of 3 lobed helices equally spaced around the circumference of the pipe and these helices all rotated through 360 degrees. The formula that governs the lobe, is given by equation (7.1) and illustrated in Figure 7.1. This only refers to the first lobe, the other two lobes are obtained by rotating the first lobe through 120° and 240°, respectively. The bold line is the out-line of the lobes. In the grid generation program, the curve stops at (0.025,120), then produces the other two by rotation. In Figure 7.1 the dashed lines that have a radii less than 0.025 m are obviously ignored in the grid generation program.

$$\rho = R \cos\left(\frac{\phi}{2}\right) \cos\left(\frac{\phi}{2} - \theta\right) + R \sqrt{\cos\left(\frac{\phi}{2}\right)^2 \cdot \cos\left(\frac{1}{2}\phi - \theta\right)^2 - \cos\phi} \quad (7.1)$$

Where,

$R=0.025\text{m}$,

θ = the angle of rotation

$\phi=2/3.\pi$

ρ = radial length from the origin.

The minimum radial length was 25 mm and the maximum was 33 mm.

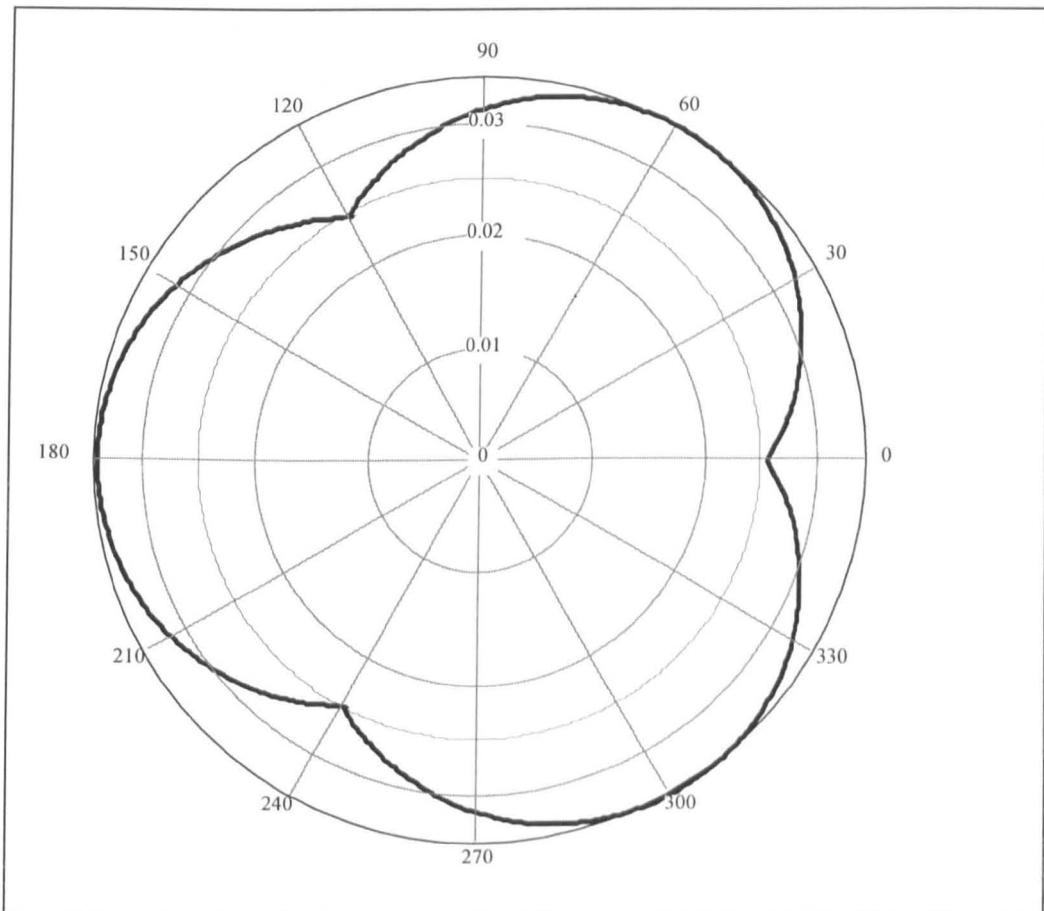


Figure 7.1 Illustration of the Geometry of the Lobes

In the case of the standard Swirly-flo pipe section (geodesic) the pitch of the helix is given by $2\pi /$ cylinder length. The brachistochrone curves similarly rotate through 2π

radians throughout the length of the pipe. In the preliminary runs all pipes were reduced to a circular cross-section through the last 30% of their length by means of a taper. With the last two runs this was not done, so that the true effect of the swirl induction could be observed without the attenuating effects of the taper. In examination of the w-velocity along the pipe, it was necessary to observe the w-velocity just away from the cylinder wall. The majority of simulations had 50 computational cells in the radial direction (J) and it was thought appropriate to choose the 45th cell in the radial direction to observe the circumferential velocity. This cell represented 0.9 of the maximum radius at any point in the pipe. As can be seen from Figure 7.1 this would not be a constant distance all along the perimeter, unless it was at the end of the taper. However, the author was interested in the flow effects at a distance away from the wall at which different pipe profiles could be sensibly compared. At the maximum radius, 33 mm, the distance away from the wall was 3.3 mm, and at the minimum radius the distance was 2.5 mm. This led to a variation of 0.8 mm, which was considered an acceptable margin. For the three runs that had less than 45 cells in the radial direction (0.6 standard Swirly-flo, 0.7 standard Swirly-flo, and 1.0 metre standard Swirly-flo pipe) with 25 cells. The 23rd cell was used which led to a variation in distance from the wall was of 0.65 mm, again acceptable. It should be noted that the incorrect characteristic length was used in 0.6 and 0.7 standard Swirly-flo pipes (500 mm, as opposed to 50 mm), however the results of these runs were noted since they still provided information, albeit incomplete.

The following two tables give the grid densities for the all the runs, whether they had tapers or not.

Length of pipe m	Pitch rad/m	Angle to the Longitudinal axis/ deg	P/D ratio	Cells (IxJxK)
0.1	62.832	57.518	2	30x50x40
0.2	31.416	38.146	4	30x50x80
0.3	20.944	27.636	6	30x50x120
0.4	15.708	21.439	8	30x50x140
0.5	12.566	17.440	10	30x50x160
0.6	10.472	14.671	12	30x25x140
0.7	8.976	12.648	14	30x26x160
0.8	7.853	11.109	16	30x50x160
0.9	6.981	9.900	18	30x50x180
1.0	6.283	8.927	20	25x25x200

Length of pipe (m)	Cells (IxJxK)
0.1	Not done because the computational cost was prohibitive
0.2	30x50x80
0.3	30x50x120
0.4	30x50x140
0.5	30x50x160

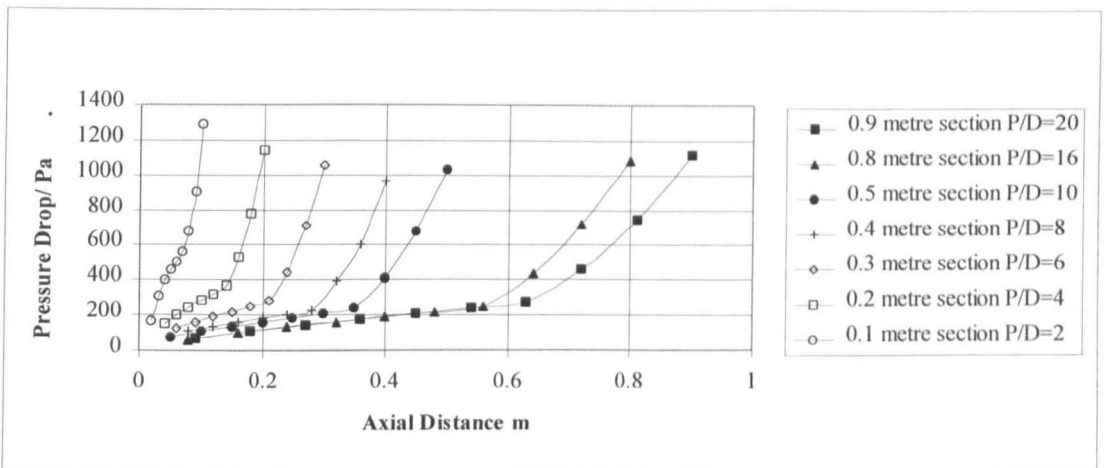


Figure 7.2 Pressure Drop against Axial Distance for Standard Swirly-flo Pipes with constant I (30) and J (25) Cell Numbers

The 0.1 metre section gave the largest w-velocity, with largest pressure drop. The 0.4 metre run produced the lowest pressure drop with a pitch/diameter ratio of 8.

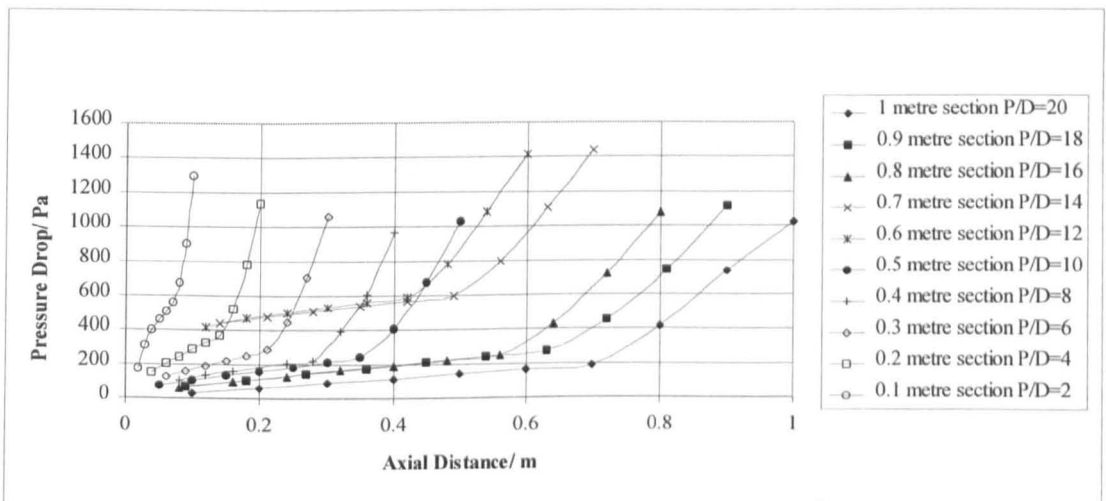


Figure 7.3 Pressure Drop against Axial Distance for All Standard Swirly-flo Pipes

Figure 7.3 graph shows that the 0.6 and 0.7 metre runs were clearly out of place, whilst the 1 metre section pipe seemed to be following the pattern of the correctly configured runs. However it shows a reduced overall pressure loss (at the last point) in comparison to the 0.9 metre curve.

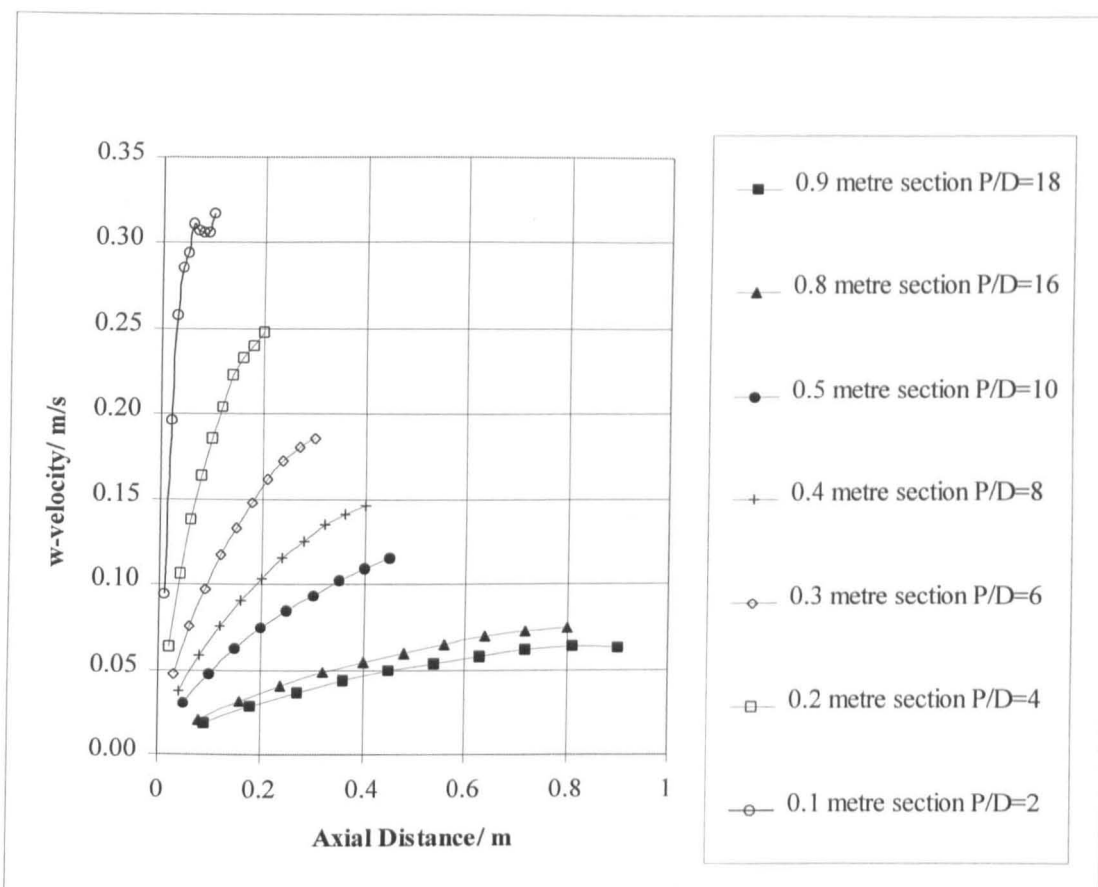


Figure 7.4 Average w-Velocity against Axial Distance for Standard Swirly-flo Pipes with constant I (30) and J (25) Cell Numbers

Figure 7.4 indicates that as the axial distance increased the amount of swirl reduced. Since all the standard pipes have a full 360° of twist, the reduction in length is bound to increase the swirling rate induced by the pipe. Note the flattening of the swirl induction effect as the standard pipe was lengthened.

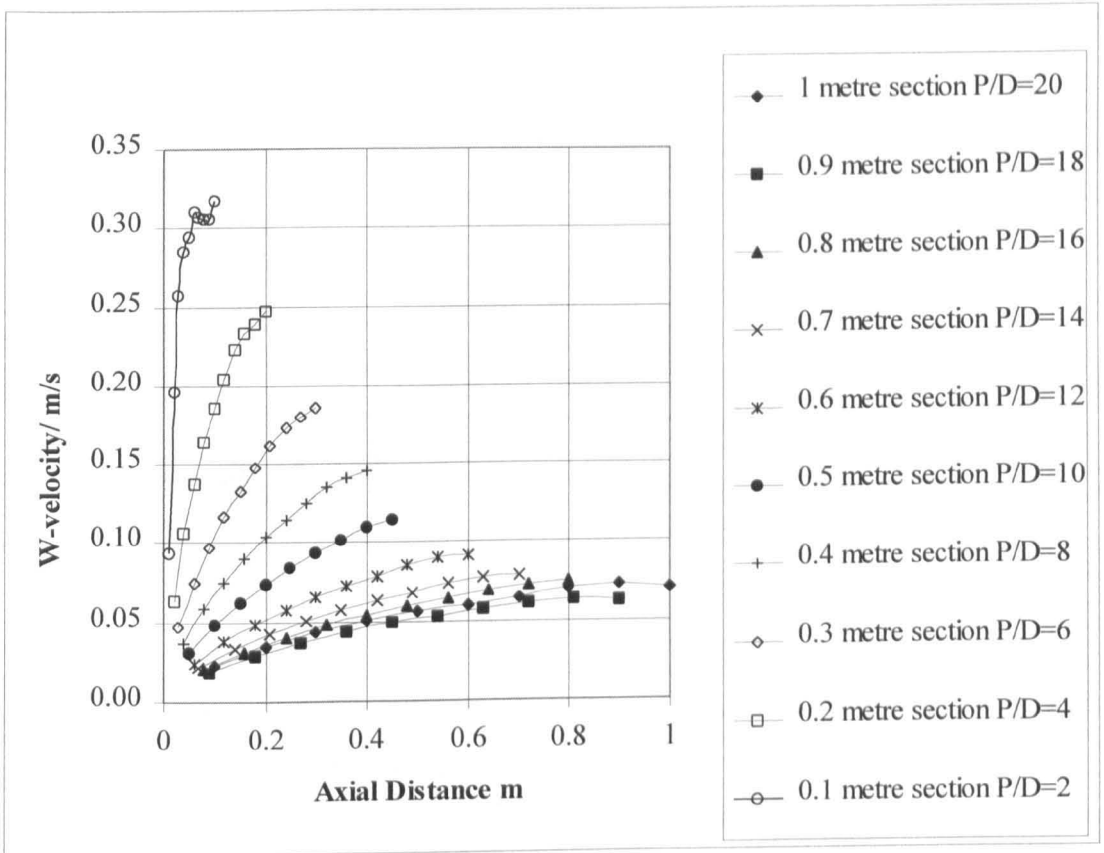


Figure 7.5 Average w-Velocity against Axial Distance for All Standard Swirly-flow Pipes

In Figure 7.5 the 0.6 and 0.7 metre runs followed similar pattern to the rest, whilst the 1 metre run showed a greater w-velocity than the 0.9 metre section.

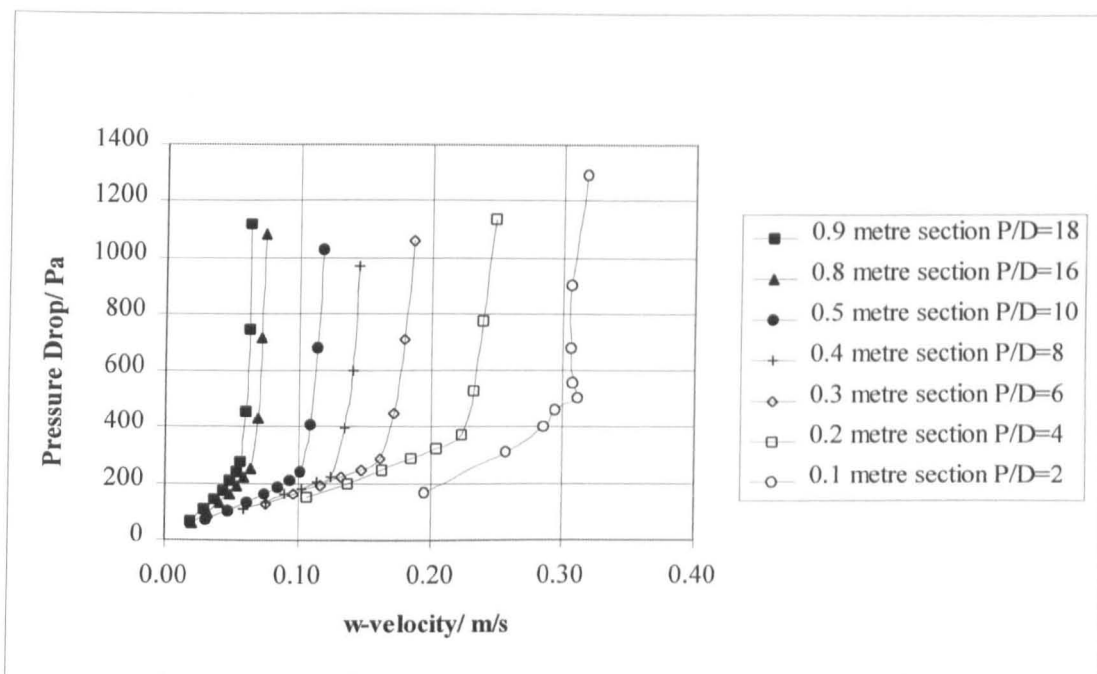


Figure 7.6 Pressure Drop against w-Velocity for Standard Swirly-flo Pipes with constant I (30) and J (25) Cell Numbers

A general summary of Figure 7.6, was that the higher the w-velocity the greater the pressure loss (measured at the last point).

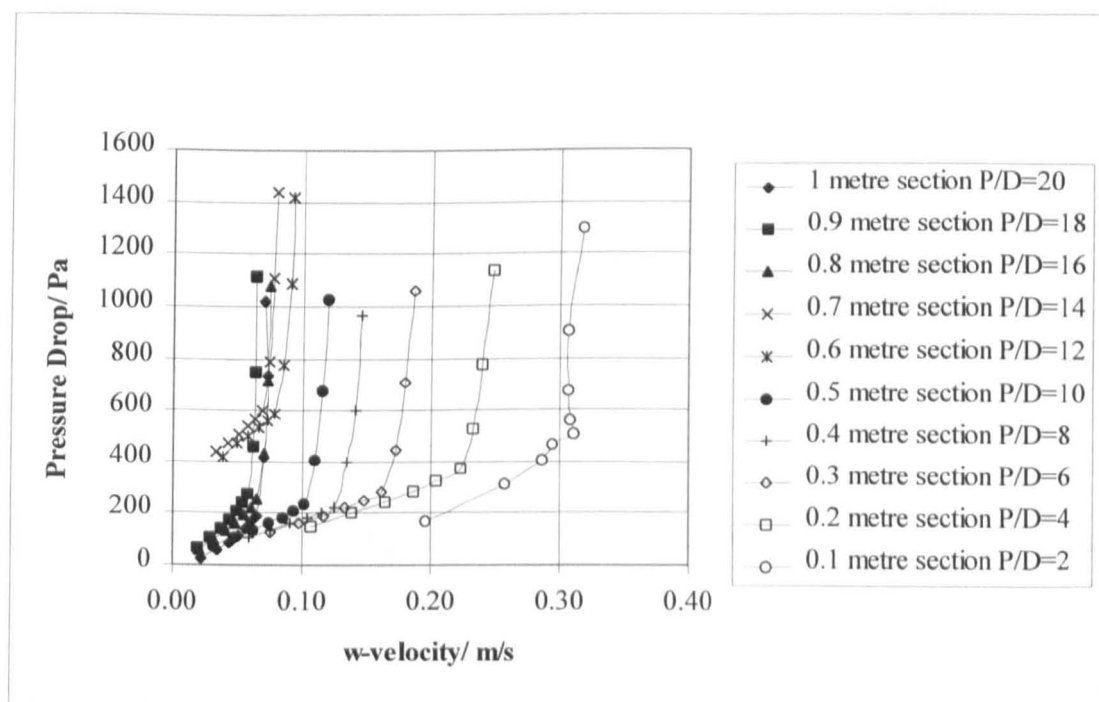


Figure 7.7 Pressure Drop against w-Velocity for All Standard Swirly-flo Pipes

As before, in Figure 7.7, the 0.7m and 0.6m runs showed a displacement of pressure drop in comparison to the other runs.

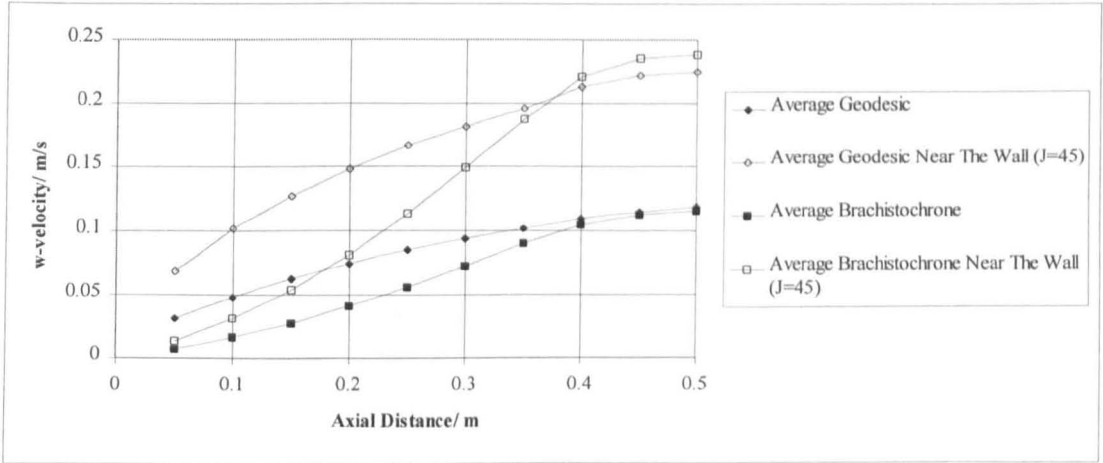


Figure 7.8 w-Velocity against Axial distance for 0.5m Standard (Geodesic) Swirly-flo Pipe and 0.5m Brachistochrone

In Figure 7.8, the average Geodesic and average Brachistochrone refer to the average w-velocity taken over the entire plane, at successive axial positions. The standard Geodesic J=45 and the Brachistochrone J=45, refer to the average of all J=45 cells taken at successive axial positions.

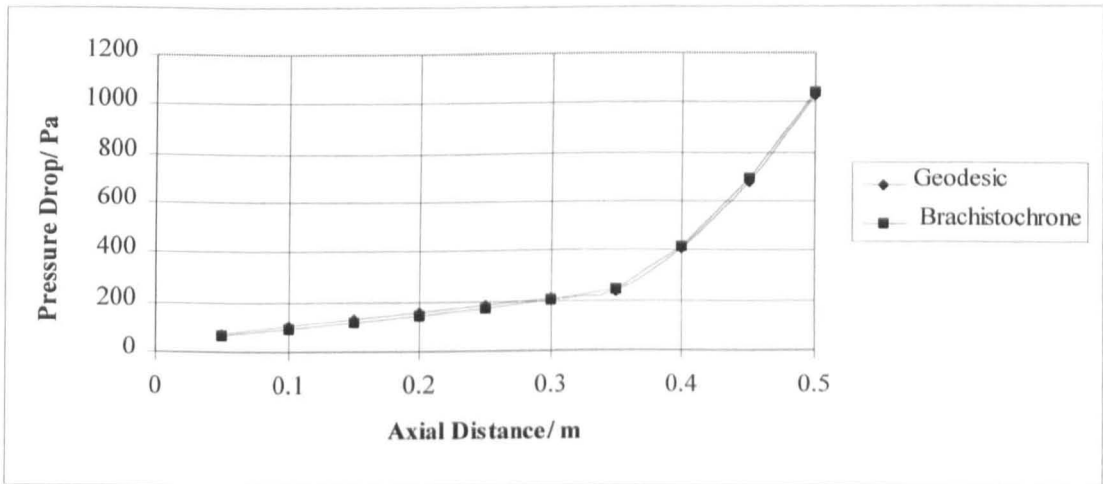


Figure 7.9 Pressure Drop Against Axial Distance for the 0.5m Standard (Geodesic) Swirly-flo pipe and the 0.5m Brachistochrone

As Figure 7.9 shows, the pressure drop for both curves was almost the same.

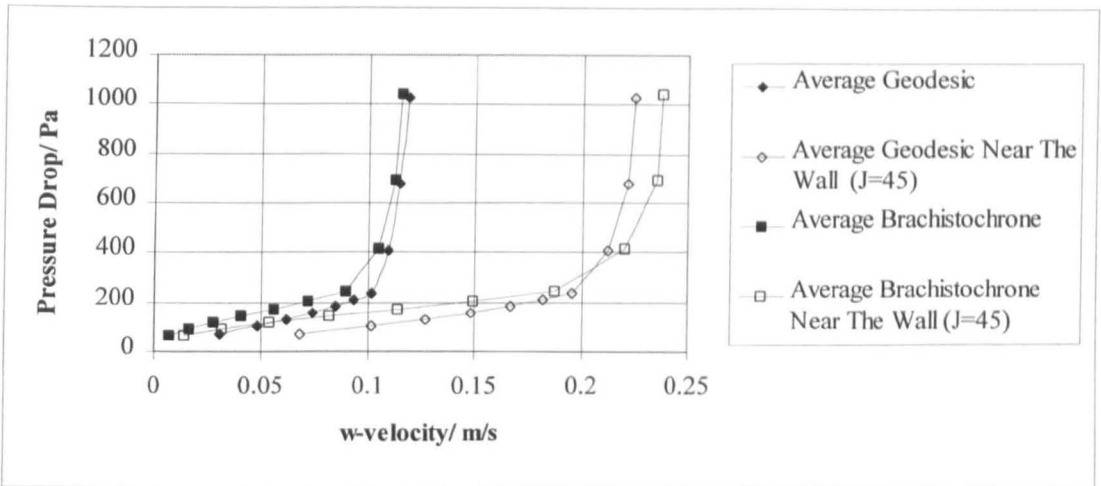


Figure 7.10 Pressure Drop Against w-Velocity for the 0.5m Standard (Geodesic) Swirly-flo pipe and the 0.5m Brachistochrone

Figure 7.10 illustrates that the w-velocity was greater nearer the wall compared to the average w-velocity, with brachistochrone being the largest.

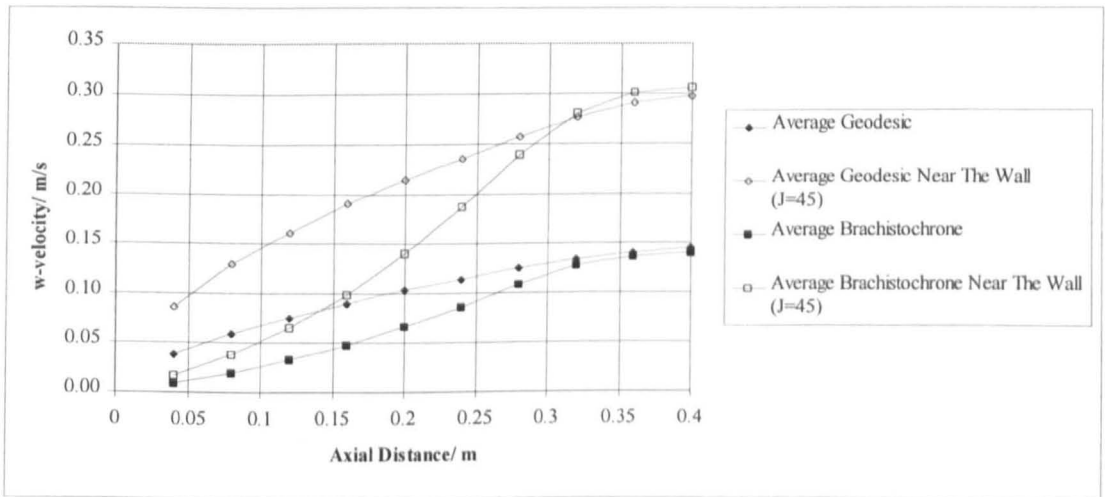


Figure 7.11 w-Velocity against Axial distance for 0.4m Standard Swirly-flo (Geodesic) Pipe and 0.4m Brachistochrone

As Figure 7.11 shows, both the 0.4 metre sections produced more swirl than the 0.5 metre sections, with J=45 brachistochrone producing slightly more swirl than the geodesic pipe. However, the average swirl across the plane was less for the brachistochrone.

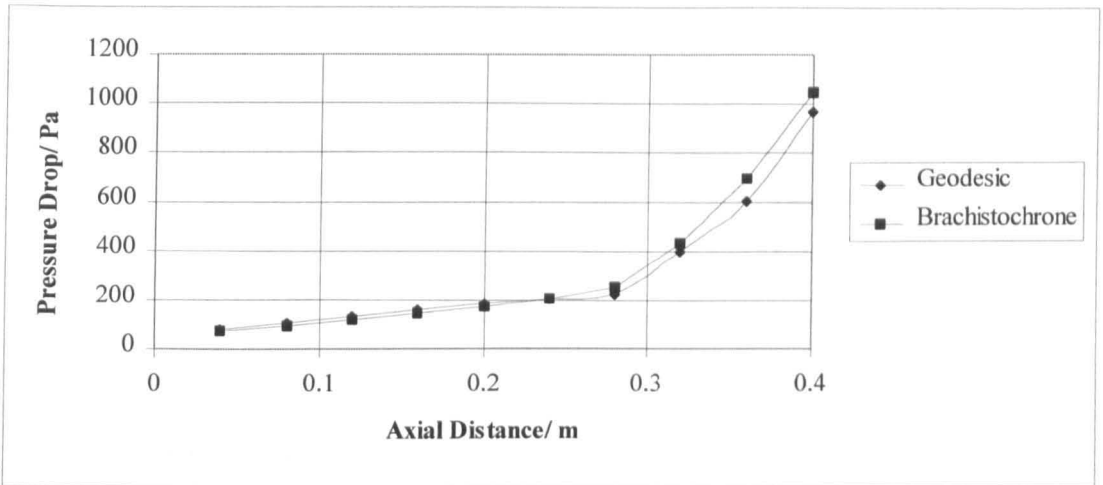


Figure 7.12 Pressure Drop Against Axial Distance for the 0.4m Standard (Geodesic) Swirly-flo pipe and the 0.4m Brachistochrone

The brachistochrone curve produced slightly more pressure loss towards the end of the pipe. (See Figure 7.12)

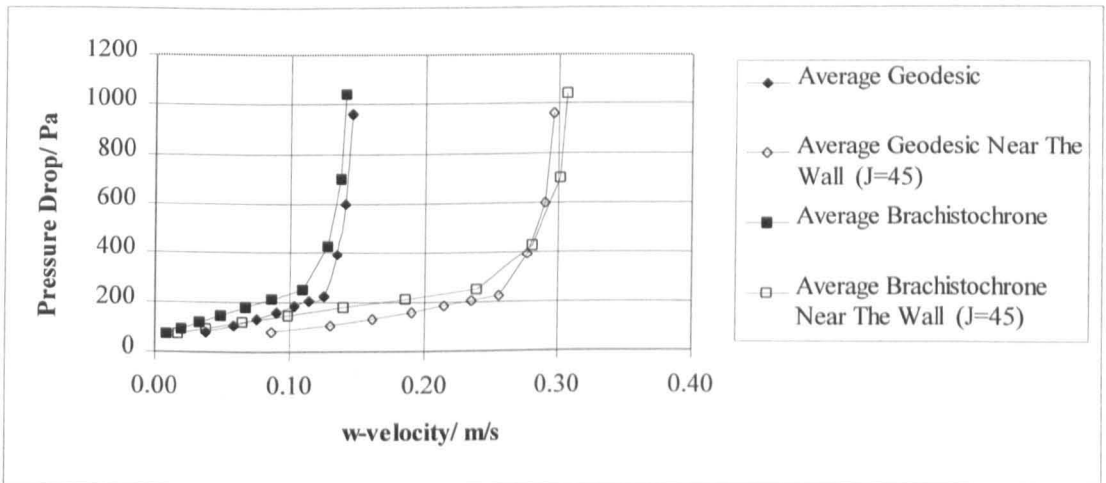


Figure 7.13 Pressure Drop Against w-Velocity for the 0.4m Standard (Geodesic) Swirly-flo pipe and the 0.4m Brachistochrone

Figure 7.13 illustrates that the w-velocity was greater nearer the wall compared to the average w-velocity, with brachistochrone being the largest.

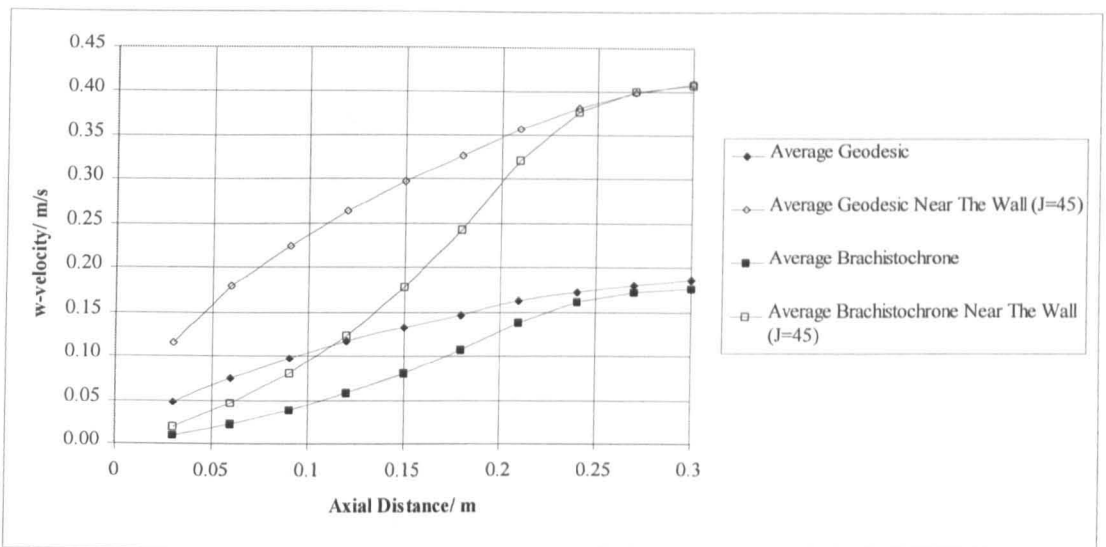


Figure 7.14 w-Velocity against Axial distance for 0.3m Standard (Geodesic) Swirly-flo Pipe and 0.3m Brachistochrone

Figure 7.14 shows that for both cases the geodesic pipe produced more swirl than the brachistochrone pipe. The average $J=45$ values were very similar at exit.

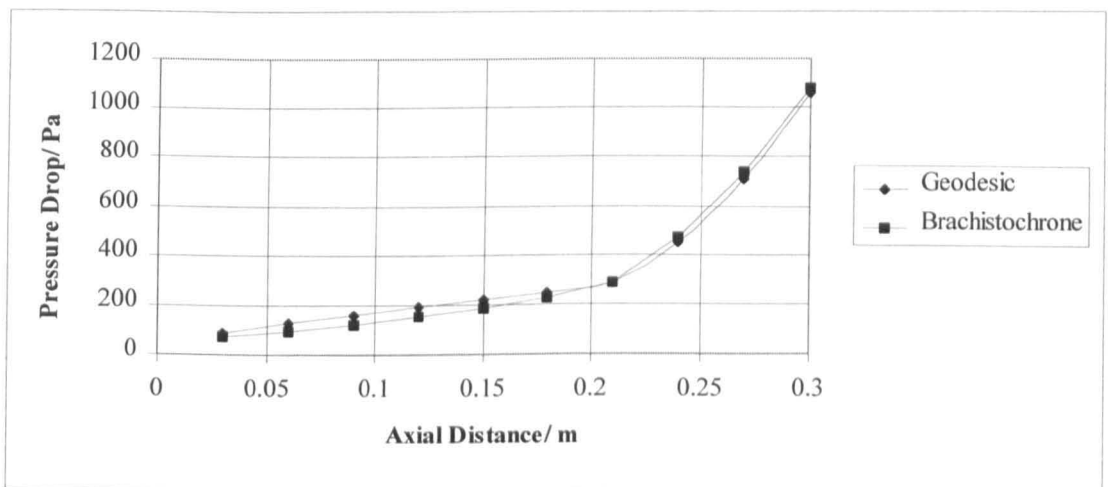


Figure 7.15 Pressure Drop Against Axial Distance for the 0.3m Standard (Geodesic) Swirly-flo pipe and the 0.3m Brachistochrone

The pressure drop for both curves was almost the same, as shown in Figure 7.15.

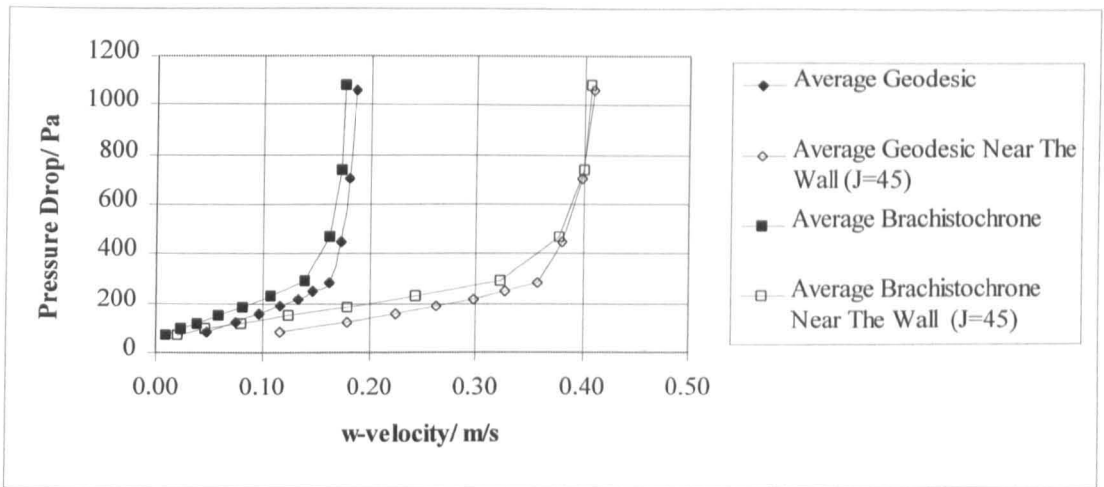


Figure 7.16 Pressure Drop Against w-Velocity for the 0.3m Standard (Geodesic) Swirly-flo pipe and the 0.3m Brachistochrone

Figure 7.16 illustrates that the w-velocity was greater nearer the wall compared to the average w-velocity. However, the difference between the two curves near the wall was negligible.

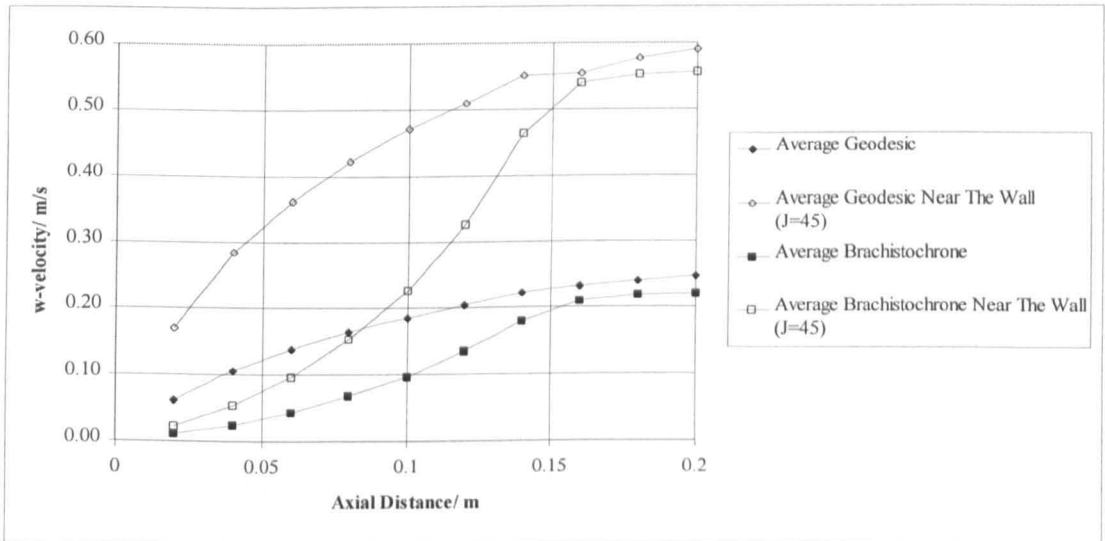


Figure 7.17 w-Velocity against Axial distance for 0.2m Standard Swirly-flo Pipe and 0.2m Brachistochrone

Figure 7.17 show that the brachistochrone curve produced slightly less swirl for the given 0.2 metre length.

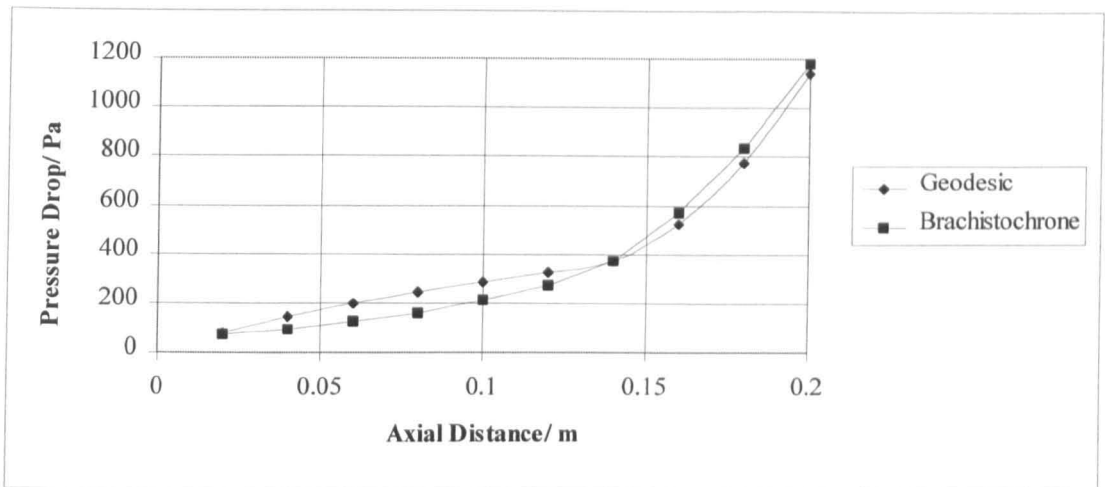


Figure 7.18 Pressure Drop Against Axial Distance for the 0.2m Standard (Geodesic) Swirly-flo pipe and the 0.2m Brachistochrone

As Figure 7.18 shows the brachistochrone curve produced slightly more pressure loss towards the end of the pipe.

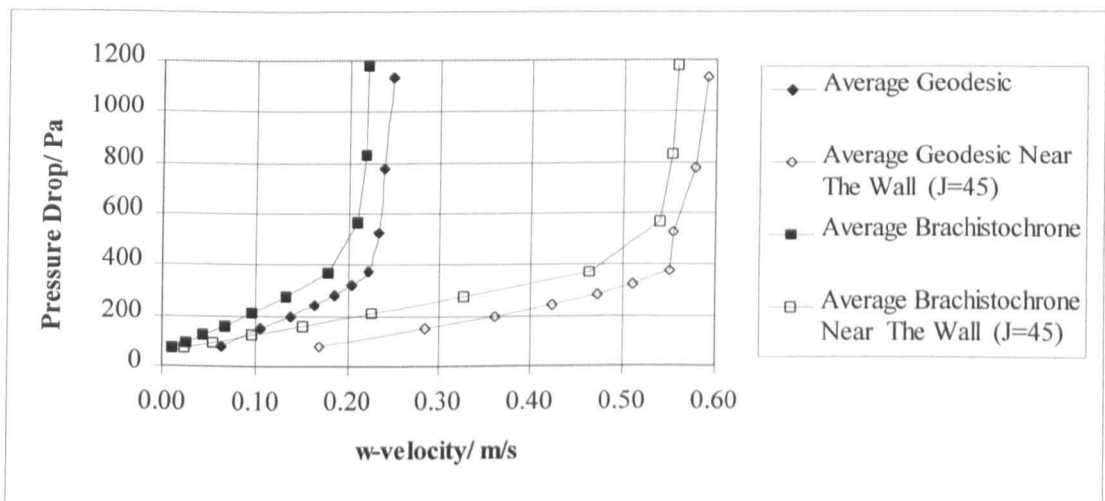


Figure 7.19 Pressure Drop Against w-Velocity for the 0.2m Standard (Geodesic) Swirly-flo pipe and the 0.2m Brachistochrone

Figure 7.19 illustrates that the w-velocity was greater nearer the wall compared to the average w-velocity. However, the difference between the two curves near the wall was larger than that for the 0.3m pipes.

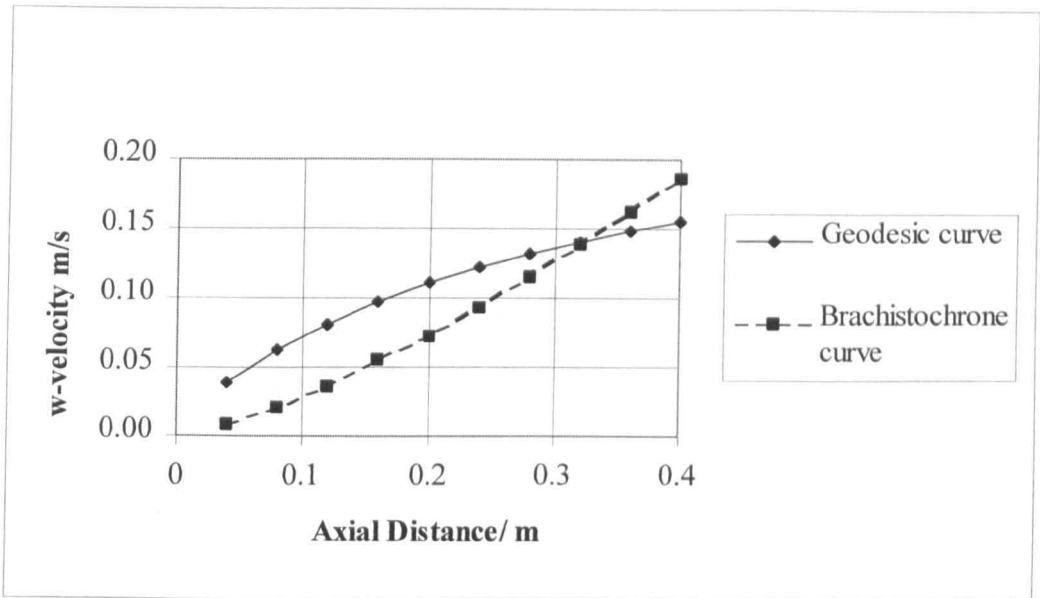


Figure 7.20 Average w-Velocity against Axial Distance for 0.4m Standard pipe and 0.4m Brachistochrone, without Tapered Ends

Figure 7.20 shows that for 0.4m length of pipe the brachistochrone produced more swirl than the standard Geodesic pipe. The brachistochrone shows an increasing gradient, whilst the converse is true for the geodesic curve.

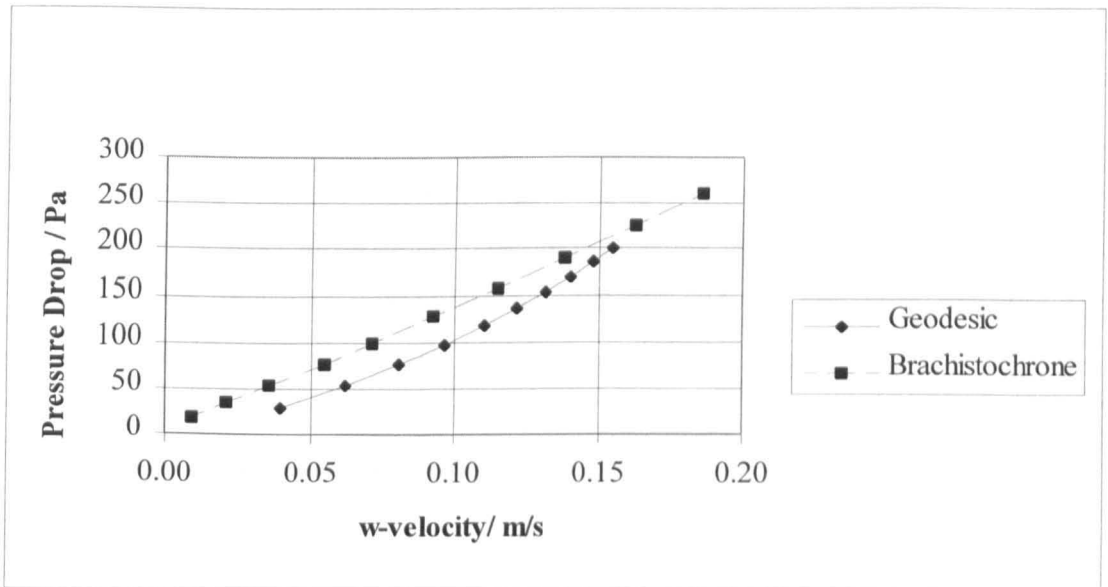


Figure 7.21 Pressure Drop against Average w-Velocity for 0.4m Standard pipe and 0.4m Brachistochrone, Without Tapered Ends

For the increase in swirl the brachistochrone suffered from a slightly increased pressure loss, of approximately 60 Pa. (See Figure 7.21)

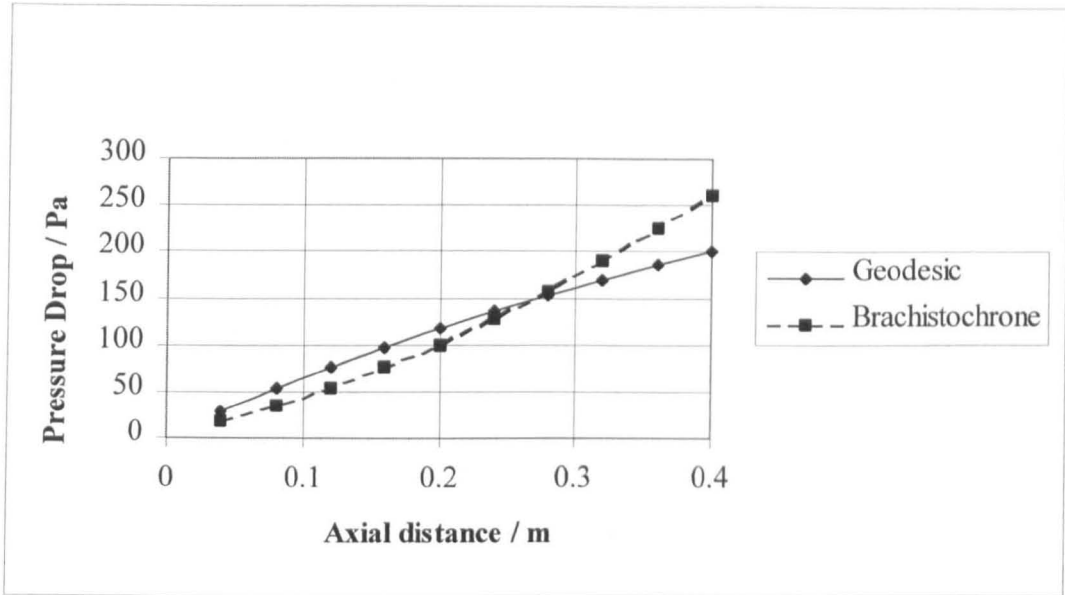


Figure 7.22 Pressure Drop against Axial Distance for 0.4m Standard pipe and 0.4m Brachistochrone, Without Tapered Ends

As outlined in Figure 7.22, the gradient of the brachistochrone was always increasing, whereas the geodesic was decreasing.

7.4 Examination of Colour Plots

The colour plots of the major parameters of interest can be found in Appendix C. The first plot for each run shows the surface grid which illustrates the external profile of the pipe. The other plots illustrate the pressure drop along the pipe followed by the plots illustrating the change in circumferential velocity and the final plot indicates the circumferential (w-velocity) at exit.

7.4.1 0.1 Metre Standard Swirly-flo Pipe

The w-velocity at exit (5-C) illustrates that the higher velocities were just away from the wall and the maximum velocity present was 0.901 m/s. Approaching the centre of the pipe the velocities become slightly negative (-0.07 m/s).

The static pressure at the wall (2-C) showed a slight rise in pressure at the entrance to the pipe, this was then followed by a rapid drop in pressure.

In examining (3-C) a region of high w-velocity was observed in one lobe about two thirds of the way along the pipe, the colour scheme indicated a velocity of 1.1 m/s. This region was also noted in (4-C).

7.4.2 0.2 Metre Standard Swirly-flo Pipe

The pressure again rose slightly at the entrance (7-C), this was followed by a gradual pressure loss, the majority of the pressure loss was in the tapered section.

Figures (8-C) and (9-C) illustrate the swirl velocity just away from the wall, again there was a region of high w-velocity, 0.845 m/s, just before the exit. Figure (10-C) shows the w-velocity at exit, where the highest velocities were near the wall. Approaching the centre the velocities became slightly negative.

7.4.3 0.3 Metre Standard Swirly-flo Pipe

The static pressure (12-C) still showed a slight pressure rise at the entrance, again with gradual losses after that.

Figures (13-C) and (14-C) show the w-velocity component just away from the wall, again one can see a region of high w-velocity (0.592 m/s) just before from the exit. At exit there was a region of high w-velocity in the top right-hand lobe of the w-velocity vector plot (15-C).

7.4.4 0.4 Metre Standard Swirly-flo Pipe

Figure (17-C) again illustrates the entrance effects, then the pipe forms a gradual pressure loss until the taper was reached, followed by a dramatic pressure drop.

As before a region of high pressure can be found just before the exit (19-C) and the region of highest w-velocity (0.418 m/s) can be found in the top right hand lobe (20-C).

7.4.5 0.5 Metre Standard Swirly-flo Pipe

Figure (22-C) shows the characteristic pressure rise at the entrance of the pipe followed by a gradual loss in pressure and finally the taper which gave the major contribution to pressure loss.

Figures (23-C) and (24-C) showing the w-velocity near the wall, again have a region of high velocity in one lobe just away from the exit (0.342 m/s). Figure (25-C) shows that as before, with the 0.4 metre standard Swirly-flo pipe, the region of high w-velocity was located in the top right-hand lobe (25-C).

7.4.6 0.6 Metre Standard Swirly-flo Pipe

The runs for 0.6m and 0.7m standard Swirly-flo pipe have slightly different grid densities because of the limited computing resources that were available. This meant the cells in the radial direction had to be reduced from 50 to 25.

The static pressure had the usual peaks in pressure at the entrance followed by the two characteristic regimes, one before the taper and one at the taper itself (26-C).

As before there was a region of high w-velocity in one lobe just before the exit (29-C), of 0.274 m/s. This is reflected in the w-velocity plot at exit (30-C); the larger w-velocities occupied slightly more than the top right hand lobe at exit.

7.4.7 0.7 Metre Standard Swirly-flo Pipe

The initial static pressure rose at the entrance. The pressure gradually dropped until the taper, where the pressure drop became larger (32-C).

As before there was a region of high w -velocity in one lobe and a maximum w -velocity of 0.202 m/s just away from the exit (33-C). On looking at the w -velocity at exit the region of the highest velocities was observed in the upper and lower right corner (35-C).

7.4.8 0.8 Metre Standard Swirly-flo Pipe

The pressure rise at the entrance was less than the 0.7 metre pipe. As before the pressure drop was gradual until the taper, where the drop became more severe (37-C).

Figures (38-C) and (39-C) show the w -velocity component near the wall. As before there was a region of high velocity in one lobe before the wall. In (39-C) the higher velocities were found to be in the upper and lower right corners of the colour plot.

7.4.9 0.9 Metre Standard Swirly-flo Pipe

Figure (42-C) illustrates the peak rises in pressure at exit which has been common throughout the standard Swirly-flo runs. As for previous runs the pressure drop was gradual all the way to the taper and the taper caused the pressure to drop dramatically.

Figures (43-C) and (44-C) again show that the higher w -velocities were in the lobes and in one of these lobes there was a region of high swirl observed (0.154 m/s) in comparison to the rest of the pipe.

Finally at the exit of the pipe the higher w -velocities occupied the upper and lower right-hand corners of the colour plot (45-C).

7.4.10 1.0 Metre Standard Swirly-flo Pipe

Figure (47-C) again shows the characteristic pressure rise at the entrance followed by the gradual drop in pressure then by the a steep drop due to the taper.

The largest w-velocity near the wall was 0.14 m/s (48-C and 49-C). No region of high pressure was noted. The w-velocity at exit was distributed all around the exit.

7.4.11 0.2 Metre Brachistochrone With End Taper

Initial rise in pressure at the entrance was less than that of the 0.2 m standard Swirly-flo pipe. The greatest pressure drop was again in the taper (52-C). Overall there was an increase of 60 Pa, compared to the 0.2 standard Swirly-flo pipe.

Comparing the w-velocities just away from the wall (53-C and 54-C), the brachistochrone had a velocity of 0.896, an increase of 0.46 m/s a second over the standard 0.2 metre Swirly-flo pipe. As with the standard pipe, a region of high w-velocity can be found in one lobe just before the exit.

In Figure (55-C) the plot of w-velocity at exit shows a reduction of the peak in comparison to the 0.2m Swirly-flo pipe.

7.4.12 0.3 Metre Brachistochrone With End Taper

Pressure rises at entrance were not as prominent as the 0.3 standard Swirly-flo pipe, and the lowest pressures in the pipe can be found at the intersection of the lobes, until the taper where the majority of pressure was lost (57-C).

The maximum w-velocity near the wall (58-C and 59-C) was 0.632 m/s compared to the standard pipe of 0.617 m/s (13-C). As before there was a region in one lobe where the

w-velocity peaked, to 0.632 m/s. Slightly negative velocities were observed near the intersection of the lobes.

At the exit the standard pipe gave (5-C) a higher peak velocity than the equivalent length brachistochrone (60-C). The region of the highest velocities were in the upper and lower right hand corner, with a peak velocity of 0.563 m/s.

7.4.13 0.4 Metre Brachistochrone With End Taper

As before the pressure rises at the entrance were less prominent than the standard pipe. The highest pressure drop was in the taper, as before. The highest pressure drop was 1020 Pa (62-C) compared with -1010 Pa for the standard pipe (17-C).

The maximum w-velocity near the wall was 0.47 m/s (63-C and 64-C), as before the peak velocity occurred in one lobe just before the exit. Slightly negative velocities can be found at the intersection of the lobes.

The maximum w-velocity at exit was 0.4 m/s (65-C) and the largest w-velocity vectors can be found on the right hand side of the exit. This was less than the 0.3 standard pipe which had a peak w-velocity of 0.92 m/s (20-C).

7.4.14 0.5 Metre Brachistochrone With End Taper

The pressure rises at the entrance were still present but reduced in magnitude compared to the previous brachistochrone pipes. The highest pressure drop again was taken by the taper, showing a peak pressure drop of 1020 Pa (67-C) and the standard pipe showed 1010 Pa.

The w-velocity near the wall (68-C) was 0.369m/s compared to 0.324 m/s of the standard pipe. The area of high w-velocity was still present as with previous brachistochrone pipes.

Figure (70-C) showed that the right hand side contained the majority of highest w-velocity vectors, with a peak of 0.294 m/s.

7.4.15 0.4 Metre Standard Swirly-flo Pipe Without Taper

Figure (72-C) shows the drop in static pressure, and it was quite uniformly distributed around the perimeter of the pipe. Slight rises in pressure at exit were seen, which was common with all the standard pipes. The maximum pressure drop was 441 Pa, with the lowest pressure drops in the region of the lobe intersections.

Figure (73-C and 74-C) showed that there was a region of high swirl very slightly before the exit, showing a w-velocity of 0.443 m/s. This was re-affirmed by the Figure (75-C).

Figure (75-C) shows the w-velocity vectors at the exit, the larger vectors were situated in the top right hand lobe of the plot, with a maximum of 0.698 m/s.

7.4.2 0.4 Metre Brachistochrone Pipe Without Taper

Figure (76-C) illustrates the surface grid of the brachistochrone pipe without taper. This is followed by Figure (77-C) the static pressure drop at the wall, indicating that the largest pressure drop regions were the intersection of the lobes. As with the standard 0.4 pipe without taper, there was no sudden rise in pressure loss at the end due to the taper; the lowest pressure determined was -410 Pa.

Figures (78-C and 79-C) indicated a region of high w-velocity at the exit of the pipe, of 0.610 m/s. The w -velocity near the wall began to increase near the exit of the pipe. This was reflected by Figure (80-C) showing that the region of highest swirl was found to be the upper right hand corner of the this vector plot.

7.5 Introduction to the CFD Results

No experimental measurements could be taken of the circumferential velocity, w -velocity, in the *Swirly-flo* pipe, so the C.F.D. method was used to provide an insight into its flow characteristics. Since the flows examined experimentally had approximately Newtonian rheology, this provided the author with some justification for the use C.F.D. in providing insight into the flow, albeit without direct validation by internal flow measurements.

In this examination the initial pipes had tapers on the end. This was, in hindsight, an error and caused the flow field to change in the last 30% of the length of each pipe. Due to this changing cross-section the dominant axial velocity also increased, with an increased pressure loss. It did, however, provide insight into the local flow conditions. The final two computational runs were performed without the taper for a cylinder length of 0.4 metre and a pitch/diameter ratio of 8. In this run the brachistochrone curve produced a slightly higher w -velocity at exit. It should also be noted that the brachistochrone provided significantly larger mechanical twist in the final plane and one can suppose an improved downstream swirl after delay has been taken into account.

7.6 Accuracy of the C.F.D. Results

7.6.1 Verification and Validation

Verification and validation are two important terms in computational modelling, and it is extremely important that the difference between these two semantic terms are understood. The terms from Roache (1997) (which Roache adopted from Boehm (1981) and Blottner (1990)) which defined verification as “solving the equations right” and validation as “solving the right equations.” The computational code defines precisely what partial differential equations are being solved and shows that they are being solved correctly, that is, usually with some order of accuracy and always consistently. As some measure of discretization Δ (mesh increment, size) approaches zero, the code produces a solution to the continuum partial differential equations; this is,

verification. Whether or not these equations and their solution bear any resemblance to a physical problem of interest to the user is subject to validation. To be exact a code cannot be validated; only a calculation (or a range of calculations) can be validated. In the words of Roache (1997) “this is a difficult concept and requires frequent re-iteration.” It must be assumed that *Fluent 4.3* was a verified code, since the user could not examine the source code to check if this was true. Validation of the *Fluent 4.3* code for rotating flow in pipes was a matter of difficulty with the regard to the turbulence model that was used. Since there was no experimental data available, the author had to improvise, which led to the use of published evidence using data from a combustor with no combustion present (see below).

7.6.2 Comparison of CFD Results with the Nearest Available Data

Hogg and Leschziner (1989) produced a paper on the “Computation of Highly Swirling Flow with a Reynolds Stress Turbulence Model”. On the swirling flow from a combustor in a jet engine without any combustion. This paper provided the nearest benchmark for the Reynolds Stress Model of Launder and Gibson (1978), for a rotating flow in a confined space. The values of the w-velocity in this paper were about 10 times higher than the ones calculated for the swirl inducing pipes, the flow therefore being considerably more severe in the combustor. The ratio of the maximum w-velocity to the maximum axial velocity is known as the degree of swirl, G (Chigier, 1964). The value of G in the combustor was about 2 and for the maximum swirl-inducing pipe about 0.5. The errors in the combustor on the whole were less than the actual measured values. Therefore it could be said that the Reynolds Stress Model (Launder and Gibson, 1978) under-predicted the values of axial and circumferential velocity. On average the under-prediction of the axial velocity was 33% and the w-velocity 25%-50 %. It was felt that the errors would not be as large as this in a swirl inducing pipe, due to the fact that the degree of swirl was less than 1. In the words of Wilcox (1991), “only qualitative agreement with measurements have been achieved” with rotating confined axial flows.

7.6.3 Grid Independence

The grid independence test was carried out on the standard 0.1 metre Swirly-flo pipe (Geodesic), in which the grid density was halved then quartered. In doing this the shape of the perimeter of the boundary became polygonal, which reduced its comparability with smoother cases. Altering the shape of the boundary would have altered the flow characteristics in the pipe. The quantities measured did seem to be converging to certain values, and it would be fair to say that the grid independence was achieved for the 0.1 metre section. This grid density was used wherever possible, but this did not necessarily mean that the same grid density could be applied to different cases and remain independent. Roache (1997) highlights that there was a problem with this type of methodology. He demonstrated the fact with two very similar aerofoil sections, in which grid independence was shown for a NACA 0012 aerofoil section. This grid was then used on a slightly thicker aerofoil (NACA 0015), and found to be lacking. Roache concluded that this approach was not justified. Therefore, the author assumed that the results of all the other grids were not necessarily grid independent solutions. To produce grid independent solutions for all grids would have been prohibitive due to the time and financial cost of using the CRAY at the Rutherford Appleton Laboratory. Hence, all the grids must be taken with caution, even though in the majority of cases the grid density was high.

7.7 Discussion of Graphical Results

Figure 7.2, provided an insight into the total pressure drop for the total length of pipe with the helix traversed through 360 degrees of rotation. The graph showed that the 0.4 metre standard Swirly-flo pipe (Geodesic) provide the least pressure drop for one rotation of 360 degrees. This was comparable to the work of Schriek *et al.*(1974) who said that the optimum pitch/diameter ratio was 8 for minimum energy requirements. The 0.4 metre pipe had a P/D of 8. On examination of Figure 7.2 the 0.7, 0.6 and 1 metre sections were out of place with the rest. This was due partly to the grid density not being the same, but primarily that the incorrect characteristic length was placed into the Computational Fluid Dynamics Package (0.5m instead of 0.05m). This could have effected the normal Reynolds stresses and caused an effective increase in pressure. The 1 metre run used considerably less number of cells which could have altered the shape of the computational domain. This could explain why the 1 metre run had slightly less pressure drop than the 0.9 metre run.

Figures 7.4 and 7.5 show how the average w-velocity across the pipe varied with the axial length. The tighter the pitch/diameter ratio (P/D), or the shorter the length, the greater the swirl. The reason for this was that the tighter the twist, or the lower the P/D, the greater the change of momentum from the axial to the circumferential direction. In Figure 7.5 the 0.6 and 0.7 metre sections were also following a similar pattern. It would seem that the error associated with the characteristic length did not adversely effect the calculation of the w-velocity. The 1 metre section on the other hand did not follow this pattern, this was probably due to the lack of cells in the circumferential and radial directions.

Figures 7.6 and 7.7 illustrate the relationship between pressure drop and average w-velocity, which show that the lower the P/D the greater the pressure loss. Again the standard 0.4 metre section shows that it produced the minimum pressure drop for the one full twist through 360 degrees. The averaged w -velocity was approximately a 1/2 of the 0.1 metre section.

7.8 Comparison between the Standard and Brachistochrone

Figures 7.8 to 7.22 show how the w -velocity, at various locations, varied with axial length for the brachistochrone and standard (geodesic) pipe lengths. On examination of the curves it was found that the gradient of the brachistochrone curve always increased as the length of the pipe was traversed, whilst with the standard Swirly-flo pipe, the gradients of curves began to reduce towards the end of the pipe. This was a function of the type of curve that governed the shape of the helix. The standard curve had a constant gradient ($2\pi/\text{cylinder length}$), whilst the gradient of the brachistochrone curve was always increasing (See Figure 7.23).

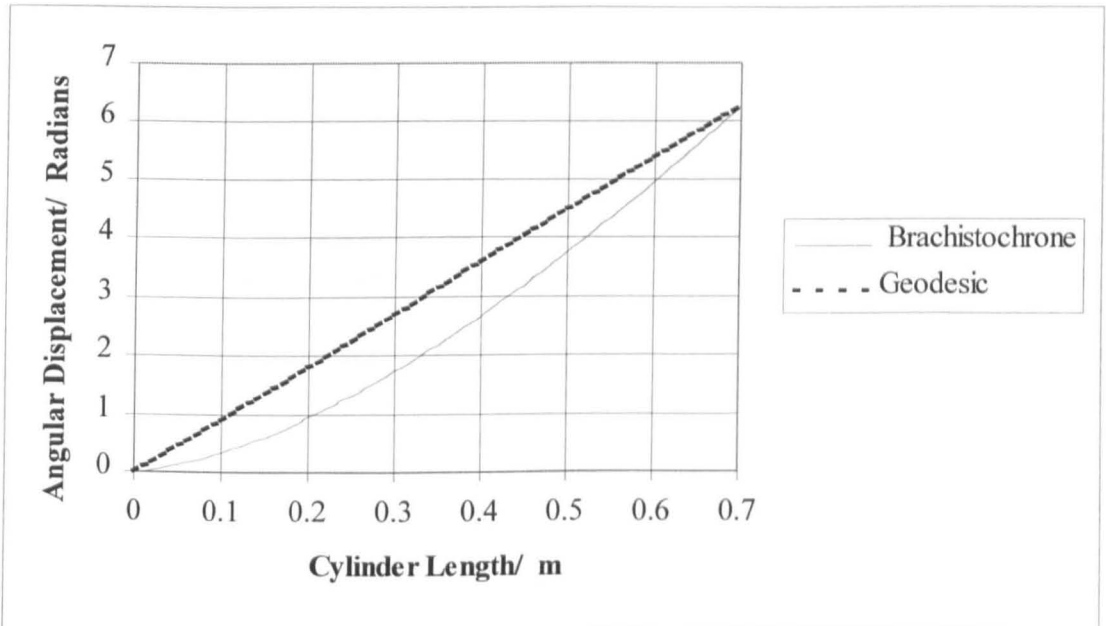


Figure 7.23 The Brachistochrone Curve and Regular Helix for a Cylinder of 0.7 m

Those values taken near the wall ($J=45$) always had a larger w -velocity than the average across a given plane in the axial direction. This would be the area of interest, just away from the wall, an ideal position to cause the suspension of particles. Figure 7.24 illustrates a typical profile of w -velocity against radius, showing the peak w -velocity was in the region of 0.8 to 0.9 of the cylinder radius. This was verified numerically, and is illustrated in Figure 7.25. On examination of the w -velocity near the wall ($J=45$ or $J=23$ cells) the magnitude was generally more than double the average w -velocity across the whole plane. This can also be seen from the colour plots in Appendix C. In the longest length the brachistochrone produced slightly more swirl (w -velocity) in both

cases, however, as the length of the pipe reduced the brachistochrone lost out to the standard Swirly-flo (geodesic) pipe.

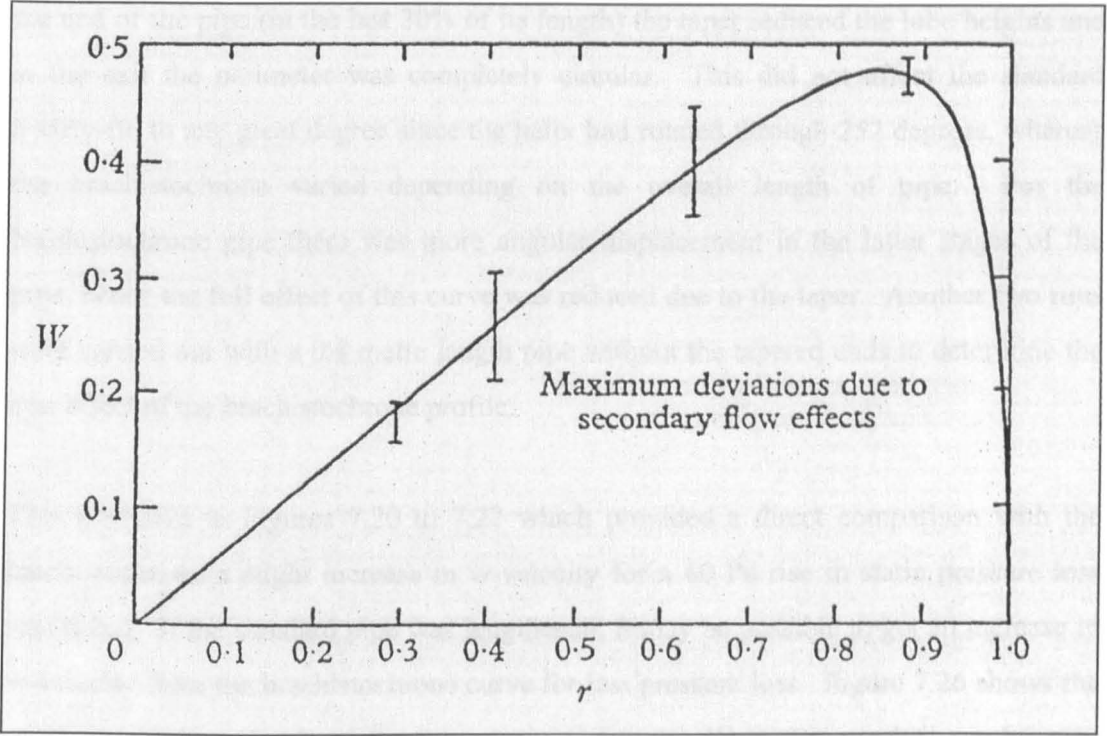


Figure 7.24 Typical w-Velocity against Radius (copied from Kreith and Sonju, 1965)

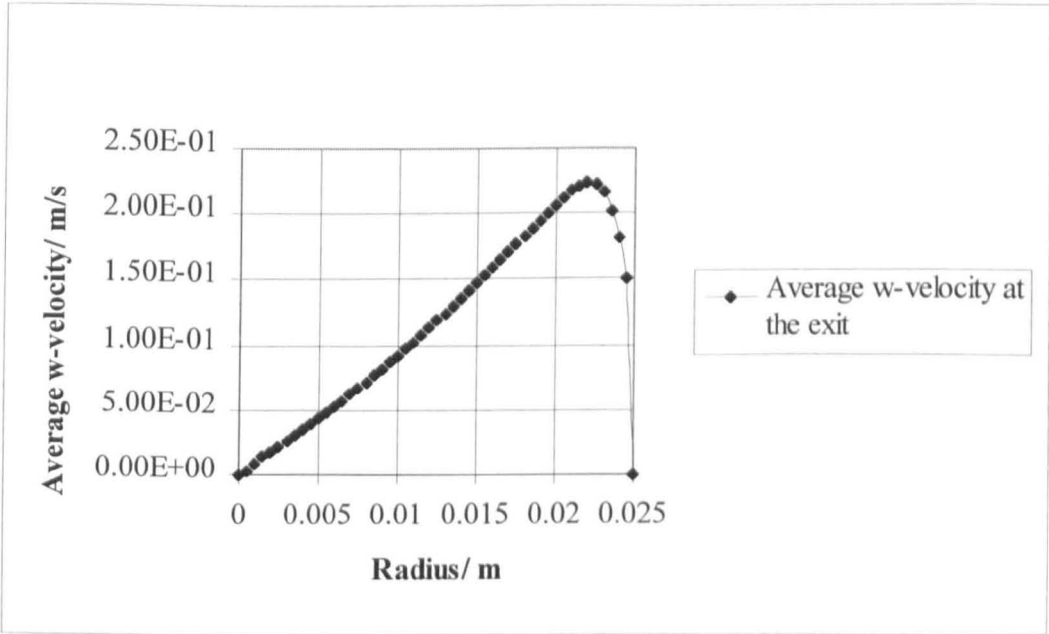


Figure 7.25 The Average profile of the w-velocity at the Exit of the 0.5 m Standard Swirly-flo pipe

Four runs were carried out comparing the brachistochrone and standard Swirly-flo sections. An unforeseen problem occurred with use of the taper which was that towards the end of the pipe (in the last 30% of its length) the taper reduced the lobe heights and at the exit the perimeter was completely circular. This did not affect the standard Swirly-flo to any great degree since the helix had rotated through 252 degrees, whereas the brachistochrone varied depending on the overall length of pipe. For the brachistochrone pipe there was more angular displacement in the latter stages of the pipe, hence the full effect of this curve was reduced due to the taper. Another two runs were carried out with a 0.4 metre length pipe without the tapered ends to determine the true effect of the brachistochrone profile.

This is shown in Figures 7.20 to 7.22 which provided a direct comparison with the brachistochrone a slight increase in w-velocity for a 60 Pa rise in static pressure loss was noted. If the standard pipe was lengthened, it may be possible to get an increase in w-velocity from the brachistochrone curve for less pressure loss. Figure 7.26 shows the geodesic curve extrapolated for a greater pipe length. From this graph it can be seen that the brachistochrone gives more w-velocity for less pressure drop.

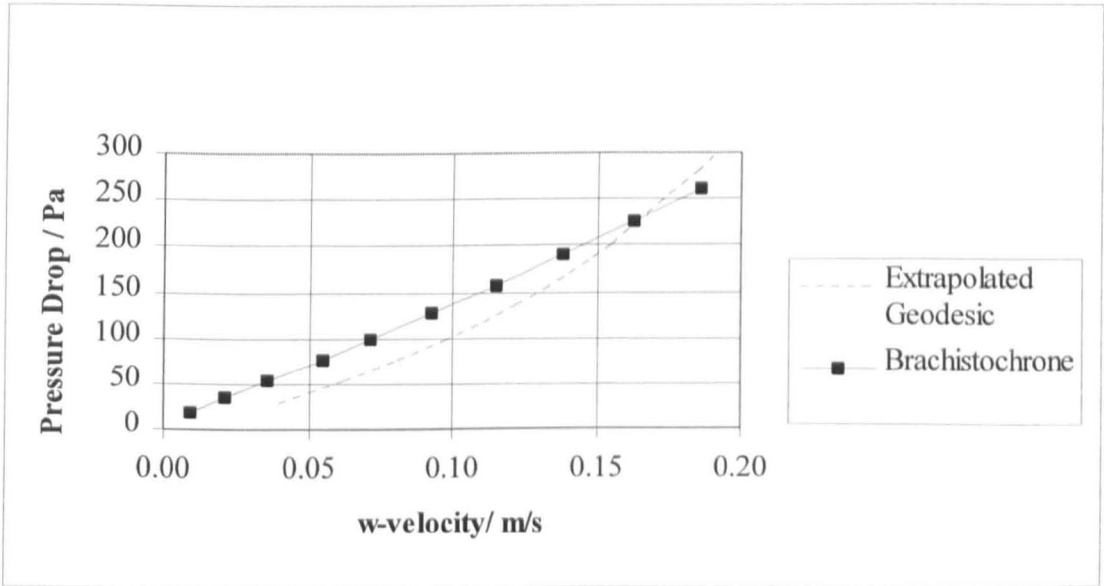


Figure 7.26 Pressure Drop against w-Velocity for 0.4m Standard pipe (Extrapolated) and 0.4m Brachistochrone, Without End Tapers

The w-velocity produced at the exit of the standard pipe was less than that with an end taper. This was due to the fact the cross-section area of the flow started to reduce in the taper and caused the axial velocity to increase, which in turn led to an increase in w-velocity.

7.9 Discussion of Colour Plots

All the computational runs had five colour plots associated with each run, namely:

- 1) surface grid,
- 2) static pressure at the pipe wall,
- 3) w-velocity -view 1,
- 4) w-velocity -view 2,
- 5) w-velocity at exit of pipe.

All the runs had a surface grid to illustrate the geometrical outline of the grid. The static pressure at the wall gave an indication of how the pressure dropped along the length of the pipe. In the early stages of the pipe, especially in the standard Swirly-flo pipe, there were slight increases in pressure, this was due to stagnation as the wall begins its twist. This generally occurred in the lobes and as one proceeded down the pipe the effects of stagnation rapidly diminished. The higher peak pressures occurred at the entrance of the Swirly-flo pipe for the shorter lengths (geodesic), which was not surprising since the pitch/diameter ratio was smaller. The brachistochrone curves on the whole did not suffer from this to the same degree. These peaks were considerably reduced, because the brachistochrone curve does not start “twisting” as early as the standard Swirly-flo pipe, thus providing better entrance conditions. For example the entrance peak pressure for the 0.5 metre brachistochrone was 59 Pa and for the 0.5 metre standard Swirly-flo was 268 Pa. Therefore, it would seem that the brachistochrone pipe produced better

entrance characteristics than the standard Swirly-flo pipe. Proceeding down the length of a standard Swirly-flo pipe the pressure drop was quite gradual until the taper began. Here the pressure increased much quicker due to the fact the cross-sectional area was reducing, causing a rise in the static pressure drop. The brachistochrone pipe showed similar characteristics, with a slightly higher pressure loss approaching the exit of the pipe. This was due to the brachistochrone curve having its greatest degree of curvature or twist near the exit of the pipe

On examination of the w-velocity plots certain characteristics were noted. The high w-velocities occurred in the lobes of the swirl-inducing pipes, whilst the lower w-velocities occurred at the lip between the lobes. There was some acceleration of the w-velocity along the length of the pipes. In the standard Swirly-flo pipe it was more gradual, but with the brachistochrone, most of the swirl was generated in the latter stages of the pipe length due to the non-linear nature of the brachistochrone curve. In all the cases with the brachistochrone and standard Swirly-flo pipes with end tapers, except the shortest standard Swirly-flo pipe, there was a peak w-velocity in just one lobe about $2/3$ down the pipe length and near the exit for the two 0.4 metre runs without tapers. In the runs with tapers the peak w-velocity in one lobe probably occurred early in the length due to the fact the axial velocity was increasing in the taper and thus caused an increased the w-velocity. The runs without tapers had to wait till almost the exit, for the peak velocity to occur. The reason for this was uncertain and requires further investigation.

The initial reasoning for having an end taper was that the swirl inducing pipe could then be fitted to a normal circular pipe and the swirl carried down the normal pipe. The exit w-velocities for the standard Swirly-flo decreased in magnitude as the pipe became longer or the pitch/diameter increased. This was expected as the helix angle reduced (pitch/diameter ratio increased) the flow, had less change in axial momentum and hence less w-velocity produced at the exit. The swirl at the exit highlights that just away from the wall there was a region of high w-velocity and as one proceeded towards the centre of the pipe the velocity reduced to very low, sometimes slightly negative, values. With longer lengths of standard Swirly-flo pipe, 0.3 m and above, a region of high w-velocity was noted in the upper right lobe, this may have been due to the fact that the swirl

velocity had not been given enough length to evenly distribute itself at the exit, as was the case with in the 0.1 metre and 0.2 metre standard Swirly-flo pipes. The brachistochrone pipes with tapers all had a region of high w-velocity situated in the upper right lobe, again this may be due to the fact that the swirl velocity had not been given enough length to evenly distribute itself at the exit. The two 0.4 metre pipes (brachistochrone and standard Swirly-flo (geodesic)) without end tapers had different characteristics due to the lack of taper. The brachistochrone had regions of high w-velocity inside the lobes, with the highest being in the upper left lobe, with a peak velocity of 0.698 m/s. The standard Swirly-flo pipe had similar characteristics in that the lobes contained high w-velocities; again the highest w-velocity occurred in the upper left lobe, with a velocity of 0.486 m/s. This was less than that produced by the brachistochrone curve. The majority of the pipes had a lobe where the w-velocity was considerably higher than the other two lobes, the reason for this is uncertain and would require further investigation.

If these locations of high w-velocity are confirmed by experiment, then these regions could prove useful in causing the suspension of particles, by having the peak w-velocity at the bottom of the swirl inducing pipe just before the exit. This would cause the particles at the bottom of the pipe to have maximum initial swirl on leaving the pipe. Following on from this if the Reynolds Stress Model proved to be accurate enough to predict major flow field characteristics, it could be used in the determination of various optima, for example, the number of ribs or lobes.

8.0 Conclusions and Recommendations

8.1 Conclusions

- 1) Advantages in creating swirl before a pipe bend have been demonstrated. Pressure loss around a bend was reduced for water and water/particle mixtures. Zones which have been associated with wear are potentially no longer vulnerable if swirl-induction is applied.
- 2) The inlet and exit orientation of a *Swirly-flo* pipe were of importance in creating the most appropriate swirl conditions at the exit of the *Swirly-flo* pipe. The transition from standard pipe to *Swirly-flo* pipe was also important.
- 3) The Computational Fluid Dynamics package, *Fluent*, qualitatively indicated that the 0.4m standard *Swirly-flo* pipe (geodesic) produced the least pressure drop for 360°. This pipe had a pitch/diameter ratio of 8, the value recommended by Schriek *et al.*,(1974)
- 4) The C.F.D. results indicated that the 0.4m brachistochrone pipe without the end taper produced more swirl than the standard *Swirly-flo* (geodesic) pipe, with a marginal increase in pressure loss at exit.
- 5) The shorter the pipe, or the smaller the pitch to diameter ratio in a geodesic pipe the greater the swirl produced with a greater pressure loss.
- 6) The thesis provided the most complete information to date on the use of swirl-inducing mechanisms in water/particle mixture flows.

8.2 Recommendations

1) The design of an improved test rig, or improvements to the existing test rig, would be an important priority. The existing rig had a minimal number of pressure transducer stations, which was considered adequate for the initial study. However, the author now considers it important to measure pressure changes radially, axially and at closer spacing. This would require a greater number of transducers at more locations. One of the aims would be to examine experimentally the flow characteristics of a swirl-inducing pipe with and without particles, in much more detail. Pressure transducers placed radially at the exit and inlet of the *Swirly-flo* pipe would provide a detailed distribution of pressure where the flow is not dominated by axial flow, but also by a significant swirl component. The sampling rate of the existing datalogger, 1 sample of all transducers every second, was considered inadequate to measure fluctuations in pressure. For example, at low velocities, saltation heaps were observed to pass a pressure transducer station in less than 1 second. The author suggests that the datalogger should sample at a rate of about 100 times per second to monitor small fluctuations in the flow field. This would allow the effect of saltation heaps on the pressure field to be measured.

The project confirmed the potential of C.F.D. in providing detailed flow information. Validation of the C.F.D. model was not possible with the existing test rig. In order to validate these C.F.D. results the modified/new test rig should have the facility to use advanced flow visualisation techniques, such as Particle Image Velocimetry (P.I.V) and Laser Doppler Anemometry (L.D.A.) which is often used in validation. New transparent swirl-inducing pipes would be manufactured so that these techniques could be used.

2) In the C.F.D. test runs it was noted that if the geodesic graph of pressure drop against w -velocity was extrapolated, as in Figure 7.25, then it would be possible to obtain more swirl from the brachistochrone than the geodesic pipe for less pressure loss. In order to test this hypothesis it would be necessary to examine the w -velocity and pressure loss

for the brachistochrone and geodesic pipes in which the total twist of the pipe is greater than 360° , possibly up to 400° .

3) In section 2.4.7 details and references are given on the decay of swirl in horizontal pipes, in which the swirl component decays in an exponential manner. In order to obtain the greatest swirl and thus keep the particles in suspension before the bend, the author recommends that the *Swirly-flo* pipe be placed as close to the bend as possible. This would produce a greater swirl on the entrance to the bend. This is illustrated in Figure 8.1.

4) In Chapter 4, the problems of sudden exit and inlet into the *Swirly-flo* pipe were mentioned. In the present long *Swirly-flo* pipe these effects can be visualised with particle laden flow. In order to reduce these pressure losses at the entrance and exit of the *Swirly-flo* pipe it would be necessary to design a smoother transition from and to the *Swirly-flo* pipe.

5) The computer and datalogger which monitored the pressure transducers in the original test rig were controlled by software which performed satisfactorily in its primary role. However, the data was stored in a format which was not easily transferable to a spreadsheet, especially with the large amounts involved. It is considered bad practice to allow for the possibility of human error in transporting data once captured. The present system was open to such errors. The author recommends, that in future, data should be placed directly into a spreadsheet, thus saving considerable processing time.

Further development is required in the measurement of the volumetric flow rate and mass flow rate, since it would be ideal if these two quantities were also datalogged. This would give the user of the test rig an indication of how the volumetric and mass flow rate is varying with time.

6) In the experimental runs on the present test rig, it could be seen that the concentration of beads varied throughout the pipelength

concentration at the top of the rig was not satisfactory when determining the characteristics of the bend and *Swirly-flo* pipe for varying concentrations. Therefore the author recommends that the concentration of beads should be determined with greater accuracy in the regions of interest, such as, the bend and in the *Swirly-flo* pipe. This would possibly prove useful in investigating the anomaly of the 2kg run, which seemed to be out of sequence, see Figure 4.9. Possible solutions to this problem of concentration measurement include image analysis.

7) Observations made indicated that the beads with swirl were more evenly distributed throughout the bend and it may be inferred that the wear would be more evenly dispersed in the bend. These observations need to be quantified by experimental methods. Once this has been achieved the experimental results could be useful in validating Computational methods in predicting bend wear.

8) Validation of the Launder and Gibson (1974) turbulence model is required for predicting velocity profiles in swirl-inducing pipes. The validation of C.F.D. solutions to low-intensity swirling flows in confined spaces is likely to be produced by the C.F.D. community as turbulence modelling evolves.

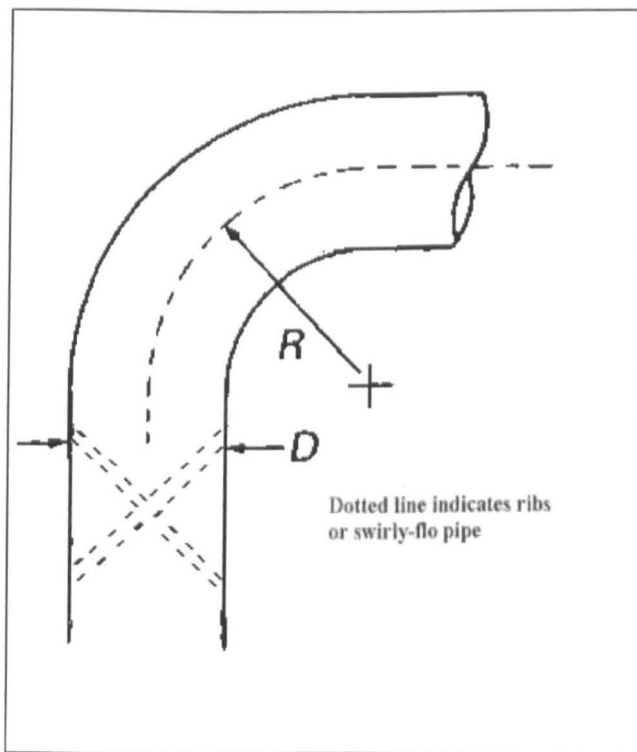


Figure 8.1 Ribs or Swirl Inducing Mechanism as an Integral Part of the Bend

9.0 References

- ABBOTT M.B. and BASCO, D.R. *Computational Fluid Dynamics An Introduction for Engineers* New York: Longman Scientific and Technical, 1989.
- ANDERSON, D.A. *Computational Fluid Mechanics and Heat Transfer* New York: Hemisphere Publishing Corporation, 1984
- ANDERSON, J.D., *Fundamentals of Aerodynamics*, Second Edition, McGraw-Hill International, pp 236-238, 1991
- BITTER, J.G.A., A Study of Erosion Phenomena. Part 1, *Wear*, 3, pp 5-21, 1963
- BITTER, J.G.A., A Study of Erosion Phenomena. Part 2, *Wear*, 6, pp 169-190, 1963a
- BLATCH, N.S., Discussion: Water filtration at Washington, D.C., *Transactions of the American Society of Civil Engineers*, volume 57, pp 400-408, 1906
- BLOTTNER, F.G., Accurate Navier-Stokes results for the hypersonic flow over a spherical nosetip. *American Institute of Aeronautics and Astronautics Journal Spacecraft Rockets*, 27(2), pp 113-122, 1990

BOEHM, B.W., *Software Engineering Economics*. New York: Prentice Hall, 1981

BOUSSINESQ J. Theorie del'Accoulement Toubillant. Mem. Pre. Par. Div. Savants a l'Academie Science, Paris, 23, 1877.

BYERLY, W.E., *Introduction of the Calculus of Variations*, Harvard University Press, 1917, p19

CHARLES, M.E., CHEH, C. H-S and CHU, L.H-L., The flow of "Settling" Slurries in Tubes with Internal Spiral Ribs, *The Canadian Journal of Chemical Engineering*, Vol 49, pp 737-741, December, 1971

CHARLES, M.E., and SINGH, V.P., The flow of sand/water slurries in horizontal pipes with internal spiral ribs - Effect of rib height, *The Canadian Journal of Chemical Engineering*, Vol. 54, pp 249-254, August, 1976

CHAMBERLAIN, A.R., Effect of boundary form on fine sand transport in twelve-inch pipes, CET No.55 ARCO, Colorado Agricultural and Mechanical College, pp 1-166, 1955

CHAMBERLAIN, A.R., GARDE, R.J., and ALBERTSON, M.L., Transport of Sediment in helical corrugated pipe, CER No. 57ARC9, Colorado Agricultural and Mechanical College, pp 1-37, 1957

CHIEN, S.F., Settling velocity of irregular shaped particles, S.P.E., 26121, Society of Petroleum Engineers, Dallas, Texas, U.S.A., 1993

CHIGIER, N.A. and BEER, J.M. Velocity and static pressure distributions in swirling air jets Issuing from annular and divergent nozzles. *Transactions of ASME Journal of Basic Engineering*. 86(4) series D, pp 788-796, 1964

COLEBROOK, C.F., Turbulent Flow in Pipes with Particular Reference to the Transition Region between the Smooth and Rough Pipe Laws, *J.Inst.Civil Engs. (London)* Vol 11, pp 133-156, 1938-1939

CHU, L. H-L., Solid liquid flows in pipes with internal spiral ribs, M.Sc. thesis, University of Toronto, Canada, 1969

DALY, B.J. and HARLOW, F.H. Transport equations for turbulence. *Physics of Fluids*. 13, pp 2634-2649, 1970

DURAND, R, Basic Relationships of the Transportation of Solids in Pipes- Experimental Research. *Proceedings of Minnesota International Hydraulics Convention*, pp 89-103, 1953

DONALDSON, C. duP. Calculation of turbulent shear flows for atmospheric and vortex motions. *American Institute of Aeronautics and Astronautics Journal*. 10, pp 4-12, 1972

EINSTEIN, A. *Ann. Phys. Leipzig* 29(371), 1906

ESDU International, Pressure losses in curved ducts: single bends, No. 83037, issued in October 1995, ESDU International Plc, 27 Corsham Street, London N1 6UA, United Kingdom

FEYNMAN,R.P., *The Feynman Lectures on Physics, Vol 2*, Addison-Wesley Publishing Company, 1967

FINNIE, I., The Mechanism of Erosion of Ductile metals, *Proceedings 3rd US Congress of Applied Mechanics*, pp 527-532, 1958

FLUENT, Fluent Incorporated, Centerra Resource Park, 10 Cavandish Court, Lebanon, New Hampshire, 03766, United States of America, 1995

FORRAY,M.J., *Variational Calculus in Science and Engineering*, McGraw-Hill Book Company, 1968

FRANKEL, N.A., AND ACRIVOS, A., On the viscosity of a concentrated suspension of solid spheres, *Chemical Engineering Science*, Vol. 22, pp 847-853, 1967

GERHART, P.M., and GROSS, P.J., *Fundamentals of Fluid Mechanics*, Addison-Wesley Publishing Company, Wokingham, England, 1985

GOLDSTEIN, H, *Classical Mechanics*, Addison-Wesley Publishing Company, pp 39-43, 1980

GORDON, H.M. and H.A., Conduit or Pipe , US patent Number. 630, 605, patented dated August 8, 1899

GOVIER, G. W., AZIZ, K., *The Flow of Complex Mixtures in Pipes*, Van Nostrand, 1972

GRAF H.,ROBINSON, M., and YUCEL, O., The Critical Deposit Velocity for Solid-Liquid Mixtures, *Proceedings of 1st International Conference of Hydraulic Transport of Solids in Pipes*, Cranfield, U.K., Hydrotransport, pp H5-77 to H5-88, 1970

GUTH E., and SIMHA, R., *Kolloid Zh.*, Vol 74, 266, 1936

HAPPEL, J., and BRENNER,H., *Low Reynolds Number Hydrodynamics*, Englewood Cliffs, NJ, Prentice-Hall, 1965

HANJALIC, K and LAUNDER,B.E. A Reynolds stress model of turbulence and its application to asymmetric shear flows. *Journal of Fluid Mechanics*. 52, pp 609-638, 1972

HAZEN, A., and HARDY, E.D., Works for the purification of water supply of Washington, D.C., *Transactions of the American Society of Civil Engineers*, paper no.1036, volume 57, pp 307-430, 1906

HINZE, J.O. *Turbulence* Second Edition, New York: McGraw-Hill,1975

HIRSCH, C., *Numerical Computation of Internal and External Flows*, John Wiley and Sons, Chichester, 1988,

HOLLINGDALE, STUART, *Makers of Mathematics*, Penguin Books, p 288, 1989

HOWARD, G.W., Transportation of sand and gravel in four inch pipe, *Transactions of the American Civil Engineers*, paper number 2101, Vol. 104, pp 1334-1380, 1939

HOWARD, G.W., Effects of rifling on four-inch pipe transporting solids, *Transactions of the American Civil Engineers*, paper number 2101, Vol. 106, pp 135-157, 1941

JEFFERY, G.B., On the motion of ellipsoidal particles immersed in a viscous liquid., *Proceedings of the Royal Society, Ser. A.*, 102, pp 161-179, 1922

JONES, T.F., *Pipe Design for improved particle distribution and reduced wear*, ECSC Research Project 7220-EA/841, 1997

JOSEPHUS, FLAVIUS, *Contra Apionem*, 1, vs 125-126, circa 100 AD translation and Greek text provided by THACKERY, H. ST. J., *Josephus, The Life, Against Apion, 1*, William Heinemann LTD, London, 1961

KITOH, O., Experimental study of turbulent swirling flow in a straight pipe, *Journal of Fluid Mechanics*, Vol. 225, pp 445-479, 1991

KOLMOGOROV, A.N., Local structure of turbulence in incompressible viscous fluid for very large Reynolds number, *Doklady AN SSSR*, Vol. 30, pp 299-303, 1941

KREITH, F., and SONJU, O.K., The decay of a turbulent swirl in a pipe, *Journal of Fluid Mechanics*, Vol. 22, part 2, pp 257-271, 1965

LAUNDER, B.E. Stress-transport closures: into the third generation. *Proceedings of the First Symposium on Turbulent Shear Flows*. New York, Springer-Verlag, 1979

- LAUNDER, B.E. and SPALDING, D.B. *Mathematical Models of Turbulence*. New York: Academic Press, 1972
- LAUNDER, B.E. and GIBSON, M.M., Ground effects on pressure fluctuations in atmospheric boundary layer, *Journal of Fluid Mechanics*, Vol 86, Pt3, pp 491-511, April 1978
- LAUNDER, B.E., RECCE, G.J., AND RODI, W., Progress in the development of Reynolds turbulence enclosure, *Journal of Fluid Mechanics*, Vol 68, Pt 3, pp 537-566, 1975
- LAUNDER, B.E., *Fifth Biennial Colloquium on Computational Fluid Dynamics*, Manchester Institute of Science and Technology, England, 1992
- LESCHZINER, M.A. and HOGG, S. Computation of highly swirling confined flow with a Reynolds stress turbulence model. *American Institute of Aeronautics and Astronautics Journal*. 27(1), pp 57-63, 1989
- LESCHZINER, M.A. Modelling engineering flows with Reynolds stress turbulence closure. *Journal of Wind Engineering and Industrial Aerodynamics*. 35, pp 21-47, 1990
- LONG, D.B., The Transport of solids in Helically Ribbed Pipes, under graduate Thesis, Department of Mining Engineering, University of Toronto, Canada, 1966
- MARKATOS, N.C. The modelling of turbulent flows. *Applied Mathematical Modelling* 10(6), pp 190-220, 1986

MATHCAD, Mathsoft Inc., 101 main Street, Cambridge, Massachusetts, 02142 USA, 1994

MELLOR, G.L. and HERRING, H.J. A survey of the mean turbulent field closure models. *American Institute of Aeronautics and Astronautics Journal*. 11, pp 590-599, 1973

MIELE, A., *Theory of Optimum Aerodynamic Shapes*, Applied Mathematics and Mechanics, Academic Press, 1965

MILLER, R.W., *Flow Measurement Engineering Handbook*. McGraw-Hill Publishing Company, 1989

MILTON, J.H., *Marine Steam Boilers*, George Newnes Limited, London, pp 65-66, 1961

MING-JAU, Y., BEDDOW, J.F., and VETTER, A.F., Effects of particle shape on solid-liquid transportation in pipes, Proceedings of the Technical Program-International Powder and Bulk Solids Handling and Processing Group, Des Plaines, IL., U.S.A., 24 -26 May 1983

MODEL 39 Power meter, Fluke corporation, P.O. Box 9090, Everett, Washington, 98206-9090, 1995

NALLASAMY, M. Turbulence models and their applications to the predication of internal flows: A Review *Computers and Fluids*. 15(2), pp 151-194, 1987

NEILSON, J.H., and GILCHRIST, A., Erosion by a Stream of Solid Particles, *Wear*, 2, pp 111-121, 1968

PATANKER, S.V. and SPALDING, D.B., A calculation procedure for heat, mass and momentum transfer in three-dimensional parabolic flows, *International Journal of Heat Transfer and Fluid Flow* 15(10), pp 1787-1806, 1972

PATANKER, S.V. Numerical Heat Transfer and Fluid Flow . New York: Hemisphere Publishing Corporation, 1980

ROACHE, P.J., Quantification of Uncertainty in Computational Fluid Dynamics, *Annual Review Fluid Mechanics*, 29, pp 123-160, 1997

ROBINSON, A.W., Delivery Pipe for Hydraulic Dredging Machines, US Patent Number 1,451,272 patented dated April 10, 1923

RODI, W. *Turbulence Models and their Applications in Hydraulics* IAHR monograph, June 1980

ROTTA, J. Statistische theorie nichthomogener turbulenz. *Z. Physics*. Vol.129, pp 547-572, 1951

RUBINI, P., Numerical Methods for Turbulent Flows. Course notes provided on the Msc in Computational Fluid Dynamics at Cranfield University, Cranfield, Bedford MK43 0AL, England. 1994

RYBICKI, E.F., and SHADLEY, J.R., *ASME Journal of Energy Resources Technology*, 114, pp 54-64, 1992

SIBULKIN, M., Unsteady, viscous, circular flow. Part 3, *Journal of Fluid Mechanics*, Vol. 11, pp 269-293, 1961

- SHOOK, C.A., and ROCO, M.C., *Slurry Flow Principles and Practice*, Butterworth-Heinemann, 1991
- SMITS, A.J. The interplay between experiments and computation in the study of turbulence. *Experimental Thermal and Fluid Science*. 5(1), pp 579-585, 1992
- SPALDING, D.B. and LAUNDER, B.E. Turbulence models and their predications to the predication of internal flows. *Heat Fluid Flow*. 2, pp 43-54, 1972
- SCHRIEK, W., SMITH, L.G., HAAS, D.B., and HUSBAND, W.H.W., The potential of helically ribbed pipes for solid transport, *CIM Bulletin*, pp 84-91, 1974
- THOMAS, D.G., Transport Characteristics of Suspensions: Part 2, Minimum Transport Velocity For Flocculated Suspensions in Horizontal Pipes *AIChE Journal* , 7(3), pp 423-430, 1961
- TIMOSHENKO, S.P., and GOODIER, J.N., *Theory of Elasticity*, 3rd Edition, McGraw-Hill Inc, pp 409-413, 1987
- TALBOT, L., Laminar swirling pipe flow, *Journal of Applied Mechanics*, Vol. 21, pp 1 -7, March 1954
- VAN LOO, A., Head of Engineering North Sea Ferries (Rotterdam, Netherlands) -Private communication, 1996

WASP, E.J., KENNY, J.P., and GANDHI, R.L. Solid-liquid Flow Slurry Pipeline Transportation Series *Series on bulk materials handling* 1(4), pp 1975-1977, 1977

WEISMAN, J., LAN, J. And DISIMILE, P., Two Phase (Air-Water) Flow Patterns and Pressure Drop in the Presence of Helical Wire Ribs, *International Journal of Multiphase Flow*, 20(5), pp 885-899, 1994

WILCOX. D.C., *Turbulence modeling for Fluid Dynamics*, Second Edition, DCW Industries, Inc., 1994

WOLFE, S.E., The Transport of Solids in Helically Ribbed Pipes, *The Canadian Mining and Metallurgical Bulletin*, Feb., pp 221-223, 1967

YUILLE, N.A., Dredger Pipe Line, US Patent Number, 1,662,178, patented dated March 13, 1928

ZENZ, F.A., and OTHMER, D.F., *Fluidization and Fluid-Particle Systems*, Reinhold Publishing Corporation, New York, 1960

ZIGH, A. Computational Study of Simultaneous Heat and Mass Transfer in turbulent Separated Flows. Ph.D. Thesis, Stevens Institute of Technology, Castle Point, Hoboken, New Jersey, U.S.A., May 1993

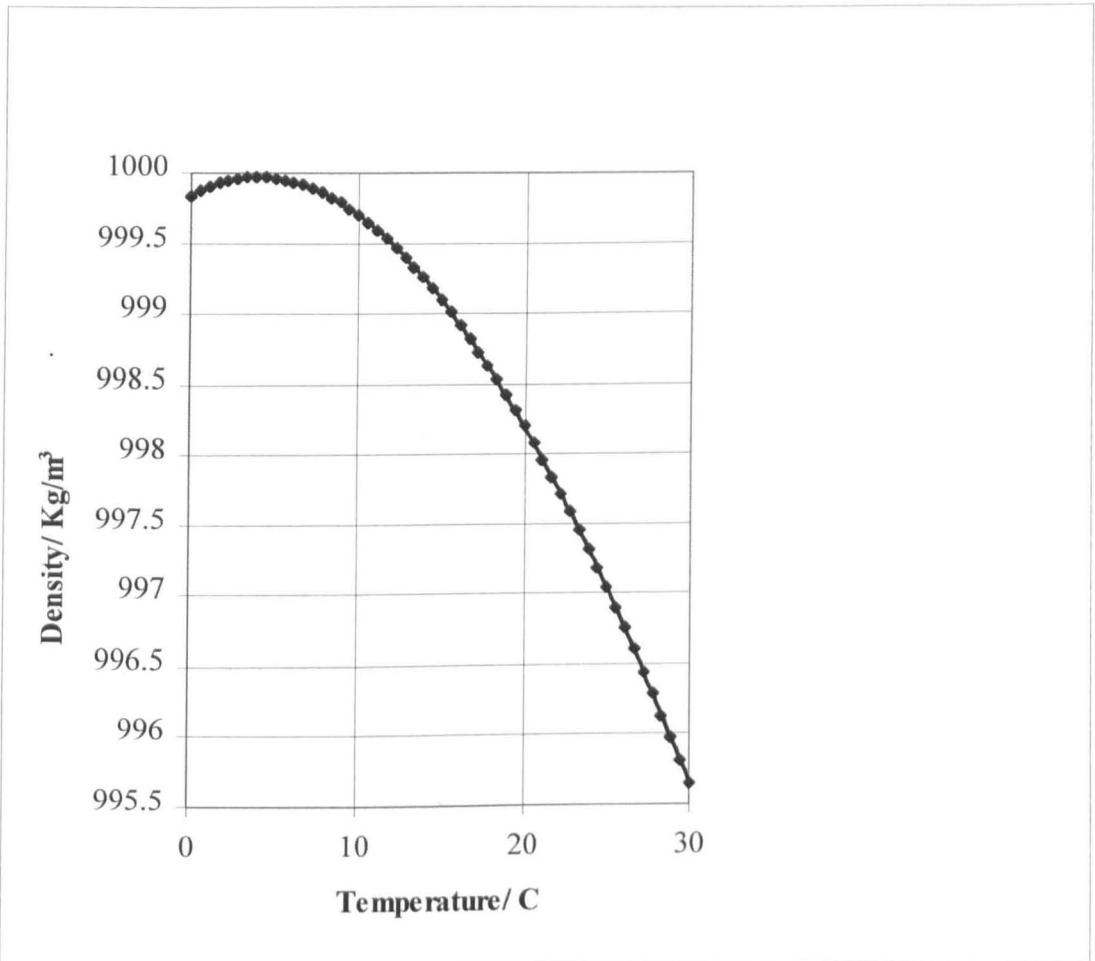
Appendix A

The relationship of density of water to temperature **1-A**

The relationship of viscosity of water to temperature **2-A**

The Variation of Water Density with Temperature

The relationship between temperature and density of water was obtained from Miller's book (Miller, 1989). The results were plotted on a graph and then polynomial equation was fitted to the results. This equation was then used in the calculation of density.



The equation of the polynomial is shown below.

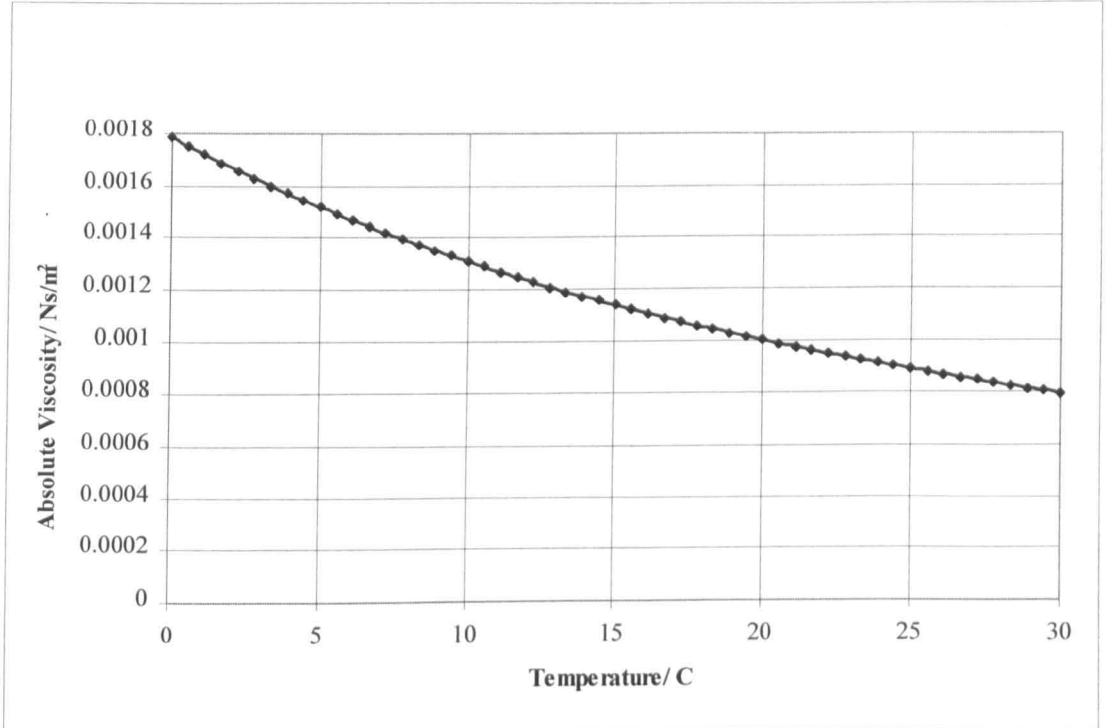
$$7E-09t^5 - 1E-06t^4 + 0.0001t^3 - 0.0091t^2 + 0.0682t + 999.84 = \text{Density of water}$$

where,

t = temperature of the water

The Variation of Water Viscosity with Temperature

The relationship between temperature and viscosity of water was obtained from Miller's book (Miller, 1989). The results were plotted on a graph and then polynomial equation was fitted to the results. This equation was then used in the calculation of viscosity.



The equation of the polynomial fit is shown below.

$$6E-14t^6 - 1E-11t^5 + 7E-10t^4 - 4E-08t^3 + 2E-06t^2 - 6E-05t + 0.0018 = \text{viscosity of the water}$$

where,

t = temperature of the water

Appendix B

Generic FORTRAN program for producing Standard Swirly-flo pipes with end tapers	1-B to 9-B
Generic FORTRAN program for producing Brachistochrone pipes with end tapers	10-B to 19-B
FORTRAN program for producing 0.4m Standard Swirly-flo pipe without end taper	20-B to 28-B
FORTRAN program for producing 0.4m Brachistochrone pipe without end taper	29-B to 39-B

```

*****
*****
*
* PROGRAM TO SAVE R,THETA,Z COORDINATES TO FLUENTFORMATTED *
* FILE *
*
*****
*****
*
* AUTHOR: BENJAMIN RAYLOR *
*
* DATE: 25 November 1996 *
*
*****
*****
*
* PURPOSE: TO PRODUCE A GRID FOR FLUENT TO USE IN THE *
* EVALUATION *
* OF HELICES IN PIPES *
*
*****
*****
*
* VARIABLES *
*
* I  NODES IN THE ANGULAR DIRECTION (INTEGER) *
* J  NODES IN THE RADIAL DIRECTION (INTEGER) *
* K  NODES IN THE AXIAL DIRECTION (INTEGER) *
* NI  MAXIMUM NUMBER OF CELLS IN THE ANGULAR DIRECTION *
* (INTEGER) *
* NJ  MAXIMUM NUMBER OF CELLS IN THE RADIAL DIRECTION *
* (INTEGER) *
* NK  MAXIMUM NUMBER OF CELLS IN THE AXIAL DIRECTION *
* (INTEGER) *
* LABEL TYPE OF CELLS (INTEGER) *
* GRDTYP GRID TYPE (INTEGER) *
* CRDSYS TYPE OF COORDINATE SYSTEM (INTEGER) *
* PRBDIM DIMENSION OF PROBLEM 2D OR 3D (INTEGER) *
* CYLLENGTH CYLINDER LENGTH IN METRES (REAL) *
* CLRADIUS  CYLINDER RADIUS IN METRES (REAL) *
* MAXCYLANGLE 2*pi In radians (REAL) *
* dx Increment in the x-direction-axial (real) *
* dt Increment in theta (real) *
* dr Increment in radius (real) *
* dp Increment in pitch (real) *
* rp taper length (real) *
* r2 Cylinder radius inside loop (real) *
* r1 set to zero only present for generality *
* r(i,j,k) Array containing r values (real) *

```

```

* x(i,j,k) Array containing x values (real) *
* y(i,j,k) Array containing y values (real) *
* z(i,j,k) Array containing z values (real) *
* gradient(i,j) Array containing gradient values for the linear *
* taper at 70 % cyllength *
* xtaper(i,j) Allows the origin for the taper to be placed at *
* cyllength70% *
* omega An angle describing one of the 3 lobes (real) *
* counter A counter (integer) *
* pitch Determines pitch of swirly-flo pipe *
*****
*****
*
* DATE OF LAST MODIFICATION: DEC 19 *
*
*****
*****
*
* ERRORS: NONE *
*
*****
*****

```

C SET INTEGERS

```

INTEGER I, J, K, NI, NJ, NK, GRDTYP, CRDSYS, PRBDIM
INTEGER COORD, LABEL, REPEAT, counter

```

C SET PARAMETERS

```

PARAMETER (GRDTYP= 2, CRDSYS = 1, PRBDIM = 3)
PARAMETER (NI =30, NJ = 50, NK =180)

```

C SET REAL VARIABLES

```

real x(ni,nj,nk), y(ni,nj,nk), z(ni,nj,nk),r(ni,nj,nk)
real gradient(ni,nj),xtaper(ni,nj)

```

C Set INTEGERS

```

integer icell(ni+1, nj+1, nk+1)

```

C REAL CONSTANTS

```

REAL CYLLENGTH,CYLRADIUS,MAXCYLANGLE

```

REAL PITCH,dp

REAL rp,pi,twopi,omega

REAL r1,r2

REAL dx,dr,dt,theta

C DEFINE REAL CONSTANTS

C CYLINDER LENGTH IN METRES

CYLENGTH = 0.9

C CYLINDER RADIUS IN METRES

CYLRADIUS = 0.025

C ANGLE OF "CYLINDER IN RADIANS

C USED FOR A FULL CYLINDER WHICH FROM 0 TO 2*PI

MAXCYLANGLE = 6.28318530718

C DEFINE SECTION FORMATS

10 FORMAT (I6, 1X, A)

20 FORMAT (80A)

30 FORMAT (A1)

40 FORMAT (10I8)

50 FORMAT (5E15.8)

60 FORMAT (20I4)

C OPEN GRID FILE

OPEN (UNIT = 4, FILE='swirl09metre.GRD', STATUS='NEW')

C WRITE FILE SECTIONS

C THESE FILE SECTIONS FOLLOW THE LAYOUT IN USER'S GUIDE
C VOLUME 4 PP B-1 TO B-16 (FLUENT VERSION 4.3)

C.1.1 FILE HEADER

```
WRITE (4, '(A10)') '#!fluent.1'
```

C.1.2 PROGRAM INFORMATION MESSAGE SECTION

```
WRITE (4, 10) 2  
WRITE (4, 20) 'Created by: SWIRL09metre.for'  
WRITE (4, 30) '#'
```

C.1.3 TITLE SECTION

```
WRITE (4, 10) 1, 'Title'  
WRITE (4, 20) '0.9 M PIPE X 50 mm bore GRID'  
WRITE (4, 30) '#'
```

C.1.4 GRID TYPE SECTION

```
WRITE (4, 10) 6, 'Grid Type'  
WRITE (4, 40) GRDTYP, CRDSYS, PRBDIM, NI, NJ, NK  
WRITE (4, 30) '#'
```

```
C *****  
C SECTIONS 1.5 - 1.9 IGNORED  
C *****
```

```
C THIS IS BASED ON THE INFORMATION PROVIDED BY DR. REN LUI  
C OF FLUENT 15/4/96. FOR BODY FITTED CO-ORDINATES THE INPUT  
C HAS TO BE IN CARTESIAN CO-ORDINATES  
C SO WE USE CYLINDRICAL POLAR CO-ORDINATES FIRST THEN  
C TRANSFER THEM INTO XYZ CARTESIAN
```

```
C SET INCREMENTAL LENGTH IN THE X-DIRECTION
```

```
dx = CYLLENGTH/real(nk-1)
```

```
C SET THE INCREMENTAL LENGTH IN THETA
```

```
dt = MAXCYLANGLE/real(ni-1)
```

C SET INTERNAL RADIUS

$$r1 = 0.0$$

C PITCH OF SWIRL

C divided by the length so that we get one full twist

C 360 degrees

$$PITCH = 8.0 * \text{atan}(1.0) / \text{cylength}$$

C CALCULATE THE INCREMENT IN PITCH

$$dp = PITCH / \text{real}(nk-1)$$

C CALCULATE 2*PI

$$\text{twopi} = 8.0 * \text{atan}(1.0)$$

C CALCULATE PI

$$pi = \text{twopi} / 2.0$$

c SET NESTED DO LOOPS FOR GRID POINTS

do k=1,nk

do j=1,nj

do i=1,ni

C TRANSLATE INTO X IN CARTESIAN GRID

$$x(i,j,k) = dx * \text{real}(k-1)$$

C CALCULATE THETA IN CYLINDRICAL COORDINATES

$$\text{theta} = dt * \text{real}(i-1)$$

C SETTING r2 TO THE BORE OF THE PIPE AND KEEPING IT
C CONSTANT PRODUCES A CYLINDER

$$r2 = \text{CYLRADIUS}$$

C TO PRODUCE THE LOBES OF THE SWIRLY FLOW PIPE
C TRIGONOMETRICAL RELATIONS WERE USED AND THE
C PROGRAM IS GENERIC FOR ANY NUMBER OF LOBES

C FORMULA FOR THE DISPLACED CIRCLE IN TERMS OF THETA

$$dr = (r2 - r1)/\text{real}(nj-1)$$

C CALCULATE RADIUS

$$r(i,j,k) = r1 + dr*\text{real}(j-1)$$

C SINCE PHI CHANGES IF STATEMENTS HAVE TO MADE
C SO THAT THE CENTRES OF THE LOBES ALTERNATE IN
C CORRECT SEQUENCE
C 3 LOBES AT AN ANGULAR DISPLACEMENT OF 120 DEG
C

IF(THETA.LE.TWOPI/3.0)THEN

$$\begin{aligned} r(i,j,k) &= r(i,j,k)*\cos(\text{TWOPI}/6.0)*\cos(\text{TWOPI}/6.0 - \text{theta}) \\ &\& +r(i,j,k)*\text{sqrt}((\cos(\text{TWOPI}/6.0))**2*(\cos(\text{TWOPI}/6.0 - \text{theta}))**2 \\ &\& -\cos(\text{TWOPI}/3.0)) \end{aligned}$$

ELSE IF((THETA.GT.TWOPI/3.0).AND.
&(THETA.LE.4.0*PI/3.0))THEN

$$\text{omega} = \text{theta} - \text{twopi}/3.0$$

$$r(i,j,k) = r(i,j,k)*\cos(\text{TWOPI}/6.0)*\cos(\text{TWOPI}/6.0 - \text{omega})$$

```

& +r(i,j,k)*sqrt((cos(TWOPI/6.0))**2*(cos(TWOPI/6.0-omega))**2
& -cos(TWOPI/3.0))

```

```

ELSE

```

```

omega = theta - 4.0*pi/3.0

```

```

r(i,j,k) = r(i,j,k)*cos(TWOPI/6.0)*cos(TWOPI/6.0 - omega)
& +r(i,j,k)*sqrt((cos(TWOPI/6.0))**2*(cos(TWOPI/6.0-omega))**2
& -cos(TWOPI/3.0))

```

```

ENDIF

```

```

c Taper for end
c This occurs at 70% of the cylinder length
c This is done by using the integer at 70%
c as a marker

```

```

IF(k.eq.real(nk*0.7))then

```

```

c calculate cell spacing radially at the exit
c this done by dividing cylradius/nj

```

```

rspacing = cylradius/real(nj)

```

```

c calculate the gradient for each (i,j) at 70% cylinder length

```

```

gradient(i,j) = (r(i,j,k)-rspacing*(j-1))/(cyllength*0.3)

```

```

c determine x(i,j,k) at taper
c This effectively moves the origin for the taper
c using a simple y=mx+c type graph

```

```

xtaper(i,j) =x(i,j,k)

```

```

endif

```

```

c The taper commences when k is greater than 70%
c overall length

```

```
if(k.gt.real(nk*0.7))then
```

```
    r(i,j,k)=r(i,j,k)-gradient(i,j)*(x(i,j,k)-xtaper(i,j))
```

```
endif
```

- c This statement stops the the nodes at the outer edge
- c falling below cylradius

```
if((j.eq.nj).and.(r(i,j,k).lt.CYLRADIUS))then
```

```
    r(i,j,k) = CYLRADIUS
```

```
endif
```

- C TRANSLATE INTO CARTESIAN CO-ORDINATES
- C INCREMENT TO PRODUCE SWIRLY PIPE
- C USING THE HELIX $\text{PHI} = \text{BZ} + \text{C}$
- C X IS EQUAL TO Z IN THE ABOVE FORMULA
- C THIS IS DUE TO THE FLUENT NOTATION

```
y(i,j,k) = r(i,j,k)*COS(theta + (pitch*x(i,j,k)))
```

```
z(i,j,k) = r(i,j,k)*SIN(theta + (pitch*x(i,j,k)))
```

```
enddo
```

```
enddo
```

```
enddo
```

C.1.10 BFC SECTION

```
WRITE (4, 10) 9, 'BFC Grid'
```

```
WRITE (4, 50) (((x(i,j,k),i=1,ni), j=1,nj), k=1,nk)
```

```
WRITE (4, 50) (((y(i,j,k),i=1,ni), j=1,nj), k=1,nk)
```

```
WRITE (4, 50) (((z(i,j,k),i=1,ni), j=1,nj), k=1,nk)
```

```
WRITE (4, 30) '#'
```

C.1.11 CELL TYPES SECTION

```
WRITE (4, 10) 11, 'Cell Types 2'  
C ONLY LIVE CELL TYPES SPECIFIED I.E. LABEL = 4  
C LOOP REPEATED TO WRITE CELL INTEGER ZONE NUMBER I.E. LABEL = 1
```

```
do i=1,ni+1  
    do j=1,nj+1  
        do k=1,nk+1  
            icell(i,j,k) = 2  
        enddo  
    enddo  
enddo
```

```
do i=2,ni  
    do j=2,nj  
        do k=2,nk  
            icell(i,j,k) = 4  
        enddo  
    enddo  
enddo
```

```
enddo  
WRITE (4, 60) (((icell(i,j,k), I = 1, NI+1), J = 1, NJ+1),  
&                K = 1, NK+1)  
WRITE (4, 60) (((1, I = 0, NI), J = 0, NJ), K = 0, NK)  
  
WRITE (4, 30) '#'
```

C.1.12 NODES SECTION

C.1.13 END-OF-FILE SECTION

```
WRITE (4, 10) -1  
WRITE (4, 30) '#'  
CLOSE (4)
```

```
END
```

```

*****
*****
*
* PROGRAM TO CALCULATE R,THETA,Z AND SAVE THEM IN CARTESIAN *
*
* COORDINATES TO FLUENT FORMATTED FILE
*
*****
*****
*
* AUTHOR: BENJAMIN RAYLOR
*
* DATE: 2 APRIL 1996
*
*****
*****
*
* PURPOSE: TO PRODUCE A GRID FOR FLUENT TO USE IN THE *
* EVALUATION OF BRACHISTOCHRONE HELICES IN PIPES
*
*****
*****
*
* VARIABLES
*
* I   NODES IN THE ANGULAR DIRECTION (INTEGER)
* J   NODES IN THE RADIAL DIRECTION (INTEGER)
* K   NODES IN THE AXIAL DIRECTION (INTEGER)
* NI  MAXIMUM NUMBER OF NODES IN THE ANGULAR DIRECTION
*(INTEGER)
* NJ  MAXIMUM NUMBER OF NODES IN THE RADIAL DIRECTION
*(INTEGER)
* NK  MAXIMUM NUMBER OF NODES IN THE AXIAL DIRECTION
*(INTEGER)
* LABEL TYPE OF CELLS (INTEGER)
* GRDTYP GRID TYPE (INTEGER)
* CRDSYS TYPE OF COORDINATE SYSTEM (INTEGER)
* PRBDIM DIMENSION OF PROBLEM 2D OR 3D (INTEGER)
*
* CYLENGTH CYLINDER LENGTH IN METRES (REAL)
* CLRADIUS CYLINDER RADIUS IN METRES (REAL)
* MAXCYL ANGLE  $2\pi$  In radians (REAL)
* dx Increment in the x-direction-axial (real)
* dt Increment in theta (real)
* dr Increment in radius (real)
* rp taper length (real)
* r2 Cylinder radius inside loop (real)
* r1 set to zero only present for generality
* r(i,j,k) Array containing r values (real)

```

```

* x(i,j,k) Array containing x values (real) *
* y(i,j,k) Array containing y values (real) *
* z(i,j,k) Array containing z values (real) *
* gradient(i,j) Array containing gradient values for a linear taper *
* at 70 % cyllength *
* xtaper(i,j) Allows the origin of the taper to be placed *
* at cyllength70% *
* omega An angle describing one of the 3 lobes (real) *
* c Constant from the brachistochrone problem (real) *
* ck Constant from the brachistochrone problem (real) *
* counter A counter (integer) *
* phi The displacement added onto theta, phi is function of axial *
* distance (real) *
* secterm,root,t3,t4 Are values that are used to break down the *
* brachistochrone equation *
*
*****
*****
*
* DATE OF LAST MODIFICATION: N/A *
*
*****
*****
*
* ERRORS: NONE *
*
*****
*****

```

C SET INTEGERS

INTEGER I, J, K, NI, NJ, NK, GRDTYP, CRDSYS, PRBDIM
 INTEGER LABEL,counter

C SET PARAMETERS

PARAMETER (GRDTYP= 2, CRDSYS = 1, PRBDIM = 3)

C SET NI,NJ,NK TO ONE PLUS THE NUMBER OF CELLS
 C YOU REQUIRE IN EACH DIRECTION

PARAMETER (NI =30, NJ = 50, NK =40)

C SET REAL VARIABLES

C THE CARESIAN COORDINATES OH THE NODES

real x(ni,nj,nk), y(ni,nj,nk), z(ni,nj,nk)
real gradient(ni,nj),xtaper(ni,nj), r(ni,nj,nk)

C CELLS

integer icell(ni+1, nj+1, nk+1)

C REAL VALUES

REAL CYLENGTH,CYLRADIUS,MAXCYLANGLE

REAL phi,rp,pi,twopi,omega

REAL r1,r2,root,secterm,t3,t4

REAL dx,dr,dt,theta,c,ck

C DEFINE REAL CONSTANTS

C CYLINDER LENGTH IN METRES

CYLENGTH = 0.9

C CYLINDER RADIUS IN METRES

CYLRADIUS = 0.025

C ANGLE OF "CYLINDER IN RADIANS"

C USED FOR A FULL CYLINDER WHICH FROM 0 TO 2*PI

MAXCYLANGLE = 6.28318530718

C DEFINE SECTION FORMATS

10 FORMAT (I6, 1X, A)

20 FORMAT (80A)

30 FORMAT (A1)

40 FORMAT (10I8)

50 FORMAT (5E15.8)

60 FORMAT (20I4)

C OPEN GRID FILE

OPEN (UNIT = 4, FILE='brach09.GRD', STATUS='NEW')

C WRITE FILE SECTIONS

C THESE FILE SECTIONS FOLLOW THE LAYOUT IN USER'S GUIDE

C VOLUME 4 PP B-1 TO B-16 (FLUENT VERSION 4.3)

C.1.1 FILE HEADER

WRITE (4, '(A10)') '#!fluent.1'

C.1.2 PROGRAM INFORMATION MESSAGE SECTION

WRITE (4, 10) 2

WRITE (4, 20) 'Created by: bracht01'

WRITE (4, 30) '#'

C.1.3 TITLE SECTION

WRITE (4, 10) 1, 'Title'

WRITE (4, 20) '0.9 M PIPE X 50 mm bore GRID'

WRITE (4, 30) '#'

C.1.4 GRID TYPE SECTION

WRITE (4, 10) 6, 'Grid Type'

WRITE (4, 40) GRDTYP, CRDSYS, PRBDIM, NI, NJ, NK

WRITE (4, 30) '#'

C *****
C SECTIONS 1.5 - 1.9 IGNORED
C *****

C THIS IS BASED ON THE INFORMATION PROVIDED BY DR. REN LUI
C OF FLUENT SHEFFIELD, 15/4/96. FOR BODY FITTED CO-ORDINATES THE
C INPUT
C HAS TO BE IN CARTESIAN CO-ORDINATES
C SO WE USE CYLINDRICAL POLAR CO-ORDINATES FIRST THEN
C TRANSFER THEM INTO XYZ CARTESIAN

C SET INCREMENTAL LENGTH IN THE X-DIRECTION

$$dx = \text{CYLLENGTH}/\text{real}(\text{nk}-1)$$

C SET THE INCREMENTAL LENGTH IN THETA

$$dt = \text{MAXCYLANGLE}/\text{real}(\text{ni}-1)$$

C SET INTERNAL RADIUS

$$r1 = 0.0$$

C CALCULATE 2*PI

$$\text{twopi} = 8.0 * \text{atan}(1.0)$$

C CALCULATE PI

$$\text{pi} = \text{twopi}/2.0$$

- c the constant from the equation 20 for the brachistochrone
- c problem This was done in Mathcad (brach9.mcd)
- c this constant changes with cylinder length and radius

$$c = 0.006760614259128$$

- c valuation of the constant K was also done in mathcad (brach9.mcd)
- c this constant changes with cylinder length and radius

$$\text{ck} = 429.5933756456777$$

c SET NESTED DO LOOPS FOR GRID POINTS

do k=1,nk

do j=1,nj

do i=1,ni

C TRANSLATE INTO X IN CARTESIAN GRID

|

$$x(i,j,k) = dx * \text{real}(k-1)$$

C CALCULATE THETA IN CYLINDRICAL COORDINATES

$$\text{theta} = dt * \text{real}(i-1)$$

C SETTING r2 TO THE BORE OF THE PIPE AND KEEPING IT
C CONSTANT PRODUCES A CYLINDER

$$r2 = \text{CYLRADIUS}$$

C TO PRODUCE THE LOBES OF THE SWIRLY FLOW PIPE
C TRIGONOMETRICAL RELATIONS WERE USED AND THE
C PROGRAM IS GENERIC FOR ANY NUMBER OF LOBES

C FORMULA FOR THE DISPLACED CIRCLE IN TERMS OF THETA

$$dr = (r2 - r1) / \text{real}(nj-1)$$

C CALCULATE RADIUS

$$r(i,j,k) = r1 + dr * \text{real}(j-1)$$

C SINCE PHI CHANGES IF STATEMENTS HAVE TO MADE
C SO THAT THE CENTRES OF THE LOBES ALTERNATE IN
C CORRECT SEQUENCE
C 3 LOBES AT AN ANGULAR DISPLACEMENT OF 120 DEG
C

IF(THETA.LE.TWOPI/3.0)THEN

$$\begin{aligned} r(i,j,k) &= r(i,j,k) * \cos(\text{TWOPI}/6.0) * \cos(\text{TWOPI}/6.0 - \text{theta}) \\ &\& + r(i,j,k) * \text{sqrt}((\cos(\text{TWOPI}/6.0)) ** 2 * (\cos(\text{TWOPI}/6.0 - \text{theta})) ** 2 \\ &\& - \cos(\text{TWOPI}/3.0)) \end{aligned}$$

```
ELSE IF((THETA.GT.TWOPI/3.0).AND.  
&(THETA.LE.4.0*PI/3.0))THEN
```

```
omega = theta - twopi/3.0
```

```
r(i,j,k) = r(i,j,k)*cos(TWOPI/6.0)*cos(TWOPI/6.0 - omega)  
& +r(i,j,k)*sqrt((cos(TWOPI/6.0))**2*(cos(TWOPI/6.0-omega))**2  
& -cos(TWOPI/3.0))
```

```
ELSE
```

```
omega = theta - 4.0*pi/3.0
```

```
r(i,j,k) = r(i,j,k)*cos(TWOPI/6.0)*cos(TWOPI/6.0 - omega)  
& +r(i,j,k)*sqrt((cos(TWOPI/6.0))**2*(cos(TWOPI/6.0-omega))**2  
& -cos(TWOPI/3.0))
```

```
ENDIF
```

- c Taper for end
- c This occurs at 70% of the cylinder length
- c This is done by using the integer at 70%
- c as a marker

```
IF(k.eq.real(nk*0.7))then
```

- c calculate cell spacing radially at the exit
- c this done by dividing cylradius/nj

```
rspacing = cylradius/real(nj)
```

- c calculate the gradient for each (i,j) at 70% cylinder length

```
gradient(i,j) = (r(i,j,k)-rspacing*(j-1))/(cyllength*0.3)
```

- c determine x(i,j,k) at taper
- c This effectively moves the origin for the taper
- c using a simple y=mx+c type graph

```
xtaper(i,j) =x(i,j,k)
```

```
endif
```

- c The taper commences when k is greater than 70%
- c overall length

```
if(k.gt.real(nk*0.7))then
```

```
  r(i,j,k)=r(i,j,k)-gradient(i,j)*(x(i,j,k)-xtaper(i,j))
```

```
endif
```

- c This statement stops the the nodes at the outer edge
- c falling below cylradius

```
if((j.eq.nj).and.(r(i,j,k).lt.CYLRADIUS))then
```

```
  r(i,j,k) = CYLRADIUS
```

```
endif
```

```
C TRANSLATE INTO CARTESIAN CO-ORDINATES  
C INCREMENT TO PRODUCE SWIRLY PIPE  
C USING THE HELIX FOR A BRACHISTOCHRONE IN A CYLINDER  
C THIS IS DUE TO THE FLUENT NOTATION  
C SINCE THE FORMULA FOR A BRACHISTRONE CURVE  
C INSIDE A CYLINDER IS RATHER COMPLICATED  
C WE WILL BREAK IT DOWN INTO SMALLER COMPONENTS
```

- c Due to the nature of the constants of the brachistrone
- c problem a slight error will occur unless phi is set to zero
- c at the k=1, or x(i,j,k)=0.0.
- c

```
if(k.eq.1)then
```

```
  phi = 0.0
```

```
else
```

- c splitting formula into parts
- c to allow easy manipulation of formulae

$$\text{ROOT} = -1.0 * \text{SQRT}(r2 * r2 * x(i,j,k) / (c * c) - x(i,j,k) * x(i,j,k))$$

$$\text{SECTERM} = 1.0 / 2.0 * r2 ** 2 / (c * c)$$

$$t3 = ((2.0 * x(i,j,k) * c * c - r2 * r2) / (r2 * r2))$$

$$t4 = \text{asin}(t3)$$

- c calculate phi temp using the temporary markers

$$\text{phi} = (\text{ROOT} + \text{SECTERM} * t4) / r2 + \text{ck}$$

endif

- c transfer into cartesian co-ordinates

$$y(i,j,k) = r(i,j,k) * \text{COS}(\text{theta} + \text{phi})$$

$$z(i,j,k) = r(i,j,k) * \text{SIN}(\text{theta} + \text{phi})$$

enddo

enddo

enddo

C.1.10 BFC SECTION

WRITE (4, 10) 9, 'BFC Grid'

WRITE (4, 50) (((x(i,j,k), i=1, ni), j=1, nj), k=1, nk)

WRITE (4, 50) (((y(i,j,k), i=1, ni), j=1, nj), k=1, nk)

WRITE (4, 50) (((z(i,j,k), i=1, ni), j=1, nj), k=1, nk)

WRITE (4, 30) '#'

C.1.11 CELL TYPES SECTION

```
WRITE (4, 10) 11, 'Cell Types 2'  
C ONLY LIVE CELL TYPES SPECIFIED I.E. LABEL = 4  
C LOOP REPEATED TO WRITE CELL INTEGER ZONE NUMBER I.E. LABEL = 1
```

```
do i=1,ni+1  
    do j=1,nj+1  
        do k=1,nk+1  
            icell(i,j,k) = 2  
        enddo  
    enddo  
enddo  
  
do i=2,ni  
    do j=2,nj  
        do k=2,nk  
            icell(i,j,k) = 4  
        enddo  
    enddo  
enddo  
  
WRITE (4, 60) (((icell(i,j,k), I = 1, NI+1), J = 1, NJ+1),  
&                K = 1, NK+1)  
WRITE (4, 60) (((1, I = 0, NI), J = 0, NJ), K = 0, NK)  
  
WRITE (4, 30) '#'
```

C.1.12 NODES SECTION

C.1.13 END-OF-FILE SECTION

```
WRITE (4, 10) -1  
WRITE (4, 30) '#'  
CLOSE (4)  
  
END
```

```

*****
*****
*****
*
* PROGRAM TO SAVE R,THETA,Z COORDINATES TO FLUENT
FORMATTED FILE
*
*****
*****
*
* AUTHOR: BENJAMIN RAYLOR
*
* DATE: 25 November 1996
*
*****
*****
*
* PURPOSE: TO PRODUCE A GRID FOR FLUENT TO USE IN THE
* EVALUATION
* OF HELICES IN PIPES WITHOUT TAPERS
*
*****
*****
*
* VARIABLES
*
* I   NODES IN THE ANGULAR DIRECTION (INTEGER)
* J   NODES IN THE RADIAL DIRECTION (INTEGER)
* K   NODES IN THE AXIAL DIRECTION (INTEGER)
* NI  MAXIMUM NUMBER OF CELLS IN THE ANGULAR DIRECTIO
(INTEGER)
* NJ  MAXIMUM NUMBER OF CELLS IN THE RADIAL DIRECTION
(INTEGER)
* NK  MAXIMUM NUMBER OF CELLS IN THE AXIAL DIRECTION
(INTEGER)
* LABEL TYPE OF CELLS (INTEGER)
* GRDTYP GRID TYPE (INTEGER)
* CRDSYS TYPE OF COORDINATE SYSTEM (INTEGER)
* PRBDIM DIMENSION OF PROBLEM 2D OR 3D (INTEGER)
* CYLLENGTH CYLINDER LENGTH IN METRES (REAL)
* CLRADIUS CYLINDER RADIUS IN METRES (REAL)
* MAXCYLANGLE 2*pi ln radians (REAL)
* dx Increment in the x-direction-axial (real)
* dt Increment in theta (real)
* dr Increment in radius (real)
* dp Increment in pitch (real)
* rp taper length (real)
* r2 Cylinder radius inside loop (real)

```

```

* r1 set to zero only present for generality *
* r(i,j,k) Array containing r values (real) *
* x(i,j,k) Array containing x values (real) *
* y(i,j,k) Array containing y values (real) *
* z(i,j,k) Array containing z values (real) *
* gradient(i,j) Array containing gradient values for the linear *
* taper at 70 % cyllength *
* xtaper(i,j) Allows the origin for the taper to be placed at *
* cyllength70% *
* omega An angle describing one of the 3 lobes (real) *
* counter A counter (integer) *
* pitch Determines pitch of swirly-flo pipe *
*****
*****
*
* DATE OF LAST MODIFICATION: DEC 1997 *
*
* modification (1) - To produce 0.4 mtre standard swirly-flo *
* without end taper *
*
*****
*****
*
* ERRORS: NONE *
*
*****
*****

```

C SET INTEGERS

```

INTEGER I, J, K, NI, NJ, NK, GRDTYP, CRDSYS, PRBDIM
INTEGER COORD, LABEL, REPEAT,counter

```

C SET PARAMETERS

```

PARAMETER (GRDTYP= 2, CRDSYS = 1, PRBDIM = 3)
PARAMETER (NI =30 , NJ = 50, NK =140)

```

C SET REAL VARIABLES

```

real x(ni,nj,nk), y(ni,nj,nk), z(ni,nj,nk),r(ni,nj,nk)
real gradient(ni,nj),xtaper(ni,nj)

```

C Set INTEGERS

integer icell(ni+1, nj+1, nk+1)

C REAL CONSTANTS

REAL CYLLENGTH,CYLRADIUS,MAXCYLANGLE

REAL PITCH,dp

REAL rp,pi,twopi,omega

REAL r1,r2

REAL dx,dr,dt,theta

C DEFINE REAL CONSTANTS

C CYLINDER LENGTH IN METRES

CYLLENGTH = 0.4

C CYLINDER RADIUS IN METRES

CYLRADIUS = 0.025

C ANGLE OF "CYLINDER IN RADIANS

C USED FOR A FULL CYLINDER WHICH FROM 0 TO 2*PI

MAXCYLANGLE = 6.28318530718

C DEFINE SECTION FORMATS

10 FORMAT (I6, 1X, A)

20 FORMAT (80A)

30 FORMAT (A1)

40 FORMAT (10I8)

50 FORMAT (5E15.8)

60 FORMAT (20I4)

C OPEN GRID FILE

```
OPEN (UNIT = 4, FILE=' swirl04metrewt.GRD', STATUS='NEW')
```

C WRITE FILE SECTIONS

C THESE FILE SECTIONS FOLLOW THE LAYOUT IN USER'S GUIDE

C VOLUME 4 PP B-1 TO B-16 (FLUENT VERSION 4.3)

C.1.1 FILE HEADER

```
WRITE (4, '(A10)') '#!fluent.1'
```

C.1.2 PROGRAM INFORMATION MESSAGE SECTION

```
WRITE (4, 10) 2
```

```
WRITE (4, 20) 'Created by: SWIRL04metrewt.for'
```

```
WRITE (4, 30) '#'
```

C.1.3 TITLE SECTION

```
WRITE (4, 10) 1, 'Title'
```

```
WRITE (4, 20) '0.4m Pipe X 50 mm without taper'
```

```
WRITE (4, 30) '#'
```

C.1.4 GRID TYPE SECTION

```
WRITE (4, 10) 6, 'Grid Type'
```

```
WRITE (4, 40) GRDTYP, CRDSYS, PRBDIM, NI, NJ, NK
```

```
WRITE (4, 30) '#'
```

C *****

C SECTIONS 1.5 - 1.9 IGNORED

C *****

C THIS IS BASED ON THE INFORMATION PROVIDED BY DR. REN LUI

C OF FLUENT 15/4/96. FOR BODY FITTED CO-ORDINATES THE INPUT

C HAS TO BE IN CARTESIAN CO-ORDINATES

C SO WE USE CYLINDRICAL POLAR CO-ORDINATES FIRST THEN

C TRANSFER THEM INTO XYZ CARTESIAN

C SET INCREMENTAL LENGTH IN THE X-DIRECTION

$$dx = CYLLENGTH/real(nk-1)$$

C SET THE INCREMENTAL LENGTH IN THETA

$$dt = MAXCYLANGLE/real(ni-1)$$

C SET INTERNAL RADIUS

$$r1 = 0.0$$

C PITCH OF SWIRL

C divided by the length so that we get one full twist

C 360 degrees

$$PITCH = 8.0*atan(1.0)/cylength$$

C CALCULATE THE INCREMENT IN PITCH

$$dp = PITCH/real(nk-1)$$

C CALCULATE 2*PI

$$twopi = 8.0*atan(1.0)$$

C CALCULATE PI

$$pi = twopi/2.0$$

c SET NESTED DO LOOPS FOR GRID POINTS

do k=1,nk

do j=1,nj

do i=1,ni

C TRANSLATE INTO X IN CARTESIAN GRID

$$x(i,j,k) = dx*real(k-1)$$

C CALCULATE THETA IN CYLINDRICAL COORDINATES

$$theta = dt*real(i-1)$$

C SETTING r2 TO THE BORE OF THE PIPE AND KEEPING IT
C CONSTANT PRODUCES A CYLINDER

$$r2 = CYLRADIUS$$

C TO PRODUCE THE LOBES OF THE SWIRLY FLOW PIPE
C TRIGONOMETRICAL RELATIONS WERE USED AND THE
C PROGRAM IS GENERIC FOR ANY NUMBER OF LOBES

C FORMULA FOR THE DISPLACED CIRCLE IN TERMS OF THETA

$$dr = (r2 - r1)/real(nj-1)$$

C CALCULATE RADIUS

$$r(i,j,k) = r1 + dr*real(j-1)$$

C SINCE PHI CHANGES IF STATEMENTS HAVE TO MADE
C SO THAT THE CENTRES OF THE LOBES ALTERNATE IN
C CORRECT SEQUENCE
C 3 LOBES AT AN ANGULAR DISPLACEMENT OF 120 DEG
C

IF(THETA.LE.TWOPI/3.0)THEN

$$\begin{aligned} r(i,j,k) &= r(i,j,k)*\cos(TWOPI/6.0)*\cos(TWOPI/6.0 -theta) \\ &\& +r(i,j,k)*\sqrt{(\cos(TWOPI/6.0))**2*(\cos(TWOPI/6.0-theta))**2} \\ &\& -\cos(TWOPI/3.0)) \end{aligned}$$

```
ELSE IF((THETA.GT.TWOPI/3.0).AND.  
&(THETA.LE.4.0*PI/3.0))THEN
```

```
    omega = theta - twopi/3.0
```

```
    r(i,j,k) = r(i,j,k)*cos(TWOPI/6.0)*cos(TWOPI/6.0 - omega)  
& +r(i,j,k)*sqrt((cos(TWOPI/6.0))**2*(cos(TWOPI/6.0-omega))**2  
& -cos(TWOPI/3.0))
```

```
ELSE
```

```
    omega = theta - 4.0*pi/3.0
```

```
    r(i,j,k) = r(i,j,k)*cos(TWOPI/6.0)*cos(TWOPI/6.0 - omega)  
& +r(i,j,k)*sqrt((cos(TWOPI/6.0))**2*(cos(TWOPI/6.0-omega))**2  
& -cos(TWOPI/3.0))
```

```
ENDIF
```

```
C    TRANSLATE INTO CARTESIAN CO-ORDINATES  
C    INCREMENT TO PRODUCE SWIRLY PIPE  
C    USING THE HELIX PHI = BZ +C  
C    X IS EQUAL TO Z IN THE ABOVE FORMULA  
C    THIS IS DUE TO THE FLUENT NOTATION
```

```
y(i,j,k) = r(i,j,k)*COS(theta + (pitch*x(i,j,k)))  
z(i,j,k) = r(i,j,k)*SIN(theta + (pitch*x(i,j,k)))
```

```
    enddo  
  
    enddo  
  
enddo
```

C.1.10 BFC SECTION

```
    WRITE (4, 10) 9, 'BFC Grid'  
    WRITE (4, 50) (((x(i,j,k),i=1,ni), j=1,nj), k=1,nk)  
    WRITE (4, 50) (((y(i,j,k),i=1,ni), j=1,nj), k=1,nk)  
    WRITE (4, 50) (((z(i,j,k),i=1,ni), j=1,nj), k=1,nk)  
  
    WRITE (4, 30) '#'
```

C.1.11 CELL TYPES SECTION

```
    WRITE (4, 10) 11, 'Cell Types 2'  
C ONLY LIVE CELL TYPES SPECIFIED I.E. LABEL = 4  
C LOOP REPEATED TO WRITE CELL INTEGER ZONE NUMBER I.E. LABEL  
= 1
```

```
    do i=1,ni+1  
  
        do j=1,nj+1  
  
            do k=1,nk+1  
  
                icell(i,j,k) = 2  
  
            enddo  
  
        enddo  
  
    enddo  
  
    do i=2,ni  
  
        do j=2,nj  
  
            do k=2,nk  
  
                icell(i,j,k) = 4
```

enddo

enddo

enddo

```
WRITE (4, 60) (((icell(i,j,k), I = 1, NI+1), J = 1, NJ+1),  
&                K = 1, NK+1)  
WRITE (4, 60) (((1, I = 0, NI), J = 0, NJ), K = 0, NK)  
  
WRITE (4, 30) '#'
```

C.1.12 NODES SECTION

C.1.13 END-OF-FILE SECTION

```
WRITE (4, 10) -1  
WRITE (4, 30) '#'  
CLOSE (4)
```

END

```

*****
*****
*
* PROGRAM TO CALCULATE R,THETA,Z AND SAVE THEM IN
*CARTESIAN
* COORDINATES TO FLUENT FORMATTED FILE
*
*****
*****
*
* AUTHOR: BENJAMIN RAYLOR
*
* DATE: 2 APRIL 1996
*
*****
*****
*
* PURPOSE: TO PRODUCE A GRID FOR FLUENT TO USE IN THE
EVALUATION
* OF BRACHISTOCHRONE HELICES IN PIPES
* WITHOUT TAPERS
*****
*****
*
* VARIABLES
*
* I   NODES IN THE ANGULAR DIRECTION (INTEGER)
* J   NODES IN THE RADIAL DIRECTION (INTEGER)
* K   NODES IN THE AXIAL DIRECTION (INTEGER)
* NI  MAXIMUM NUMBER OF NODES IN THE ANGULAR DIRECTION
(INTEGER)
* NJ  MAXIMUM NUMBER OF NODES IN THE RADIAL DIRECTION
(INTEGER)
* NK  MAXIMUM NUMBER OF NODES IN THE AXIAL DIRECTION
(INTEGER)
* LABEL TYPE OF CELLS (INTEGER)
* GRDTYP GRID TYPE (INTEGER)
* CRDSYS TYPE OF COORDINATE SYSTEM (INTEGER)
* PRBDIM DIMENSION OF PROBLEM 2D OR 3D (INTEGER)
*
* CYLLENGTH CYLINDER LENGTH IN METRES (REAL)
* CLRADIUS  CYLINDER RADIUS IN METRES (REAL)
* MAXCYLANGLE 2*pi ln radians (REAL)
* dx Increment in the x-direction-axial (real)
* dt Increment in theta (real)
* dr Increment in radius (real)
* rp taper length (real)
* r2 Cylinder radius inside loop (real)

```

```

* r1 set to zero only present for generality
* r(i,j,k) Array containing r values (real)
* x(i,j,k) Array containing x values (real)
* y(i,j,k) Array containing y values (real)
* z(i,j,k) Array containing z values (real)
* gradient(i,j) Array containing gradient values for a linear taper
* at 70 % cyllength
* xtaper(i,j) Allows the origin of the taper to be placed
* at cyllength70%
* omega An angle describing one of the 3 lobes (real)
* c Constant from the brachistochrone problem (real)
* ck Constant from the brachistochrone problem (real)
* counter A counter (integer)
* phi The displacement added onto theta, phi is function of axial
* distance (real)
* secterm,root,t3,t4 Are values that are used to break down the
* brachistochrone equation
*
*****
*****
*
* DATE OF LAST MODIFICATION: DEC 1997
*
* Modification (1) To produce a 0.4 metre Brachistochrone
* without end taper
*
*****
*****
*
* ERRORS: NONE
*
*****
*****

```

C SET INTEGERS

```

INTEGER I, J, K, NI, NJ, NK, GRDTYP, CRDSYS, PRBDIM
INTEGER LABEL,counter

```

C SET PARAMETERS

```

PARAMETER (GRDTYP= 2, CRDSYS = 1, PRBDIM = 3)

```

```

C SET NI,NJ,NK TO ONE PLUS THE NUMBER OF CELLS
C YOU REQUIRE IN EACH DIRECTION

```

PARAMETER (NI =30, NJ = 50, NK =140)

- C SET REAL VARIABLES
- C THE CARESIAN COORDINATES OH THE NODES

real x(ni,nj,nk), y(ni,nj,nk), z(ni,nj,nk)
real gradient(ni,nj),xtaper(ni,nj), r(ni,nj,nk)

- C CELLS

integer icell(ni+1, nj+1, nk+1)

- C REAL VALUES

REAL CYLLENGTH,CYLRADIUS,MAXCYLANGLE

REAL phi,rp,pi,twopi,omega

REAL r1,r2,root,secterm,t3,t4

REAL dx,dr,dt,theta,c,ck

- C DEFINE REAL CONSTANTS

- C CYLINDER LENGTH IN METRES

CYLLENGTH = 0.4

- C CYLINDER RADIUS IN METRES

CYLRADIUS = 0.025

- C ANGLE OF "CYLINDER IN RADIANS"
- C USED FOR A FULL CYLINDER WHICH FROM 0 TO 2*PI

MAXCYLANGLE = 6.28318530718

- C DEFINE SECTION FORMATS

```
10 FORMAT (I6, 1X, A)
20 FORMAT (80A)
30 FORMAT (A1)
40 FORMAT (10I8)
50 FORMAT (5E15.8)
60 FORMAT (20I4)
```

C OPEN GRID FILE

```
OPEN (UNIT = 4, FILE='brach04.GRD', STATUS='NEW')
```

```
C WRITE FILE SECTIONS
C THESE FILE SECTIONS FOLLOW THE LAYOUT IN USER'S GUIDE
C VOLUME 4 PP B-1 TO B-16 (FLUENT VERSION 4.3)
```

C.1.1 FILE HEADER

```
WRITE (4, '(A10)') '#!fluent.1'
```

C.1.2 PROGRAM INFORMATION MESSAGE SECTION

```
WRITE (4, 10) 2
WRITE (4, 20) 'Created by: bracht04'
WRITE (4, 30) '#'
```

C.1.3 TITLE SECTION

```
WRITE (4, 10) 1, 'Title'
WRITE (4, 20) '1M PIPE X 50 mm bore GRID'
WRITE (4, 30) '#'
```

C.1.4 GRID TYPE SECTION

```
WRITE (4, 10) 6, 'Grid Type'
WRITE (4, 40) GRDTYP, CRDSYS, PRBDIM, NI, NJ, NK
WRITE (4, 30) '#'
```

```
C *****
C SECTIONS 1.5 - 1.9 IGNORED
C *****
```

C THIS IS BASED ON THE INFORMATION PROVIDED BY DR. REN LUI
C OF FLUENT SHEFFIELD, 15/4/96. FOR BODY FITTED CO-ORDINATES
THE INPUT
C HAS TO BE IN CARTESIAN CO-ORDINATES
C SO WE USE CYLINDRICAL POLAR CO-ORDINATES FIRST THEN
C TRANSFER THEM INTO XYZ CARTESIAN

C SET INCREMENTAL LENGTH IN THE X-DIRECTION

$$dx = CYLLENGTH/real(nk-1)$$

C SET THE INCREMENTAL LENGTH IN THETA

$$dt = MAXCYLANGLE/real(ni-1)$$

C SET INTERNAL RADIUS

$$r1 = 0.0$$

C CALCULATE 2*PI

$$twopi = 8.0 * atan(1.0)$$

C CALCULATE PI

$$pi = twopi/2.0$$

c the constant from the equation 20 for the brachistochrone
c problem This was done in Mathcad (brach4.mcd)
c this constant changes with cylinder length and radius

$$c = 0.021130559837260$$

c valuation of the constant K was also done in mathcad (brach1.mcd)
c this constant changes with cylinder length and radius

$$ck = 43.97520604974775$$

c SET NESTED DO LOOPS FOR GRID POINTS

do k=1,nk

do j=1,nj

do i=1,ni

C TRANSLATE INTO X IN CARTESIAN GRID

$x(i,j,k) = dx * \text{real}(k-1)$

C CALCULATE THETA IN CYLINDRICAL COORDINATES

$\text{theta} = dt * \text{real}(i-1)$

C SETTING r2 TO THE BORE OF THE PIPE AND KEEPING IT
C CONSTANT PRODUCES A CYLINDER

$r2 = \text{CYLRADIUS}$

C TO PRODUCE THE LOBES OF THE SWIRLY FLOW PIPE
C TRIGONOMETRICAL RELATIONS WERE USED AND THE
C PROGRAM IS GENERIC FOR ANY NUMBER OF LOBES

C FORMULA FOR THE DISPLACED CIRCLE IN TERMS OF THETA

$dr = (r2 - r1) / \text{real}(nj-1)$

C CALCULATE RADIUS

$r(i,j,k) = r1 + dr * \text{real}(j-1)$

C SINCE PHI CHANGES IF STATEMENTS HAVE TO MADE
C SO THAT THE CENTRES OF THE LOBES ALTERNATE IN
C CORRECT SEQUENCE
C 3 LOBES AT AN ANGULAR DISPLACEMENT OF 120 DEG

C

IF(THETA.LE.TWOPI/3.0)THEN

r(i,j,k) = r(i,j,k)*cos(TWOPI/6.0)*cos(TWOPI/6.0 -theta)
& +r(i,j,k)*sqrt((cos(TWOPI/6.0))**2*(cos(TWOPI/6.0-theta))**2
& -cos(TWOPI/3.0))

ELSE IF((THETA.GT.TWOPI/3.0).AND.
&(THETA.LE.4.0*PI/3.0))THEN

omega = theta - twopi/3.0

r(i,j,k) = r(i,j,k)*cos(TWOPI/6.0)*cos(TWOPI/6.0 -omega)
& +r(i,j,k)*sqrt((cos(TWOPI/6.0))**2*(cos(TWOPI/6.0-omega))**2
& -cos(TWOPI/3.0))

ELSE

omega = theta - 4.0*pi/3.0

r(i,j,k) = r(i,j,k)*cos(TWOPI/6.0)*cos(TWOPI/6.0 - omega)
& +r(i,j,k)*sqrt((cos(TWOPI/6.0))**2*(cos(TWOPI/6.0-omega))**2
& -cos(TWOPI/3.0))

ENDIF

c Taper for end
c This occurs at 70% of the cylinder length
c This is done by using the integer at 70%
c as a marker

IF(k.eq.real(nk*0.7))then

c calculate cell spacing radially at the exit
c this done by dividing cylradius/nj

rspacing = cylradius/real(nj)

c calculate the gradient for each (i,j) at 70% cylinder length

$$\text{gradient}(i,j) = (r(i,j,k) - \text{rspacing} * (j-1)) / (\text{cyllength} * 0.3)$$

c determine x(i,j,k) at taper

c This effectively moves the origin for the taper

c using a simple $y=mx+c$ type graph

$$\text{xtaper}(i,j) = x(i,j,k)$$

endif

c The taper commences when k is greater than 70%

c overall length

if(k.gt.real(nk*0.7))then

$$r(i,j,k) = r(i,j,k) - \text{gradient}(i,j) * (x(i,j,k) - \text{xtaper}(i,j))$$

endif

c This statement stops the the nodes at the outer edge

c falling below cylradius

if((j.eq.nj).and.(r(i,j,k).lt.CYLRADIUS))then

$$r(i,j,k) = \text{CYLRADIUS}$$

endif

C TRANSLATE INTO CARTESIAN CO-ORDINATES
C INCREMENT TO PRODUCE SWIRLY PIPE
C USING THE HELIX FOR A BRACHISTOCHRONE IN A CYLINDER
C THIS IS DUE TO THE FLUENT NOTATION
C SINCE THE FORMULA FOR A BRACHISTRONE CURVE
C INSIDE A CYLINDER IS RATHER COMPLICATED
C WE WILL BREAK IT DOWN INTO SMALLER COMPONENTS

c Due to the nature of the constants of the brachistrone
 c problem a slight error will occur unless phi is set to zero
 c at the k=1, or $x(i,j,k)=0.0$.

c

if(k.eq.1)then

phi = 0.0

else

c splitting formula into parts
 c to allow easy manipulation of formulae

ROOT = $-1.0 * \text{SQRT}(r2 * r2 * x(i,j,k) / (c * c) - x(i,j,k) * x(i,j,k))$

SECTERM = $1.0 / 2.0 * r2 ** 2 / (c * c)$

t3 = $((2.0 * x(i,j,k) * c * c - r2 * r2) / (r2 * r2))$

t4 = $\text{asin}(t3)$

c calculate phi temp using the temporary markers

phi = $(\text{ROOT} + \text{SECTERM} * t4) / r2 + ck$

endif

c transfer into cartesian co-ordinates

$y(i,j,k) = r(i,j,k) * \text{COS}(\text{theta} + \text{phi})$

$z(i,j,k) = r(i,j,k) * \text{SIN}(\text{theta} + \text{phi})$

enddo

enddo

enddo

C.1.10 BFC SECTION

```
WRITE (4, 10) 9, 'BFC Grid'  
WRITE (4, 50) (((x(i,j,k),i=1,ni), j=1,nj), k=1,nk)  
WRITE (4, 50) (((y(i,j,k),i=1,ni), j=1,nj), k=1,nk)  
WRITE (4, 50) (((z(i,j,k),i=1,ni), j=1,nj), k=1,nk)  
  
WRITE (4, 30) '#'
```

C.1.11 CELL TYPES SECTION

```
WRITE (4, 10) 11, 'Cell Types 2'  
C ONLY LIVE CELL TYPES SPECIFIED I.E. LABEL = 4  
C LOOP REPEATED TO WRITE CELL INTEGER ZONE NUMBER I.E. LABEL  
= 1
```

```
do i=1,ni+1  
    do j=1,nj+1  
        do k=1,nk+1  
            icell(i,j,k) = 2  
        enddo  
    enddo  
enddo  
  
do i=2,ni  
    do j=2,nj  
        do k=2,nk  
            icell(i,j,k) = 4  
        enddo  
    enddo  
enddo  
  
& WRITE (4, 60) (((icell(i,j,k), I = 1, NI+1), J = 1, NJ+1),  
                K = 1, NK+1)  
WRITE (4, 60) (((1, I = 0, NI), J = 0, NJ), K = 0, NK)
```

WRITE (4, 30) '#'

C.1.12 NODES SECTION

C.1.13 END-OF-FILE SECTION

WRITE (4, 10) -1

WRITE (4, 30) '#'

CLOSE (4)

END

APPENDIX C

0.1 metre pipe X 50 mm Nominal Bore Standard Swirly-flo Pipe - With End Taper - Grid	1-C
0.1 metre pipe X 50 mm Nominal Bore Standard Swirly-flo Pipe - With End Taper - Static Pressure (Pa) at the wall	2-C
0.1 metre pipe X 50 mm Nominal Bore Standard Swirly-flo Pipe - With End Taper - W-velocity (m/s) at J=45 - View 1	3-C
0.1 metre pipe X 50 mm Nominal Bore Standard Swirly-flo Pipe - With End Taper - W-velocity (m/s) at J=45 - View 2	4-C
0.1 metre pipe X 50 mm Nominal Bore Standard Swirly-flo Pipe - With End Taper - W-Velocity at Exit	5-C
0.2 metre pipe X 50 mm Nominal Bore Standard Swirly-flo Pipe - With End Taper - Grid	6-C
0.2 metre pipe X 50 mm Nominal Bore Standard Swirly-flo Pipe - With End Taper - Static Pressure (Pa) at the wall	7-C
0.2 metre pipe X 50 mm Nominal Bore Standard Swirly-flo Pipe - With End Taper - W-velocity (m/s) at J=45 - View 1	8-C
0.2 metre pipe X 50 mm Nominal Bore Standard Swirly-flo Pipe - With End Taper - W-velocity (m/s) at J=45 - View 2	9-C
0.2 metre pipe X 50 mm Nominal Bore Standard Swirly-flo Pipe - With End Taper - W-Velocity at Exit	10-C
0.3 metre pipe X 50 mm Nominal Bore Standard Swirly-flo Pipe - With End Taper - Grid	11-C
0.3 metre pipe X 50 mm Nominal Bore Standard Swirly-flo Pipe - With End Taper - Static Pressure (Pa) at the wall	12-C
0.3 metre pipe X 50 mm Nominal Bore Standard Swirly-flo Pipe - With End Taper - W-velocity (m/s) at J=45 - View 1	13-C
0.3 metre pipe X 50 mm Nominal Bore Standard Swirly-flo Pipe - With End Taper - W-velocity (m/s) at J=45 - View 2	14-C
0.3 metre pipe X 50 mm Nominal Bore Standard Swirly-flo Pipe - With End Taper - W-Velocity at Exit	15-C

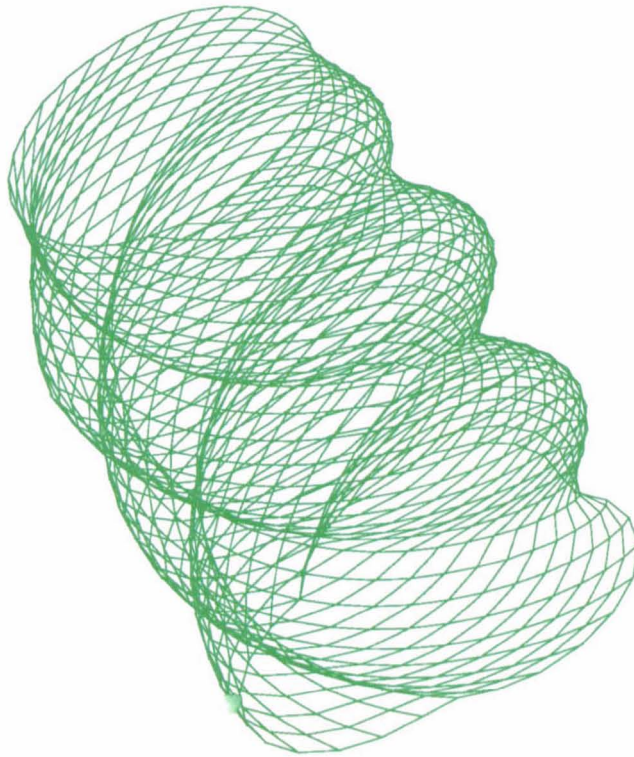
0.4 metre pipe X 50 mm Nominal Bore Standard Swirly-flo Pipe - With End Taper - Grid	16-C
0.4 metre pipe X 50 mm Nominal Bore Standard Swirly-flo Pipe - With End Taper - Static Pressure (Pa) at the wall	17-C
0.4 metre pipe X 50 mm Nominal Bore Standard Swirly-flo Pipe - With End Taper - W-velocity (m/s) at J=45 - View 1	18-C
0.4 metre pipe X 50 mm Nominal Bore Standard Swirly-flo Pipe - With End Taper - W-velocity (m/s) at J=45 - View 2	19-C
0.4 metre pipe X 50 mm Nominal Bore Standard Swirly-flo Pipe - With End Taper - W-Velocity at Exit	20-C
0.5 metre pipe X 50 mm Nominal Bore Standard Swirly-flo Pipe - With End Taper - Grid	21-C
0.5 metre pipe X 50 mm Nominal Bore Standard Swirly-flo Pipe - With End Taper - Static Pressure (Pa) at the wall	22-C
0.5 metre pipe X 50 mm Nominal Bore Standard Swirly-flo Pipe - With End Taper - W-velocity (m/s) at J=45 - View 1	23-C
0.5 metre pipe X 50 mm Nominal Bore Standard Swirly-flo Pipe - With End Taper - W-velocity (m/s) at J=45 - View 2	24-C
0.5 metre pipe X 50 mm Nominal Bore Standard Swirly-flo Pipe - With End Taper - W-Velocity at Exit	25-C
0.6 metre pipe X 50 mm Nominal Bore Standard Swirly-flo Pipe - With End Taper - Grid	26-C
0.6 metre pipe X 50 mm Nominal Bore Standard Swirly-flo Pipe - With End Taper - Static Pressure (Pa) at the wall	27-C
0.6 metre pipe X 50 mm Nominal Bore Standard Swirly-flo Pipe - With End Taper - W-velocity (m/s) at J=23 - View 1	28-C
0.6 metre pipe X 50 mm Nominal Bore Standard Swirly-flo Pipe - With End Taper - W-velocity (m/s) at J=23 - View 2	29-C
0.6 metre pipe X 50 mm Nominal Bore Standard Swirly-flo Pipe - With End Taper - W-Velocity at Exit	30-C

0.7 metre pipe X 50 mm Nominal Bore Standard Swirly-flo Pipe - With End Taper - Grid	31-C
0.7 metre pipe X 50 mm Nominal Bore Standard Swirly-flo Pipe - With End Taper - Static Pressure (Pa) at the wall	32-C
0.7 metre pipe X 50 mm Nominal Bore Standard Swirly-flo Pipe - With End Taper - W-velocity (m/s) at J=23 - View 1	33-C
0.7 metre pipe X 50 mm Nominal Bore Standard Swirly-flo Pipe - With End Taper - W-velocity (m/s) at J=23 - View 2	34-C
0.7 metre pipe X 50 mm Nominal Bore Standard Swirly-flo Pipe - With End Taper - W-Velocity at Exit	35-C
0.8 metre pipe X 50 mm Nominal Bore Standard Swirly-flo Pipe - With End Taper - Grid	36-C
0.8 metre pipe X 50 mm Nominal Bore Standard Swirly-flo Pipe - With End Taper - Static Pressure (Pa) at the wall	37-C
0.8 metre pipe X 50 mm Nominal Bore Standard Swirly-flo Pipe - With End Taper - W-velocity (m/s) at J=23 - View 1	38-C
0.8 metre pipe X 50 mm Nominal Bore Standard Swirly-flo Pipe - With End Taper - W-velocity (m/s) at J=23 - View 2	39-C
0.8 metre pipe X 50 mm Nominal Bore Standard Swirly-flo Pipe - With End Taper - W-Velocity at Exit	40-C
0.9 metre pipe X 50 mm Nominal Bore Standard Swirly-flo Pipe - With End Taper - Grid	41-C
0.9 metre pipe X 50 mm Nominal Bore Standard Swirly-flo Pipe - With End Taper - Static Pressure (Pa) at the wall	42-C
0.9 metre pipe X 50 mm Nominal Bore Standard Swirly-flo Pipe - With End Taper - W-velocity (m/s) at J=23 - View 1	43-C
0.9 metre pipe X 50 mm Nominal Bore Standard Swirly-flo Pipe - With End Taper - W-velocity (m/s) at J=23 - View 2	44-C
0.9 metre pipe X 50 mm Nominal Bore Standard Swirly-flo Pipe - With End Taper - W-Velocity at Exit	45-C

1.0 metre pipe X 50 mm Nominal Bore Standard Swirly-flo Pipe - With End Taper - Grid	46-C
1.0 metre pipe X 50 mm Nominal Bore Standard Swirly-flo Pipe - With End Taper - Static Pressure (Pa) at the wall	47-C
1.0 metre pipe X 50 mm Nominal Bore Standard Swirly-flo Pipe - With End Taper - W-velocity (m/s) at J=23 - View 1	48-C
1.0 metre pipe X 50 mm Nominal Bore Standard Swirly-flo Pipe - With End Taper - W-velocity (m/s) at J=23 - View 2	49-C
1.0 metre pipe X 50 mm Nominal Bore Standard Swirly-flo Pipe - With End Taper - W-Velocity at Exit	50-C
0.2 Pipe X 50 mm Bore Brachistochrone - With End Taper - Grid	51-C
0.2 Pipe X 50 mm Bore Brachistochrone - With End Taper - Static Pressure (Pa) at the wall	52-C
0.2 Pipe X 50 mm Bore Brachistochrone - With End Taper W-velocity (m/s) at J=45 - View 1	53-C
0.2 Pipe X 50 mm Bore Brachistochrone - With End Taper - W-velocity (m/s) at J=45 - View 2	54-C
0.2 Pipe X 50 mm Bore Brachistochrone - With End Taper - With End Taper - W-Velocity at Exit	55-C
0.3 Pipe X 50 mm Bore Brachistochrone - With End Taper - Grid	56-C
0.3 Pipe X 50 mm Bore Brachistochrone - With End Taper - Static Pressure (Pa) at the wall	57-C
0.3 Pipe X 50 mm Bore Brachistochrone - With End Taper W-velocity (m/s) at J=45 - View 1	58-C
0.3 Pipe X 50 mm Bore Brachistochrone - With End Taper - W-velocity (m/s) at J=45 - View 2	59-C
0.3 Pipe X 50 mm Bore Brachistochrone - With End Taper - W-Velocity at Exit	60-C

0.4 Pipe X 50 mm Bore Brachistochrone - With End Taper - Grid	61-C
0.4 Pipe X 50 mm Bore Brachistochrone - With End Taper - Static Pressure (Pa) at the wall	62-C
0.4 Pipe X 50 mm Bore Brachistochrone - With End Taper W-velocity (m/s) at J=45 - View 1	63-C
0.4 Pipe X 50 mm Bore Brachistochrone - With End Taper - W-velocity (m/s) at J=45 - View 2	64-C
0.4 Pipe X 50 mm Bore Brachistochrone - With End Taper - With End Taper - W-Velocity at Exit	65-C
0.5 Pipe X 50 mm Bore Brachistochrone - With End Taper - Grid	66-C
0.5 Pipe X 50 mm Bore Brachistochrone - With End Taper - Static Pressure (Pa) at the wall	67-C
0.5 Pipe X 50 mm Bore Brachistochrone - With End Taper W-velocity (m/s) at J=45 - View 1	68-C
0.5 Pipe X 50 mm Bore Brachistochrone - With End Taper - W-velocity (m/s) at J=45 - View 2	69-C
0.5 Pipe X 50 mm Bore Brachistochrone -With End Taper - W-Velocity at Exit	70-C
0.4 metre pipe X 50 mm Nominal Bore Standard Swirly-flo Pipe - Without End Taper - Grid	71-C
0.4 metre pipe X 50 mm Nominal Bore Standard Swirly-flo Pipe - Without End Taper - Static Pressure (Pa) at the wall	72-C
0.4 metre pipe X 50 mm Nominal Bore Standard Swirly-flo Pipe - Without End Taper - W-velocity (m/s) at J=45 - View 1	73-C
0.4 metre pipe X 50 mm Nominal Bore Standard Swirly-flo Pipe - Without End Taper - W-velocity (m/s) at J=45 - View 2	74-C
0.4 metre pipe X 50 mm Nominal Bore Standard Swirly-flo Pipe - Without End Taper - W-Velocity at Exit	75-C
0.4 Pipe X 50 mm Bore Brachistochrone - Without End Taper - Grid	76-C

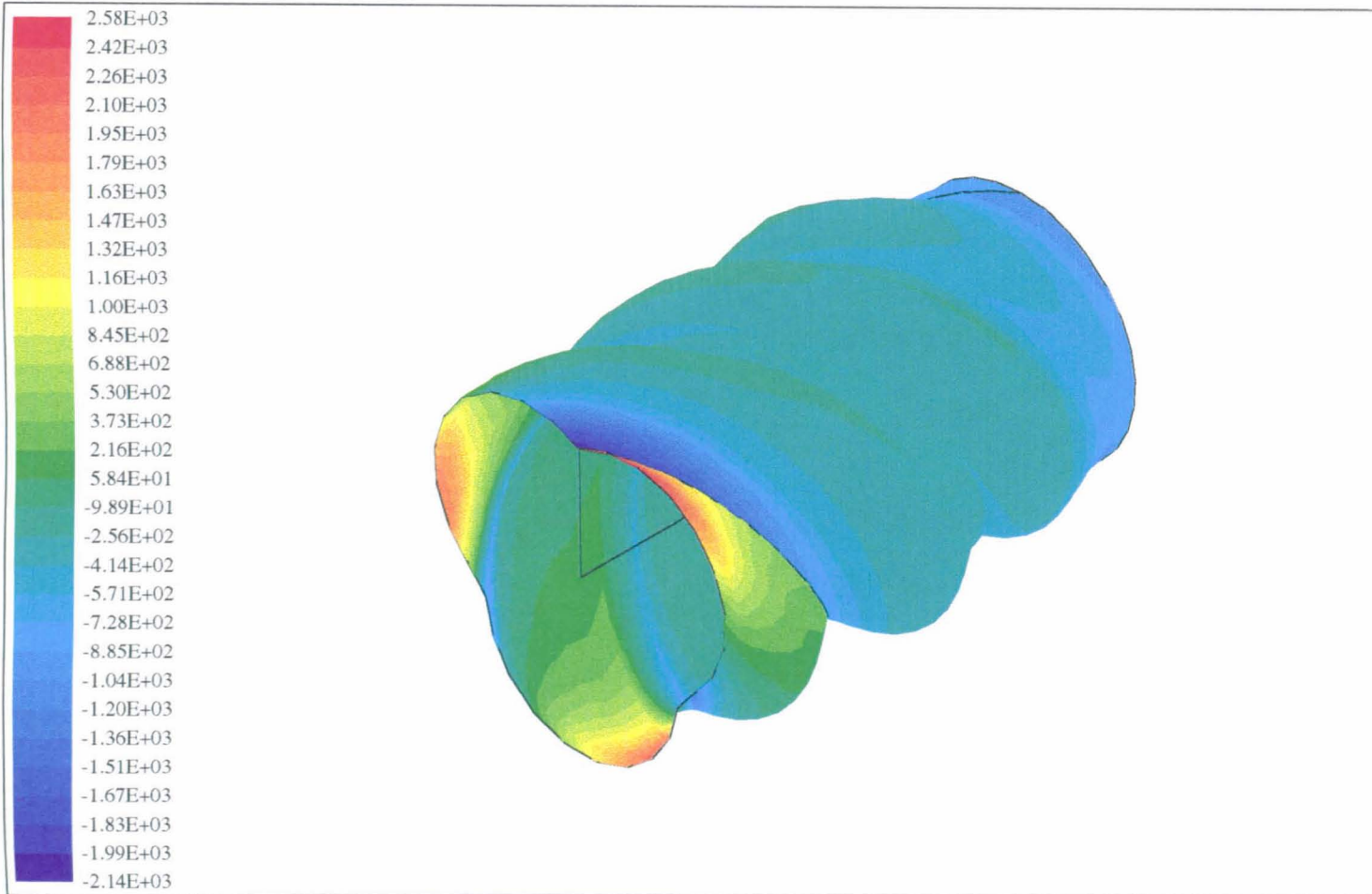
0.4 Pipe X 50 mm Bore Brachistochrone - Without End Taper - Static Pressure (Pa) at the wall	77-C
0.4 Pipe X 50 mm Bore Brachistochrone - Without End Taper W-velocity (m/s) at J=23 - View 1	78-C
0.4 Pipe X 50 mm Bore Brachistochrone - Without End Taper - W-velocity (m/s) at J=23 - View 2	79-C
0.4 Pipe X 50 mm Bore Brachistochrone - Without End Taper - W-Velocity at Exit	80-C



0.1 M Pipe X 50 mm Nominal Bore Standard Swirly-flo Grid
With End Taper Grid (30 X 50 X 40)

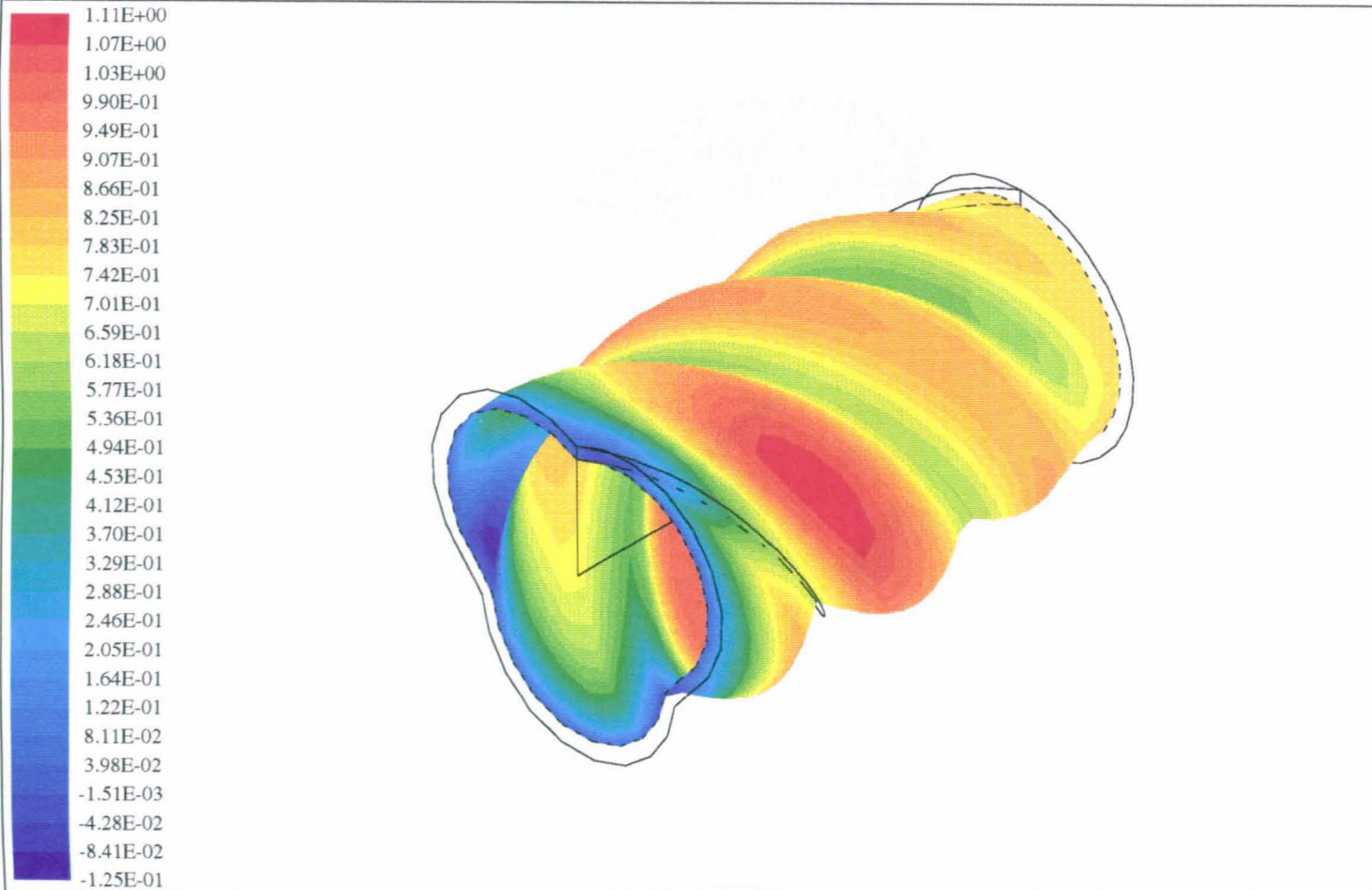


2-C



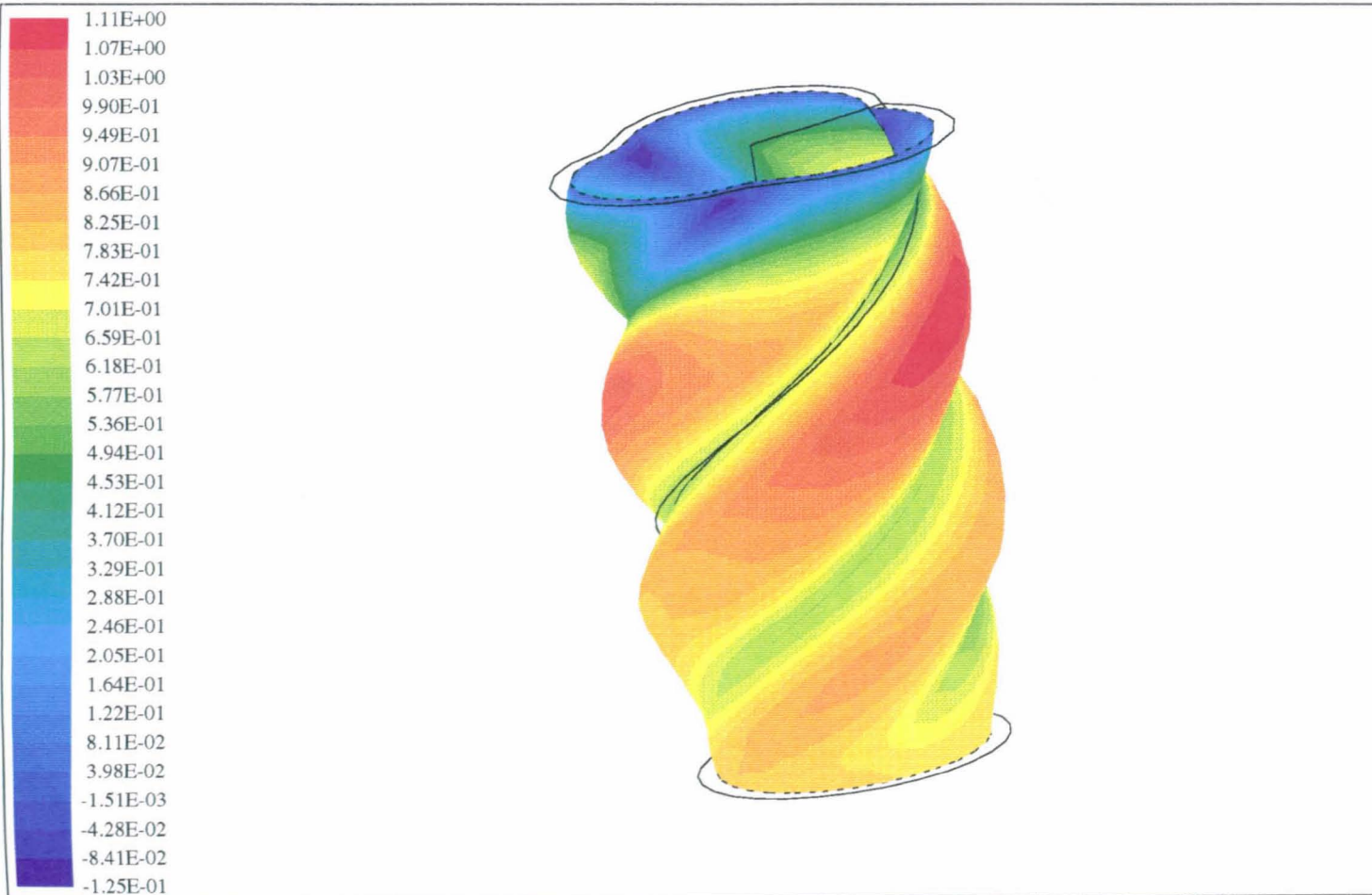
0.1 M Pipe X 50 mm Nominal Bore Standard Swirly-flo Pipe
With End Taper Static Pressure (Pa) at the Wall
Lmax = 2.576E+03 Lmin = -2.144E+03

3-C



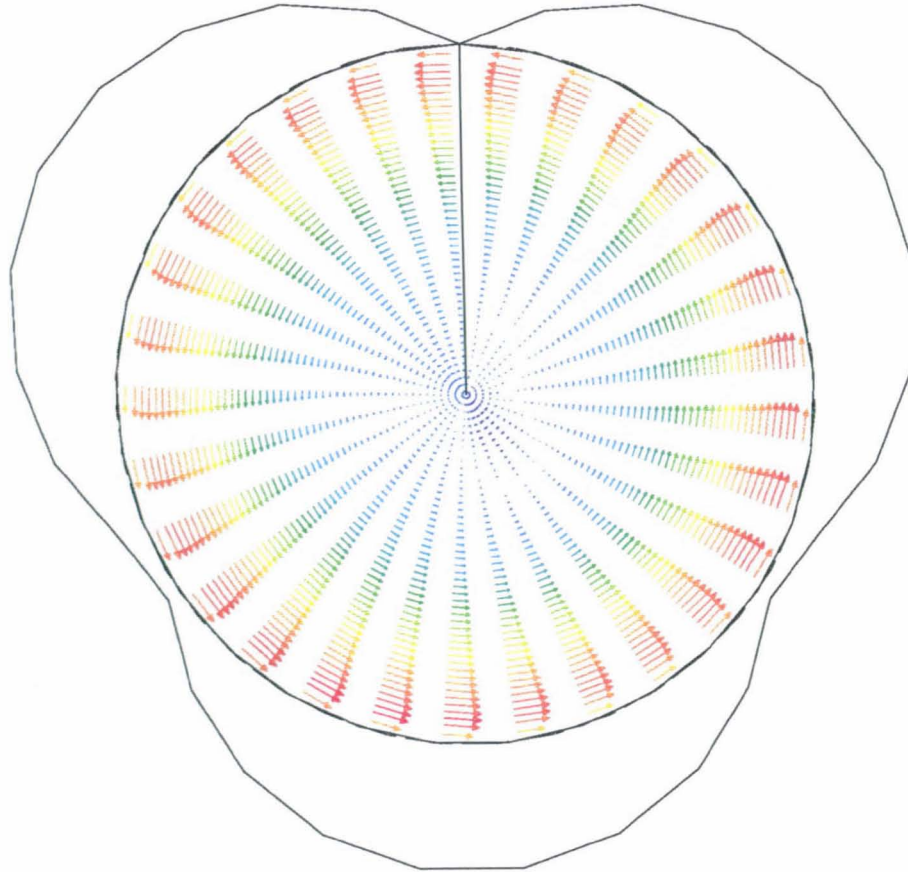
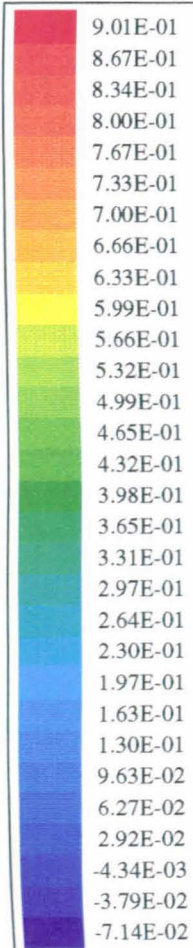
0.1 M Pipe X 50 mm Nominal Bore Standard Swirly-flo Pipe
With End Taper W-Velocity (M/S) at J=45- View 1
Lmax = 1.114E+00 Lmin = -1.254E-01

4-C

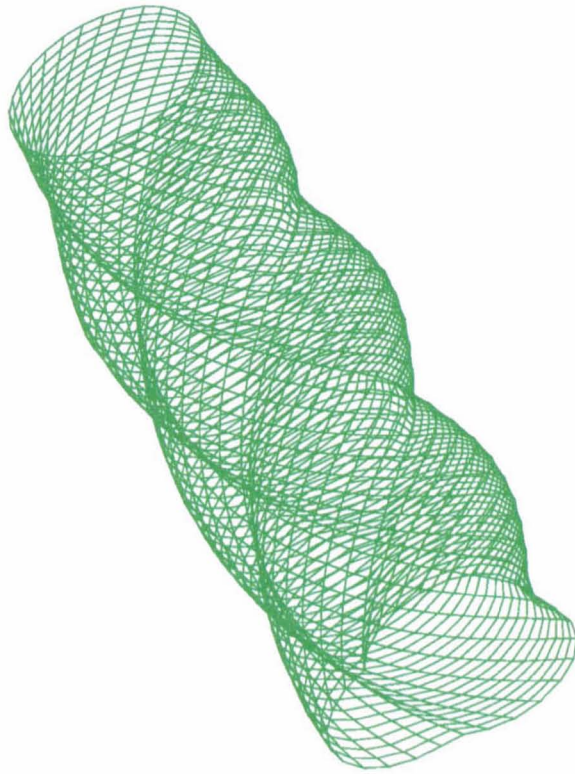


0.1 M Pipe X 50 mm Nominal Bore Standard Swirly-flo Pipe
With End Taper W-Velocity (M/S) at J=45- View 2
Lmax = 1.114E+00 Lmin = -1.254E-01

S-C



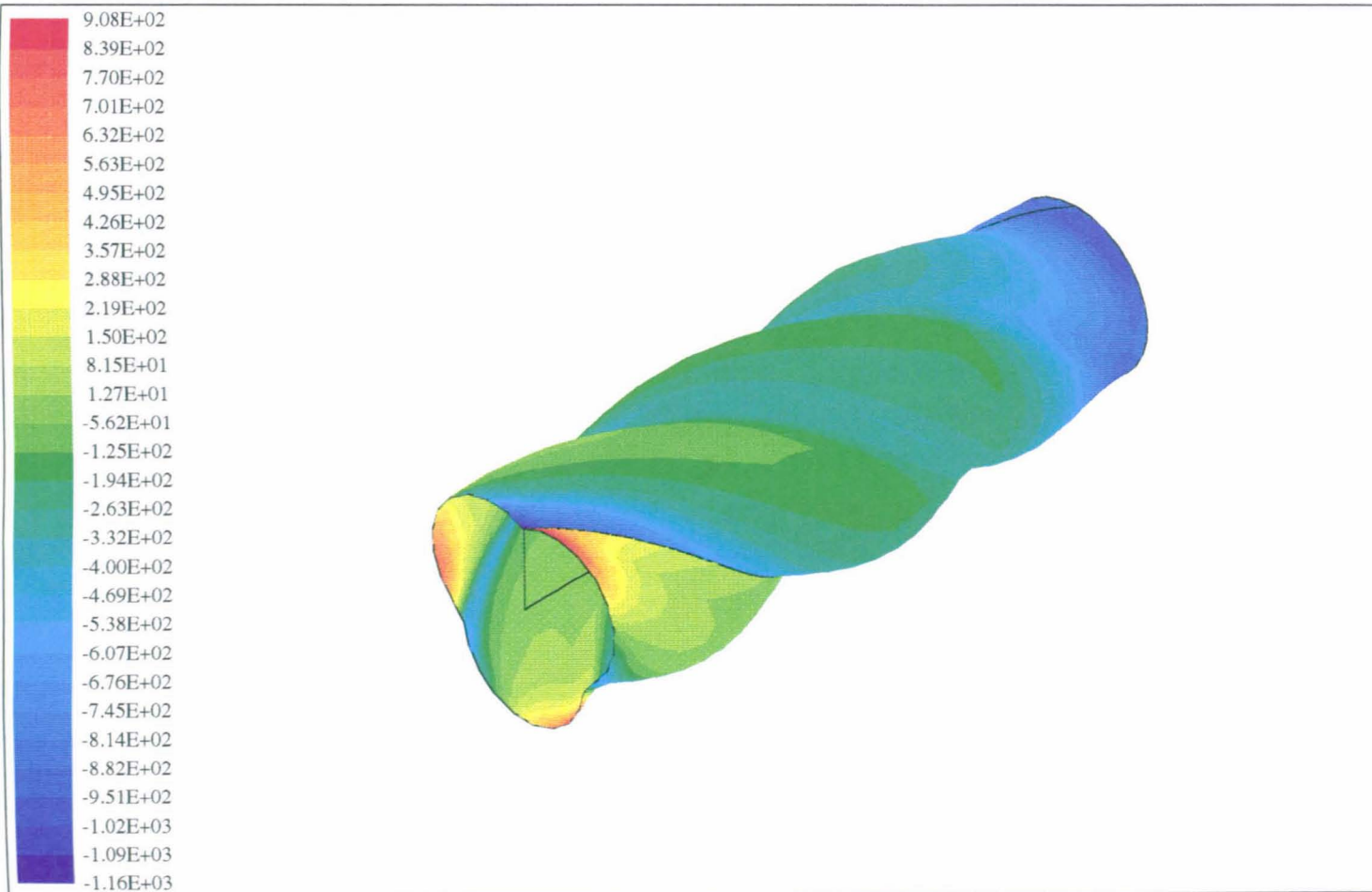
0.1 M Pipe X 50 mm Nominal Bore Standard Swirly-flo Pipe
With End Taper W-Velocity (M/S) at Exit
Lmax = 9.010E-01 Lmin = -7.140E-02



0.2 M PIPE X 50 mm Bore Standard Swirly-flo
With End Taper Grid (30 X 50 X 80)

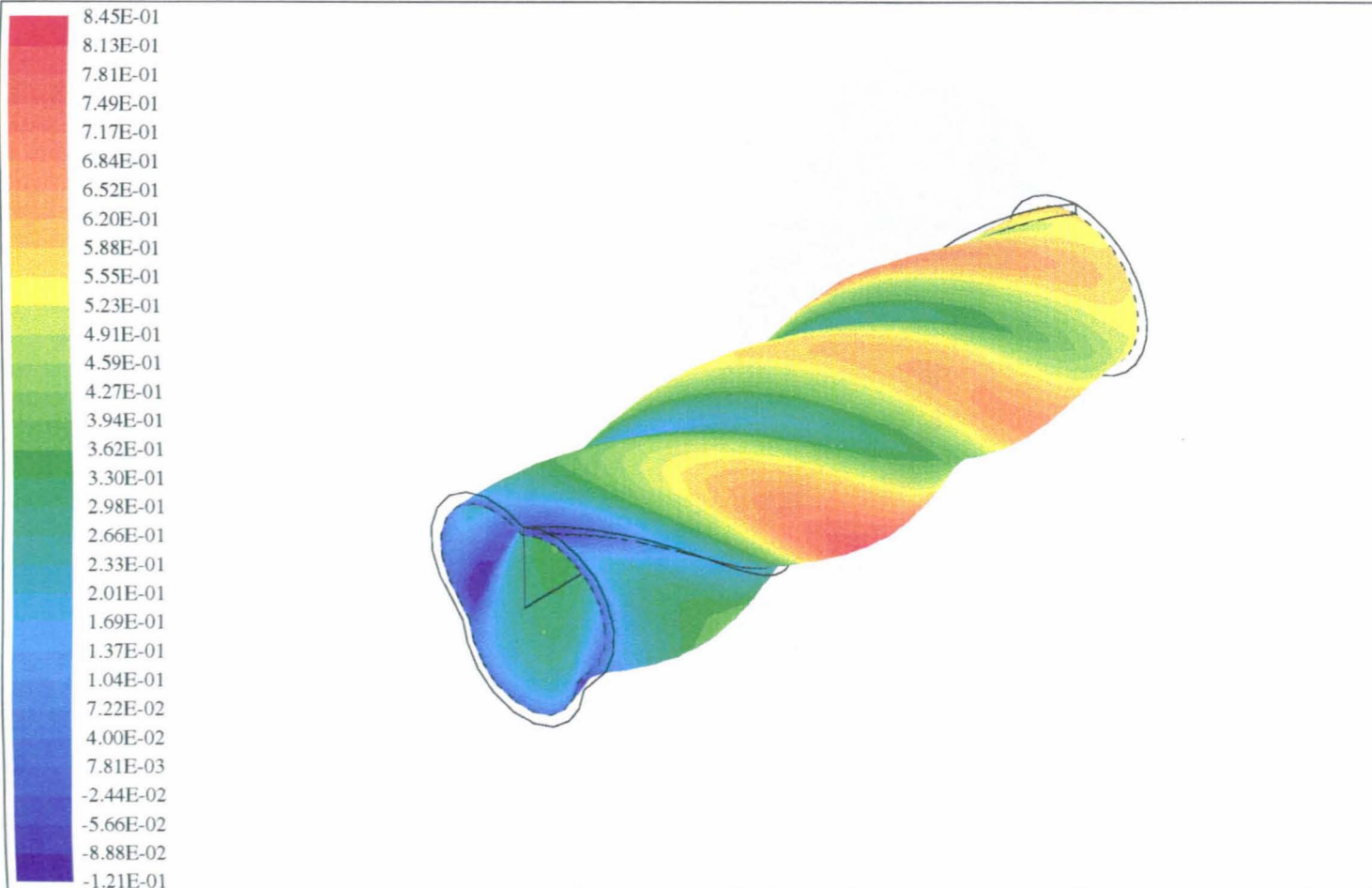


7-C



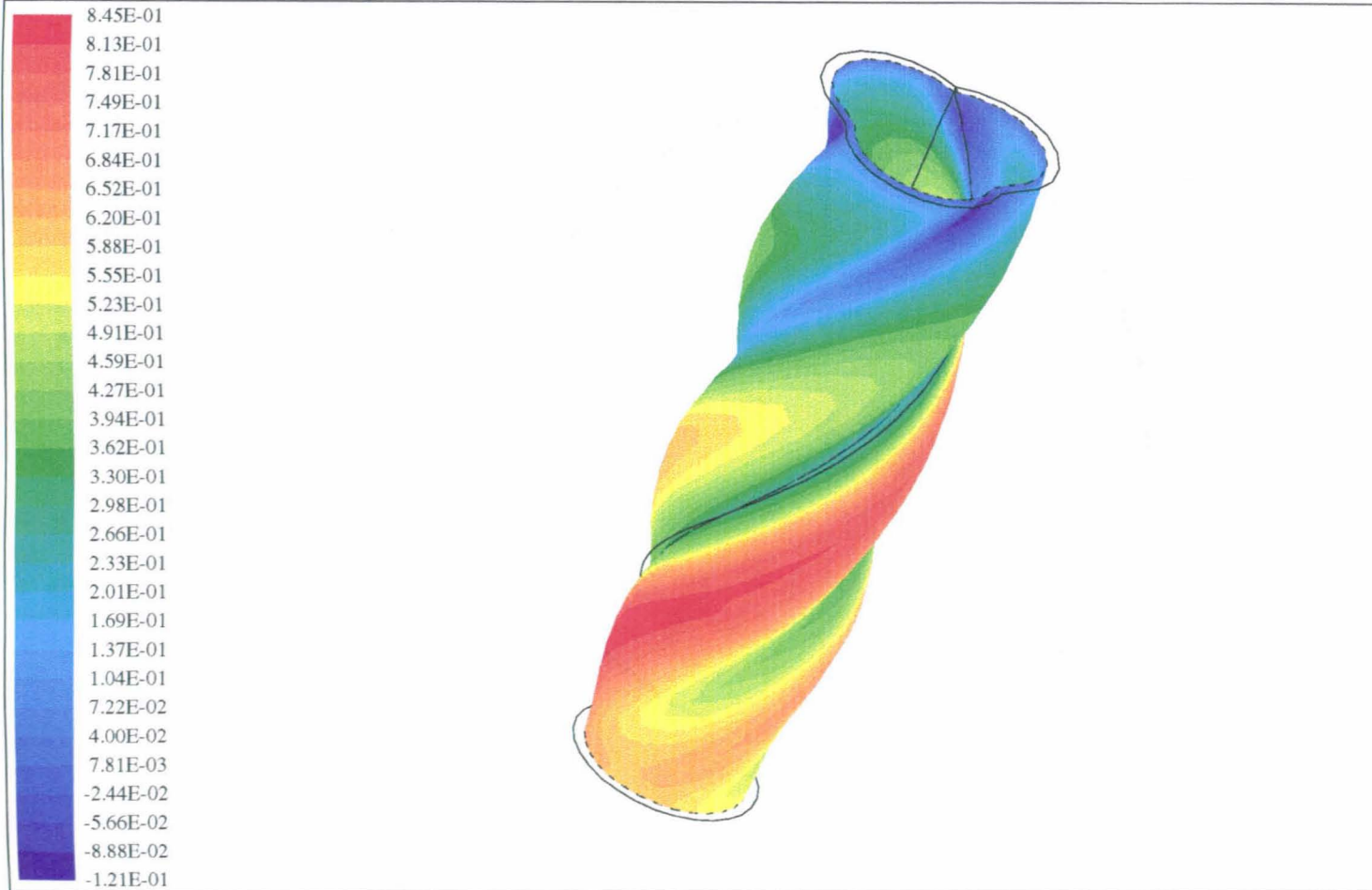
0.2 M PIPE X 50 mm Bore Standard Swirly-flo Pipe
With End Taper Static Pressure (Pa) at the Wall
Lmax = 9.077E+02 Lmin = -1.158E+03

8-C



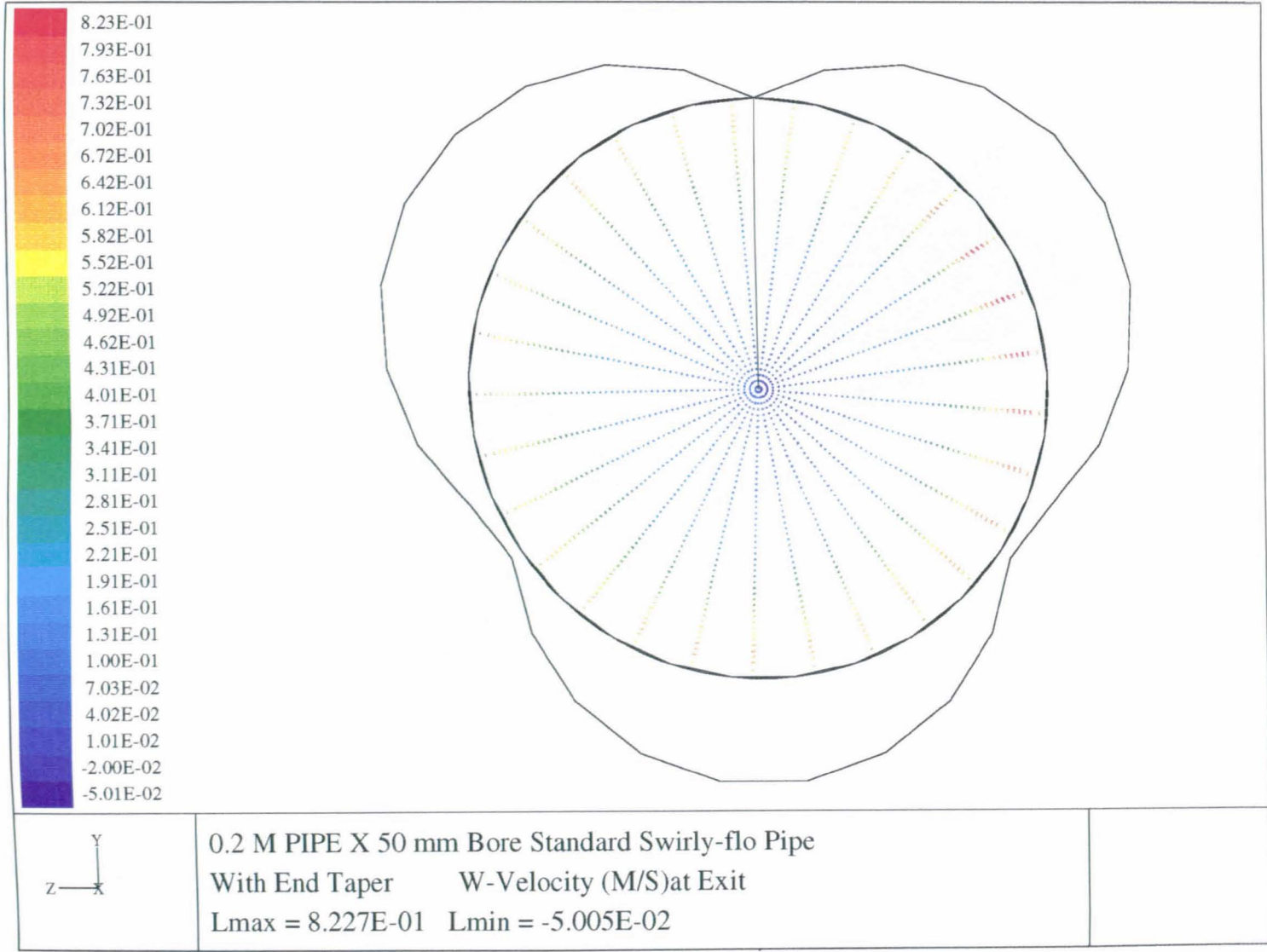
0.2 M PIPE X 50 mm Bore Standard Swirly-flo Pipe
With End Taper W-Velocity (M/S)at J=45- View 1
Lmax = 8.454E-01 Lmin = -1.210E-01

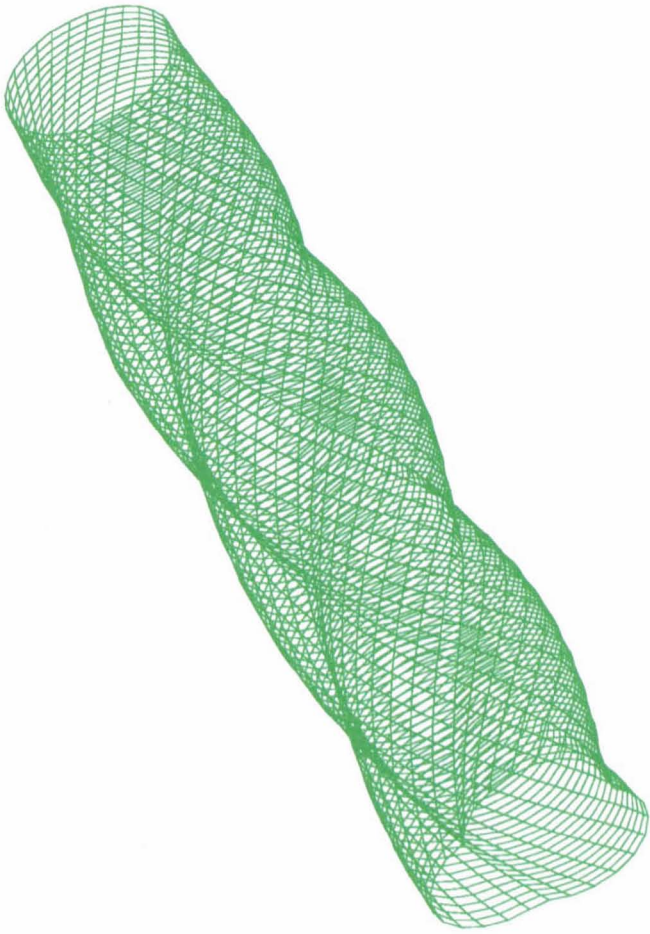
9-C



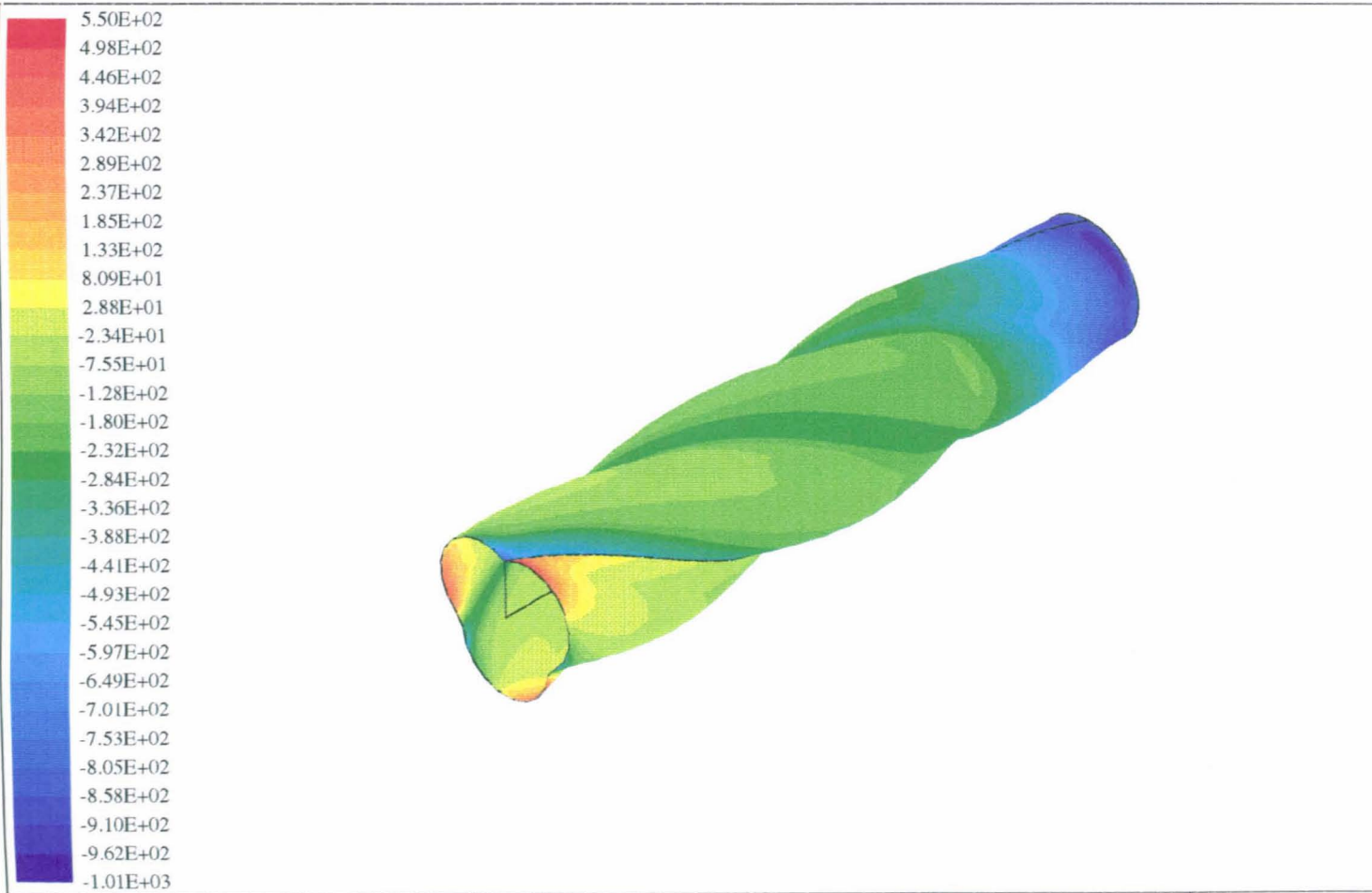
0.2 M PIPE X 50 mm Bore Standard Swirly-flo
With End Taper W-Velocity (M/S) at J=45- View 2
Lmax = 8.454E-01 Lmin = -1.210E-01

10-C



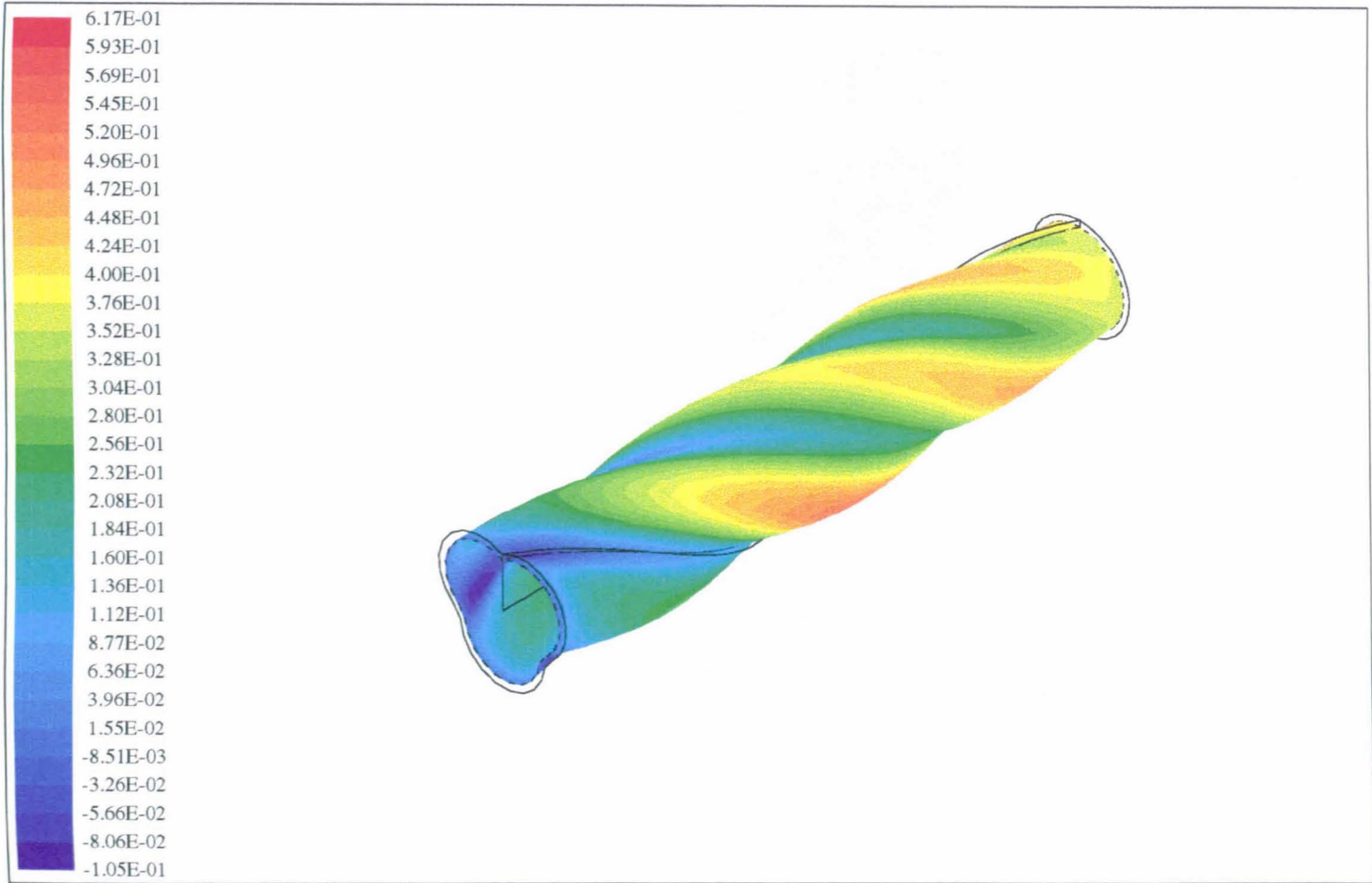
	<p>0.3 M Pipe X 50 mm Bore Standard Swirly-flo Pipe With End Taper Grid (30 X 50 X 120)</p>	
--	--	---

12-C



0.3 M Pipe X 50 mm Bore Standard Swirly-flo Pipe
With End Taper Static Pressure (Pa)
Lmax = 5.502E+02 Lmin = -1.014E+03

13-C



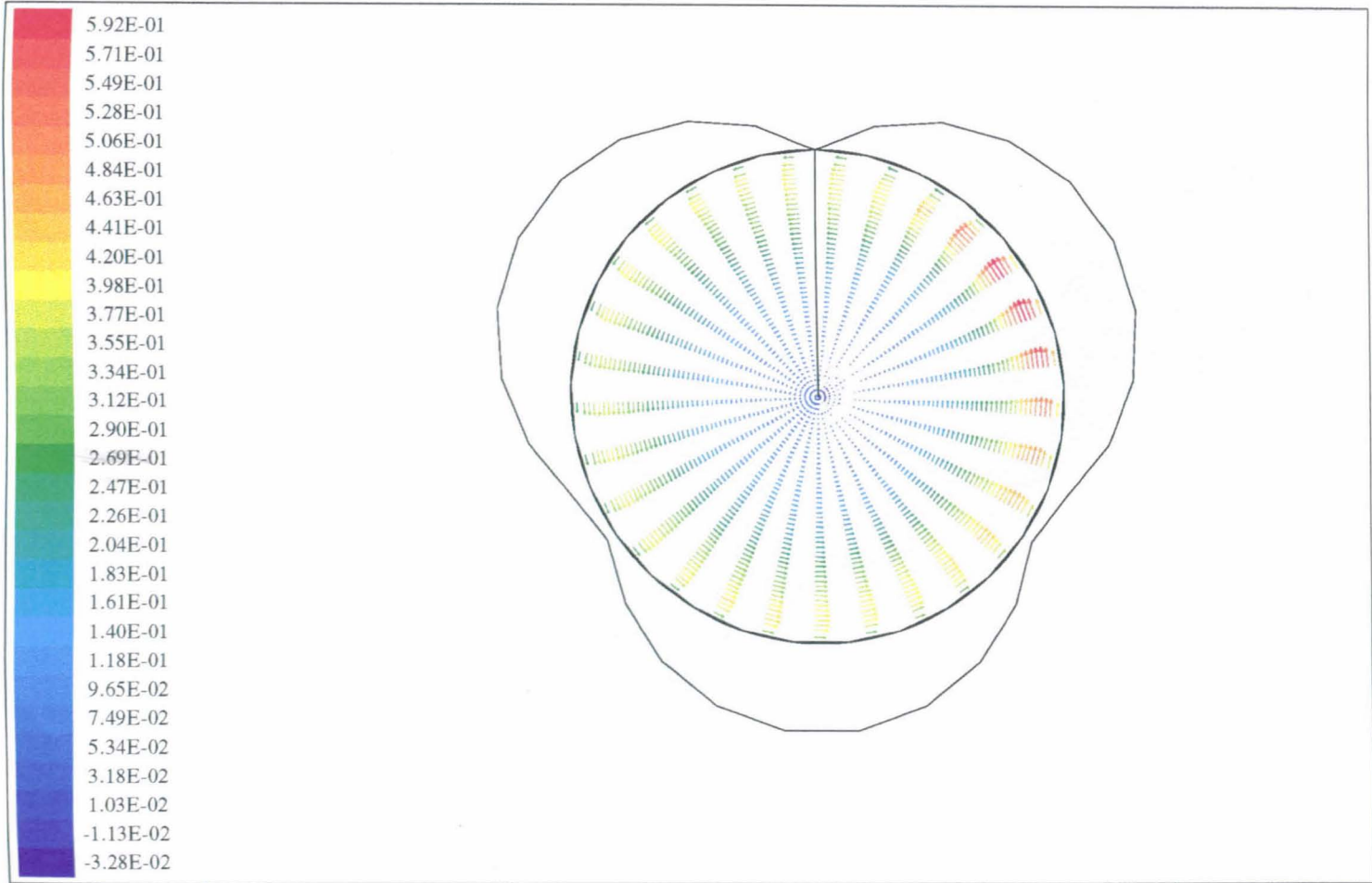
0.3 M Pipe X 50 mm Bore Standard SWirly-flo Pipe
With End Taper W-Velocity (M/S)at J=45- View 1
Lmax = 6.167E-01 Lmin = -1.047E-01

14-C

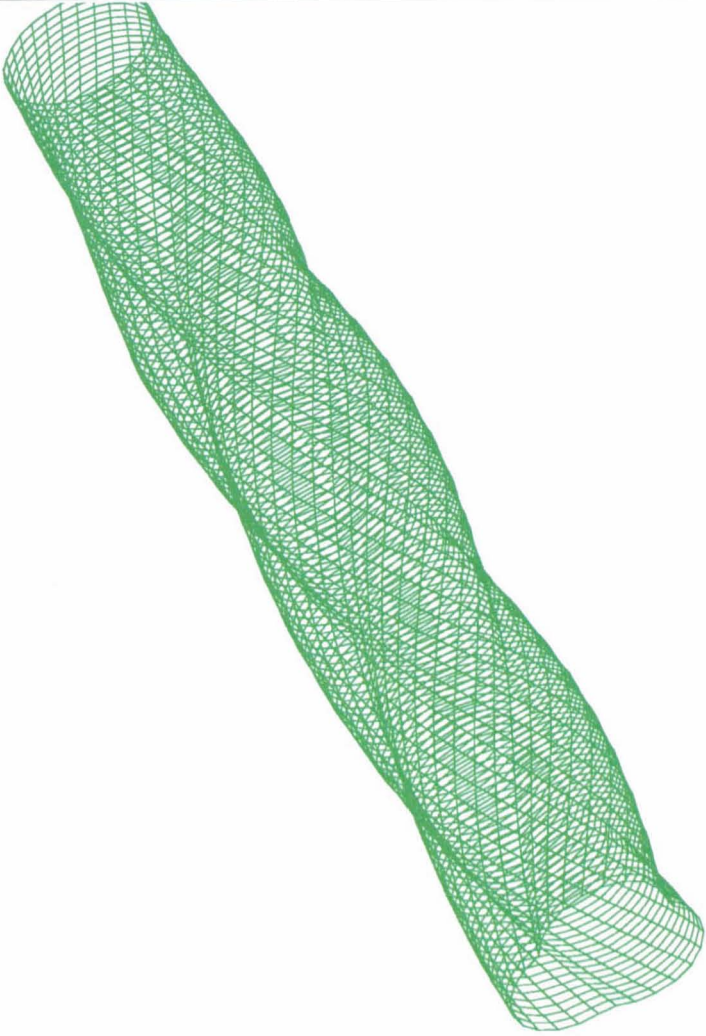


0.3 M Pipe X 50 mm Bore Standard Swirly-flo Pipe
With End Taper W-Velocity (M/S) at J=45- View 2
Lmax = 6.167E-01 Lmin = -1.047E-01

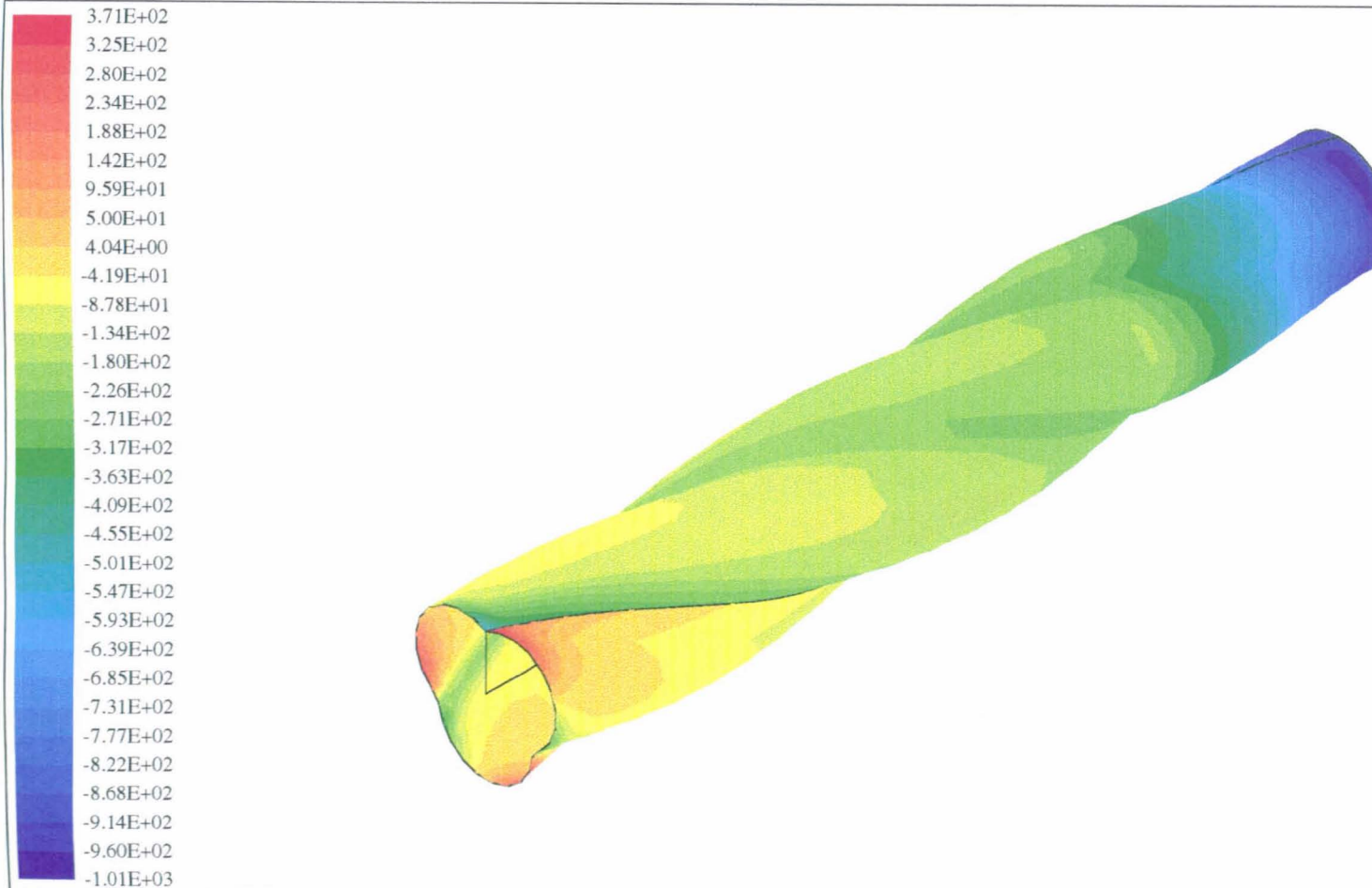
IS-C



0.3 M Pipe X 50 mm Bore Standard Swirly-flo Pipe
With End Taper W-Velocity (M/S)at Exit
Lmax = 5.922E-01 Lmin = -3.283E-02

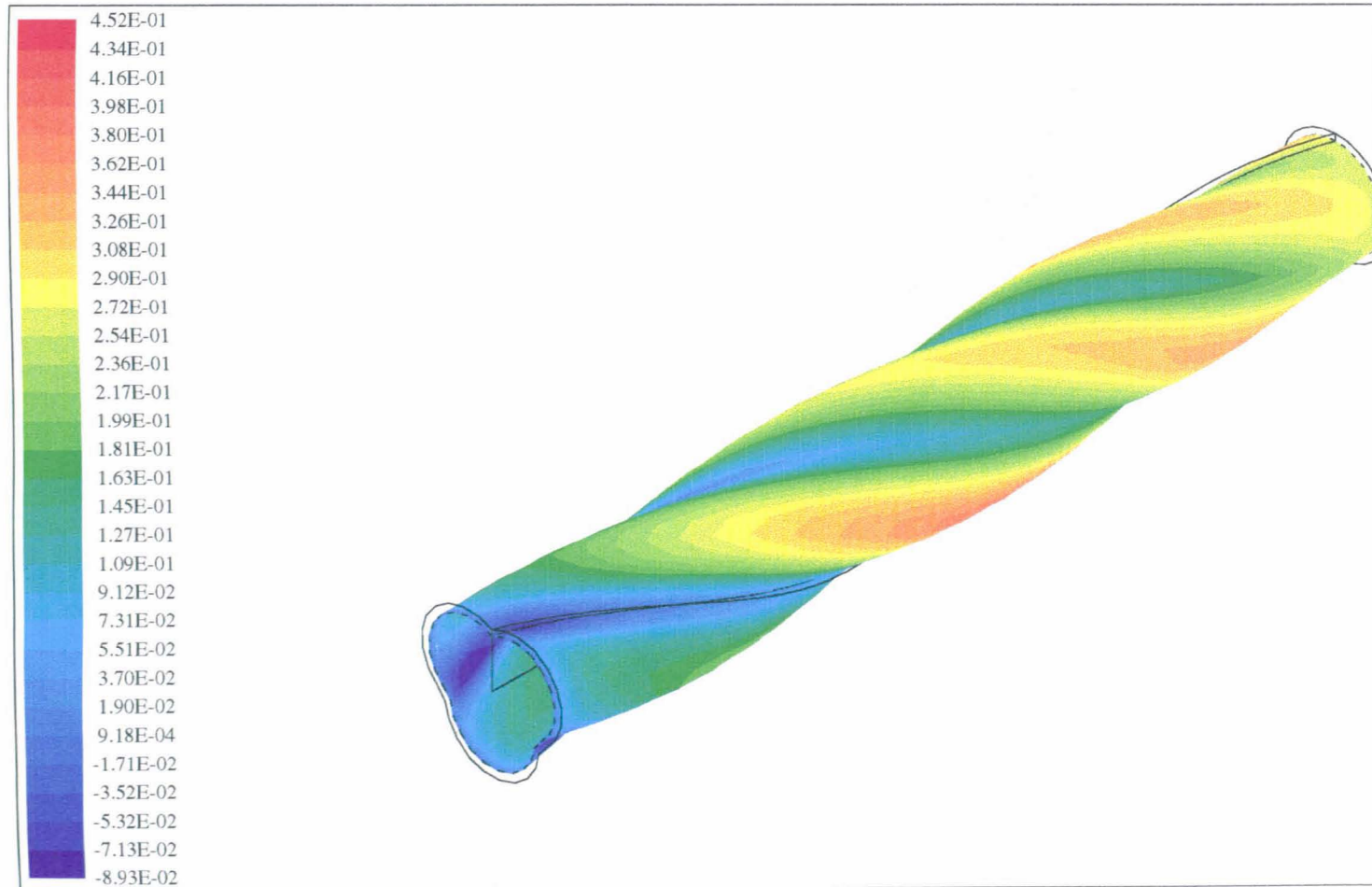
	<p data-bbox="1159 766 1241 1594">0.4M Pipe X 50 mm Nominal Bore Standard Swirly-flo Grid With End Taper Grid (30 X 50 X 140)</p> 
---	--

17-C



0.4 M Pipe X 50 mm Nominal Bore Standard Swirly-flo Pipe
With End Taper Static Pressure (Pa)at the Wall
Lmax = 3.714E+02 Lmin = -1.006E+03

18-C



0.4 M Pipe X 50 mm Nominal Bore Standard Swirly-flo Pipe

W-Velocity (M/S)at J=45- View 1

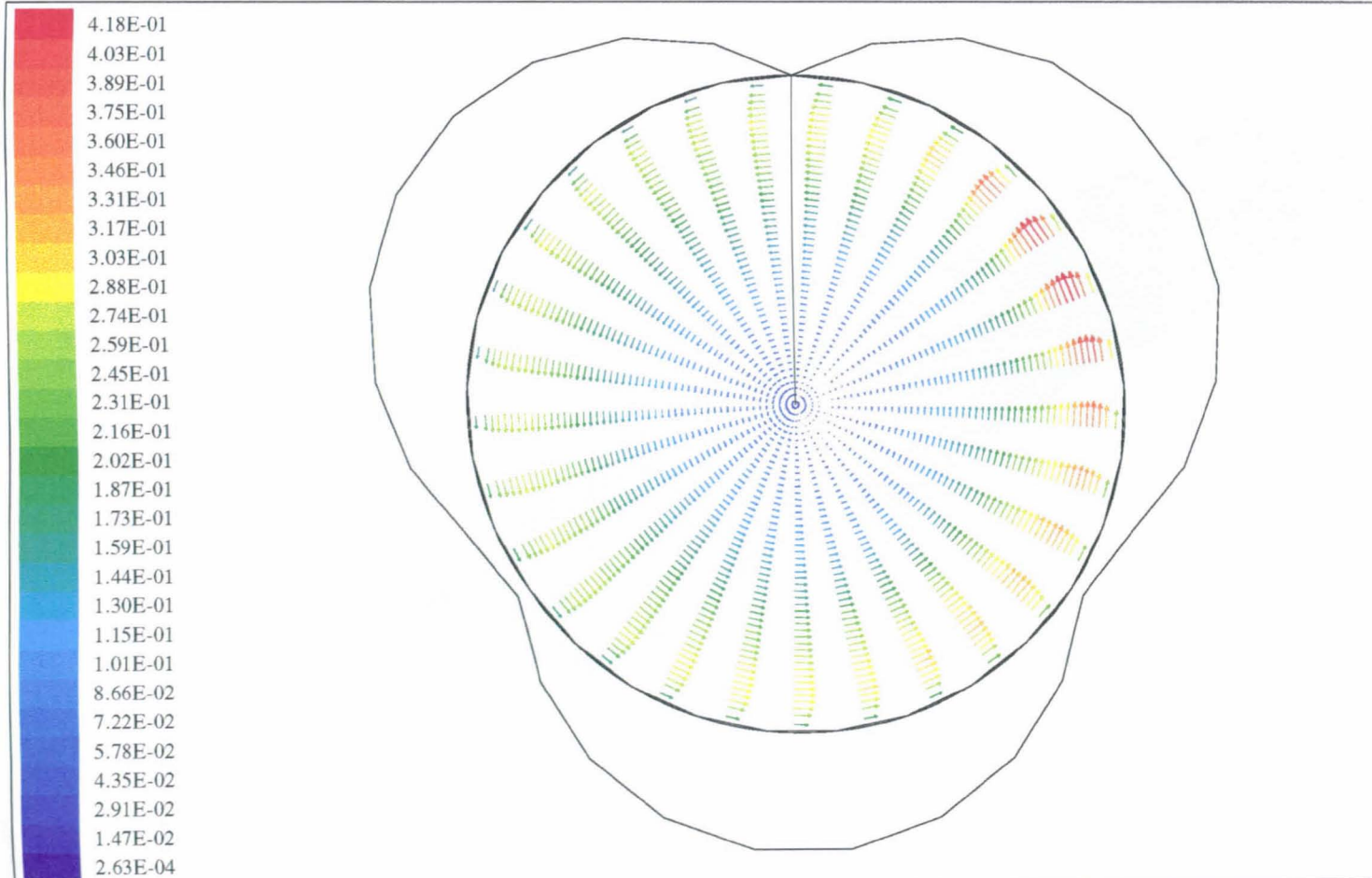
Lmax = 4.521E-01 Lmin = -8.932E-02

19-C

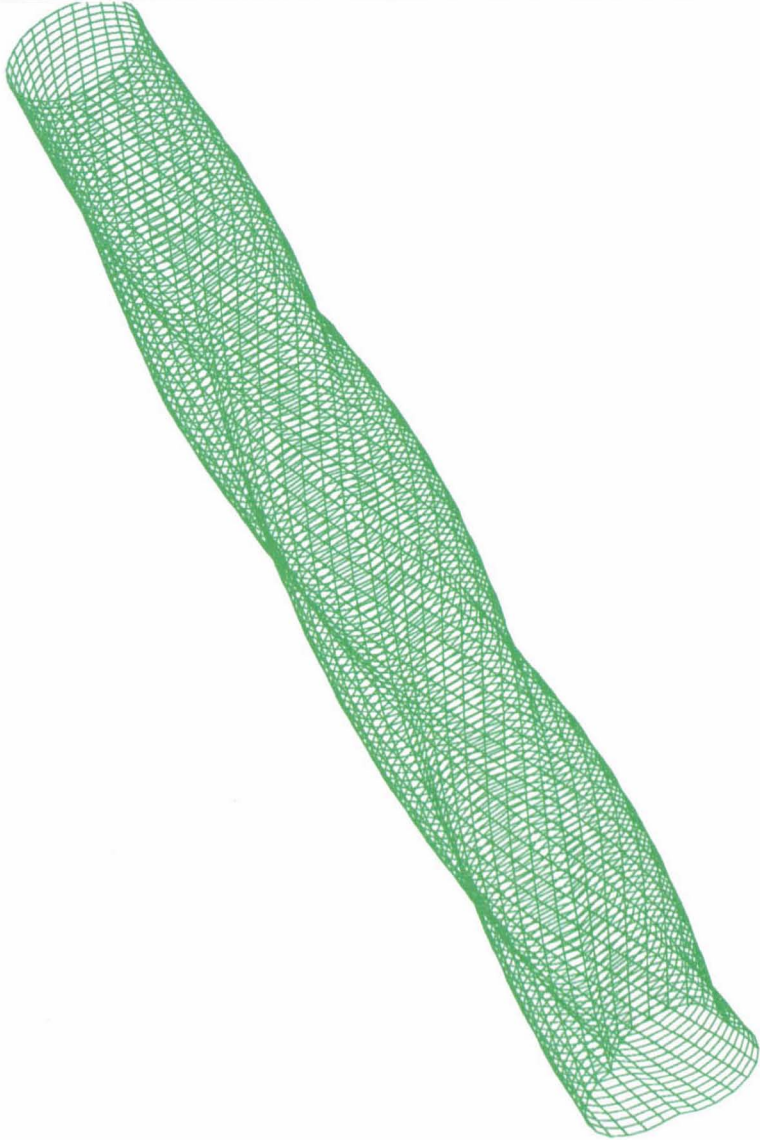


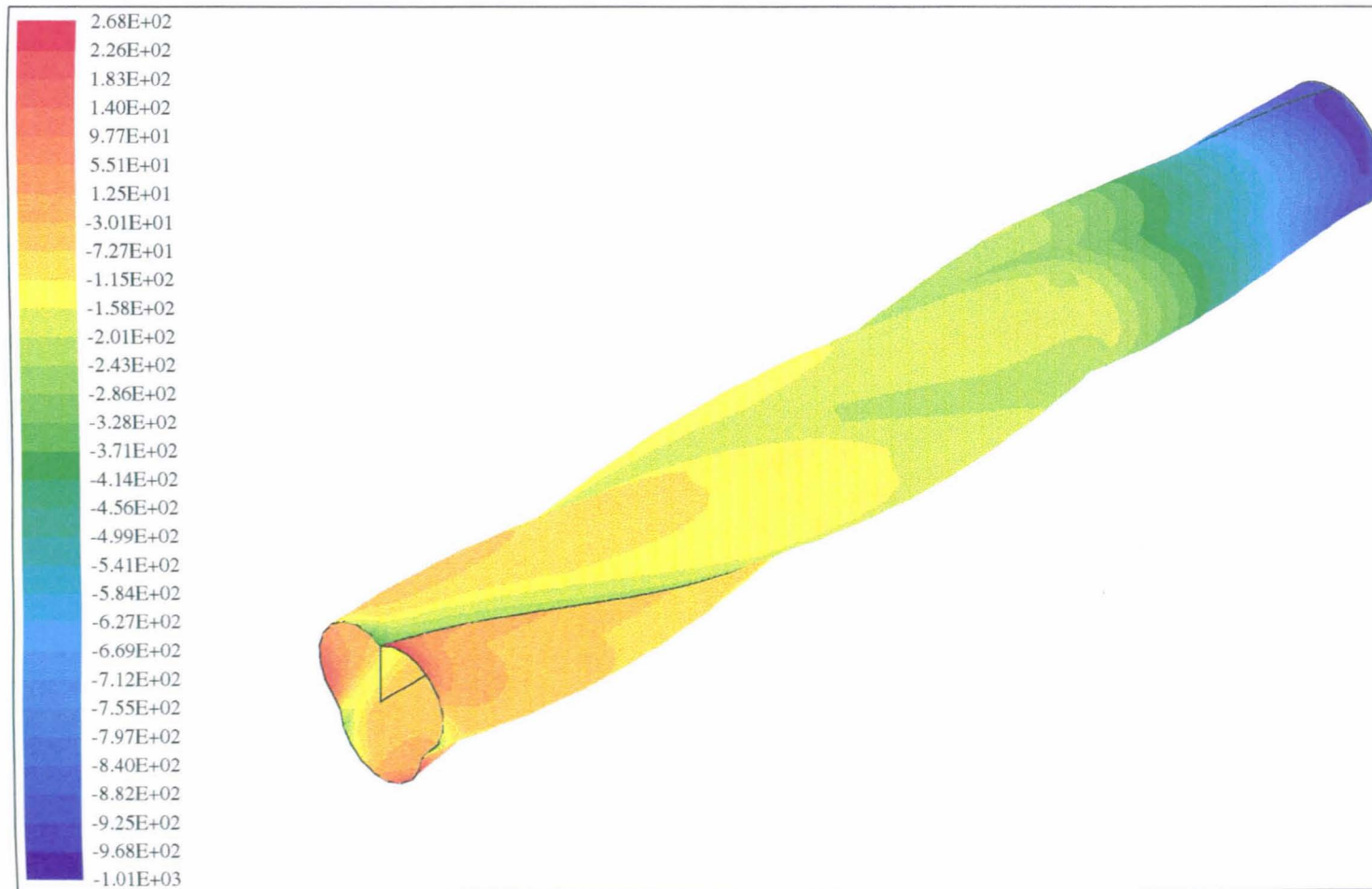
0.4 M Pipe X 50 mm Nominal Bore Standard Swirly-flo Pipe
With End Taper W-Velocity (M/S) at J=45- View 2
Lmax = 4.521E-01 Lmin = -8.932E-02

20-C



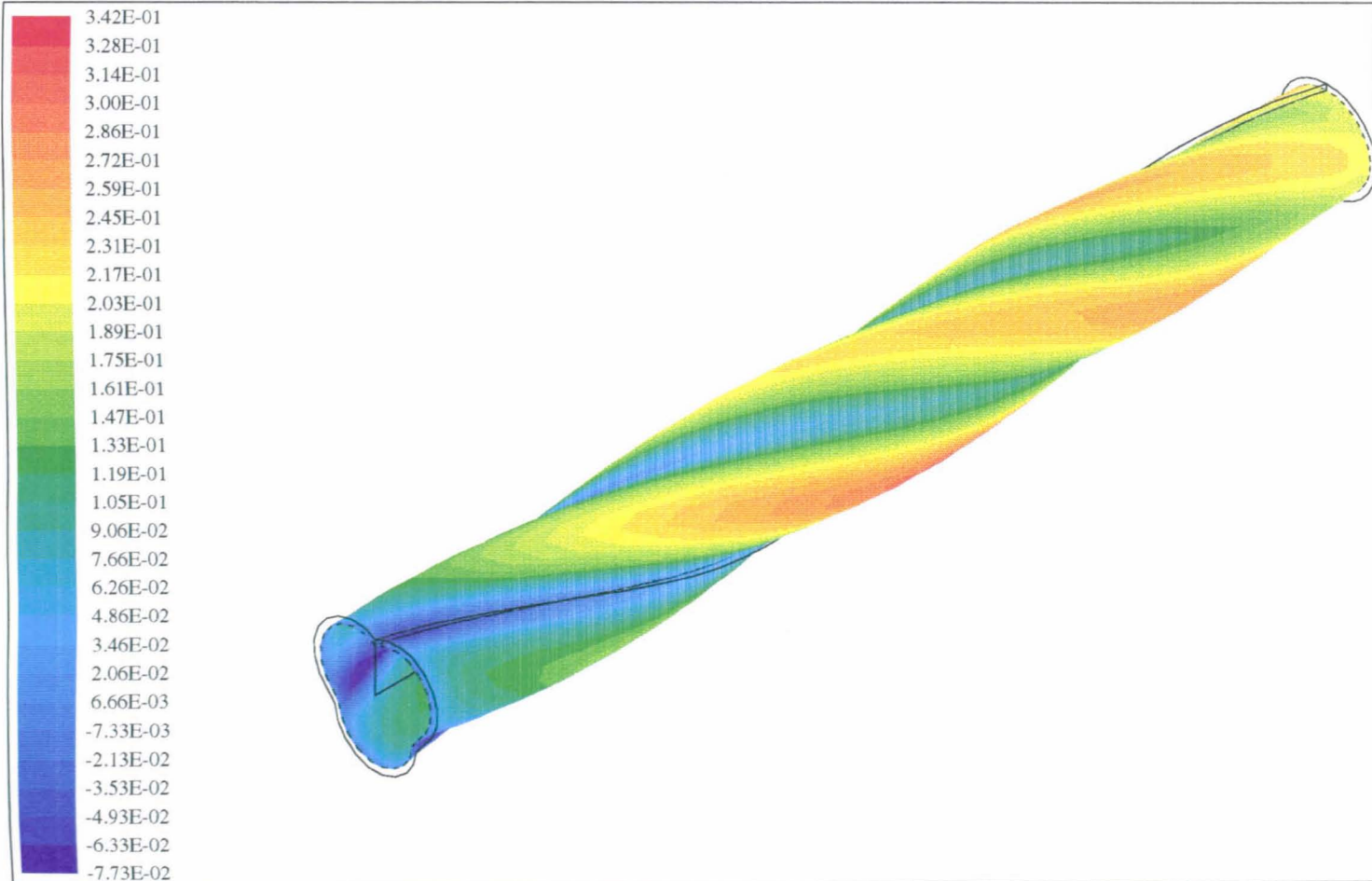
0.4 M Pipe X 50 mm Nominal Bore Standard Swirly-flo Pipe
With End Taper W-Velocity (M/S)at Exit
Lmax = 4.178E-01 Lmin = 2.635E-04

	<p>0.5 M Pipe X 50 mm Nominal Bore Standard Swirly-flo Pipe With End Taper Grid (30 X 50 X 150)</p>	
---	--	---



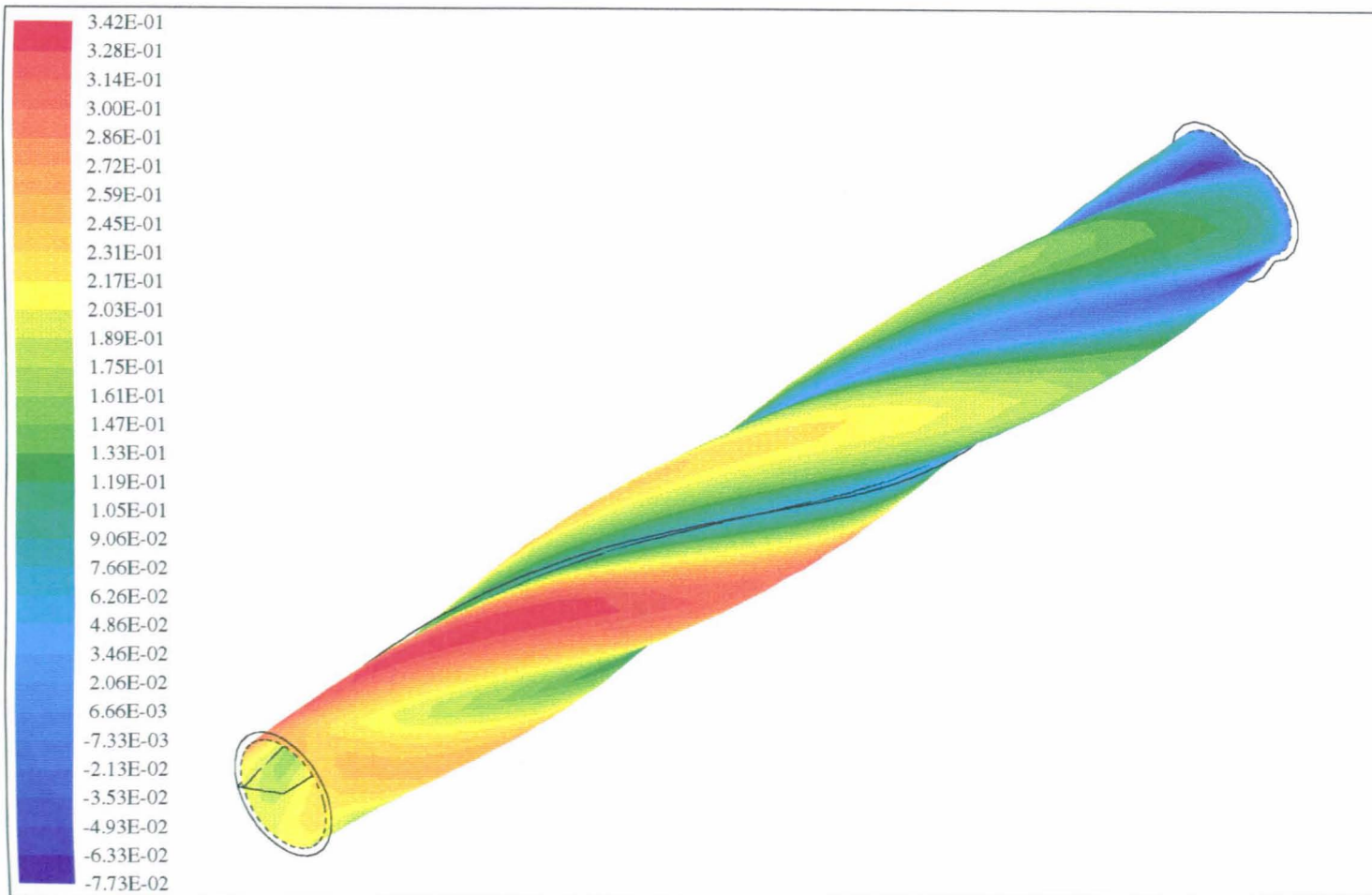
0.5 M Pipe X 50 mm Nominal Bore Standard Swirly-flo Pipe
 With End Taper Static Pressure (Pa) at Exit
 Lmax = 2.682E+02 Lmin = -1.010E+03

23-C



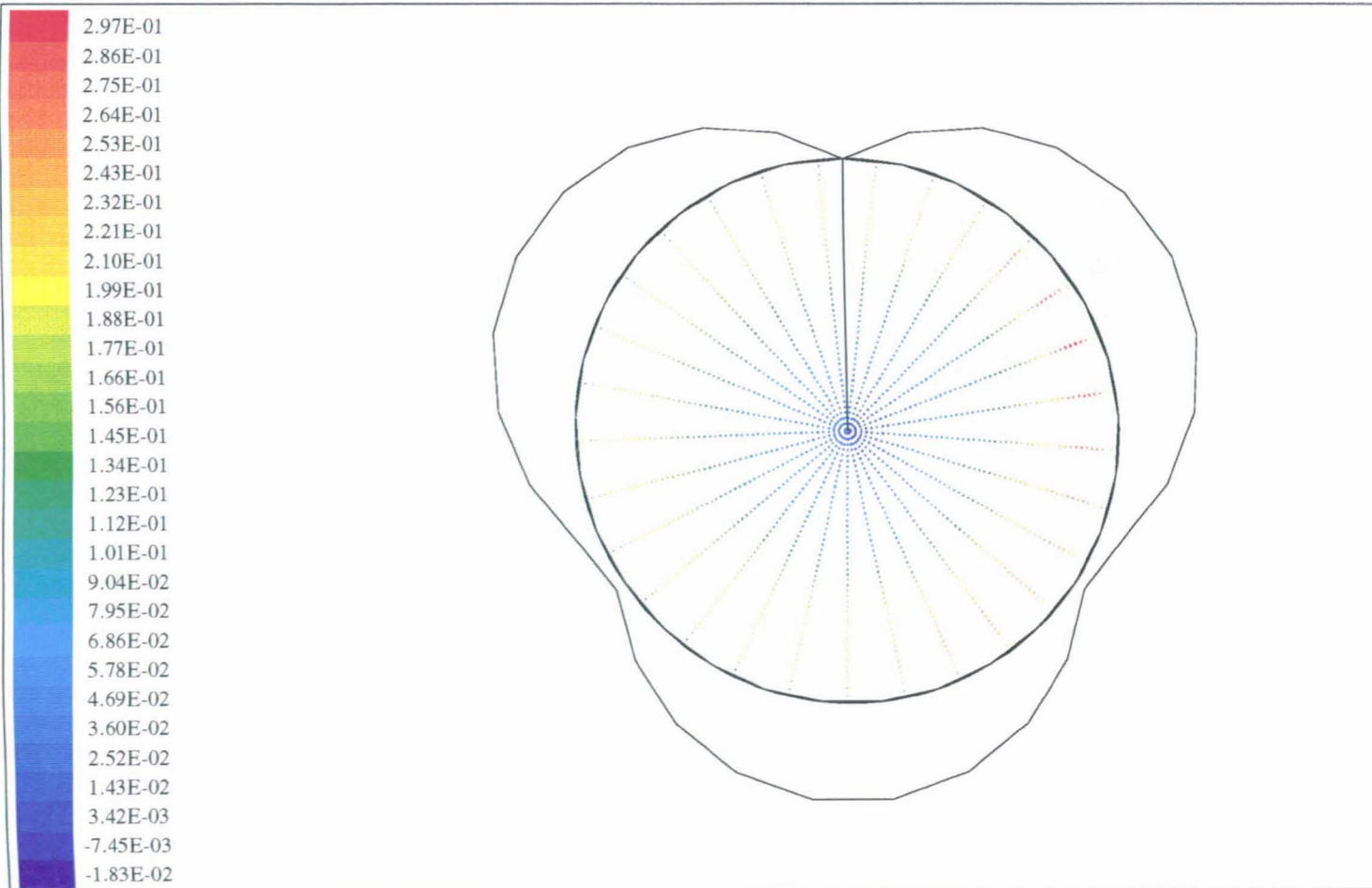
0.5 M Pipe X 50 mm Nominal Bore Standard Swirly-flo Pipe
With End Taper W-Velocity (M/S) at J=45- View 1
Lmax = 3.424E-01 Lmin = -7.729E-02

24-C

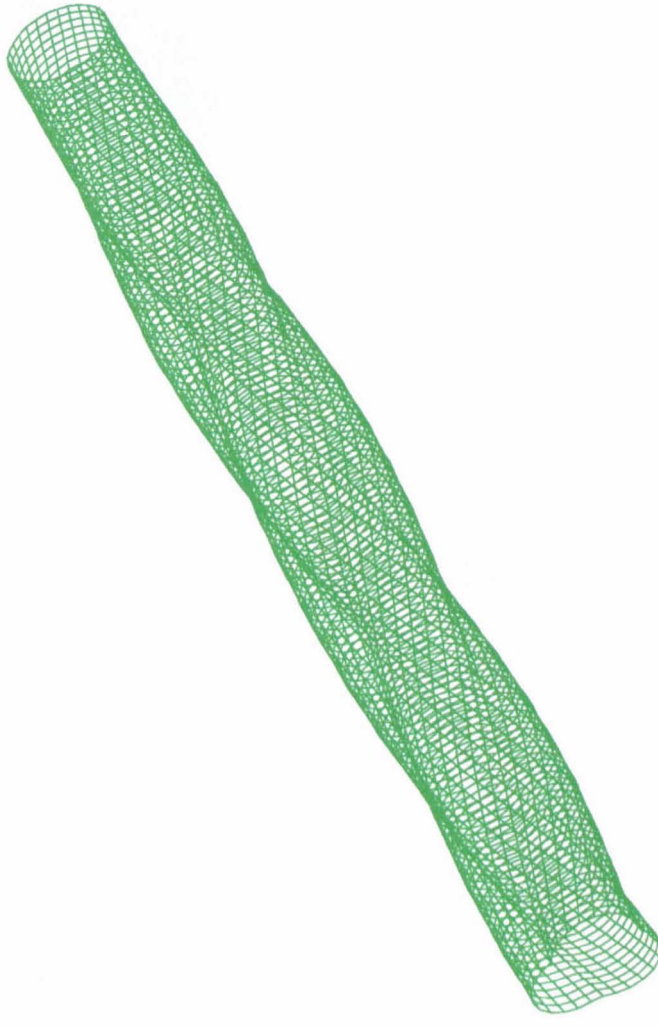


0.5 M Pipe X 50 mm Nominal Bore Standard Swirly-flo Pipe
With End Taper W-Velocity (M/S) at J=45- View 2
Lmax = 3.424E-01 Lmin = -7.729E-02

25-C



0.5 M Pipe X 50 mm Nominal Bore Standard Swirly-flo Pipe
With End Taper W-Velocity (M/S) at Exit
Lmax = 2.969E-01 Lmin = -1.832E-02

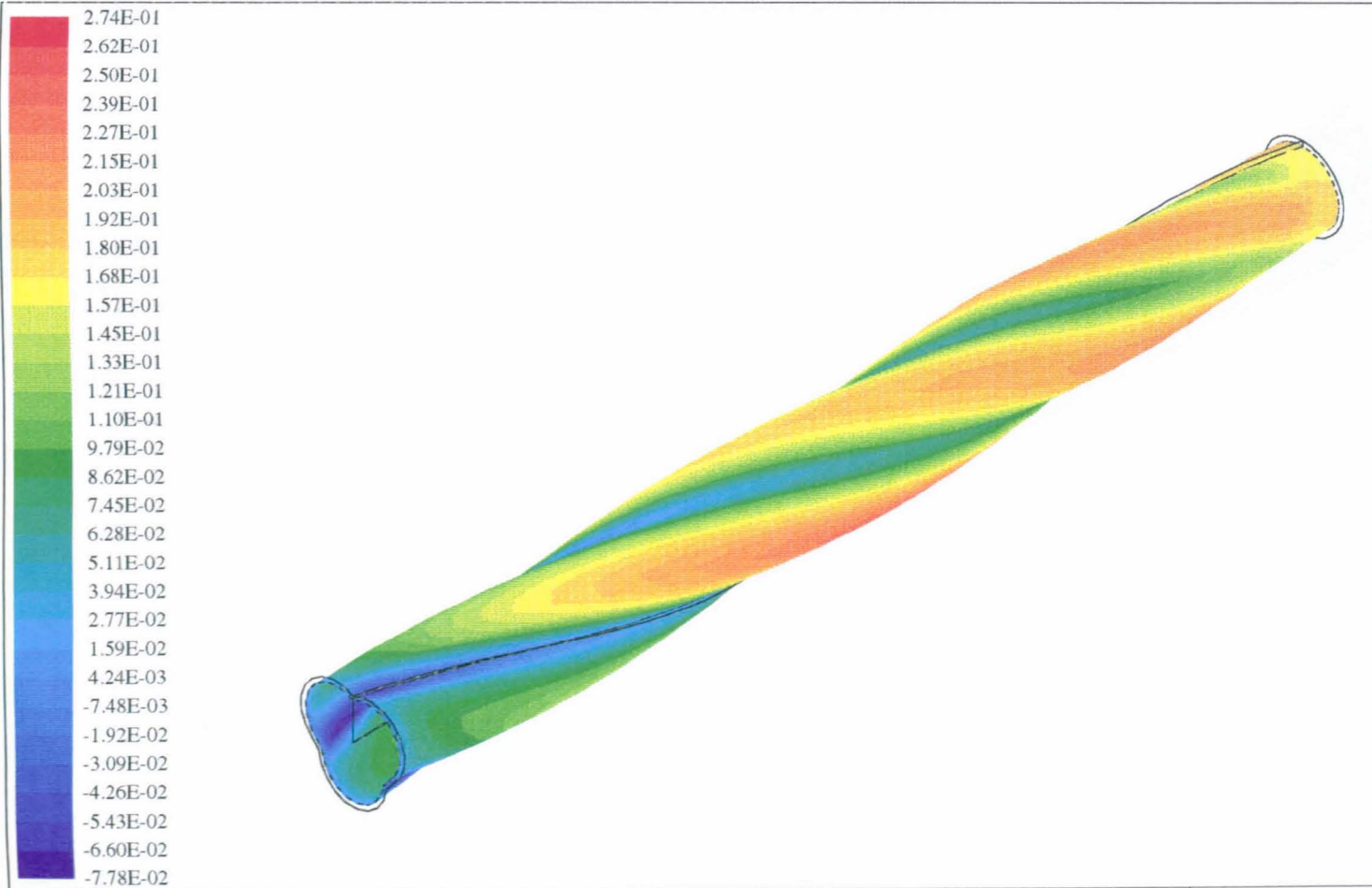
		<p>0.6M Pipe X 50 mm Nominal Bore Standard Swirly-flo Pipe With End Taper Grid (30 X 25 X 140)</p>	
---	--	---	---

27-C



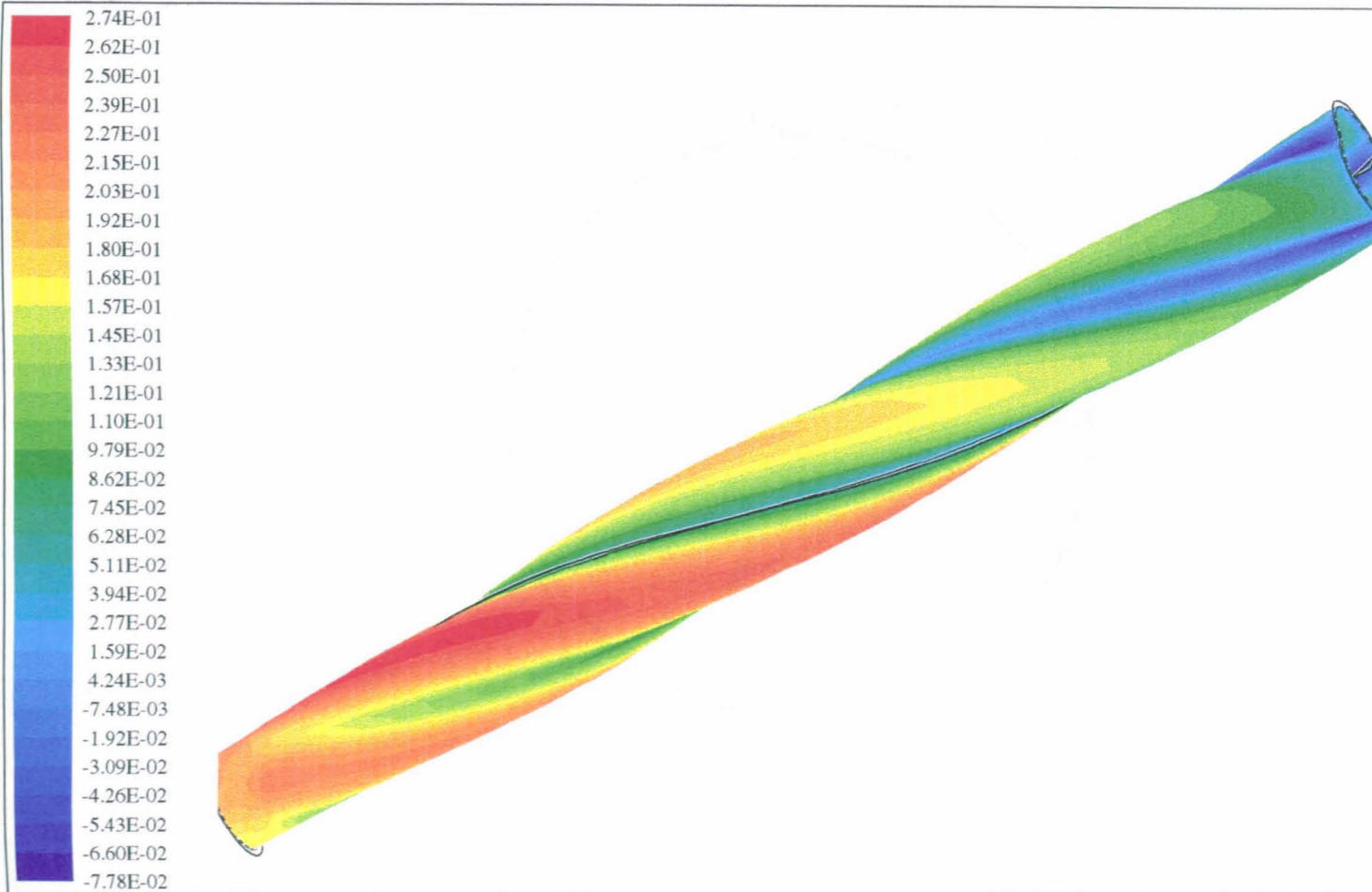
0.6M Pipe X 50 mm Nominal Bore Standard Swirly-flo Pipe
With End Taper Static Pressure (Pa)at the Wall
Lmax = 1.949E+02 Lmin = -8.958E+02

28-C



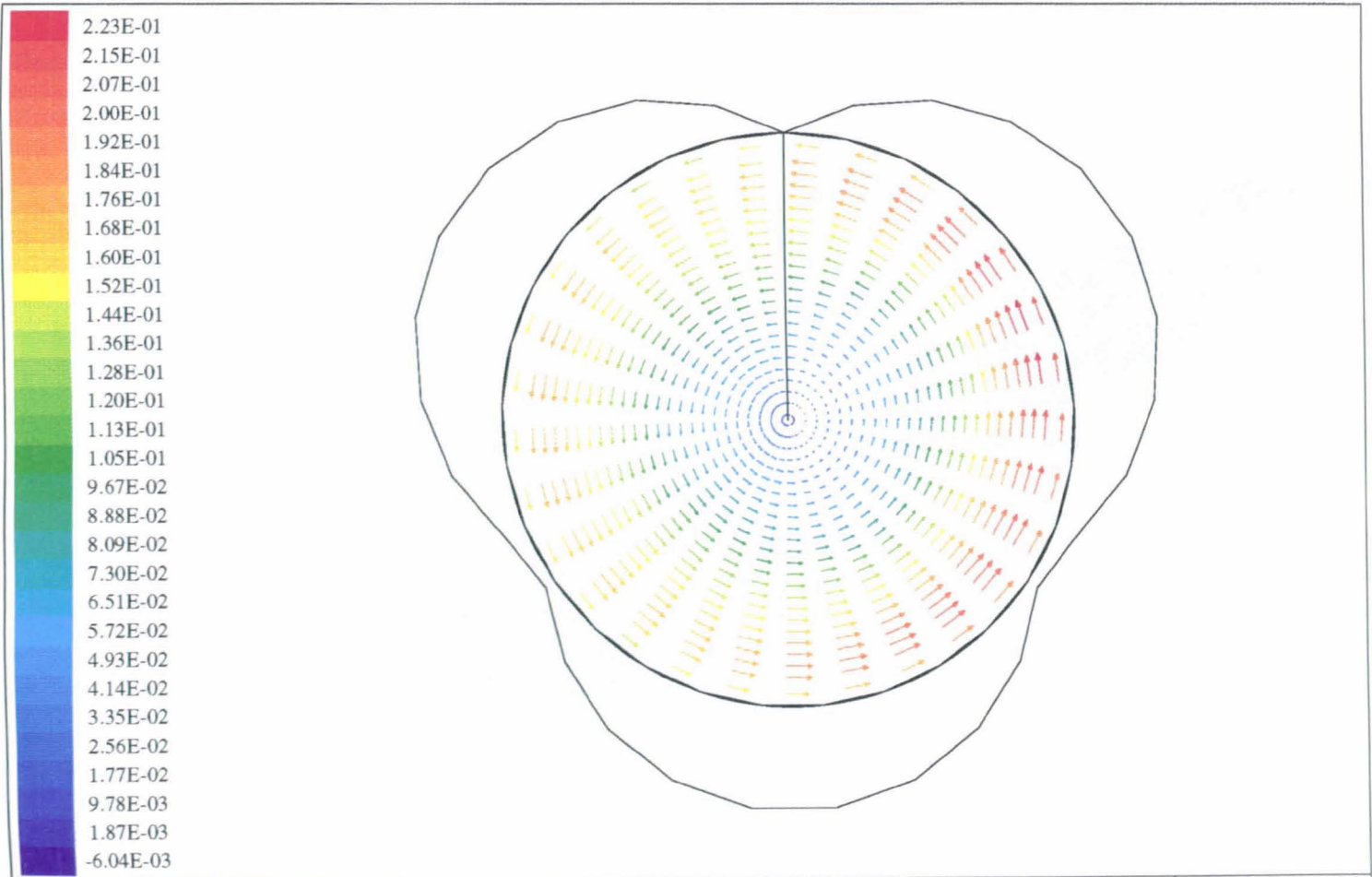
0.6M Pipe X 50 mm Nominal Bore Standard Swirly-flo Pipe
With End Taper W-Velocity (M/S) at J=23- View 1
Lmax = 2.737E-01 Lmin = -7.776E-02

29-C

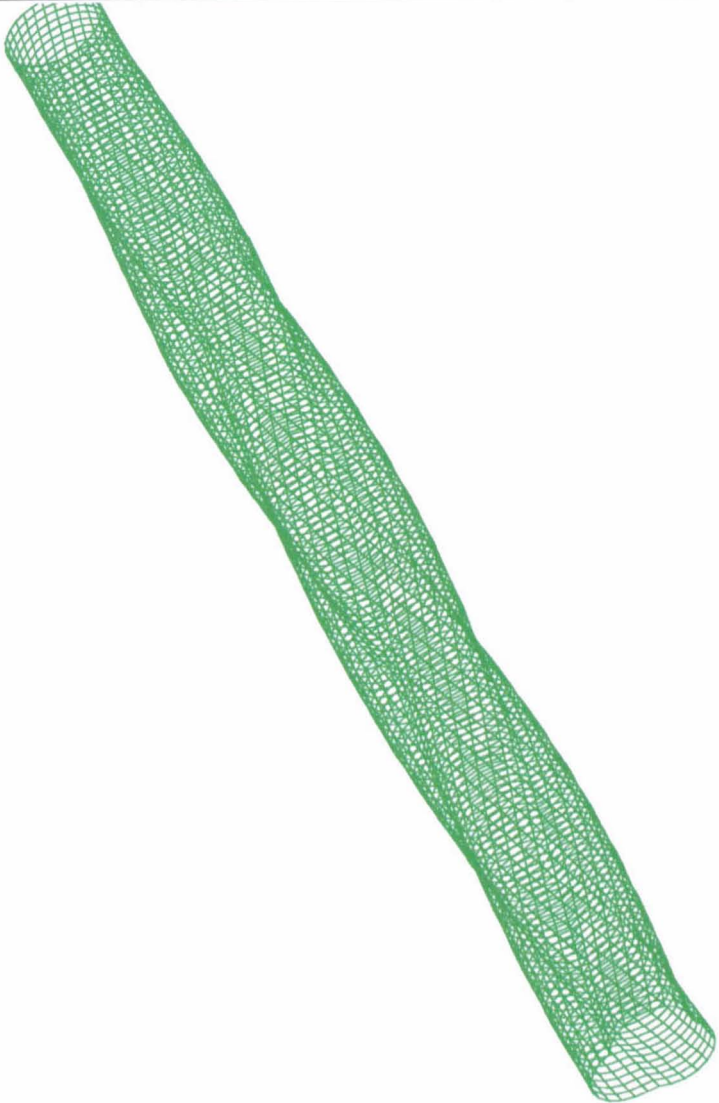


0.6 M Pipe X 50 mm Nominal Bore Standard Swirly-flo Pipe
With End Taper W-Velocity (M/S) at J=23- View 2
Lmax = 2.737E-01 Lmin = -7.776E-02

30-C



0.6M Pipe X 50 mm Nomial Bore Standard Swirly-flo Pipe
With End Taper W-Velocity (M/S)
Lmax = 2.233E-01 Lmin = -6.036E-03

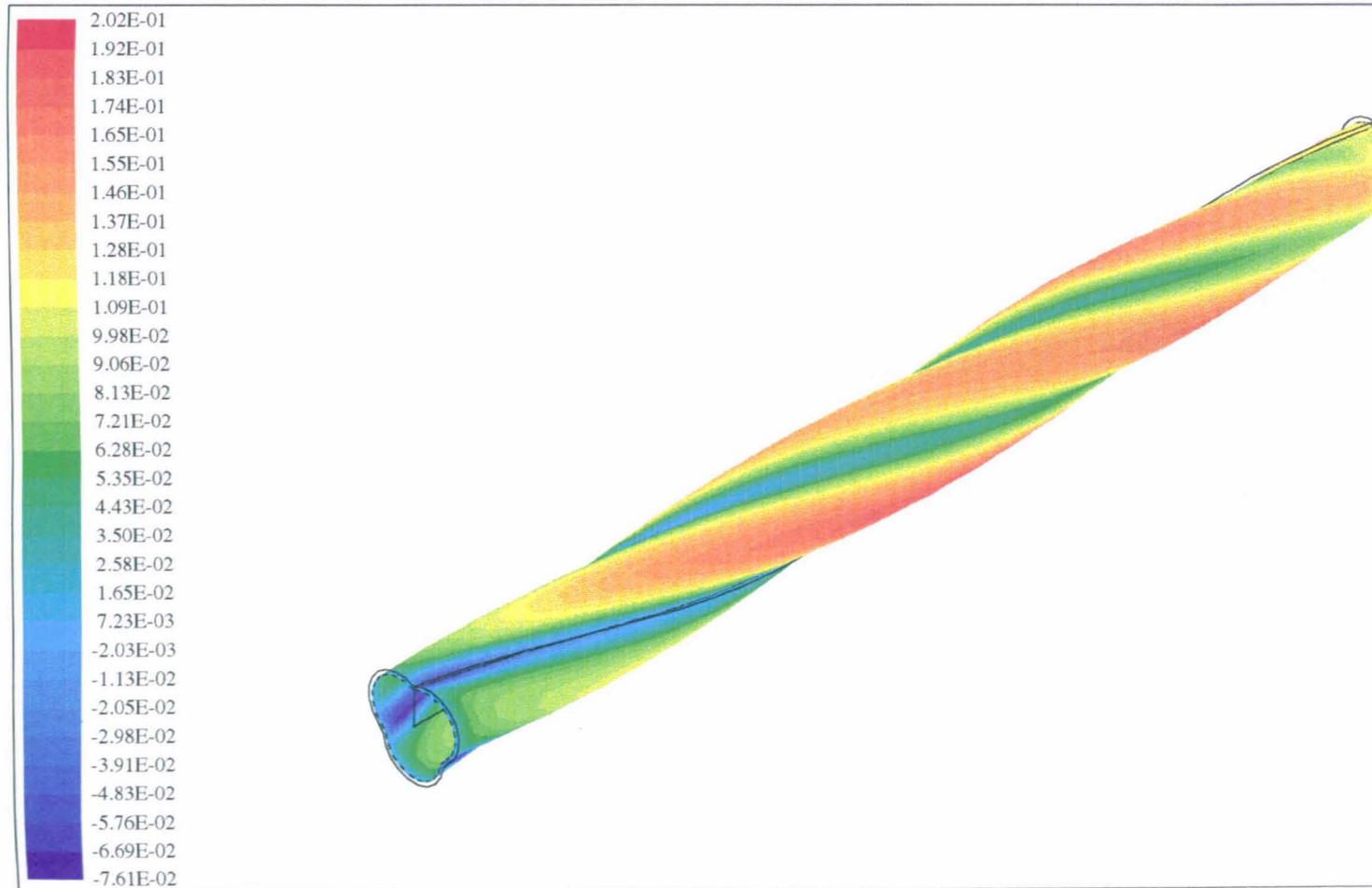
	<p>0.7M Pipe X 50 mm Nominal Bore Standard Swirly-flo Pipe With End Taper Grid (30 X 25 X 160)</p>	
---	---	---

32-C



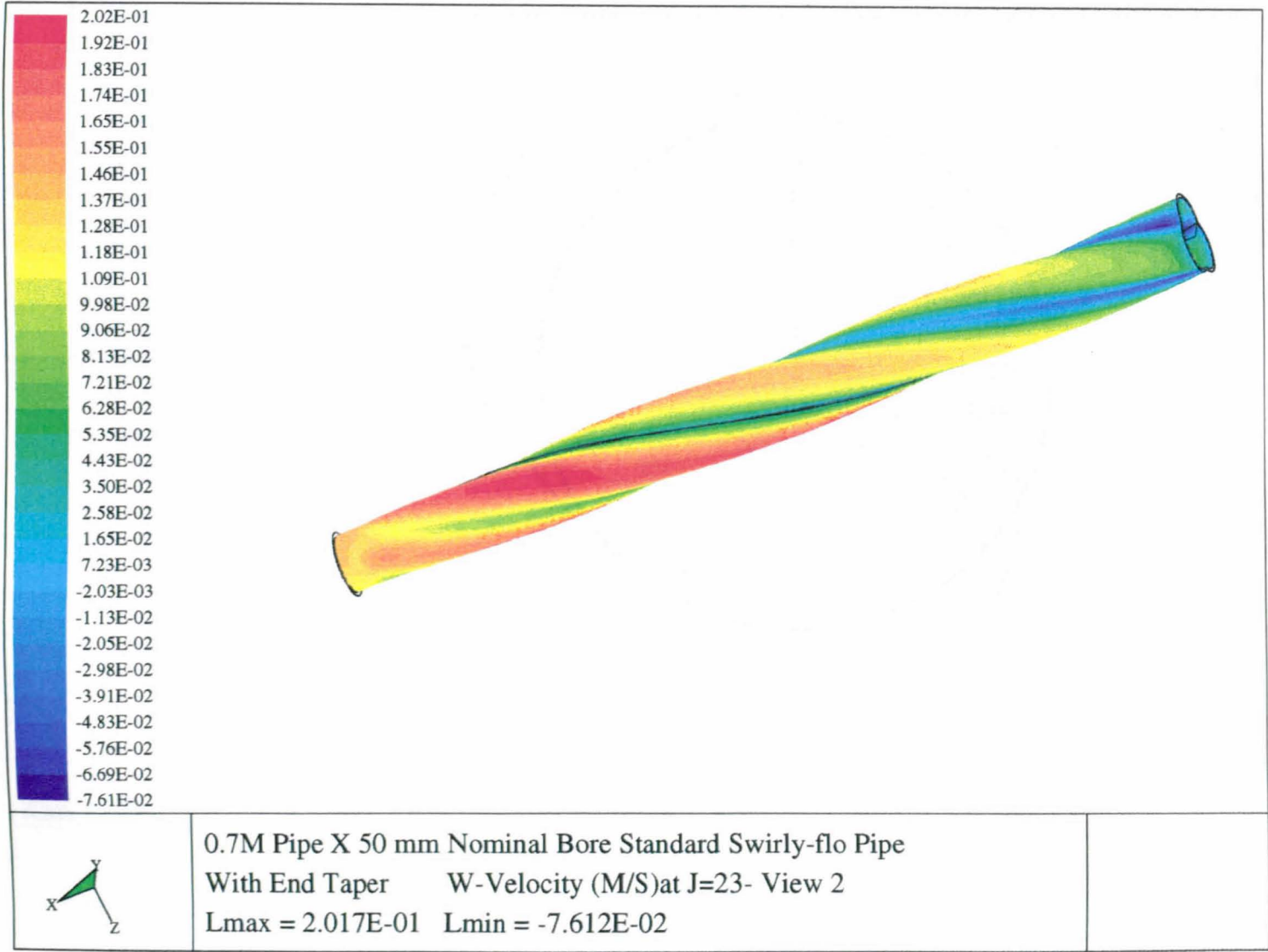
0.7M Pipe X 50 mm Nominal Bore Standard Swirly-flo
With End Taper Static Pressure (Pa)at the Wall
Lmax = -1.839E+02 Lmin = -1.420E+03

33-C

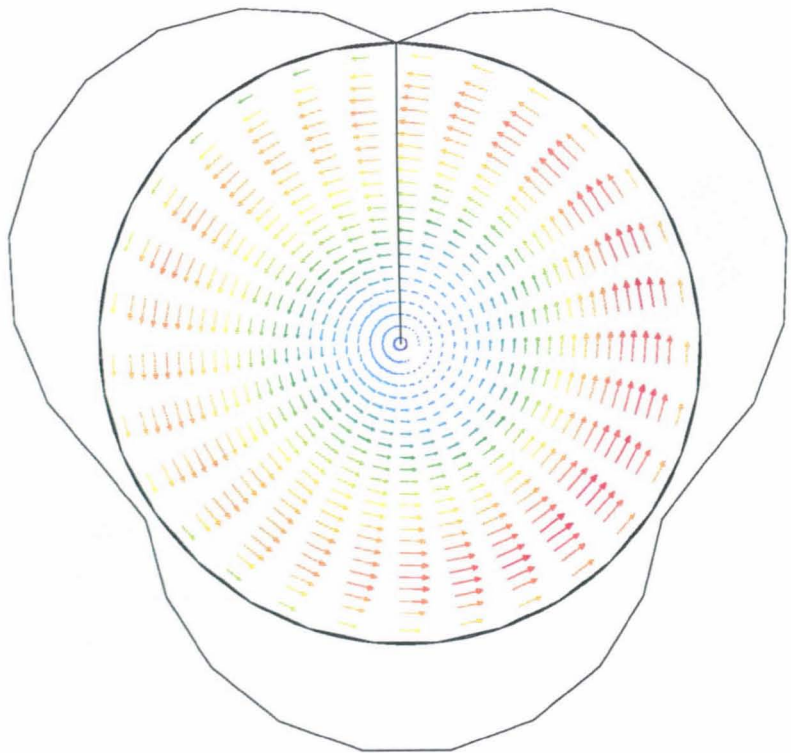
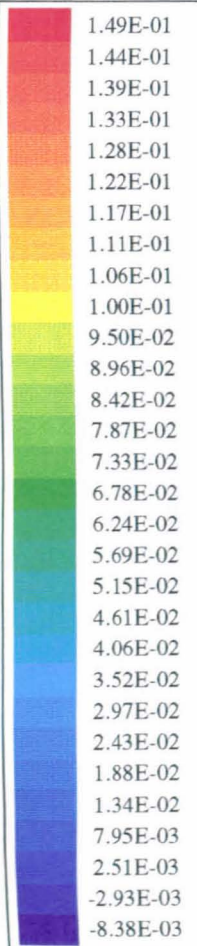


0.7M Pipe X 50 mm Nominal Bore Standard Swirly-flo Pipe
With End Taper W-Velocity (M/S)at J=23- View 1
Lmax = 2.017E-01 Lmin = -7.612E-02

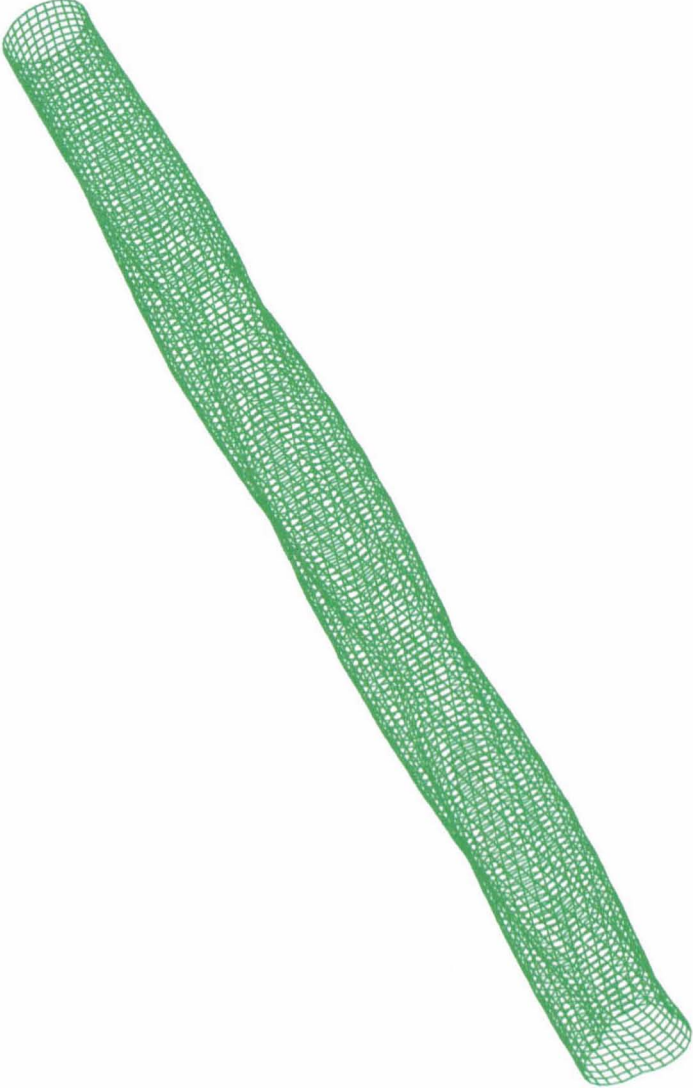
34-C



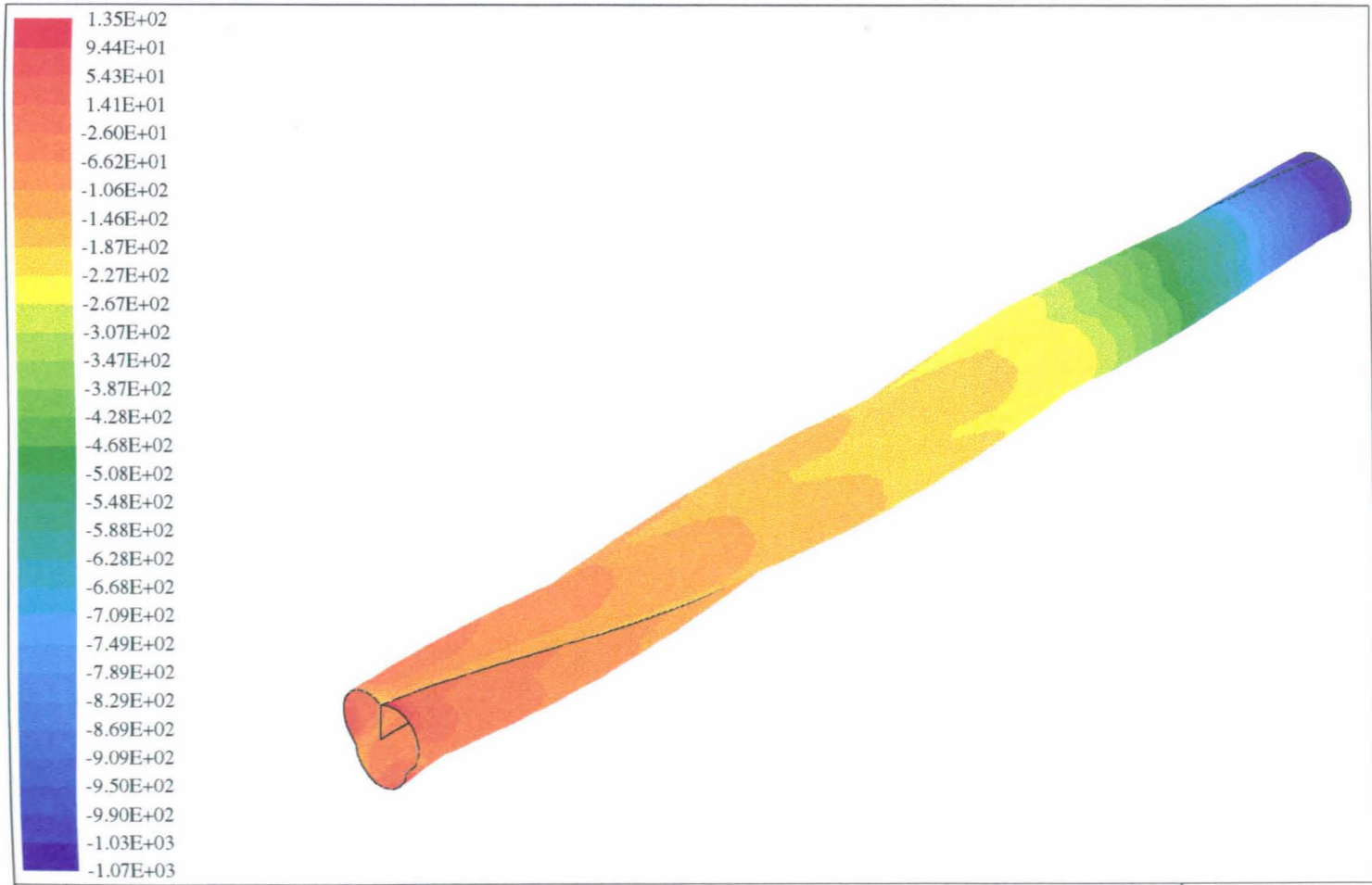
35-C



0.7M Pipe X 50 mm Nominal Bore Standard Swirly-flo Pipe
With End Taper W-Velocity (M/S) at Exit
Lmax = 1.495E-01 Lmin = -8.376E-03

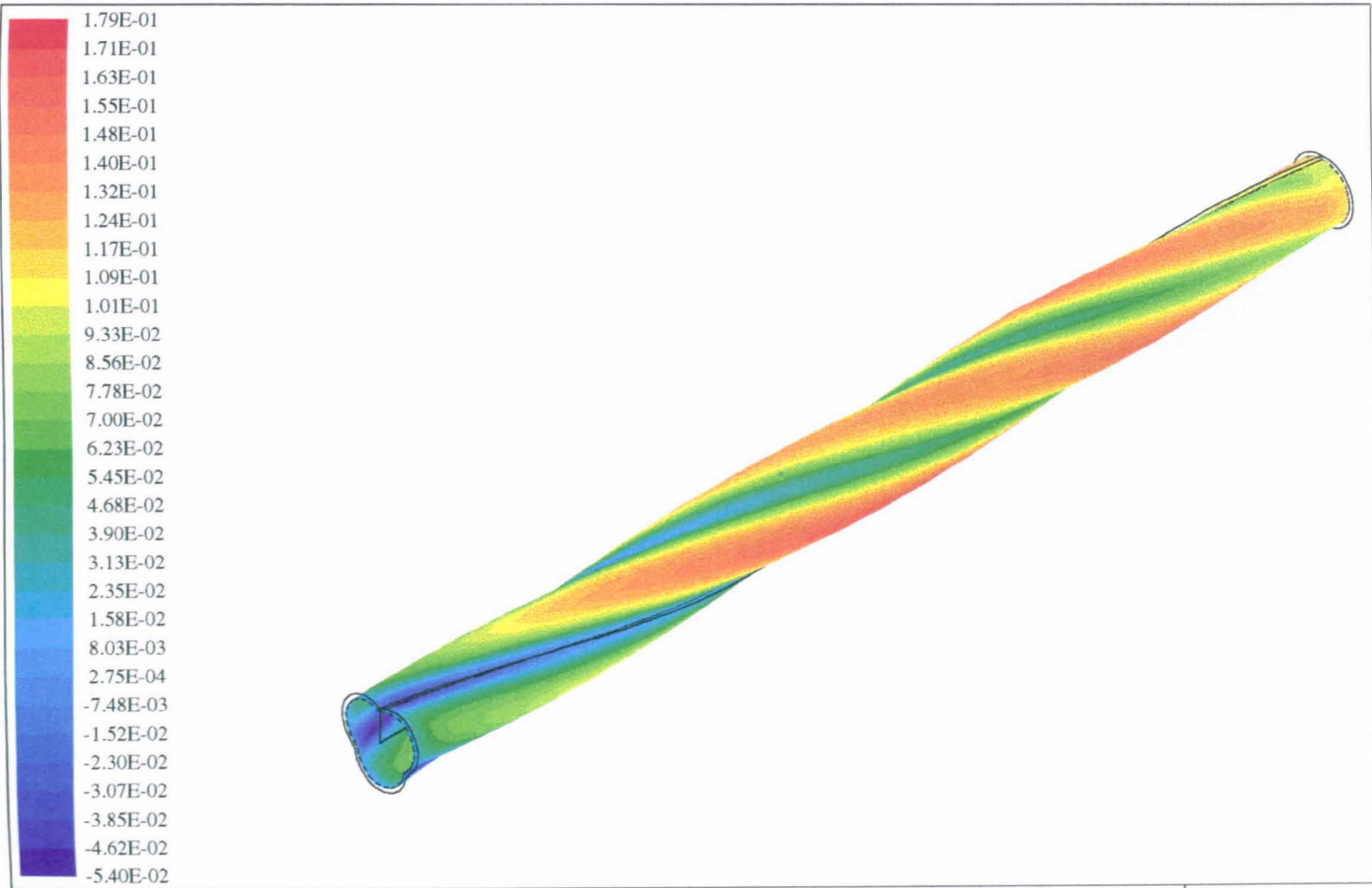
	<p>0.8M Pipe X 50 mm Nominal Bore Standard Swirly-flo Pipe With End Taper Grid (30 X 50 X 160)</p>	
---	---	---

37-C



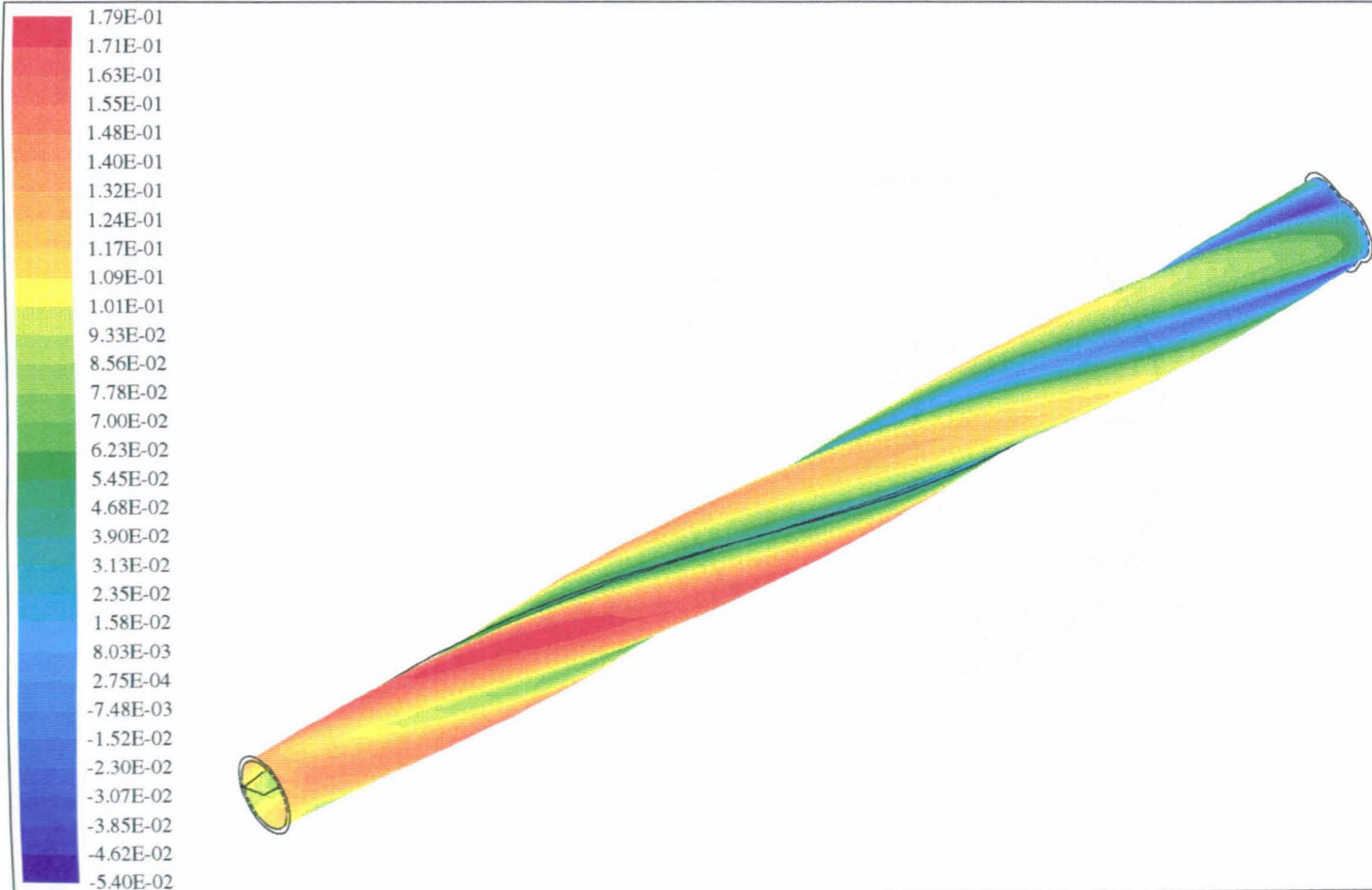
0.8 M PIPE X 50 mm Nominal Bore Standard Swirly-flo Pipe
With End Taper Static Pressure (Pa)at Exit
Lmax = 1.346E+02 Lmin = -1.070E+03

38-C



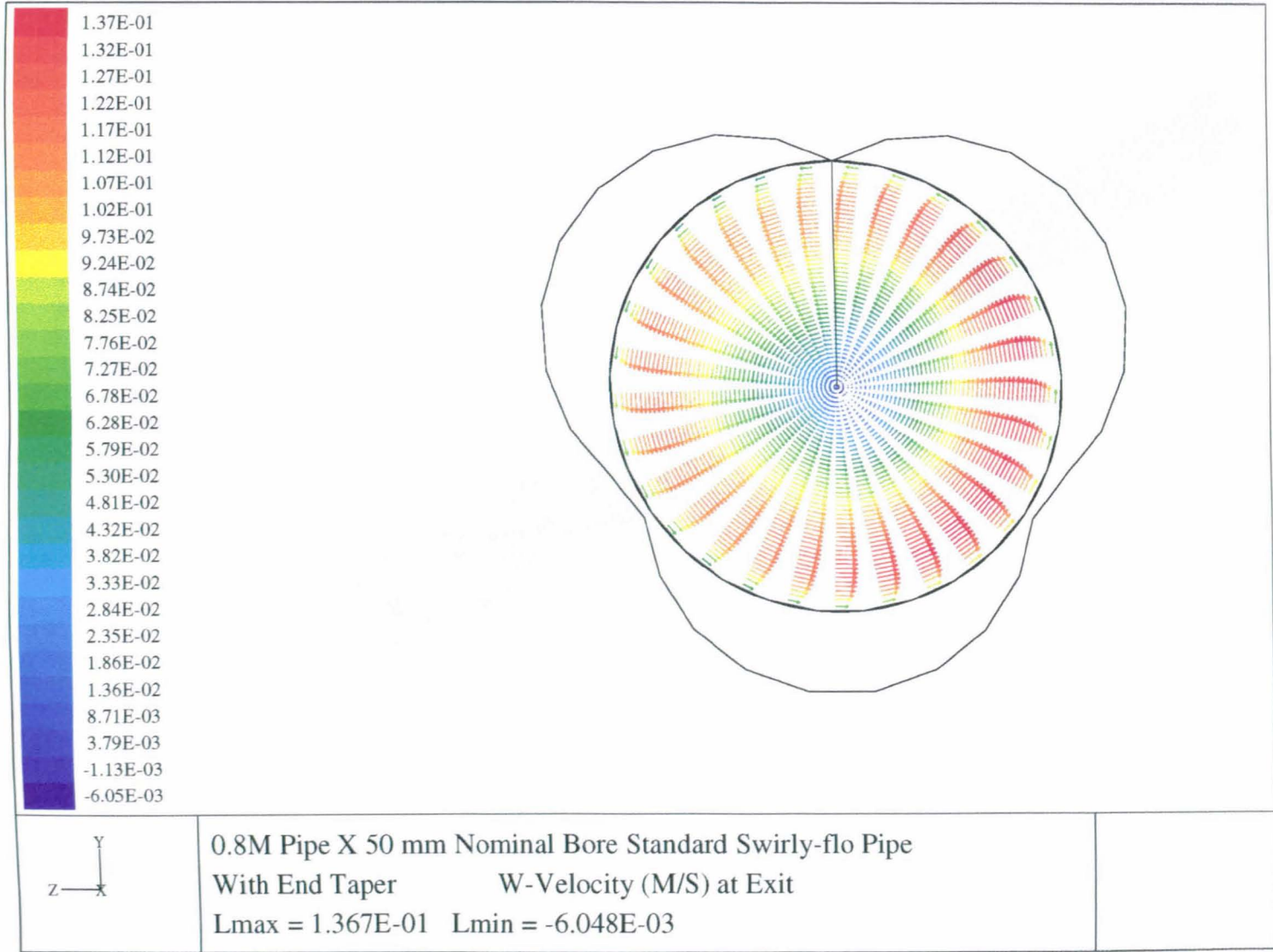
0.8M Pipe X 50 mm Nominal Bore Standard Swirly-flo Pipe
With End Taper W-Velocity (M/S) at J=45- View 1
Lmax = 1.786E-01 Lmin = -5.399E-02

39-C



0.8M Pipe X 50 mm Nominal Bore Standard Swirly-flo Pipe
With End Taper W-Velocity (M/S) at J=45- View 2
Lmax = 1.786E-01 Lmin = -5.399E-02

40-C



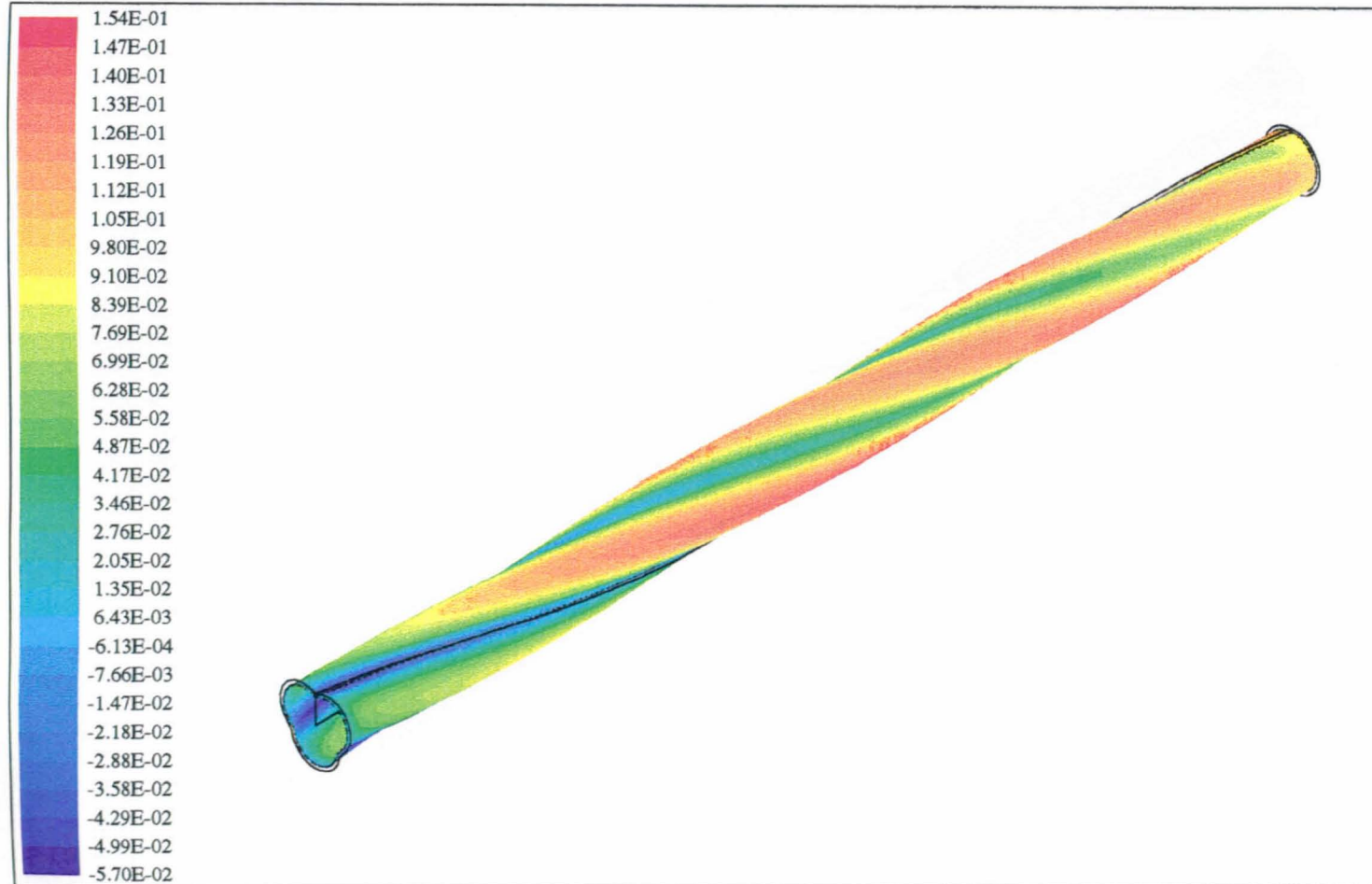
	<p data-bbox="1167 752 1249 1575">0.9 M Pipe X 50 mm Nominal Bore Standard Swirly-flo Pipe With End Taper Grid (30 X 50 X 180)</p> 
---	---

42-C



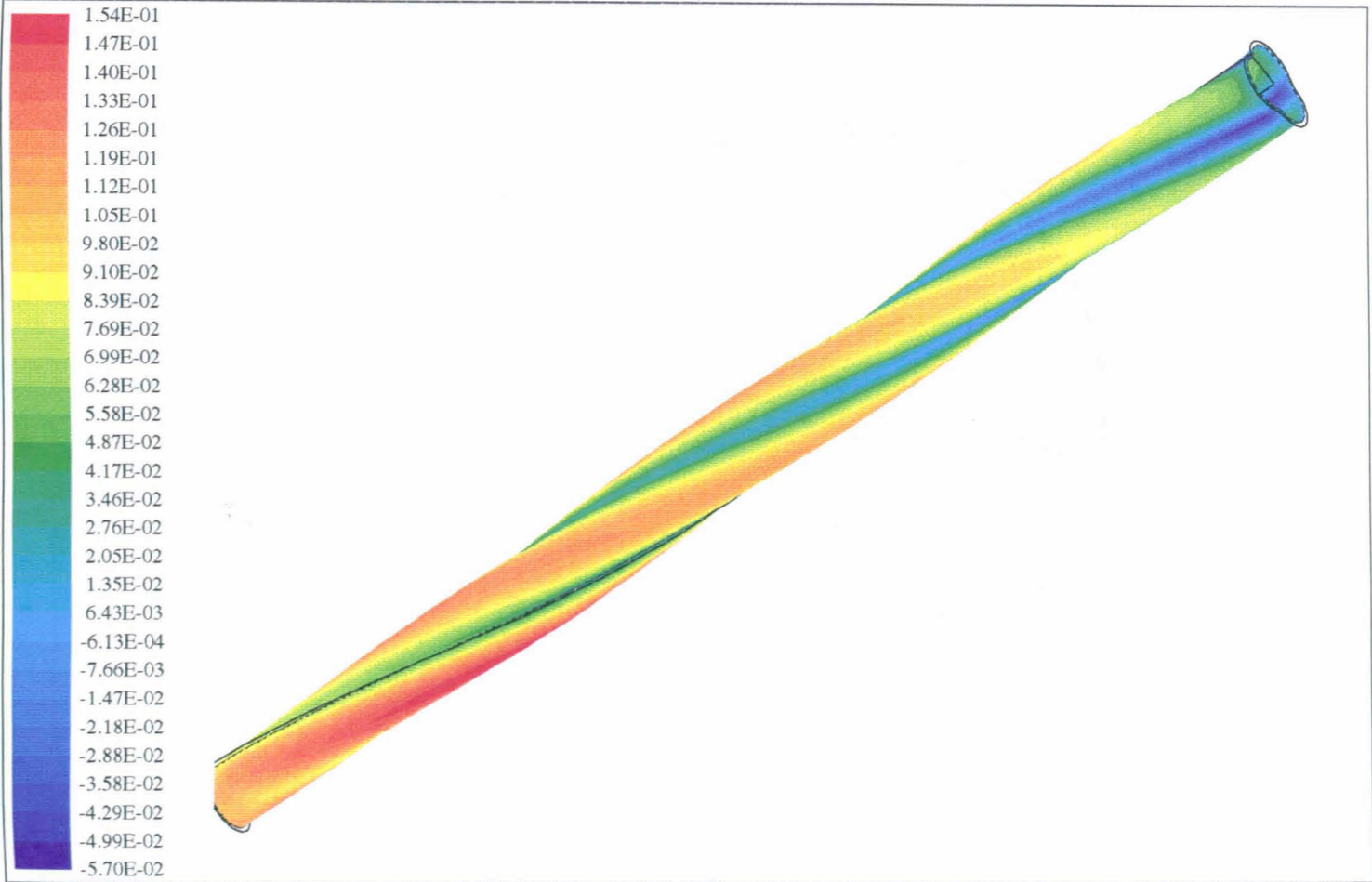
0.9M Pipe X 50 mm Nominal Bore Standard Swirly-flo Pipe
With End Taper Static Pressure (Pa) at the Wall
Lmax = 1.058E+02 Lmin = -1.114E+03

43-C



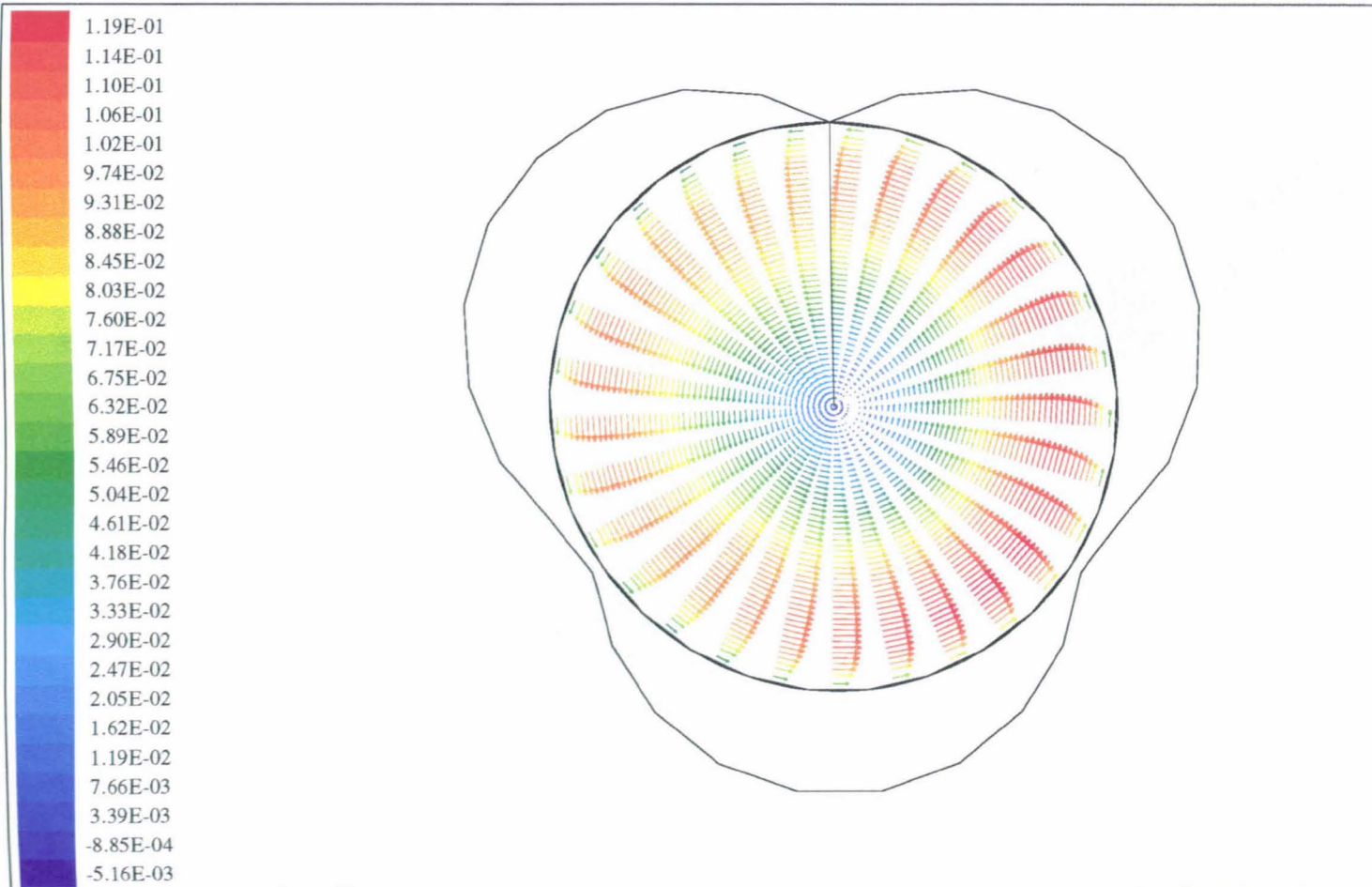
0.9M Pipe X 50 mm Nominal Bore Standard Swirly-flo Pipe
With End Taper W-Velocity (M/S) at J=45- View 1
Lmax = 1.544E-01 Lmin = -5.699E-02

44-C

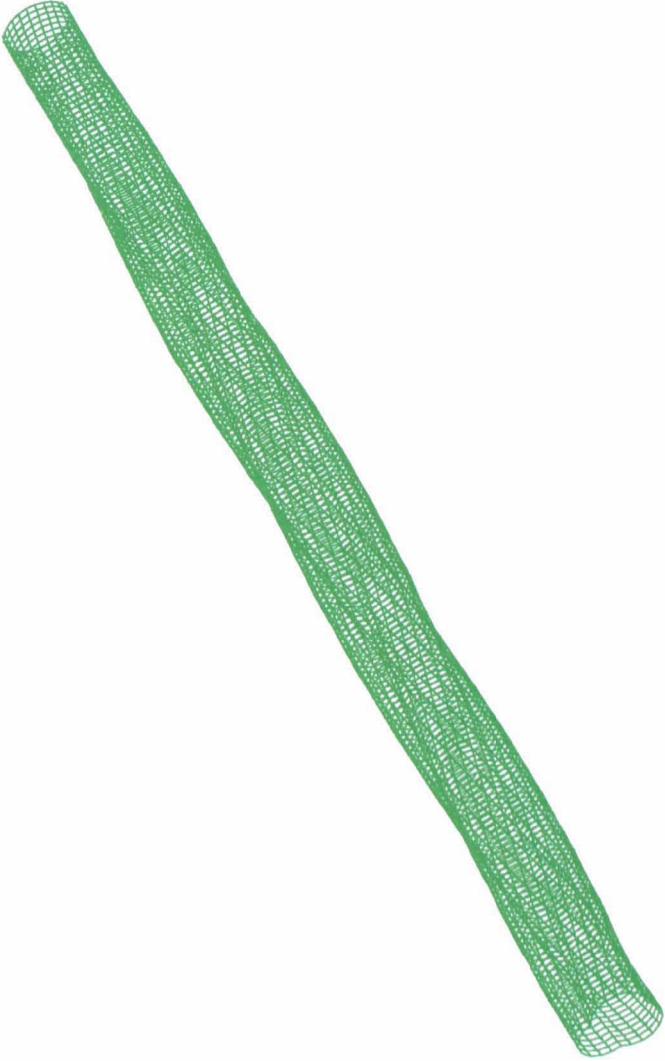


0.9M Pipe X 50 mm Nominal Bore Standard Swirly-flo Pipe
With End Taper W-Velocity (M/S) at J=45- View 2
Lmax = 1.544E-01 Lmin = -5.699E-02

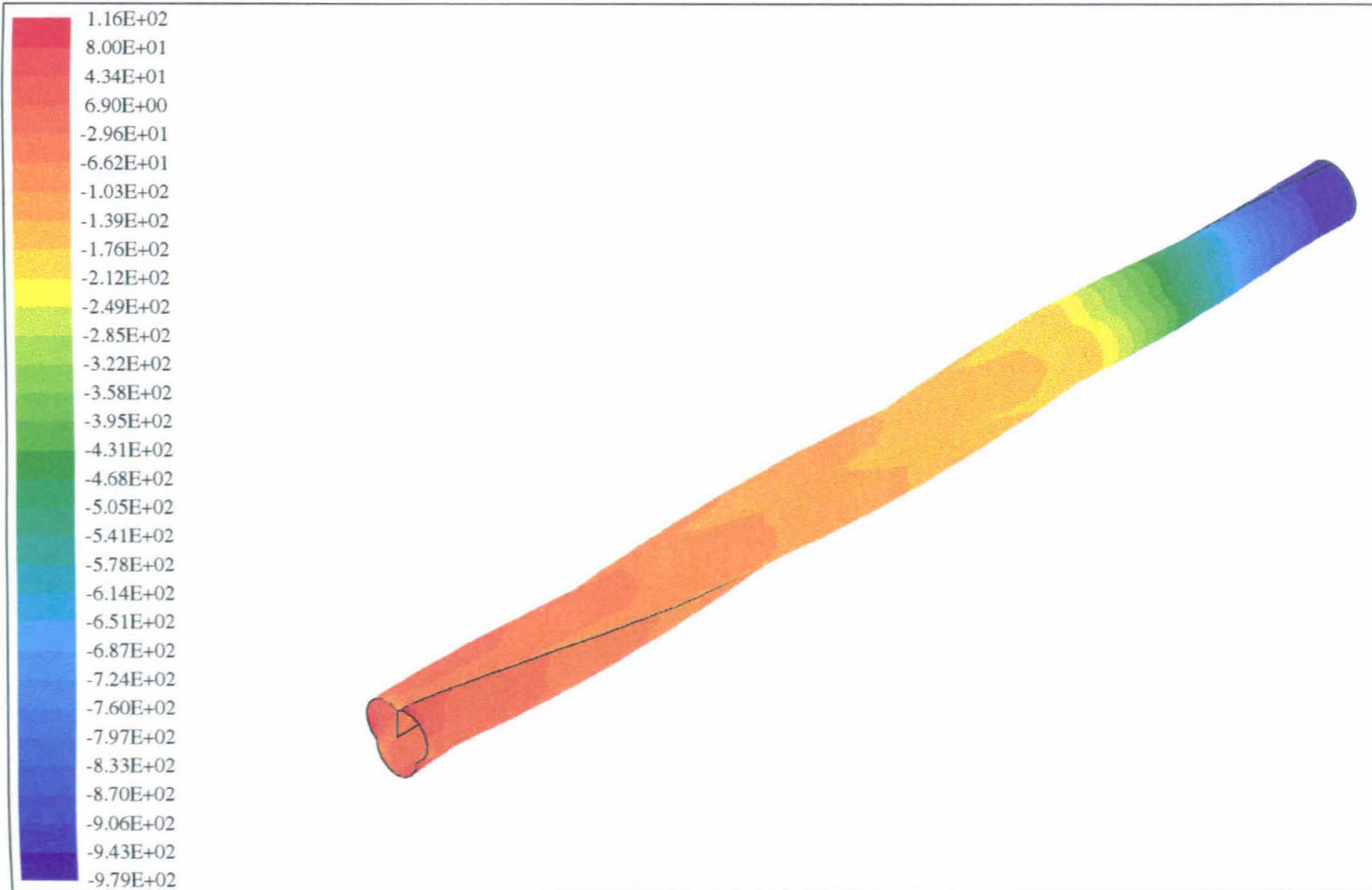
45-C



0.9M Pipe X 50 mm Nominal Bore Standard Swirly-flo Pipe
With End Taper W-Velocity (M/S) at Exit
Lmax = 1.187E-01 Lmin = -5.156E-03

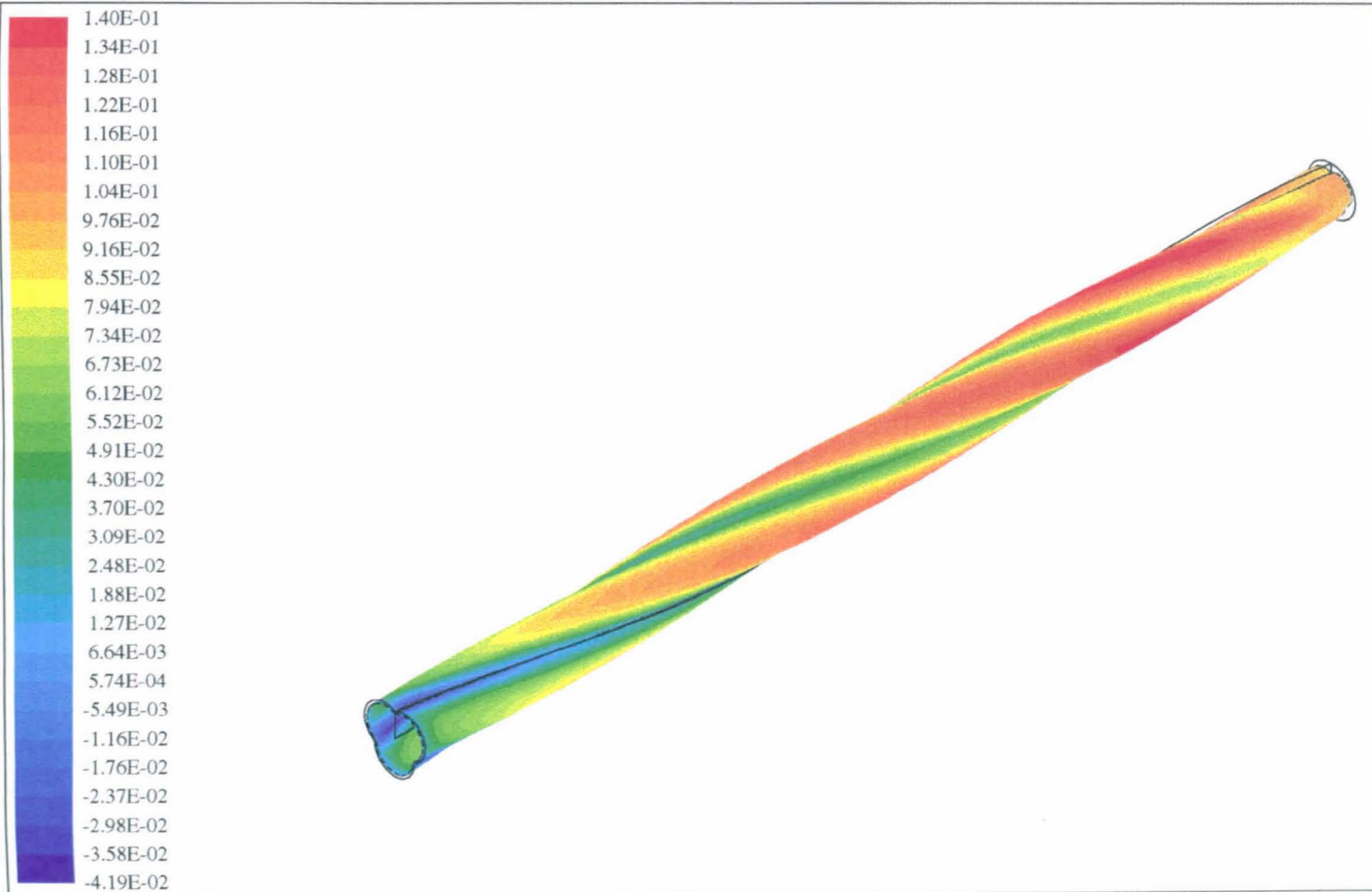
		<p>1M Pipe X 50 mm Nominal Bore Standard Swirly-flo Pipe With End Taper Grid (25 X 25 X 200)</p>	
---	--	---	---

47-C



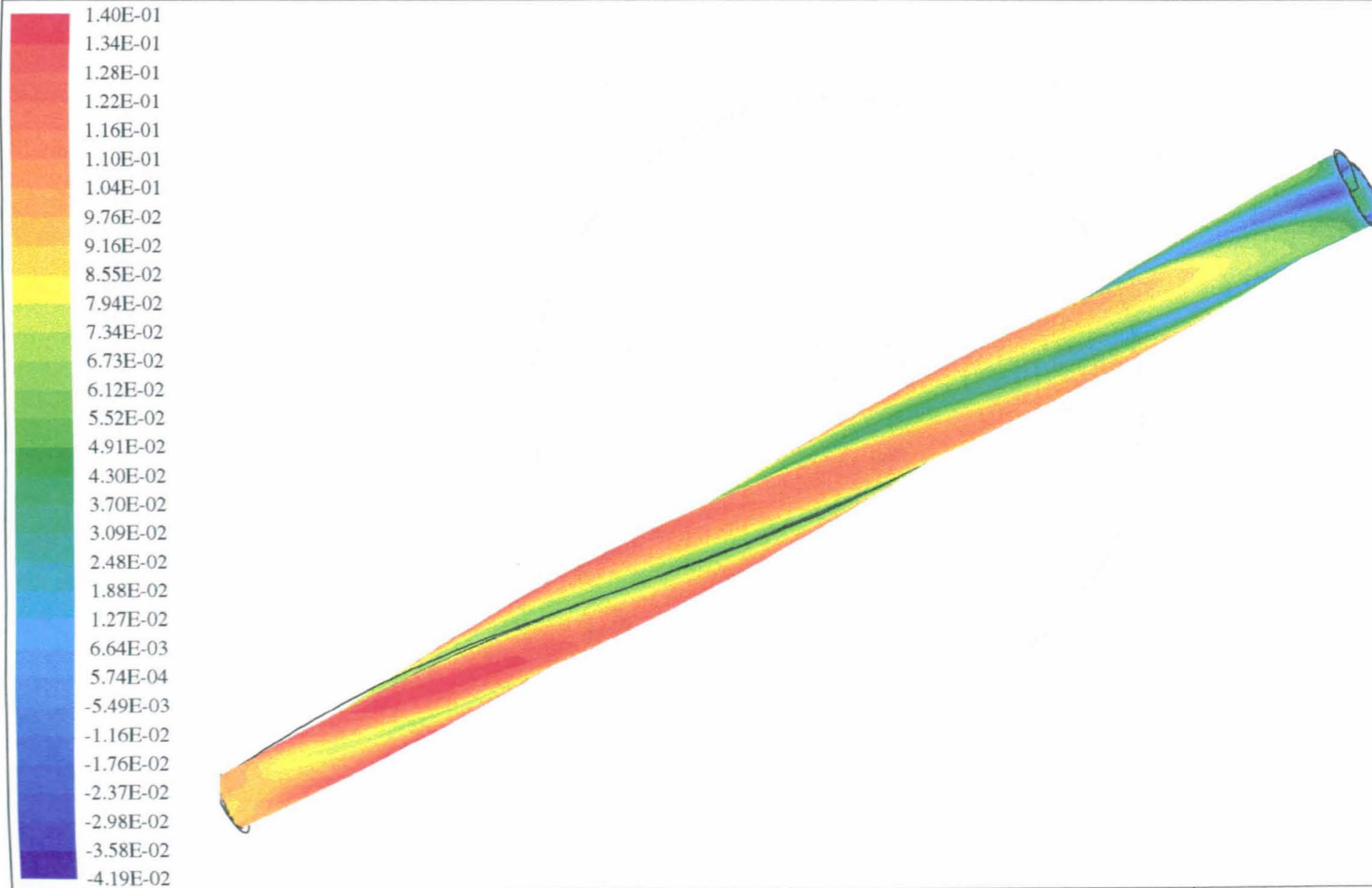
1M Pipe X 50 mm Nominal Bore Standard Swirly-flo Pipe
With End Taper Static Pressure (Pa) at the Wall
Lmax = 1.165E+02 Lmin = -9.794E+02

48-C



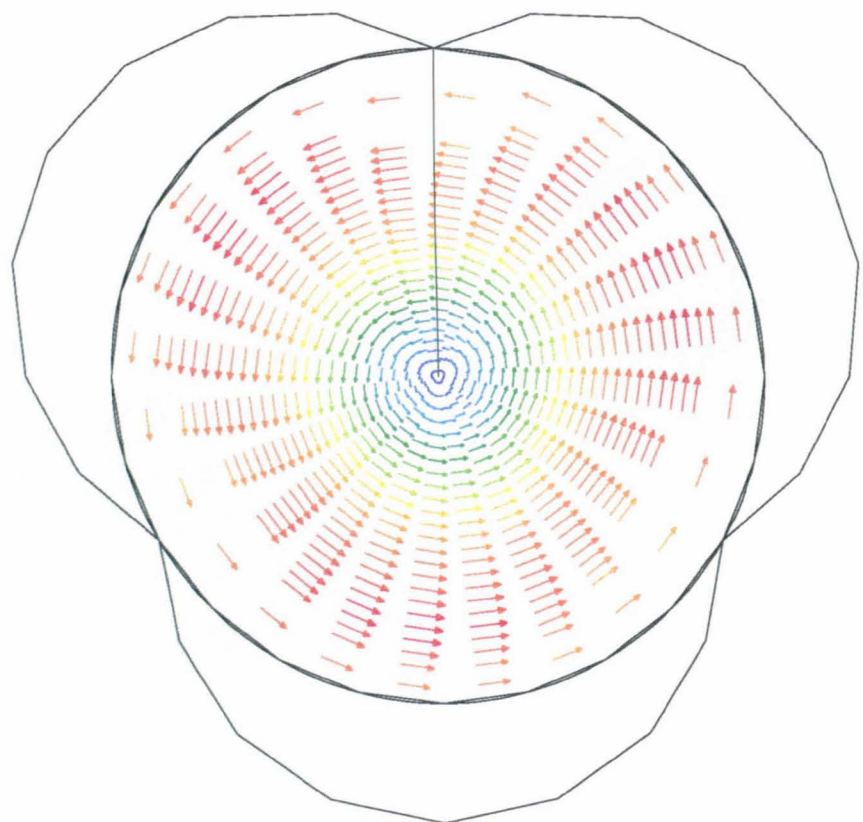
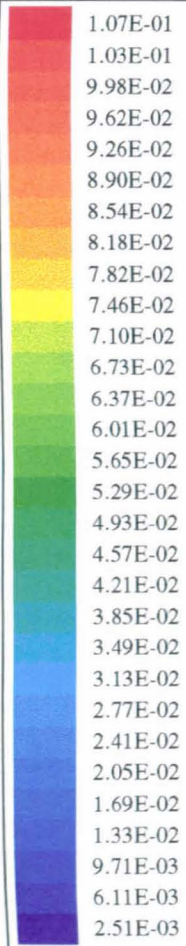
1M Pipe X 50 mm Nominal Bore Standard Swirly-flo Pipe
With End Taper W-Velocity (M/S) at J=23- View 1
Lmax = 1.401E-01 Lmin = -4.189E-02

49-C



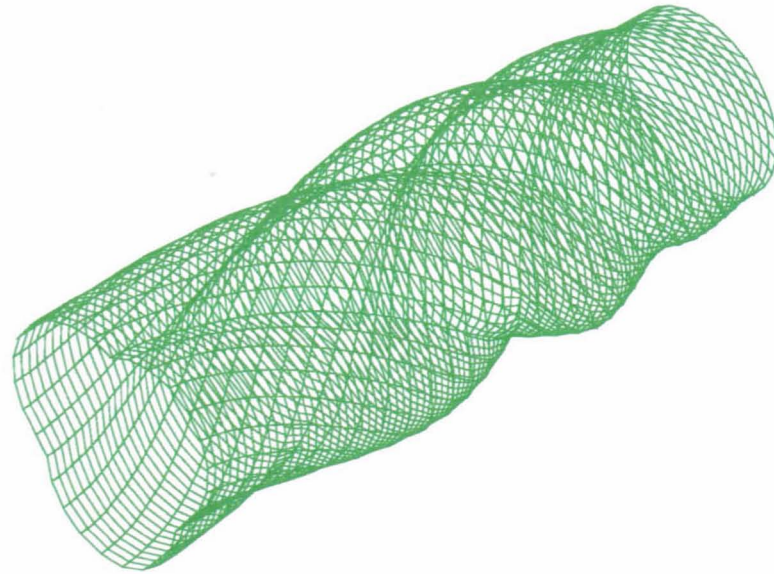
1M Pipe X 50 mm Nominal Bore Standard Swirly-flo Pipe
With End Taper W-Velocity (M/S) at J=23- View 2
Lmax = 1.401E-01 Lmin = -4.189E-02

50-C



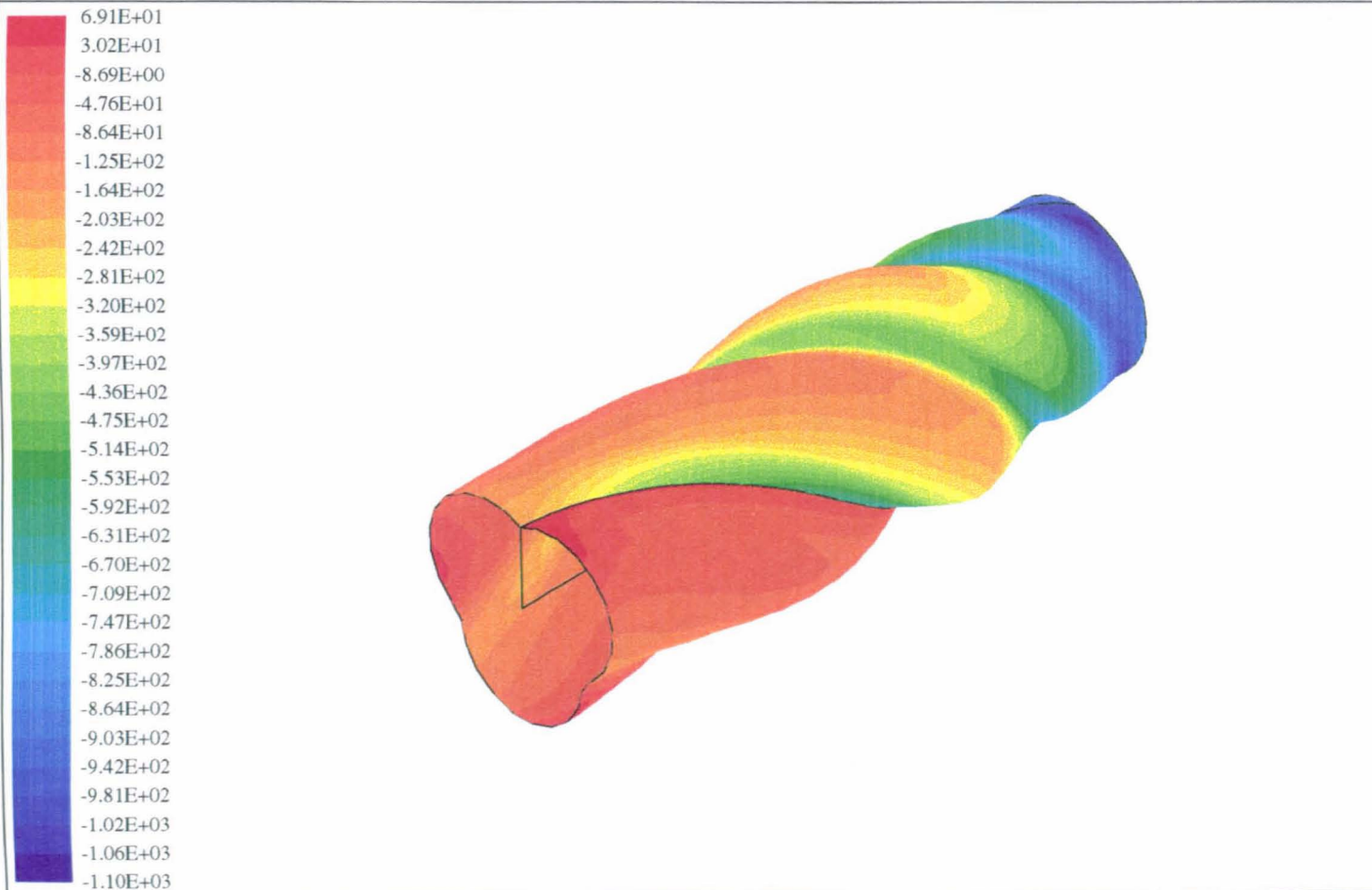
1M Pipe X 50 mm Nominal Bore Swirly-flo Pipe
With End Taper W-Velocity (M/S) at Exit
Lmax = 1.070E-01 Lmin = 2.508E-03

SI-C



0.2 M PIPE X 50 mm Bore Brachistochrone With End Taper
Grid (30 X 50 X 80)

52-C

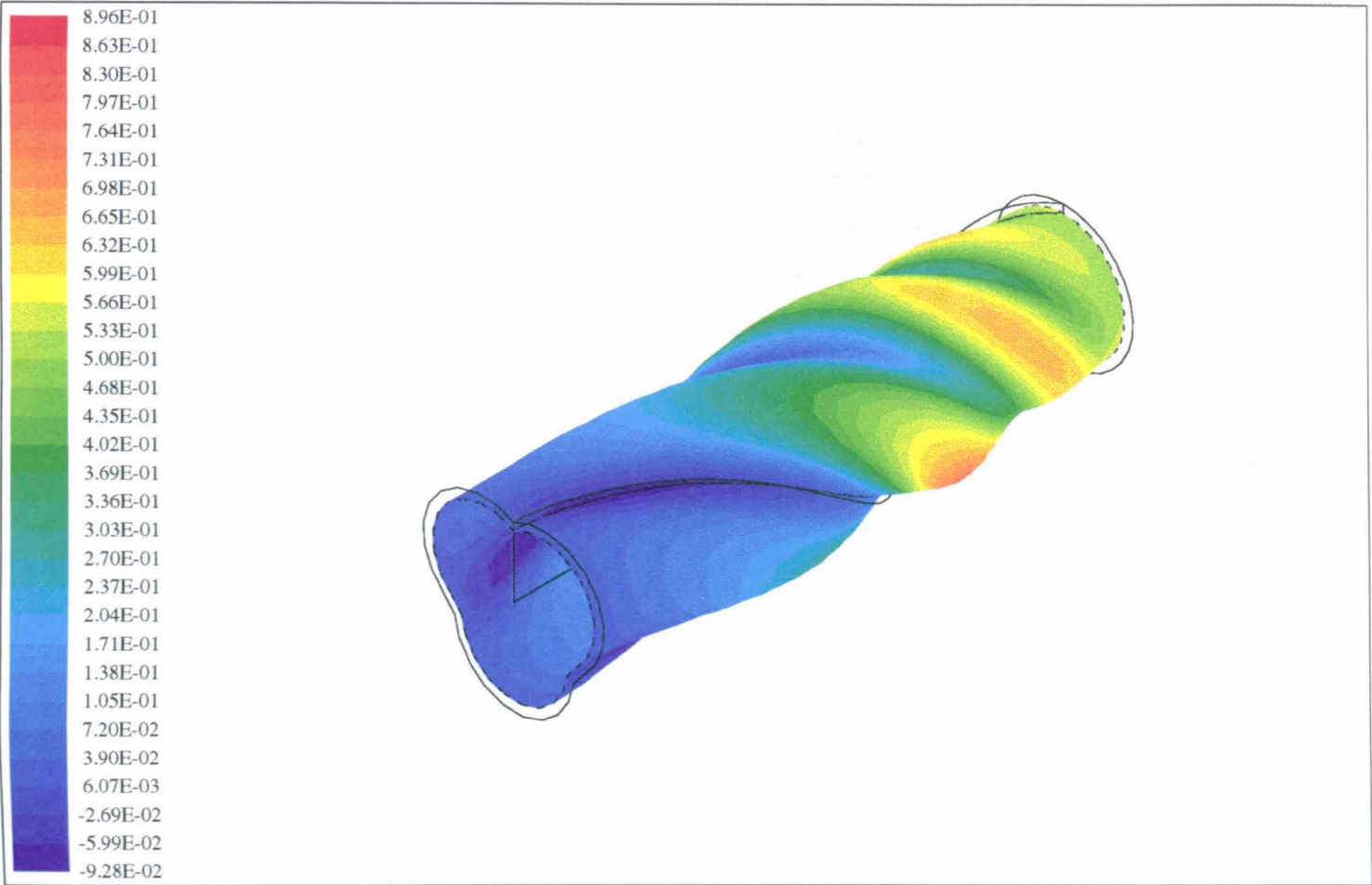


0.2 M PIPE X 50 mm Bore Brachistochrone With End Taper

Static Pressure (Pa) at Wall

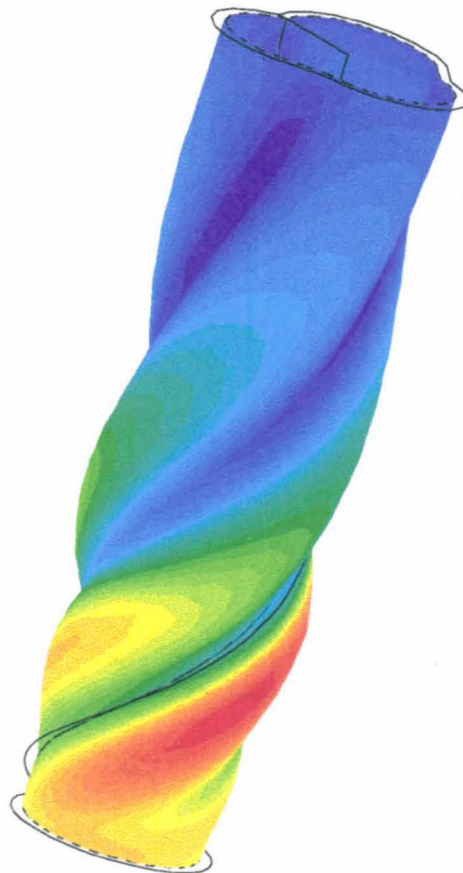
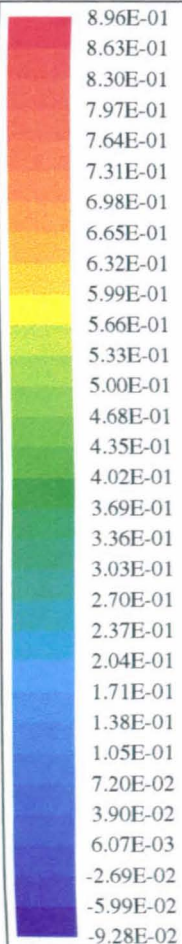
Lmax = 6.907E+01 Lmin = -1.097E+03

53-C



0.2 M PIPE X 50 mm Nominal Bore Brachistochrone With End Taper
W-Velocity (M/S) at J=45- View 1
Lmax = 8.960E-01 Lmin = -9.281E-02

54-C

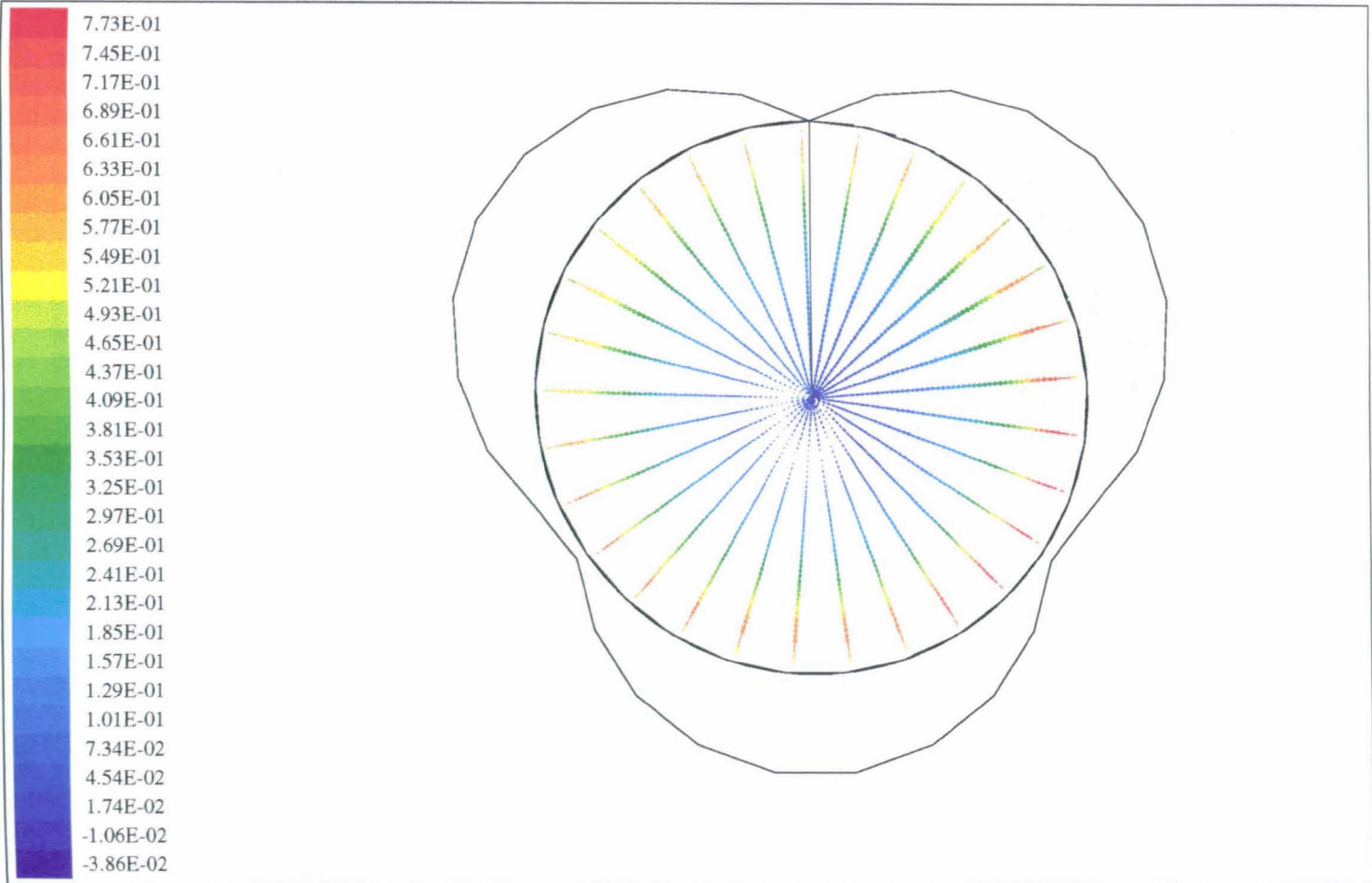


0.2 M PIPE X 50 mm Nominal Bore Brachistochrone With End Taper

W-Velocity (M/S) at J=45- View 2

Lmax = 8.960E-01 Lmin = -9.281E-02

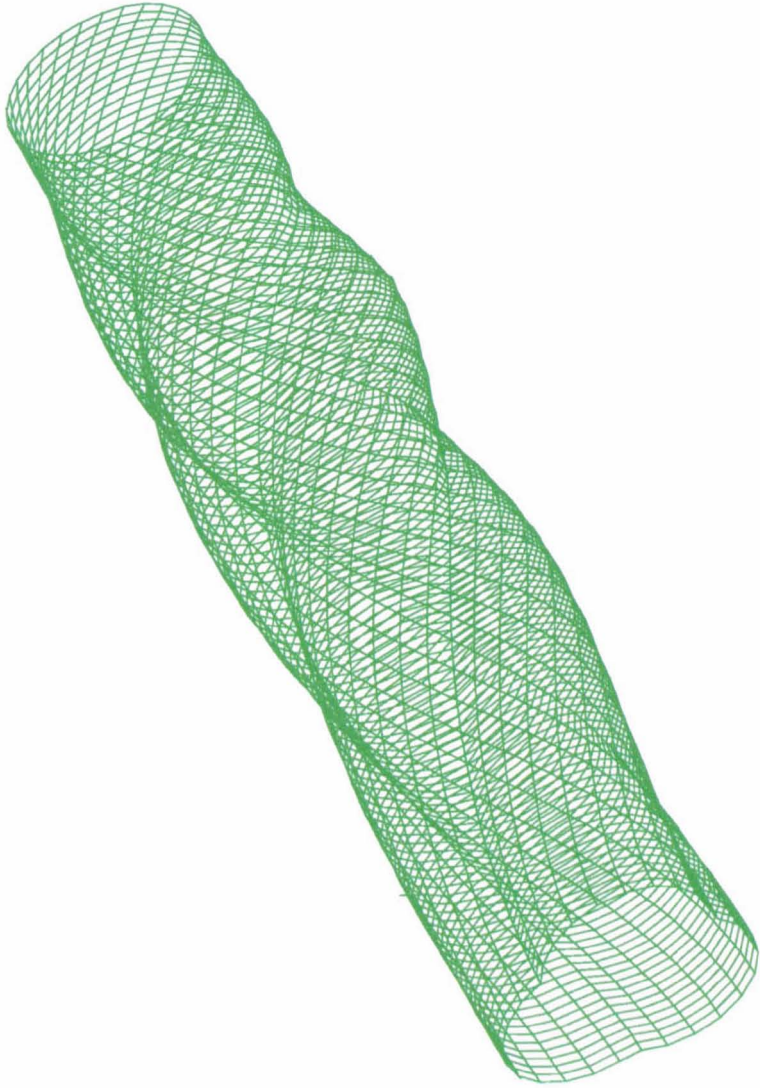
SS-C



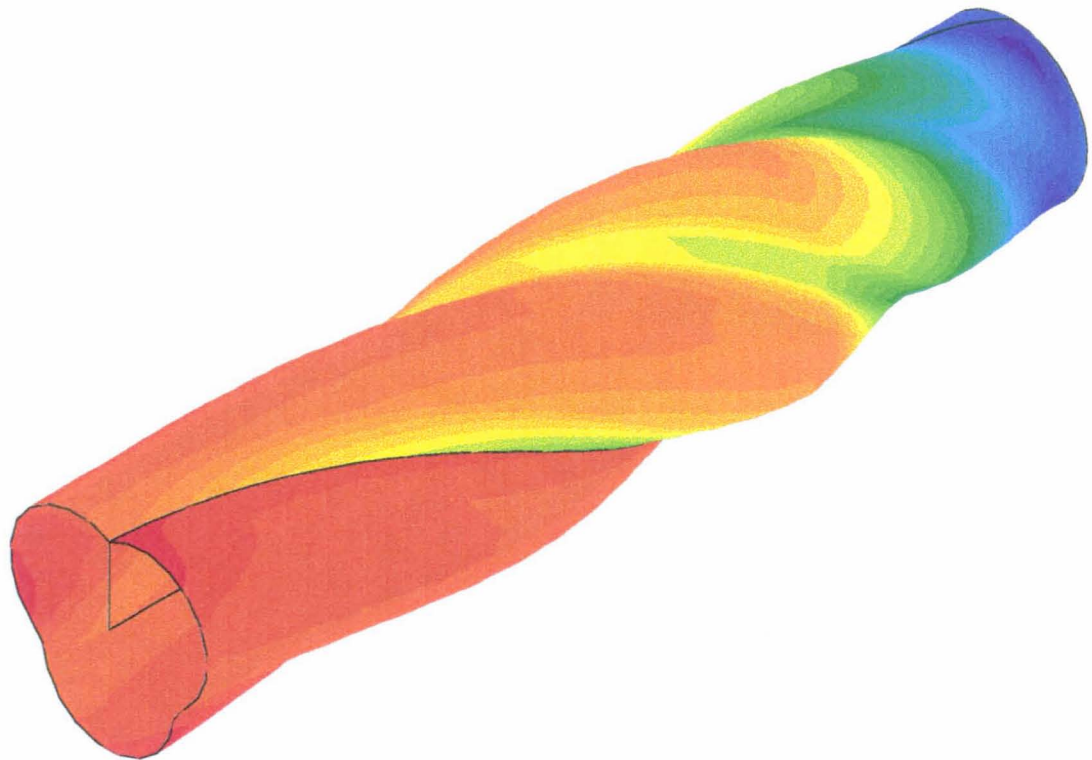
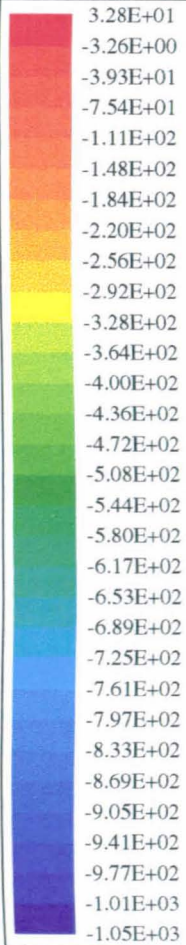
0.2 M PIPE X 50 mm Nominal Bore Brachistochrone With End Taper

W-Velocity (M/S) at Exit

Lmax = 7.731E-01 Lmin = -3.858E-02

	<p data-bbox="1149 760 1237 1590">0.3 M PIPE X 50 mm Bore Brachistochrone With End Taper Grid (30 X 50 X 120)</p> 
---	---

S7-C

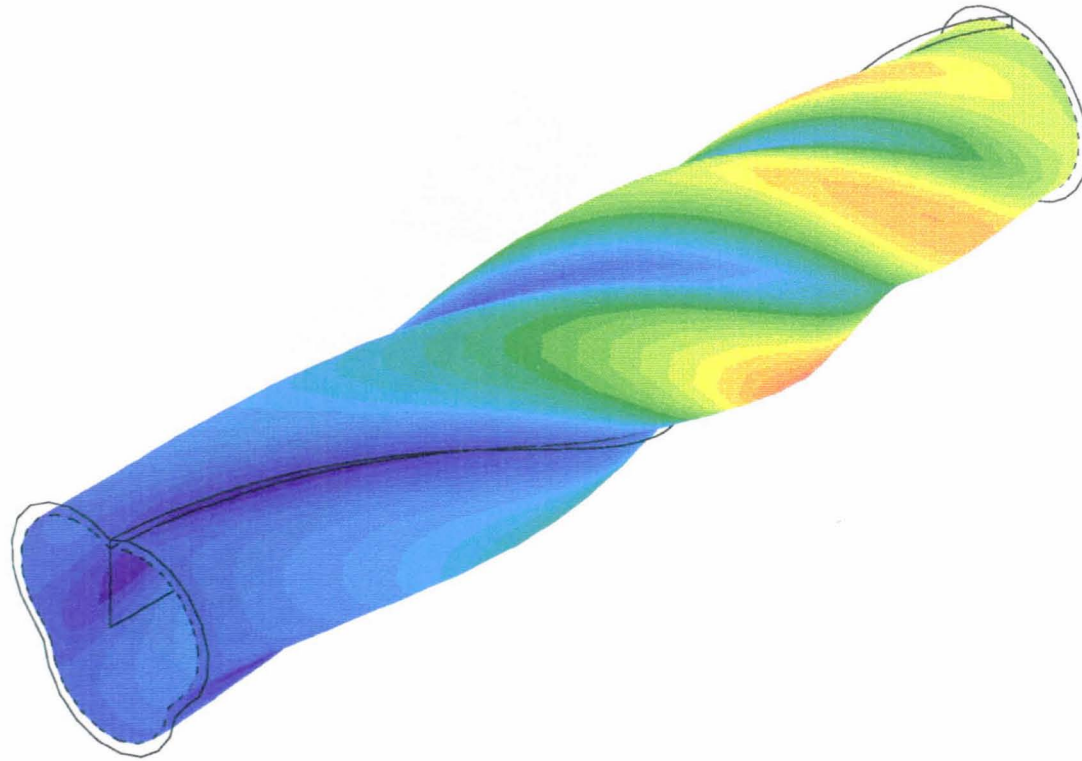
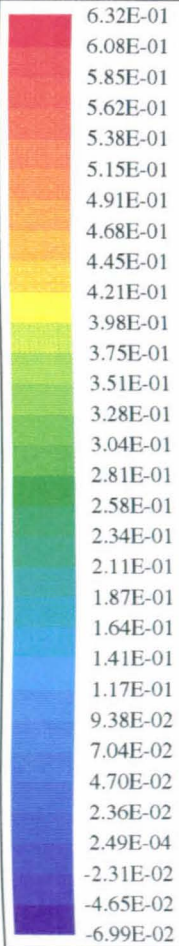


0.3 M PIPE X 50 mm Bore Brachistochrone With End Taper

Static Pressure (Pa)at Wall

Lmax = 3.281E+01 Lmin = -1.049E+03

58-C

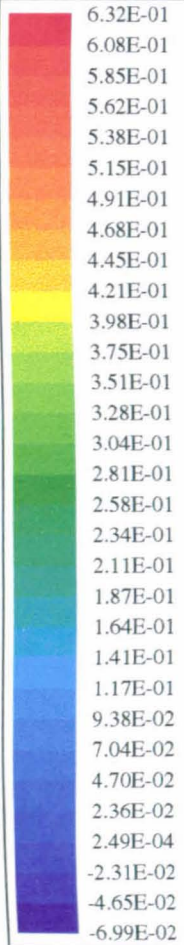


0.3 M PIPE X 50 mm Bore Brachistochrone With End Taper

W-Velocity (M/S) at J=45- View 1

Lmax = 6.319E-01 Lmin = -6.993E-02

59-C

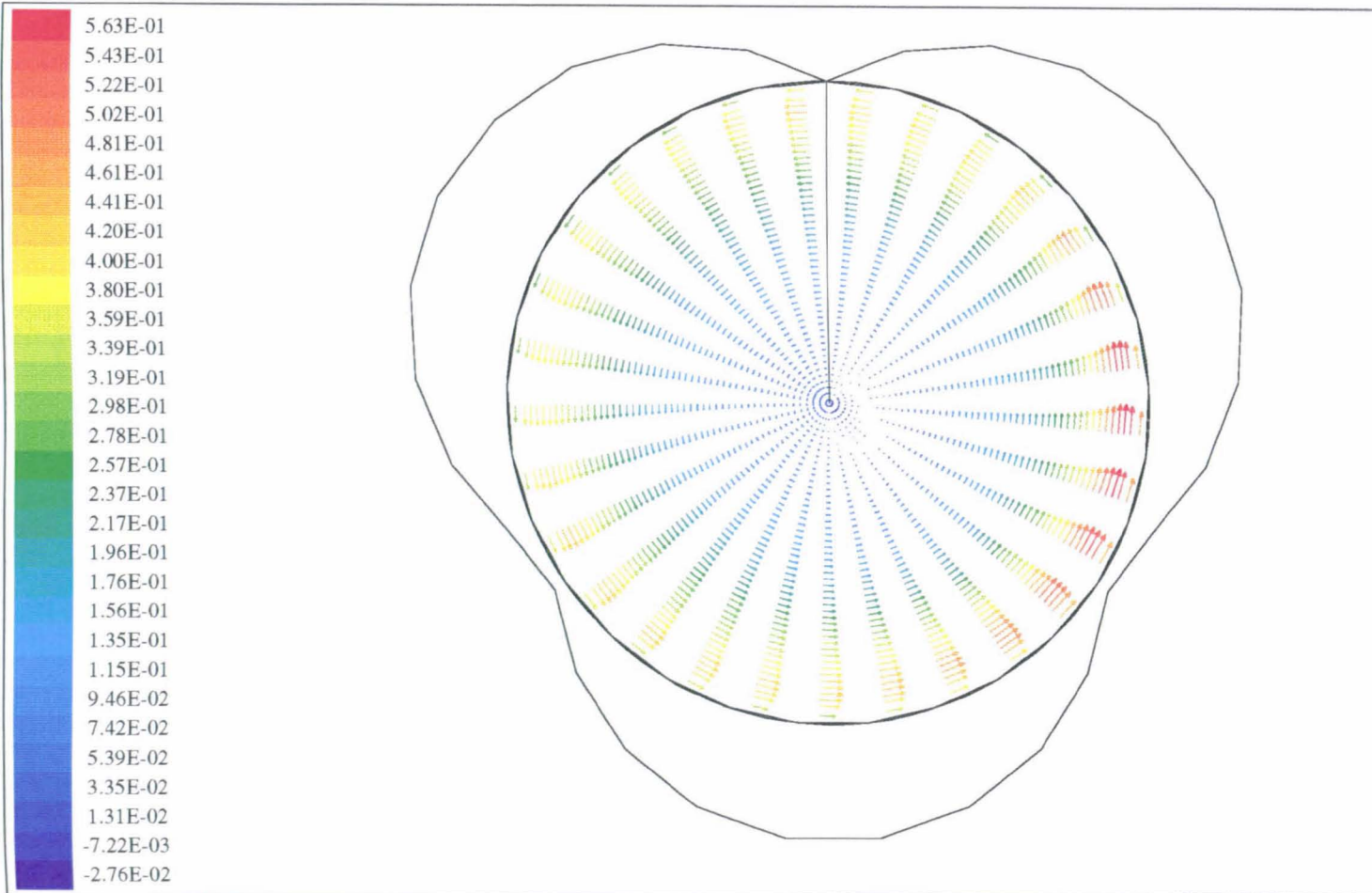


0.3 M PIPE X 50 mm Bore Brachistochrone With End Taper

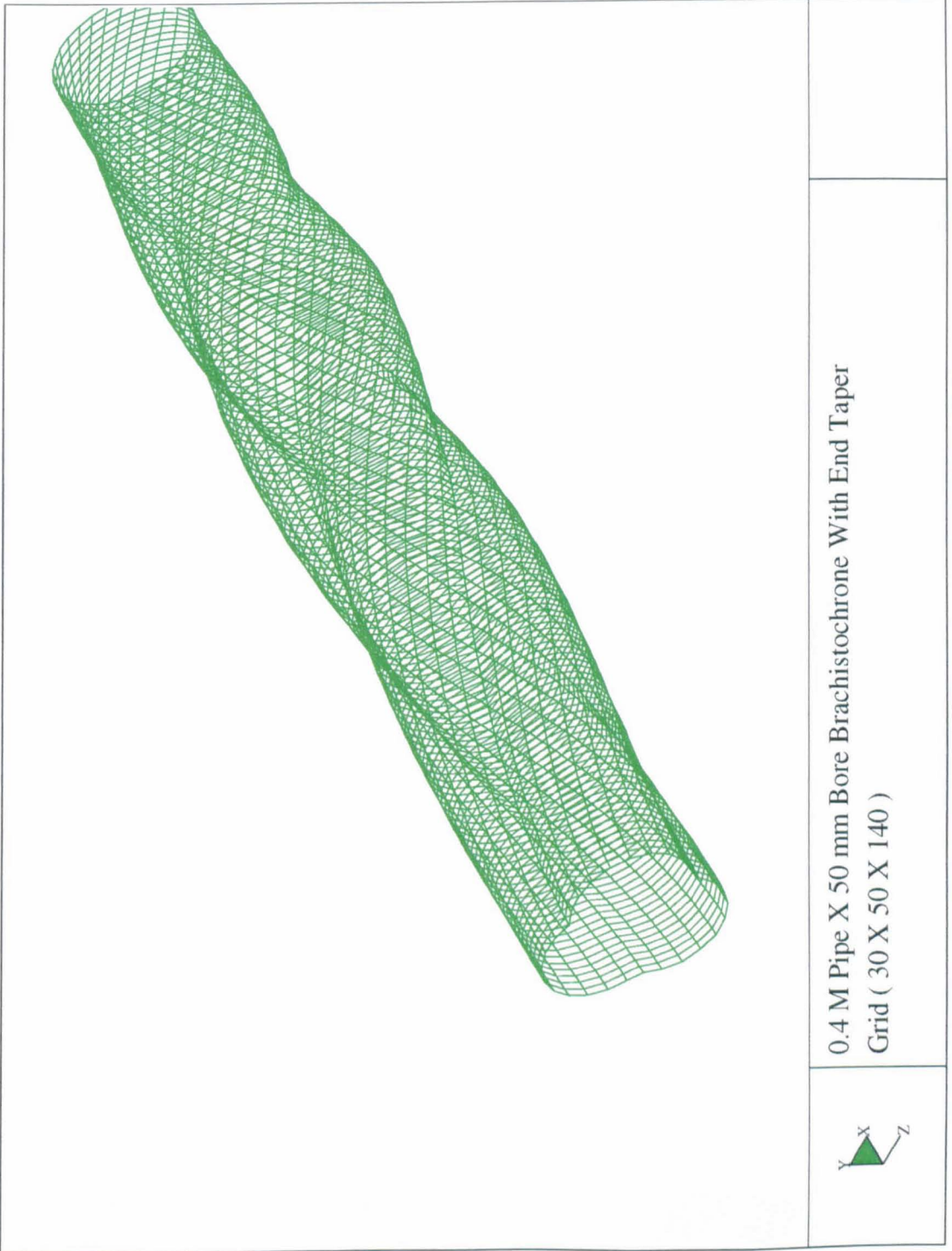
W-Velocity (M/S) at J=45- View 2

Lmax = 6.319E-01 Lmin = -6.993E-02

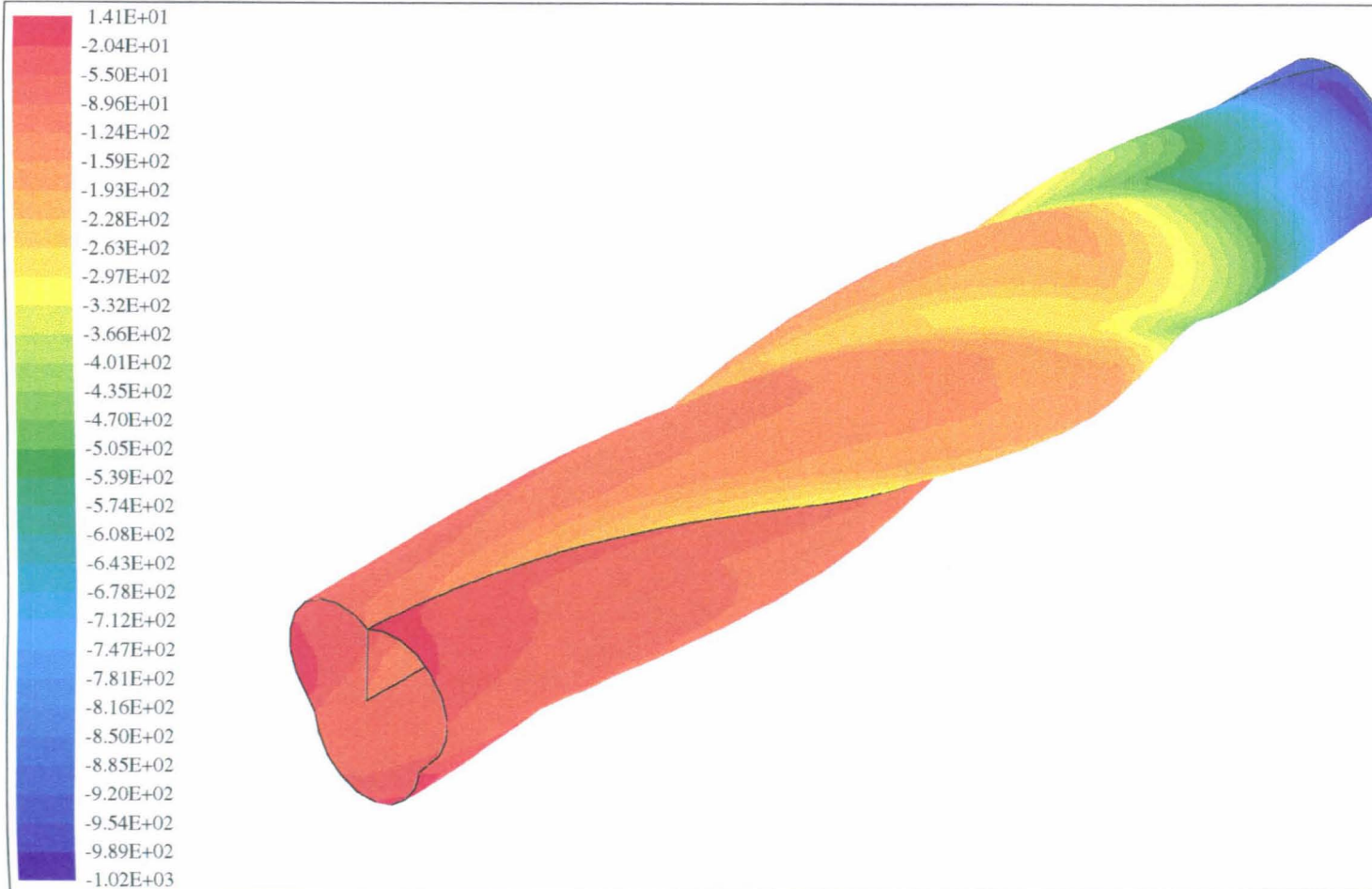
60-C



0.3 M PIPE X 50 mm Bore Brachistochrone With End Taper
W-Velocity (M/S)at Exit
Lmax = 5.629E-01 Lmin = -2.758E-02



62-C

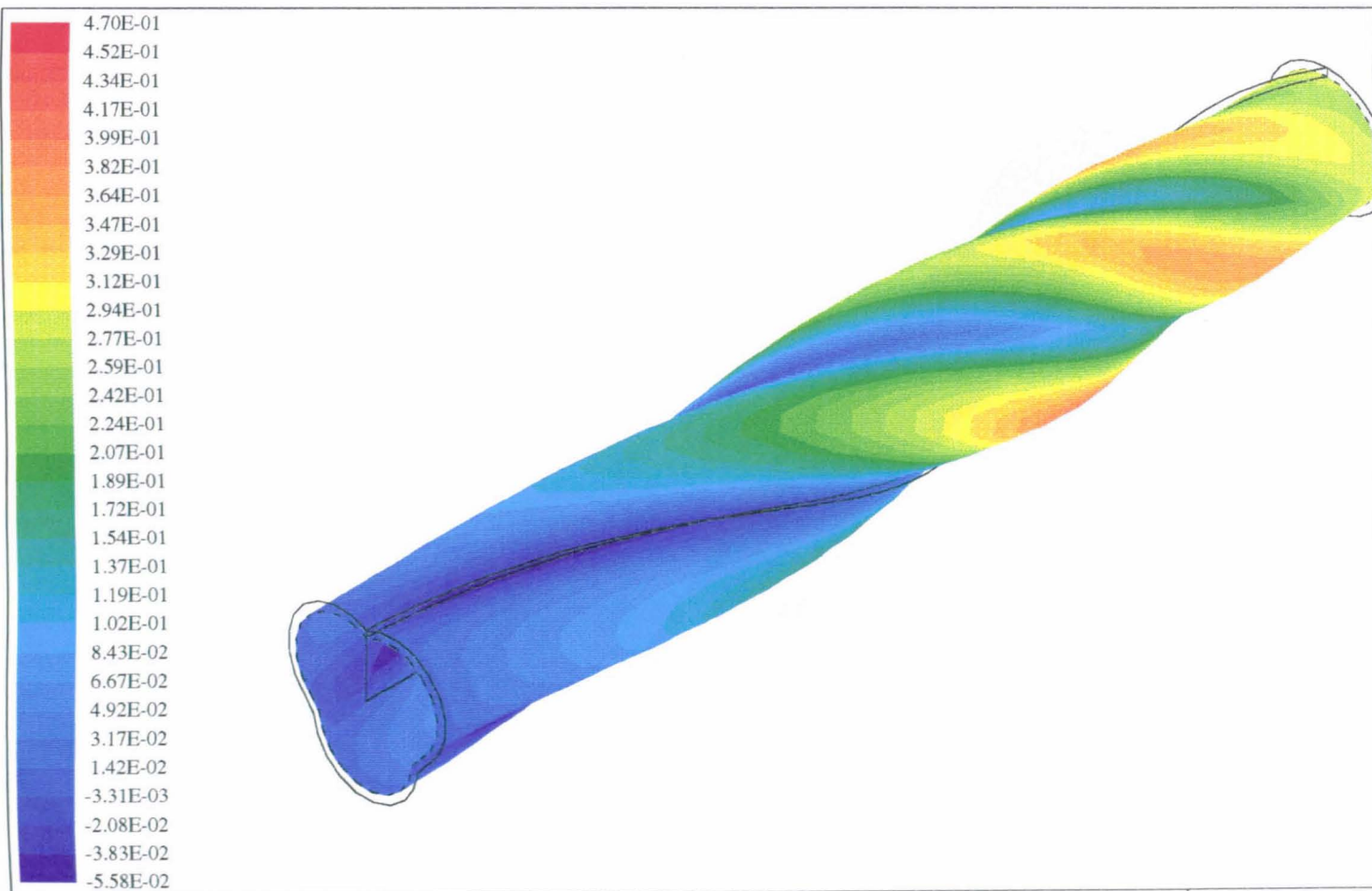


0.4 M Pipe X 50 mm Bore Brachistochrone With End Taper

Static Pressure (Pa)at the Wall

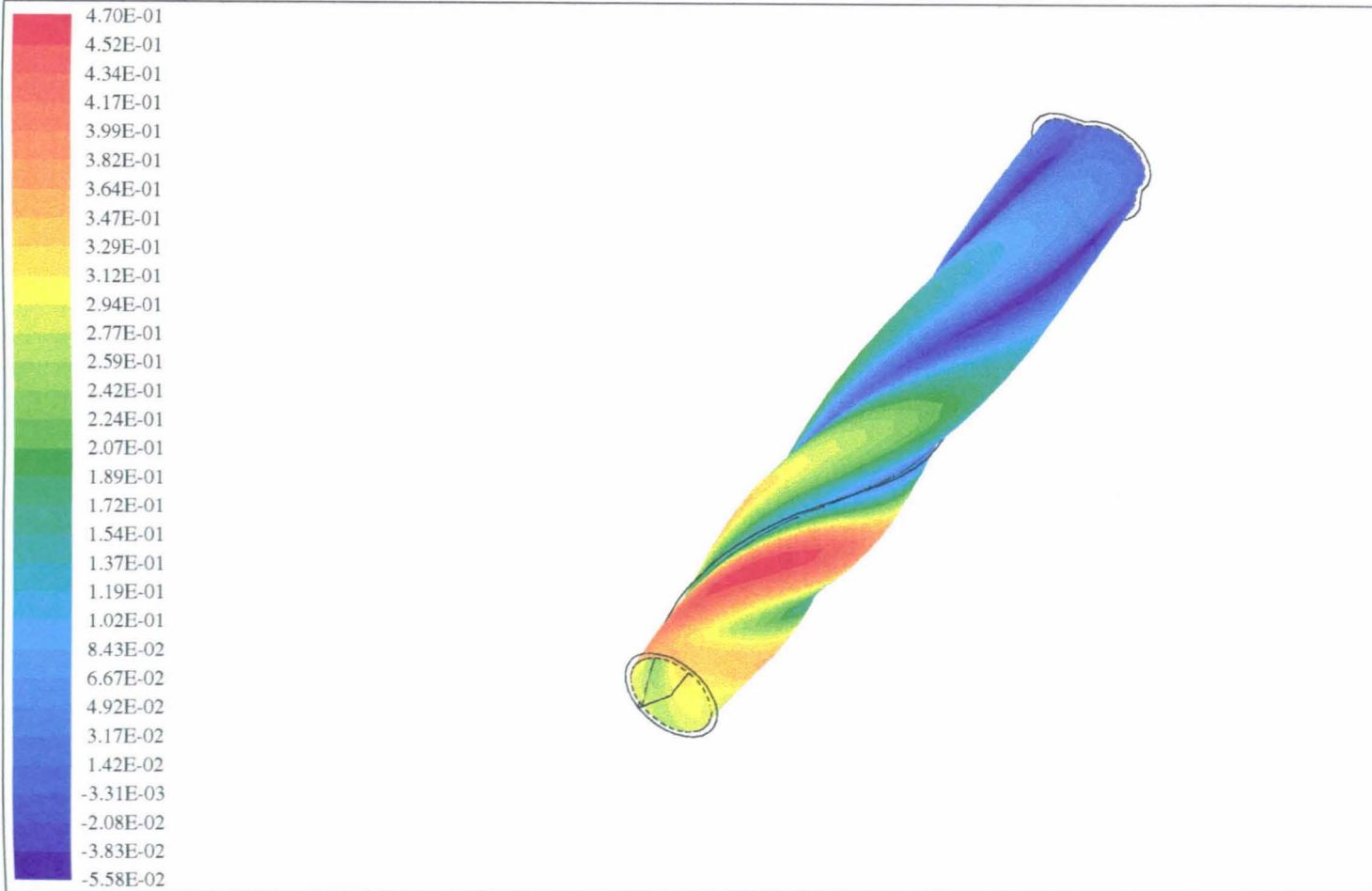
Lmax = 1.414E+01 Lmin = -1.023E+03

63-C



0.4M Pipe X 50 mm Bore Brachistochrone With End Taper
W-Velocity (M/S) at J=45- View 1
Lmax = 4.695E-01 Lmin = -5.584E-02

64-C

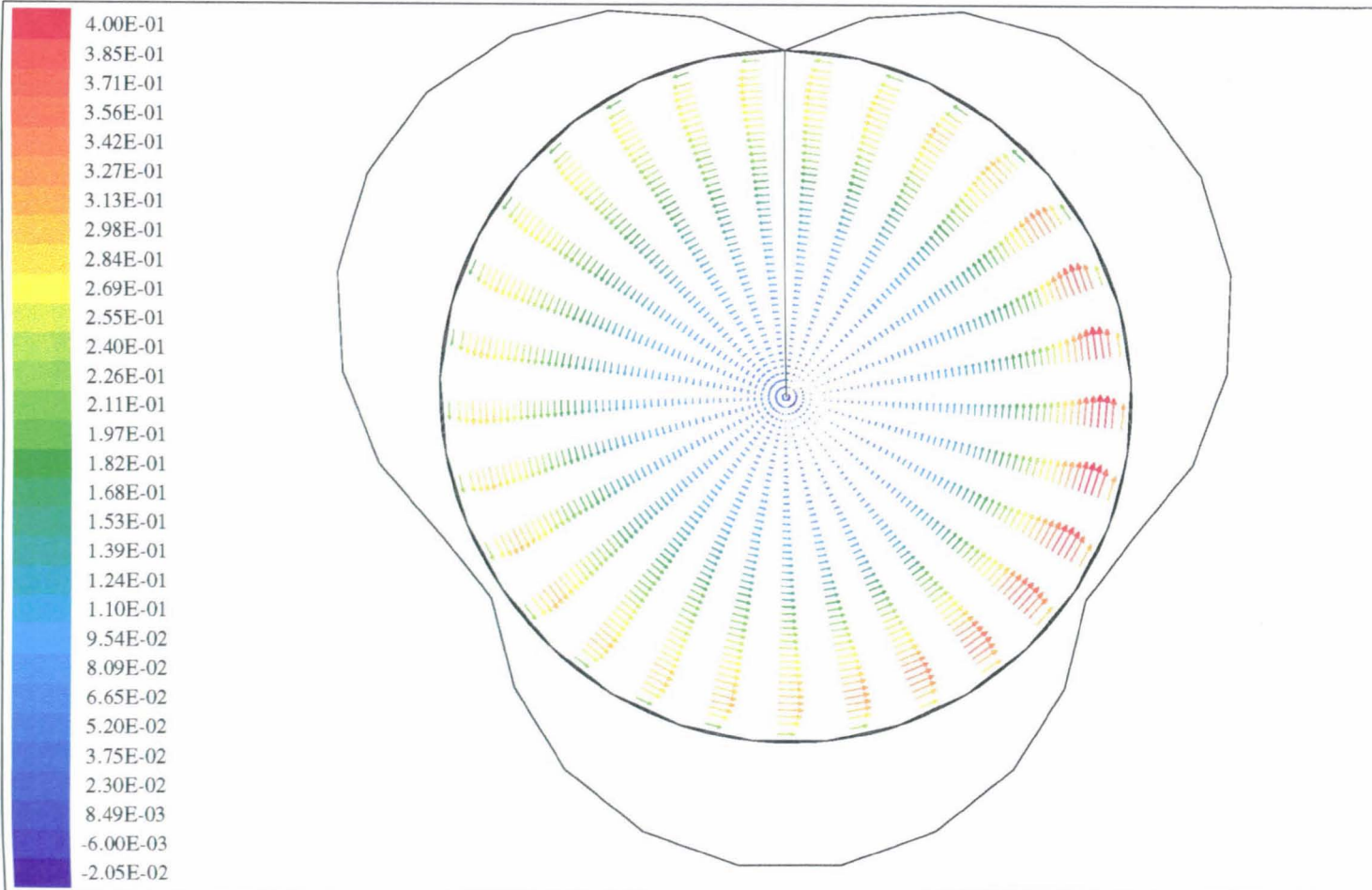


0.4M Pipe X 50 mm Bore Brachistochrone With End Taper

W-Velocity (M/S)at J=45- View 2

Lmax = 4.695E-01 Lmin = -5.584E-02

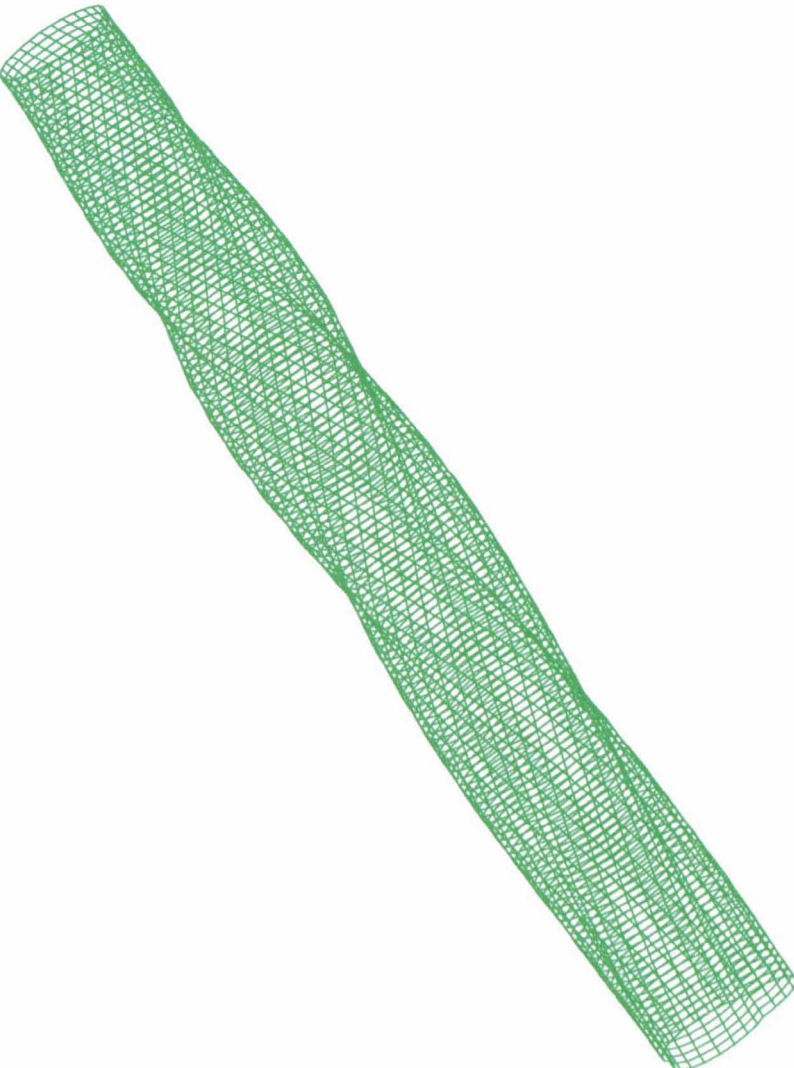
65-C



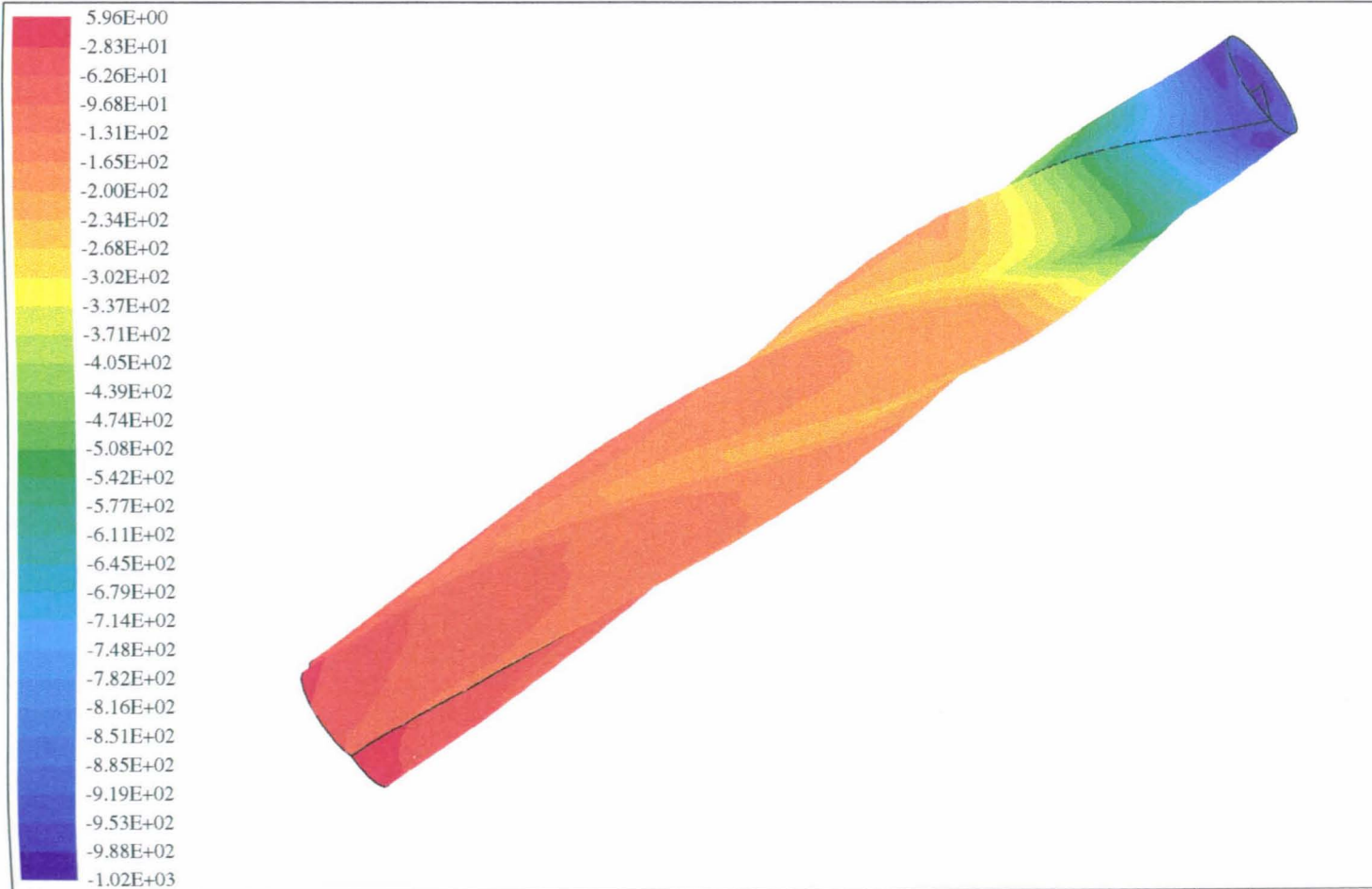
0.4 M Pipe X 50 mm Bore Brachistochrone With End Taper

W-Velocity (M/S)at Exit

Lmax = 3.997E-01 Lmin = -2.049E-02

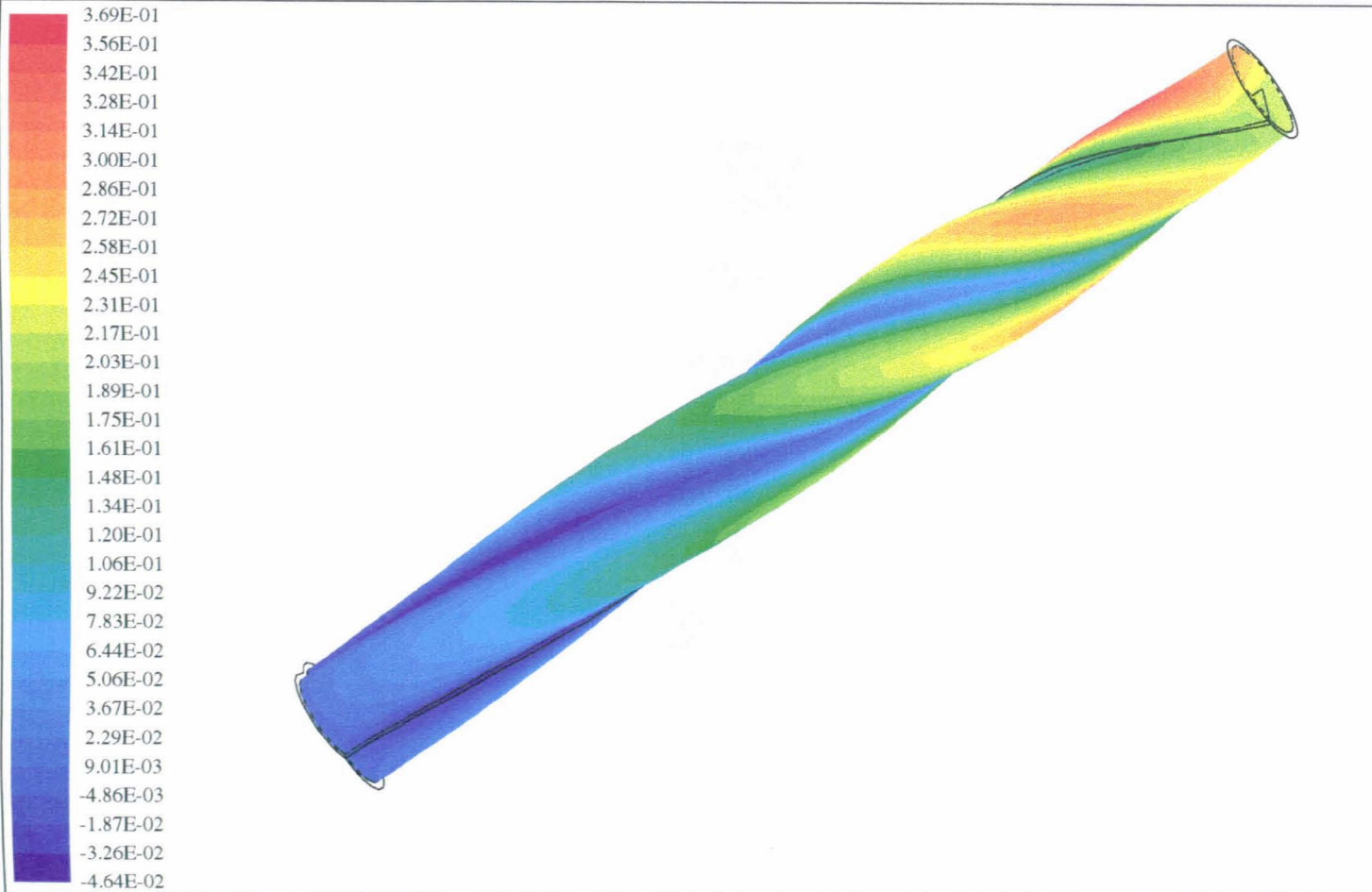
	 <p data-bbox="1173 991 1255 1584">0.5 M Pipe X 50 mm Bore Brachistochrone With End Taper Grid (30 X 50 X 150)</p>
---	---

67-C



0.5M Pipe X 50 mm Bore Brachistochrone
With End Taper Static Pressure (Pa)at the Wall
Lmax = 5.963E+00 Lmin = -1.022E+03

68-C

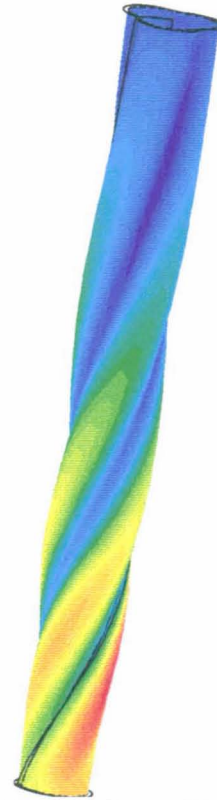
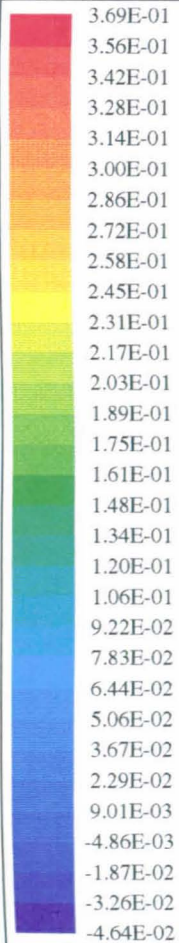


0.5M Pipe X 50 mm Bore Brachistochrone With End Taper

W-Velocity (M/S)at J=45- View 1

Lmax = 3.694E-01 Lmin = -4.644E-02

0-69

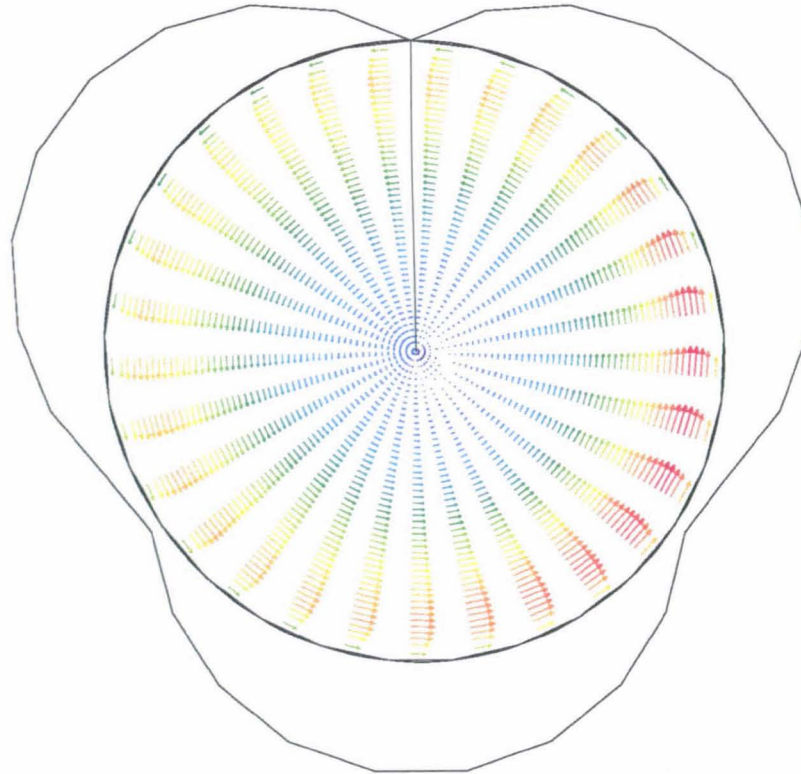
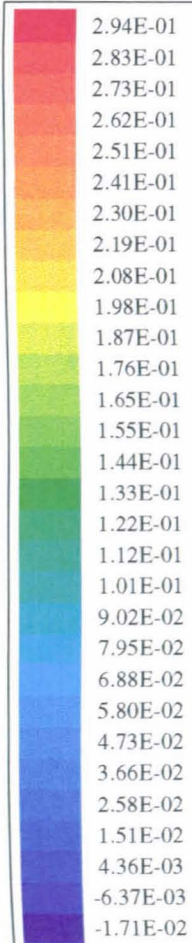


0.5 M Pipe X 50 mm Bore Brachistochrone With End Taper

W-Velocity (M/S) at J=45- View 2

Lmax = 3.694E-01 Lmin = -4.644E-02

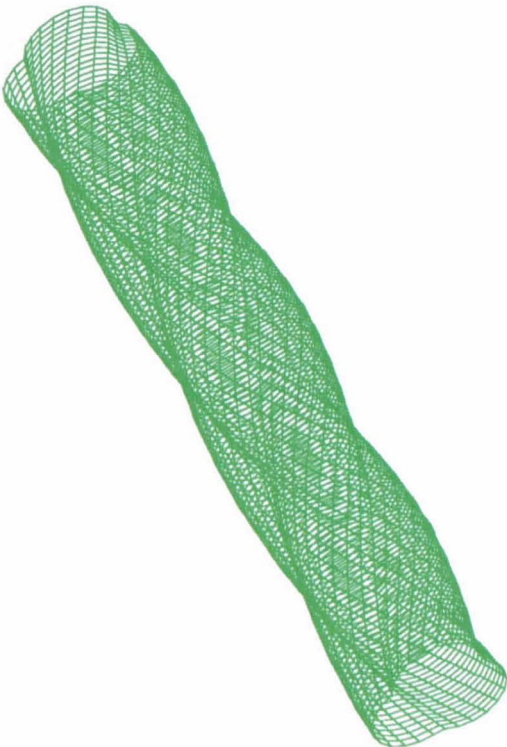
70-C



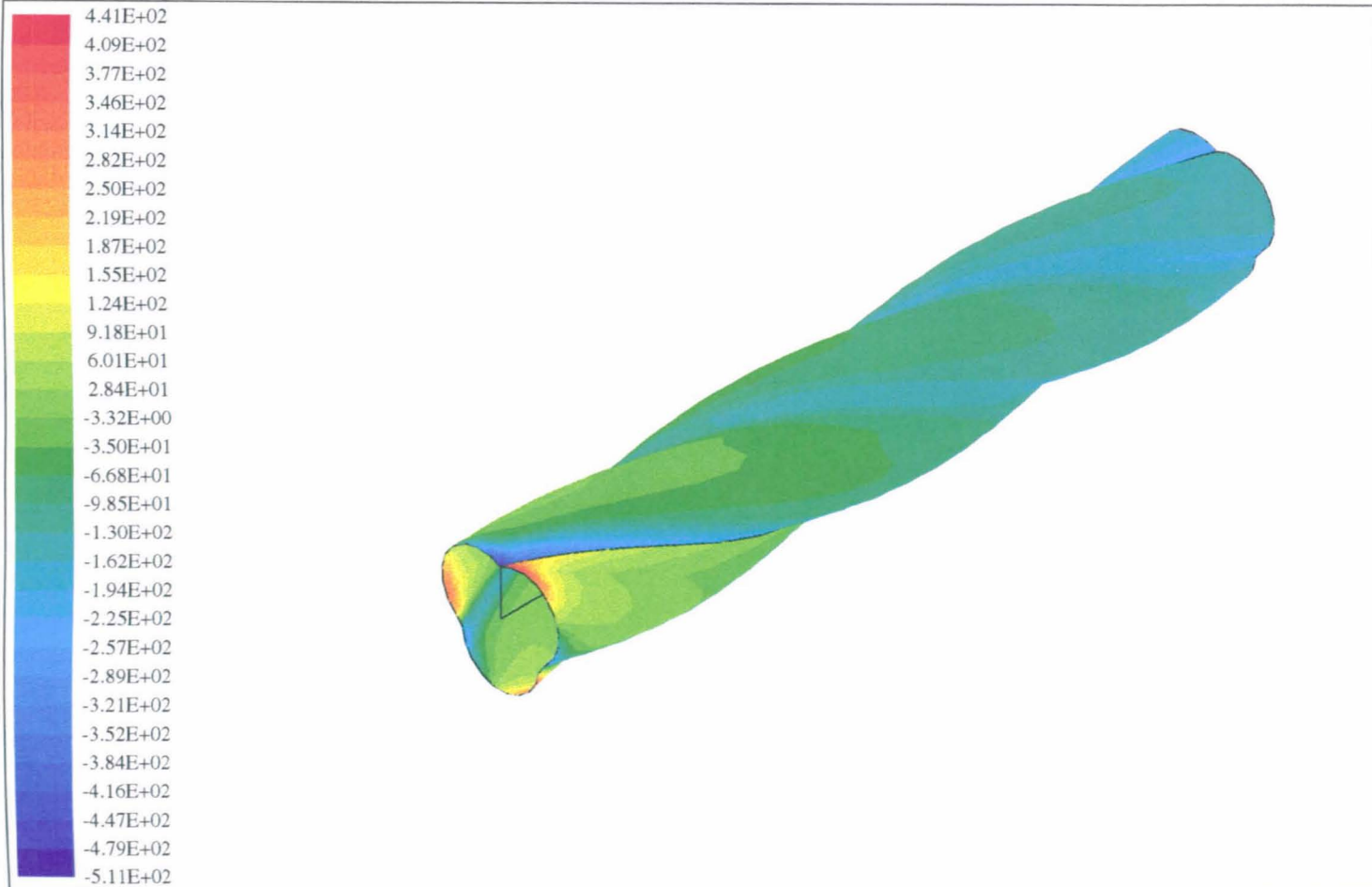
0.5M Pipe X 50 mm Bore Brachistochrone With End Taper

W-Velocity (M/S) at Exit

Lmax = 2.942E-01 Lmin = -1.710E-02

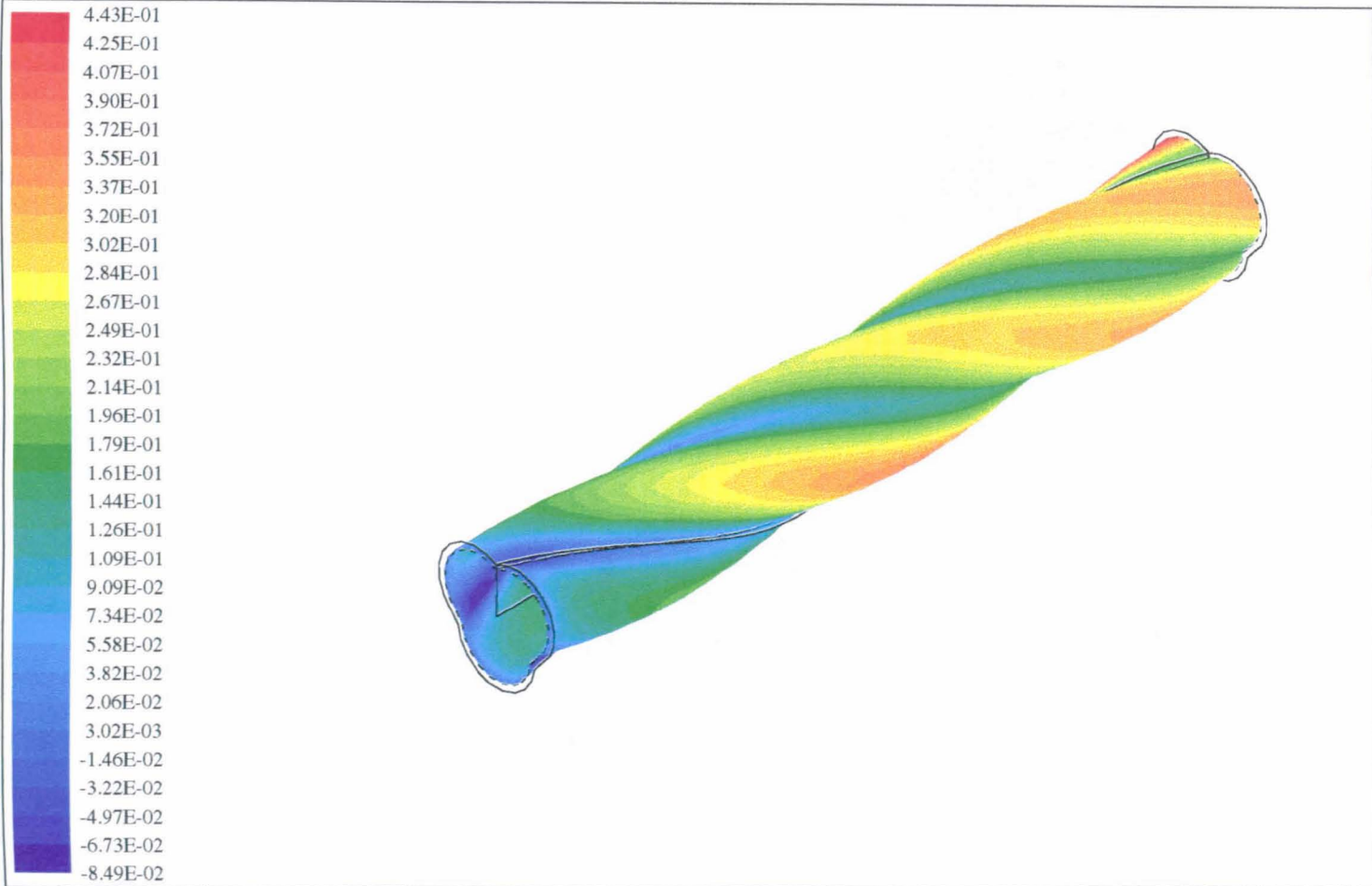
	<p>0.4m Pipe X 50 mm Nominal Bore Standard Swirly-flo Grid Without End Taper Grid (30 X 50 X 140)</p>	
--	---	---

72-C



0.4m Pipe X 50 mm Nominal Bore Standard Swirly-flo Pipe
Without Taper Static Pressure (Pa)
Lmax = 4.407E+02 Lmin = -5.108E+02

73-C



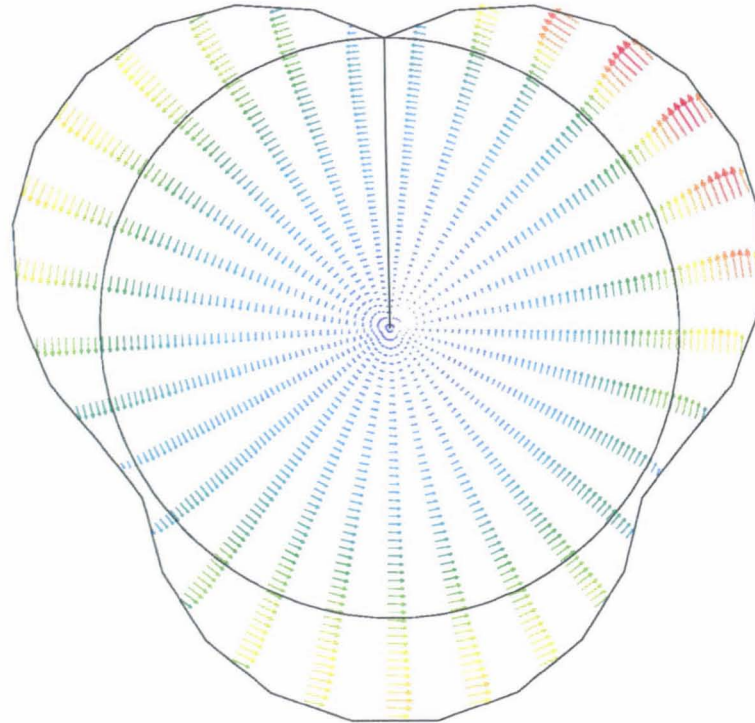
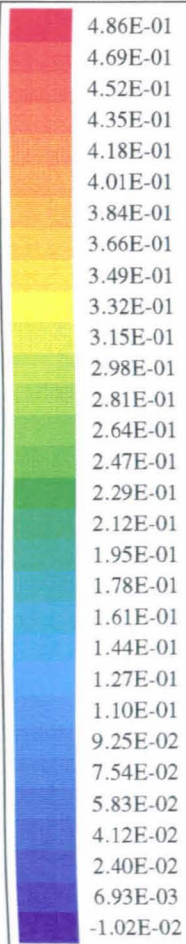
0.4m Pipe X 50 mm Nominal Bore Standard SWirly-flo Pipe
Without End Taper W-Velocity (M/S) at J=45- View 1
Lmax = 4.427E-01 Lmin = -8.491E-02

74-C

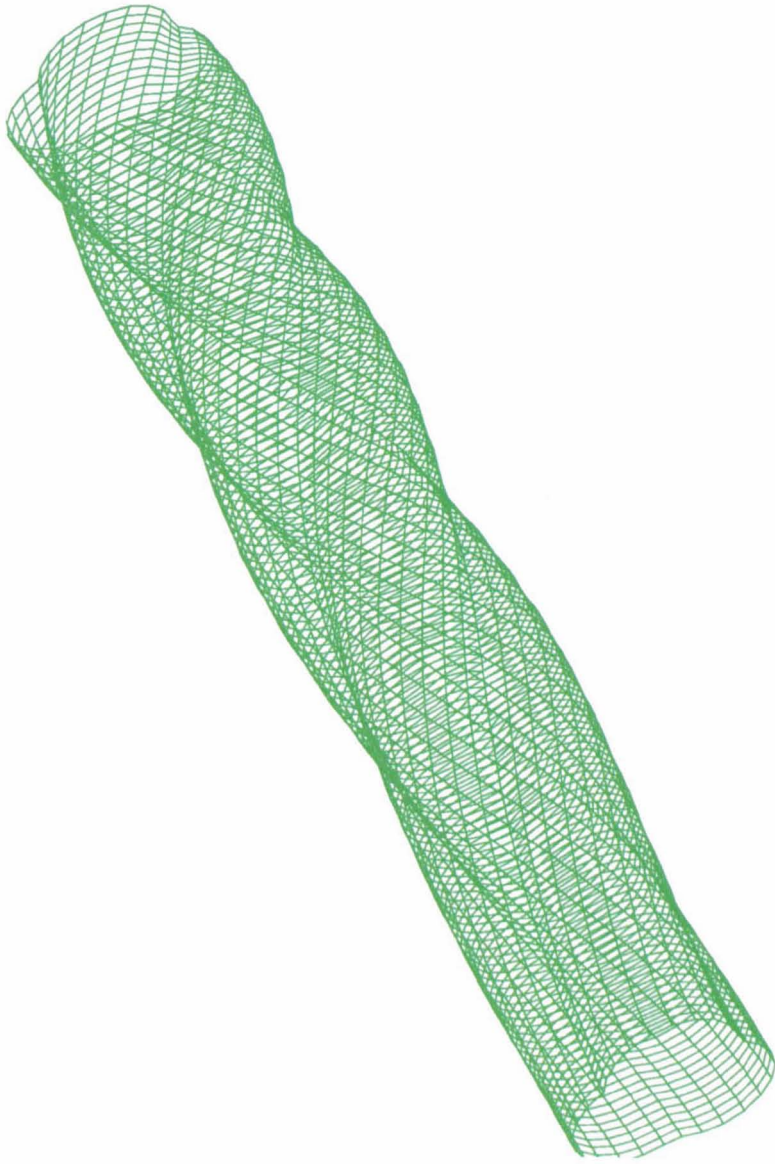


0.4m Pipe X 50 mm Nominal Bore Standard Swirly-flo Pipe
Without End Taper W-Velocity (M/S) at J=45- View 2
Lmax = 4.427E-01 Lmin = -8.491E-02

75-C



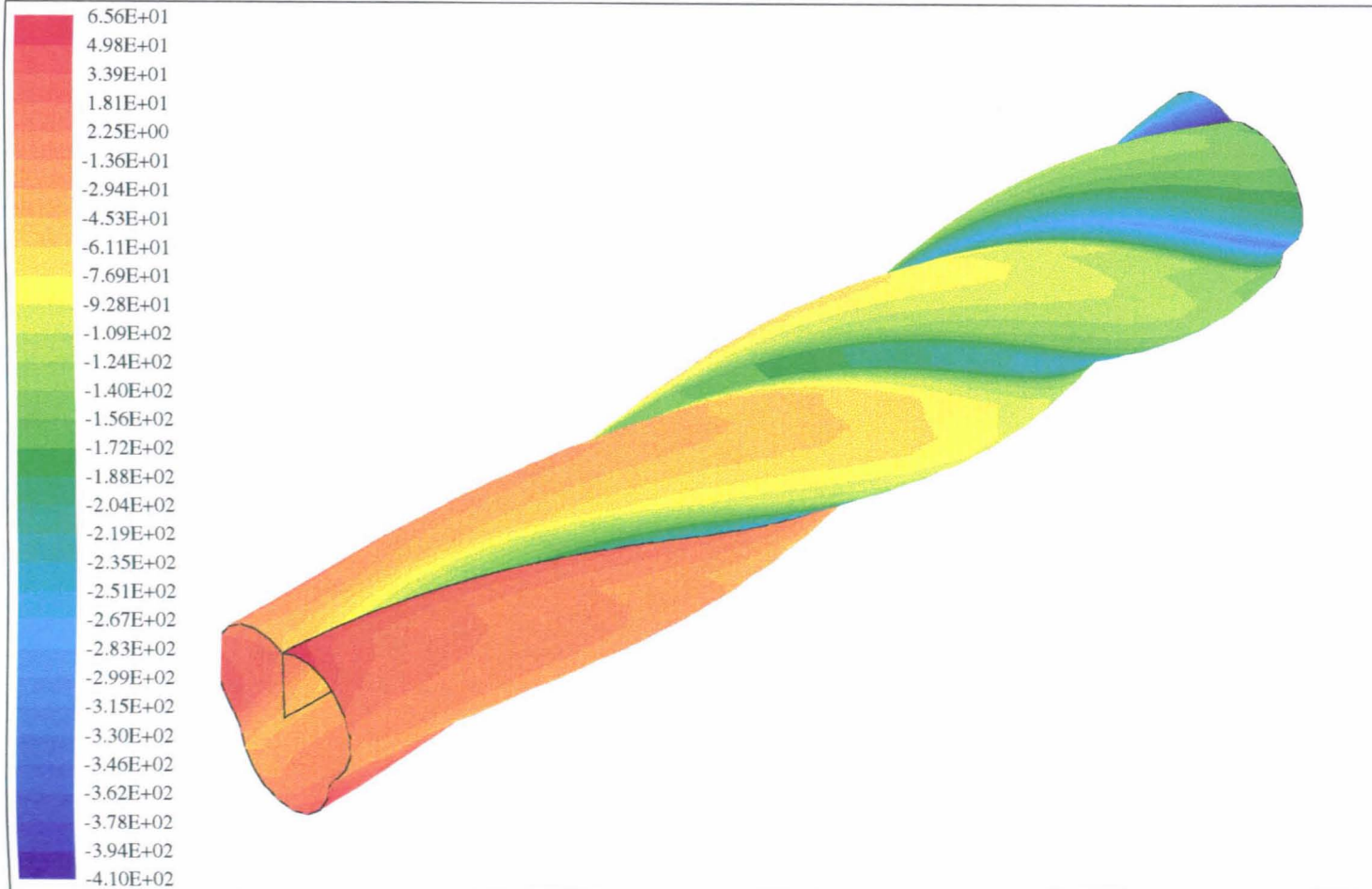
0.4m Pipe X 50 mm Nominal Bore Standard Swirly-flo Pipe
Without End Taper W-Velocity (M/S) at Exit
Lmax = 4.863E-01 Lmin = -1.019E-02



0.4M Pipe X 50 mm Bore Brachistochrone
Without End Taper Grid (30 X 50 X 140)

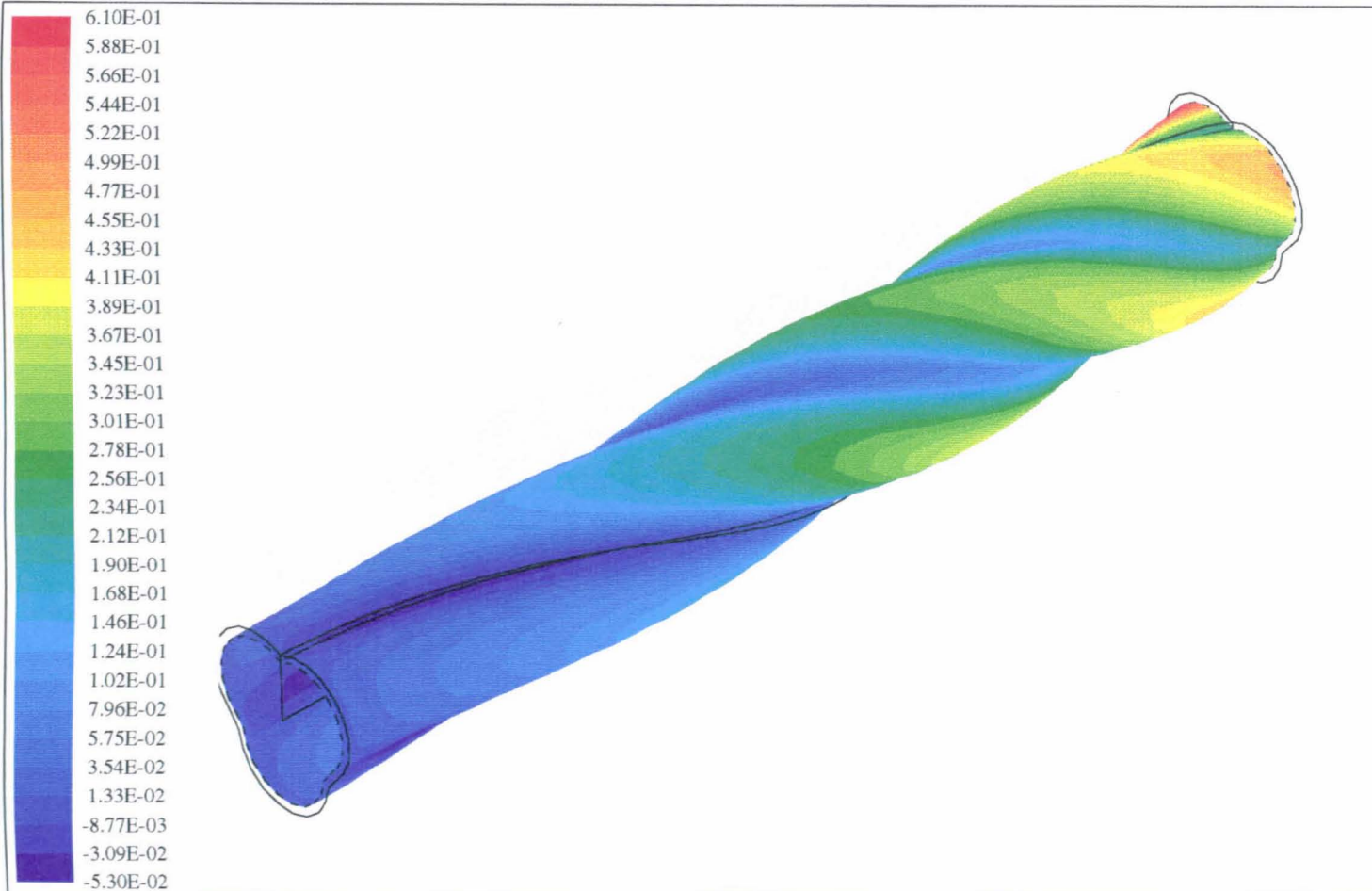


77-C



0.4M PIPE X 50 mm bore Brachistochrone
Without End Taper Static Pressure (Pa) at the Wall
Lmax = 6.560E+01 Lmin = -4.095E+02

78-C

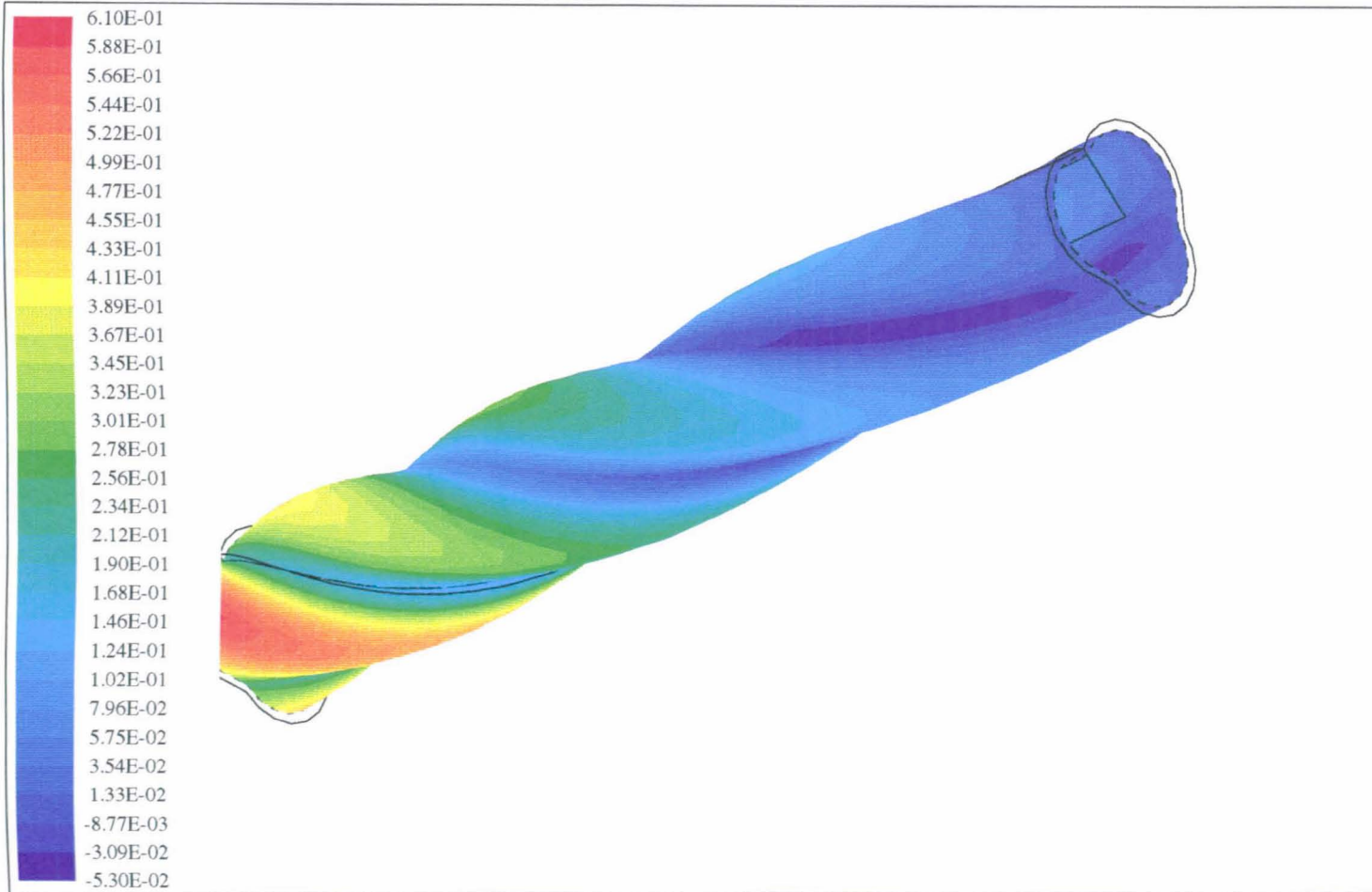


0.4M PIPE X 50 mm bore Brachistochrone Without End Taper

W-Velocity (M/S) at J=45- View 1

Lmax = 6.099E-01 Lmin = -5.296E-02

79-C

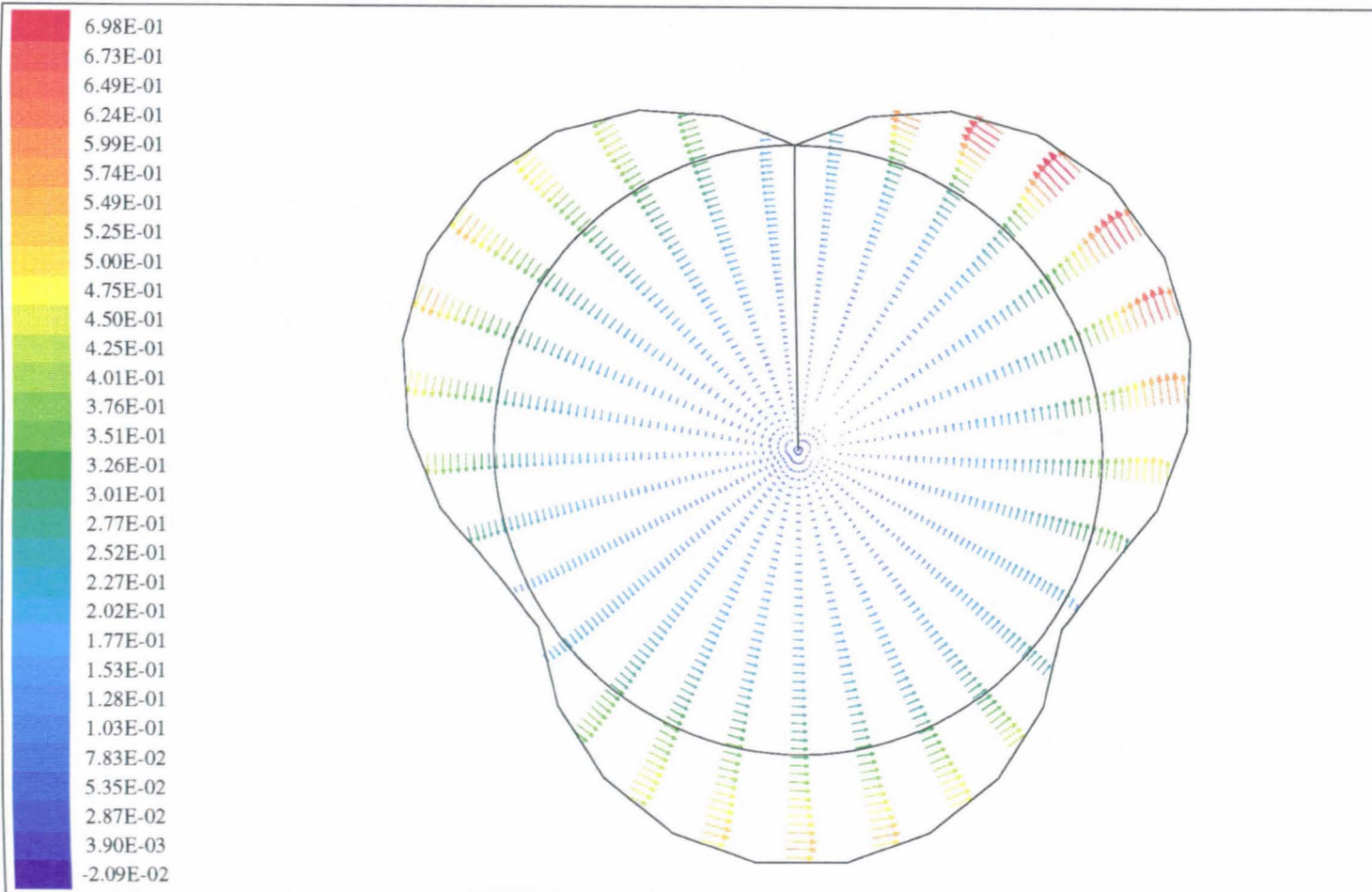


0.4M PIPE X 50 mm bore Brachistochrone Without End Taper

W-Velocity (M/S) at J=45- View 2

Lmax = 6.099E-01 Lmin = -5.296E-02

80-C



0.4M PIPE X 50 mm bore Brachistochrone Without End Taper

W-Velocity (M/S) at Exit

Lmax = 6.981E-01 Lmin = -2.090E-02

Appendix D The Experimental Pressure Results with Graphs

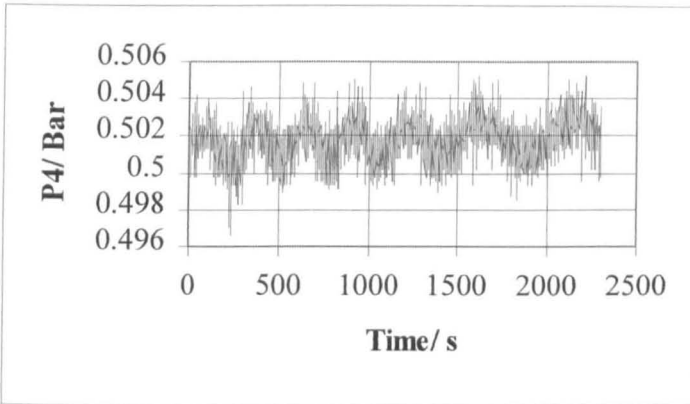
Standard water runs	Water I to Water XXXV
Short <i>Swirly-flo</i> water runs	Water XXXVI to Water LXVII
Medium <i>Swirly-flo</i> water runs	Water LXVIII to Water CIII
Long <i>Swirly-flo</i> water runs	Water CIV to Water CXXXIX
Standard Pipe Arrangement with 2kg	I to XXXVI
Standard Pipe Arrangement with 4kg	XXXVII to LXXII
Standard Pipe Arrangement with 6kg	LXXIII to CIX
Standard Pipe Arrangement with 8kg	CX to CXLV
Long <i>Swirly-flo</i> Pipe Arrangement (pos 1)	CXLVI to CLXCV
Long <i>Swirly-flo</i> Pipe Arrangement (pos 2)	CLXCVI to CCXXXV
Long <i>Swirly-flo</i> Pipe Arrangement (pos 3)	CCXXXVI to CCLXV
Long <i>Swirly-flo</i> Pipe Arrangement (pos 4)	CCLXVI to CCC
Long <i>Swirly-flo</i> Pipe Arrangement (pos 5)	CCCI to CCCXXXVI
Long <i>Swirly-flo</i> Pipe Arrangement (pos 6)	CCCXXXVII to CCCLXXII
Long <i>Swirly-flo</i> Pipe Arrangement (optimum position) 4Kg	CCCLXXIII to CCCXCVIII
Long <i>Swirly-flo</i> Pipe Arrangement (optimum position) 6Kg	CCCXCIX to CDXXVI
Long <i>Swirly-flo</i> Pipe Arrangement (optimum position) 8Kg	CDXXVII to CDLIV

Standard Pipe Arrangement

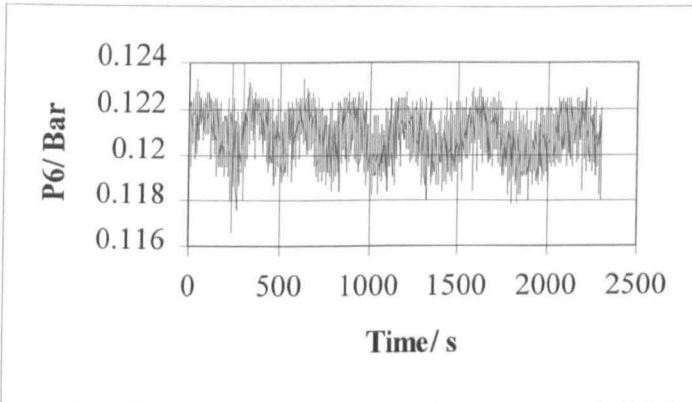
Run: water20

Volumetric Flow: 1.009 l/s

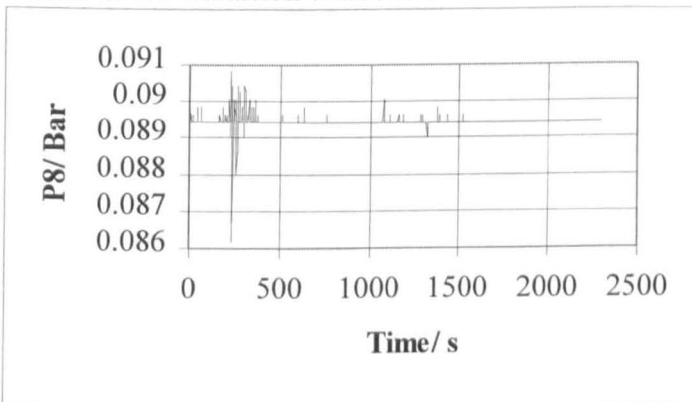
Number of Data of Points:2302



Water I P4 variation with time



Water II P6 variation with time



Water III P8 variation with time

	p1	p2	p3	p4	p5	p6	p7	p8
mean	0.499067	0.505548	0.502901	0.501795	0.484286	0.120857	0.092682	0.089439
median	0.49907	0.50562	0.50287	0.50198	0.4843	0.12089	0.0927	0.08943
mode	0.49907	0.50706	0.50287	0.50259	0.4845	0.12068	0.09188	0.08943
standard deviation	7.97E-05	0.001462	0.001276	0.001138	0.00114	0.001019	0.00088	0.000121
variance	6.35E-09	2.14E-06	1.63E-06	1.3E-06	1.3E-06	1.04E-06	7.75E-07	1.46E-08
skew	-27.5108	-0.03576	-0.18907	-0.28487	0.181905	-0.27555	0.074742	-7.07845
kurtosis	1011.789	-0.41587	-0.07271	0.134312	0.504472	-0.40387	0.386985	279.737

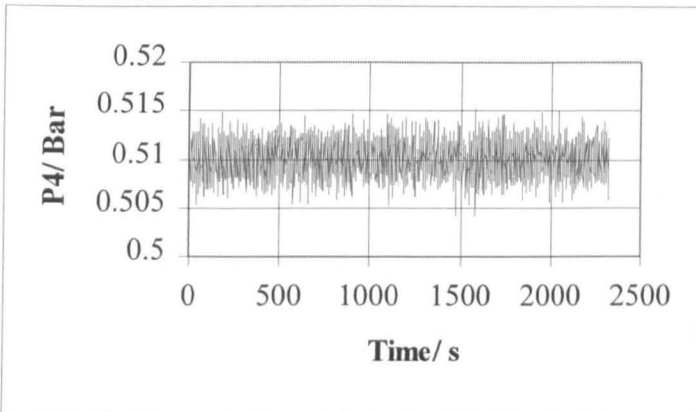
Water IV Pressure Readings and Statistical Data

Standard Pipe Arrangement

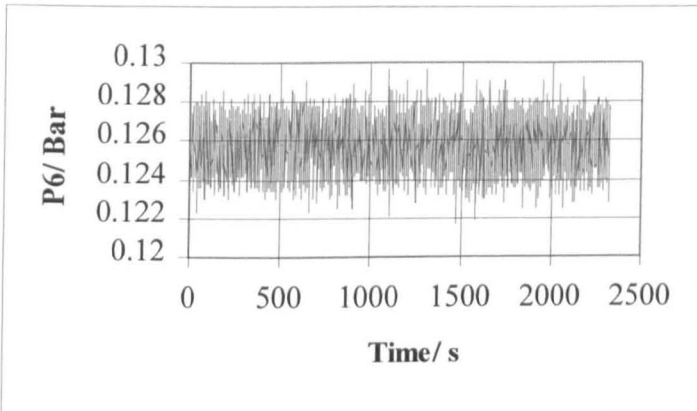
Run: water25

Volumetric Flow: 1.421 l/s

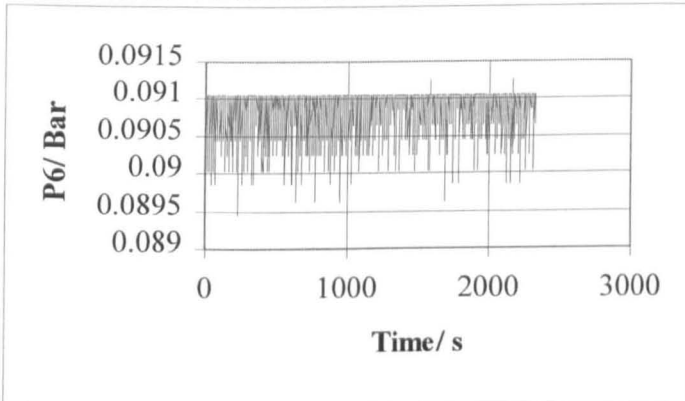
Number of Data of Points:2326



Water V P4 variation with time



Water VI P6 variation with time



Water VII P8 variation with time

	p1	p2	p3	p4	p5	p6	p7	p8
mean	0.537702	0.517711	0.512168	0.510024	0.491819	0.125818	0.098052	0.090904
median	0.53794	0.5179	0.51207	0.50996	0.49187	0.1258	0.09822	0.09106
mode	0.53999	0.51851	0.51289	0.51078	0.49269	0.1258	0.09843	0.09106
standard deviation	0.001966	0.001646	0.001737	0.00176	0.001726	0.00137	0.001323	0.000271
variance	3.86E-06	2.71E-06	3.02E-06	3.1E-06	2.98E-06	1.88E-06	1.75E-06	7.33E-08
skew	-0.68928	-0.05583	-0.02112	-0.0345	-0.05249	-0.07165	-0.18712	-1.97058
kurtosis	-0.29505	0.280306	-0.23905	-0.34374	-0.38066	-0.59872	-0.50043	3.679977

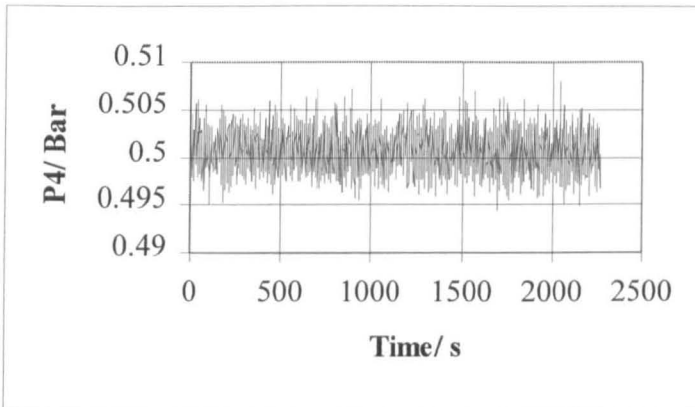
Water VIII Pressure Readings and Statistical Data

Standard Pipe Arrangement

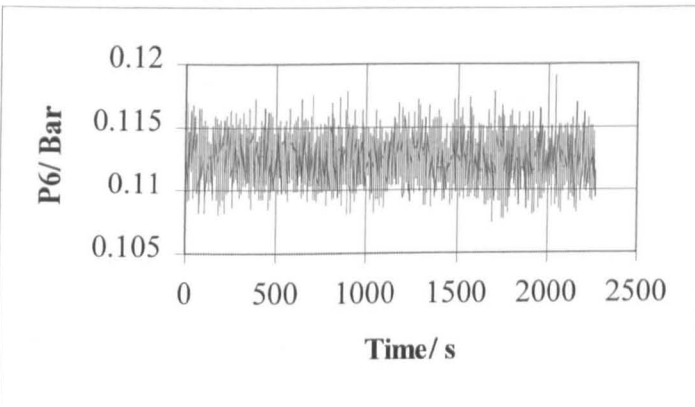
Run: water30

Volumetric Flow: 1.839 l/s

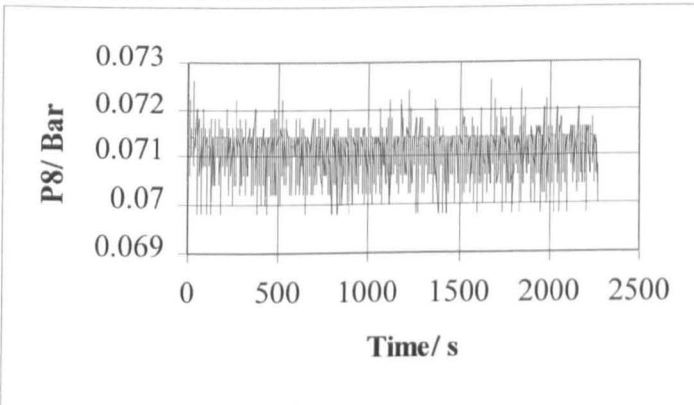
Number of Data of Points:2265



Water IX P4 variation with time



Water X P6 variation with time



Water XI P8 variation with time

	p1	p2	p3	p4	p5	p6	p7	p8
mean	0.577734	0.514635	0.504125	0.500784	0.481611	0.112508	0.084085	0.07116
median	0.57784	0.51463	0.50409	0.50075	0.48143	0.1125	0.08411	0.07142
mode	0.57784	0.51422	0.50368	0.50034	0.48082	0.11291	0.0839	0.07142
standard deviation	0.002368	0.002342	0.002096	0.002019	0.002053	0.001804	0.001699	0.000423
variance	5.61E-06	5.48E-06	4.39E-06	4.08E-06	4.21E-06	3.25E-06	2.89E-06	1.79E-07
skew	0.137192	5.61E-05	0.072978	0.049136	0.081237	0.037509	0.033548	-0.91916
kurtosis	-0.47158	-0.03006	-0.13424	-0.10899	-0.11814	-0.31476	-0.34275	1.087337

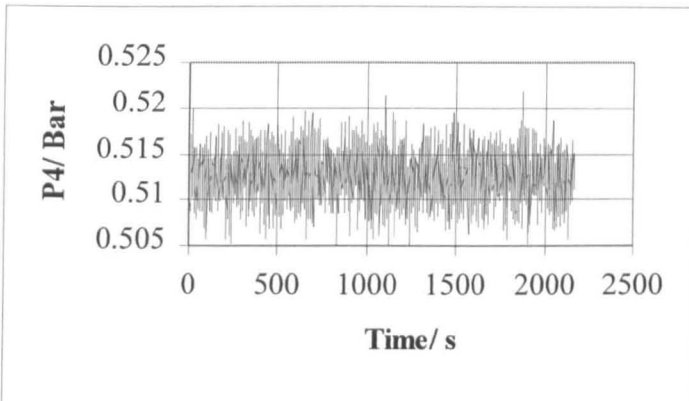
Water XII Pressure Readings and Statistical Data

Standard Pipe Arrangement

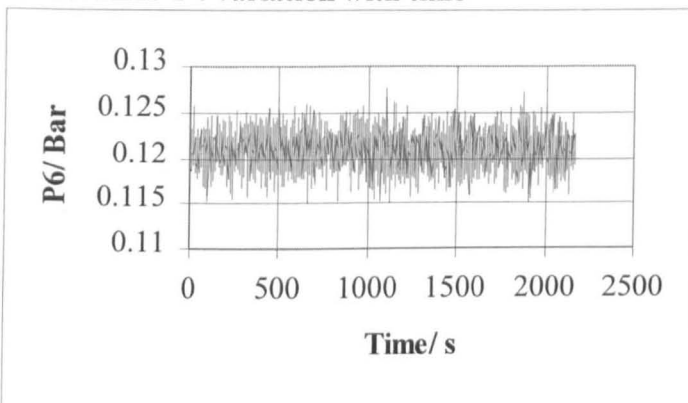
Run: water35

Volumetric Flow: 2.24 l/s

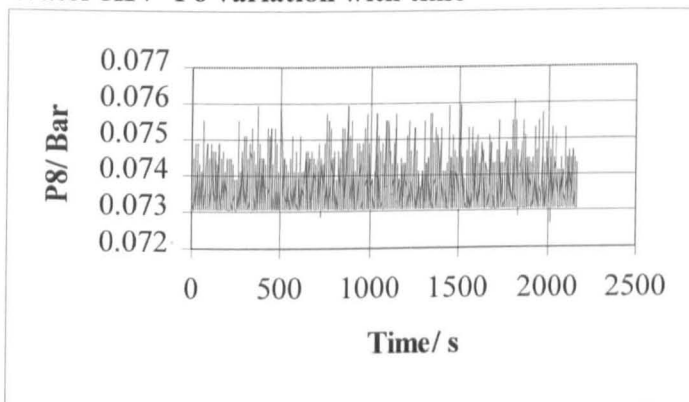
Number of Data of Points:2164



Water XIII P4 variation with time



Water XIV P6 variation with time



Water XV P8 variation with time

	p1	p2	p3	p4	p5	p6	p7	p8
mean	0.637068	0.531372	0.517023	0.51252	0.492829	0.120946	0.091828	0.073571
median	0.63717	0.5314	0.51698	0.51262	0.49289	0.12089	0.09188	0.07347
mode	0.63717	0.53161	0.5176	0.51262	0.49432	0.12068	0.09249	0.07306
standard deviation	0.002042	0.00312	0.002596	0.002534	0.002464	0.001914	0.001866	0.000596
variance	4.17E-06	9.73E-06	6.74E-06	6.42E-06	6.07E-06	3.66E-06	3.48E-06	3.55E-07
skew	-0.37593	0.076188	0.041753	0.013038	-0.0187	-0.05489	0.008315	1.3183
kurtosis	0.479915	0.151724	0.125218	0.054923	0.051494	0.014902	0.024802	1.384795

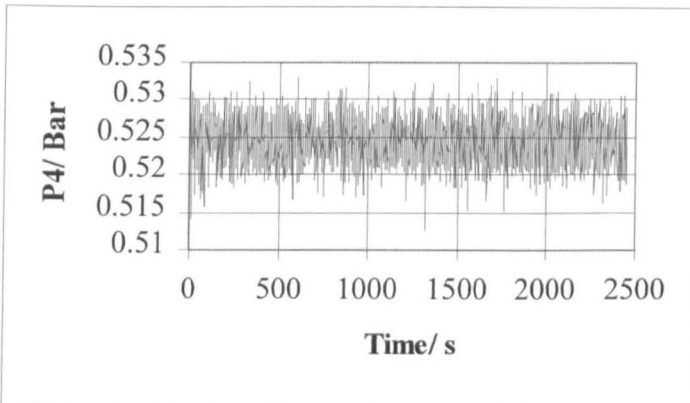
Water XVI Pressure Readings and Statistical Data

Standard Pipe Arrangement

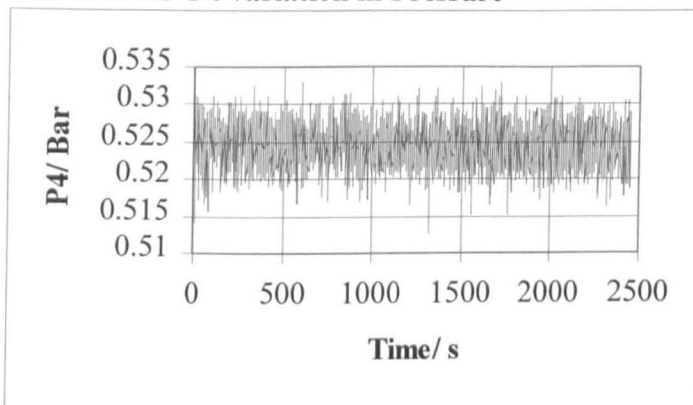
Run: water40

Volumetric Flow: 2.602 l/s

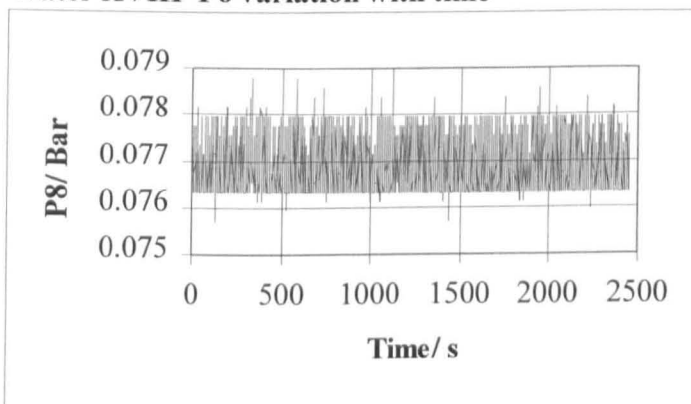
Number of Data of Points:2444



Water XVII P4 variation in Pressure



Water XVIII P6 variation with time



Water XIX P8 variation with time

	p1	p2	p3	p4	p5	p6	p7	p8
mean	0.698094	0.548579	0.529931	0.524519	0.504243	0.129334	0.099964	0.076875
median	0.69854	0.54859	0.52987	0.52448	0.50414	0.12928	0.09986	0.07674
mode	0.69854	0.5492	0.52905	0.52366	0.50435	0.12907	0.10006	0.07633
standard deviation	0.00266	0.003755	0.002977	0.002864	0.002783	0.002064	0.001996	0.00057
variance	7.08E-06	1.41E-05	8.86E-06	8.2E-06	7.75E-06	4.26E-06	3.98E-06	3.25E-07
skew	-0.10572	-0.06455	-0.0019	-0.03484	-0.05658	-0.01138	-0.05398	0.716479
kurtosis	-0.07744	0.023288	-0.03839	-0.11505	-0.10777	-0.10054	-0.01284	-0.66085

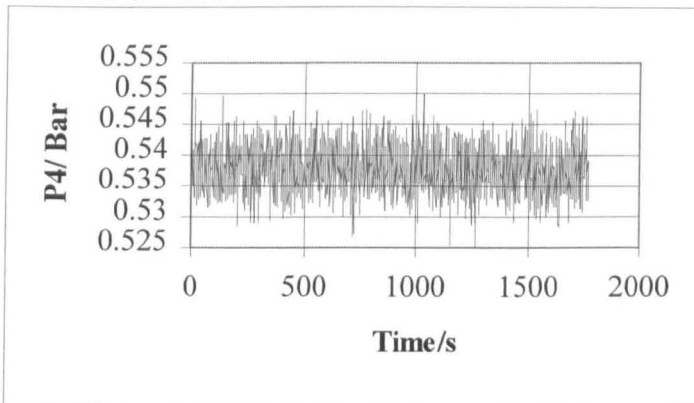
Water XX Pressure Readings and Statistical Data

Standard Pipe Arrangement

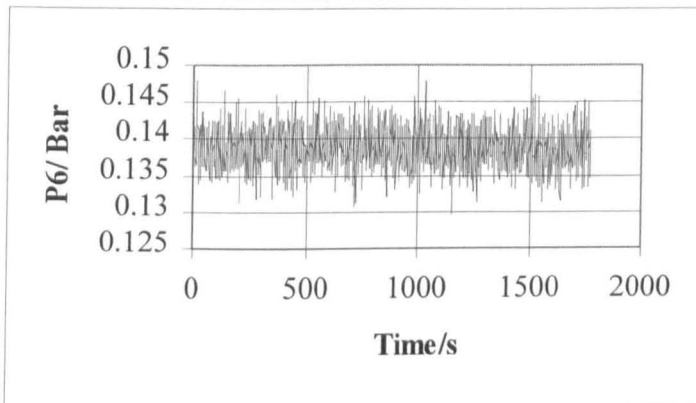
Run: water45

Volumetric Flow: 2.928 l/s

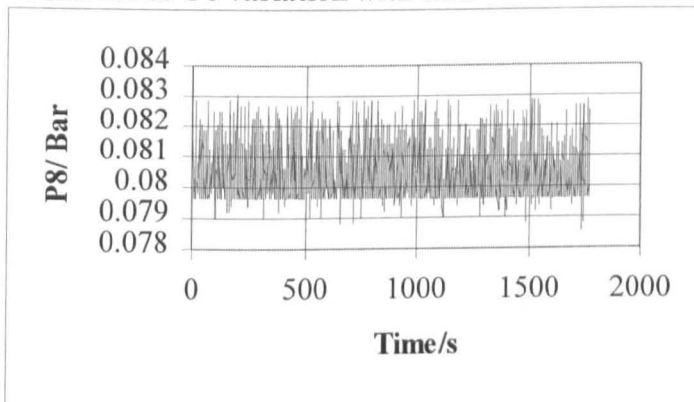
Number of Data of Points:1771



Water XXI P4 variation with time



Water XXII P6 variation with time



XXIII P8 variation with time

	p1	p2	p3	p4	p5	p6	p7	p8
mean	0.767371	0.567363	0.544456	0.537789	0.516984	0.138849	0.109152	0.08046
median	0.76708	0.5672	0.5444	0.53778	0.51683	0.13889	0.10907	0.08022
mode	0.76912	0.56659	0.54521	0.53799	0.51683	0.13889	0.10927	0.07961
standard deviation	0.002942	0.004624	0.003855	0.003618	0.003561	0.002623	0.002591	0.000888
variance	8.63E-06	2.13E-05	1.48E-05	1.31E-05	1.27E-05	6.88E-06	6.71E-06	7.89E-07
skew	-0.10379	0.12198	0.10027	0.09314	0.068622	0.032199	-0.00499	0.840602
kurtosis	0.006884	-0.01585	-0.01312	-0.01141	-0.05764	0.035809	-0.01087	-0.1351

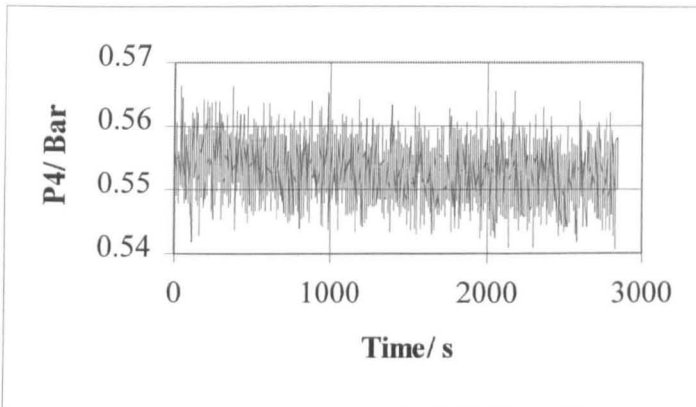
XXIV Pressure Readings and Statistical Data

Standard Pipe Arrangement

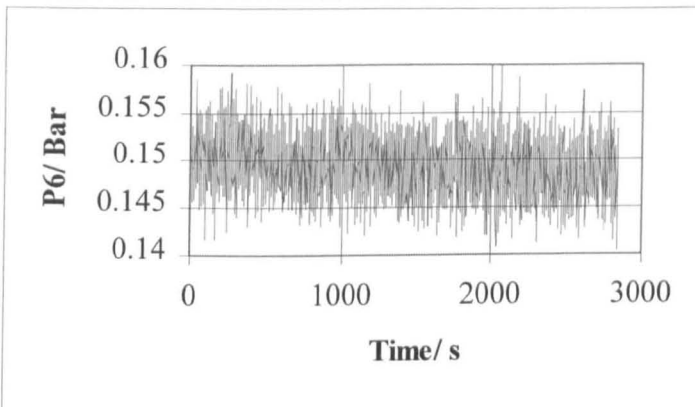
Run: water50

Volumetric Flow: 3.241 l/s

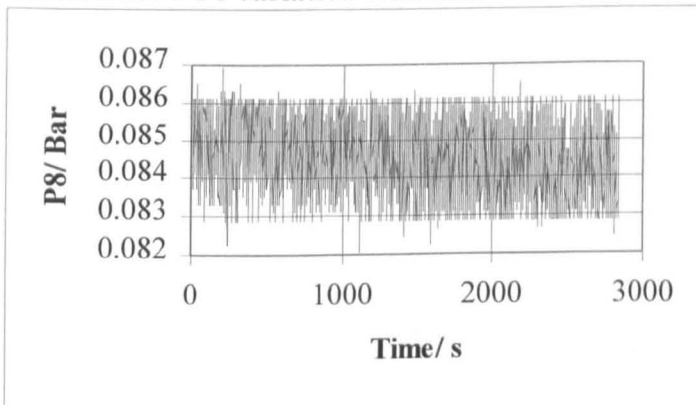
Number of Data of Points:2839



Water XXV P4 variation with time



Water XXVI P6 variation with time



Water XXVII P8 variation with time

	p1	p2	p3	p4	p5	p6	p7	p8
mean	0.851538	0.588854	0.560782	0.552853	0.531462	0.149422	0.119439	0.08453
median	0.85096	0.58868	0.56076	0.55272	0.53135	0.14932	0.1195	0.08452
mode	0.85096	0.58787	0.55872	0.55272	0.53258	0.14851	0.11909	0.08452
standard deviation	0.004619	0.005371	0.004168	0.004038	0.003959	0.002895	0.002851	0.000923
variance	2.13E-05	2.88E-05	1.74E-05	1.63E-05	1.57E-05	8.38E-06	8.13E-06	8.52E-07
skew	0.279536	0.087296	0.06794	0.095816	0.076023	0.057555	0.100686	-0.01782
kurtosis	-0.14573	-0.02551	-0.11204	-0.12892	-0.1493	-0.05784	-0.04004	-0.80776

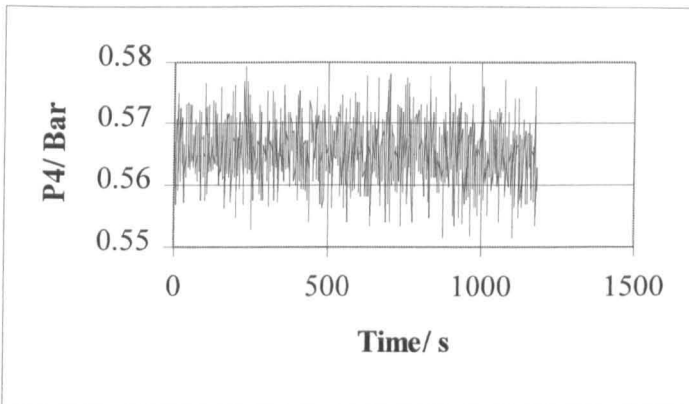
Water XXVIII Pressure Readings and Statistical Data

Standard Pipe Arrangement

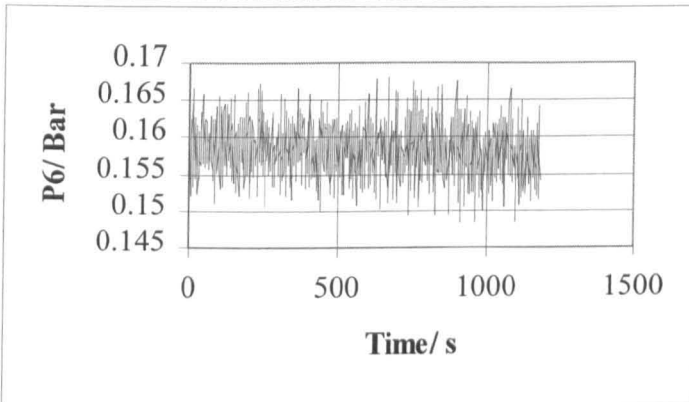
Run: water55

Volumetric Flow: 3.556 l/s

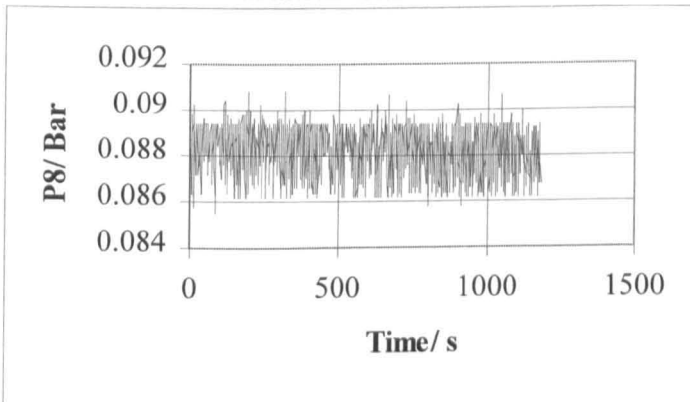
Number of Data of Points:1181



Water XXIX P4 variation with time



Water XXX P6 variation with time



Water XXXI P8 variation with time

	p1	p2	p3	p4	p5	p6	p7	p8
mean	0.920637	0.606816	0.574108	0.565439	0.543536	0.158261	0.128249	0.088217
median	0.92051	0.60689	0.57406	0.5654	0.54342	0.15812	0.1283	0.0884
mode	0.92051	0.60792	0.57447	0.5656	0.54445	0.1573	0.1283	0.08943
standard deviation	0.004293	0.006391	0.004864	0.004575	0.00449	0.003317	0.003272	0.001067
variance	1.84E-05	4.08E-05	2.37E-05	2.09E-05	2.02E-05	1.1E-05	1.07E-05	1.14E-06
skew	0.015454	0.009855	0.029813	-0.02189	-0.00823	0.06872	0.028731	-0.34092
kurtosis	0.053551	-0.03944	0.143132	0.135001	0.167177	0.107586	0.117806	-0.86013

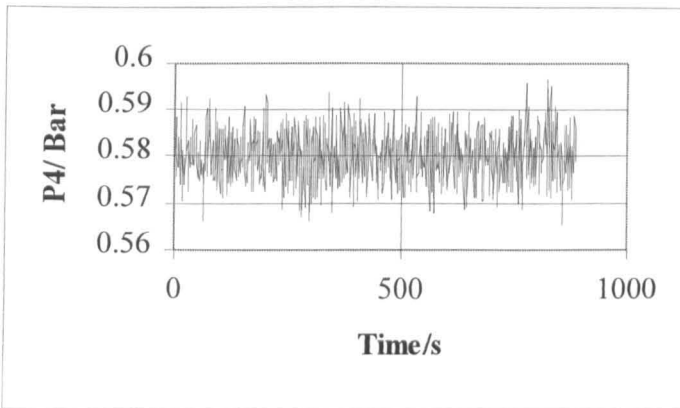
Water XXXII Pressure Readings and Statistical Data

Standard Pipe Arrangement

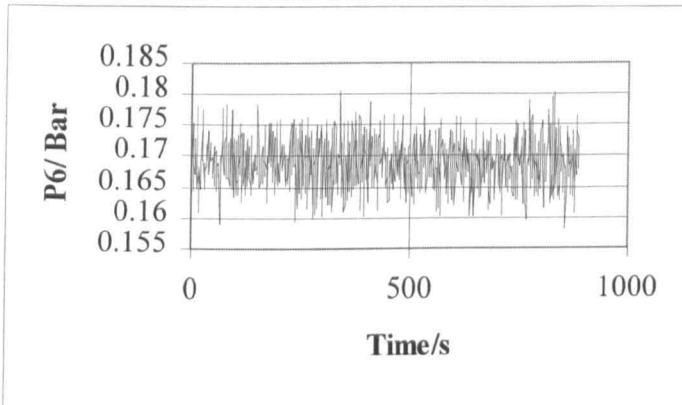
Run: water60

Volumetric Flow: 3.873 l/s

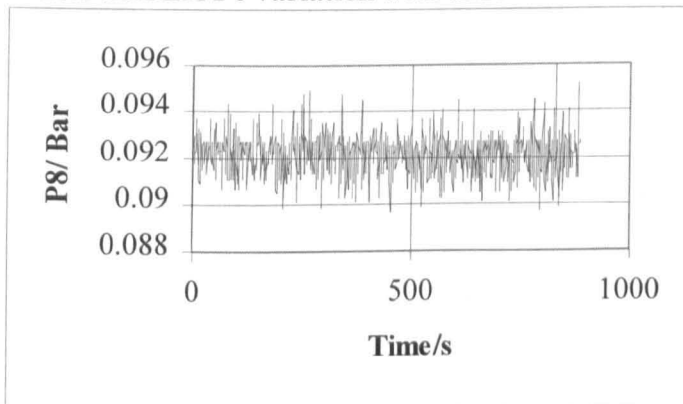
Number of Data of Points:885



Water XXXIII P4 variation with time



Water XXXIII P6 variation with time



Water XXXIV P8 variation with time

	p1	p2	p3	p4	p5	p6	p7	p8
mean	1.005983	0.628236	0.590074	0.580153	0.557669	0.168895	0.138554	0.092145
median	1.00542	0.62858	0.59022	0.58013	0.55774	0.16896	0.13853	0.09229
mode	1.00644	0.63062	0.58981	0.57767	0.56061	0.16937	0.13812	0.0927
standard deviation	0.004379	0.006885	0.005474	0.005225	0.005165	0.003897	0.003706	0.000842
variance	1.92E-05	4.74E-05	3E-05	2.73E-05	2.67E-05	1.52E-05	1.37E-05	7.09E-07
skew	0.094647	-0.06044	-0.01237	0.042635	0.026285	0.054626	0.012602	0.024987
kurtosis	-0.12839	-0.05887	-0.23229	-0.25741	-0.29769	-0.29419	-0.31855	0.891787

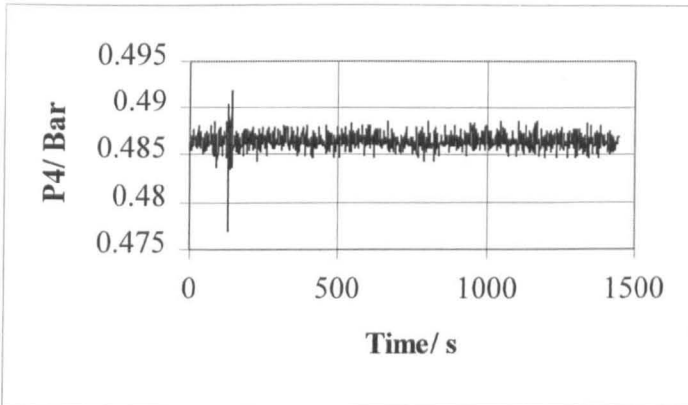
Water XXXV Pressure Readings and Statistical Data

Short Swirly-flo Pipe

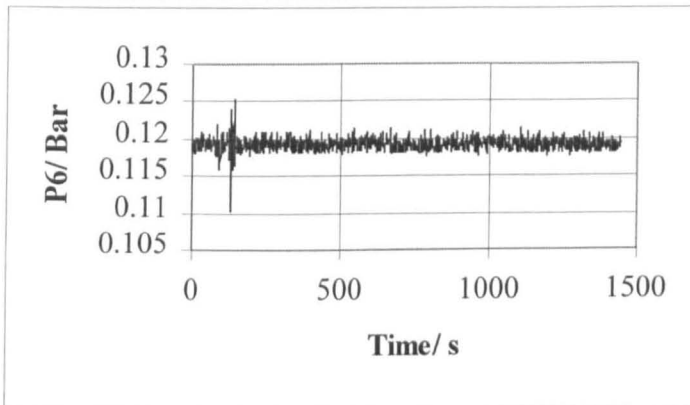
Run: Water 20

Volumetric Flow: 0.868 l/s

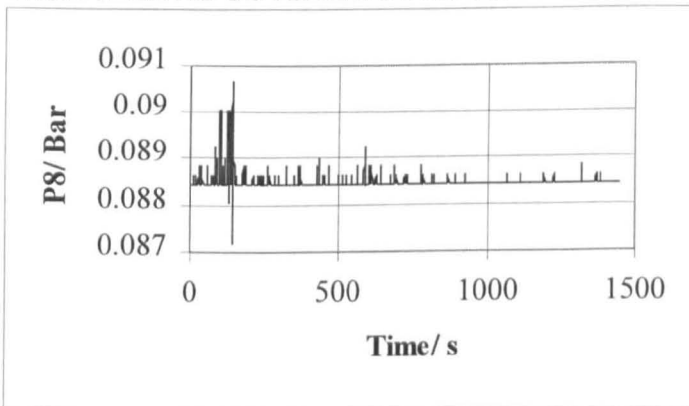
Number of Data Points: 1446



Water XXXVI P4 variation with time



Water XXXVII P6 variation with time



Water XXXVIII P8 variation with time

	p1	p2	p3	p4	p5	p6	p7	p8
mean	0.490979	0.504514	0.503616	0.486569	0.48117	0.119269	0.094097	0.088461
mode	0.4908	0.50378	0.50368	0.48623	0.48123	0.11925	0.09434	0.08843
modal	0.4908	0.50378	0.50368	0.48623	0.48123	0.11925	0.09434	0.08843
standard deviatio	0.002321	0.000944	0.000729	0.00079	0.000907	0.000773	0.000739	0.000157
variance	5.39E-06	8.9E-07	5.31E-07	6.25E-07	8.22E-07	5.97E-07	5.46E-07	2.45E-08
skew	-0.07019	0.914786	-0.9472	-0.99046	-0.4317	-0.68427	-1.18944	6.912738
kurtosis	-0.96783	0.261036	11.41329	17.99668	8.570774	17.8983	19.80424	73.48142

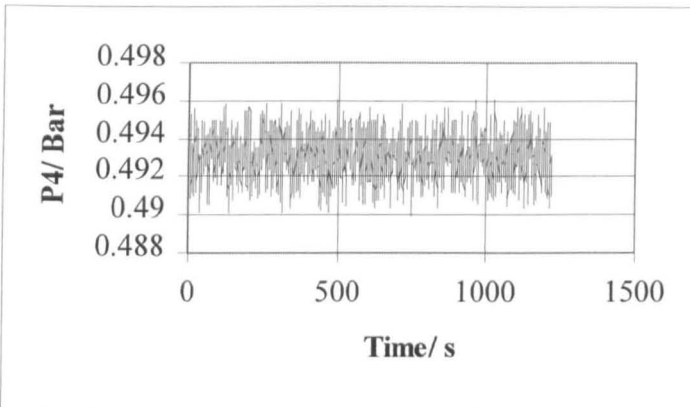
Water XXXIX Pressure Reading and Statistical Results

Short Swirly-flo Pipe

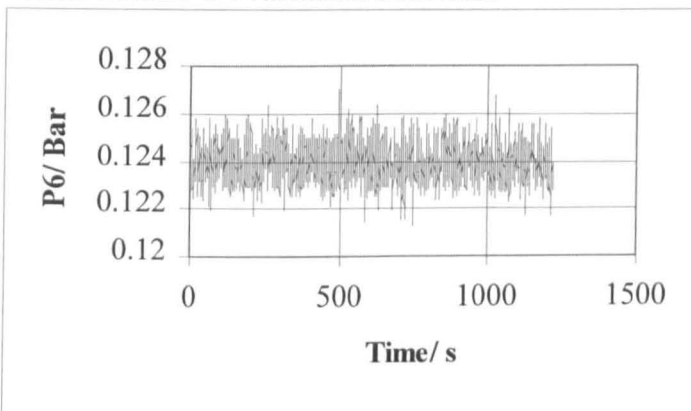
Run: Water 25

Volumetric Flow: 1.27 l/s

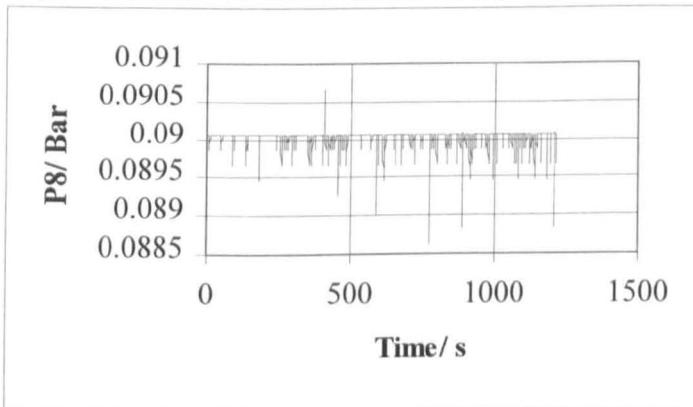
Number of Data Points: 1215



Water XXXX P4 variation with time



Water XXXXI P6 variation with time



Water XXXXII P8 variation with time

	p1	p2	p3	p4	p5	p6	p7	p8
mean	0.527623	0.517853	0.513881	0.493065	0.487945	0.123955	0.098488	0.090031
mode	0.52762	0.51851	0.51432	0.49277	0.48778	0.12355	0.09843	0.09006
median	0.52762	0.5181	0.51412	0.49298	0.48778	0.12396	0.09843	0.09006
standard deviation	5.06E-05	0.001143	0.001094	0.001192	0.001088	0.000885	0.000842	0.000116
variance	2.56E-09	1.31E-06	1.2E-06	1.42E-06	1.18E-06	7.84E-07	7.09E-07	1.36E-08
skew	20.07479	-0.51083	-0.31764	-0.06551	-0.17423	0.167302	-0.36973	-5.56407
kurtosis	401.6584	0.596196	-0.10055	-0.36851	0.105306	-0.29464	0.375493	45.96873

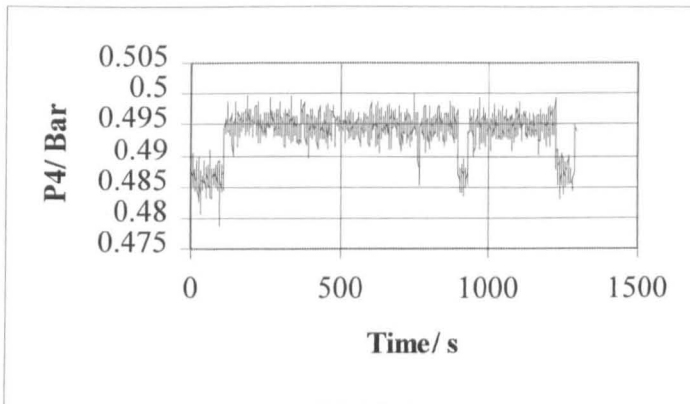
Water XXXXIII Pressure readings and Statistical Data

Short Swirly-flo Pipe

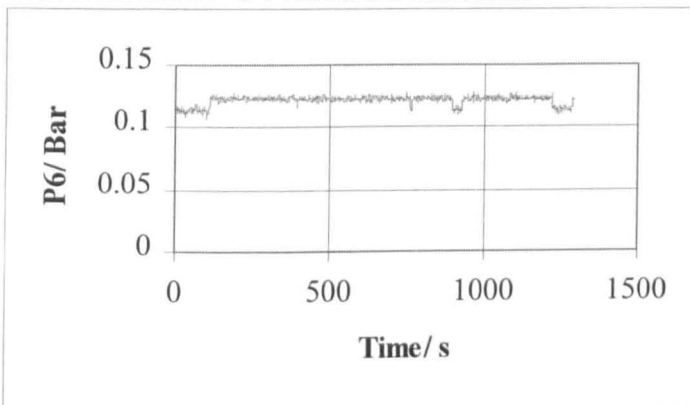
Run: Water 30

Volumetric Flow: 1.68 l/s

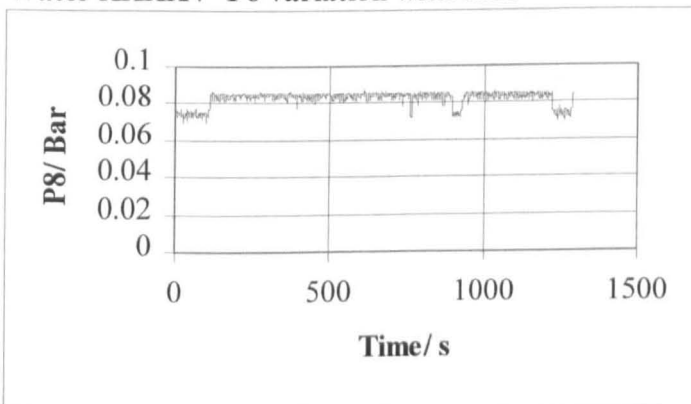
Number of Data Points:1292



Water XXXXIV P4 variation with time



Water XXXXV P6 variation with time



Water XXXXVI P8 variation with time

	p1	p2	p3	p4	p5	p6	p7	p8
mean	0.574017	0.526836	0.51917	0.493616	0.488333	0.121781	0.095747	0.08247
mode	0.57672	0.52731	0.52087	0.49605	0.49003	0.12252	0.09843	0.08515
median	0.57468	0.52751	0.52005	0.49461	0.48941	0.12293	0.097	0.08372
standard deviation	0.002489	0.003192	0.00335	0.003513	0.003632	0.003689	0.003729	0.003777
variance	6.2E-06	1.02E-05	1.12E-05	1.23E-05	1.32E-05	1.36E-05	1.39E-05	1.43E-05
skew	-1.13583	-1.28286	-1.5327	-1.55348	-1.60049	-1.76834	-1.72412	-1.98872
kurtosis	0.446378	0.837963	1.125935	1.110507	1.122072	1.332702	1.197468	1.428545

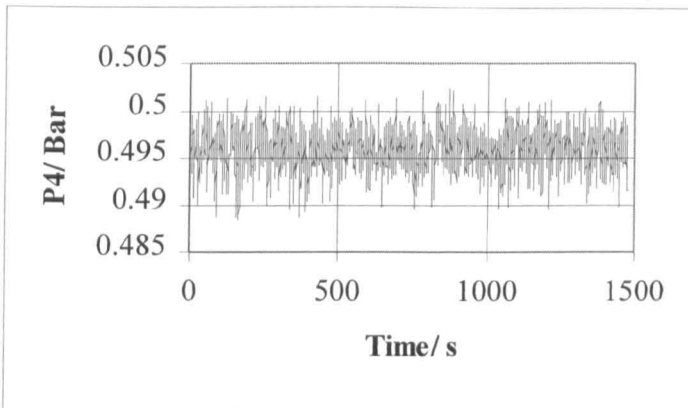
Water XXXXVII Pressure Readings and Statistical Data

Short Swirly-flo Pipe

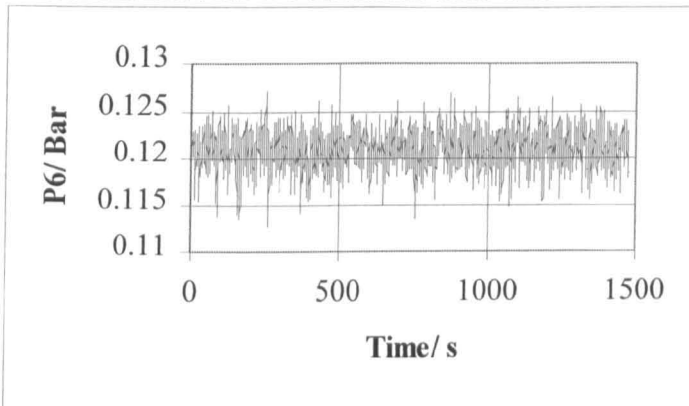
Run: Water 35

Volumetric Flow: 2.069 l/s

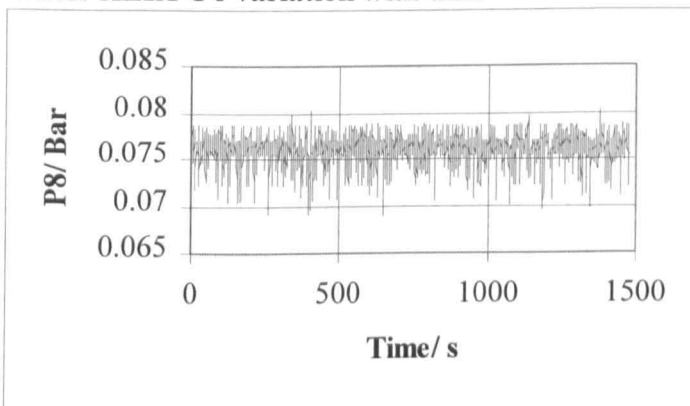
Number of Data Points:1478



Water XXXXVIII P4 variation with time



Water XLIX P6 variation with time



Water L P8 variation with time

	p1	p2	p3	p4	p5	p6	p7	p8
mean	0.625864	0.538443	0.526745	0.495912	0.490514	0.120997	0.094434	0.076002
mode	0.62582	0.53815	0.52762	0.49625	0.49105	0.12191	0.09515	0.07533
median	0.62582	0.53836	0.5268	0.49605	0.49064	0.12109	0.09454	0.07636
standard deviatio	0.000234	0.002279	0.002133	0.002223	0.002282	0.002116	0.002102	0.001717
variance	5.46E-08	5.2E-06	4.55E-06	4.94E-06	5.21E-06	4.48E-06	4.42E-06	2.95E-06
skew	4.795627	0.053932	-0.21111	-0.20618	-0.1852	-0.34923	-0.28674	-1.06811
kurtosis	28.37206	0.285441	0.252993	0.288818	0.25148	0.344684	0.269866	1.719579

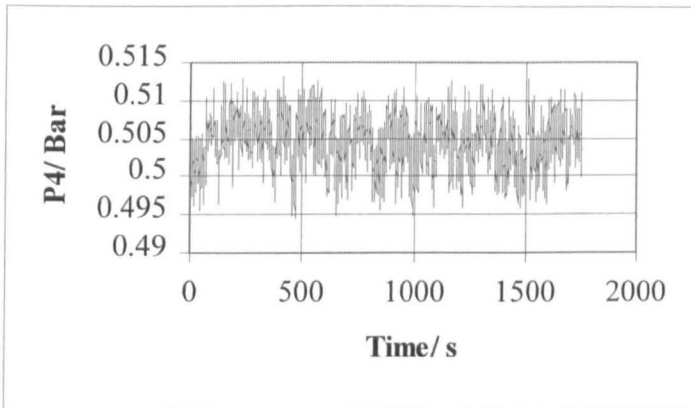
Water LI Pressure Readings and Statistical Data

Short Swirly-flo Pipe

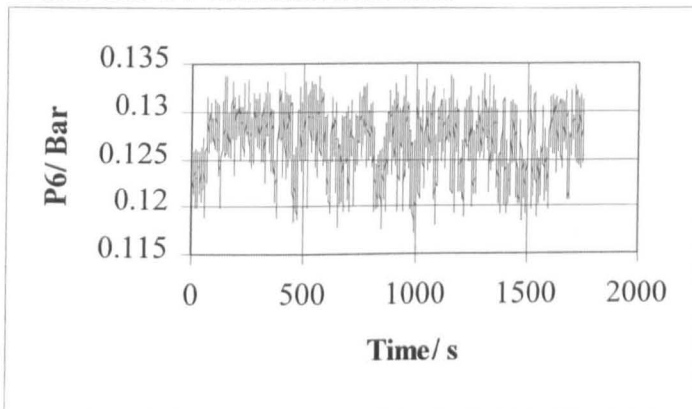
Run: Water 40

Volumetric Flow: 2.386 l/s

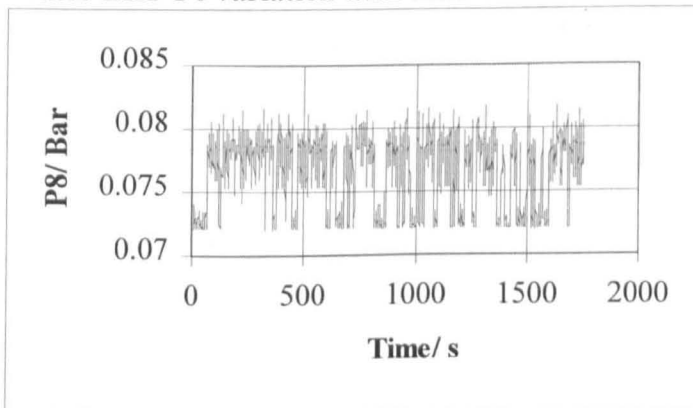
Number of Data Points:1756



Water LII P4 variation with time



Water LIII P6 variation with time



Water LIV P8 variation with time

	p1	p2	p3	p4	p5	p6	p7	p8
mean	0.688877	0.555697	0.54024	0.504607	0.499133	0.126773	0.099962	0.076554
mode	0.6872	0.55718	0.54133	0.50587	0.50046	0.12907	0.10088	0.07861
median	0.68924	0.55595	0.54051	0.50484	0.49944	0.12723	0.10047	0.0784
standard deviatio	0.001674	0.003283	0.003323	0.003448	0.003429	0.003206	0.003206	0.00292
variance	2.8E-06	1.08E-05	1.1E-05	1.19E-05	1.18E-05	1.03E-05	1.03E-05	8.53E-06
skew	-0.0822	-0.23895	-0.24938	-0.25671	-0.28343	-0.35802	-0.36736	-0.5389
kurtosis	-0.84517	-0.26445	-0.34631	-0.39678	-0.44047	-0.54032	-0.54706	-1.33442

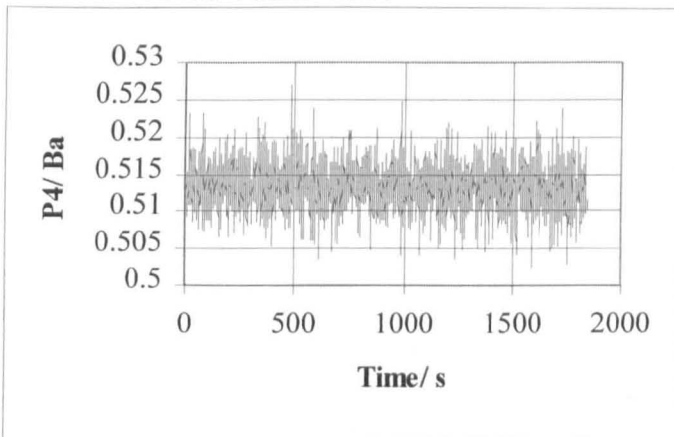
Water LV Pressure readings and Statistical Data

Short *Swirly-flo* Pipe

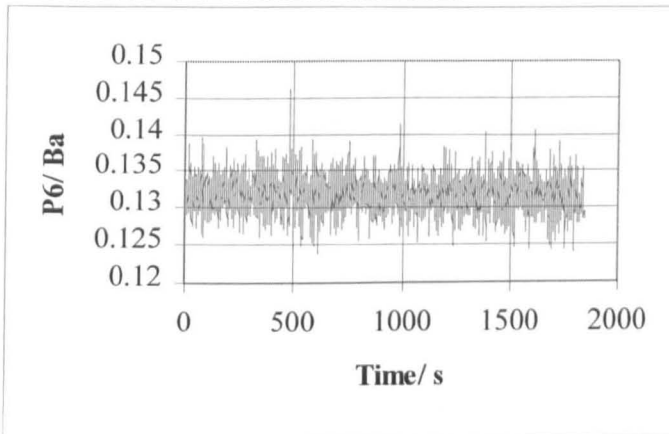
Run: Water 45

Volumetric Flow: 2.74 l/s

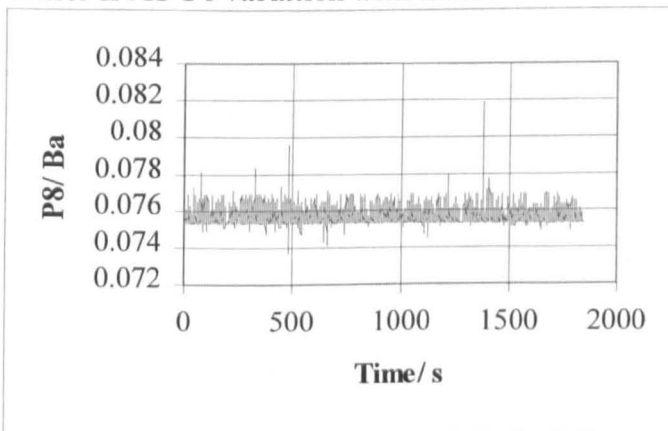
Number of Data Points: 1844



Water LVI P4 variation with time



Water LVII P6 variation with time



Water LVIII P8 variation with time

	p1	p2	p3	p4	p5	p6	p7	p8
mean	0.759381	0.574923	0.555249	0.513444	0.507595	0.131839	0.104678	0.075719
mode	0.75982	0.57416	0.55483	0.51446	0.5066	0.13153	0.10518	0.07533
median	0.75982	0.57498	0.55524	0.51344	0.50762	0.13173	0.10457	0.07554
standard deviatio	0.001467	0.003446	0.003266	0.003294	0.003142	0.002611	0.002551	0.000569
variance	2.15E-06	1.19E-05	1.07E-05	1.08E-05	9.87E-06	6.82E-06	6.51E-06	3.23E-07
skew	0.048047	0.029774	0.033454	0.045317	0.108097	0.172575	0.209435	2.402207
kurt	0.299081	0.186778	0.271862	0.239184	0.438445	0.530217	0.634896	14.76572

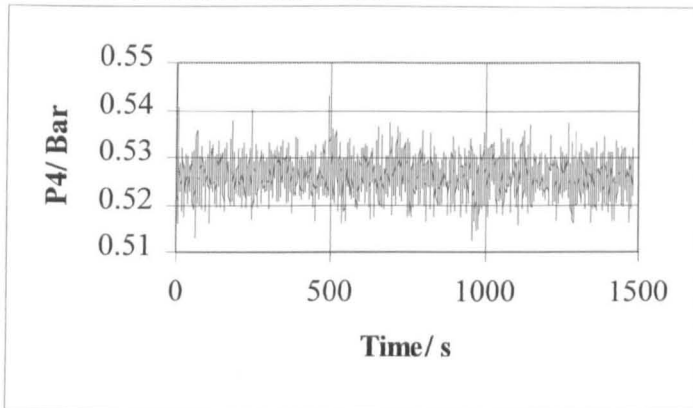
Water LIX Pressure readings and Statistical Data

Short Swirly-flo Pipe

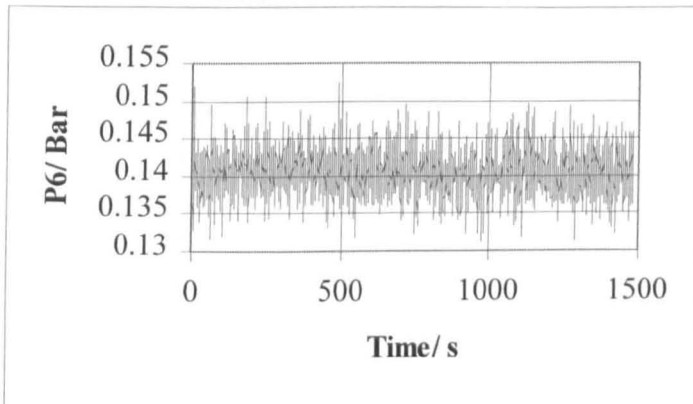
Run: Water 50

Volumetric Flow: 3.073 l/s

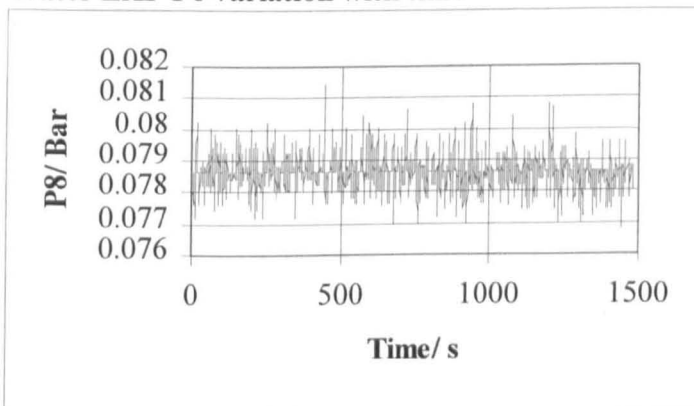
Number of Data Points: 1483



Water LX P4 variation with time



Water LXI P6 variation with time



Water LXII P8 variation with time

	p1	p2	p3	p4	p5	p6	p7	p8
mean	0.836518	0.597872	0.573315	0.525989	0.519839	0.140677	0.113316	0.078591
mode	0.83654	0.59625	0.57222	0.52653	0.51949	0.14114	0.11357	0.07861
median	0.83654	0.59769	0.57324	0.52591	0.5199	0.14073	0.11336	0.07861
standard deviatio	0.001781	0.00428	0.003958	0.00402	0.00401	0.003272	0.003197	0.000475
variance	3.17E-06	1.83E-05	1.57E-05	1.62E-05	1.61E-05	1.07E-05	1.02E-05	2.25E-07
skew	-0.16323	-0.00671	0.097829	0.065451	0.10254	0.082346	0.070915	0.395715
kurtosis	0.173123	0.208488	0.350338	0.13389	0.122294	-0.02281	-0.02256	4.126828

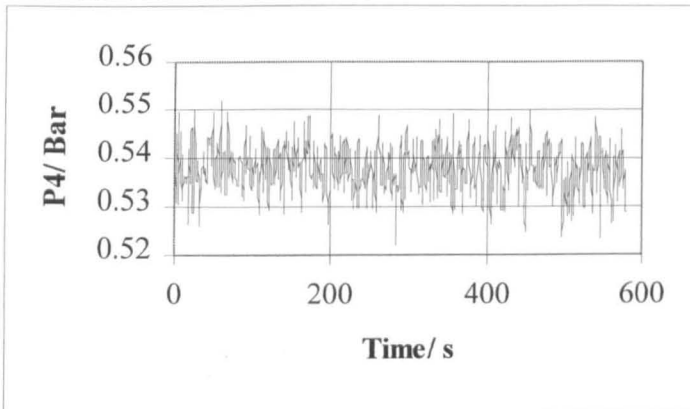
Water LXIII Pressure Readings and Statistical Data

Short Swirly-flo Pipe

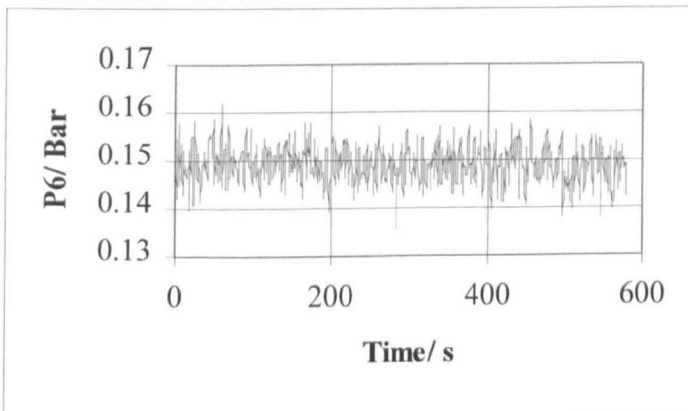
Run: Water 55

Volumetric Flow: 3.33 l/s

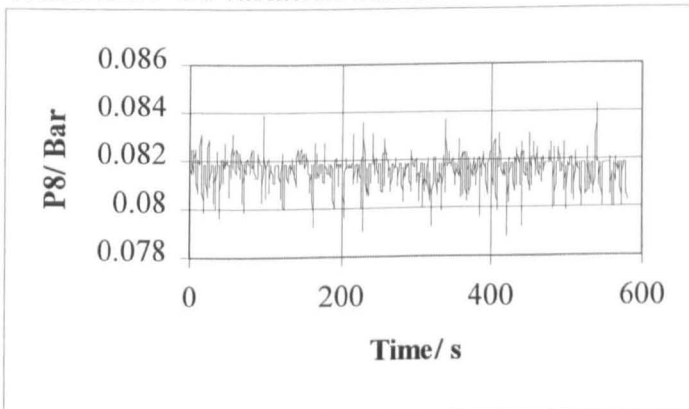
Number of Data Points: 580



Water LXIV P4 variation with time



Water LXV P6 variation with time



Water LXVI P8 variation with time

	p1	p2	p3	p4	p5	p6	p7	p8
mean	0.907225	0.620003	0.590472	0.537618	0.531494	0.148976	0.121431	0.081619
mode	0.90815	0.62121	0.589	0.53839	0.52869	0.14789	0.12236	0.08188
median	0.90713	0.6204	0.59043	0.53758	0.53156	0.14912	0.12155	0.08188
standard deviatio	0.00173	0.005111	0.004857	0.005037	0.004955	0.004009	0.003936	0.000684
variance	2.99E-06	2.61E-05	2.36E-05	2.54E-05	2.46E-05	1.61E-05	1.55E-05	4.68E-07
skew	-0.27662	-0.1946	-0.02182	-0.06444	-0.03806	-0.04021	-0.05307	-0.85071
kurtosis	-0.02758	-0.2141	-0.04318	-0.14492	-0.11061	-0.09687	-0.08	2.298411

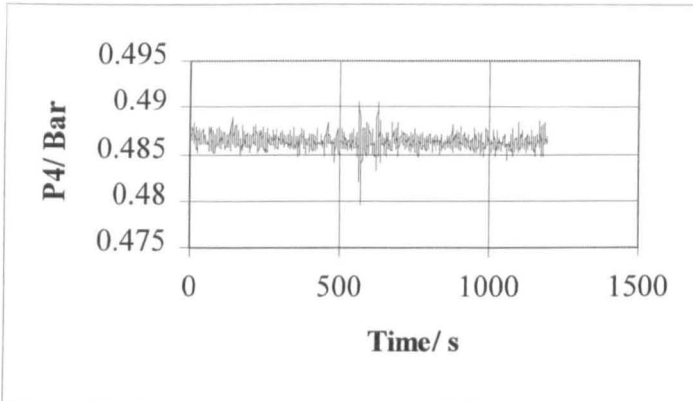
Water LXVII Pressure Readings and Statistical Data

Medium Swirly-flo Pipe

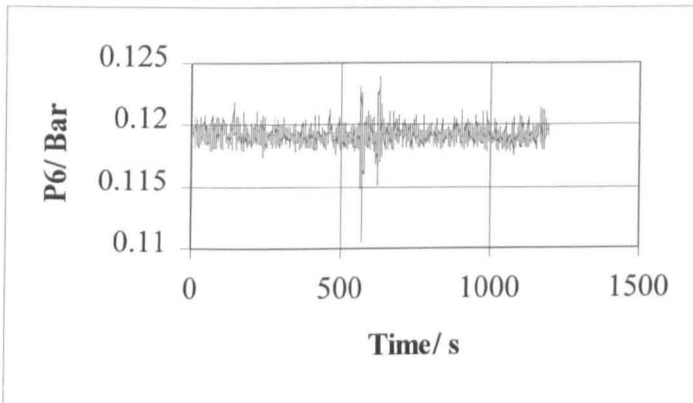
Run: Water20

Volumetric Flow: 0.881 l/s

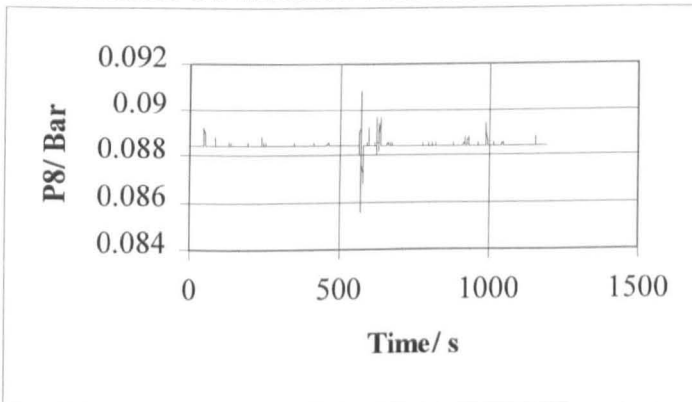
Number of Data Points: 1194



Water LXVIII P4 variation with time



Water LXIX P6 variation with time



Water LXX P8 variation with time

	p1	p2	p3	p4	p5	p6	p7	p8
mean	0.493247	0.505515	0.504166	0.486462	0.481099	0.119218	0.093817	0.088443
mode	0.49489	0.50706	0.5045	0.48623	0.48123	0.11925	0.09352	0.08843
median	0.49387	0.50542	0.5043	0.48623	0.48102	0.11925	0.09393	0.08843
standard deviatio	0.001748	0.001056	0.000681	0.000778	0.000905	0.000815	0.000804	0.00016
variance	3.06E-06	1.12E-06	4.64E-07	6.06E-07	8.19E-07	6.65E-07	6.46E-07	2.57E-08
skew	-1.0344	-0.07756	-0.68508	-0.3978	-0.08621	-0.73006	-1.13001	-0.82529
kurtosis	0.434254	-1.12677	9.481718	7.819137	4.823862	13.54034	15.09324	153.6302

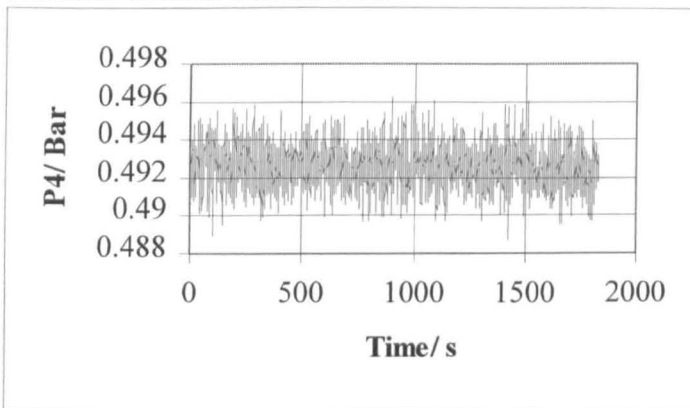
Water LXXI Pressure Results and Statistical Data

Medium *Swirly-flo* Pipe

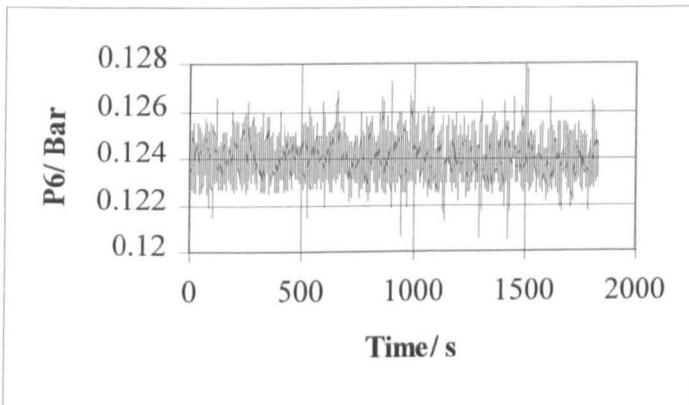
Run: Water25

Volumetric Flow: 1.28 l/s

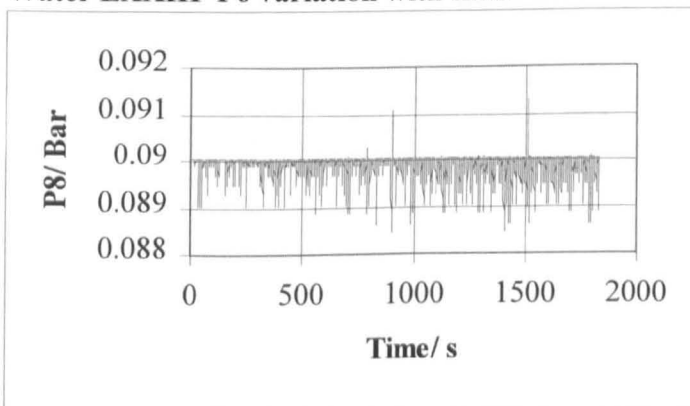
Number of Data Points: 1830



Water LXXII P4 variation with time



Water LXXIII P6 variation with time



Water LXXIV P8 variation with time

	p1	p2	p3	p4	p5	p6	p7	p8
mean	0.527643	0.518912	0.515023	0.492633	0.487788	0.124006	0.098335	0.089911
mode	0.52762	0.51851	0.51432	0.49277	0.48778	0.12355	0.09843	0.09006
median	0.52762	0.51851	0.51494	0.49277	0.48778	0.12396	0.09843	0.09006
standard deviatio	0.000155	0.001064	0.001021	0.001165	0.001074	0.000906	0.000887	0.000286
variance	2.39E-08	1.13E-06	1.04E-06	1.36E-06	1.15E-06	8.22E-07	7.88E-07	8.16E-08
skew	6.932887	0.243773	-0.10034	-0.00235	-0.13378	0.155739	-0.38185	-2.12513
kurtosis	49.97377	1.307373	0.646398	0.016734	0.50792	0.093313	0.757003	5.37426

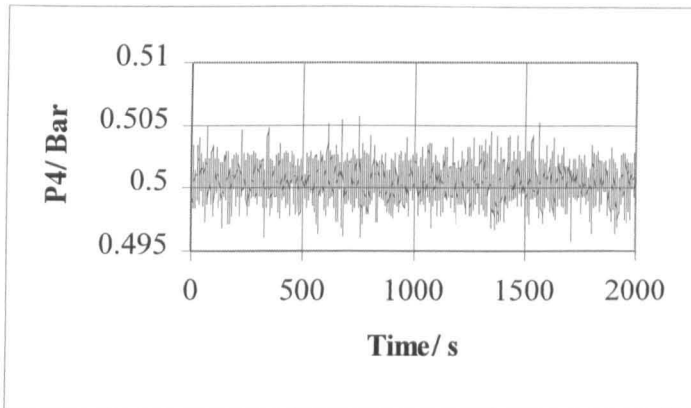
Water LXXV Pressure Results and Statistical Data

Medium Swirly-flo Pipe

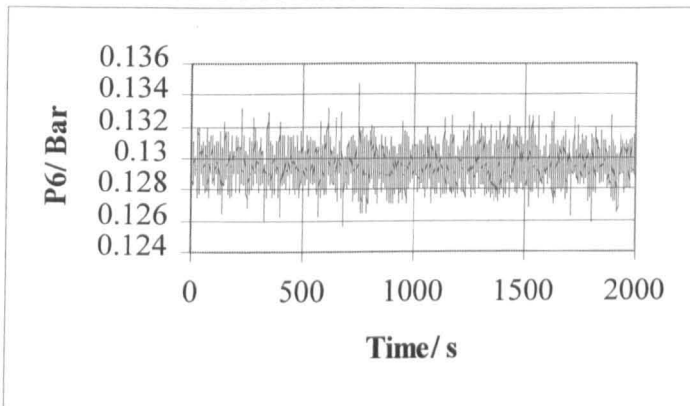
Run: Water 30

Volumetric Flow: 1.69 l/s

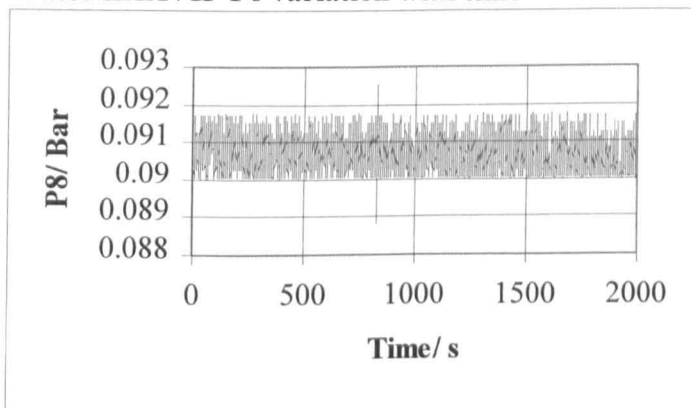
Number of Data Points: 1994



Water LXXVI P4 variation with time



Water LXXVII P6 variation with time



Water LXXVIII P8 variation with time

	p1	p2	p3	p4	p5	p6	p7	p8
mean	0.576779	0.535102	0.528152	0.500505	0.495819	0.129553	0.103431	0.090697
mode	0.57672	0.53488	0.52742	0.49993	0.49555	0.12907	0.10354	0.09006
median	0.57672	0.53508	0.52803	0.50055	0.49575	0.12948	0.10354	0.09068
standard deviat	0.00027	0.001589	0.001255	0.001402	0.001275	0.001103	0.001166	0.000513
variance	7.27E-08	2.52E-06	1.58E-06	1.97E-06	1.63E-06	1.22E-06	1.36E-06	2.63E-07
skew	3.967177	0.105346	0.015264	-0.04558	0.087189	0.170263	0.034993	0.378863
kurtosis	19.59079	-0.03076	0.584667	0.116565	0.454461	0.537231	-0.23192	-0.90017

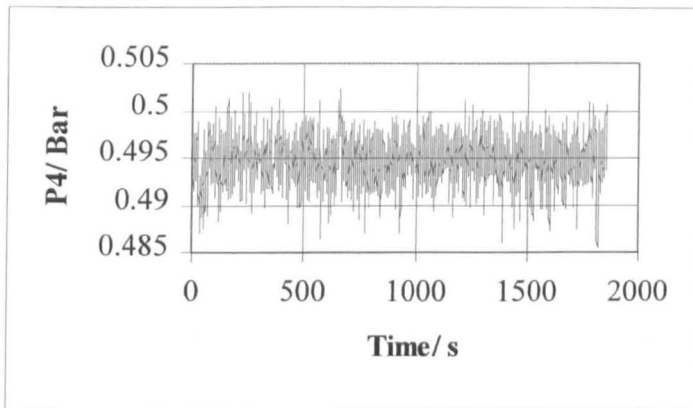
Water LXXIX Pressure Results and Statistical Data

Medium Swirly-flo Pipe

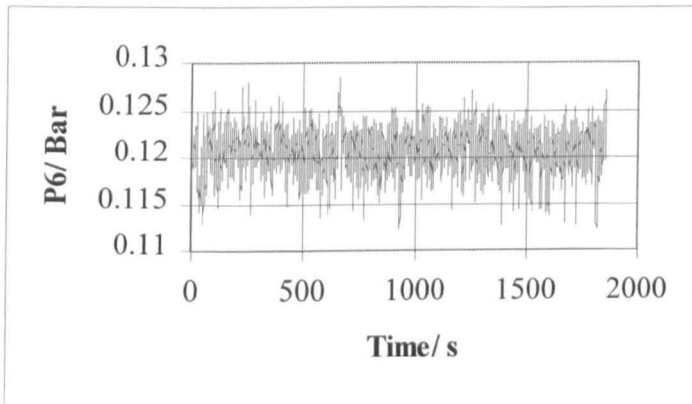
Run: Water 35

Volumetric Flow: 2.038 l/s

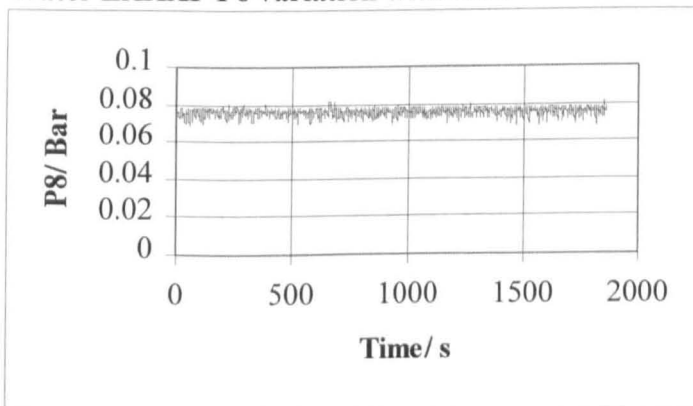
Number of Data Points: 1858



Water LXXX P4 variation with time



Water LXXXI P6 variation with time



Water LXXXII P8 variation with time

	p1	p2	p3	p4	p5	p6	p7	p8
mean	0.62643	0.541157	0.529517	0.494756	0.489966	0.120761	0.094092	0.075833
mode	0.62582	0.54183	0.53069	0.49584	0.49003	0.12252	0.09515	0.07533
median	0.62582	0.54122	0.52967	0.49482	0.49003	0.12109	0.09434	0.07615
standard deviatio	0.00094	0.002605	0.002338	0.002525	0.002529	0.00243	0.002417	0.002216
variance	8.83E-07	6.79E-06	5.47E-06	6.38E-06	6.4E-06	5.91E-06	5.84E-06	4.91E-06
skew	1.636757	-0.16843	-0.22641	-0.29739	-0.38489	-0.51313	-0.46805	-0.83207
kurtosis	3.376043	-0.16061	0.491724	0.240835	0.418283	0.510925	0.499981	0.82727

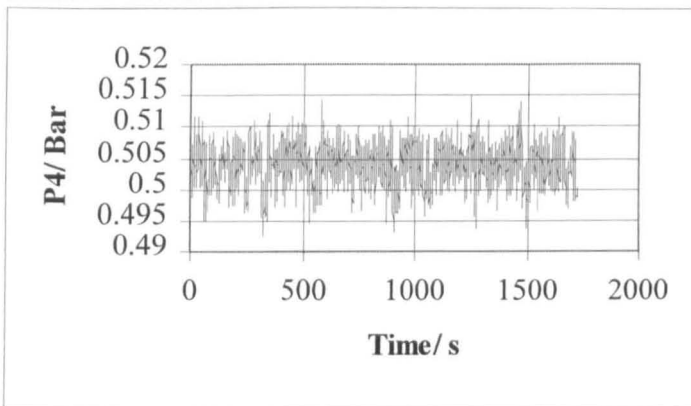
Water LXXXIII Pressure Readings and Statistical Data

Medium Swirly-flo Pipe

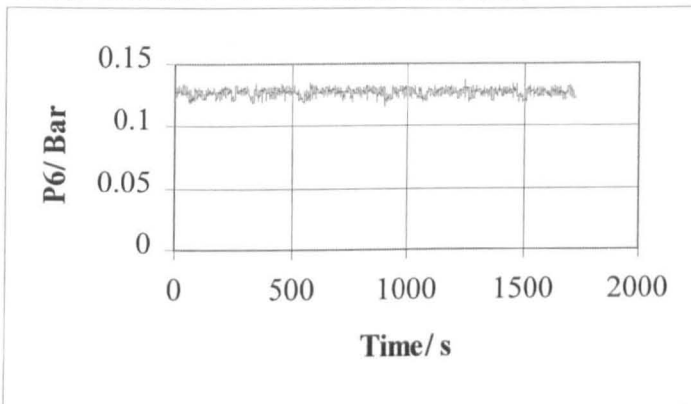
Run: Water 40

Volumetric Flow: 2.372 l/s

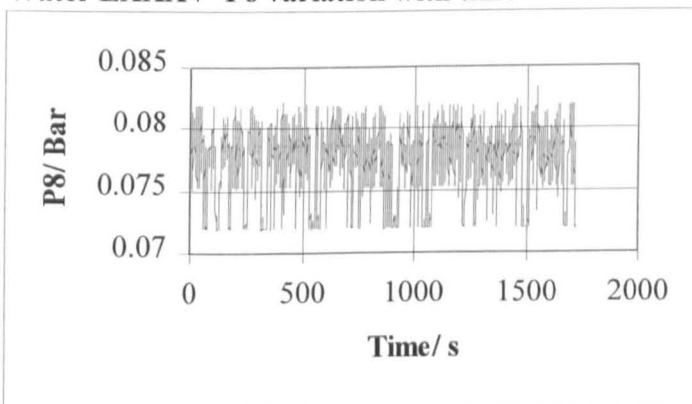
Number of Data Points: 1727



Water LXXXIV P4 variation with time



Water LXXXV P6 variation with time



Water LXXXVI P8 variation with time

	p1	p2	p3	p4	p5	p6	p7	p8
mean	0.690368	0.559968	0.544854	0.503714	0.499318	0.127145	0.100246	0.077205
mode	0.69129	0.55943	0.54542	0.50443	0.49964	0.12846	0.10088	0.07861
median	0.69129	0.56004	0.54521	0.50402	0.49964	0.12743	0.10068	0.07861
standard deviatio	0.001396	0.003182	0.003173	0.003345	0.003227	0.003006	0.003004	0.002852
variance	1.95E-06	1.01E-05	1.01E-05	1.12E-05	1.04E-05	9.04E-06	9.02E-06	8.13E-06
skew	-0.90786	-0.24364	-0.29549	-0.2273	-0.34419	-0.39146	-0.416	-0.71178
kurtosis	0.455013	0.076531	0.03857	-0.01515	0.00249	-0.08378	-0.09798	-0.59952

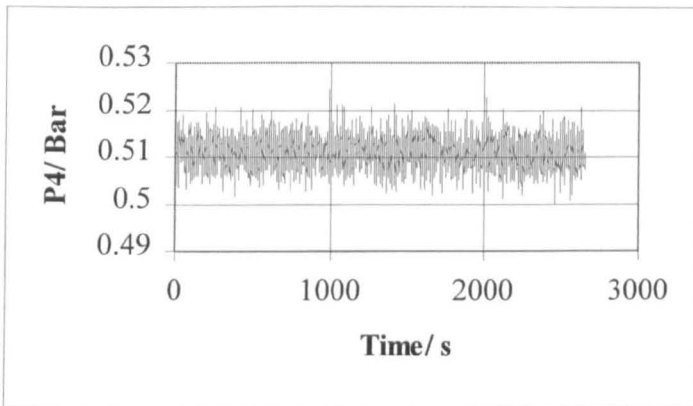
Water LXXXVII Pressure Results and Statistical Data

Medium Swirly-flo Pipe

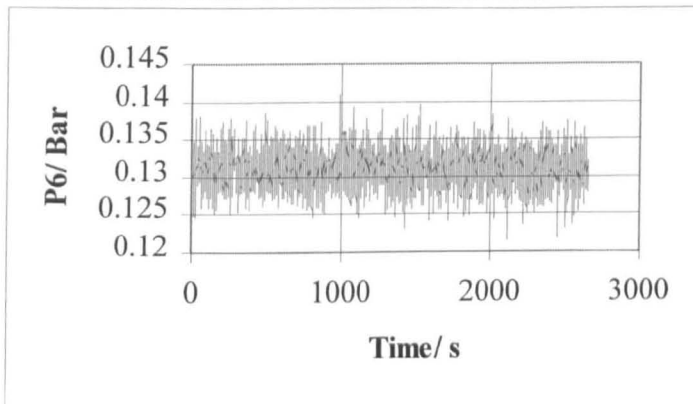
Run: Water 45

Volumetric Flow: 2.75 l/s

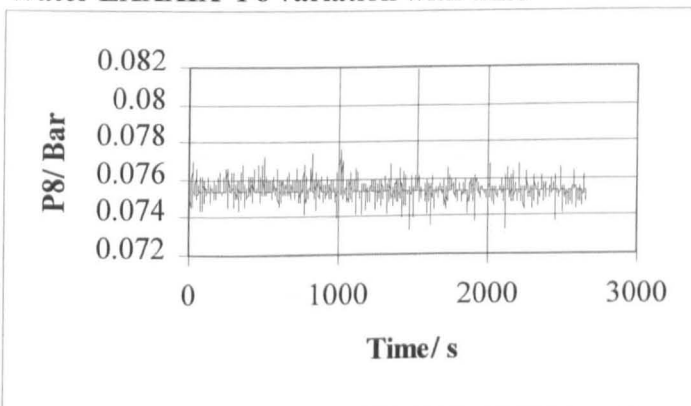
Number of Data Points: 2652



Water LXXXVIII P4 variation with time



Water LXXXIX P6 variation with time



Water XC P8 variation with time

	p1	p2	p3	p4	p5	p6	p7	p8
mean	0.761534	0.579382	0.56006	0.511005	0.506812	0.131059	0.103855	0.075361
mode	0.76187	0.57948	0.55913	0.51221	0.50742	0.13071	0.10436	0.07533
median	0.76187	0.57927	0.55994	0.51098	0.5068	0.13112	0.10375	0.07533
standard deviatio	0.001529	0.003399	0.0031	0.003249	0.003008	0.002494	0.002433	0.000334
variance	2.34E-06	1.16E-05	9.61E-06	1.06E-05	9.05E-06	6.22E-06	5.92E-06	1.12E-07
skew	0.084102	0.091748	0.047409	0.066157	0.052095	0.055277	0.077947	3.287558
kurtosis	-0.22397	0.031099	0.10222	0.092575	0.216514	0.1861	0.185021	61.4865

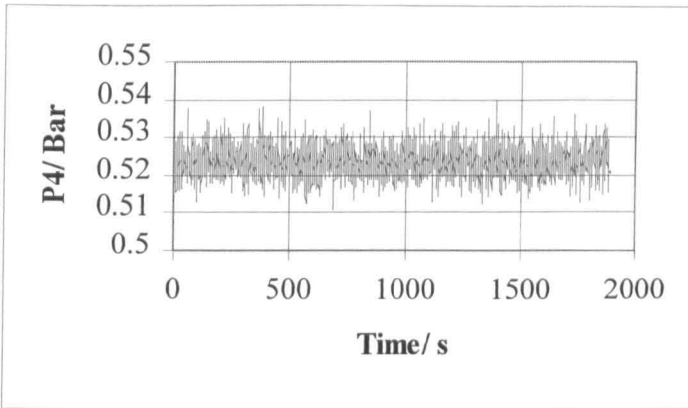
Water XCI Pressure Results and Statistical Data

Medium Swirly-flo Pipe

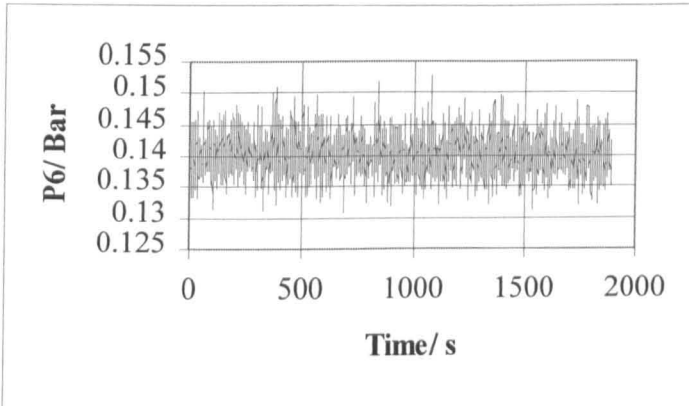
Run: Water 50

Volumetric Flow: 3.078 l/s

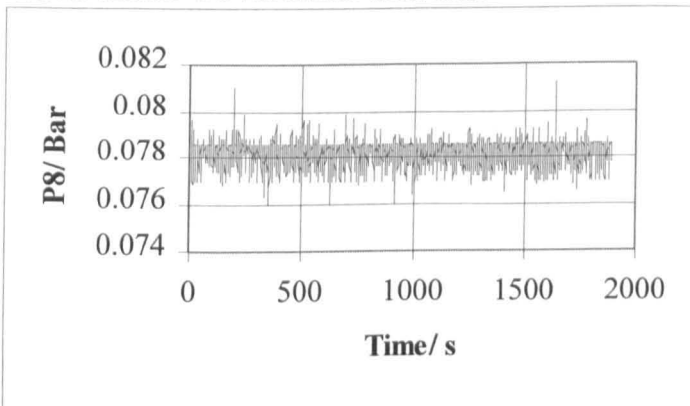
Number of Data Points: 1890



Water XCII P4 variation with time



Water XCIII P6 variation with time



Water XCIV P8 variation with time

	p1	p2	p3	p4	p5	p6	p7	p8
mean	0.842608	0.604766	0.580318	0.523782	0.519721	0.140254	0.112899	0.078252
mode	0.84268	0.60485	0.57918	0.52407	0.5199	0.14012	0.11295	0.07861
median	0.84268	0.60464	0.5802	0.52387	0.51969	0.14012	0.11275	0.0784
standard deviatio	0.00159	0.004363	0.004023	0.004106	0.003961	0.003246	0.003189	0.000546
variance	2.53E-06	1.9E-05	1.62E-05	1.69E-05	1.57E-05	1.05E-05	1.02E-05	2.98E-07
skew	0.163856	0.219722	0.237887	0.156607	0.199506	0.131958	0.104737	-0.76645
kurtosis	0.21651	0.146408	0.069228	0.161231	0.184024	0.207432	0.247705	1.273933

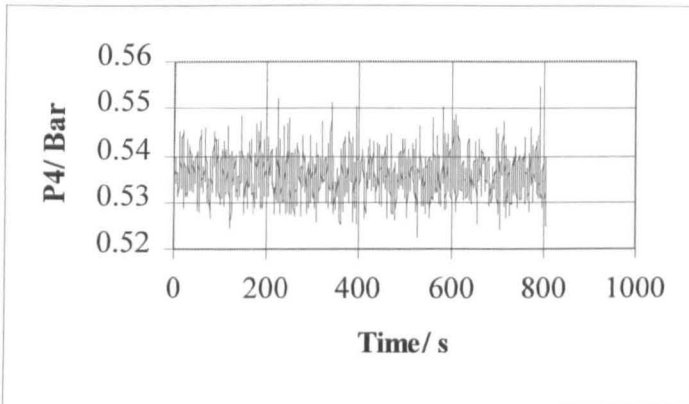
Water XCV Pressure Results and Statistical Data

Medium Swirly-flo Pipe

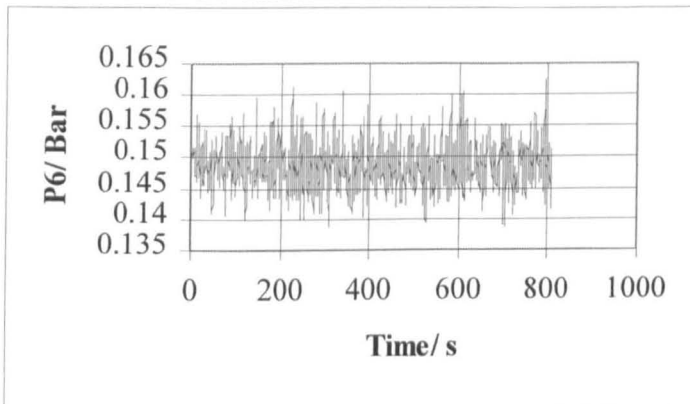
Run: Water 55

Volumetric Flow: 3.72 l/s

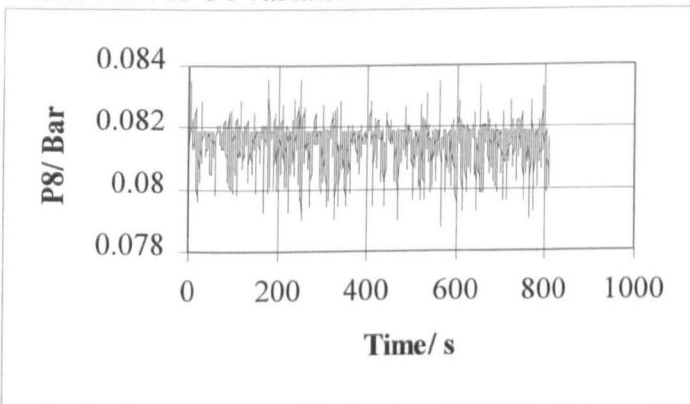
Number of Data Points: 808



Water XCVI P4 variation with time



Water XCVII P6 variation with time



Water XCVIII P8 variation with time

	p1	p2	p3	p4	p5	p6	p7	p8
mean	0.917607	0.628725	0.5992	0.535733	0.531905	0.148856	0.121338	0.081471
mode	0.91838	0.62837	0.59759	0.53451	0.53299	0.15117	0.11991	0.08188
median	0.91735	0.62858	0.59882	0.53533	0.53156	0.14871	0.12114	0.08168
standard deviatio	0.002265	0.005283	0.004808	0.00495	0.00481	0.003885	0.003842	0.000766
variance	5.13E-06	2.79E-05	2.31E-05	2.45E-05	2.31E-05	1.51E-05	1.48E-05	5.86E-07
skew	-0.22297	0.280661	0.3572	0.371421	0.285202	0.229587	0.25107	-0.99957
kurtosis	-0.07815	0.226516	0.287211	0.122126	0.113856	0.09768	0.109915	1.196034

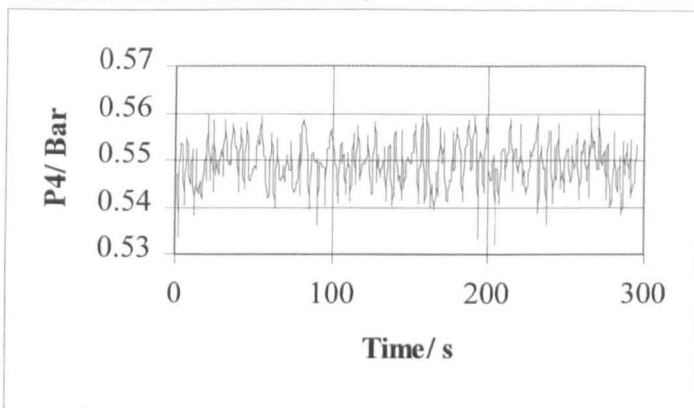
Water XCIX Pressure Results and Statistical Data

Medium Swirly-flo Pipe

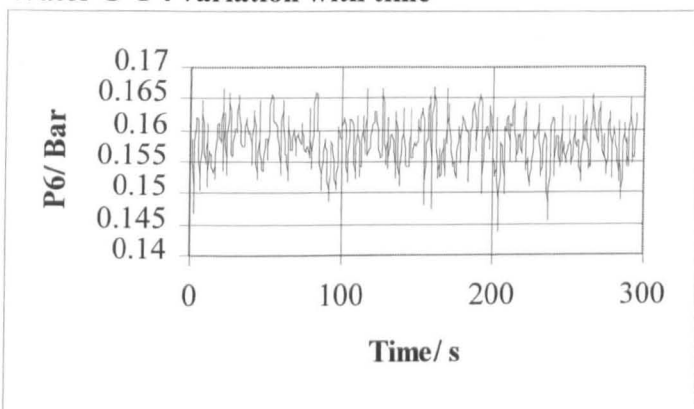
Run: Water 60

Volumetric Flow: 3.709 l/s

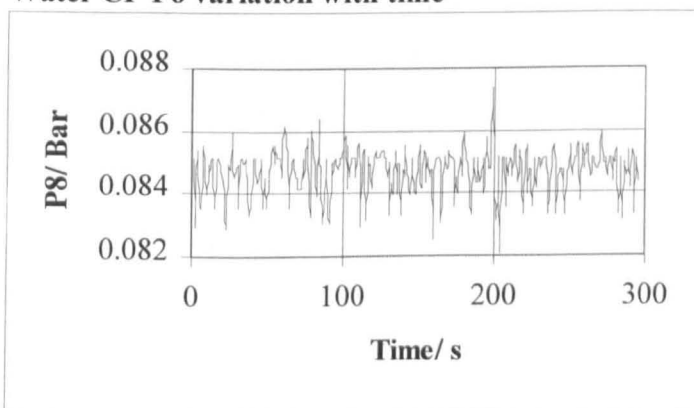
Number of Data Points: 295



Water C P4 variation with time



Water CI P6 variation with time



Water CII P8 variation with time

	p1	p2	p3	p4	p5	p6	p7	p8
mean	1.000855	0.654321	0.619798	0.548991	0.544869	0.158061	0.130323	0.084704
median	1.00123	0.65436	0.61989	0.54903	0.54506	0.15812	0.13055	0.08495
mode	1.00021	0.65088	0.62234	0.54781	0.54506	0.15833	0.12748	0.08515
standard deviatio	0.002264	0.006008	0.005348	0.005357	0.005044	0.004134	0.004023	0.000717
variance	5.13E-06	3.61E-05	2.86E-05	2.87E-05	2.54E-05	1.71E-05	1.62E-05	5.14E-07
skew	-0.16294	-0.12347	-0.23155	-0.21616	-0.26874	-0.29493	-0.34097	-0.66225
kurtosis	0.502061	0.26378	0.093703	-0.06384	0.160956	0.175723	0.312773	1.006603

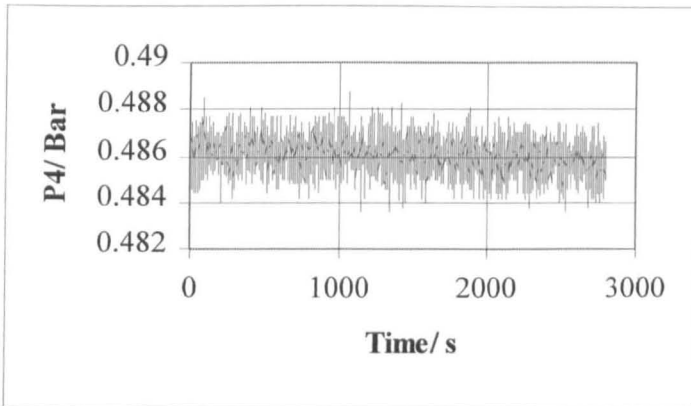
Water CIII Pressure Results and Statistical Data

Long Swirly-flo Pipe

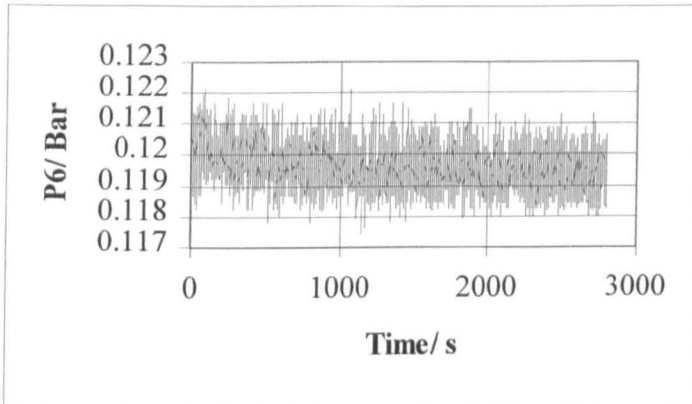
Run: Water 20

Volumetric Flow: 0.852 l/s

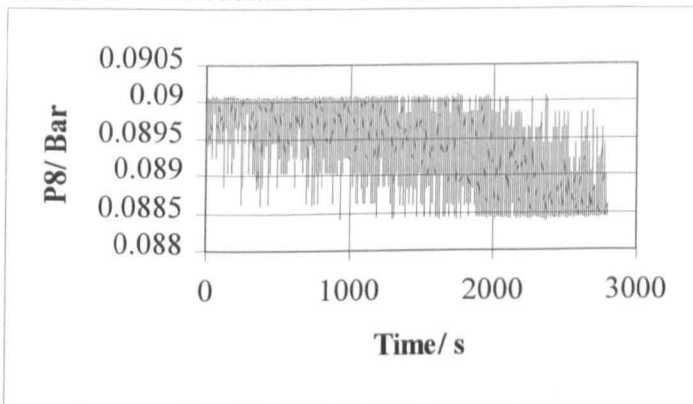
Number of Data Points: 2798



Water CIV P4 variation with time



Water CV P6 variation with time



Water CVI P8 variation with time

	p1	p2	p3	p4	p5	p6	p7	p8
mean	0.488893	0.504456	0.503629	0.486064	0.481356	0.11961	0.092818	0.089403
mode	0.49089	0.50378	0.50348	0.48623	0.48143	0.11925	0.09315	0.09006
median	0.48884	0.50419	0.50368	0.48623	0.48143	0.11946	0.09295	0.08945
standard deviatio	0.001922	0.000919	0.000658	0.000706	0.000811	0.000748	0.000521	0.000567
variance	3.7E-06	8.44E-07	4.33E-07	4.99E-07	6.58E-07	5.59E-07	2.71E-07	3.21E-07
skew	-0.86736	1.005528	-0.24519	-0.24026	0.090618	0.322493	-0.29077	-0.38546
kurtosis	0.038834	0.401712	0.202887	0.621032	-0.55012	-0.13437	1.022217	-1.23721

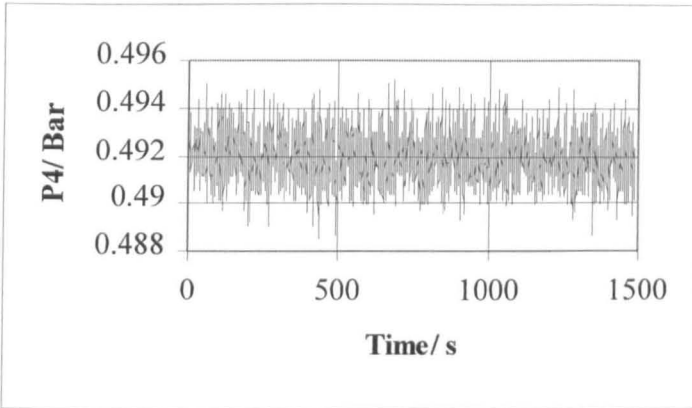
Water CVII Pressure Results and Statistical Data

Long Swirly-flo Pipe

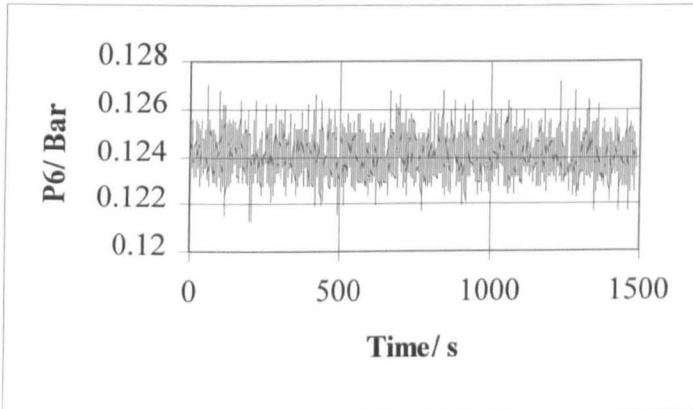
Run: Water 25

Volumetric Flow: 1.26 l/s

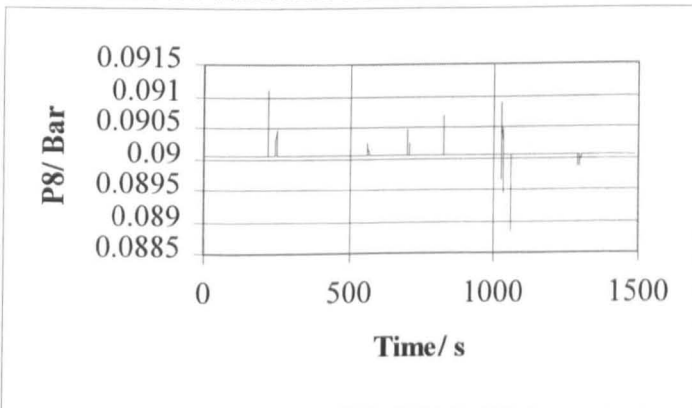
Number of Data Points: 1486



Water CVIII P4 variation with time



Water CIX P6 variation with time



Water CX P8 variation with time

	p1	p2	p3	p4	p5	p6	p7	p8
mean	0.523627	0.517375	0.513489	0.491993	0.48788	0.1241	0.097101	0.090062
mode	0.52362	0.51851	0.51432	0.49277	0.48778	0.12355	0.09725	0.09006
median	0.52362	0.51769	0.5135	0.49195	0.48798	0.12416	0.09704	0.09006
standard deviation	9.15E-05	0.001221	0.001152	0.001147	0.001124	0.000907	0.000858	6.07E-05
variance	8.37E-09	1.49E-06	1.33E-06	1.32E-06	1.26E-06	8.23E-07	7.37E-07	3.68E-09
skew	14.79914	-0.51526	-0.22903	0.058324	-0.16301	0.14374	-0.21987	1.537486
kurtosis	245.8038	-0.27899	-0.19933	-0.33925	0.060436	-0.09359	0.185196	227.9948

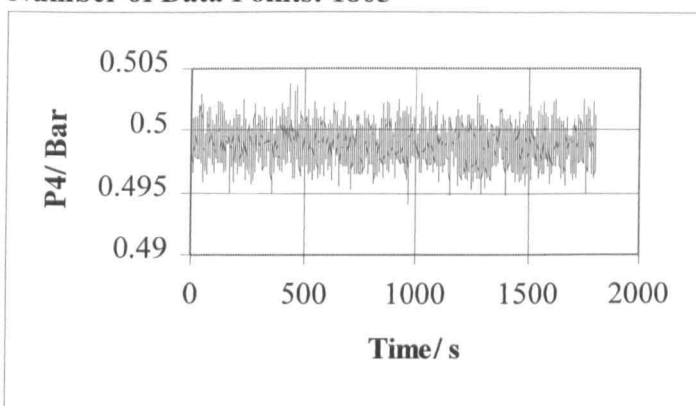
Water CXI Pressure Results and Statistical Data

Long Swirly-flo Pipe

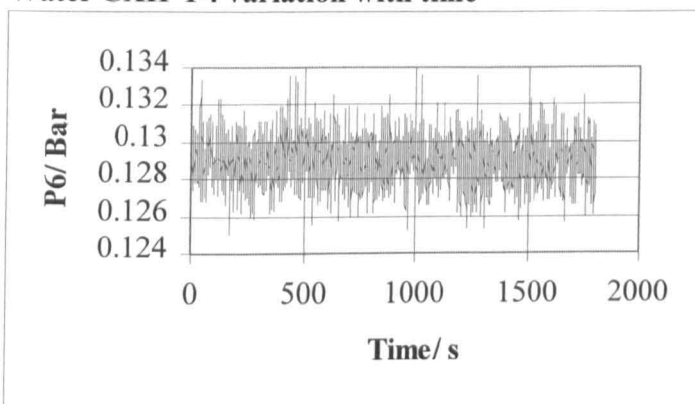
Run: Water 30

Volumetric Flow: 1.664 l/s

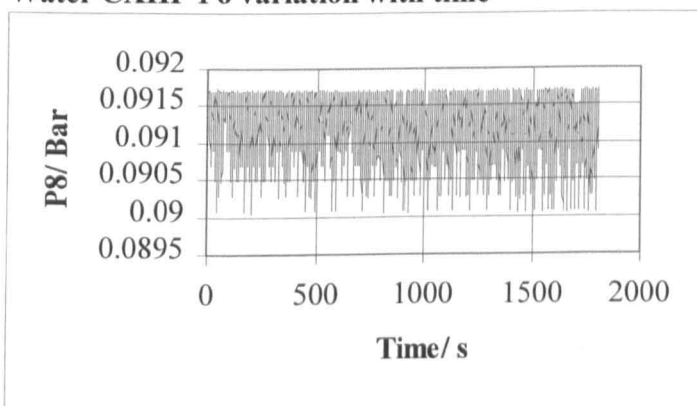
Number of Data Points: 1805



Water CXII P4 variation with time



Water CXIII P6 variation with time



Water CXIV P8 variation with time

	p1	p2	p3	p4	p5	p6	p7	p8
mean	0.568099	0.530985	0.524392	0.499013	0.495145	0.129067	0.101754	0.091238
median	0.56761	0.5312	0.52435	0.49911	0.49514	0.12907	0.10175	0.09129
mode	0.56761	0.53161	0.52414	0.49932	0.49535	0.12907	0.10113	0.0917
standard deviation	0.001757	0.001429	0.001444	0.001457	0.001437	0.001243	0.001288	0.000452
variance	3.09E-06	2.04E-06	2.09E-06	2.12E-06	2.06E-06	1.54E-06	1.66E-06	2.05E-07
skew	0.164244	-0.10186	0.013723	-0.00824	-0.10565	0.035583	-0.00401	-0.79463
kurtosis	0.016751	0.321657	-0.18922	-0.24762	0.062794	0.337441	-0.07219	-0.34341

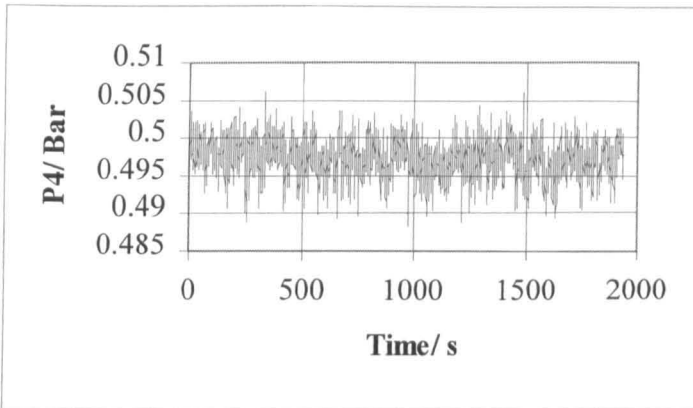
Water CXV Pressure Results and Statistical Data

Long Swirly-flo Pipe

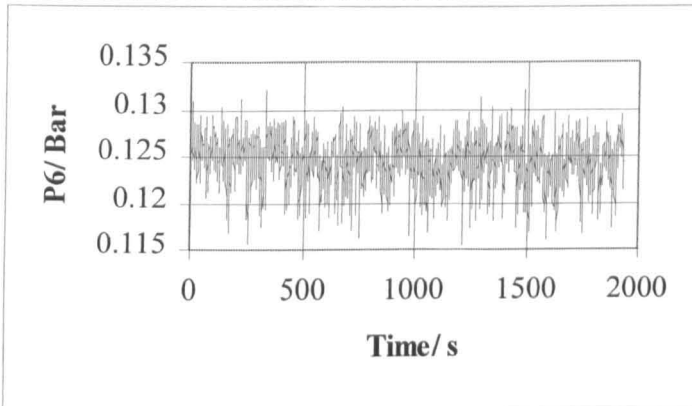
Run: Water 35

Volumetric Flow: 2.031 l/s

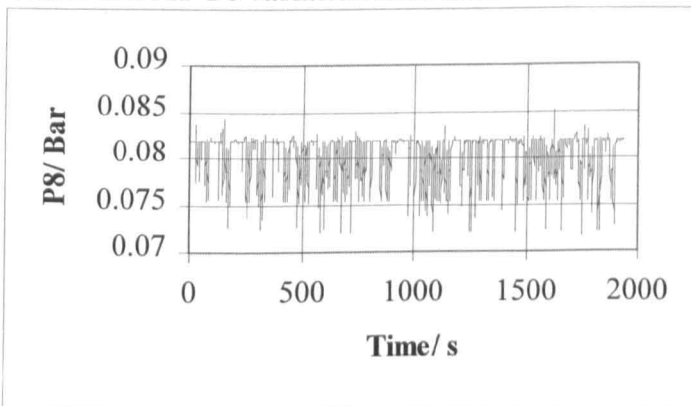
Number of Data Points: 1936



Water CXVI P4 variation with time



Water CXVII P6 variation with time



Water CXVIII P8 variation with time

	p1	p2	p3	p4	p5	p6	p7	p8
mean	0.623294	0.53881	0.528041	0.497369	0.493676	0.124536	0.09663	0.080342
mode	0.62182	0.53815	0.52905	0.49809	0.49432	0.12518	0.09725	0.08188
median	0.62285	0.53877	0.52823	0.49748	0.49391	0.12477	0.09704	0.08188
standard deviatio	0.00139	0.002542	0.002446	0.002558	0.002599	0.002444	0.002404	0.00217
variance	1.93E-06	6.46E-06	5.98E-06	6.55E-06	6.75E-06	5.97E-06	5.78E-06	4.71E-06
skew	0.814604	-0.07646	-0.27801	-0.29479	-0.33399	-0.50269	-0.53548	-1.36188
kurtosis	0.217083	0.066269	0.347929	0.250136	0.305036	0.51709	0.599203	1.394477

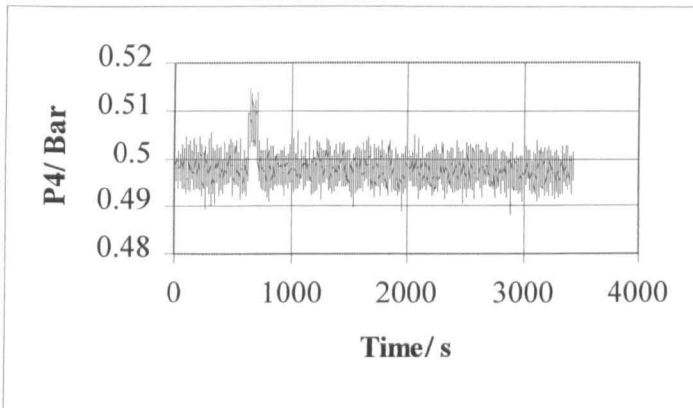
Water CXIX Pressure Results and Statistical Data

Long Swirly-flo Pipe

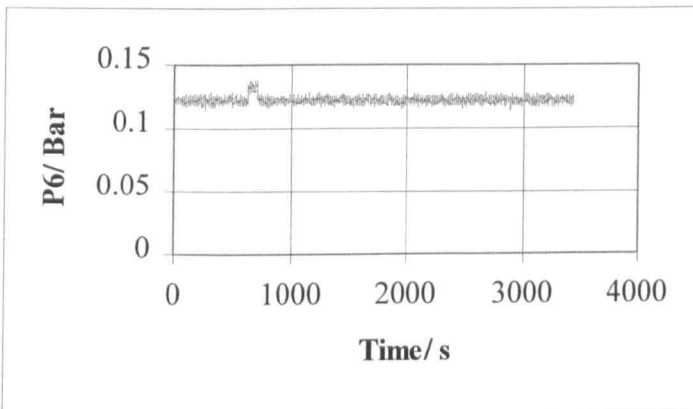
Run: Water 40

Volumetric Flow: 2.353 l/s

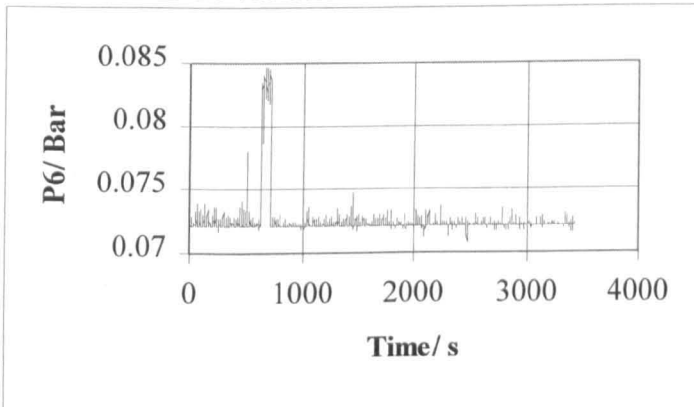
Number of Data Points: 2439



Water CXX P4 variation with time



Water CXXI P6 variation with time



Water CXXII P8 variation with time

	p1	p2	p3	p4	p5	p6	p7	p8
mean	0.684495	0.549172	0.534047	0.497923	0.49445	0.122443	0.094469	0.0724
mode	0.6832	0.55002	0.53437	0.49789	0.49432	0.12252	0.095	0.07206
median	0.68422	0.549	0.53396	0.49768	0.49432	0.12232	0.09438	0.07206
standard deviation	0.001602	0.00294	0.002858	0.002834	0.002873	0.002547	0.002514	0.001713
variance	2.57E-06	8.64E-06	8.17E-06	8.03E-06	8.25E-06	6.49E-06	6.32E-06	2.93E-06
skew	0.224468	0.501584	0.74302	0.893254	0.888576	1.344361	1.487859	6.06372
kurtosis	-0.72117	1.124903	1.949538	2.886904	2.869865	5.104883	5.716866	35.78215

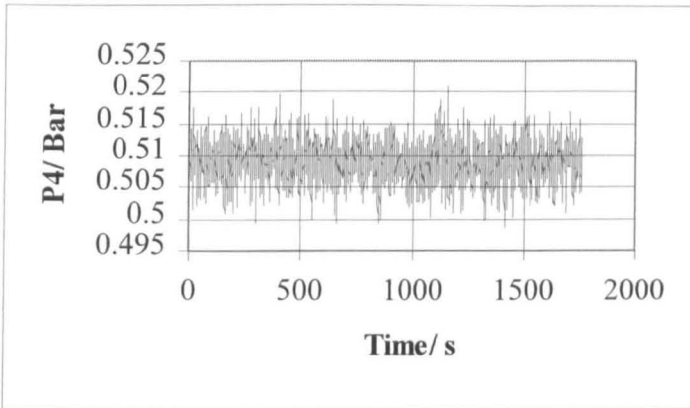
Water CXXIII Pressure Results and Statistical Data

Long Swirly-flo Pipe

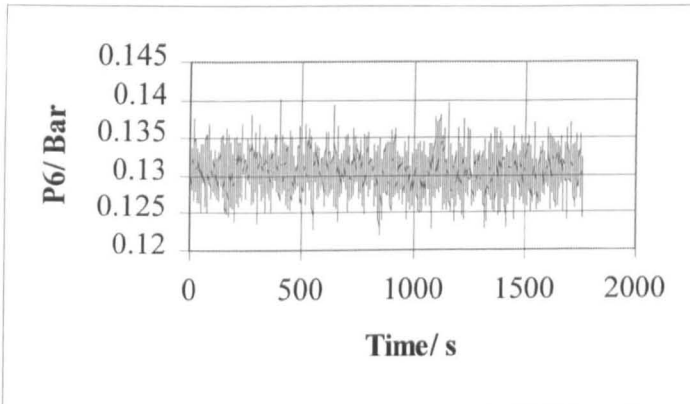
Run: Water 45

Volumetric Flow: 2.692 l/s

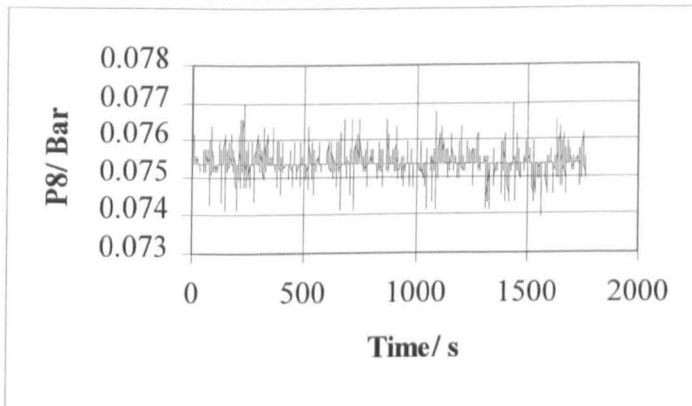
Number of Data Points: 1763



Water CXXIV P4 variation with time



Water CXXV P6 variation with time



Water CXXVI P8 variation with time

	p1	p2	p3	p4	p5	p6	p7	p8
mean	0.752918	0.569508	0.550871	0.508919	0.505522	0.130543	0.102385	0.075344
mode	0.75276	0.56945	0.54951	0.50852	0.50578	0.13091	0.10318	0.07533
median	0.75276	0.56945	0.55074	0.50873	0.50557	0.1305	0.10236	0.07533
standard deviation	0.001593	0.003467	0.003323	0.003236	0.003145	0.002563	0.002512	0.000261
variance	2.54E-06	1.2E-05	1.1E-05	1.05E-05	9.89E-06	6.57E-06	6.31E-06	6.82E-08
skew	-0.06684	0.171926	0.028288	0.016369	-0.03437	0.032248	0.046038	0.446493
kurtosis	0.054971	0.208718	0.048545	0.069471	0.155906	0.160506	0.092948	9.583371

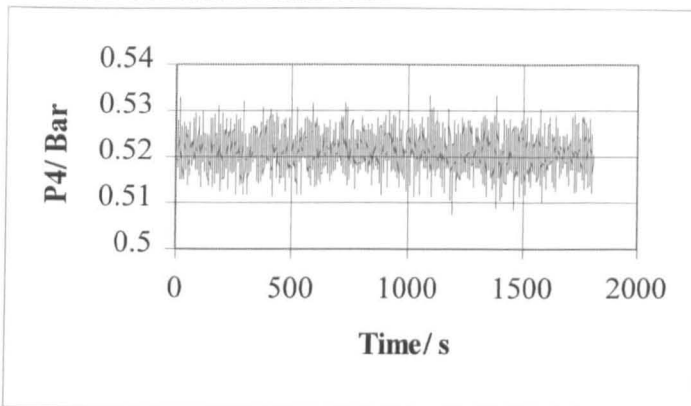
Water CXXVII Pressure Results and Statistical Data

Long Swirly-flo Pipe

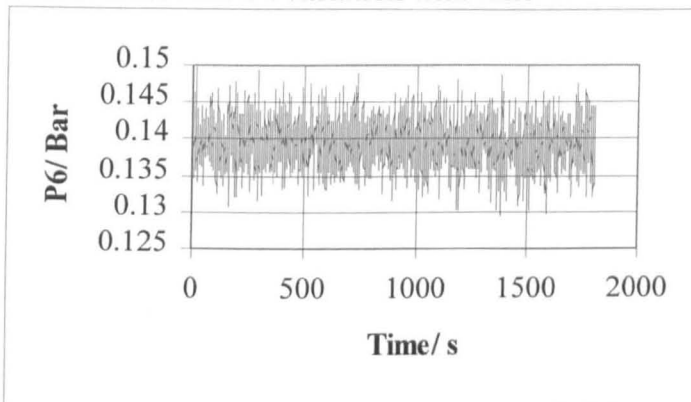
Run: Water 50

Volumetric Flow: 2.958 l/s

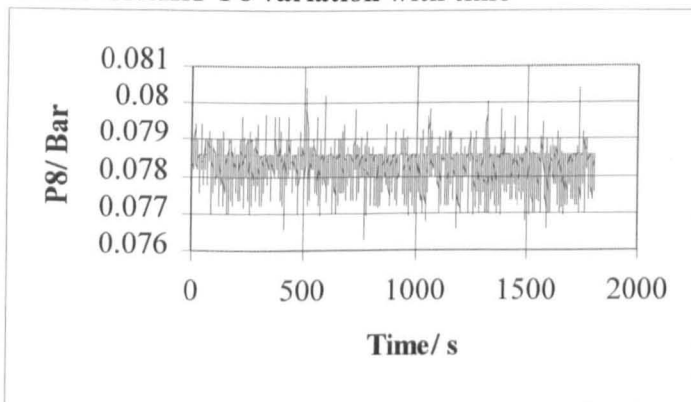
Number of Data Points: 1806



Water CXXVIII P4 variation with time



Water CXXIX P6 variation with time



Water CXXX P8 variation with time

	p1	p2	p3	p4	p5	p6	p7	p8
mean	0.83064	0.592119	0.568725	0.521138	0.517653	0.139521	0.111141	0.078361
mode	0.8305	0.59319	0.56792	0.521	0.51805	0.1395	0.11075	0.07861
median	0.8305	0.59216	0.56874	0.521	0.51764	0.1395	0.11116	0.07861
standard deviation	0.001791	0.004343	0.003938	0.003887	0.003887	0.00318	0.003119	0.000497
variance	3.21E-06	1.89E-05	1.55E-05	1.51E-05	1.51E-05	1.01E-05	9.73E-06	2.47E-07
skew	-0.07564	0.024502	0.008056	-0.01196	0.044989	0.029383	0.006086	-0.91468
kurtosis	0.133629	0.017022	0.070586	-0.03575	-0.00202	-0.04493	-0.00506	1.674236

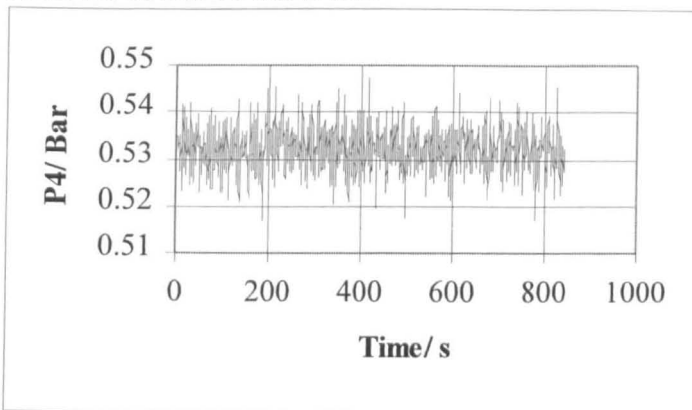
Water CXXXI Pressure Results and Statistical Data

Long Swirly-flo Pipe

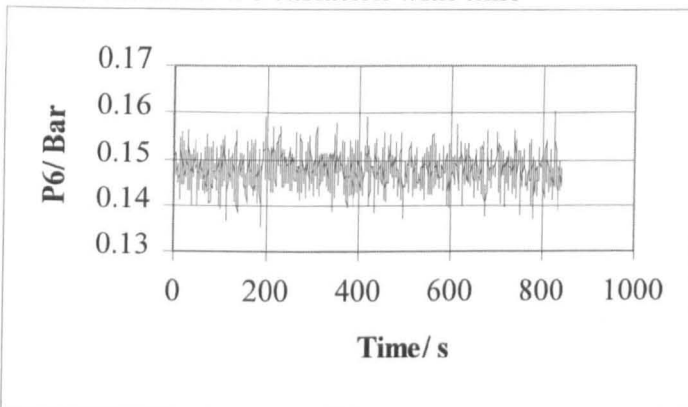
Run: Water 55

Volumetric Flow: 3.303 l/s

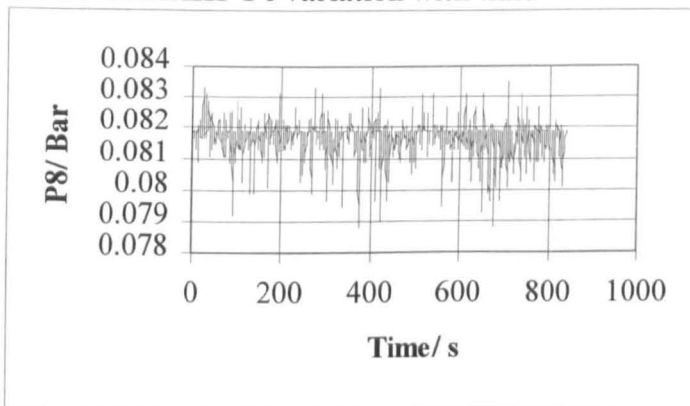
Number of Data Points: 842



Water CXXXII P4 variation with time



Water CXXXIII P6 variation with time



Water CXXXIV P8 variation with time

	p1	p2	p3	p4	p5	p6	p7	p8
mean	0.896943	0.612677	0.584861	0.532134	0.52892	0.147825	0.119253	0.081696
mode	0.89801	0.61569	0.58511	0.53205	0.5289	0.15055	0.1177	0.08188
median	0.89699	0.61262	0.58511	0.53226	0.5289	0.14779	0.11914	0.08188
standard deviatio	0.002175	0.005115	0.004764	0.004694	0.004764	0.003865	0.00382	0.000564
variance	4.73E-06	2.62E-05	2.27E-05	2.2E-05	2.27E-05	1.49E-05	1.46E-05	3.18E-07
skew	0.027784	-0.00187	-0.04081	-0.0016	-0.01363	-0.0225	-0.00502	-1.4619
kurtosis	0.011255	-0.20612	-0.09294	0.046317	-0.11011	-0.02041	-0.03715	5.185571

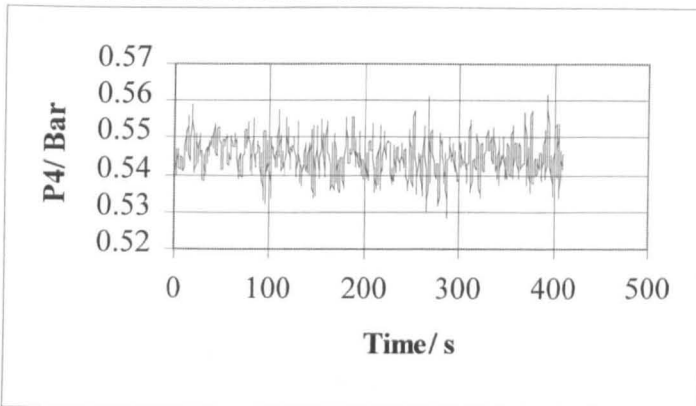
Water CXXXV Pressure Results and Statistical Data

Long Swirly-flo Pipe

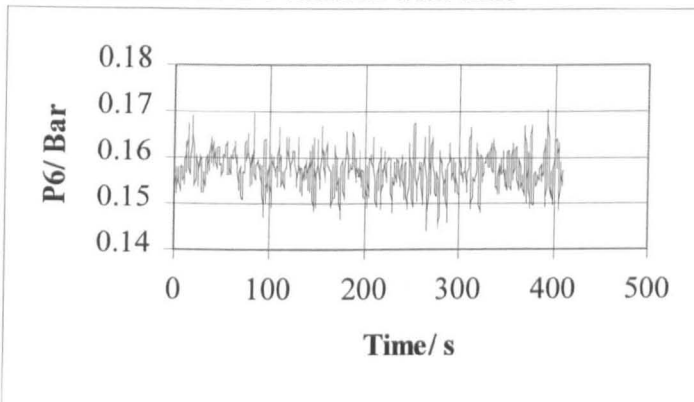
Run: Water 60

Volumetric Flow: 3.583 l/s

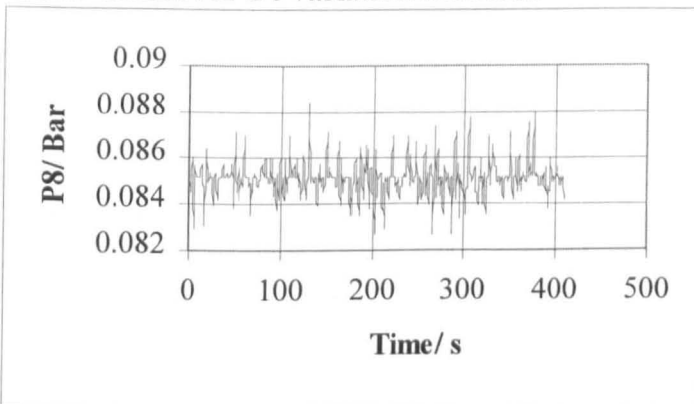
Number of Data Points: 410



Water CXXXVI P4 variation with time



Water CXXXVII P6 variation with time



Water CXXXVIII P8 variation with time

	p1	p2	p3	p4	p5	p6	p7	p8
mean	0.978275	0.636528	0.603533	0.54491	0.541901	0.157314	0.128516	0.085105
mode	0.97882	0.64106	0.60332	0.54781	0.54342	0.1571	0.12875	0.08515
median	0.97882	0.63635	0.60352	0.545045	0.54219	0.1573	0.12875	0.08515
standard deviatio	0.002493	0.005922	0.005414	0.005469	0.005393	0.004461	0.004377	0.000747
variance	6.21E-06	3.51E-05	2.93E-05	2.99E-05	2.91E-05	1.99E-05	1.92E-05	5.59E-07
skew	-0.23298	0.248387	0.051294	0.038315	-0.06103	-0.00856	-0.04693	0.466444
kurtosis	-0.22161	0.165382	0.014717	-0.05066	-0.06901	-0.05205	-0.07623	3.263099

Water CXXXIX Pressure Results and Statistical Data

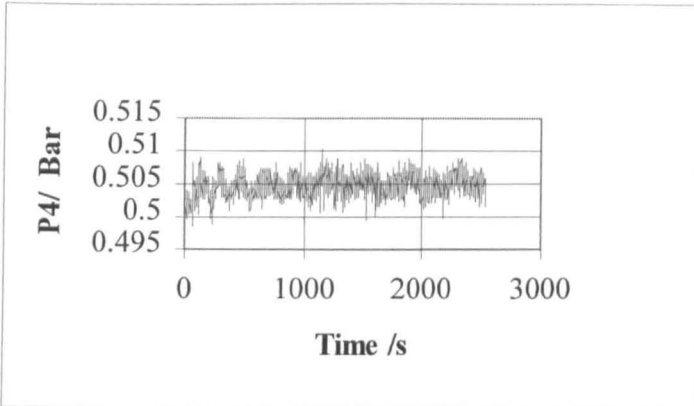
Standard Pipe Arrangement

Run: 2kgstd20

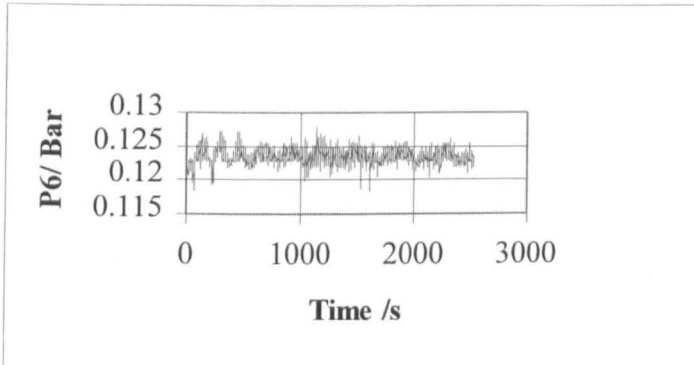
Volumetric Flow: 0.952 l/s

Mass Flow: 0.976 Kg/s

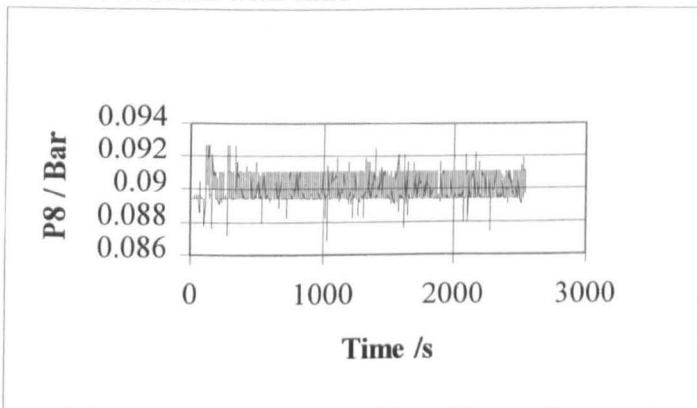
Number of Data Points: 2530



I P4 variation with time



II P6 variation with time



III P8 variation with time

	p1	p2	p3	p4	p5	p6	p7	p8
mean	0.499371	0.511738	0.507296	0.504771	0.48825	0.123353	0.095452	0.089944
median	0.49907	0.51176	0.50757	0.50484	0.48818	0.12314	0.09536	0.08943
mode	0.49907	0.51033	0.50778	0.50587	0.48778	0.12252	0.09515	0.08943
standard deviation	0.000755	0.001603	0.001602	0.00162	0.00156	0.001072	0.001186	0.000701
variance	5.69E-07	2.57E-06	2.57E-06	2.63E-06	2.43E-06	1.15E-06	1.41E-06	4.92E-07
skew	3.126792	-0.16589	-0.29304	-0.19502	-0.20259	0.229389	-0.09897	0.770316
kurtosis	11.24855	-0.12822	0.069468	-0.12998	0.092289	0.939136	0.81883	0.290947

IV Pressure Readings and Statistical Data

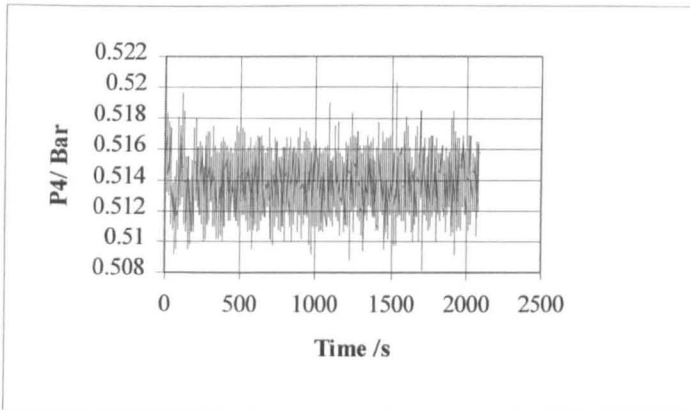
Standard Pipe Arrangement

Run: 2kgstd25

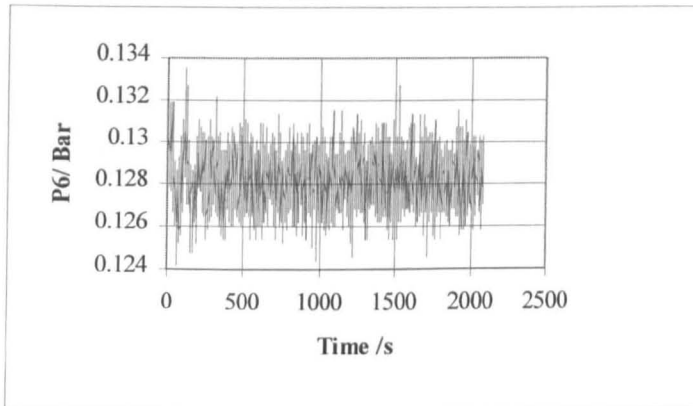
Volumetric Flow: 1.385 l/s

Mass Flow: 1.415 Kg/s

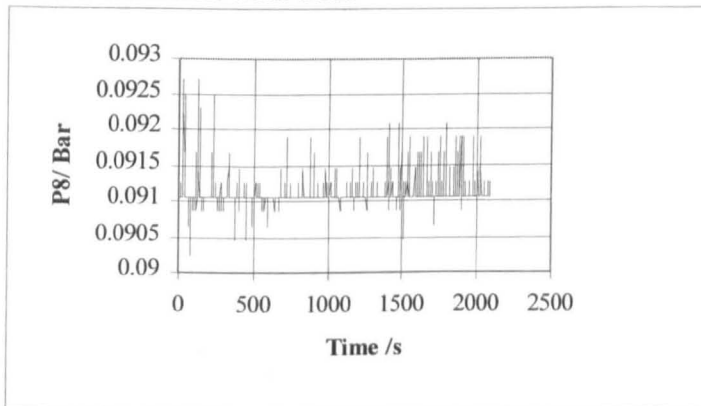
Number of Data Points: 2086



V P4 variation with time



VI P6 variation with time



VII P8 variation with time

	p1	p2	p3	p4	p5	p6	p7	p8
mean	0.53988	0.524057	0.517047	0.51377	0.496103	0.128255	0.100279	0.091091
median	0.53999	0.52424	0.51698	0.51384	0.49616	0.12825	0.10027	0.09106
mode	0.53999	0.52506	0.51739	0.51384	0.49637	0.12907	0.10006	0.09106
standard deviation	0.000506	0.001534	0.001625	0.001664	0.001595	0.001273	0.001207	0.000166
variance	2.56E-07	2.35E-06	2.64E-06	2.77E-06	2.54E-06	1.62E-06	1.46E-06	2.76E-08
skew	-4.37322	-0.07076	0.130036	0.053006	0.073564	0.041398	0.111861	5.489836
kurtosis	35.77456	0.437445	0.010563	-0.16678	0.049571	-0.01441	0.126073	41.88804

VIII Pressure Readings and Statistical Data

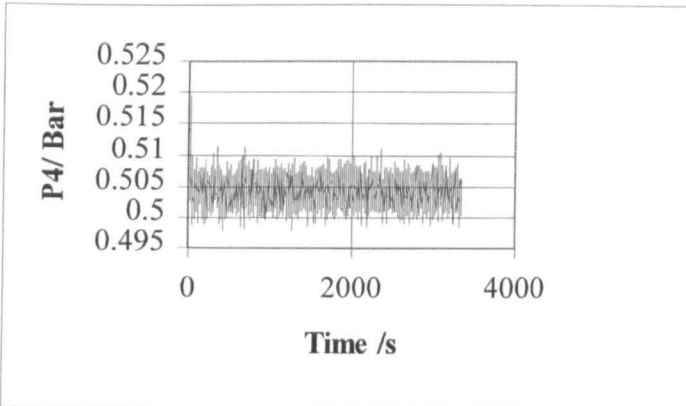
Standard Pipe Arrangement

Run: 2kgstd30

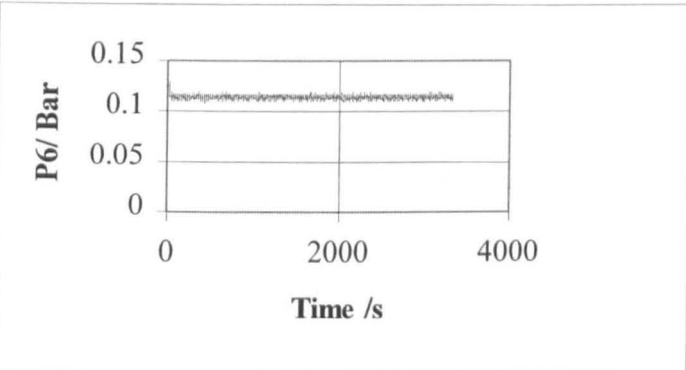
Volumetric Flow: 1.824 l/s

Mass Flow: 1.866 Kg/s

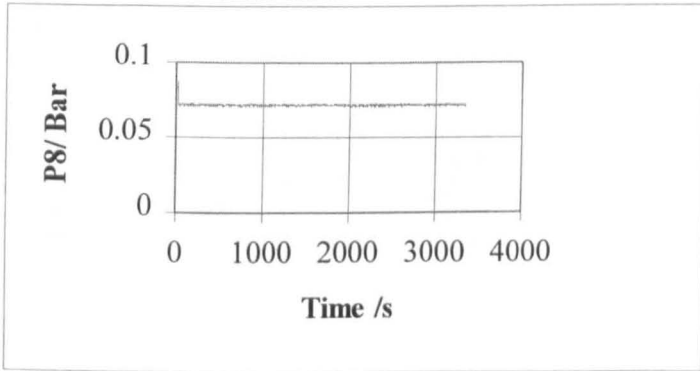
Number of Data Points:3332



IX P4 variation with time



X P6 variation with time



XI P8 variation with time

	p1	p2	p3	p4	p5	p6	p7	p8
mean	0.58075	0.520224	0.50877	0.504197	0.485673	0.114625	0.085839	0.0718
median	0.58091	0.52015	0.5088	0.50402	0.48552	0.11455	0.08574	0.07142
mode	0.58091	0.51994	0.509	0.50321	0.48532	0.11414	0.08533	0.07142
standard deviation	0.002477	0.00242	0.002344	0.002322	0.002379	0.002141	0.00207	0.001315
variance	6.14E-06	5.85E-06	5.5E-06	5.39E-06	5.66E-06	4.58E-06	4.29E-06	1.73E-06
skew	-0.0085	0.867121	1.022399	1.145852	1.093351	1.603851	1.889113	9.517022
kurtosis	0.097379	3.913889	4.894877	5.580246	5.190259	9.331928	11.62575	103.1061

XII Pressure Readings and Statistical Data

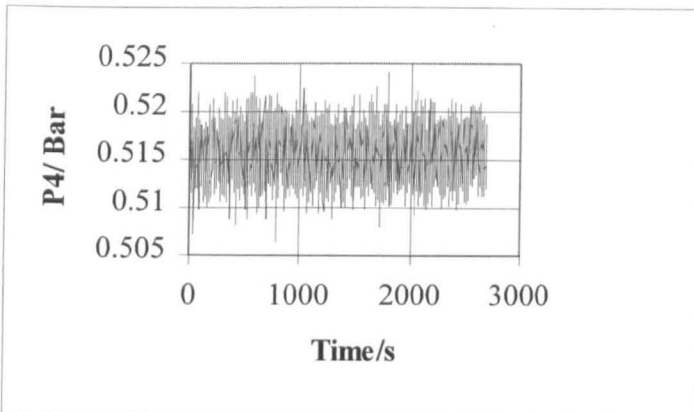
Standard Pipe Arrangement

Run: 2kgstd35

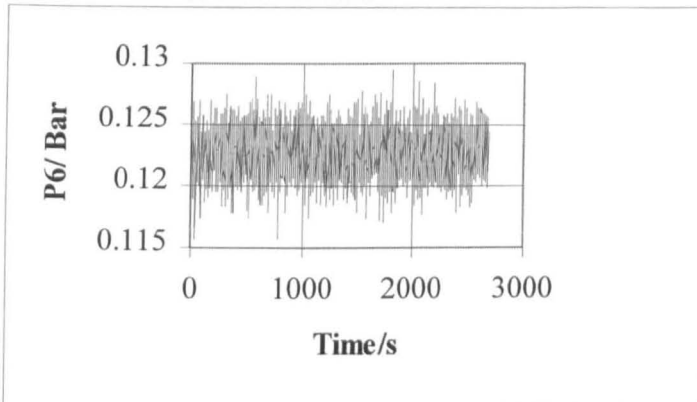
Volumetric Flow: 2.216 l/s

Mass Flow: 2.273 Kg/s

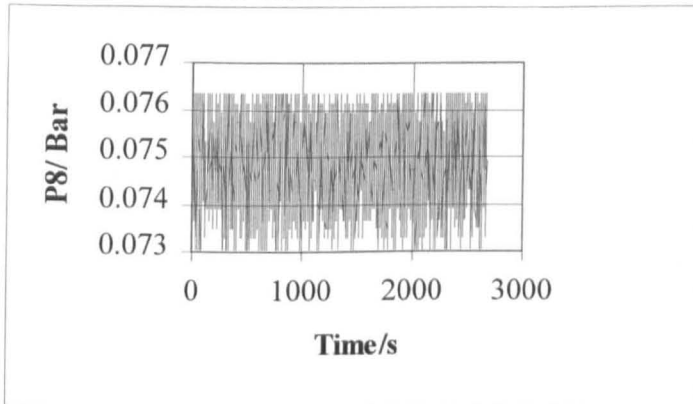
Number of Data Points: 2681



XIII P4 variation with time



XIV P6 variation with time



XV P8 variation with time

	p1	p2	p3	p4	p5	p6	p7	p8
mean	0.638773	0.535972	0.521107	0.51567	0.496483	0.122752	0.093354	0.074811
median	0.63921	0.5359	0.52107	0.51569	0.49637	0.12273	0.09331	0.0747
mode	0.63819	0.5359	0.52189	0.51548	0.49596	0.12293	0.09352	0.0747
standard deviation	0.002082	0.003077	0.002554	0.002454	0.002386	0.001817	0.001794	0.000835
variance	4.34E-06	9.47E-06	6.52E-06	6.02E-06	5.69E-06	3.3E-06	3.22E-06	6.97E-07
skew	0.069898	0.101291	0.005828	-0.03193	-0.00141	-0.04117	0.001448	-0.07288
kurtosis	0.930848	-0.06463	-0.11734	-0.07498	-0.03774	0.116894	0.000296	-0.64537

XVI Pressure Readings and Statistical Data

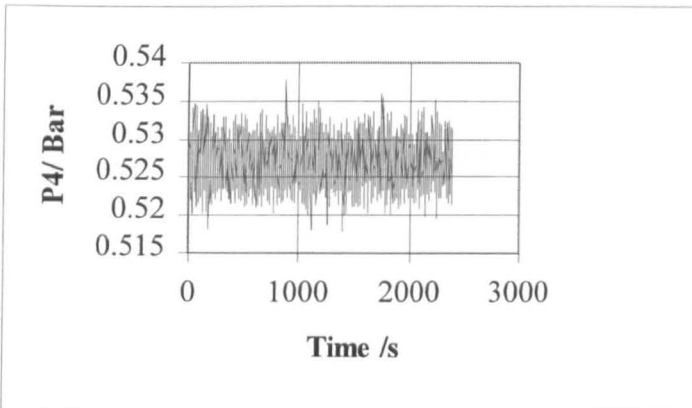
Standard Pipe Arrangement

Run: 2kgstd40

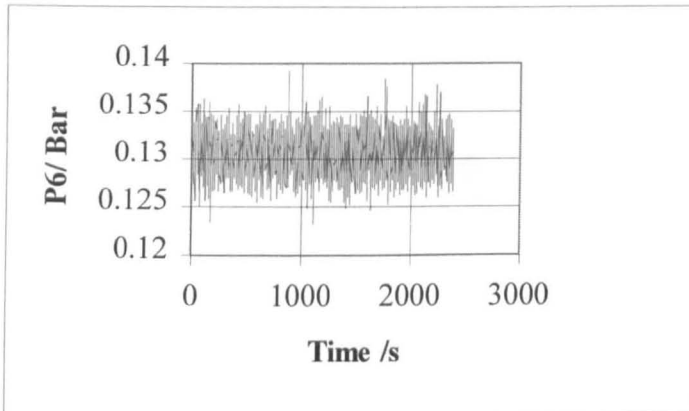
Volumetric Flow: 2.566 l/s

Mass Flow: 2.637 Kg/s

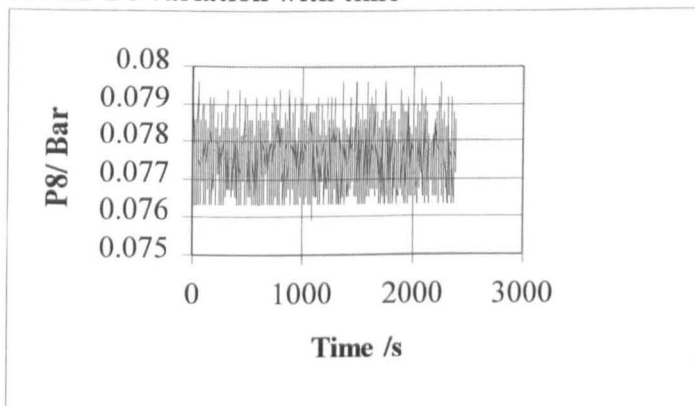
Number of Data Points: 2389



XVII P4 variation with time



XVIII P6 variation with time



XIX P8 variation with time

	p1	p2	p3	p4	p5	p6	p7	p8
mean	0.699675	0.552294	0.533315	0.527067	0.507284	0.130633	0.100933	0.077652
median	0.69956	0.55227	0.53335	0.52714	0.50721	0.1305	0.10088	0.07777
mode	0.69956	0.55247	0.53478	0.52735	0.50782	0.13091	0.10027	0.07797
standard deviation	0.002561	0.00358	0.002964	0.002817	0.002733	0.002084	0.001988	0.000625
variance	6.56E-06	1.28E-05	8.78E-06	7.93E-06	7.47E-06	4.34E-06	3.95E-06	3.91E-07
skew	-0.25902	0.085225	0.112202	0.028783	0.04611	0.103036	0.058178	-0.19576
kurtosis	0.16277	-0.18896	-0.18912	-0.13527	-0.05791	0.063556	0.169185	0.12908

XX Pressure Readings and Statistical Data

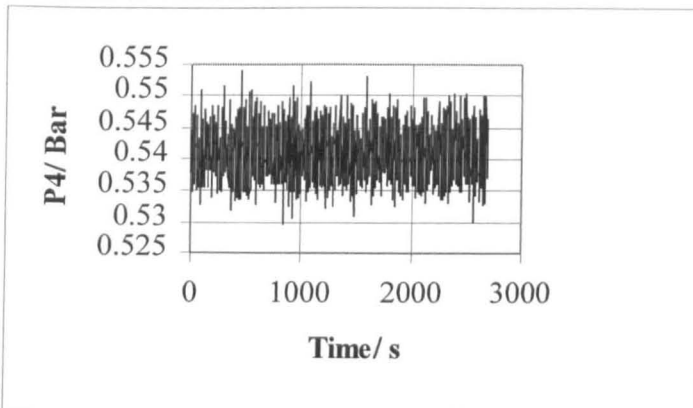
Standard Pipe Arrangement

Run: 2kgstd45

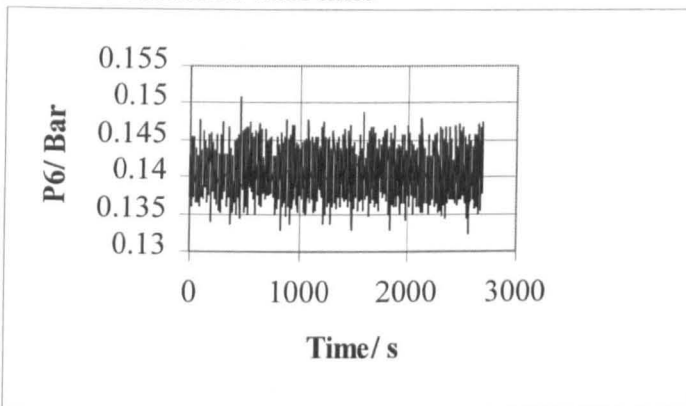
Volumetric Flow: 2.941 l/s

Mass Flow: 3.021 Kg/s

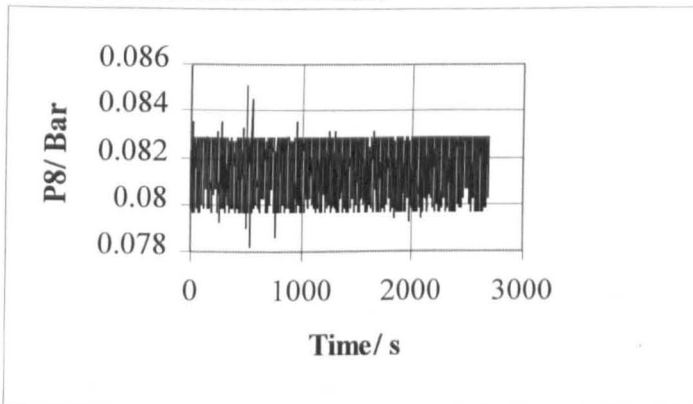
Number of Data Points:2689



XXI P4 variation with time



XXII P6 variation with time



XXIII P8 variation with time

	p1	p2	p3	p4	p5	p6	p7	p8
mean	0.774232	0.571996	0.548696	0.541079	0.520782	0.140591	0.110542	0.081517
median	0.77424	0.57191	0.54849	0.54105	0.52071	0.14053	0.1105	0.08165
mode	0.77424	0.57252	0.54808	0.54024	0.52276	0.14032	0.11091	0.08288
standard deviation	0.002763	0.004528	0.003665	0.003431	0.003389	0.002531	0.002474	0.001022
variance	7.63E-06	2.05E-05	1.34E-05	1.18E-05	1.15E-05	6.4E-06	6.12E-06	1.04E-06
skew	0.01526	0.199227	0.157546	0.159904	0.147169	0.133883	0.089967	-0.27099
kurtosis	0.311326	0.081946	-0.02569	-0.02928	-0.00458	-0.02058	-0.02765	-0.95106

XXIV Pressure Readings and Statistical Data

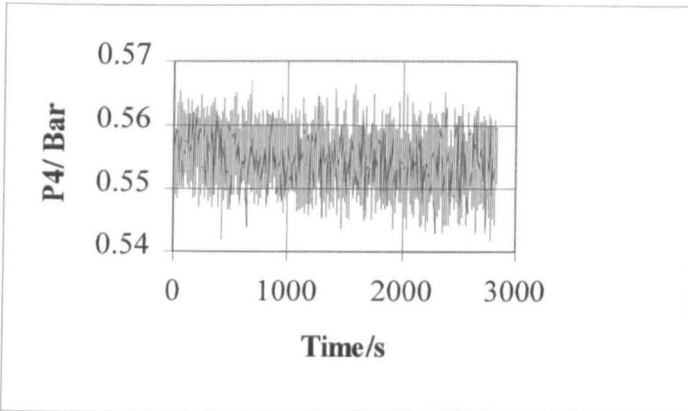
Standard Pipe Arrangement

Run: 2kgstd50

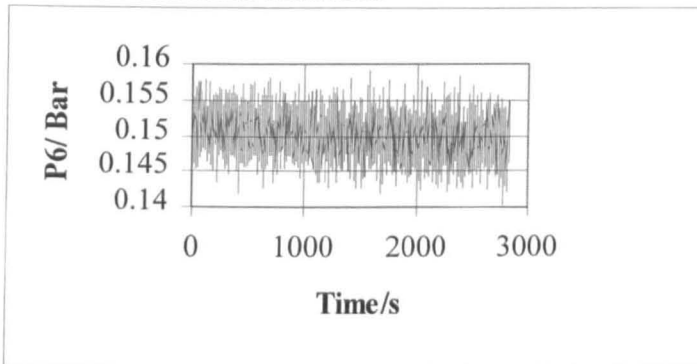
Volumetric Flow: 3.324 l/s

Mass Flow: 3.339 Kg/s

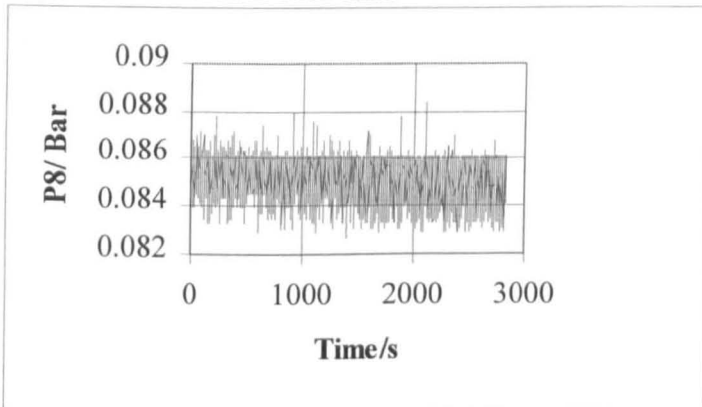
Number of Data Points:2829



XXV P4 variation with time



XXVI P6 variation with time



XXVII P8 variation with time

	p1	p2	p3	p4	p5	p6	p7	p8
mean	0.849923	0.590801	0.563016	0.554475	0.533707	0.150048	0.119844	0.085191
median	0.84891	0.59073	0.56301	0.55435	0.53381	0.14994	0.1197	0.08534
mode	0.84891	0.59032	0.56199	0.55394	0.53401	0.14973	0.11868	0.08615
standard deviation	0.005648	0.005318	0.004129	0.004012	0.00392	0.002844	0.002812	0.000872
variance	3.19E-05	2.83E-05	1.71E-05	1.61E-05	1.54E-05	8.09E-06	7.91E-06	7.61E-07
skew	0.277439	-0.03114	-0.02844	0.000926	-0.01455	0.034432	0.076098	-0.44677
kurtosis	-0.35521	-0.06806	-0.07784	-0.16957	-0.16852	-0.11306	-0.12289	-0.42919

XXVIII Pressure Readings and Statistical Data

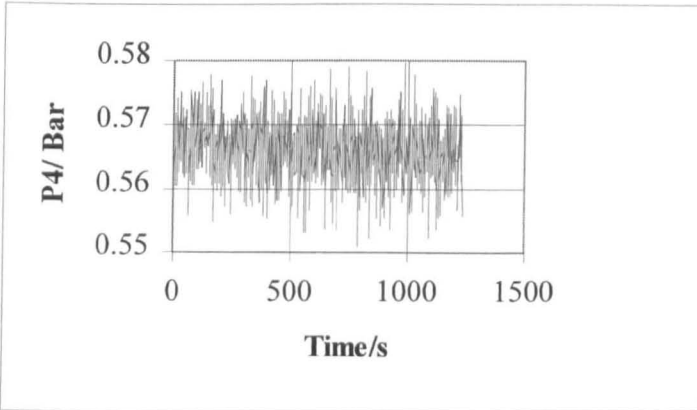
Standard Pipe Arrangement

Run: 2kgstd55

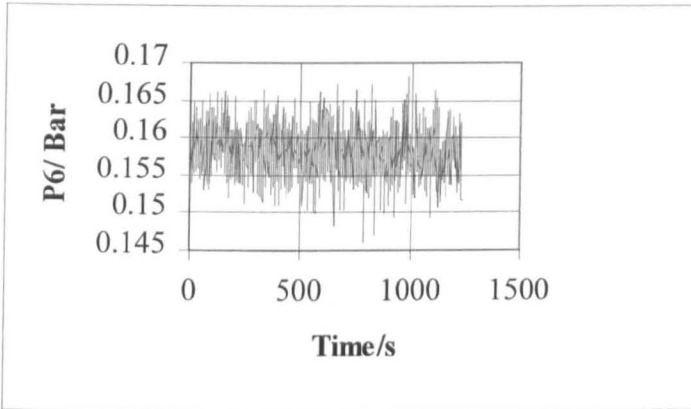
Volumetric Flow: 3.523 l/s

Mass Flow: 3.64 Kg/s

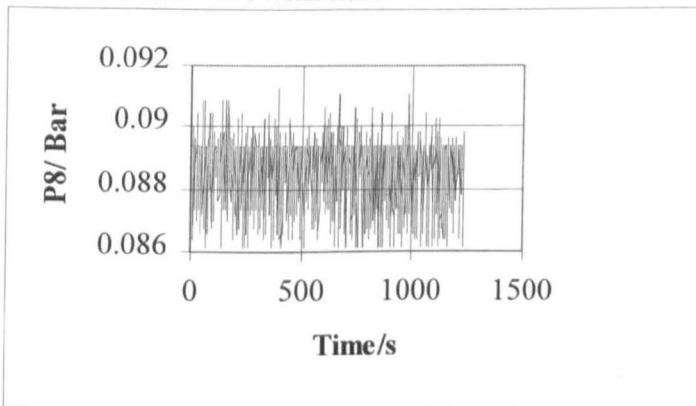
Number of Data Points:1235



IXXX P4 variation with time



XXX P6 variation with time



XXXI P8 variation with time

	p1	p2	p3	p4	p5	p6	p7	p8
mean	0.917176	0.607498	0.575315	0.566122	0.544835	0.158262	0.128113	0.088566
median	0.91745	0.60751	0.57529	0.56622	0.54485	0.15812	0.12809	0.08881
mode	0.91847	0.60648	0.57447	0.56663	0.54506	0.15812	0.12768	0.08943
standard deviation	0.004361	0.006279	0.004727	0.004433	0.004338	0.003198	0.003171	0.001054
variance	1.9E-05	3.94E-05	2.23E-05	1.97E-05	1.88E-05	1.02E-05	1.01E-05	1.11E-06
skew	-0.03718	-0.03501	-0.0343	-0.10567	-0.08157	-0.0471	-0.09242	-0.59095
kurtosis	-0.24962	-0.03836	0.162728	0.214966	0.219578	0.159144	0.140124	-0.43488

XXXII Pressure Readings and Statistical Data

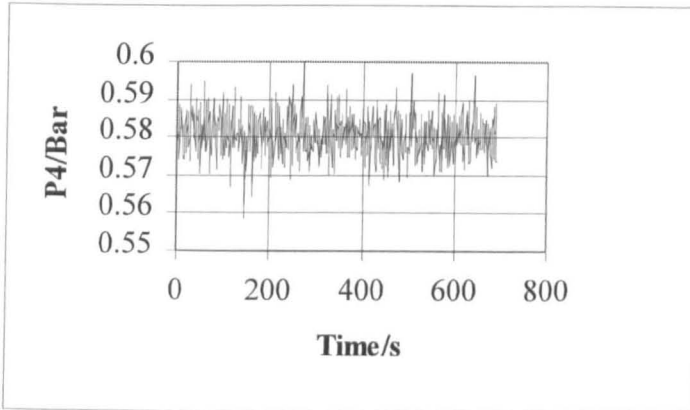
Standard Pipe Arrangement

Run: 2kgstd60

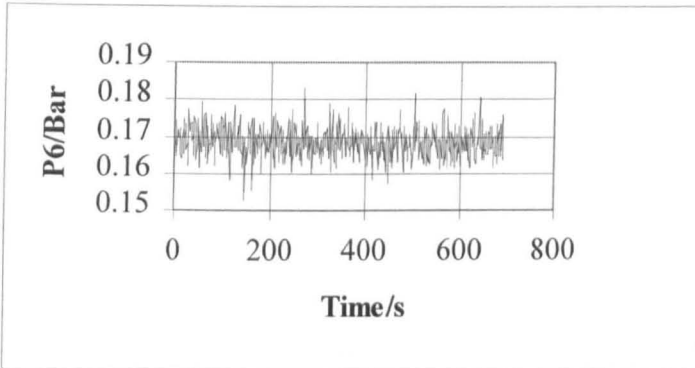
Volumetric Flow: 3.76 l/s

Mass Flow: 3.908 Kg/s

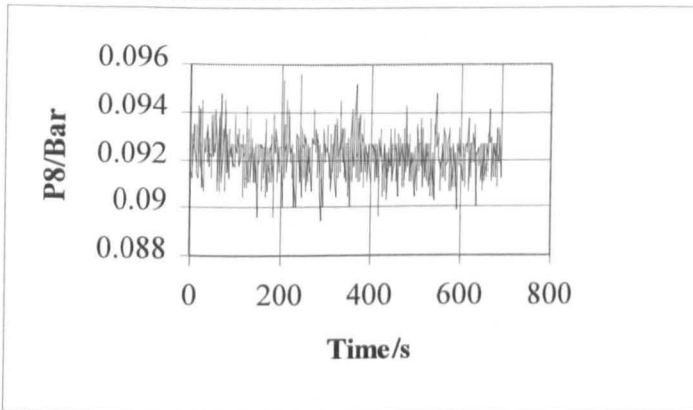
Number of Data Points:691



XXXIII P4 variation with time



XXXIV P6 variation with time



XXXV P8 variation with time

	p1	p2	p3	p4	p5	p6	p7	p8
mean	0.999177	0.628681	0.591019	0.580638	0.558701	0.168514	0.137976	0.092189
median	0.99928	0.62858	0.59063	0.58033	0.55836	0.16835	0.13791	0.09229
mode	0.99928	0.62981	0.59002	0.57808	0.55836	0.16815	0.13934	0.0927
standard deviation	0.004851	0.007259	0.005652	0.005379	0.005279	0.003916	0.003723	0.000925
variance	2.35E-05	5.27E-05	3.19E-05	2.89E-05	2.79E-05	1.53E-05	1.39E-05	8.56E-07
skew	-0.05231	0.082721	0.074092	0.077547	0.046854	0.065443	0.049255	0.210137
kurtosis	-0.13798	0.425328	0.285365	0.302179	0.291152	0.550406	0.528863	0.939915

XXXVI Pressure Readings and Statistical Data

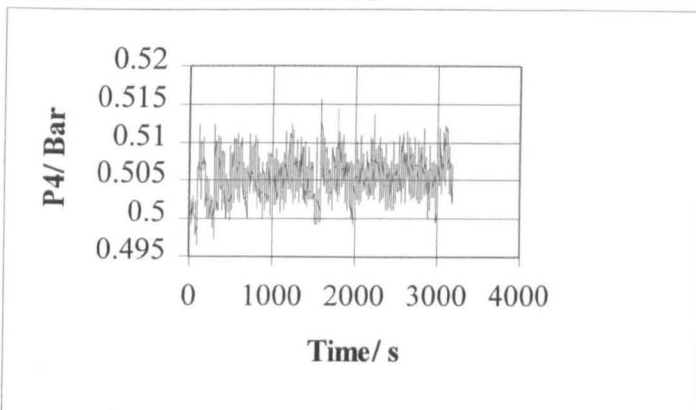
Standard Pipe Arrangement

Run: 4kgstd20

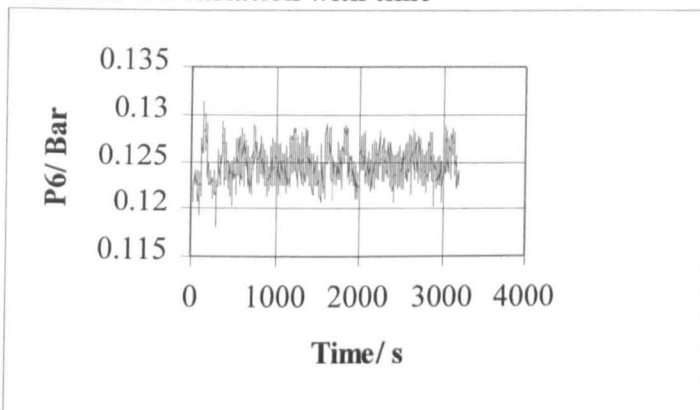
Volumetric Flow: 0.888 l/s

Mass Flow: 0.916 Kg/s

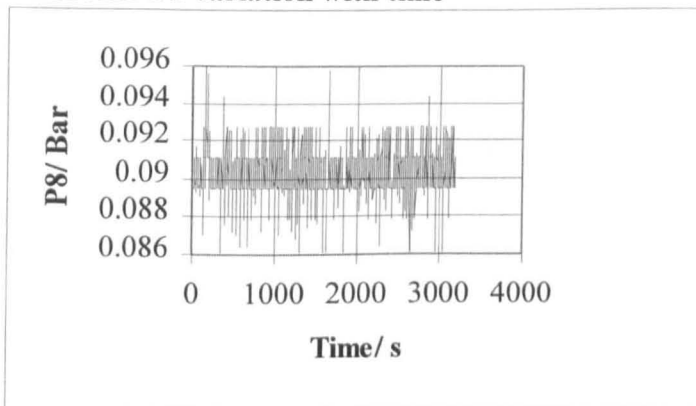
Number of Data Points:3192



XXXVII P4 variation with time



XXXVIII P6 variation with time



XXXIX P8 variation with time

	p1	p2	p3	p4	p5	p6	p7	p8
mean	0.501406	0.514076	0.508603	0.50558	0.489288	0.124602	0.097075	0.090215
median	0.50112	0.51401	0.50859	0.50566	0.48921	0.12457	0.0972	0.08984
mode	0.49907	0.5136	0.50778	0.50587	0.48778	0.12252	0.09843	0.08943
standard deviation	0.002126	0.002166	0.002598	0.002605	0.002485	0.001695	0.001796	0.001059
variance	4.52E-06	4.69E-06	6.75E-06	6.79E-06	6.17E-06	2.87E-06	3.23E-06	1.12E-06
skew	0.776346	-0.42776	-0.23294	-0.02707	0.022655	0.123028	-0.25128	0.605598
kurtosis	-0.15728	2.324992	0.502053	0.119683	0.066416	-0.01821	-0.1854	1.854944

XXXX Pressure Readings and Statistical Data

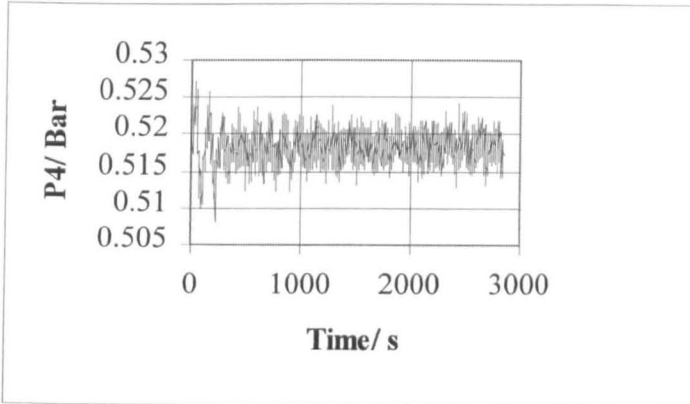
Standard Pipe Arrangement

Run: 4kgstd25

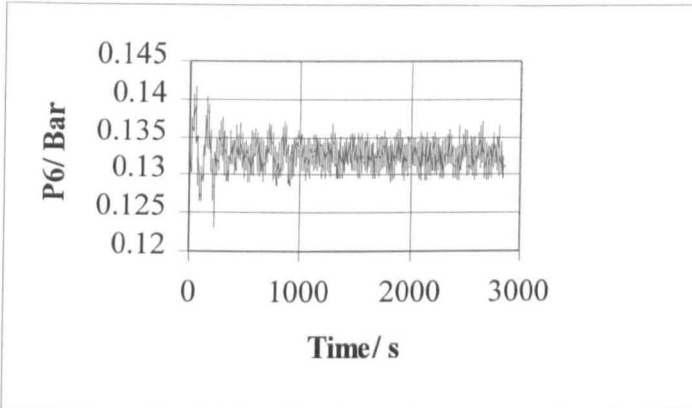
Volumetric Flow: 1.312 l/s

Mass Flow: 1.349 Kg/s

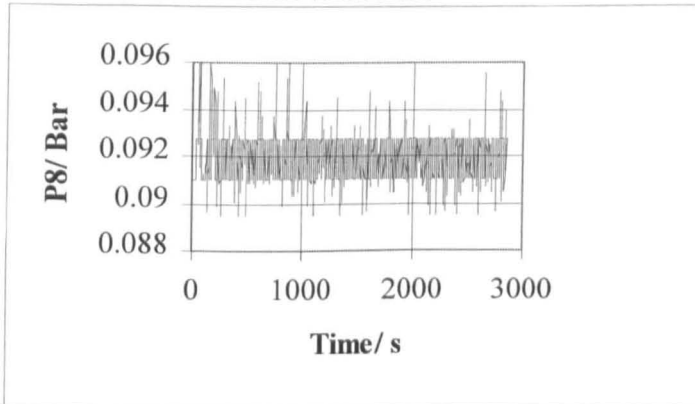
Number of Data Points: 2854



XXXXI P4 variation with time



XXXXII P6 variation with time



XXXXIII P8 variation with time

	p1	p2	p3	p4	p5	p6	p7	p8
mean	0.540718	0.532795	0.522563	0.518243	0.50149	0.132728	0.103851	0.091976
median	0.53999	0.53263	0.52251	0.51814	0.50148	0.13275	0.10395	0.09209
mode	0.53999	0.53161	0.5223	0.51794	0.50087	0.13234	0.10497	0.0927
standard deviation	0.001072	0.001763	0.002114	0.002083	0.002068	0.001811	0.00179	0.000838
variance	1.15E-06	3.11E-06	4.47E-06	4.34E-06	4.28E-06	3.28E-06	3.2E-06	7.02E-07
skew	1.871092	-0.04846	0.064693	-0.18646	-0.01605	0.19205	-0.31656	0.317892
kurtosis	4.526125	0.681567	1.283266	1.603637	1.266936	1.530085	1.835422	1.012649

XXXXIV Pressure Readings and Statistical Data

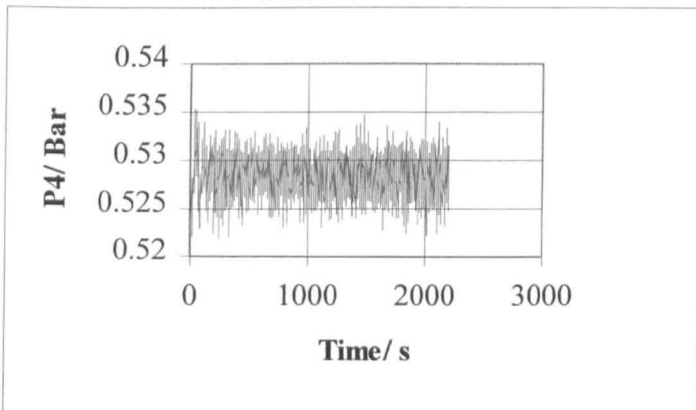
Standard Pipe Arrangement

Run: 4kgstd30

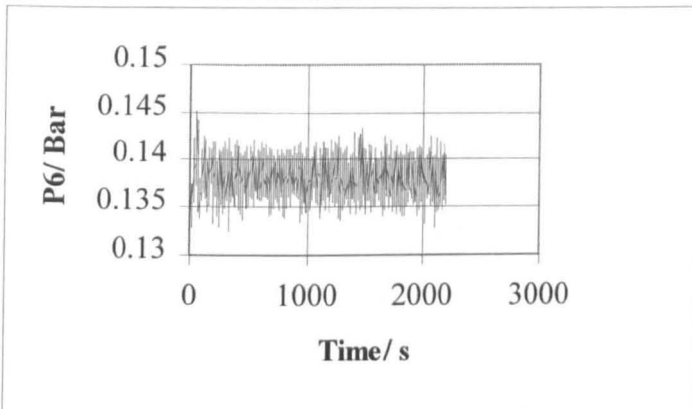
Volumetric Flow: 1.766 l/s

Mass Flow: 1.809 Kg/s

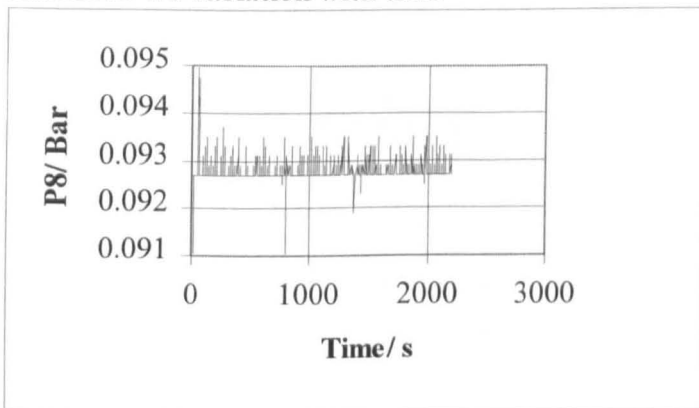
Number of Data Points: 2199



XXXXV P4 variation with time



XXXXVI P6 variation with time



XXXXVII P8 variation with time

	p1	p2	p3	p4	p5	p6	p7	p8
mean	0.589484	0.546701	0.53341	0.528344	0.51037	0.138066	0.109356	0.092741
median	0.58909	0.54674	0.53335	0.52837	0.51028	0.13807	0.10927	0.0927
mode	0.58909	0.54654	0.53335	0.52837	0.51069	0.13787	0.10968	0.0927
standard deviation	0.000763	0.00209	0.002036	0.002031	0.002053	0.001789	0.001786	0.000175
variance	5.82E-07	4.37E-06	4.15E-06	4.13E-06	4.21E-06	3.2E-06	3.19E-06	3.05E-08
skew	1.948573	-0.00738	0.069251	-0.00876	0.068146	0.041032	0.015413	4.424019
kurtosis	4.485922	0.234985	0.044911	0.070684	-0.00037	-0.08766	-0.14906	49.86235

XXXXVIII Pressure Readings and Statistical Data

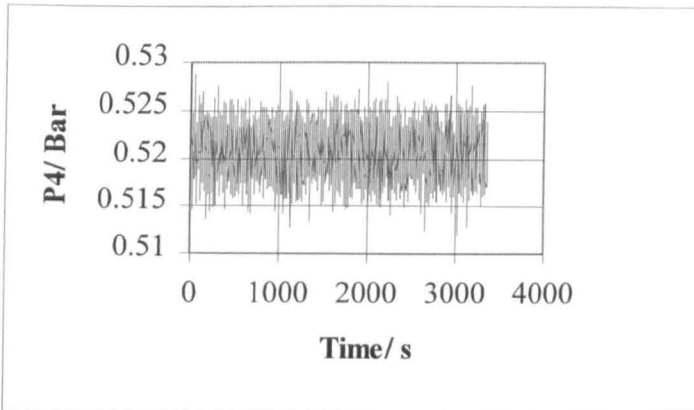
Standard Pipe Arrangement

Run: 4kgstd35

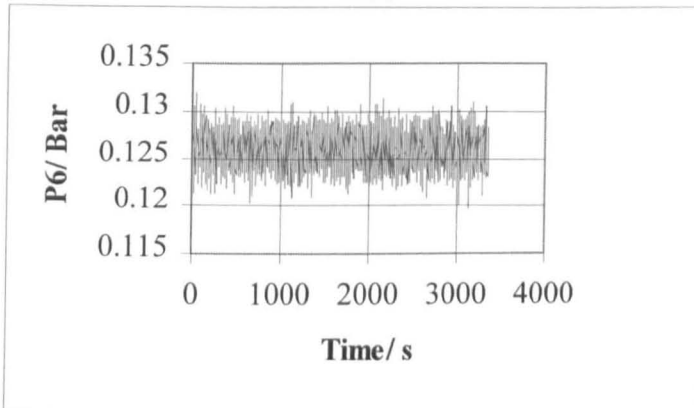
Volumetric Flow: 2.159 l/s

Mass Flow: 2.246 Kg/s

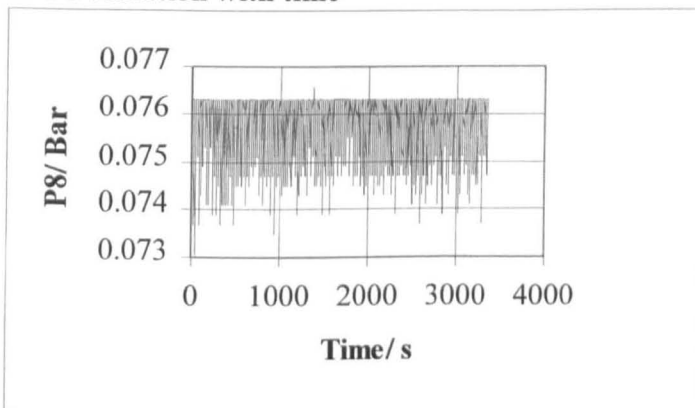
Number of Data Points:3344



XLIX P4 variation with time



L P6 variation with time



LI P8 variation time

	p1	p2	p3	p4	p5	p6	p7	p8
mean	0.640796	0.544255	0.527098	0.520686	0.501964	0.126008	0.096625	0.075857
median	0.64023	0.54429	0.52721	0.5208	0.5021	0.126	0.09659	0.07613
mode	0.64023	0.54429	0.52742	0.5208	0.50169	0.12621	0.09618	0.07633
standard deviation	0.00231	0.003014	0.002422	0.00235	0.002329	0.001732	0.001725	0.000561
variance	5.33E-06	9.09E-06	5.87E-06	5.52E-06	5.42E-06	3E-06	2.97E-06	3.15E-07
skew	0.441027	-0.06889	-0.07376	-0.01151	-0.03894	-0.03109	-0.06241	-1.21846
kurtosis	0.319516	-0.06133	0.057711	0.019937	-0.01708	-0.04569	-0.15726	0.918418

LII Pressure Readings and Statistical Data

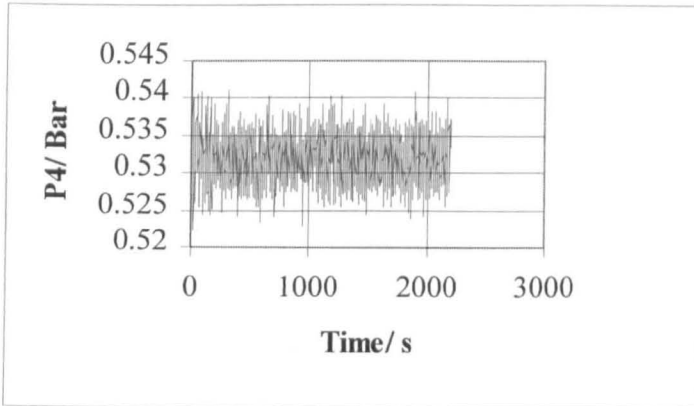
Standard Pipe Arrangement

Run: 4kgstd40

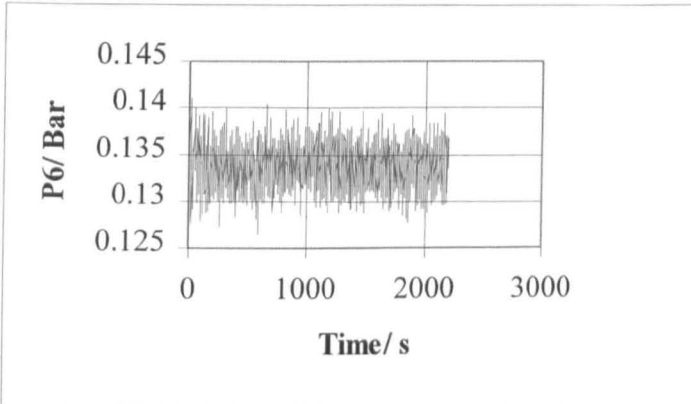
Volumetric Flow: 2.547 l/s

Mass Flow: 2.638 Kg/s

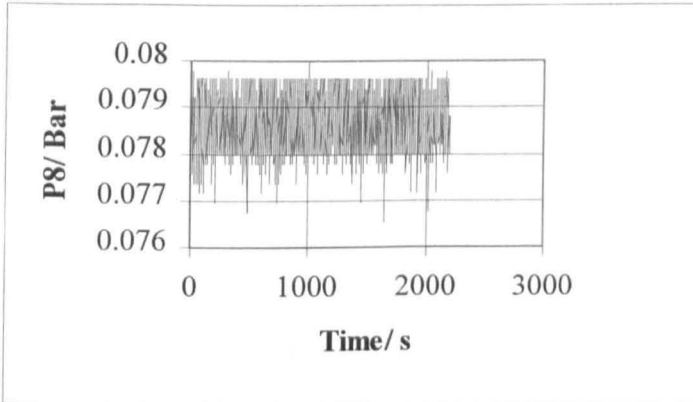
Number of Data Points:2196



LIII P4 variation with time



LIV P6 variation with time



LV P8 variation with time

	p1	p2	p3	p4	p5	p6	p7	p8
mean	0.701293	0.559669	0.539261	0.53194	0.512565	0.13381	0.104053	0.078662
median	0.70161	0.55963	0.53928	0.53185	0.51253	0.13398	0.10416	0.07858
mode	0.70161	0.55861	0.53969	0.53205	0.51273	0.13398	0.10457	0.07797
standard deviation	0.002513	0.003548	0.003024	0.002786	0.002803	0.002111	0.002045	0.00062
variance	6.31E-06	1.26E-05	9.15E-06	7.76E-06	7.86E-06	4.46E-06	4.18E-06	3.84E-07
skew	-0.12776	0.088388	0.072195	0.056148	0.076511	0.016162	0.095517	0.019982
kurtosis	0.105413	0.227656	0.164329	0.186462	0.048292	0.021141	0.043995	-1.02214

LVI Pressure Readings and Statistical Data

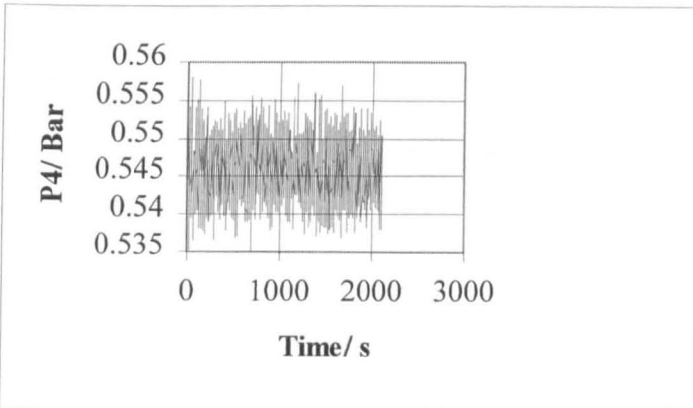
Standard Pipe Arrangement

Run: 4kgstd45

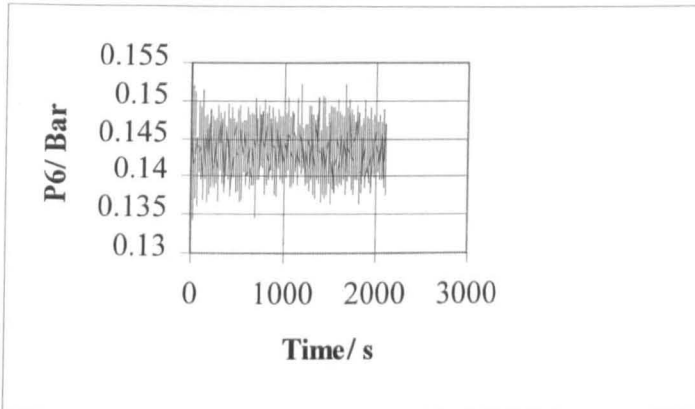
Volumetric Flow: 2.912 l/s

Mass Flow: 3.013 Kg/s

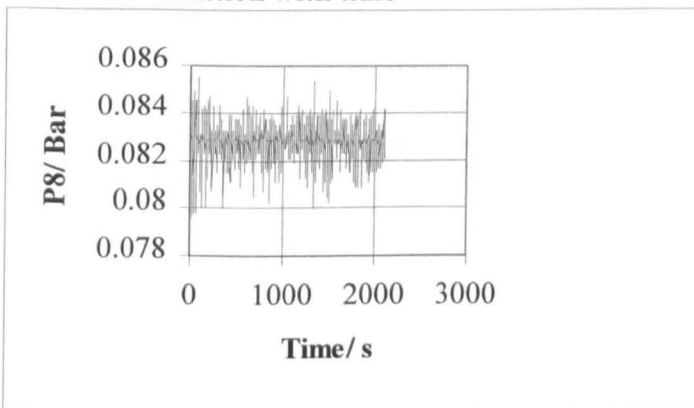
Number of Data Points:2114



LVII P4 variation with time



LVIII P6 variation with time



LIX P8 variation with time

	p1	p2	p3	p4	p5	p6	p7	p8
mean	0.77531	0.578813	0.554372	0.54581	0.525893	0.143498	0.113401	0.082795
median	0.77526	0.57866	0.55442	0.54576	0.52583	0.14339	0.11336	0.08288
mode	0.77526	0.57661	0.55299	0.54576	0.52603	0.1436	0.11336	0.08288
standard deviation	0.002651	0.004396	0.003628	0.003442	0.003396	0.002541	0.002456	0.000533
variance	7.03E-06	1.93E-05	1.32E-05	1.19E-05	1.15E-05	6.46E-06	6.03E-06	2.84E-07
skew	0.024263	0.158449	0.075877	0.130719	0.136675	0.078914	0.058089	-1.10838
kurtosis	0.2747	0.164023	0.023722	0.101223	0.112812	0.167814	0.254673	6.984059

LX Pressure Readings and Statistical Data

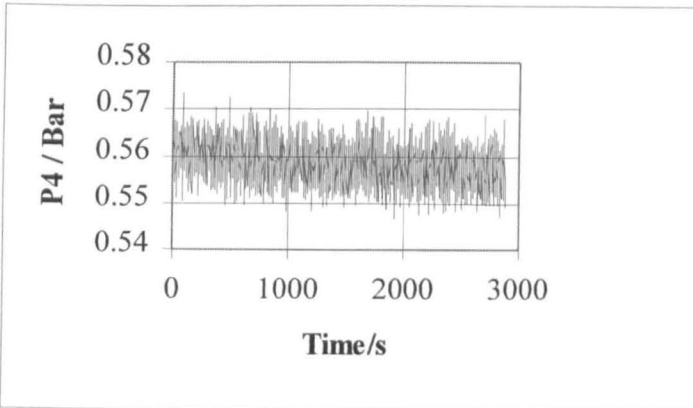
Standard Pipe Arrangement

Run: 4kgstd50

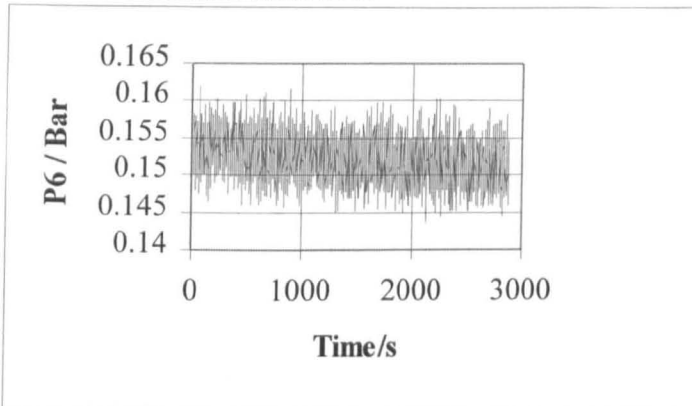
Volumetric Flow: 3.22 l/s

Mass Flow: 3.316 Kg/s

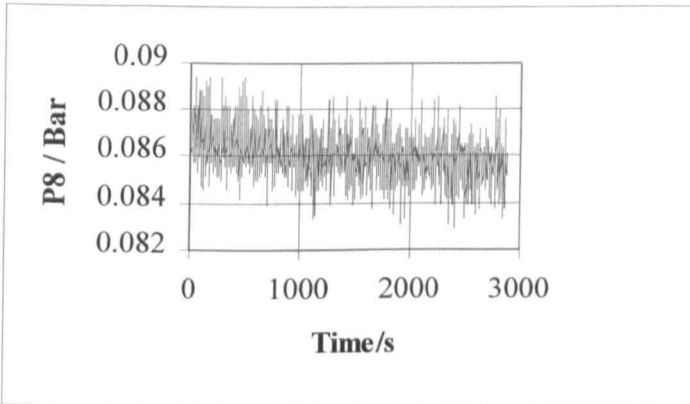
Number of Data Points:2877



LXI P4 variation with time



LXII P6 variation with time



LXIII P8 variation with time

	p1	p2	p3	p4	p5	p6	p7	p8
mean	0.846137	0.596179	0.56752	0.55834	0.537879	0.152232	0.121891	0.086071
median	0.84482	0.59605	0.56751	0.55844	0.5379	0.15219	0.12195	0.08615
mode	0.84277	0.59584	0.56792	0.55885	0.53831	0.15239	0.12236	0.08615
standard deviation	0.006363	0.005377	0.004101	0.003978	0.003858	0.002839	0.002814	0.000758
variance	4.05E-05	2.89E-05	1.68E-05	1.58E-05	1.49E-05	8.06E-06	7.92E-06	5.74E-07
skew	0.660032	0.153386	0.121088	0.079827	0.078245	0.095152	0.108648	0.196155
kurtosis	-0.06736	0.046382	-0.07474	-0.13376	-0.13284	-0.075	-0.11526	2.646911

LXIV Pressure Readings and Statistical Data

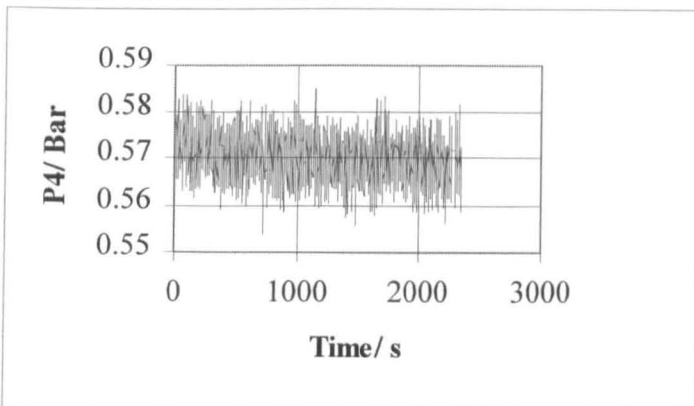
Standard Pipe Arrangement

Run: 4kgstd55

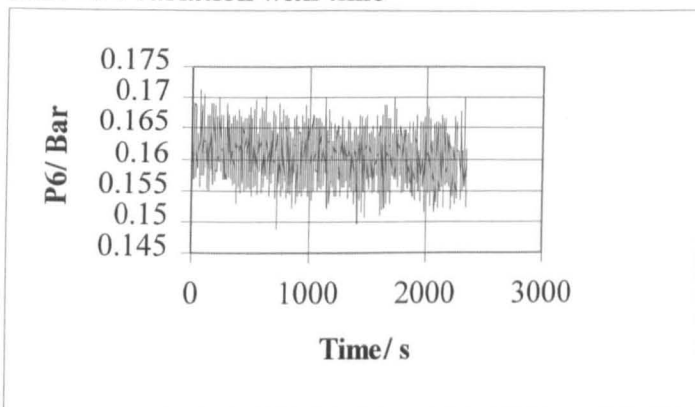
Volumetric Flow: 3.45 l/s

Mass Flow: 3.571 Kg/s

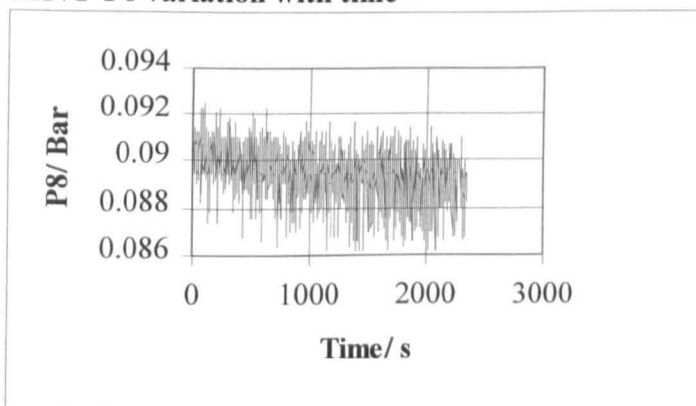
Number of Data Points:2344



LXV P4 variation with time



LXVI P6 variation with time



LXVII P8 variation with time

	p1	p2	p3	p4	p5	p6	p7	p8
mean	0.916508	0.613726	0.580433	0.570383	0.549349	0.160722	0.130328	0.089475
median	0.9154	0.61344	0.5804	0.57051	0.54936	0.16078	0.13034	0.08943
mode	0.91131	0.61283	0.58163	0.57174	0.55058	0.1614	0.13096	0.08943
standard deviation	0.00846	0.006289	0.004885	0.004552	0.004455	0.003329	0.003228	0.000912
variance	7.16E-05	3.95E-05	2.39E-05	2.07E-05	1.98E-05	1.11E-05	1.04E-05	8.31E-07
skew	0.487487	0.042085	0.016265	-0.01637	0.003148	-0.00959	-0.05582	-0.45607
kurtosis	-0.52658	-0.15673	-0.11925	0.00368	0.004481	0.018352	0.080486	1.494557

LXVIII Pressure Readings and Statistical Data

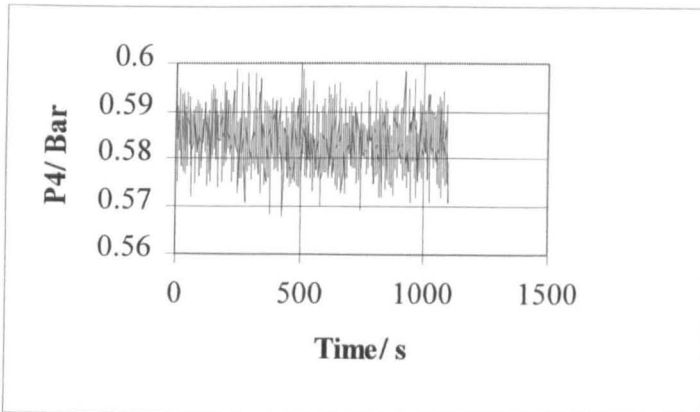
Standard Pipe Arrangement

Run: 4kgstd60

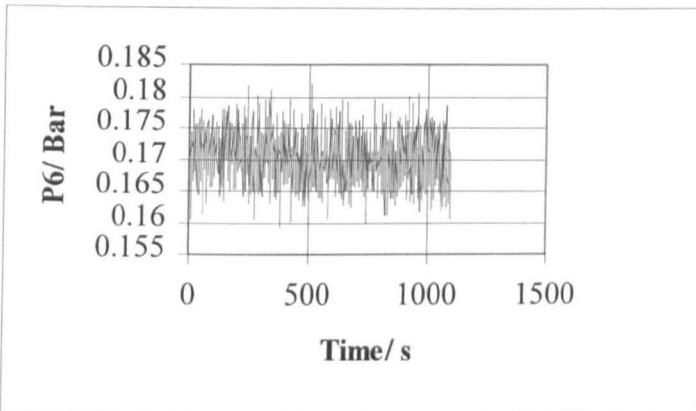
Volumetric Flow:3.751 l/s

Mass Flow: 3.903 Kg/s

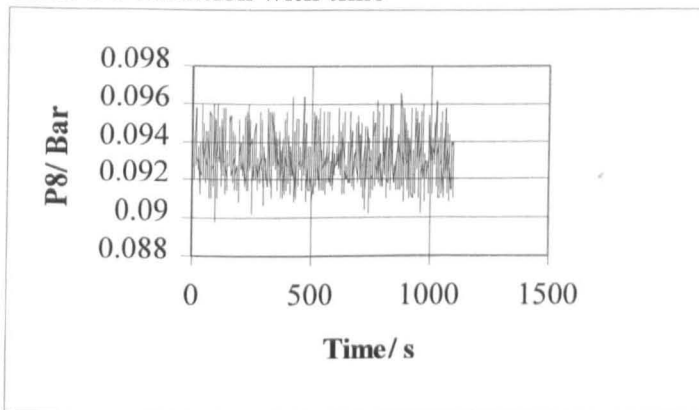
Number of Data Points:1097



LXIX P4 variation with time



LXX P6 variation with time



LXXI P8 variation with time

	p1	p2	p3	p4	p5	p6	p7	p8
mean	0.994931	0.63323	0.595094	0.584002	0.562435	0.170394	0.1396	0.092987
median	0.99519	0.63308	0.59493	0.58402	0.56245	0.17019	0.13955	0.0927
mode	0.99416	0.63308	0.59472	0.58218	0.56286	0.16978	0.13955	0.0927
standard deviation	0.00433	0.007185	0.005527	0.005235	0.00516	0.003852	0.003661	0.001108
variance	1.87E-05	5.16E-05	3.05E-05	2.74E-05	2.66E-05	1.48E-05	1.34E-05	1.23E-06
skew	0.006835	0.089917	0.039592	0.043701	0.038888	0.091598	0.050564	0.721255
kurtosis	0.19758	0.201336	0.04169	-0.07049	-0.11002	-0.10262	-0.14851	0.551093

LXXII Pressure Readings and Statistical Data

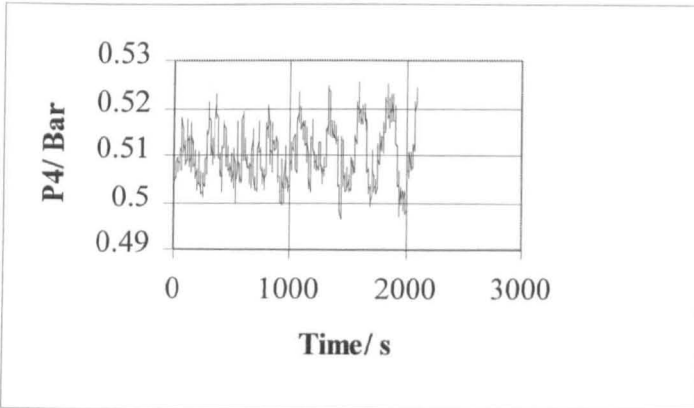
Standard Pipe Arrangement

Run: 6kgstd20

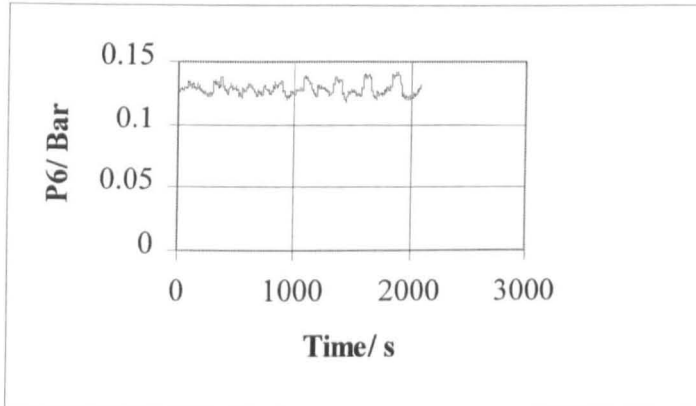
Volumetric Flow:0.827 l/s

Mass Flow: 0.849 Kg/s

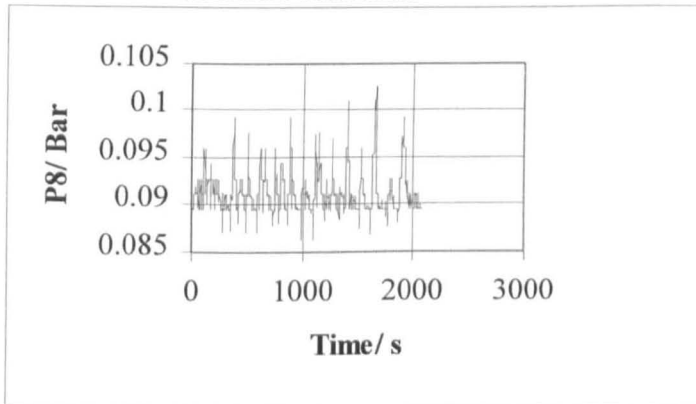
Number of Data Points:2088



LXXIII P4 variation with time



LXXIV P6 variation with time



LXXV P8 variation with time

	p1	p2	p3	p4	p5	p6	p7	p8
mean	0.505758	0.522798	0.514446	0.510244	0.494233	0.128372	0.099336	0.091164
median	0.50726	0.52301	0.51422	0.50965	0.49391	0.12784	0.09863	0.09086
mode	0.50726	0.52506	0.51105	0.51078	0.49105	0.12907	0.09515	0.08943
standard deviation	0.002554	0.003869	0.005805	0.005644	0.005434	0.00465	0.004726	0.002163
variance	6.52E-06	1.5E-05	3.37E-05	3.19E-05	2.95E-05	2.16E-05	2.23E-05	4.68E-06
skew	-1.28925	-0.28419	0.179568	0.300289	0.228943	0.623314	0.730939	1.547041
kurtosis	0.972482	-0.01471	-0.59871	-0.55465	-0.54135	-0.06463	0.137318	2.81444

LXXVI Pressure Readings and Statistical Data

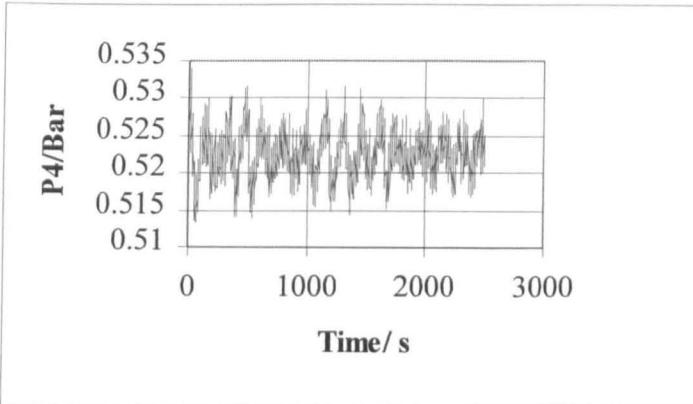
Standard Pipe Arrangement

Run: 6kgstd25

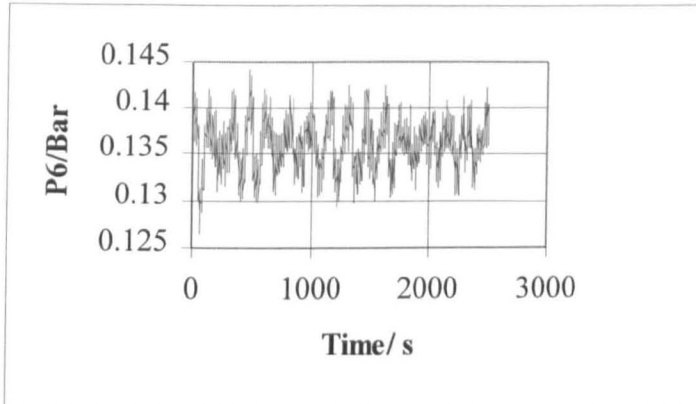
Volumetric Flow:1.244 l/s

Mass Flow: 1.293 Kg/s

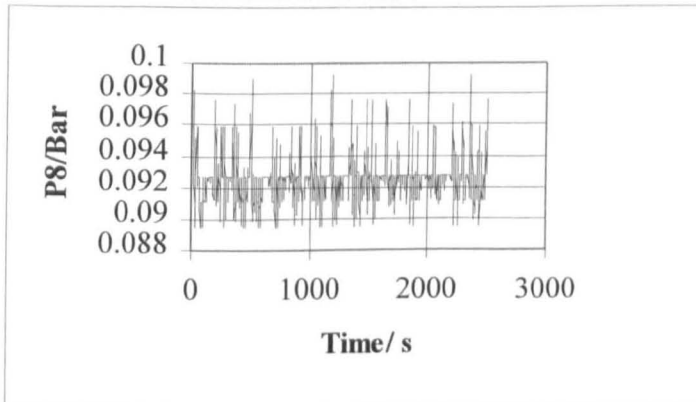
Number of Data Points:2496



LXXVII P4 variation with time



LXXIX P6 variation with time



LXXX P8 variation with time

	p1	p2	p3	p4	p5	p6	p7	p8
mean	0.545152	0.54113	0.527927	0.522614	0.505712	0.136188	0.107506	0.09256
median	0.5451	0.54122	0.52803	0.52264	0.50578	0.13623	0.10763	0.0927
mode	0.54817	0.53815	0.52823	0.52387	0.50414	0.13562	0.10825	0.0927
standard deviation	0.002659	0.002405	0.002954	0.003021	0.002935	0.002636	0.002686	0.001378
variance	7.07E-06	5.78E-06	8.73E-06	9.13E-06	8.61E-06	6.95E-06	7.22E-06	1.9E-06
skew	-0.13979	-0.11769	-0.11175	0.017909	-0.06887	-0.12789	-0.11085	1.20002
kurtosis	-0.77775	-0.08657	0.333729	0.10379	0.133817	-0.13996	-0.27742	2.743485

LXXXI Pressure Readings and Statistical Data

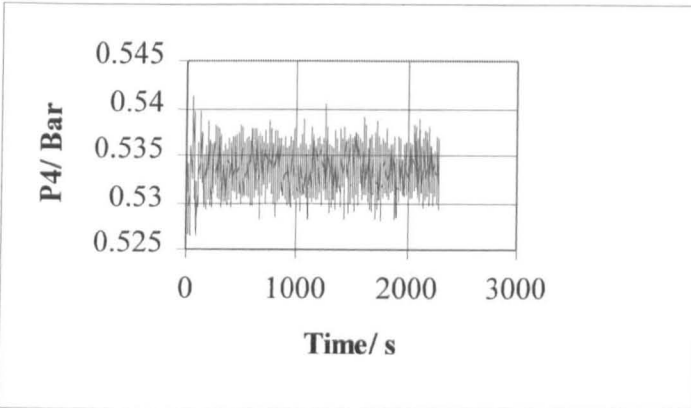
Standard Pipe Arrangement

Run: 6kgstd30

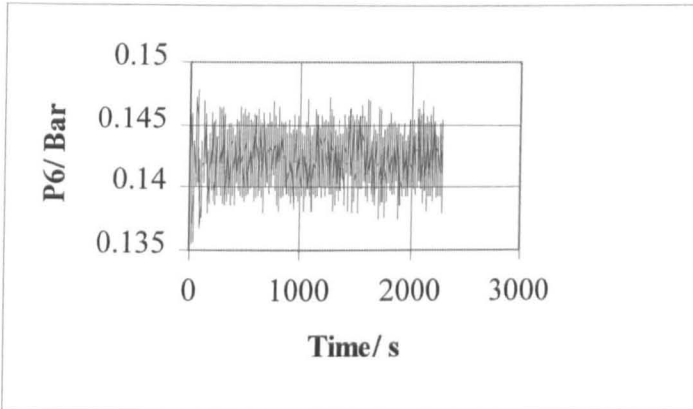
Volumetric Flow: 1.743 l/s

Mass Flow: 1.814 Kg/s

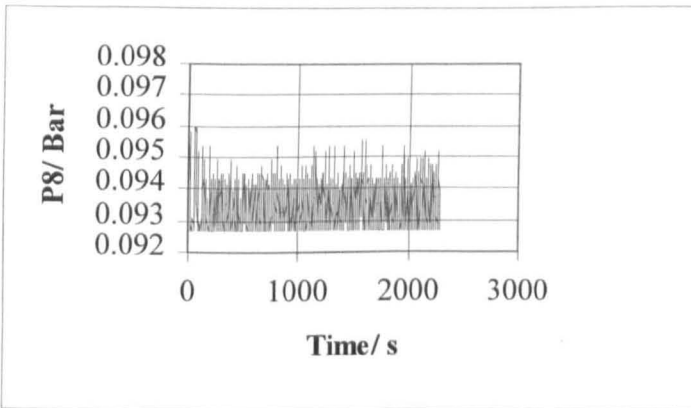
Number of Data Points:2284



LXXXII P4 variation with time



LXXXIII P6 variation with time



LXXXIV P8 variation with time

	p1	p2	p3	p4	p5	p6	p7	p8
mean	0.591303	0.556015	0.539905	0.533518	0.51571	0.142261	0.113265	0.093516
median	0.59113	0.55616	0.5399	0.53348	0.5158	0.14216	0.11336	0.09352
mode	0.59113	0.55718	0.54051	0.53369	0.51621	0.14339	0.11398	0.0927
standard deviation	0.001755	0.00203	0.002056	0.002036	0.002106	0.001879	0.001826	0.00063
variance	3.08E-06	4.12E-06	4.23E-06	4.15E-06	4.44E-06	3.53E-06	3.34E-06	3.97E-07
skew	0.742461	-0.01087	-0.10403	-0.02802	-0.04107	-0.00762	-0.0315	0.780332
kurtosis	0.303249	0.394673	0.402573	0.13154	0.043961	-0.03111	0.044634	1.113912

LXXXV Pressure Readings and Statistical Data

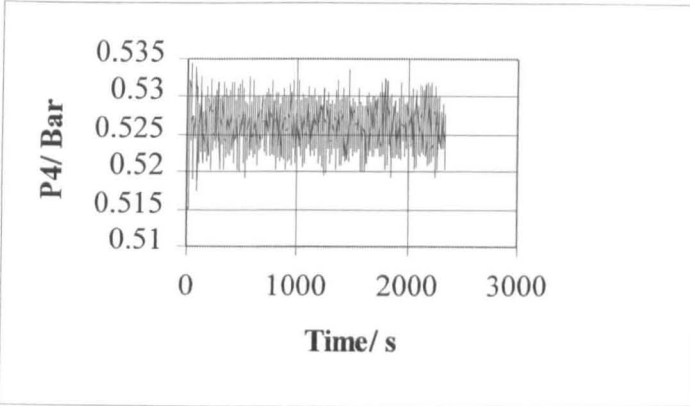
Standard Pipe Arrangement

Run: 6kgstd35

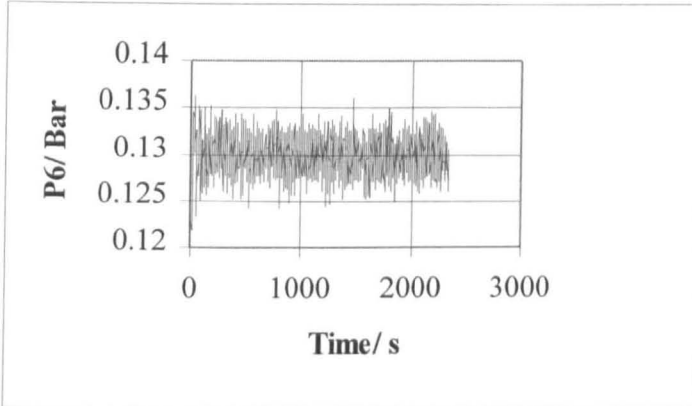
Volumetric Flow: 2.157 l/s

Mass Flow: 2.237 Kg/s

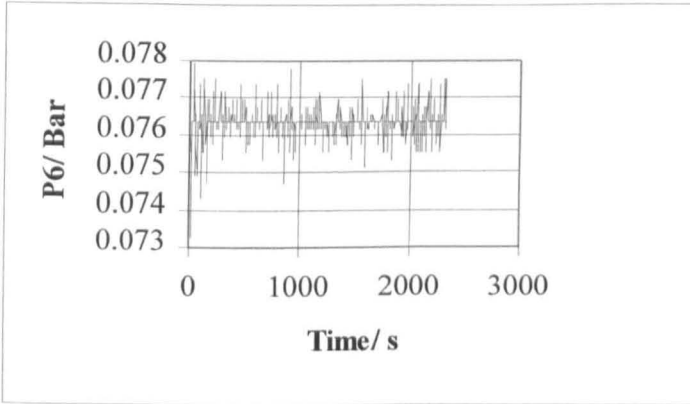
Number of Data Points:2336



LXXXVI P4 variation with time



LXXXVII P6 variation with time



LXXXVIII P8 variation with time

	p1	p2	p3	p4	p5	p6	p7	p8
mean	0.643472	0.55349	0.533512	0.52621	0.507417	0.129838	0.10007	0.076321
median	0.6433	0.5535	0.53355	0.52632	0.50742	0.12989	0.10006	0.07633
mode	0.6433	0.55391	0.53376	0.5253	0.50803	0.12989	0.09925	0.07633
standard deviation	0.002691	0.003012	0.00264	0.002509	0.002421	0.001893	0.001824	0.000257
variance	7.24E-06	9.07E-06	6.97E-06	6.3E-06	5.86E-06	3.58E-06	3.33E-06	6.6E-08
skew	0.169889	-0.03964	-0.09786	-0.14282	-0.11472	-0.00129	-0.04525	-1.40544
kurtosis	-0.28911	0.224788	0.455835	0.44882	0.565721	0.428912	0.640899	24.67838

LXXXIX Pressure Readings and Statistical Data

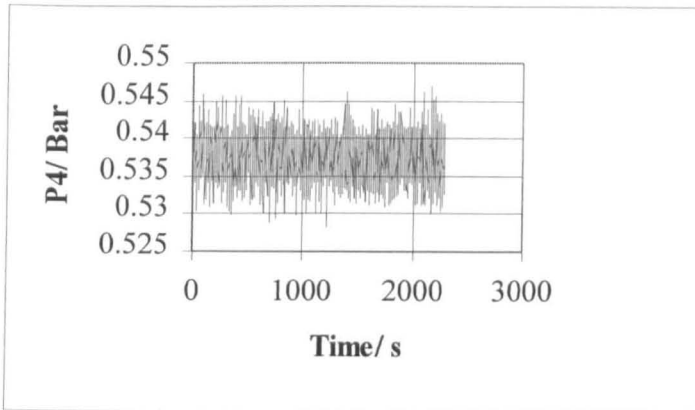
Standard Pipe Arrangement

Run: 6kgstd40

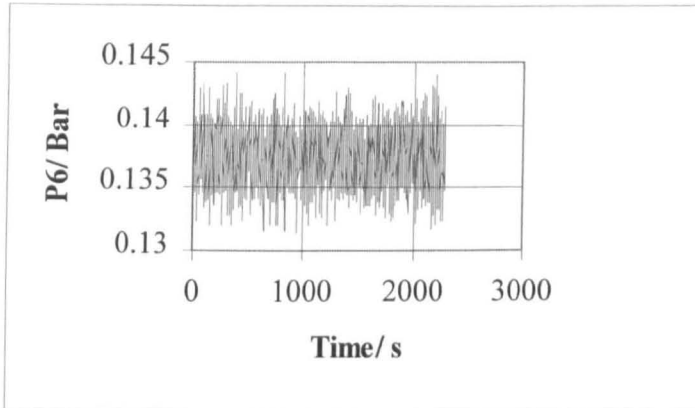
Volumetric Flow: 2.527 l/s

Mass Flow: 2.636 Kg/s

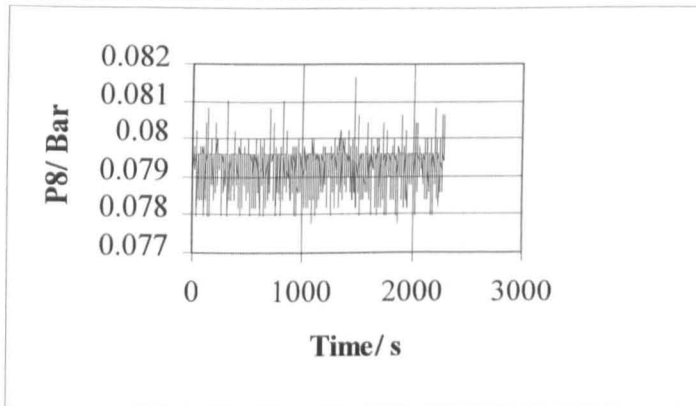
Number of Data Points:2290



XC P4 variation with time



XCI P6 variation with time



XCII P8 variation with time

	p1	p2	p3	p4	p5	p6	p7	p8
mean	0.703263	0.568229	0.545654	0.537285	0.517999	0.137357	0.107273	0.079397
median	0.70366	0.56823	0.54562	0.53737	0.51805	0.13725	0.10722	0.07961
mode	0.70366	0.56925	0.54583	0.53839	0.51744	0.13644	0.10702	0.07961
standard deviation	0.002329	0.003472	0.00292	0.002803	0.002777	0.002058	0.00203	0.000412
variance	5.42E-06	1.21E-05	8.95E-06	7.86E-06	7.71E-06	4.24E-06	4.12E-06	1.7E-07
skew	-0.04245	0.094863	0.062738	0.082126	0.050325	0.053354	0.033053	-1.21512
kurtosis	0.619569	0.031134	-0.01607	-0.02584	-0.01706	0.00541	-0.04459	2.943194

XCIII Pressure Readings and Statistical Data

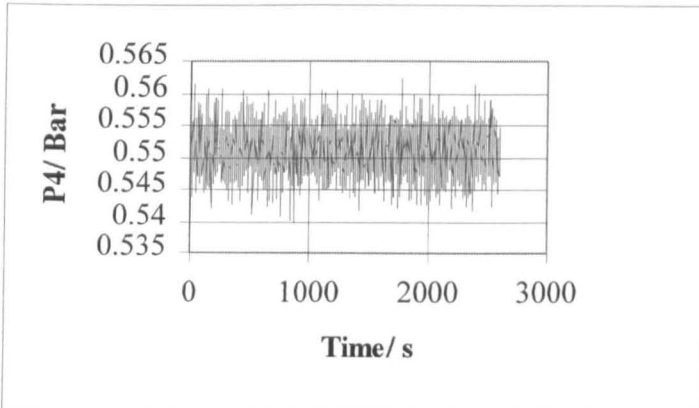
Standard Pipe Arrangement

Run: 6kgstd45

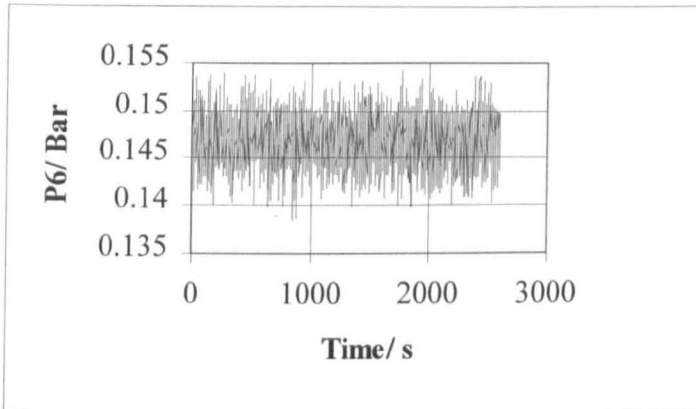
Volumetric Flow:2.91 Kg/s

Mass Flow: 3.03 l/s

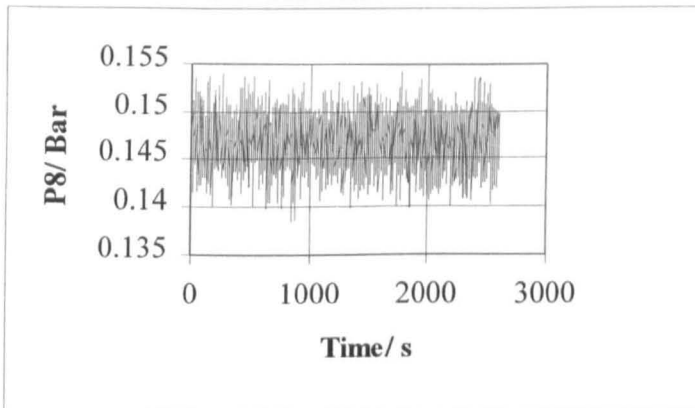
Number of Data Points:2597



XCIV P4 variation with time



XCIV P6 variation with time



XCVI P8 variation with time

	p1	p2	p3	p4	p5	p6	p7	p8
mean	0.777177	0.586806	0.56043	0.551073	0.531213	0.146872	0.116475	0.083477
median	0.77731	0.58684	0.56056	0.55108	0.53115	0.14687	0.11643	0.08329
mode	0.77731	0.58746	0.56076	0.55128	0.53053	0.14769	0.11745	0.08288
standard deviation	0.002726	0.004098	0.003331	0.003264	0.003219	0.002431	0.00235	0.000635
variance	7.43E-06	1.68E-05	1.11E-05	1.07E-05	1.04E-05	5.91E-06	5.52E-06	4.03E-07
skew	0.214826	-0.03221	-0.03319	0.00763	-0.01186	-0.07108	0.001794	0.807902
kurtosis	0.146168	0.045322	0.167525	0.108562	0.058263	-0.03555	-0.0106	-0.0693

XCVII Pressure Readings and Statistical Data

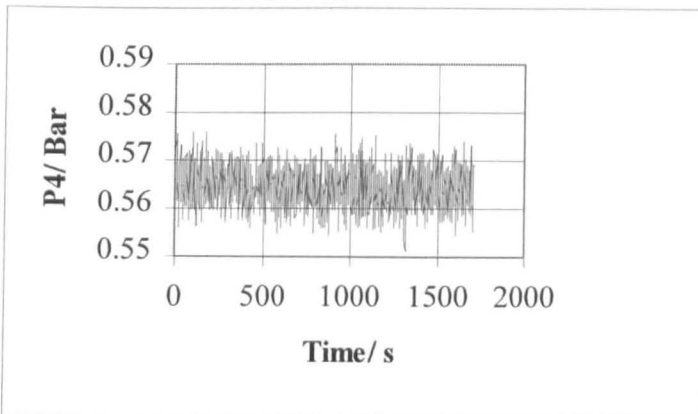
Standard Pipe Arrangement

Run: 6kgstd50

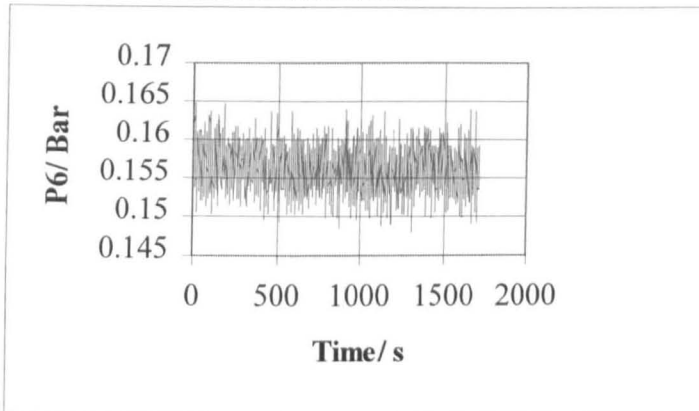
Volumetric Flow:3.207 l/s

Mass Flow: 3.342 Kg/s

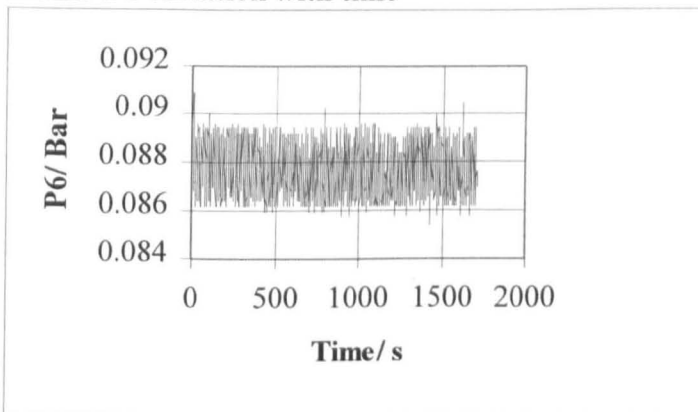
Number of Data Points:2597



XCVIII P4 variation with time



XCIX P6 variation with time



C P8 variation with time

	p1	p2	p3	p4	p5	p6	p7	p8
mean	0.854202	0.605234	0.574446	0.564527	0.544021	0.156176	0.125683	0.087671
median	0.85402	0.60505	0.57447	0.56458	0.54404	0.15628	0.12564	0.08759
mode	0.85402	0.60362	0.57406	0.56397	0.54342	0.15628	0.12461	0.08615
standard deviation	0.00467	0.005058	0.003961	0.003771	0.003704	0.002751	0.002755	0.001053
variance	2.18E-05	2.56E-05	1.57E-05	1.42E-05	1.37E-05	7.57E-06	7.59E-06	1.11E-06
skew	0.087238	0.163122	0.167729	0.09108	0.106443	0.071869	0.037809	0.141234
kurtosis	-0.0249	0.064126	0.145508	0.10192	0.080644	0.030078	-0.05036	-1.06349

CI Pressure Readings and Statistical Data

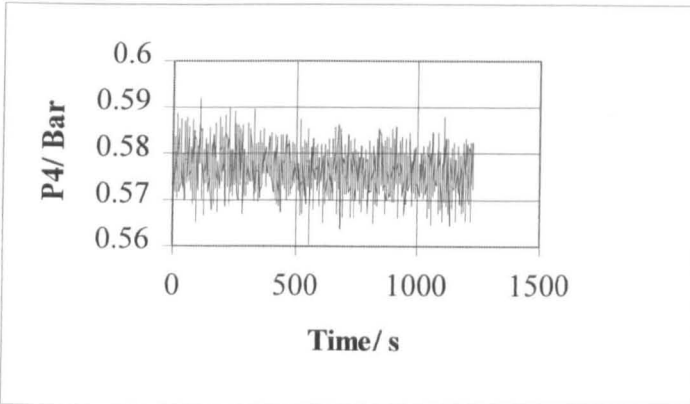
Standard Pipe Arrangement

Run: 6kgstd55

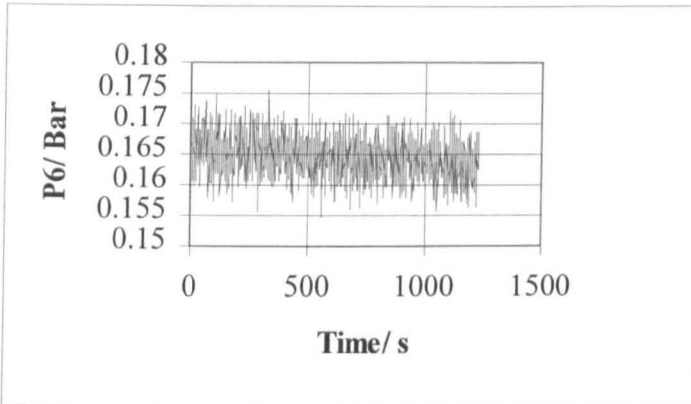
Volumetric Flow: 3.506 l/s

Mass Flow: 3.634 Kg/s

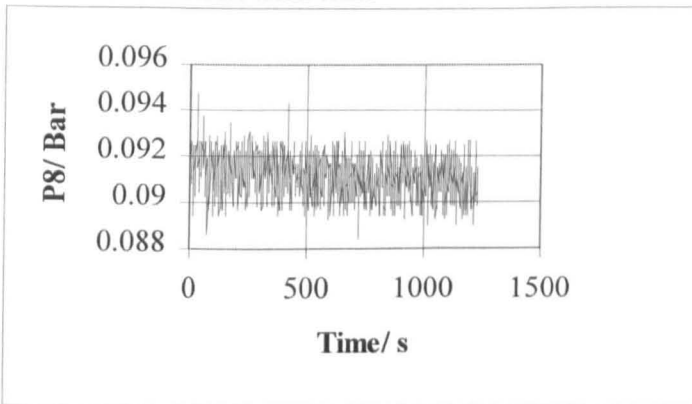
Number of Data Points:1229



CII P4 variation with time



CIII P6 variation with time



CIV P8 variation with time

	p1	p2	p3	p4	p5	p6	p7	p8
mean	0.924285	0.622561	0.587432	0.576505	0.555479	0.164669	0.134	0.091181
median	0.92358	0.62244	0.58756	0.57645	0.55549	0.16467	0.13403	0.09106
mode	0.91949	0.62224	0.58797	0.57645	0.5557	0.16528	0.1328	0.09106
standard deviation	0.00718	0.006188	0.004818	0.004493	0.004416	0.003286	0.00315	0.000884
variance	5.16E-05	3.83E-05	2.32E-05	2.02E-05	1.95E-05	1.08E-05	9.92E-06	7.81E-07
skew	0.304459	0.031933	0.018202	0.054476	0.05156	0.024169	-0.00345	-0.01066
kurtosis	-0.52345	-0.09934	-0.02377	0.021175	-0.0069	-0.05557	-0.02802	-0.17204

CV Pressure Readings and Statistical Data

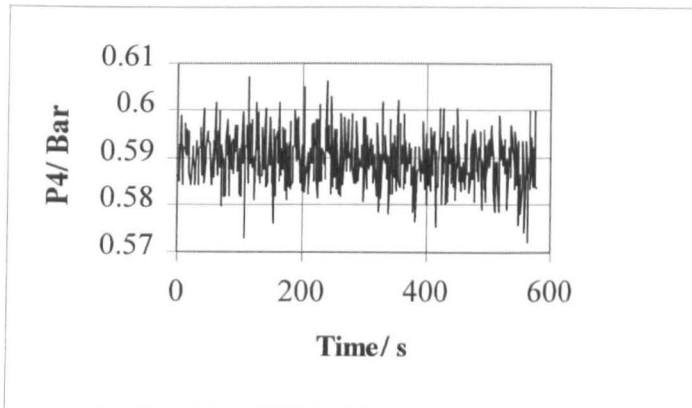
Standard Pipe Arrangement

Run: 6kgstd60

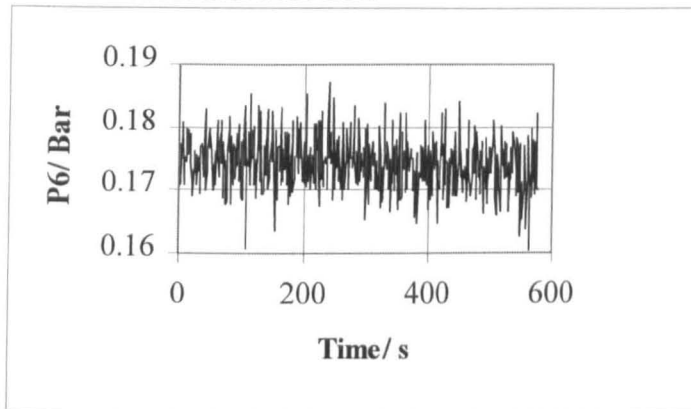
Volumetric Flow: 3.8 l/s

Mass Flow: 3.395 Kg/s

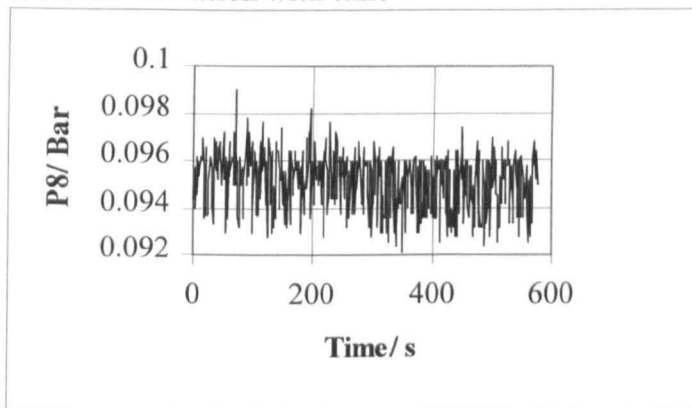
Number of Data Points:577



CVI P4 variation with time



CVII P6 variation with time



CVIII P8 variation with time

	p1	p2	p3	p4	p5	p6	p7	p8
mean	1.000138	0.641202	0.601612	0.589912	0.568353	0.174284	0.143155	0.095118
median	0.99928	0.64085	0.60147	0.58974	0.56818	0.17408	0.14303	0.09536
mode	0.99928	0.63983	0.60086	0.58913	0.57043	0.17531	0.14364	0.09597
standard deviation	0.00517	0.007215	0.005656	0.005403	0.005338	0.004094	0.003867	0.001196
variance	2.67E-05	5.21E-05	3.2E-05	2.92E-05	2.85E-05	1.68E-05	1.5E-05	1.43E-06
skew	0.168098	0.075348	0.012688	0.014271	0.00382	0.045348	0.028812	-0.37138
kurtosis	0.18045	-0.05655	0.179679	0.207639	0.180909	0.221554	0.309734	-0.53559

CIX Pressure Readings and Statistical Data

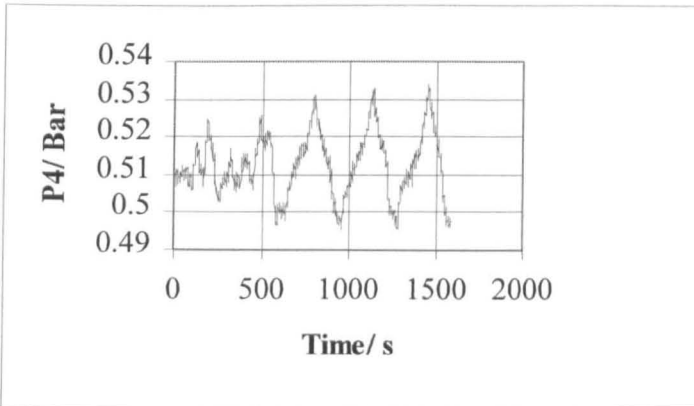
Standard Pipe Arrangement

Run: 8kgstd20

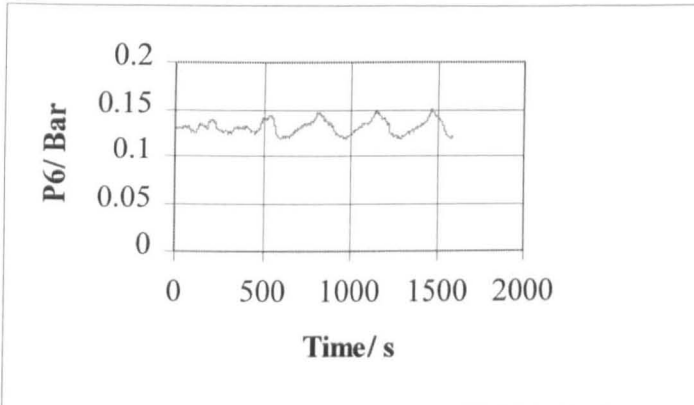
Volumetric Flow: 0.739 l/s

Mass Flow: 0.757 Kg/s

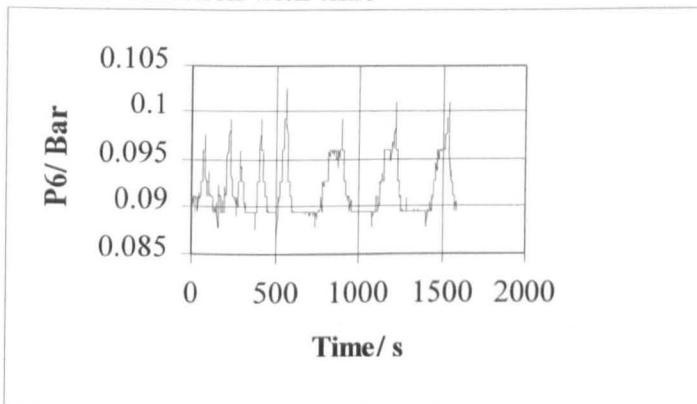
Number of Data Points:1588



CX P4 variation with time



CXI P6 variation with time



CXII P8 variation with time

	p1	p2	p3	p4	p5	p6	p7	p8
mean	0.508747	0.525832	0.517331	0.512466	0.496027	0.130789	0.102837	0.091742
median	0.50726	0.52588	0.51719	0.512	0.49555	0.13009	0.10231	0.09086
mode	0.50726	0.53161	0.51432	0.51078	0.49432	0.1258	0.09843	0.08943
standard deviation	0.0033	0.005275	0.008492	0.008319	0.008178	0.007453	0.007497	0.002872
variance	1.09E-05	2.78E-05	7.21E-05	6.92E-05	6.69E-05	5.55E-05	5.62E-05	8.25E-06
skew	0.212218	-0.27759	0.007826	0.164488	0.122886	0.399358	0.429065	1.033087
kurtosis	0.785455	-0.59386	-0.37383	-0.46027	-0.4716	-0.53761	-0.52243	0.038232

CXIII Pressure Readings and Statistical Data

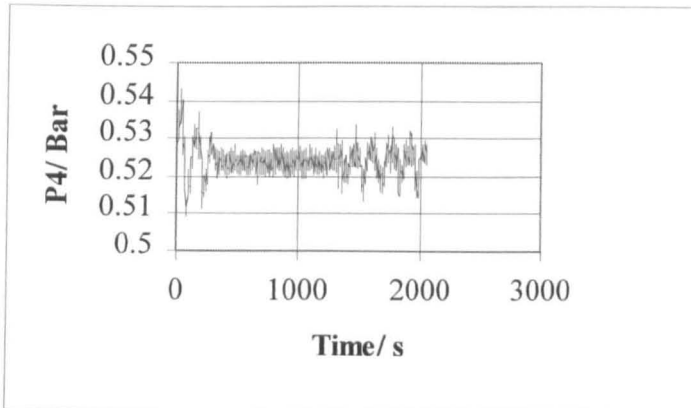
Standard Pipe Arrangement

Run: 8kgstd25

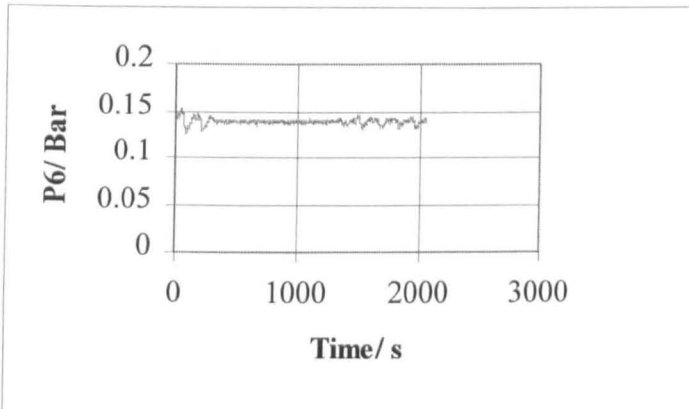
Volumetric Flow: 1.206 l/s

Mass Flow: 1.252 Kg/s

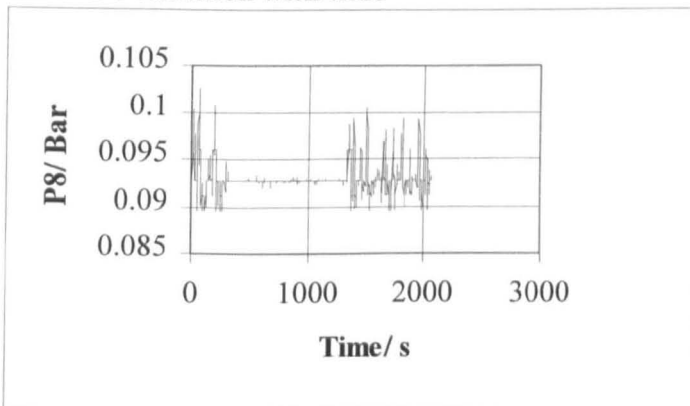
Number of Data Points:2057



CXIV P4 variation with time



CXV P6 variation with time



CXVI P8 variation with time

	p1	p2	p3	p4	p5	p6	p7	p8
mean	0.549573	0.544057	0.529911	0.524057	0.507129	0.138305	0.110315	0.092908
median	0.54919	0.54409	0.52987	0.52407	0.50721	0.13828	0.1105	0.0927
mode	0.54817	0.5447	0.52987	0.52387	0.50742	0.13848	0.11152	0.0927
standard deviation	0.002634	0.002862	0.00374	0.003714	0.003623	0.003271	0.003305	0.001547
variance	6.94E-06	8.19E-06	1.4E-05	1.38E-05	1.31E-05	1.07E-05	1.09E-05	2.39E-06
skew	0.103264	0.617145	0.58029	0.31647	0.248409	-0.12981	-0.14218	1.965756
kurtosis	1.161168	3.357042	3.892871	2.822107	2.796986	1.944199	1.959537	6.23026

CXVII Pressure Readings and Statistical Data

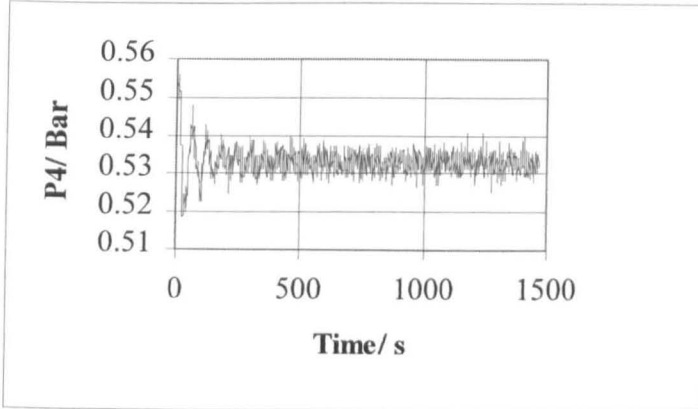
Standard Pipe Arrangement

Run: 8kgstd30

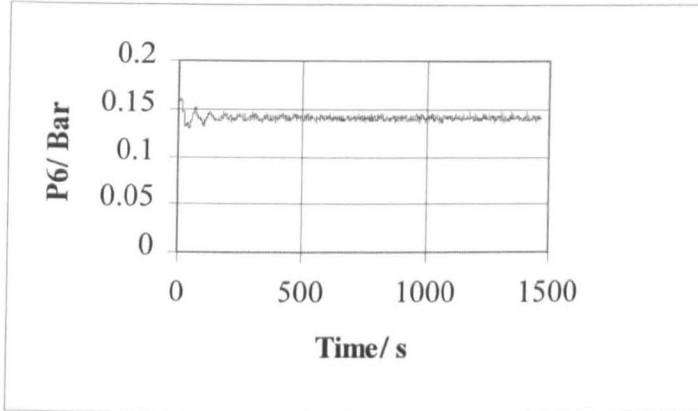
Volumetric Flow: 1.669 l/s

Mass Flow: 1.74 Kg/s

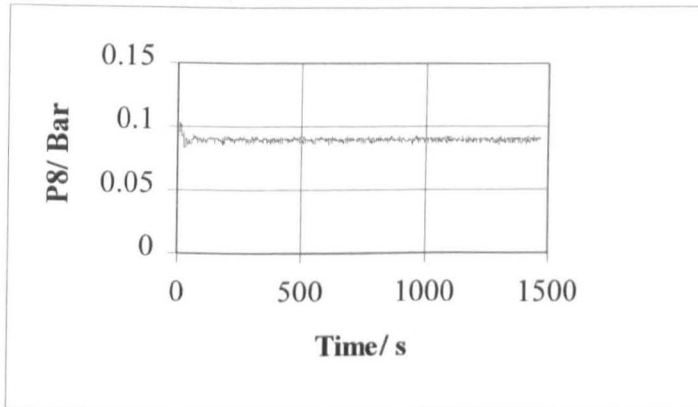
Number of Data Points:1468



CXVIII P4 variation with time



CXIX P6 variation with time



CXX P8 variation with time

	p1	p2	p3	p4	p5	p6	p7	p8
mean	0.594008	0.558733	0.540216	0.533134	0.515214	0.140848	0.112211	0.089493
median	0.5942	0.55861	0.5401	0.53308	0.51519	0.14073	0.11213	0.08943
mode	0.5942	0.55779	0.5401	0.53185	0.51499	0.14032	0.11213	0.08943
standard deviation	0.002947	0.003163	0.003612	0.003565	0.003616	0.003144	0.003163	0.001645
variance	8.69E-06	1E-05	1.3E-05	1.27E-05	1.31E-05	9.88E-06	1E-05	2.7E-06
skew	0.577269	0.165369	1.04046	1.231864	1.275881	1.548345	1.650501	1.464665
kurtosis	0.762776	6.951634	8.710702	8.800725	8.803548	9.44248	10.27465	11.44972

CXXI Pressure Readings and Statistical Data

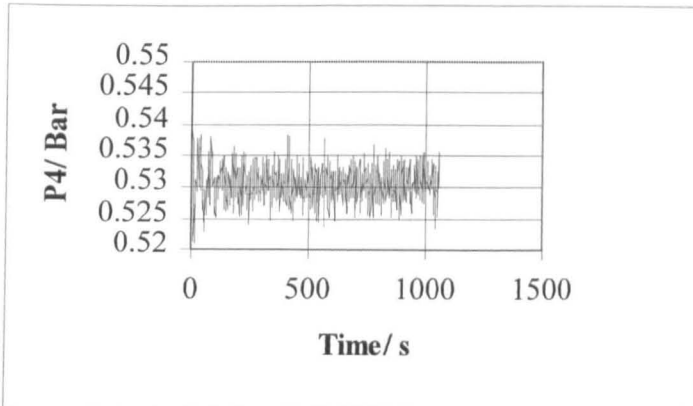
Standard Pipe Arrangement

Run: 8kgstd35

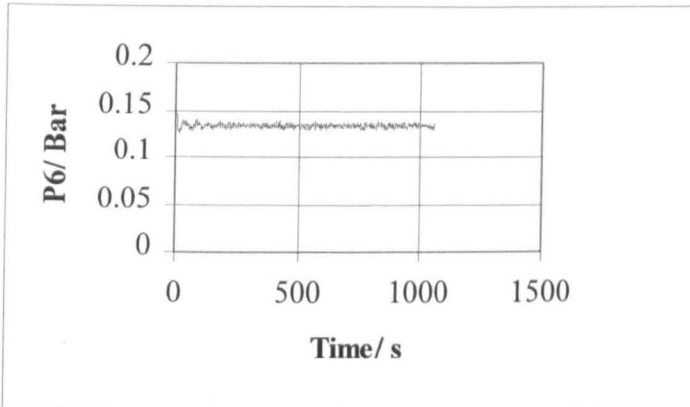
Volumetric Flow: 2.14 l/s

Mass Flow: 2.236 Kg/s

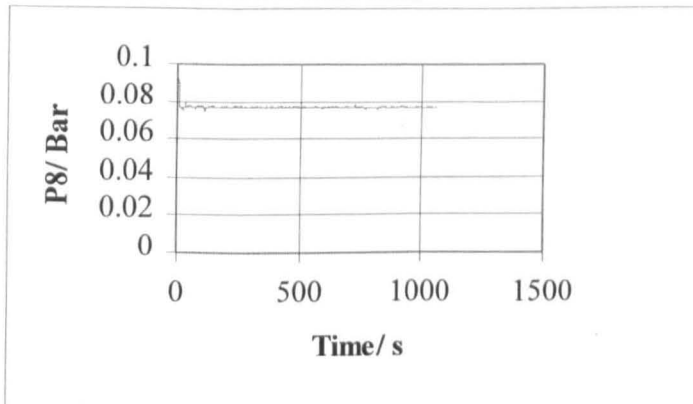
Number of Data Points:1057



CXXII P4 variation with time



CXXIII P6 variation with time



CXXIV P8 variation with time

	p1	p2	p3	p4	p5	p6	p7	p8
mean	0.648237	0.560647	0.538648	0.530641	0.511755	0.133268	0.103805	0.076668
median	0.64842	0.56066	0.53867	0.53062	0.51171	0.13316	0.10375	0.07633
mode	0.64944	0.55882	0.53867	0.53144	0.51089	0.13378	0.10334	0.07633
standard deviation	0.002932	0.002967	0.002811	0.00262	0.002606	0.002222	0.002194	0.001261
variance	8.6E-06	8.81E-06	7.9E-06	6.86E-06	6.79E-06	4.94E-06	4.81E-06	1.59E-06
skew	-0.3941	-0.10988	0.05684	0.16135	0.283702	1.114906	1.285315	10.2764
kurtosis	-0.08972	0.111637	1.035626	1.714405	1.842665	7.936661	9.519251	125.4925

CXXV Pressure Readings and Statistical Data

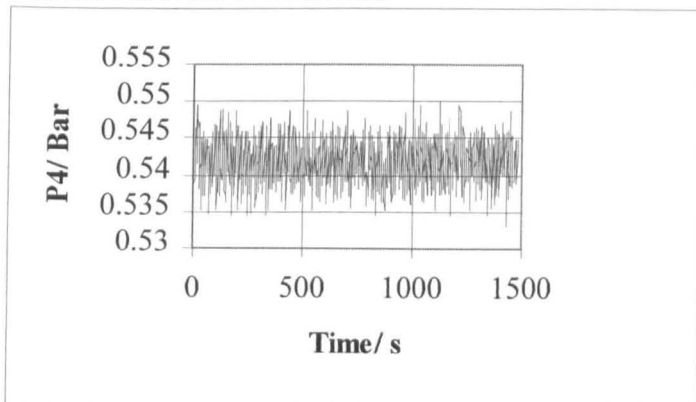
Standard Pipe Arrangement

Run: 8kgstd40

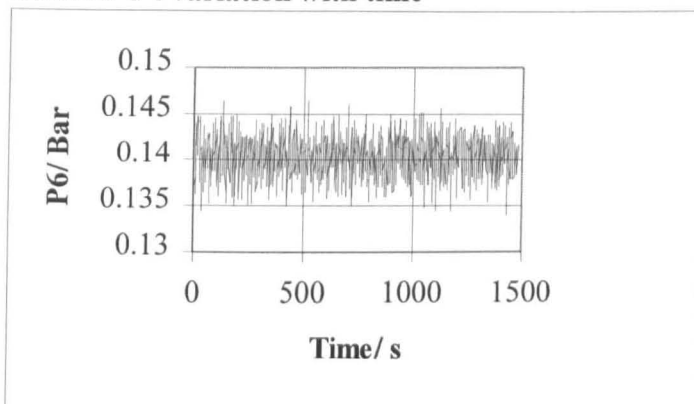
Volumetric Flow: 2.485 l/s

Mass Flow: 2.593 Kg/s

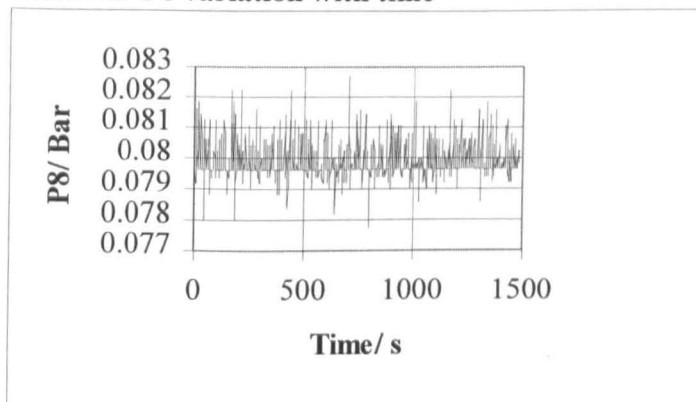
Number of Data Points:1481



CXXVI P4 variation with time



CXXVII P6 variation with time



CXXVIII P8 variation with time

	p1	p2	p3	p4	p5	p6	p7	p8
mean	0.706195	0.575073	0.550663	0.541756	0.522331	0.140398	0.110605	0.079819
median	0.7057	0.57498	0.55074	0.54187	0.52235	0.14053	0.1107	0.07961
mode	0.70672	0.57457	0.55135	0.54228	0.52255	0.13971	0.11173	0.07961
standard deviation	0.002502	0.003408	0.00296	0.002769	0.002735	0.002056	0.002033	0.000492
variance	6.26E-06	1.16E-05	8.76E-06	7.67E-06	7.48E-06	4.23E-06	4.13E-06	2.42E-07
skew	0.056737	0.008481	-0.01114	-0.02742	-0.01196	-0.1136	-0.14887	1.793683
kurtosis	-0.00812	-0.135	-0.1966	-0.2031	-0.14417	-0.10792	-0.11288	5.472336

CXXIX Pressure Readings and Statistical Data

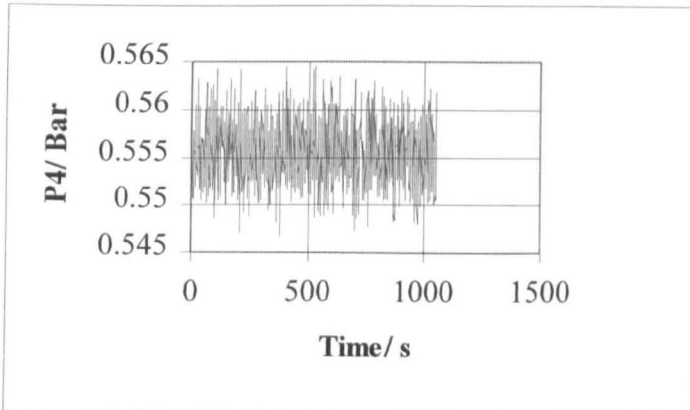
Standard Pipe Arrangement

Run: 8kgstd45

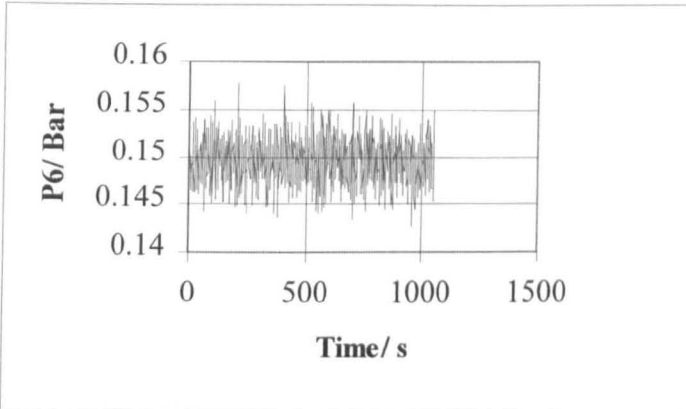
Volumetric Flow: 2.874 l/s

Mass Flow: 2.996 Kg/s

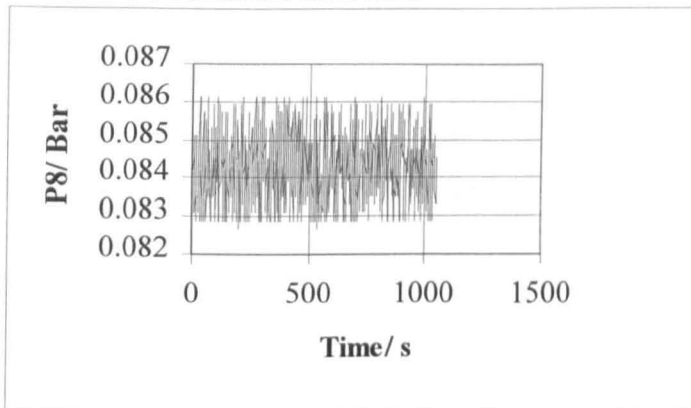
Number of Data Points:1047



CXXX P4 variation with time



CXXXI P6 variation with time



CXXXII P8 variation with time

	p1	p2	p3	p4	p5	p6	p7	p8
Mean	0.779689	0.593371	0.565321	0.555691	0.535659	0.149758	0.119479	0.084312
median	0.77935	0.59339	0.56526	0.55558	0.53565	0.14973	0.1195	0.08431
mode	0.77935	0.59421	0.56608	0.5566	0.53422	0.14871	0.1195	0.08452
Standard deviation	0.002992	0.003959	0.003216	0.00317	0.003121	0.002316	0.002313	0.000838
variance	8.95E-06	1.57E-05	1.03E-05	1.01E-05	9.74E-06	5.36E-06	5.35E-06	7.02E-07
skew	0.081642	0.075672	0.10156	0.043674	0.022118	-0.01534	0.016898	0.121401
kurtosis	-0.34347	-0.20645	-0.20133	-0.23666	-0.16031	-0.04971	-0.09225	-0.59726

CXXXIII Pressure Readings and Statistical Data

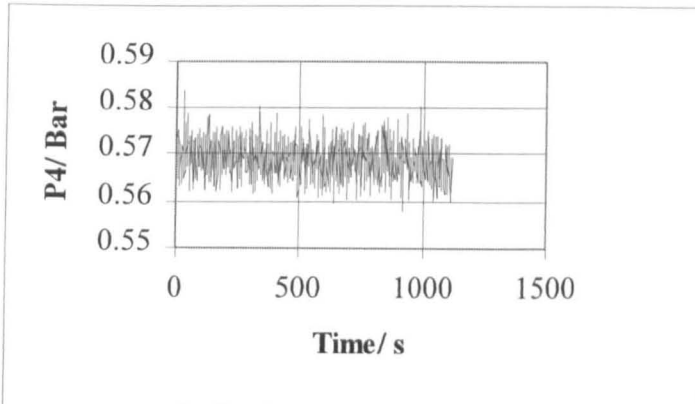
Standard Pipe Arrangement

Run: 8kgstd50

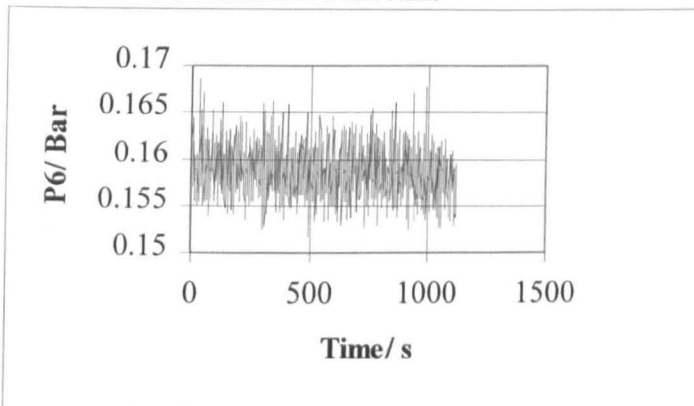
Volumetric Flow: 3.254 l/s

Mass Flow: 3.419 Kg/s

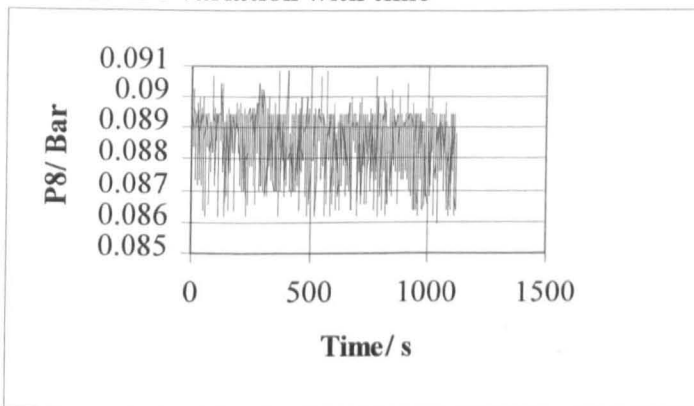
Number of Data Points:1118



CXXXIV P4 variation with time



CXXXV P6 variation with time



CXXXVI P8 variation with time

	p1	p2	p3	p4	p5	p6	p7	p8
mean	0.85771	0.611766	0.579386	0.568986	0.548242	0.158816	0.128411	0.088561
median	0.85812	0.6118	0.57938	0.56888	0.54813	0.15874	0.1283	0.08881
mode	0.85812	0.61426	0.57836	0.56847	0.54833	0.15894	0.1283	0.08943
standard deviation	0.003904	0.004963	0.003883	0.003585	0.003507	0.00266	0.002623	0.000967
variance	1.52E-05	2.46E-05	1.51E-05	1.29E-05	1.23E-05	7.08E-06	6.88E-06	9.35E-07
skew	0.092114	0.124626	0.134522	0.110239	0.129865	0.144989	0.079445	-0.71231
kurtosis	-0.28932	0.128876	0.040109	0.066877	0.070202	0.02755	-0.04204	-0.24878

CXXXVII Pressure Readings and Statistical Data

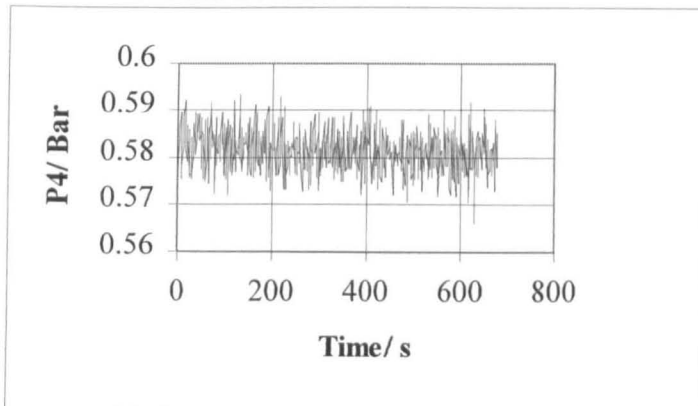
Standard Pipe Arrangement

Run: 8kgstd55

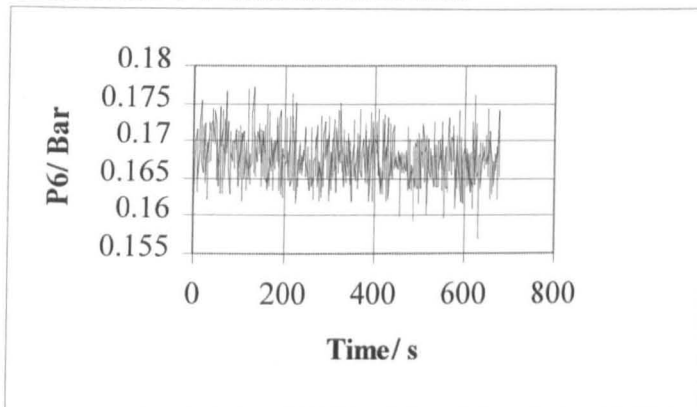
Volumetric Flow: 3.514 l/s

Mass Flow: 3.648 Kg/s

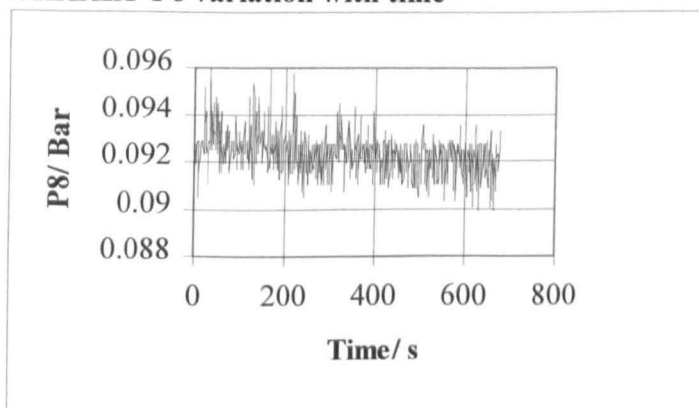
Number of Data Points:677



CXXXVIII P4 variation with time



CXXXIX P6 variation with time



CXL P8 variation with time

	p1	p2	p3	p4	p5	p6	p7	p8
mean	0.928975	0.629209	0.592894	0.581576	0.560365	0.167752	0.136993	0.0923
median	0.92819	0.62899	0.59268	0.58146	0.5602	0.16753	0.13689	0.0925
mode	0.92665	0.62796	0.59084	0.5834	0.5602	0.16753	0.13607	0.0927
standard deviation	0.006341	0.005752	0.004509	0.004314	0.00424	0.003134	0.00299	0.000861
variance	4.02E-05	3.31E-05	2.03E-05	1.86E-05	1.8E-05	9.82E-06	8.94E-06	7.42E-07
skew	0.156172	0.064413	0.040133	0.091877	0.08985	0.162261	0.15111	0.38395
kurtosis	-0.71325	-0.06923	-0.13384	-0.24247	-0.22865	-0.08738	-0.16084	1.628725

CXLI Pressure Readings and Statistical Data

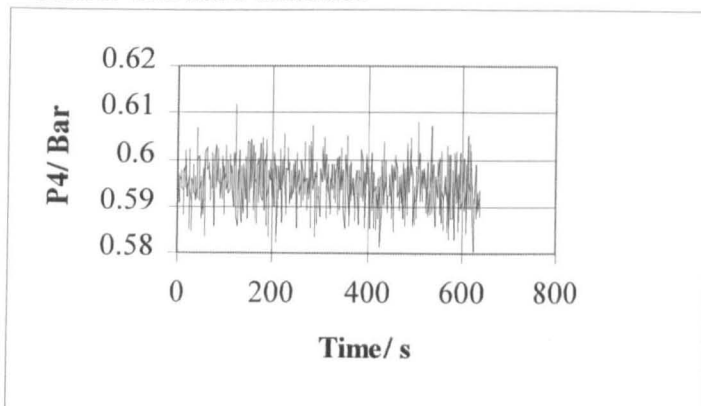
Standard Pipe Arrangement

Run: 8kgstd60

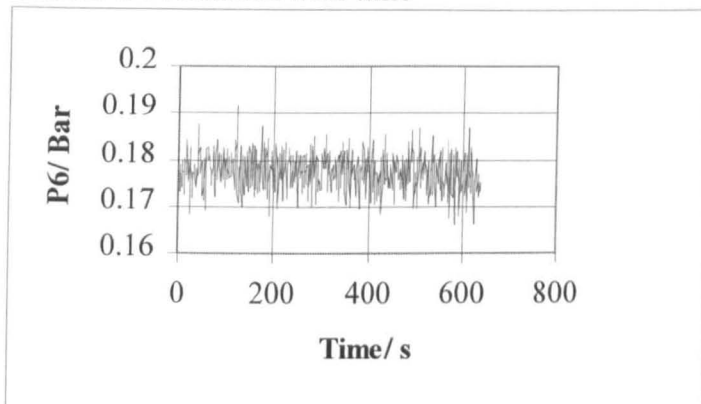
Volumetric Flow: 3.802 l/s

Mass Flow: 3.975 Kg/s

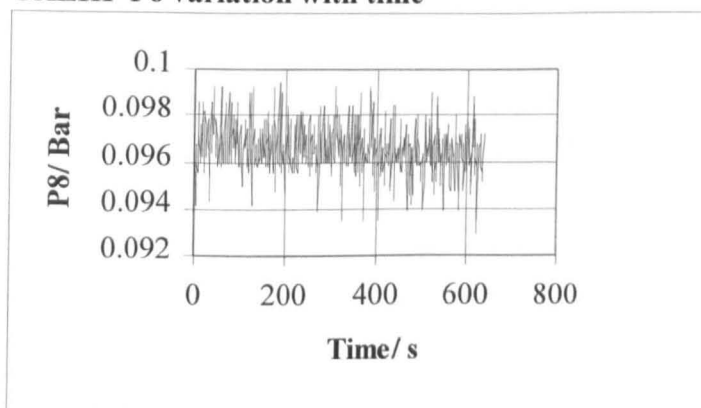
Number of Data Points:639



CXLII P4 variation with time



CXLIII P6 variation with time



CXLIV P8 variation with time

	p1	p2	p3	p4	p5	p6	p7	p8
mean	1.003011	0.647157	0.606732	0.594759	0.572998	0.177371	0.145997	0.096574
median	1.00337	0.64699	0.60659	0.59465	0.57288	0.17735	0.1461	0.09638
mode	1.00439	0.65006	0.60598	0.59527	0.57002	0.17797	0.14712	0.09597
standard deviation	0.005549	0.006527	0.005147	0.004886	0.004815	0.003708	0.003471	0.001017
variance	3.08E-05	4.26E-05	2.65E-05	2.39E-05	2.32E-05	1.37E-05	1.2E-05	1.03E-06
skew	0.066719	0.032293	0.00619	-0.06402	-0.08116	-0.0502	-0.02326	0.176236
kurtosis	-0.34652	-0.19856	-0.14354	-0.11439	-0.08072	0.157786	0.288107	0.578791

CXLV Pressure Readings and Statistical Data

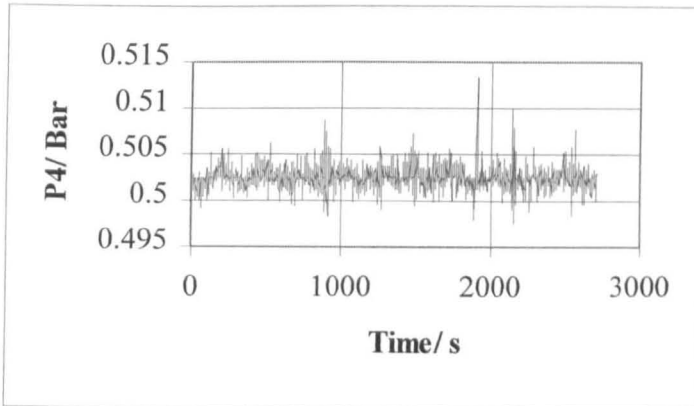
Long Swirly-flo Pipe Arrangement (pos 1)

Run: 2kglsf20

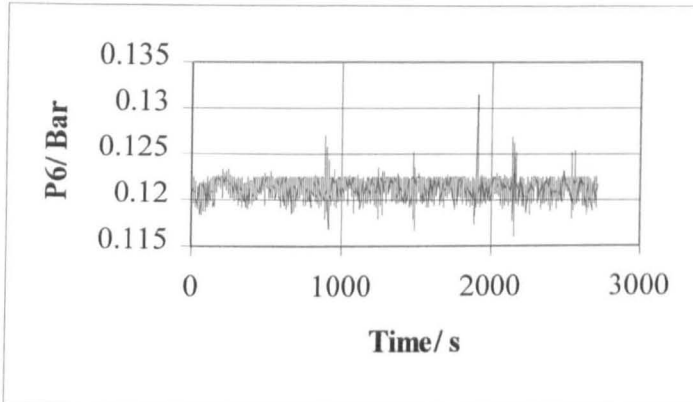
Volumetric Flow: 0.841 l/s

Mass Flow: 0.867 Kg/s

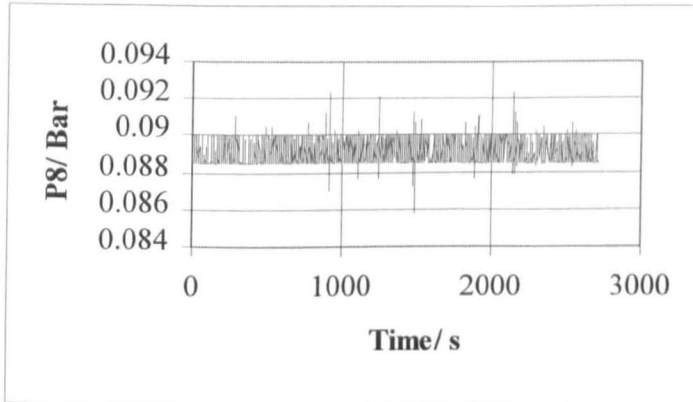
Number of Data Points:2713



CXLVI P4 variation with time



CXLVII P6 variation with time



CXLVIII P8 variation with time

	p1	p2	p3	p4	p5	p6	p7	p8
mean	0.496015	0.507198	0.505408	0.502541	0.48343	0.121359	0.095765	0.089146
median	0.496	0.50706	0.50512	0.50259	0.48348	0.1215	0.0957	0.08904
mode	0.49703	0.50706	0.5045	0.50259	0.4845	0.12252	0.09488	0.08843
standard deviation	0.001927	0.001279	0.00131	0.001017	0.001133	0.001059	0.000929	0.000676
variance	3.71E-06	1.64E-06	1.72E-06	1.03E-06	1.28E-06	1.12E-06	8.62E-07	4.57E-07
skew	-0.47803	-0.08615	0.484284	0.715076	0.397243	-0.02657	1.200751	0.325788
kurtosis	0.350777	1.338766	0.975695	8.618137	5.997436	4.241834	8.167287	-0.64242

CXLIX Pressure Readings and Statistical Data

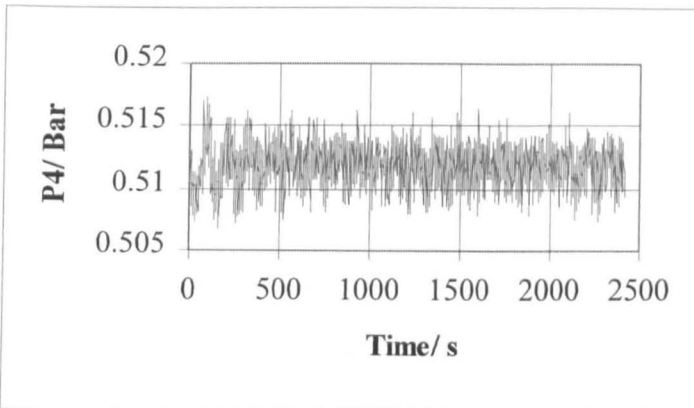
Long Swirly-flo Pipe Arrangement (pos 1)

Run: 2kglsf25

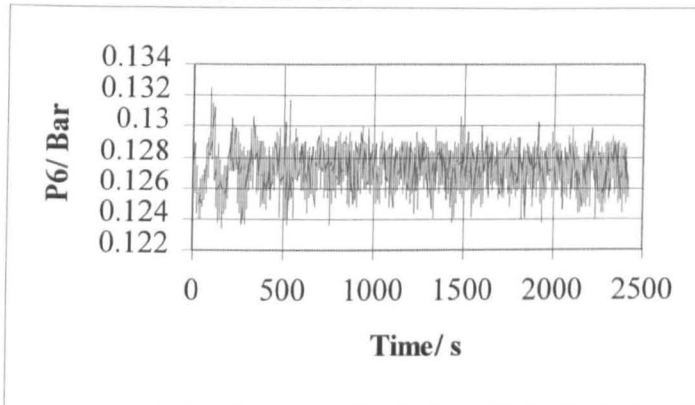
Volumetric Flow: 1.23 l/s

Mass Flow: 1.259 Kg/s

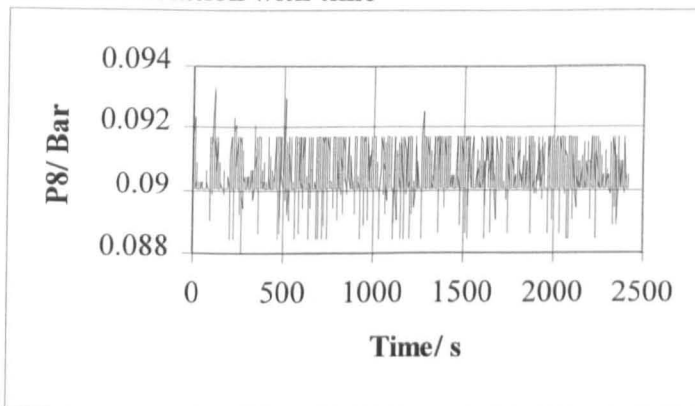
Number of Data Points:2414



CL P4 variation with time



CLI P6 variation with time



CLII P8 variation with time

	p1	p2	p3	p4	p5	p6	p7	p8
mean	0.529619	0.523532	0.517896	0.511841	0.492819	0.127249	0.101831	0.090536
median	0.52976	0.52363	0.5178	0.5118	0.49289	0.12723	0.10184	0.09006
mode	0.53078	0.52506	0.5176	0.51078	0.49432	0.12682	0.10143	0.09006
standard deviation	0.001868	0.001525	0.001554	0.001546	0.001555	0.001251	0.001177	0.000729
variance	3.49E-06	2.33E-06	2.42E-06	2.39E-06	2.42E-06	1.57E-06	1.38E-06	5.32E-07
skew	-0.44545	-0.22193	0.131504	-0.07058	-0.05471	-0.10925	-0.23403	0.401641
kurtosis	-0.25504	-0.20088	-0.0408	0.161788	-0.17808	-0.04198	0.554459	-0.13203

CLIII Pressure Readings and Statistical Data

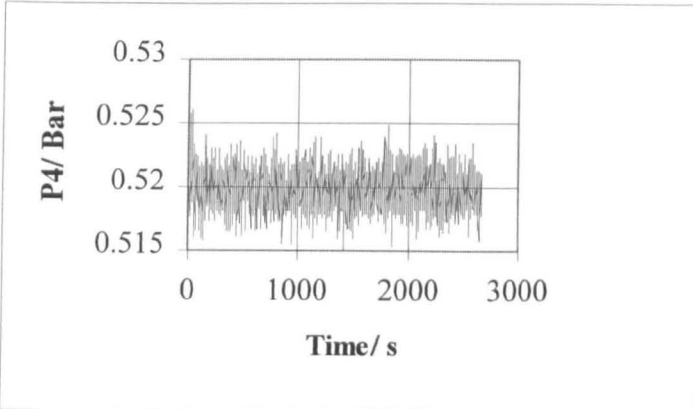
Long Swirly-flo Pipe Arrangement (pos 1)

Run: 2kglsf30

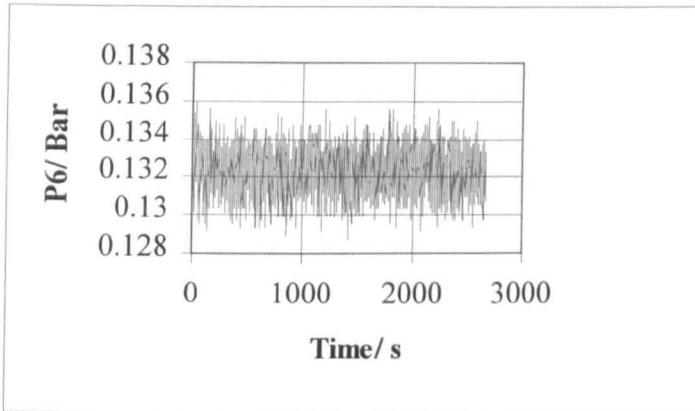
Volumetric Flow: 1.667 l/s

Mass Flow: 1.72 Kg/s

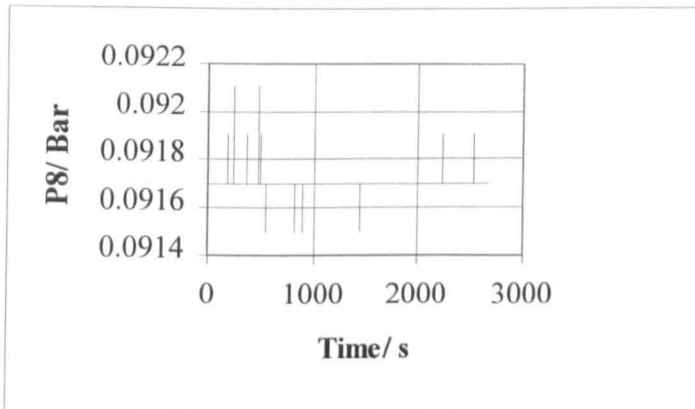
Number of Data Points:2666



CLIV P4 variation with time



CLV P6 variation with time



CLVI P8 variation with time

	p1	p2	p3	p4	p5	p6	p7	p8
mean	0.575562	0.538457	0.530127	0.519805	0.500794	0.132279	0.106475	0.0917
median	0.57579	0.53836	0.53008	0.51978	0.50087	0.13234	0.10654	0.0917
mode	0.57477	0.53815	0.52967	0.51957	0.50087	0.13234	0.10654	0.0917
standard deviation	0.001853	0.001808	0.001457	0.001393	0.001403	0.001136	0.001102	1.64E-05
variance	3.43E-06	3.27E-06	2.12E-06	1.94E-06	1.97E-06	1.29E-06	1.21E-06	2.69E-10
kurtosis	0.069954	0.590396	0.345402	0.418534	0.125406	-0.07334	-0.34435	373.9031

CLVII Pressure Readings and Statistical Data

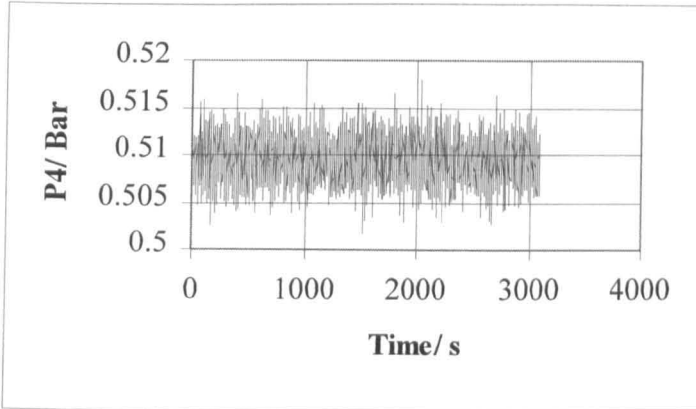
Long Swirly-flo Pipe Arrangement (pos 1)

Run: 2kglsf35

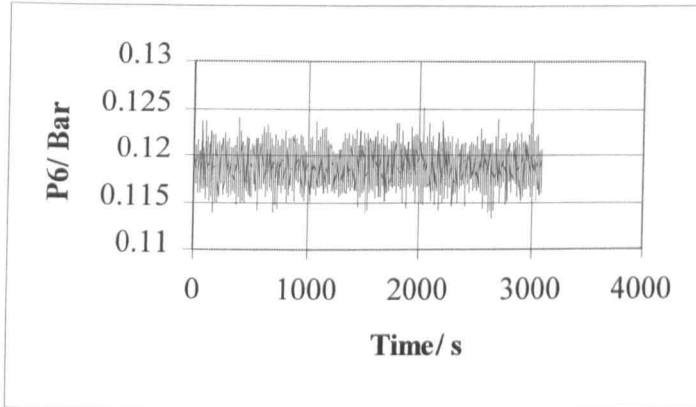
Volumetric Flow: 2.048 l/s

Mass Flow: 2.107 Kg/s

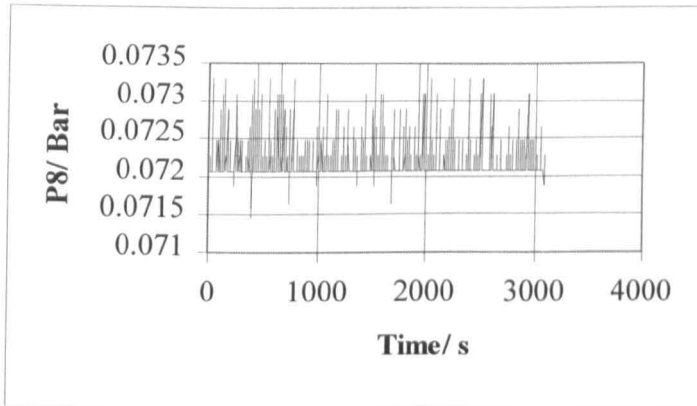
Number of Data Points:3094



CLVIII P4 variation with time



CLIX P6 variation with time



CLX P8 variation with time

	p1	p2	p3	p4	p5	p6	p7	p8
mean	0.623065	0.539086	0.526382	0.509474	0.490589	0.118847	0.092395	0.072104
mode	0.62182	0.53815	0.52742	0.50996	0.49125	0.11823	0.09161	0.07206
median	0.62285	0.53897	0.52639	0.50955	0.49064	0.11884	0.09243	0.07206
standard deviation	0.001408	0.002842	0.002276	0.002207	0.002138	0.001645	0.001539	0.000167
variance	1.98E-06	8.07E-06	5.18E-06	4.87E-06	4.57E-06	2.71E-06	2.37E-06	2.79E-08
skew	1.255927	0.131517	0.024755	0.05904	0.041031	0.036919	0.089971	4.650205
kurtosis	1.659309	-0.10653	-0.01843	-0.03473	-0.02654	-0.06286	-0.069	24.94093

CLXI Pressure Readings and Statistical Data

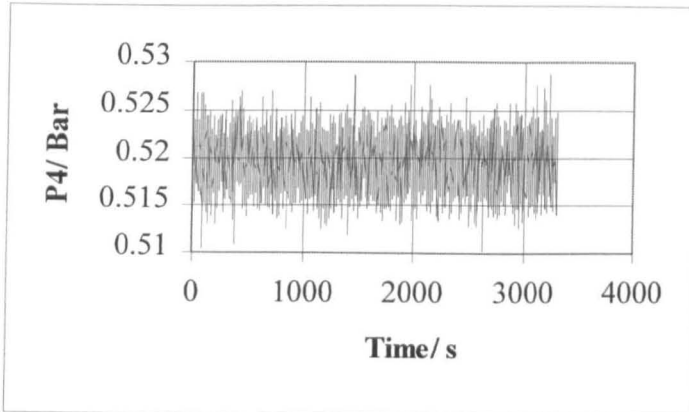
Long Swirly-flo Pipe Arrangement (pos 1)

Run: 2kglsf40

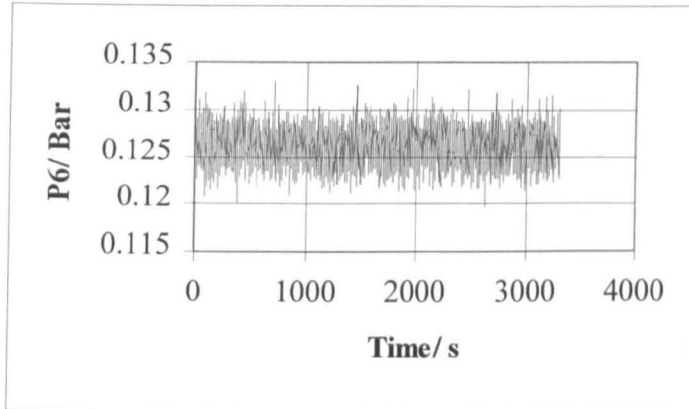
Volumetric Flow: 2.387 l/s

Mass Flow: 2.465 Kg/s

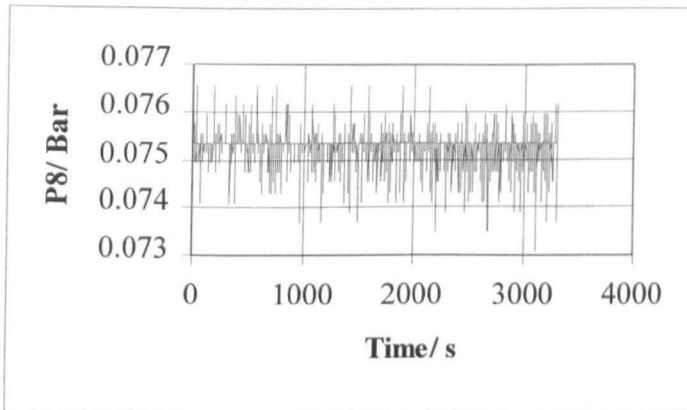
Number of Data Points:3313



CLXII P4 variation with time



CLXIII P6 variation with time



CLXIV P8 variation time

	p1	p2	p3	p4	p5	p6	p7	p8
mean	0.685894	0.557434	0.541215	0.519464	0.500686	0.126111	0.099588	0.075284
median	0.68627	0.55738	0.54133	0.51957	0.50066	0.12621	0.09959	0.07533
mode	0.68627	0.55697	0.54112	0.51957	0.50066	0.12682	0.09979	0.07533
standard deviation	0.001589	0.003322	0.002803	0.00254	0.002491	0.001826	0.00181	0.000244
variance	2.53E-06	1.1E-05	7.86E-06	6.45E-06	6.2E-06	3.33E-06	3.27E-06	5.95E-08
skew	-0.6589	0.033954	0.019143	-0.01259	0.010931	-0.01287	-0.05034	-2.00242
kurtosis	0.6399	-0.02068	-0.00208	-0.03434	-0.06111	-0.11969	-0.16901	14.53269

CLXV Pressure Readings and Statistical Data

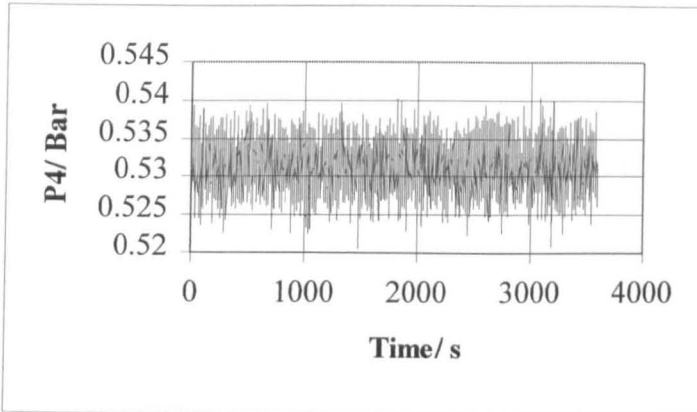
Long Swirly-flo Pipe Arrangement (pos 1)

Run: 2kglsf45

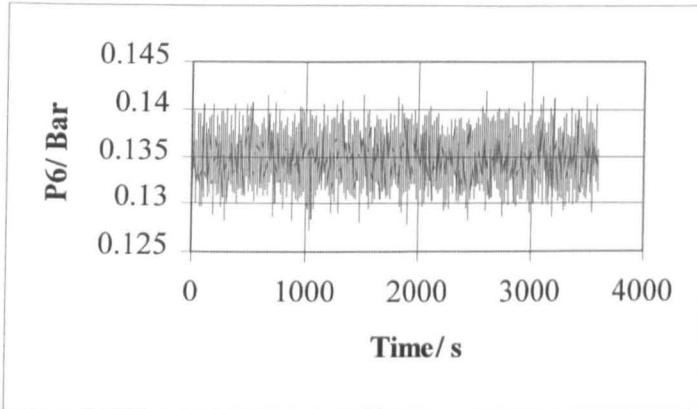
Volumetric Flow: 2.762 l/s

Mass Flow: 2.817 Kg/s

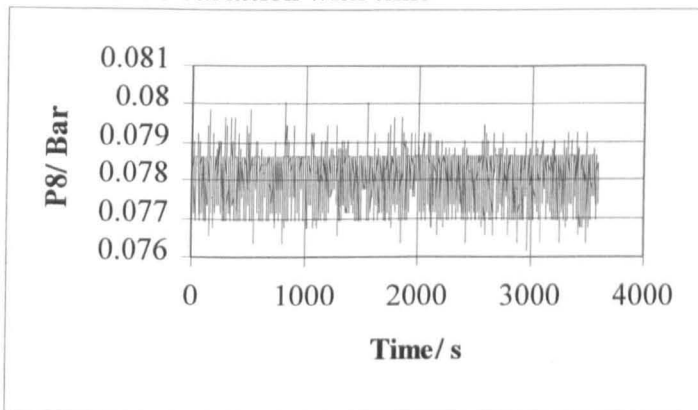
Number of Data Points:3588



CLXVI P4 variation with time



CLXVII P6 variation with time



CLXVIII P8 variation with time

	p1	p2	p3	p4	p5	p6	p7	p8
mean	0.757001	0.579599	0.559506	0.531451	0.512813	0.134899	0.108144	0.078239
mode	0.75685	0.57968	0.55892	0.53103	0.51233	0.13439	0.10797	0.07861
median	0.75685	0.57968	0.55954	0.53144	0.51273	0.1348	0.10818	0.0784
standard deviation	0.002318	0.003993	0.003181	0.002896	0.002857	0.002163	0.00212	0.000539
variance	5.37E-06	1.59E-05	1.01E-05	8.39E-06	8.16E-06	4.68E-06	4.49E-06	2.9E-07
skew	0.248634	0.008286	-0.07197	-0.03069	0.005299	-0.01251	0.039982	-1.0322
kurtosis	0.165662	-0.01126	-0.02917	0.010821	-0.06647	-0.02336	-0.03075	0.542582

CLXIX Pressure Readings and Statistical Data

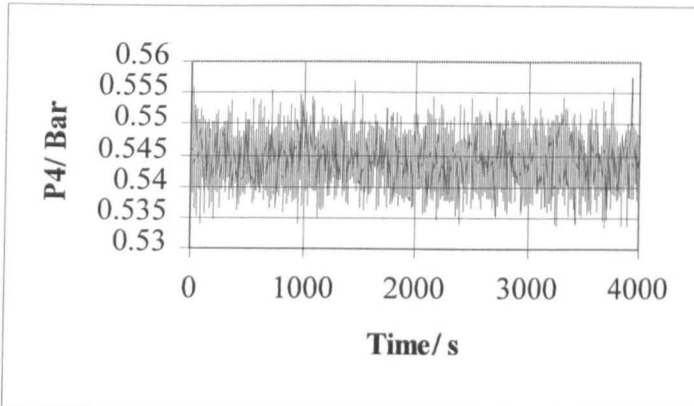
Long Swirly-flo Pipe Arrangement (pos 1)

Run: 2kglsf50

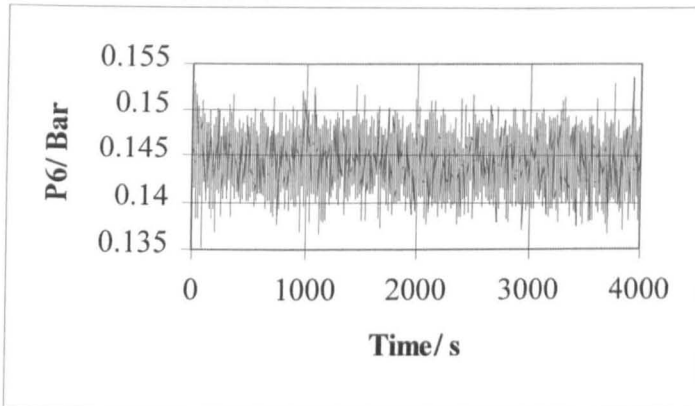
Volumetric Flow: 3.762 l/s

Mass Flow: 3.175 Kg/s

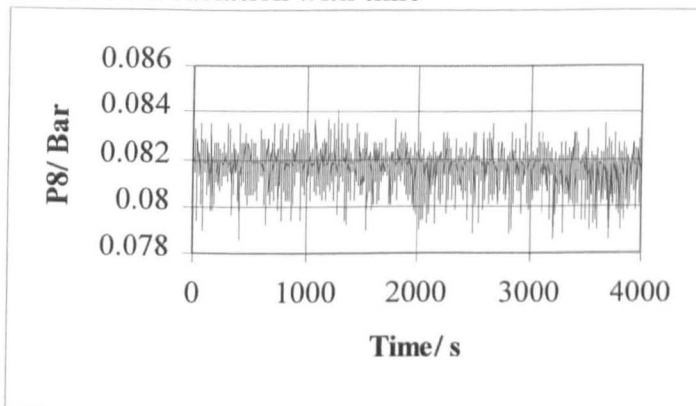
Number of Data Points:4000



CLXX P4 variation with time



CLXXI P6 variation with time



CLXXII P8 variation with time

	p1	p2	p3	p4	p5	p6	p7	p8
mean	0.840061	0.603351	0.578266	0.544167	0.52584	0.144288	0.117472	0.081701
median	0.8397	0.60321	0.57815	0.54412	0.52583	0.14421	0.11739	0.08188
mode	0.8397	0.60178	0.57856	0.54453	0.52521	0.14298	0.11616	0.08188
standard deviation	0.002738	0.004838	0.003785	0.003475	0.003407	0.002516	0.002417	0.000586
variance	7.5E-06	2.34E-05	1.43E-05	1.21E-05	1.16E-05	6.33E-06	5.84E-06	3.44E-07
skew	0.065377	0.148182	0.132672	0.103022	0.100135	0.110998	0.112858	-1.28998
kurtosis	0.053547	-0.07701	-0.04671	0.041103	-0.00154	-0.02954	0.05057	4.302255

CLXXIII Pressure readings and Statistical Data

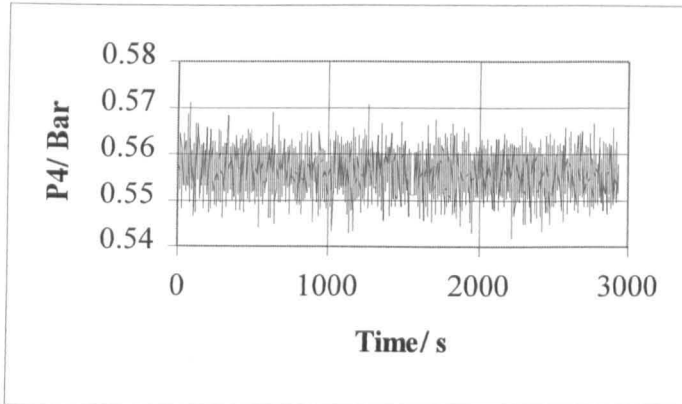
Long Swirly-flo Pipe Arrangement (pos 1)

Run: 2kglsf55

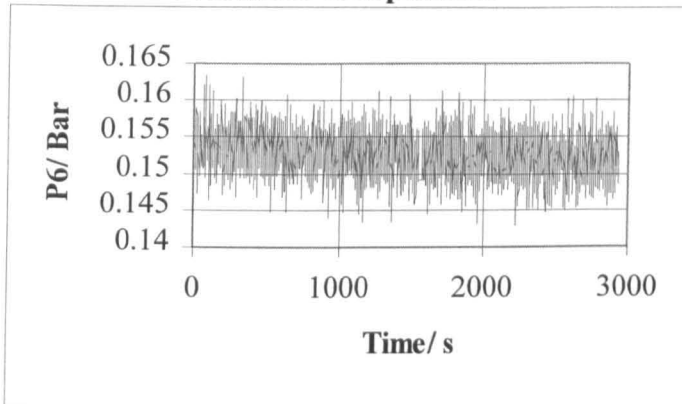
Volumetric Flow: 3.426 l/s

Mass Flow: 3.456 Kg/s

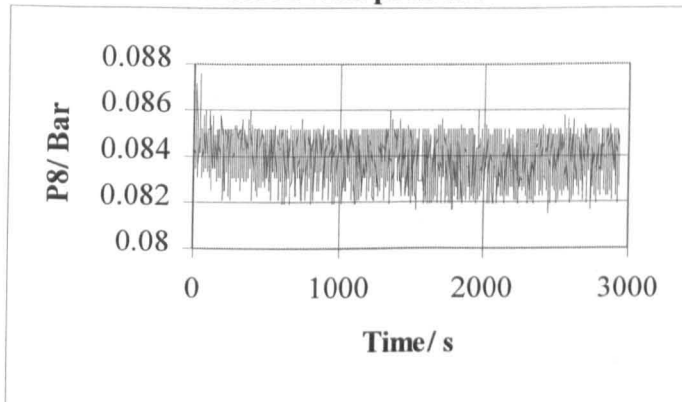
Number of Data Points:2938



CLXXIV P4 variation with pressure



CLXXV P6 variation with pressure



CLXXVI P8 variation with pressure

	p1	p2	p3	p4	p5	p6	p7	p8
mean	0.917763	0.626629	0.595827	0.556039	0.539058	0.152693	0.126218	0.083992
mode	0.91745	0.62633	0.59575	0.5566	0.53851	0.15219	0.12618	0.08515
median	0.91745	0.62674	0.59575	0.55609	0.53913	0.1526	0.12618	0.08413
standard deviation	0.004617	0.005445	0.004186	0.003945	0.003823	0.002825	0.002784	0.000883
variance	2.13E-05	2.96E-05	1.75E-05	1.56E-05	1.46E-05	7.98E-06	7.75E-06	7.79E-07
skew	0.097839	-0.0437	-0.02823	-0.0549	-0.04961	-0.01859	-0.01387	-0.32659
kurtosis	-0.29509	0.181113	0.160378	0.140935	0.201944	0.194957	0.07366	-0.51967

CLXXVII Pressure Readings and Statistical Data

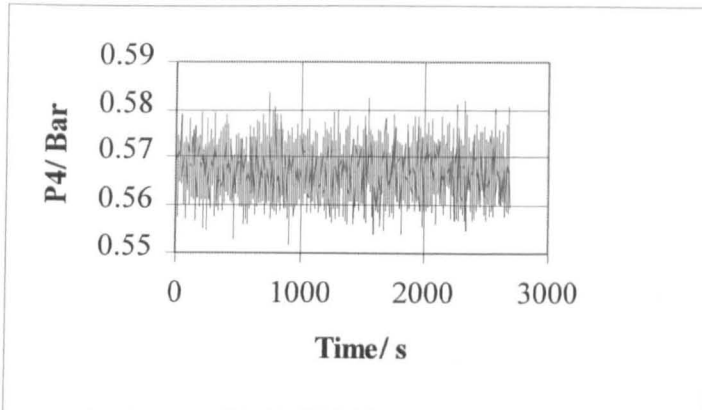
Long Swirly-flo Pipe Arrangement (pos 1)

Run: 2kglsf60

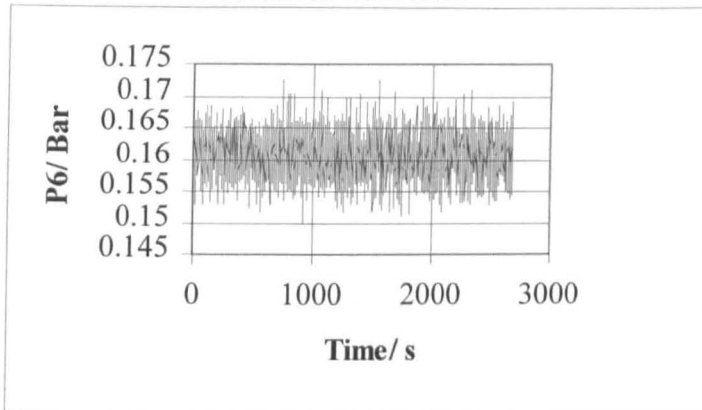
Volumetric Flow: 3.623 l/s

Mass Flow: 3.666 Kg/s

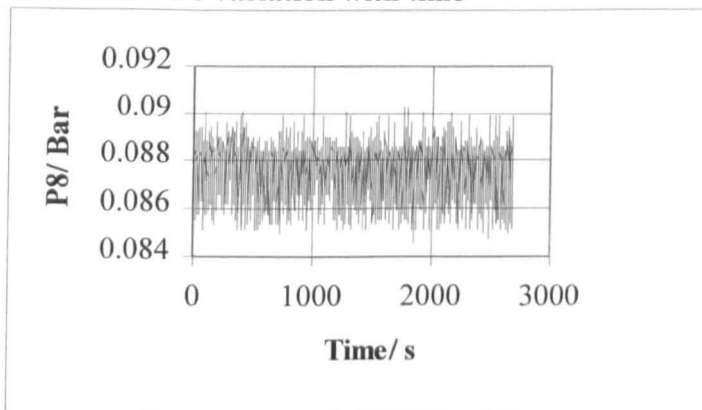
Number of Data Points:2684



CLXXVIII P4 variation with time



CLXXXIX P6 variation with time



CLXC P8 variation with time

	p1	p2	p3	p4	p5	p6	p7	p8
mean	0.988559	0.64637	0.612042	0.567347	0.549679	0.160773	0.134459	0.087745
median	0.98905	0.64638	0.61191	0.56745	0.54976	0.16078	0.13457	0.08802
mode	0.98905	0.64495	0.61068	0.56622	0.54976	0.16119	0.13457	0.08843
standard deviation	0.003963	0.006474	0.005056	0.00452	0.004413	0.003273	0.003171	0.000983
variance	1.57E-05	4.19E-05	2.56E-05	2.04E-05	1.95E-05	1.07E-05	1.01E-05	9.67E-07
skew	-0.15767	0.075594	0.104906	0.040128	0.078904	0.05831	0.018795	-0.78499
kurtosis	0.272667	-0.09637	-0.05006	-0.03915	0.013354	0.018479	0.040406	0.128698

CLXCI Pressure Readings and Statistical Data

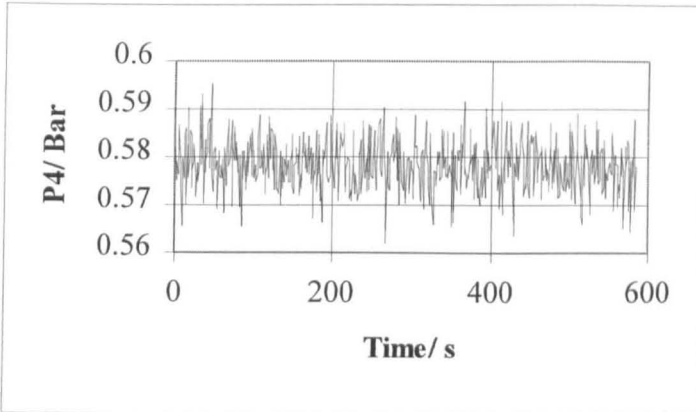
Long Swirly-flo Pipe Arrangement (pos 1)

Run: 2kglsf65

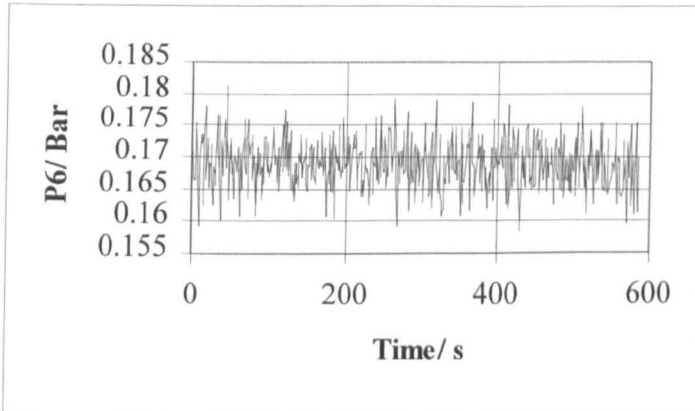
Volumetric Flow: 3.837 l/s

Mass Flow: 3.875 Kg/s

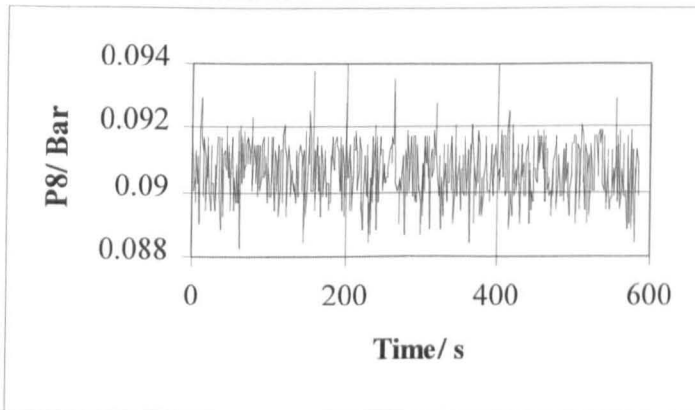
Number of Data Points:586



CLXCII P4 variation with time



CLXCIII P6 variation with time



CLXCIV P8 variation with time

	p1	p2	p3	p4	p5	p6	p7	p8
mean	1.063753	0.666449	0.628446	0.578306	0.560506	0.168958	0.142228	0.090659
median	1.06372	0.66622	0.62828	0.57829	0.5604	0.16896	0.14214	0.09068
mode	1.0627	0.66459	0.63093	0.58136	0.56163	0.16794	0.14153	0.0917
standard deviation	0.004911	0.00718	0.005673	0.005158	0.005062	0.003726	0.003506	0.000892
variance	2.41E-05	5.16E-05	3.22E-05	2.66E-05	2.56E-05	1.39E-05	1.23E-05	7.95E-07
skew	0.053646	0.084051	0.023118	0.033574	0.020768	0.031922	0.018199	-0.08175
kurtosis	-0.34066	0.314583	0.237126	0.166983	0.098831	0.056953	0.123156	-0.33916

CLXCV Pressure Readings and Statistical Data

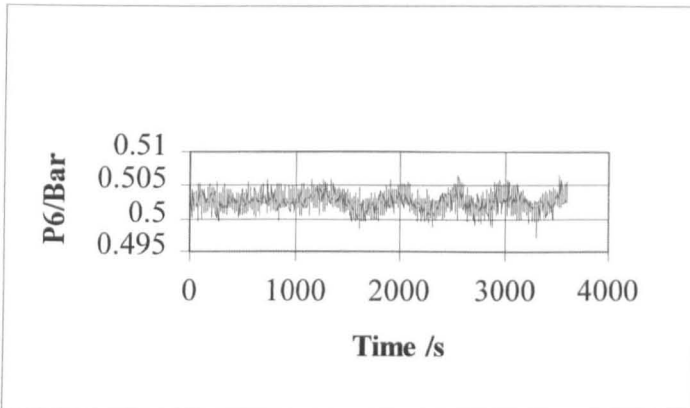
Long Swirly-flo Pipe Arrangement (pos 2)

Run: 2kglsf20

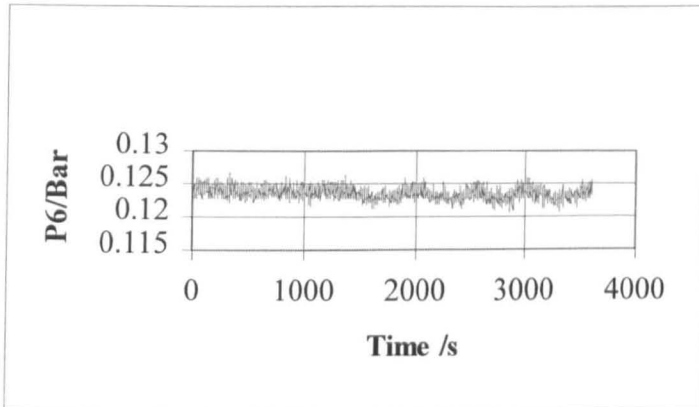
Volumetric Flow: 0.896 l/s

Mass Flow: 0.9162 Kg/s

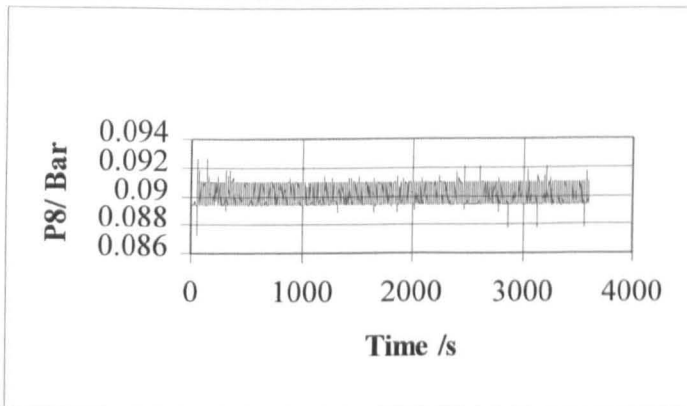
Number of Data Points:3600



CLXCVI P4 variation with time



CLXCVII P6 variation time



CLXCVIII P8 variation with time

	p1	p2	p3	p4	p5	p6	p7	p8
mean	0.499078	0.513032	0.509293	0.50257	0.487755	0.123386	0.095607	0.090042
median	0.49907	0.5134	0.50921	0.50259	0.48778	0.12334	0.09536	0.08984
mode	0.49907	0.5136	0.509	0.50259	0.48778	0.12252	0.09515	0.08943
standard deviation	9.75E-05	0.001377	0.001325	0.001106	0.001304	0.000877	0.0009	0.000677
variance	9.52E-09	1.9E-06	1.76E-06	1.22E-06	1.7E-06	7.69E-07	8.1E-07	4.58E-07
skew	14.18048	-0.24167	-0.16808	0.008025	-0.21494	0.395756	0.31762	0.537622
kurtosis	225.2547	0.012517	-0.05157	0.870103	0.19857	-0.1585	0.693843	-0.94386

CLXCIX Pressure Readings and Statistical Data

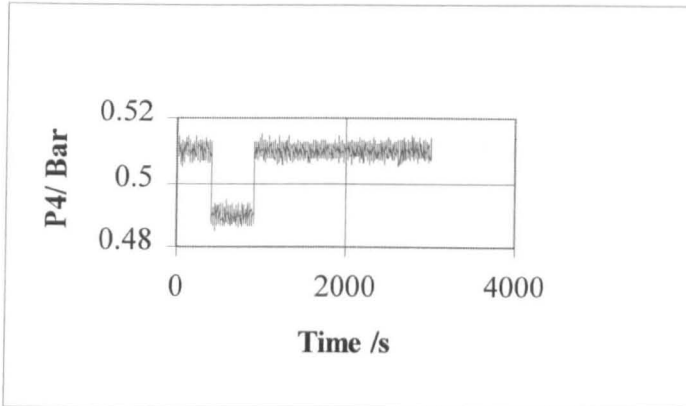
Long Swirly-flo Pipe Arrangement (pos 2)

Run: 2kglsf25

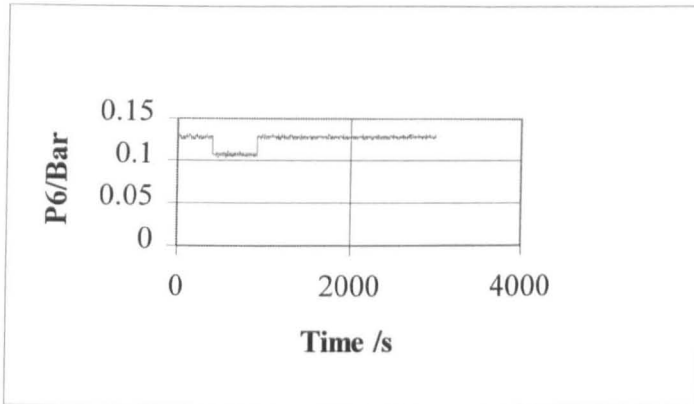
Volumetric Flow: 1.318 l/s

Mass Flow: 1.357 Kg/s

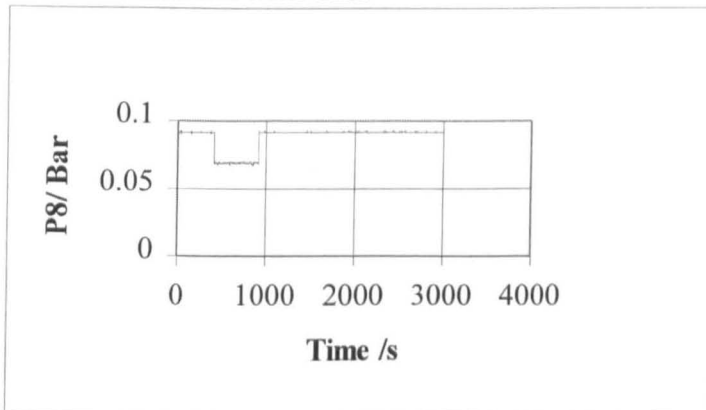
Number of Data Points:3002



CC P4 variation with time



CCI P6 variation with time



CCII P8 variation with time

	p1	p2	p3	p4	p5	p6	p7	p8
mean	0.537385	0.517222	0.523615	0.506636	0.491046	0.124482	0.096486	0.087475
median	0.53999	0.52005	0.52608	0.50955	0.49412	0.12764	0.09966	0.09106
mode	0.53999	0.52087	0.52506	0.51078	0.49473	0.12907	0.09945	0.09106
standard deviation	0.004652	0.007306	0.006787	0.007719	0.007777	0.00811	0.008126	0.008269
variance	2.17E-05	5.35E-05	4.61E-05	5.97E-05	6.06E-05	6.59E-05	6.62E-05	6.85E-05
skew	-1.76575	-1.64041	-1.63953	-1.65373	-1.66613	-1.71956	-1.73151	-1.77706
kurtosis	1.522646	1.027824	1.05835	1.030694	1.04936	1.103659	1.13393	1.157822

CCIII Pressure Readings and Statistical Data

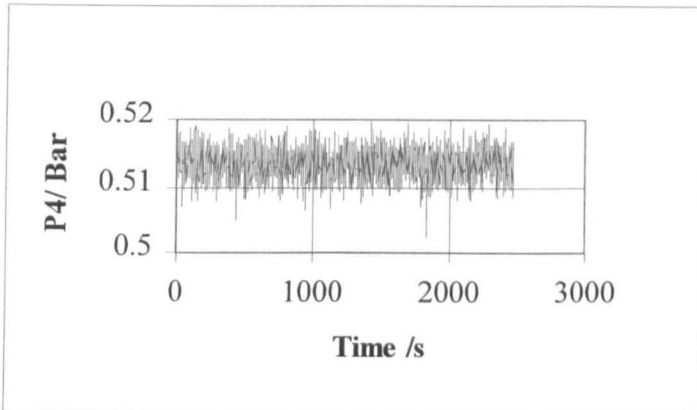
Long Swirly-flo Pipe Arrangement (pos 2)

Run: 2kglsf30

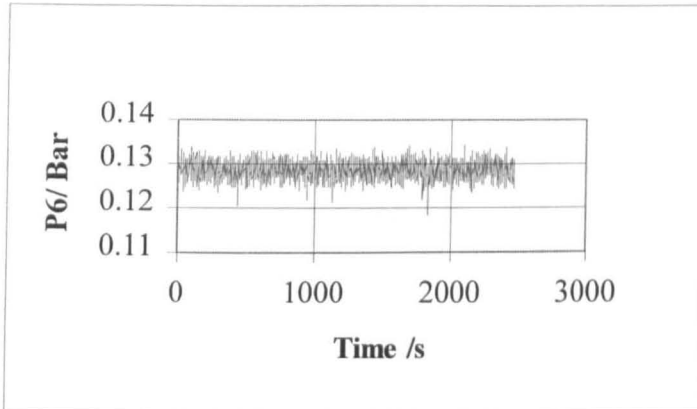
Volumetric Flow: 1.756 l/s

Mass Flow: 1.81 Kg/s

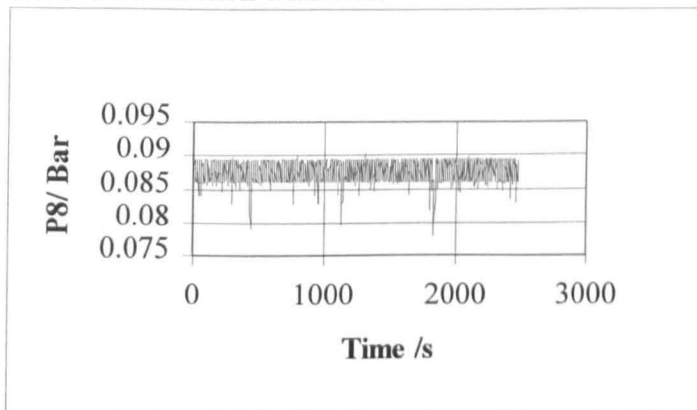
Number of Data Points:2469



CCIV P4 variation with time



CCV P6 variation with time



CCVI P8 variation with time

	p1	p2	p3	p4	p5	p6	p7	p8
mean	0.587214	0.538178	0.528717	0.513389	0.497692	0.128575	0.100076	0.087519
median	0.58807	0.53815	0.52885	0.51344	0.4978	0.12866	0.10006	0.08759
mode	0.58909	0.53815	0.52844	0.51344	0.4978	0.12846	0.10006	0.08615
standard deviation	0.001743	0.002185	0.002011	0.002178	0.002137	0.001927	0.001896	0.001498
variance	3.04E-06	4.77E-06	4.04E-06	4.74E-06	4.57E-06	3.71E-06	3.59E-06	2.24E-06
skew	-0.90821	0.030169	-0.19538	-0.26247	-0.24892	-0.3483	-0.46553	-1.1289
kurtosis	0.445437	0.518959	0.682011	0.531987	0.652037	0.964395	1.262608	3.99636

CCVII Pressure Readings and Statistical Readings

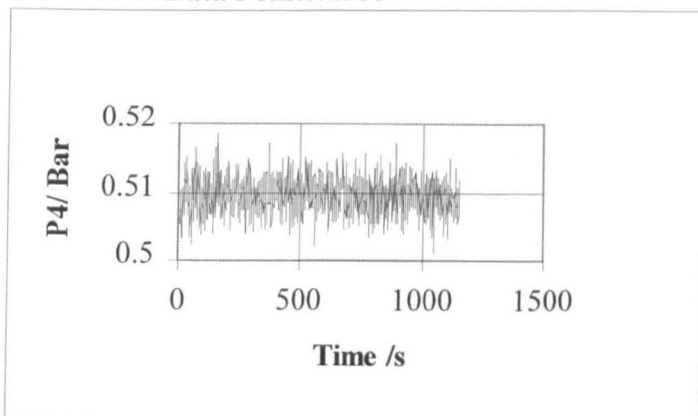
Long Swirly-flo Pipe Arrangement (pos 2)

Run: 2kglsf35

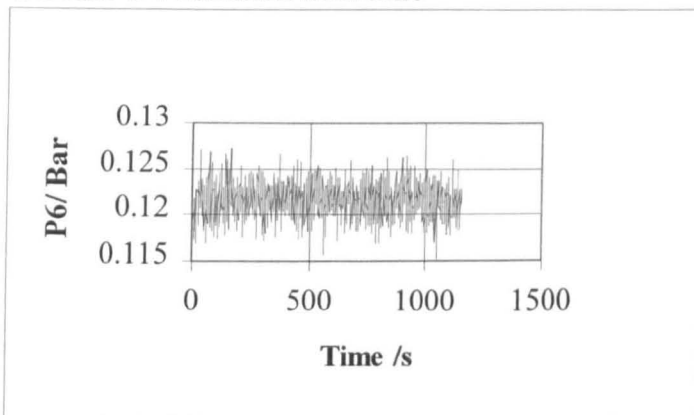
Volumetric Flow: 2.155 l/s

Mass Flow: 2.207 Kg/s

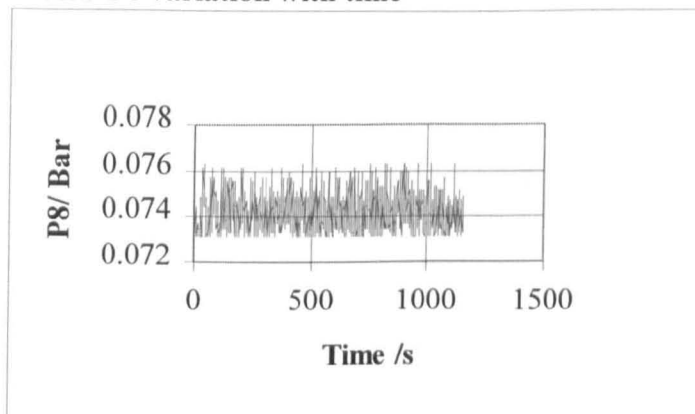
Number of Data Points:1155



CCVIII P4 variation with time



CCIX P6 variation with time



CCX P8 variation with time

	p1	p2	p3	p4	p5	p6	p7	p8
mean	0.638996	0.545096	0.530993	0.509352	0.493815	0.121567	0.092351	0.074183
median	0.63921	0.54511	0.53089	0.50934	0.49391	0.1215	0.09229	0.07408
mode	0.63819	0.54511	0.53048	0.50852	0.49309	0.12089	0.09249	0.07306
standard deviation	0.002076	0.003146	0.002556	0.002442	0.00235	0.0018	0.00175	0.000786
variance	4.31E-06	9.9E-06	6.53E-06	5.96E-06	5.52E-06	3.24E-06	3.06E-06	6.18E-07
skew	0.245058	0.058888	0.117933	0.059526	0.020961	-0.00643	0.052156	0.453124
kurtosis	0.808468	0.138094	0.1577	0.128508	0.155947	0.095101	0.107654	-0.40051

CCXI Pressure Readings and Statistical Data

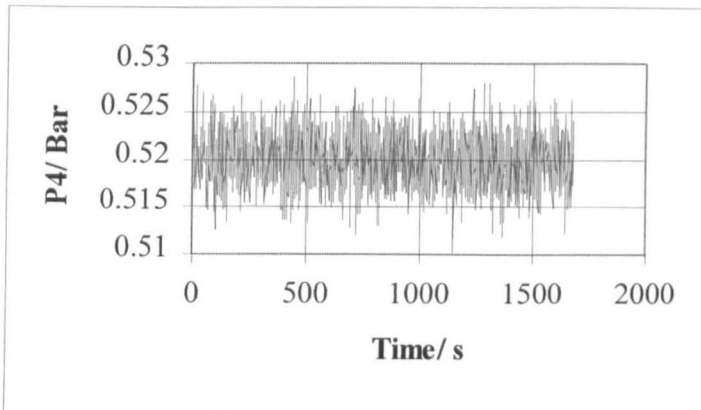
Long Swirly-flo Pipe Arrangement (pos 2)

Run: 2kglsf40

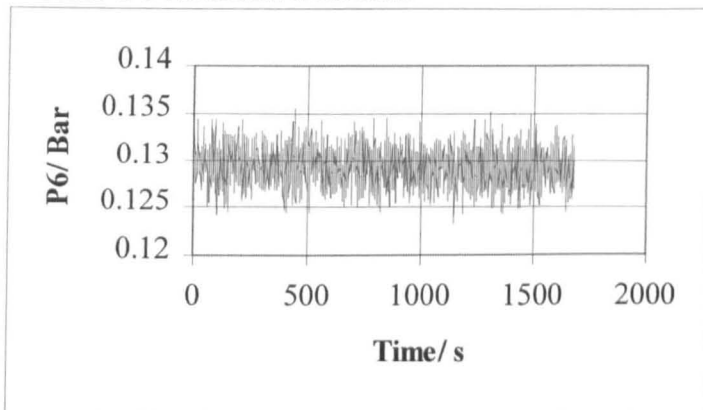
Volumetric Flow: 2.49 l/s

Mass Flow: 2.54 Kg/s

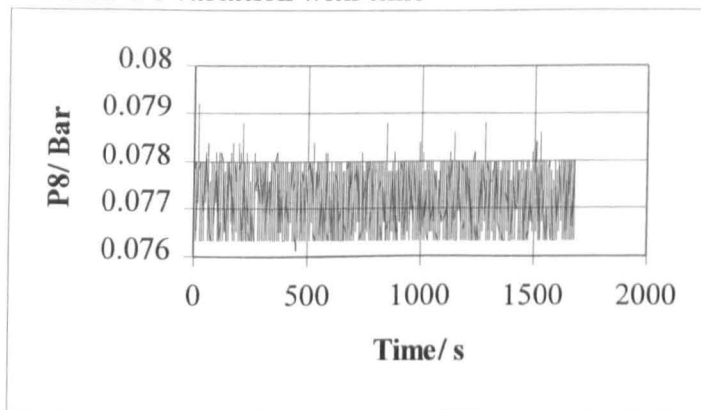
Number of Data Points:1682



CCXII P4 variation with time



CCXIII P6 variation with time



CCXIV P8 variation with time

	p1	p2	p3	p4	p5	p6	p7	p8
mean	0.701107	0.564402	0.54694	0.519987	0.504467	0.129284	0.09983	0.077192
median	0.70161	0.56434	0.54685	0.51998	0.50455	0.12928	0.09986	0.07715
mode	0.70161	0.56475	0.54726	0.51998	0.50414	0.12907	0.10027	0.07797
standard deviation	0.002431	0.003607	0.003018	0.002709	0.00263	0.001923	0.00186	0.000618
variance	5.91E-06	1.3E-05	9.11E-06	7.34E-06	6.92E-06	3.7E-06	3.46E-06	3.82E-07
skew	-0.17468	0.056919	0.016221	-0.00478	-0.03403	0.045091	0.025203	-0.00746
kurtosis	0.353372	-0.05443	-0.07914	-0.02778	-0.0422	-0.0295	0.051781	-1.3009

CCXV Pressure Readings and Statistical Data

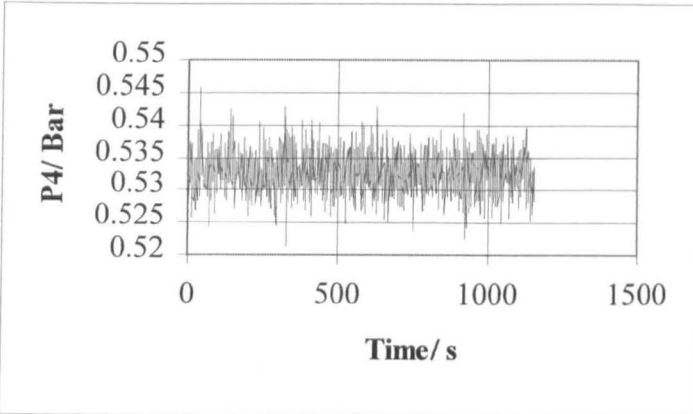
Long Swirly-flo Pipe Arrangement (pos 2)

Run: 2kglsf45

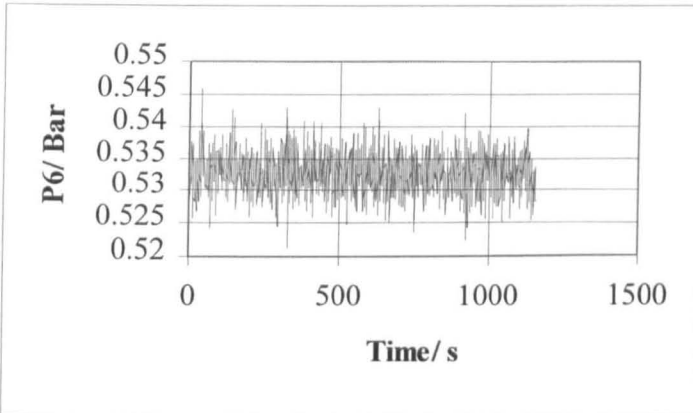
Volumetric Flow: 2.864 l/s

Mass Flow: 2.928 Kg/s

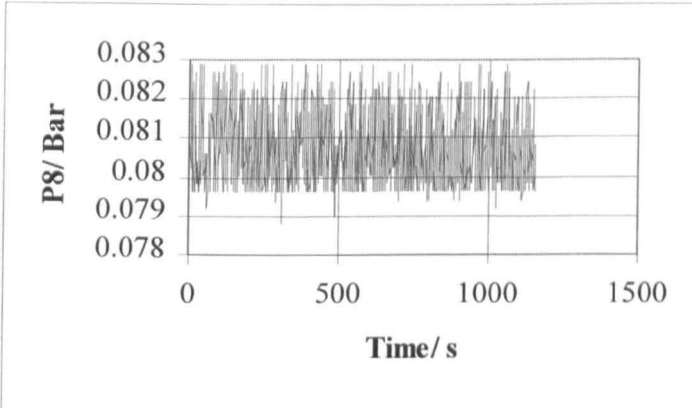
Number of Data Points:1158



CCXV P4 variation with time



CCXVI P6 variation with time



CCXVII P8 variation with time

	p1	p2	p3	p4	p5	p6	p7	p8
mean	0.776646	0.588145	0.566096	0.532697	0.517329	0.138784	0.108968	0.080726
mode	0.77731	0.58868	0.56506	0.53267	0.51826	0.13869	0.10845	0.07961
median	0.77628	0.58828	0.56608	0.53267	0.51724	0.13869	0.10886	0.08063
standard deviation	0.00283	0.00443	0.00345	0.00318	0.003154	0.002377	0.002325	0.000971
variance	0.002829	0.004428	0.003449	0.003179	0.003152	0.002376	0.002324	0.000971
skew	0.08788	-0.04857	0.033447	0.072278	0.091091	0.13966	0.095022	0.514751
kurtosis	0.192081	0.147616	0.220779	0.341623	0.278617	0.439011	0.313354	-0.83322

CCXVIII Pressure Readings and Statistical Data

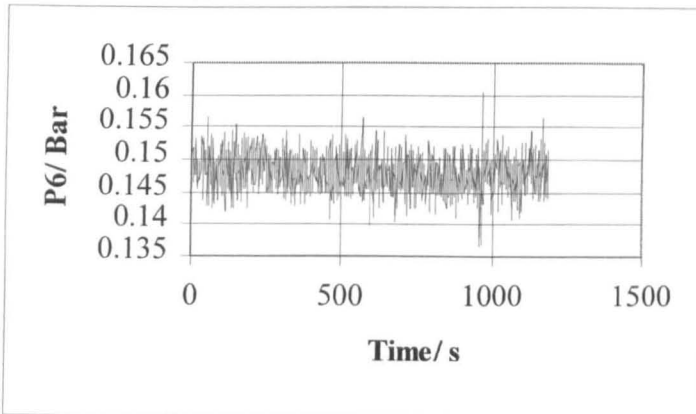
Long Swirly-flo Pipe Arrangement (pos 2)

Run: 2kglsf50

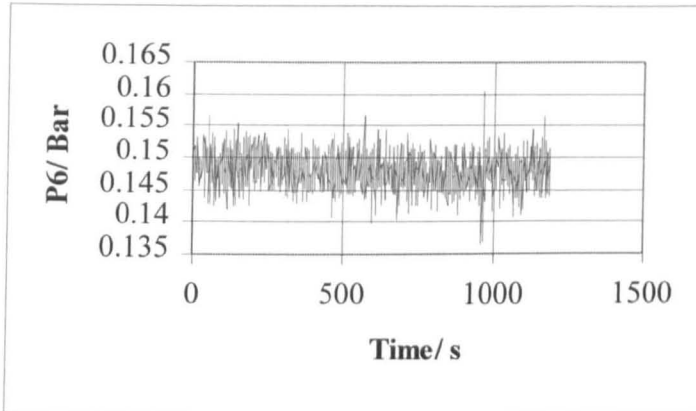
Volumetric Flow: 3.168 l/s

Mass Flow: 3.168 Kg/s

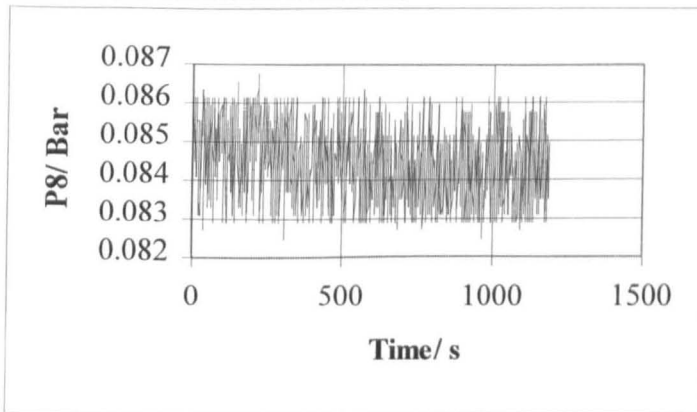
Number of Data Points:1188



CCXIX P4 variation with time



CCXX P6 variation with time



CCXXI P8 variation with time

	p1	p2	p3	p4	p5	p6	p7	p8
mean	0.854947	0.611371	0.584344	0.545073	0.53008	0.148086	0.117983	0.084427
median	0.85402	0.61119	0.58429	0.54494	0.53012	0.1481	0.11786	0.08452
mode	0.85198	0.61078	0.58409	0.54596	0.5291	0.14769	0.11643	0.08452
standard deviation	0.005331	0.005495	0.004285	0.003912	0.003851	0.002815	0.002771	0.000974
variance	2.84E-05	3.02E-05	1.84E-05	1.53E-05	1.48E-05	7.93E-06	7.68E-06	9.48E-07
skew	-0.11219	0.086216	0.005609	0.064377	-0.01142	-0.03774	0.009685	0.108128
kurtosis	2.253598	0.925458	0.854053	0.655197	0.573056	0.302773	0.147682	-0.93992

CCXXII Pressure Readings and Statistical Data

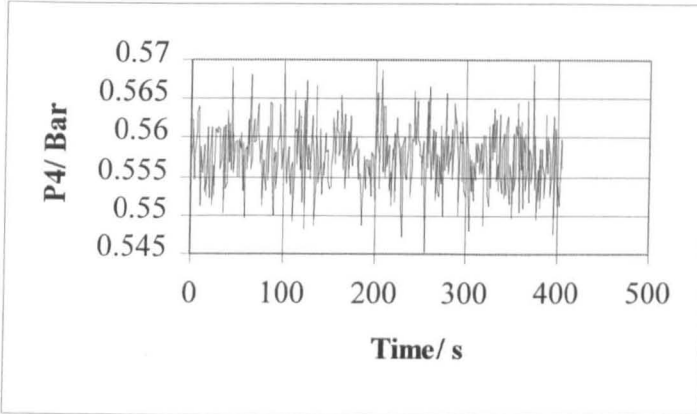
Long Swirly-flo Pipe Arrangement (pos 2)

Run: 2kgl5f55

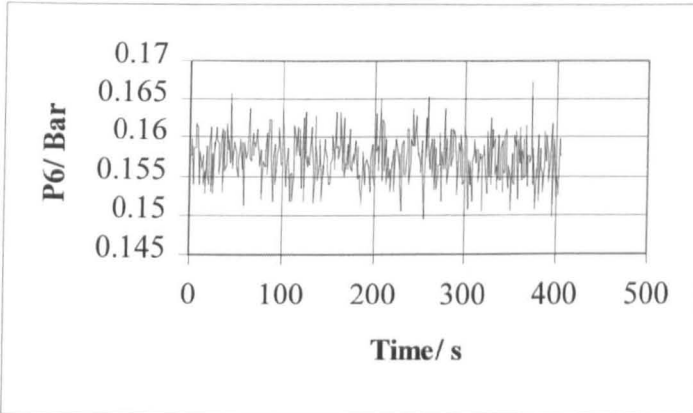
Volumetric Flow: 3.446 l/s

Mass Flow: 3.518 Kg/s

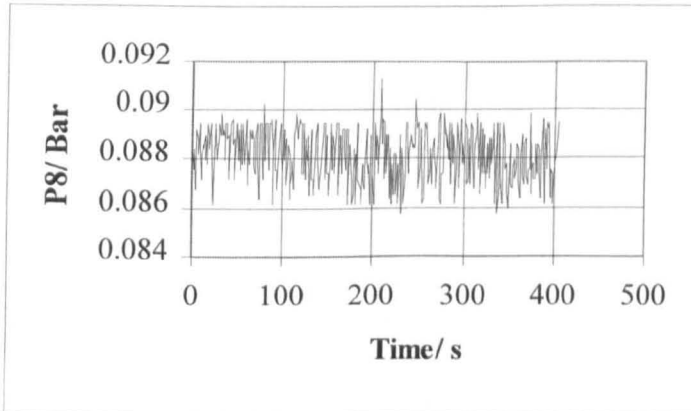
Number of Data Points:405



CCXXIII P4 variation with time



CCXXIX P6 variation with time



CCXXX P8 variation with time

	p1	p2	p3	p4	p5	p6	p7	p8
mean	0.931012	0.634094	0.602312	0.557565	0.542628	0.157297	0.127123	0.088162
median	0.93074	0.6339	0.60229	0.55763	0.5426	0.1573	0.12707	0.0882
mode	0.93279	0.63553	0.59943	0.55722	0.54424	0.15669	0.12789	0.08943
standard deviation	0.004944	0.005809	0.004498	0.004155	0.003992	0.003019	0.003012	0.001071
variance	2.44E-05	3.37E-05	2.02E-05	1.73E-05	1.59E-05	9.11E-06	9.07E-06	1.15E-06
skew	0.030624	0.150842	0.070306	0.083328	0.113801	0.076125	0.068369	-0.23888
kurtosis	-0.5251	0.104516	0.038319	0.079295	0.076507	0.011292	0.05082	-0.86088

CCXXXI Pressure Readings and Statistical Data

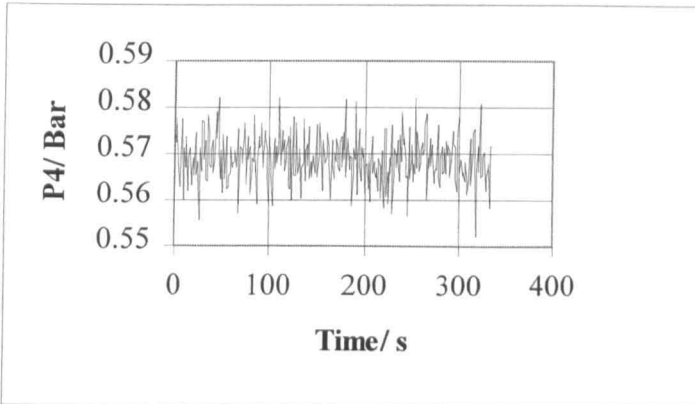
Long Swirly-flo Pipe Arrangement (pos 2)

Run: 2kglsf60

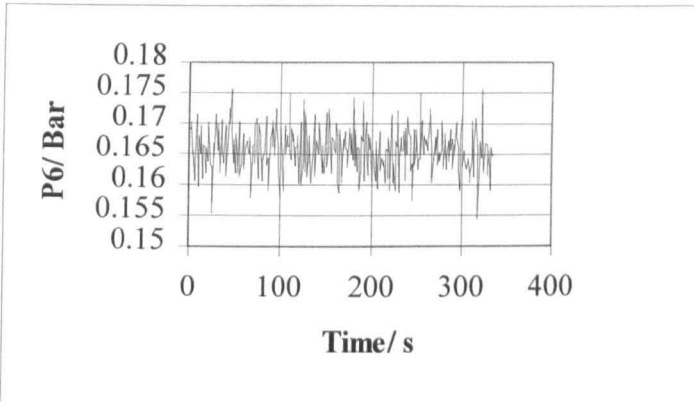
Volumetric Flow: 3.696 l/s

Mass Flow: 3.784 Kg/s

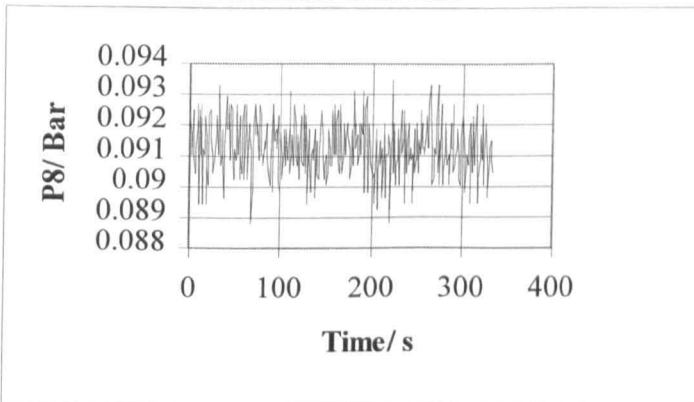
Number of Data Points:335



CCXXXII P4 variation with time



CCXXXIII P6 variation with time



CCXXXIV P8 variation with time

	p1	p2	p3	p4	p5	p6	p7	p8
mean	0.9981	0.654777	0.618753	0.568774	0.553892	0.165669	0.135262	0.091258
median	0.99826	0.65477	0.61866	0.56847	0.55386	0.16569	0.13525	0.09127
mode	1.0003	0.65558	0.616	0.56929	0.55079	0.16631	0.13587	0.09106
standard deviation	0.004463	0.006881	0.005513	0.00499	0.004842	0.003607	0.00345	0.000917
variance	1.99E-05	4.73E-05	3.04E-05	2.49E-05	2.34E-05	1.3E-05	1.19E-05	8.41E-07
skew	-0.18285	-0.18325	-0.02557	0.011674	-0.01847	0.057204	-0.00682	-0.01476
kurtosis	0.126389	0.311862	0.108624	0.269108	0.229651	0.050593	-0.01967	-0.43455

CCXXXV Pressure Readings and Statistical Data

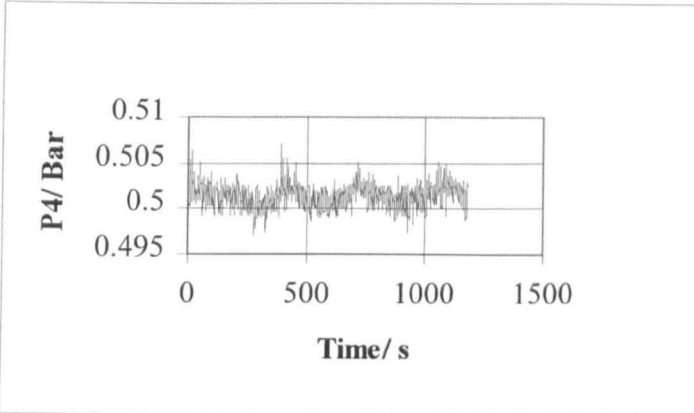
Long Swirly-flo Pipe Arrangement (pos 3)

Run: 2kglsf20

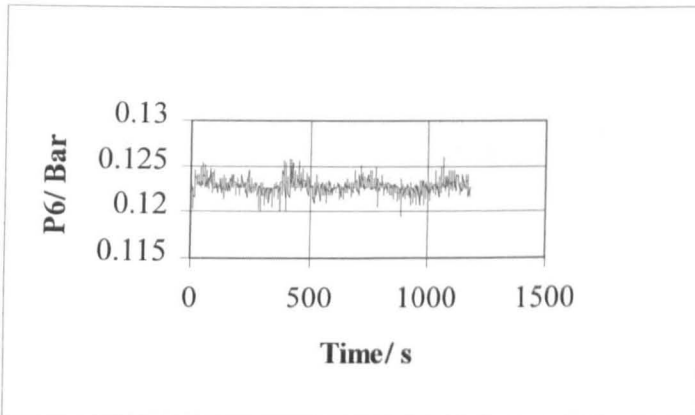
Volumetric Flow: 0.878 l/s

Mass Flow: 0.893 Kg/s

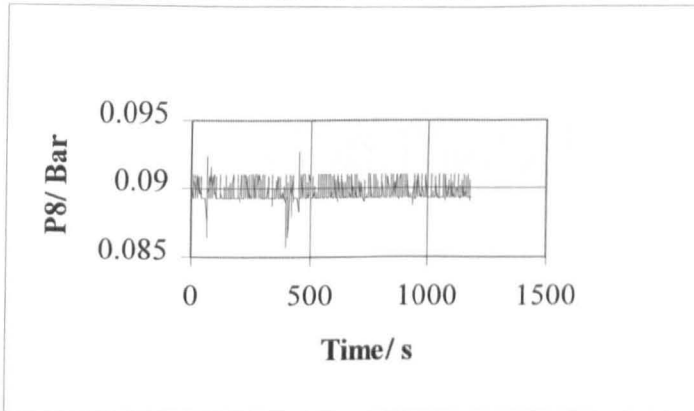
Number of Data Points:1180



CCXXXVI P4 variation with time



CCXXXVII P6 variation with time



CCXXXVIII P6 variation with time

	p1	p2	p3	p4	p5	p6	p7	p8
mean	0.499041	0.511553	0.508021	0.501446	0.486874	0.12273	0.095098	0.089781
median	0.49907	0.51135	0.50798	0.50157	0.48696	0.12252	0.09515	0.08943
mode	0.49907	0.51033	0.50778	0.50259	0.48778	0.12252	0.09515	0.08943
standard deviation	0.000188	0.001511	0.001452	0.00129	0.001414	0.000804	0.000896	0.000625
variance	3.54E-08	2.28E-06	2.11E-06	1.66E-06	2E-06	6.46E-07	8.03E-07	3.91E-07
skew	-7.2679	0.153777	-0.03851	-0.01227	0.084395	0.414621	0.350637	0.647466
kurtosis	58.09141	-0.22508	0.443859	0.428965	0.193067	1.693354	0.921517	3.350079

CCXXXIV Pressure Readings and Statistical Data

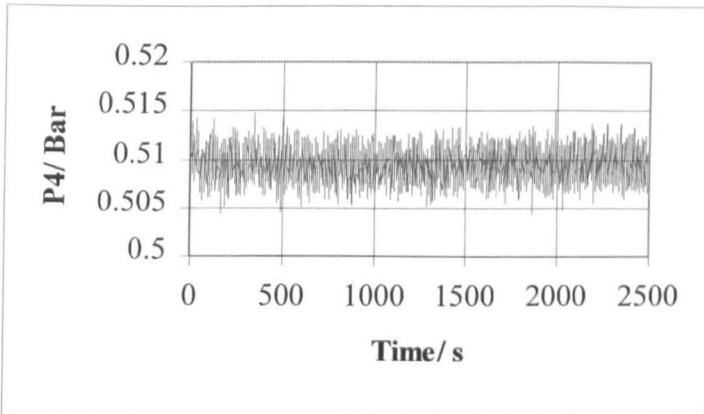
Long Swirly-flo Pipe Arrangement (pos 3)

Run: 2kglsf25

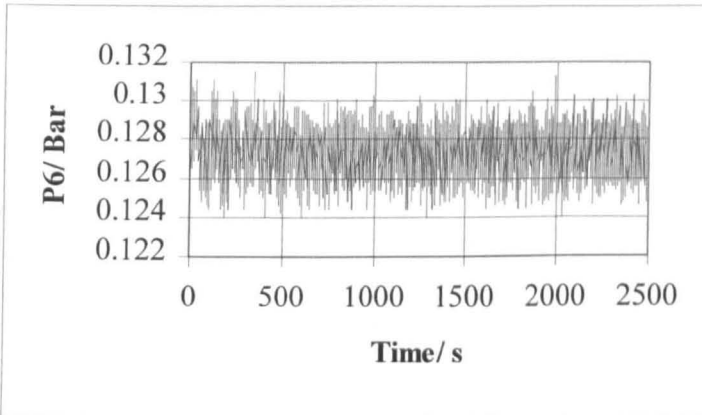
Volumetric Flow: 1.31 l/s

Mass Flow: 1.347 Kg/s

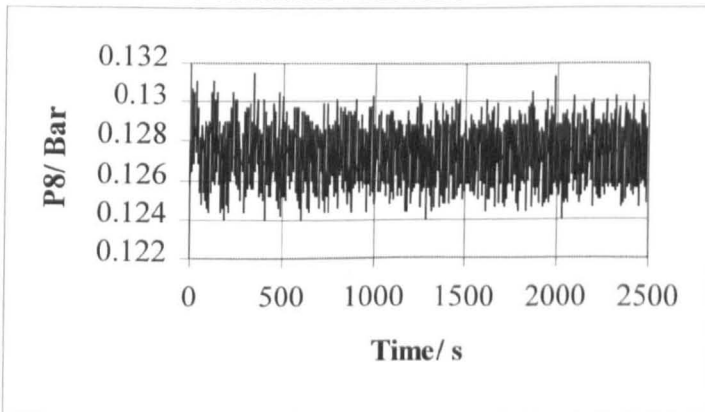
Number of Data Points:2493



CCXXXV P4 variation with time



CCXXXVI P6 variation with time



CCXXXVII P8 variation with time

	p1	p2	p3	p4	p5	p6	p7	p8
mean	0.536613	0.526218	0.519894	0.50948	0.494689	0.127379	0.099846	0.090957
median	0.53692	0.52608	0.51985	0.50955	0.49473	0.12743	0.09986	0.09106
mode	0.53692	0.52506	0.52026	0.51078	0.49555	0.12825	0.10006	0.09106
standard deviation	0.002131	0.001489	0.001654	0.00165	0.001582	0.001273	0.001181	0.000324
variance	4.54E-06	2.22E-06	2.74E-06	2.72E-06	2.5E-06	1.62E-06	1.39E-06	1.05E-07
skew	-0.26	0.209261	-0.00045	-0.02276	-0.0741	-0.11796	-0.05412	-2.17024
kurtosis	-0.67748	0.115867	-0.35052	-0.36843	-0.27378	-0.46078	-0.19338	9.646436

CCXXXVIII Pressure and Statistical Data

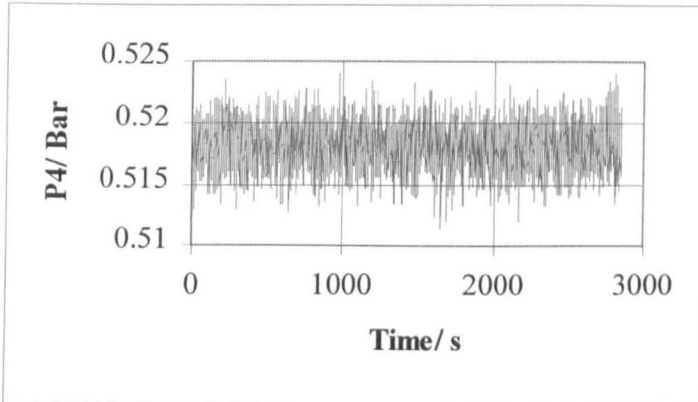
Long Swirly-flo Pipe Arrangement (pos 3)

Run: 2kglf30

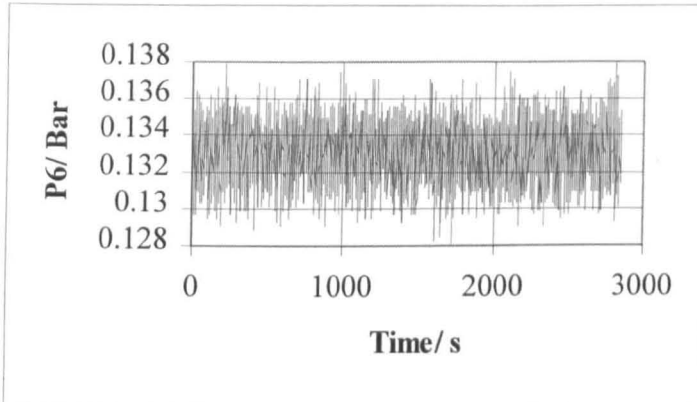
Volumetric Flow: 1.735 l/s

Mass Flow: 1.794 Kg/s

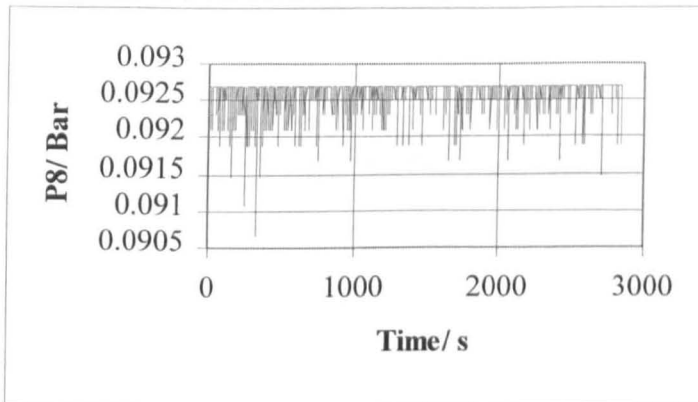
Number of Data Points:2847



CCXXXIX P4 variation with time



CCXXXX P6 variation with time



CCXXXI P8 variation with time

	p1	p2	p3	p4	p5	p6	p7	p8
mean	0.587364	0.54265	0.533175	0.51812	0.5031	0.133038	0.10498	0.092646
median	0.58807	0.54265	0.53314	0.51814	0.50312	0.13296	0.10497	0.0927
mode	0.58909	0.5447	0.53273	0.51814	0.50291	0.13296	0.10559	0.0927
standard deviation	0.001606	0.002112	0.001864	0.001842	0.001871	0.001579	0.001561	0.00016
variance	2.58E-06	4.46E-06	3.48E-06	3.39E-06	3.5E-06	2.49E-06	2.44E-06	2.57E-08
skew	-0.91443	-0.16874	0.027184	0.004165	0.008121	0.021052	0.050392	-4.10982
kurtosis	0.49892	-0.27249	-0.15374	-0.04851	-0.20066	-0.38295	-0.42232	23.0868

CCXXXXII Pressure Readings with Statistical Data

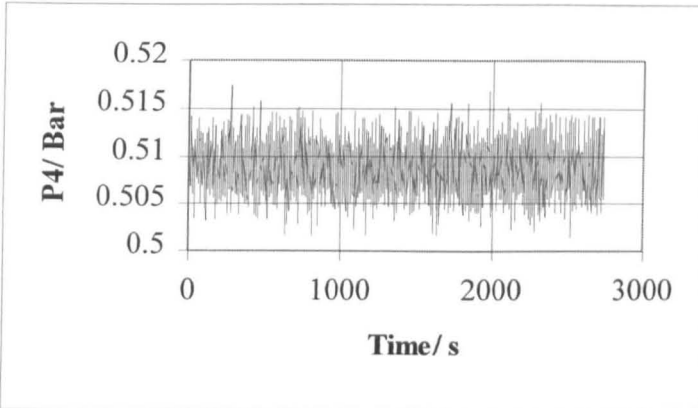
Long Swirly-flo Pipe Arrangement (pos 3)

Run: 2kglf35

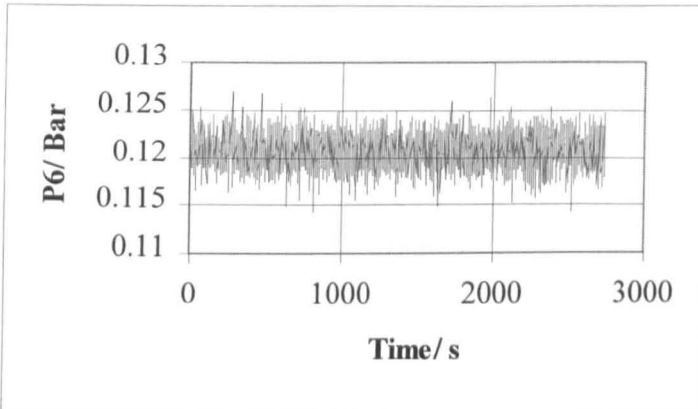
Volumetric Flow: 2.144 l/s

Mass Flow: 2.205 Kg/s

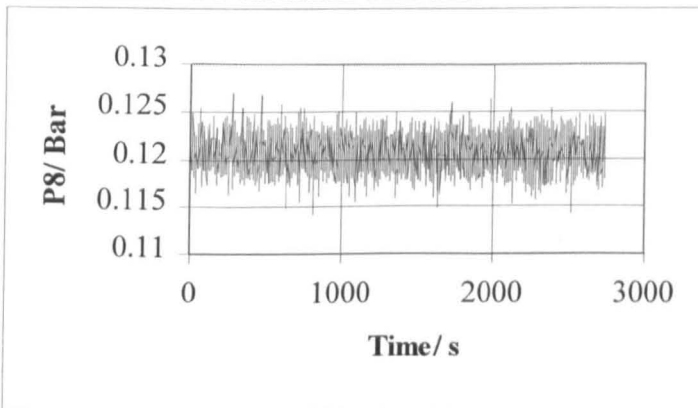
Number of Data Points:2735



CCXXXIII P4 variation with time



CCXXXIV P6 variation with time



CCXXXV P8 variation with time

	p1	p2	p3	p4	p5	p6	p7	p8
mean	0.637031	0.544781	0.530771	0.508819	0.493951	0.120747	0.091784	0.073424
median	0.63717	0.5447	0.53069	0.50873	0.49391	0.12068	0.09188	0.07327
mode	0.63819	0.54409	0.53048	0.50873	0.49432	0.12191	0.09188	0.07306
standard deviation	0.002148	0.003041	0.002464	0.002366	0.002274	0.001751	0.001708	0.000489
variance	4.62E-06	9.25E-06	6.07E-06	5.6E-06	5.17E-06	3.07E-06	2.92E-06	2.39E-07
skew	-0.2779	0.055923	0.165944	0.077122	0.001168	-0.06087	0.000356	1.437701
kurtosis	0.357068	0.001182	0.112113	-0.08453	0.030794	-0.00934	0.035429	1.504969

CCXXXVI Pressure Readings and Statistical Data

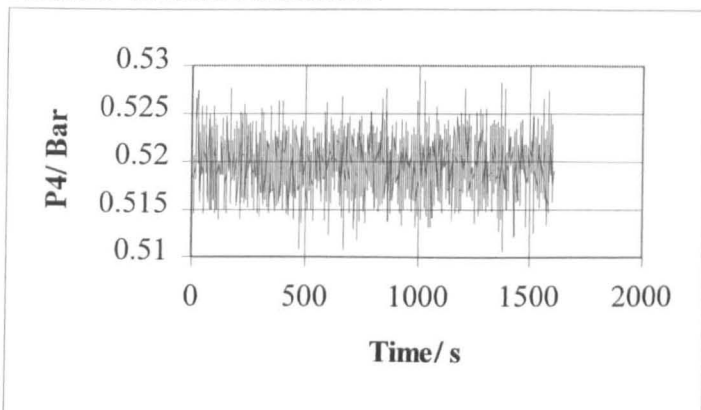
Long Swirly-flo Pipe Arrangement (pos 3)

Run: 2kglsf40

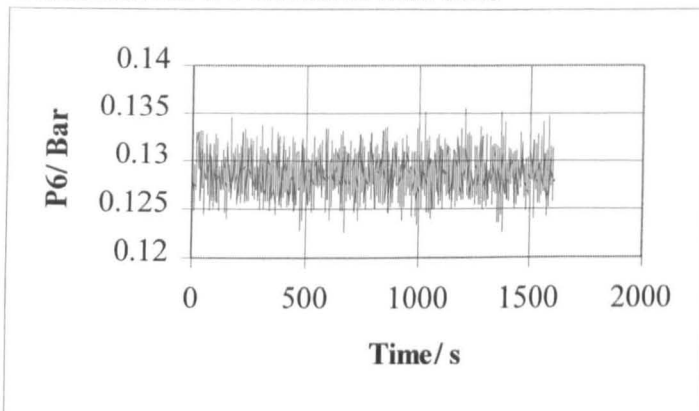
Volumetric Flow: 2.485 l/s

Mass Flow: 2.559 Kg/s

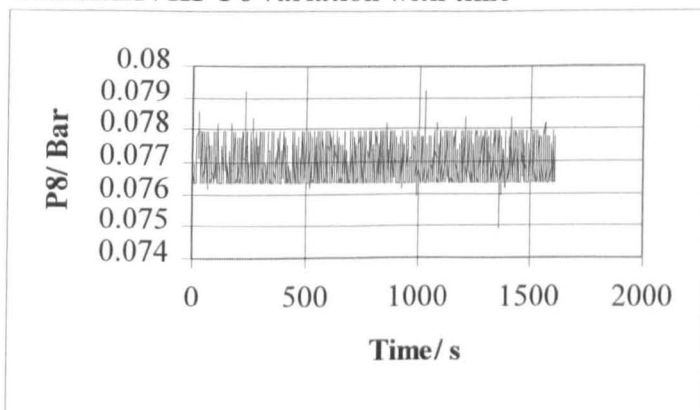
Number of Data Points:1607



CCXXXXVII P4 variation with time



CCXXXXVIII P6 variation with time



CCXLIX P8 variation with time

	p1	p2	p3	p4	p5	p6	p7	p8
mean	0.699055	0.564406	0.547063	0.519736	0.504805	0.128688	0.099465	0.076906
median	0.69956	0.56434	0.54706	0.51978	0.50476	0.12866	0.09945	0.07674
mode	0.69956	0.56495	0.54603	0.51916	0.50435	0.12907	0.09925	0.07633
standard deviation	0.002505	0.003466	0.002968	0.002678	0.002618	0.001934	0.001877	0.000586
variance	6.27E-06	1.2E-05	8.81E-06	7.17E-06	6.85E-06	3.74E-06	3.52E-06	3.43E-07
skew	-0.27573	0.104594	0.054938	-0.00203	0.015123	0.087154	0.022858	0.631241
kurtosis	0.066934	0.079185	0.078055	0.118375	0.132712	0.17943	0.194735	-0.68454

CCL Pressure Readings and Statistical Data

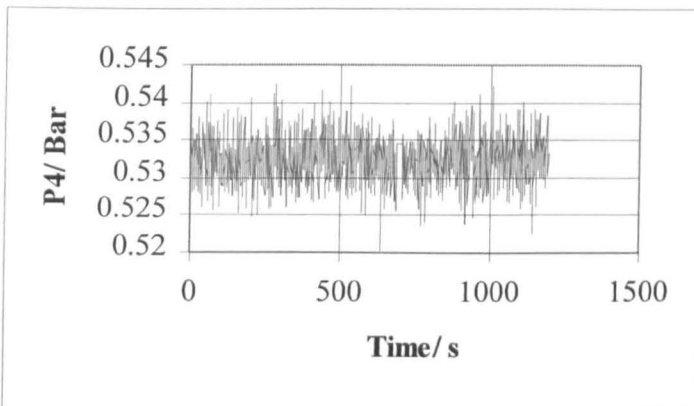
Long Swirly-flo Pipe Arrangement (pos 3)

Run: 2kglsf45

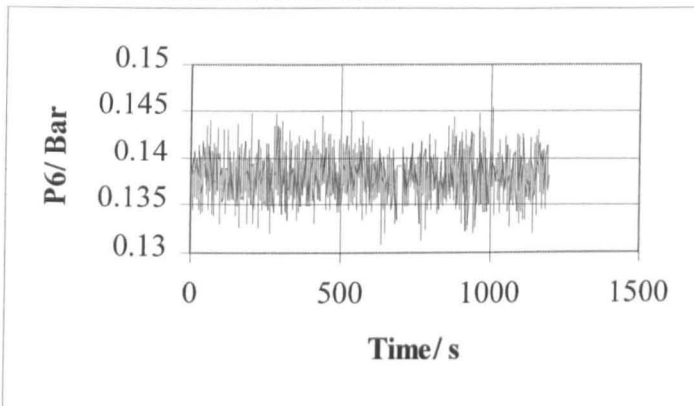
Volumetric Flow: 2.854 l/s

Mass Flow: 2.927 Kg/s

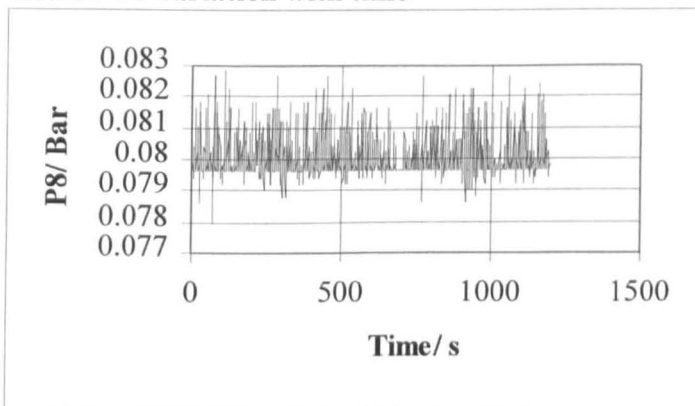
Number of Data Points:1197



CCLI P4 variation with time



CCLII P6 variation with time



CCLIII P8 variation with time

	p1	p2	p3	p4	p5	p6	p7
mean	0.775348	0.588246	0.566323	0.532393	0.517658	0.138027	0.108386
median	0.77526	0.58828	0.56629	0.53246	0.51764	0.13807	0.10845
mode	0.77526	0.58991	0.56915	0.53123	0.51969	0.13869	0.10866
standard standard	0.002646	0.004257	0.003364	0.003077	0.00307	0.002275	0.002219
variance	7E-06	1.81E-05	1.13E-05	9.47E-06	9.42E-06	5.18E-06	4.92E-06
skew	0.057968	0.038971	0.043066	0.087241	0.098075	0.115222	0.142247
kurtosis	-0.0301	-0.02682	0.145595	0.217915	0.085333	0.05982	0.041112

CCLIV Pressure Readings and Statistical Data

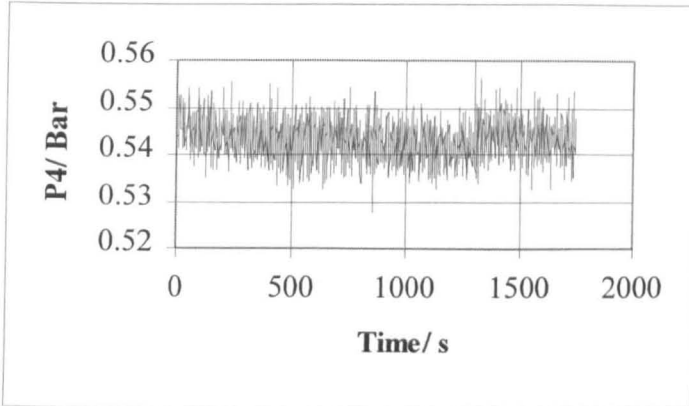
Long Swirly-flo Pipe Arrangement (pos 3)

Run: 2kglsf50

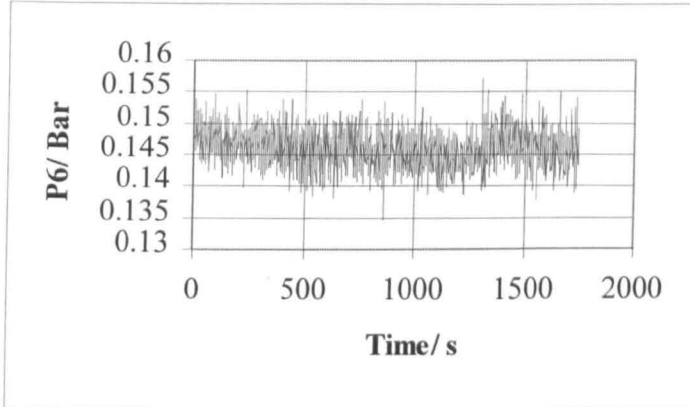
Volumetric Flow: 3.147 l/s

Mass Flow: 3.243 Kg/s

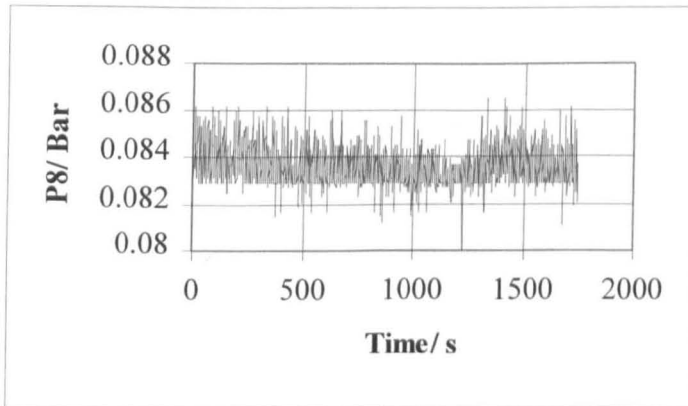
Number of Data Points:1752



CCLV P6 variation with time



CCLVI P6 variation with time



CCLLVII P8 variation with time

	p1	p2	p3	p4	p5	p6	p7	p8
mean	0.842034	0.608266	0.582164	0.54324	0.528746	0.14615	0.116259	0.083563
median	0.84175	0.60812	0.58224	0.5431	0.52869	0.14605	0.11623	0.08329
mode	0.83357	0.60628	0.58429	0.54494	0.52828	0.14564	0.11602	0.08288
standard deviation	0.007625	0.005708	0.004476	0.00399	0.00394	0.002902	0.002813	0.000817
variance	5.81E-05	3.26E-05	2E-05	1.59E-05	1.55E-05	8.42E-06	7.91E-06	6.67E-07
skew	0.245996	0.110975	0.087335	0.077585	0.063183	0.023585	0.069246	0.708446
kurtosis	-0.34752	-0.03871	-0.00641	0.095297	0.16134	0.083252	0.22828	0.622948

CCLLVIII Pressure Readings and Statistica Data

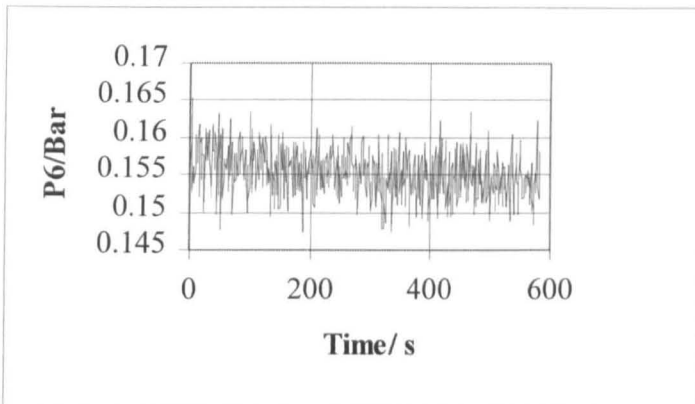
Long Swirly-flo Pipe Arrangement (pos 3)

Run: 2kgl55

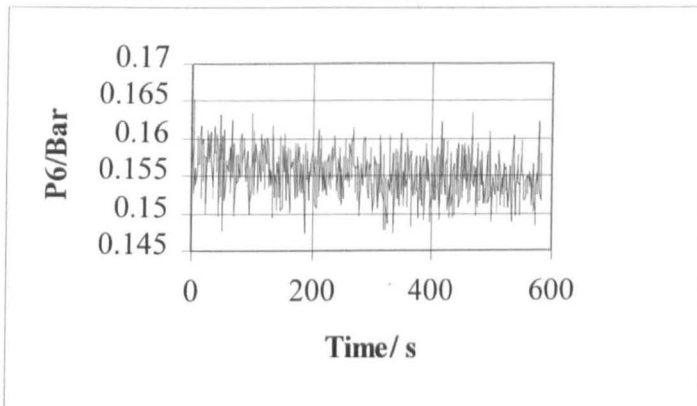
Volumetric Flow: 3.334 l/s

Mass Flow: 3.423 Kg/s

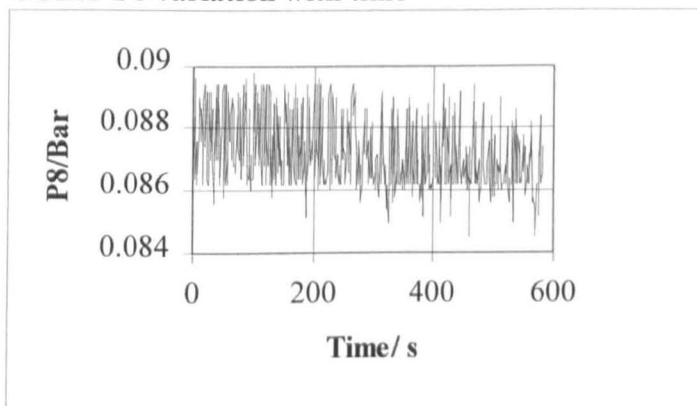
Number of Data Points:582



CCLIX P4 variation with time



CCLX P6 variation with time



CCLXI P8 variation with time

	p1	p2	p3	p4	p5	p6	p7	p8
mean	0.91674	0.630999	0.600035	0.555704	0.541227	0.155297	0.125244	0.087139
median	0.91642	0.63093	0.60004	0.55578	0.54117	0.15526	0.12543	0.08677
mode	0.91131	0.63513	0.60066	0.55783	0.54097	0.15669	0.12564	0.08615
standard deviation	0.008643	0.006215	0.00486	0.004364	0.004229	0.003131	0.003125	0.001132
variance	7.47E-05	3.86E-05	2.36E-05	1.9E-05	1.79E-05	9.8E-06	9.76E-06	1.28E-06
skew	0.223259	0.035235	0.029598	0.014329	0.021273	0.028904	-0.01385	0.571889
kurtosis	-0.85371	0.285269	-0.04649	-0.21131	-0.24143	-0.30425	-0.30465	-0.64445

CCLXII Pressure Readings and Statistical Data

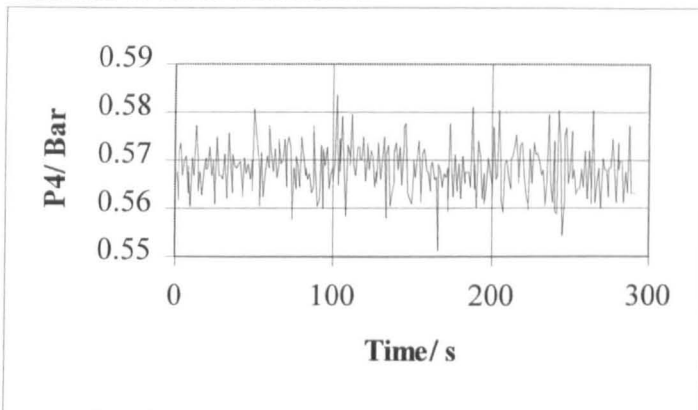
Long Swirly-flo Pipe Arrangement (pos 3)

Run: 2kglsf60

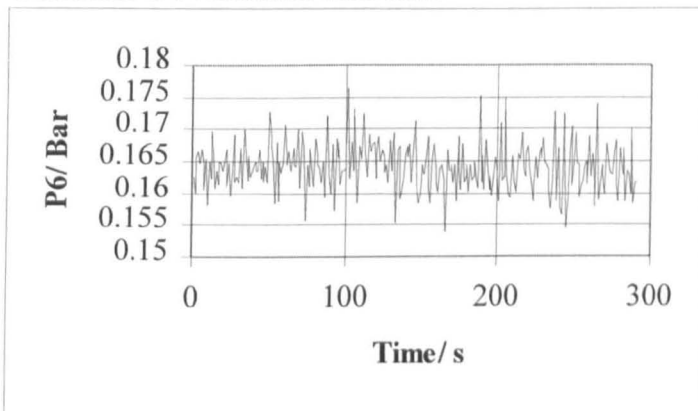
Volumetric Flow: 3.696 l/s

Mass Flow: 3.784 Kg/s

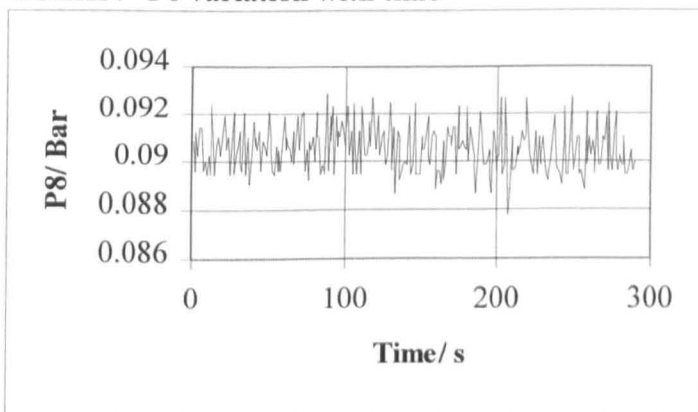
Number of Data Points:291



CCLXIII P4 variation with time



CCLXIV P6 variation with time



CCLXV P8 variation with time

	p1	p2	p3	p4	p5	p6	p7	p8
mean	0.992611	0.654217	0.618382	0.568115	0.553588	0.164214	0.133979	0.090553
median	0.99314	0.65436	0.61825	0.56806	0.55365	0.16426	0.13382	0.09045
mode	0.99416	0.65129	0.61743	0.5699	0.55406	0.16262	0.13321	0.09106
standard deviation	0.005695	0.007117	0.005604	0.005098	0.004929	0.003721	0.003566	0.000958
variance	3.24E-05	5.07E-05	3.14E-05	2.6E-05	2.43E-05	1.38E-05	1.27E-05	9.17E-07
skew	-0.29225	0.109546	0.165818	0.130966	0.189088	0.293933	0.251801	0.260163
kurtosis	-0.38195	-0.03738	0.02093	0.221094	0.337864	0.428445	0.405771	-0.43466

CCLXV Pressure Readings and Statistical Data

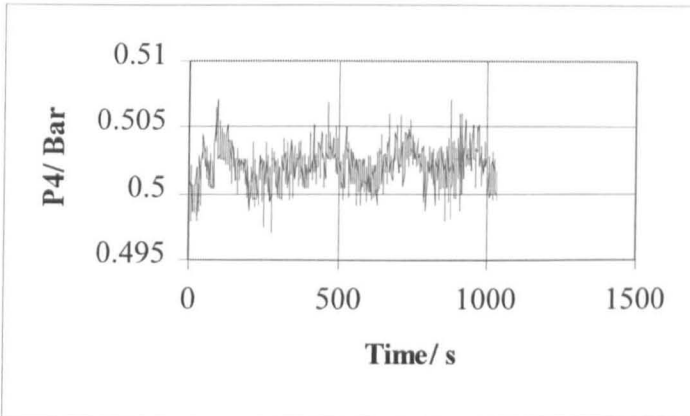
Long Swirly-flo Pipe Arrangement (pos 4)

Run: 2kglsf20

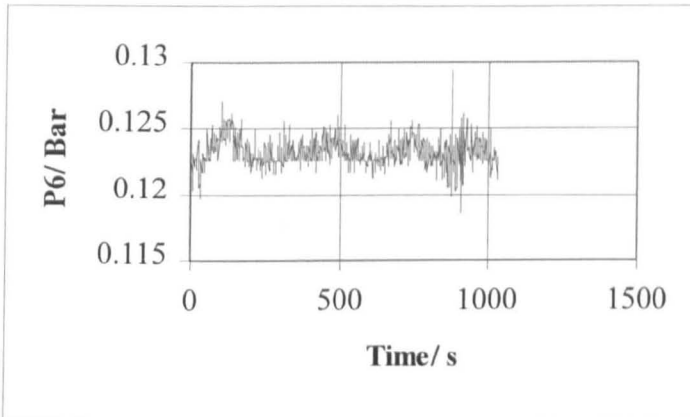
Volumetric Flow: 0.889 l/s

Mass Flow: 0.907 Kg/s

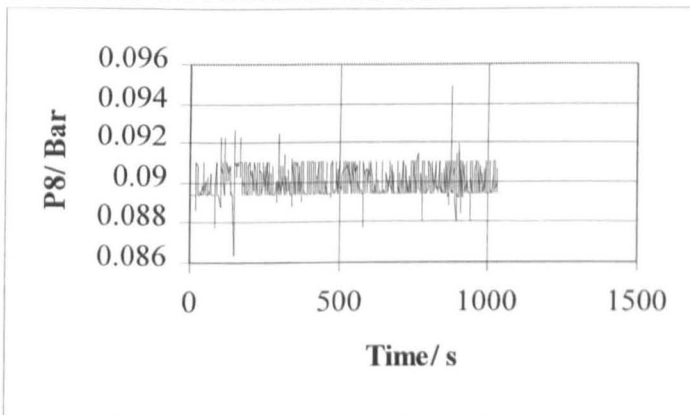
Number of Data Points:1031



CCLXVI P4 variation with time



CCLXVII P6 variation with time



CCLXVIII P8 variation with time

	p1	p2	p3	p4	p5	p6	p7	p8
mean	0.49905	0.512493	0.508435	0.502091	0.48721	0.123224	0.0947	0.089998
median	0.49907	0.51258	0.50839	0.50218	0.48737	0.12314	0.09475	0.08963
mode	0.49907	0.5136	0.50778	0.50259	0.48778	0.12252	0.09515	0.08943
standard deviation	0.000184	0.00164	0.001635	0.001429	0.001548	0.00101	0.001114	0.000721
variance	3.4E-08	2.69E-06	2.67E-06	2.04E-06	2.4E-06	1.02E-06	1.24E-06	5.21E-07
skew	-13.8956	-0.1241	-0.01804	-0.03164	-0.03502	0.434635	-0.09289	0.742335
kurtosis	254.2848	0.037053	0.301575	0.796822	0.140185	2.161469	2.354099	2.190959

CCLXIX Pressure Readings and Statistical Data

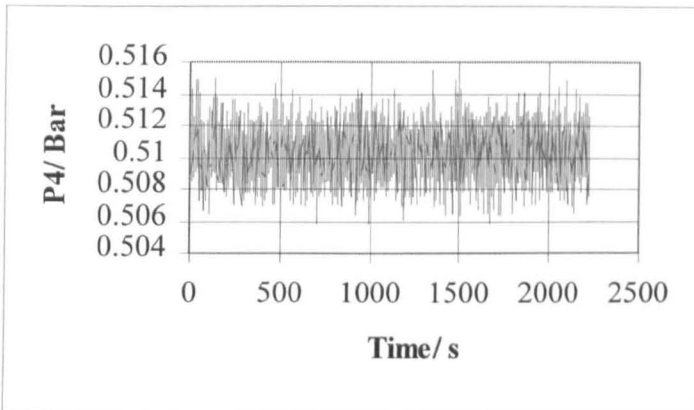
Long Swirly-flo Pipe Arrangement (pos 4)

Run: 2kglsf25

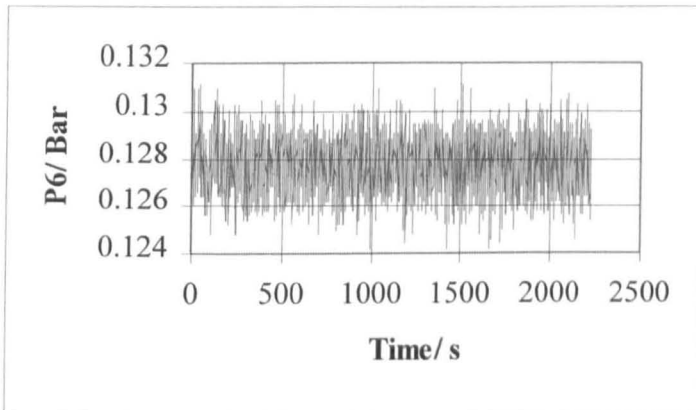
Volumetric Flow: 1.321 l/s

Mass Flow: 1.358 Kg/s

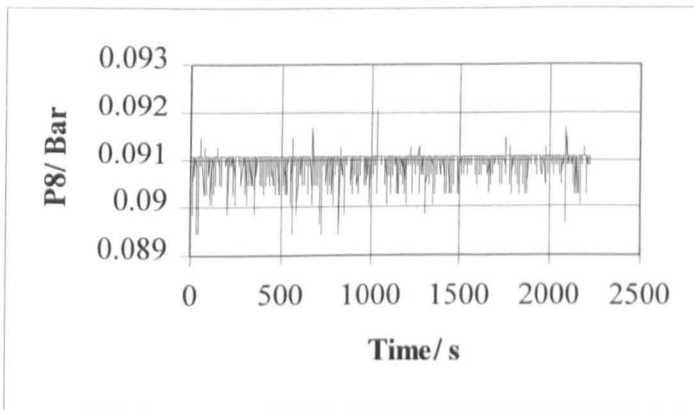
Number of Data Points:2226



CCLXX P4 variation with time



CCLXXI P6 variation with time



CCLXXII P8 variation with time

	p1	p2	p3	p4	p5	p6	p7	p8
mean	0.537718	0.52719	0.52045	0.510346	0.495133	0.127796	0.099662	0.090971
median	0.53794	0.52731	0.52046	0.51037	0.49514	0.12784	0.09966	0.09106
mode	0.53999	0.52833	0.52087	0.51078	0.49473	0.12846	0.09925	0.09106
standard deviation	0.001903	0.001609	0.001598	0.001578	0.001485	0.00116	0.001081	0.000227
variance	3.62E-06	2.59E-06	2.55E-06	2.49E-06	2.2E-06	1.35E-06	1.17E-06	5.16E-08
skew	-0.64585	0.115313	-0.05962	-0.04535	-0.08457	-0.12015	-0.07206	-2.86308
kurtosis	-0.31096	-0.16131	-0.20881	-0.25717	-0.09113	-0.22472	0.029978	10.62032

CCLXXIII Pressure Readings and Statistical Data

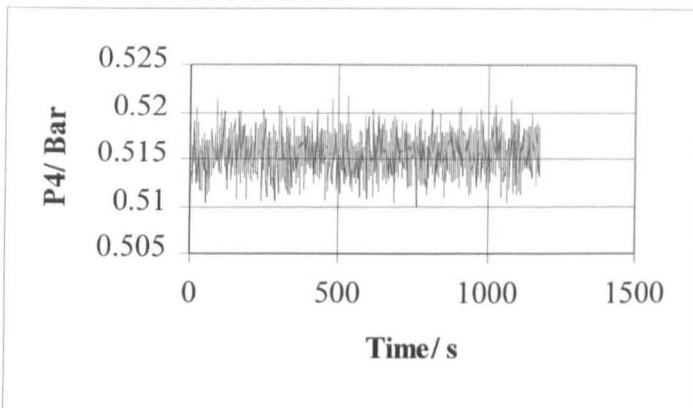
Long Swirly-flo Pipe Arrangement (pos 4)

Run: 2kglsf30

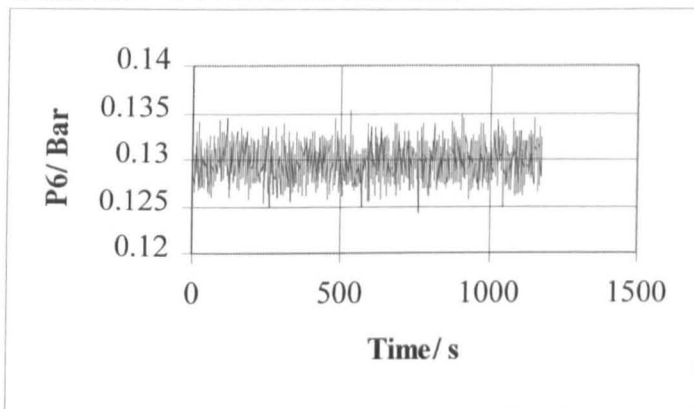
Volumetric Flow: 1.768 l/s

Mass Flow: 1.812 Kg/s

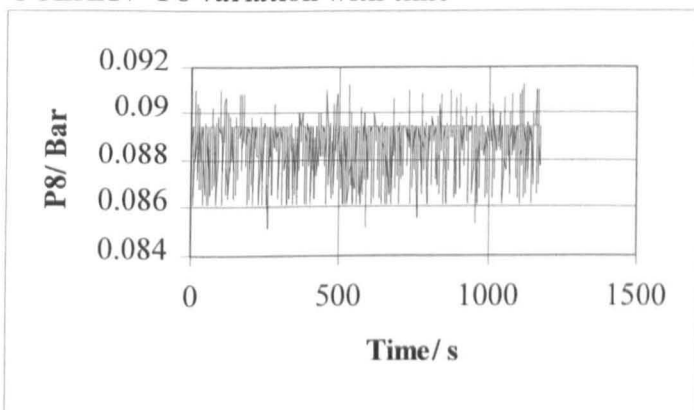
Number of Data Points:1177



CCLXXIV P4 variation with time



CCLXXV P6 variation with time



CCLXXVI P8 variation with time

	p1	p2	p3	p4	p5	p6	p7	p8
mean	0.586432	0.540585	0.530572	0.515575	0.500065	0.129846	0.101216	0.08877
median	0.58704	0.54061	0.53048	0.51569	0.50005	0.12989	0.10129	0.08922
mode	0.58704	0.54122	0.53048	0.5163	0.50066	0.1305	0.1015	0.08943
standard deviation	0.001999	0.002145	0.001975	0.002093	0.002093	0.001862	0.001808	0.001083
variance	4E-06	4.6E-06	3.9E-06	4.38E-06	4.38E-06	3.47E-06	3.27E-06	1.17E-06
skew	-0.61009	0.004208	0.057511	0.039584	0.078462	0.033251	0.005093	-1.04308
kurtosis	0.002107	-0.08019	-0.05983	-0.30957	-0.3061	-0.47848	-0.38299	0.560832

CCLXXVII Pressure Readings and Statistical Data

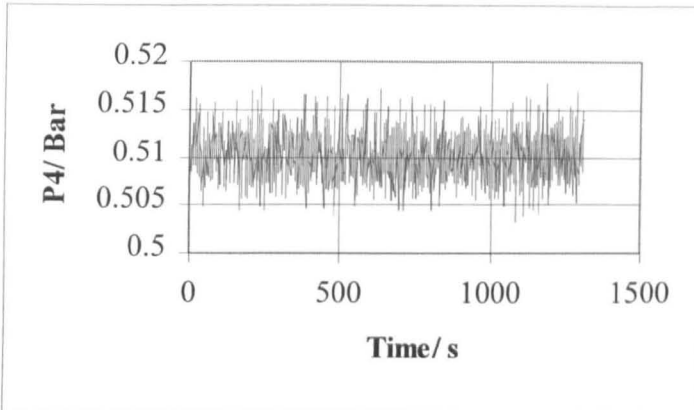
Long Swirly-flo Pipe Arrangement (pos 4)

Run: 2kglf35

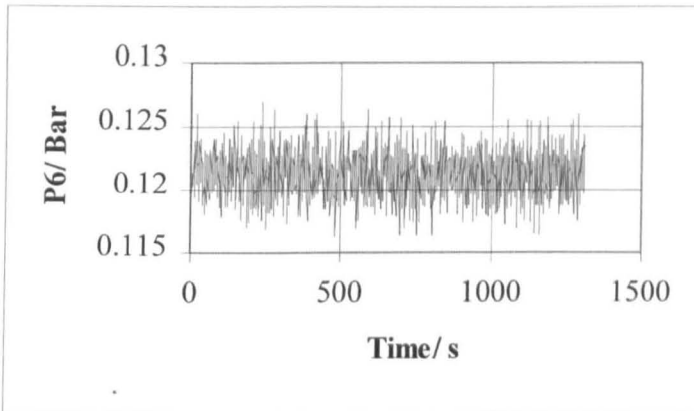
Volumetric Flow: 2.15 l/s

Mass Flow: 2.206 Kg/s

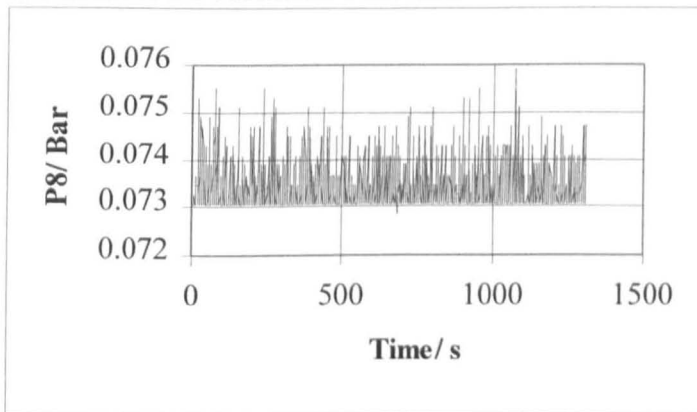
Number of Data Points:1312



CCLXXVIII P4 variation with time



CCLXXIX P6 variation with time



CCLXXX P8 variation with time

	p1	p2	p3	p4	p5	p6	p7	p8
mean	0.637524	0.546399	0.531717	0.510307	0.494744	0.121326	0.091886	0.073421
median	0.63717	0.54634	0.53171	0.51016	0.49473	0.1213	0.09188	0.07327
mode	0.63819	0.54552	0.53171	0.50975	0.49514	0.12089	0.09209	0.07306
standard deviation	0.002046	0.003071	0.002507	0.002381	0.002267	0.00175	0.001701	0.000494
variance	4.19E-06	9.43E-06	6.29E-06	5.67E-06	5.14E-06	3.06E-06	2.89E-06	2.44E-07
skew	-0.15938	0.087934	0.180549	0.085894	0.06026	-0.00086	0.033318	1.629022
kurtosis	0.767843	-0.23218	-0.10039	-0.06559	0.017095	0.030896	-0.01403	2.439566

CCLXXXI Pressure Readings and Statistical Data

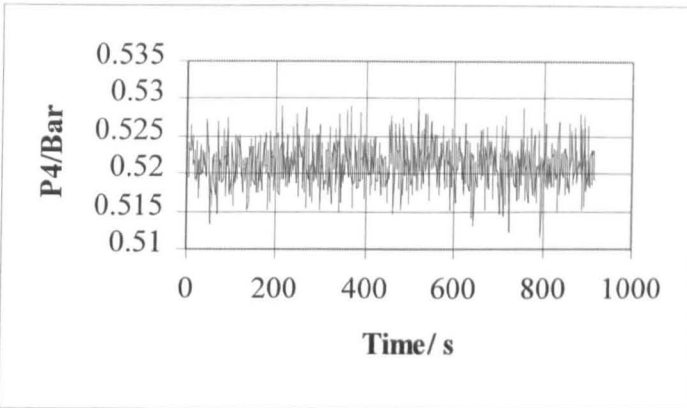
Long Swirly-flo Pipe Arrangement (pos 4)

Run: 2kglsf40

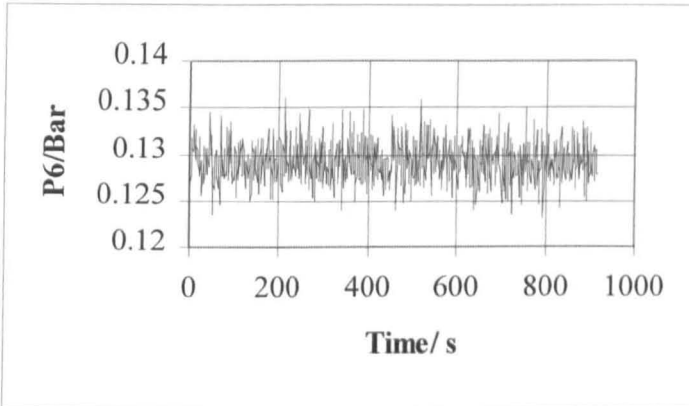
Volumetric Flow:2.481 l/s

Mass Flow: 2.569 Kg/s

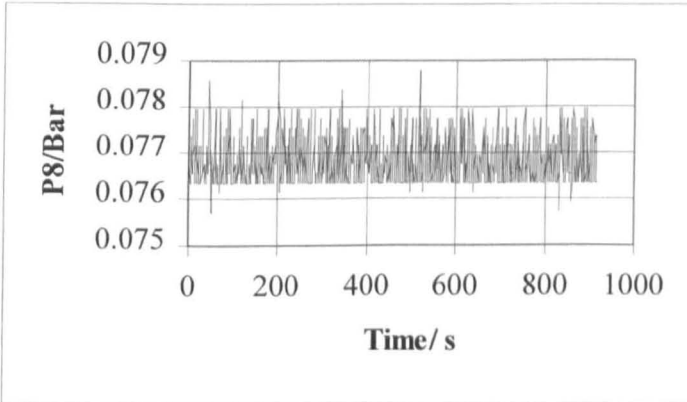
Number of Data Points:916



CCLXXXII P4 variation with time



CCLXXXIII P6 variation with time



CCLXXXIV P8 variation with time

	p1	p2	p3	p4	p5	p6	p7	p8
mean	0.6994	0.566246	0.548125	0.52133	0.505589	0.129244	0.099522	0.076809
median	0.69956	0.56618	0.54808	0.52141	0.50557	0.12928	0.09966	0.07674
mode	0.70059	0.56577	0.5491	0.52182	0.50496	0.12948	0.09925	0.07633
standard deviation	0.002576	0.00368	0.003106	0.002776	0.00269	0.001994	0.001931	0.000525
variance	6.66E-06	1.35E-05	9.62E-06	7.67E-06	7.21E-06	3.96E-06	3.71E-06	2.74E-07
skew	-0.24337	0.129201	0.066025	-0.02564	-0.01728	0.095163	0.019944	0.890761
kurtosis	-0.05986	0.375032	0.16228	0.184851	0.195592	0.211635	0.295829	-0.12672

CCLXXXV Pressure Readings and Statistical Data

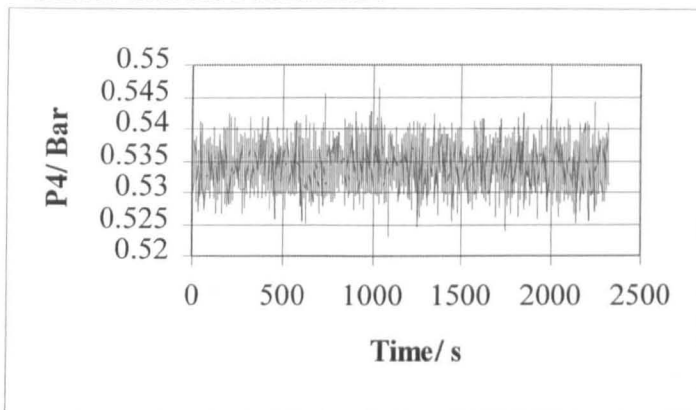
Long Swirly-flo Pipe Arrangement (pos 4)

Run: 2kglsf45

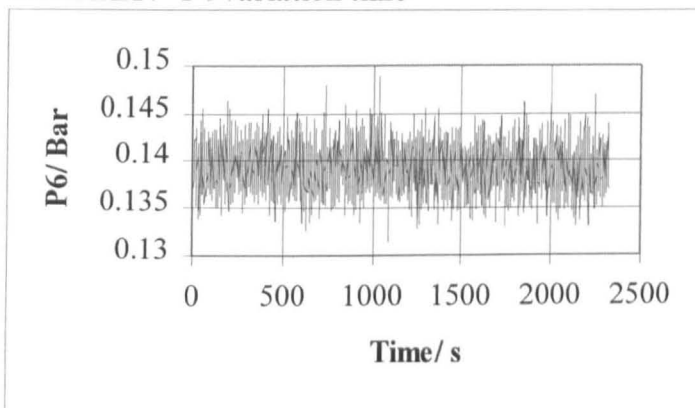
Volumetric Flow: 2.892 l/s

Mass Flow: 2.969 Kg/s

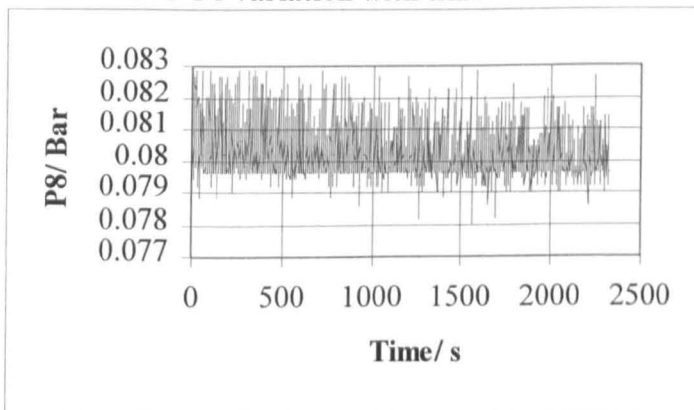
Number of Data Points:2324



CCLXXXV P4 variation time



CCLXXXVI P6 variation with time



CCLXXXVII P8 variation with time

	p1	p2	p3	p4	p5	p6	p7	p8
mean	0.775234	0.591646	0.56799	0.534231	0.520014	0.139396	0.109045	0.080174
median	0.77526	0.59175	0.56792	0.5343	0.5201	0.1395	0.10907	0.07981
mode	0.77526	0.59216	0.56895	0.53471	0.52092	0.1391	0.10968	0.07961
standard deviation	0.002724	0.004323	0.003405	0.003169	0.003165	0.002354	0.002302	0.000769
variance	7.42E-06	1.87E-05	1.16E-05	1E-05	1E-05	5.54E-06	5.3E-06	5.91E-07
skew	0.049809	-0.04635	0.004428	0.041819	0.047132	0.07791	0.049832	1.26427
kurtosis	0.374143	-0.01447	-0.0654	-0.01591	-0.02161	0.051845	-0.00915	1.242499

CCLXXXVIII Pressure Readings and Statistical Data

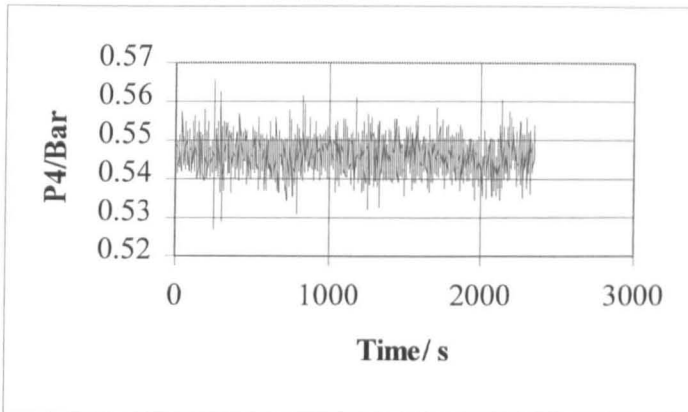
Long Swirly-flo Pipe Arrangement (pos 4)

Run: 2kglsf50

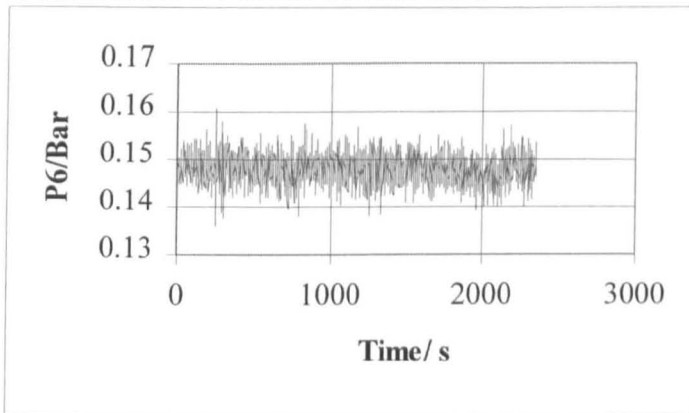
Volumetric Flow: 3.236 l/s

Mass Flow: 3.324 Kg/s

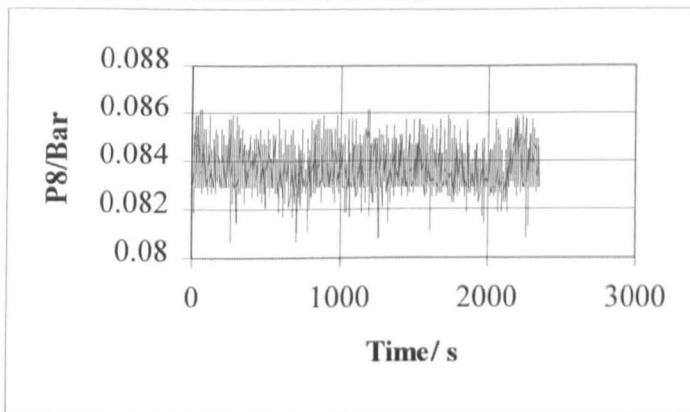
Number of Data Points:2345



CCLXXXIX P4 variation with time



CCLXC P6 variation with time



CCLXCI P8 variation with time

	p1	p2	p3	p4	p5	p6	p7	p8
mean	0.849834	0.613852	0.585784	0.546092	0.531934	0.147921	0.117801	0.083587
median	0.84993	0.61385	0.58593	0.54617	0.53197	0.14789	0.11766	0.08349
mode	0.85096	0.61303	0.58756	0.5476	0.53135	0.14871	0.11664	0.08288
standard deviation	0.005963	0.005753	0.004444	0.004042	0.003961	0.0029	0.002844	0.000812
variance	3.56E-05	3.31E-05	1.98E-05	1.63E-05	1.57E-05	8.41E-06	8.09E-06	6.59E-07
skew	-0.25008	-0.05167	-0.05836	0.032754	0.00644	-0.02219	0.042011	0.583325
kurtosis	0.071036	0.892098	0.780812	0.851983	0.678978	0.363194	0.319558	0.291764

CCLXCII Pressure Readings and Statistical Data

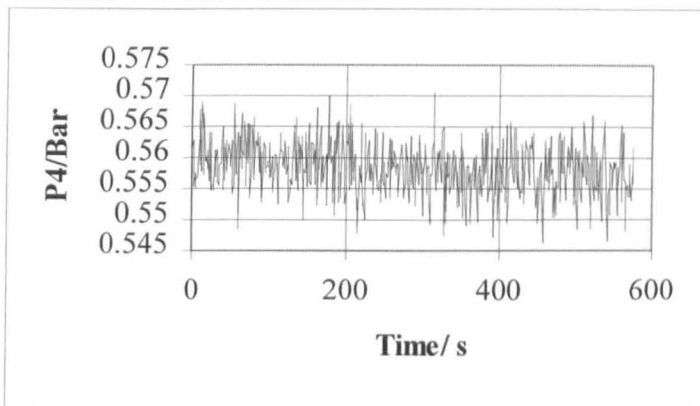
Long Swirly-flo Pipe Arrangement (pos 4)

Run: 2kglsf55

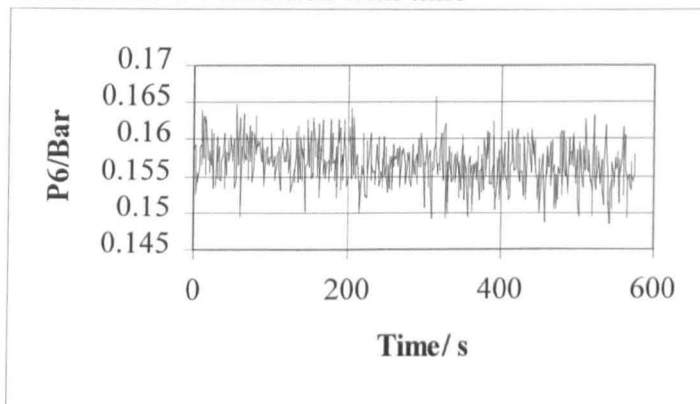
Volumetric Flow: 3.502 l/s

Mass Flow: 3.588 Kg/s

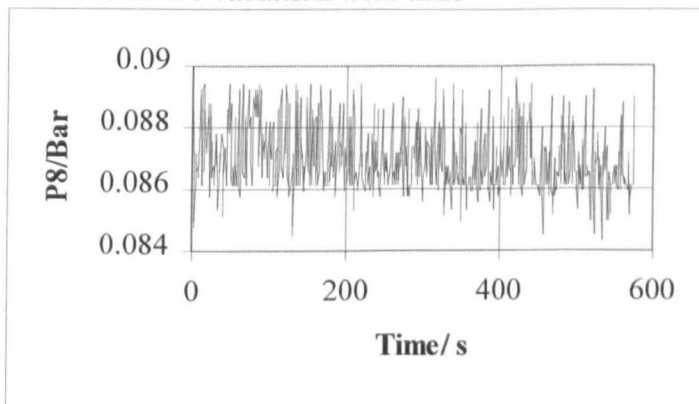
Number of Data Points:576



CCLXCIII P4 variation with time



CCLXCIV P6 variation with time



CCLXCIV P8 variation with time

	p1	p2	p3	p4	p5	p6	p7	p8
mean	0.923061	0.636097	0.603379	0.558232	0.543983	0.156704	0.126518	0.086963
median	0.92256	0.63594	0.60342	0.55824	0.54404	0.15669	0.12646	0.08656
mode	0.92051	0.63819	0.60413	0.55926	0.54404	0.15649	0.12502	0.08615
standard deviation	0.007159	0.005767	0.00456	0.004166	0.003973	0.002973	0.002975	0.001079
variance	5.13E-05	3.33E-05	2.08E-05	1.74E-05	1.58E-05	8.84E-06	8.85E-06	1.16E-06
skew	0.170698	0.057773	0.030258	-0.02162	-0.09134	-0.02476	-0.03723	0.629526
kurtosis	-0.73279	-0.04751	-0.08128	0.023016	0.113364	0.036554	0.032456	-0.31312

CCLXCVI Pressure Readings and Statistical Data

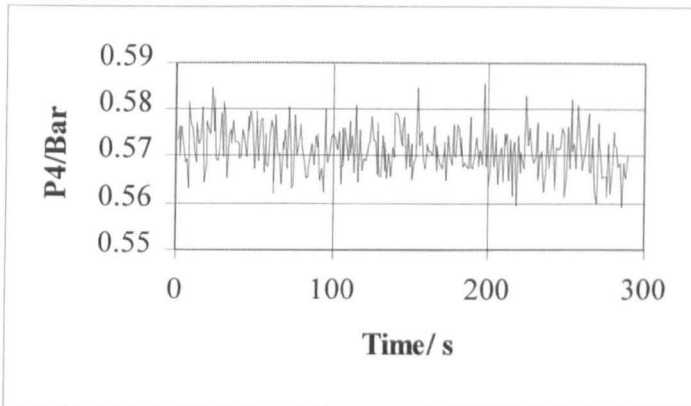
Long Swirly-flo Pipe Arrangement (pos 4)

Run: 2kglsf60

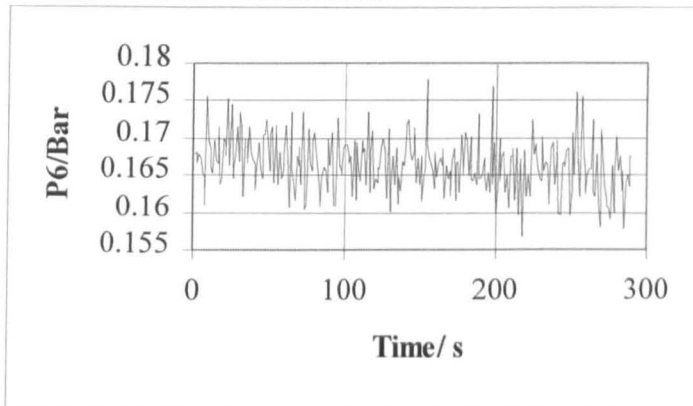
Volumetric Flow: 3.722 l/s

Mass Flow: 3.811 Kg/s

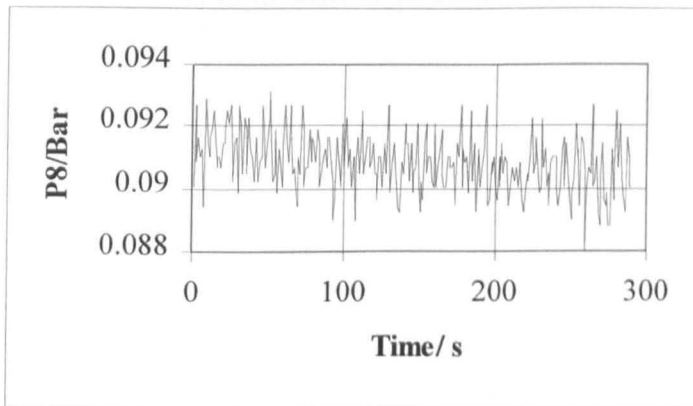
Number of Data Points:290



CCLXCVII P4 variation with time



CCLXCVIII P6 variation with time



CCLXCIX P8 variation with time

	p1	p2	p3	p4	p5	p6	p7	p8
mean	1.003022	0.660166	0.622767	0.571463	0.557099	0.16646	0.135953	0.090832
median	1.00235	0.66008	0.62255	0.57133	0.55672	0.16641	0.13587	0.09086
mode	0.99621	0.65456	0.61907	0.57481	0.5602	0.16446	0.13668	0.09106
standard deviation	0.007107	0.007028	0.005638	0.004939	0.004899	0.003618	0.00345	0.000931
variance	5.05E-05	4.94E-05	3.18E-05	2.44E-05	2.4E-05	1.31E-05	1.19E-05	8.67E-07
skew	0.323131	0.011571	0.064283	0.119304	0.202148	0.225459	0.203183	0.074141
kurtosis	-0.46694	-0.405	-0.32173	-0.18166	-0.1514	0.185241	0.141414	-0.32011

CCC Pressure Readings and Statistical Data

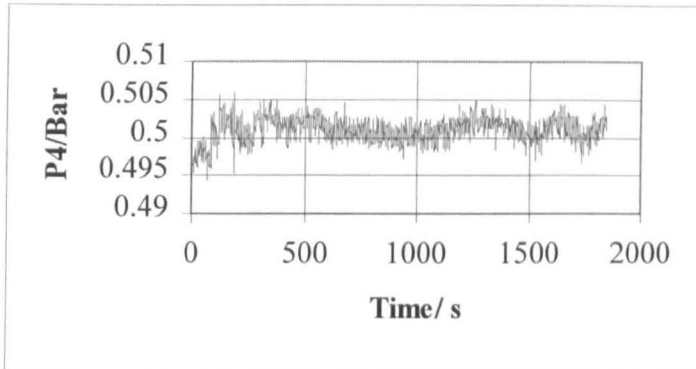
Long Swirly-flo Pipe Arrangement (pos 5)

Run: 2kglsf20

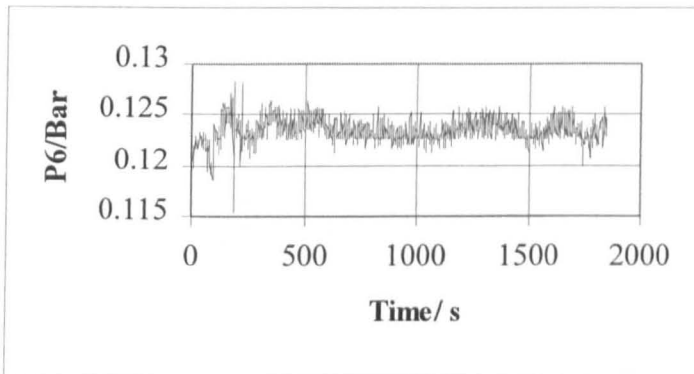
Volumetric Flow: 0.905 l/s

Mass Flow: 0.929 Kg/s

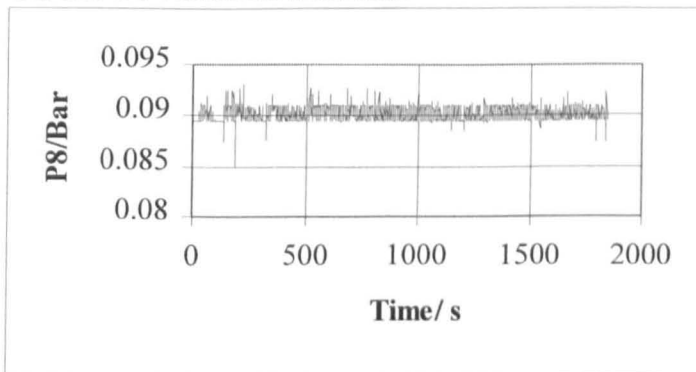
Number of Data Points:1848



CCCI P4 variation with time



CCCII P6 variation with time



CCCIII P8 variation with time

	p1	p2	p3	p4	p5	p6	p7	p8
mean	0.499098	0.513286	0.509136	0.501001	0.487716	0.123413	0.095162	0.090202
median	0.49907	0.5136	0.50921	0.50116	0.48778	0.12334	0.09515	0.09004
mode	0.49907	0.5136	0.50778	0.50259	0.48778	0.12252	0.09515	0.08943
standard deviation	0.000483	0.001813	0.001682	0.001556	0.001611	0.001103	0.001187	0.000734
variance	2.33E-07	3.29E-06	2.83E-06	2.42E-06	2.6E-06	1.22E-06	1.41E-06	5.38E-07
skew	20.33455	-0.63211	-0.3413	-0.49073	-0.33974	-0.14859	-0.47094	0.095088
kurtosis	454.005	2.336385	0.696985	0.530664	0.558359	2.547311	2.868114	1.080226

CCCIV Pressure Readings and Statistical Data

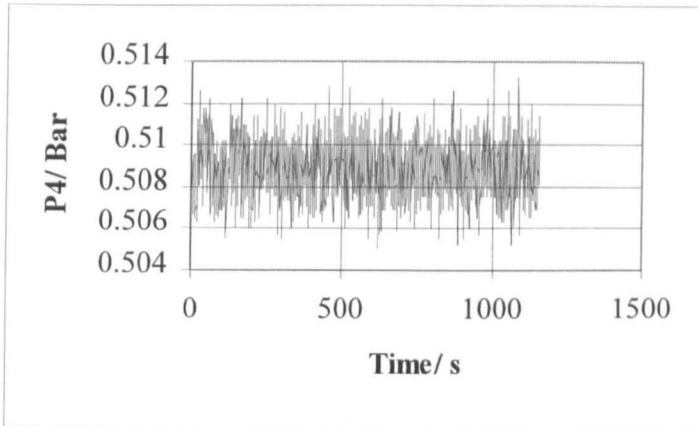
Long Swirly-flo Pipe Arrangement (pos 5)

Run: 2kglsf25

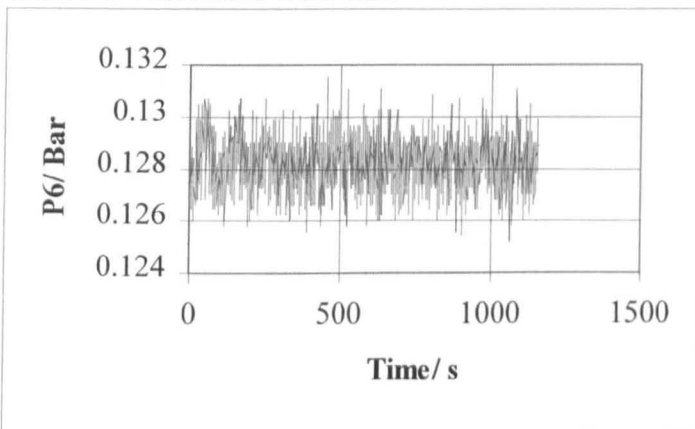
Volumetric Flow: 1.33 l/s

Mass Flow: 1.364 Kg/s

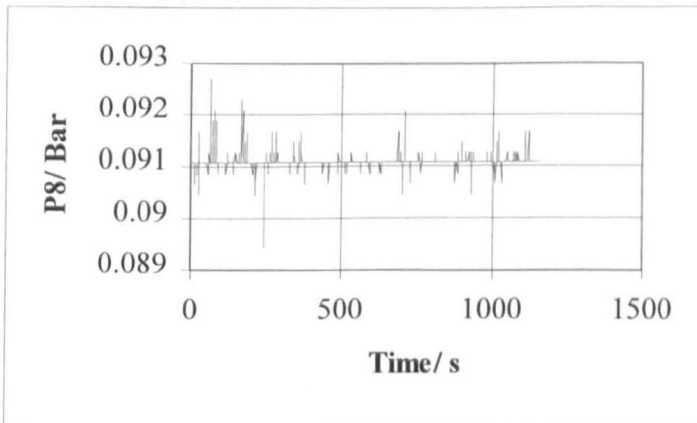
Number of Data Points:1159



CCCV P4 variation with time



CCCVI P6 variation with time



CCCVII P8 variation with time

	p1	p2	p3	p4	p5	p6	p7	p8
mean	0.539066	0.527875	0.520935	0.508829	0.495551	0.128234	0.099997	0.091071
median	0.53999	0.52813	0.52087	0.50893	0.49555	0.12825	0.09986	0.09106
mode	0.53999	0.52833	0.52087	0.50893	0.49555	0.12846	0.10006	0.09106
standard deviation	0.001337	0.001541	0.001434	0.001409	0.001318	0.001035	0.000964	0.000143
variance	1.79E-06	2.37E-06	2.06E-06	1.98E-06	1.74E-06	1.07E-06	9.29E-07	2.05E-08
skew	-1.79835	-0.00611	-0.05182	0.094044	0.004583	-0.07451	0.028072	2.658728
kurtosis	3.625903	-0.33063	-0.15325	-0.3133	0.028115	-0.19428	-0.11032	49.49604

CCCVIII Pressure Readings and Statistical Data

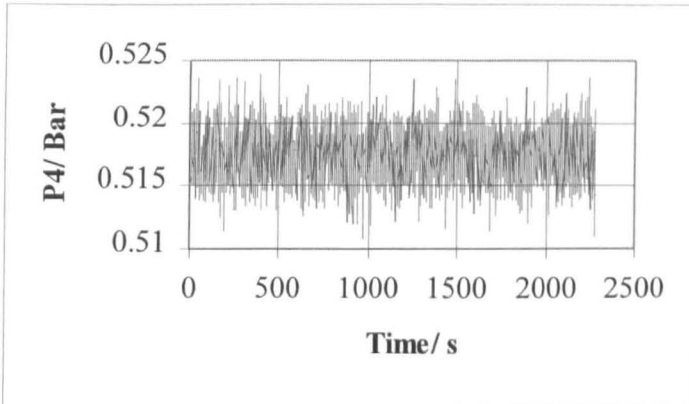
Long Swirly-flo Pipe Arrangement (pos 5)

Run: 2kglf30

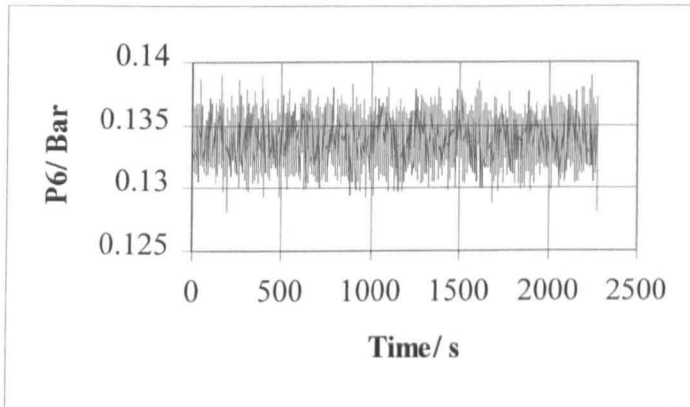
Volumetric Flow: 1.761 l/s

Mass Flow: 1.811 Kg/s

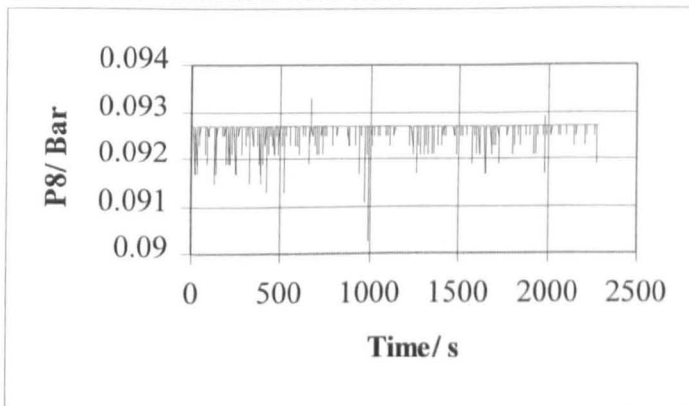
Number of Data Points:2280



CCCIX P4 variation with time



CCCX P6 variation with time



CCCXI P8 variation with time

	p1	p2	p3	p4	p5	p6	p7	p8
mean	0.588498	0.544279	0.534187	0.517496	0.503963	0.133851	0.105299	0.092663
median	0.58909	0.54429	0.53417	0.51753	0.50394	0.13398	0.10538	0.0927
mode	0.58909	0.5447	0.53396	0.51773	0.50332	0.13419	0.10641	0.0927
standard deviation	0.00099	0.002063	0.002033	0.002078	0.002083	0.001813	0.001781	0.000155
variance	9.8E-07	4.26E-06	4.13E-06	4.32E-06	4.34E-06	3.29E-06	3.17E-06	2.41E-08
skew	-1.94309	-0.06841	0.042587	-0.00546	-0.01607	-0.04583	-0.03152	-6.03635
kurtosis	4.267023	0.230724	-0.23595	-0.26883	-0.35684	-0.53906	-0.54699	51.44116

CCCXII Pressure Readings and Statistical Data

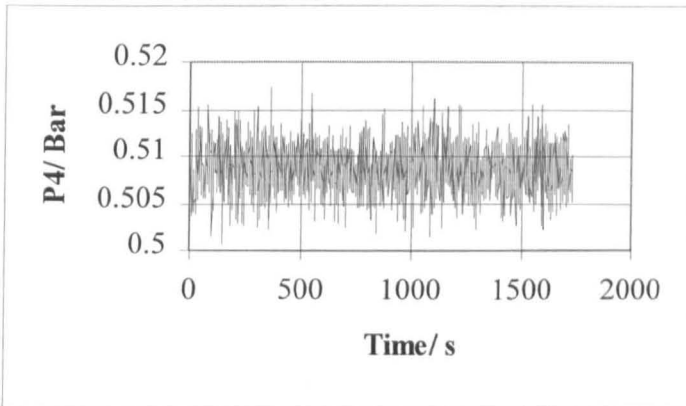
Long Swirly-flo Pipe Arrangement (pos 5)

Run: 2kglsf35

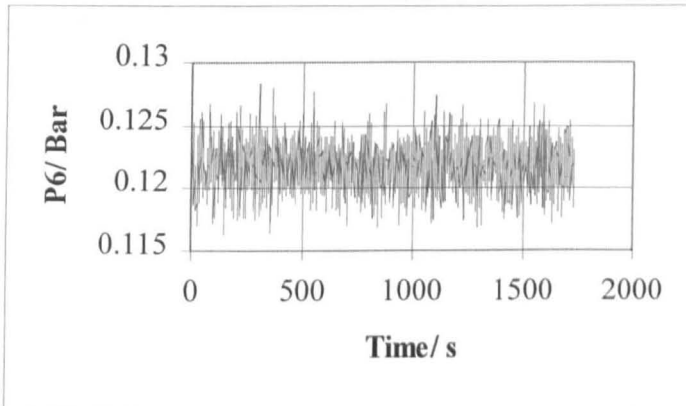
Volumetric Flow: 2.175 l/s

Mass Flow: 2.23 Kg/s

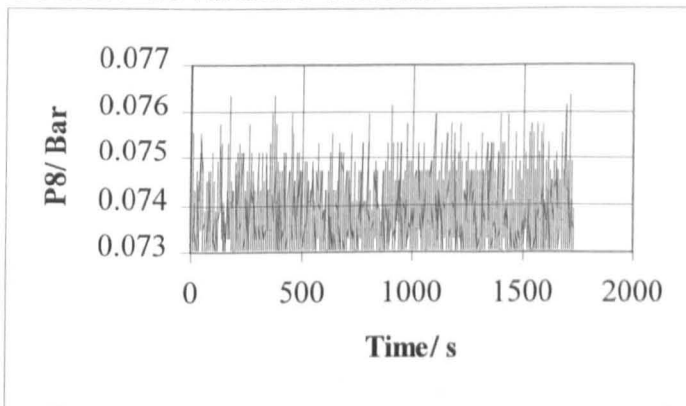
Number of Data Points:1731



CCCXIII P4 variation with time



CCCXIV P6 variation with time



CCCXV P8 variation with time

	p1	p2	p3	p4	p5	p6	p7	p8
mean	0.638671	0.546788	0.532073	0.508625	0.495153	0.121799	0.092407	0.073806
median	0.63819	0.54674	0.53192	0.50852	0.49514	0.12191	0.09249	0.07367
mode	0.63819	0.54695	0.5311	0.50975	0.49575	0.12252	0.09311	0.07306
standard deviation	0.002079	0.003169	0.002592	0.002448	0.002346	0.001791	0.001756	0.000677
variance	4.32E-06	1E-05	6.72E-06	5.99E-06	5.51E-06	3.21E-06	3.08E-06	4.58E-07
skew	0.309391	0.054296	0.113841	0.039241	0.008856	-0.00253	0.070064	0.877116
kurtosis	0.954234	0.138595	0.058817	0.007361	0.11829	0.119568	0.084653	0.279324

CCCXVI Pressure Readings and Statistical Data

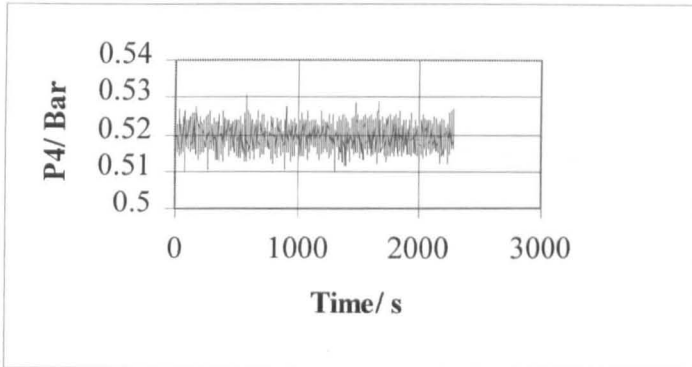
Long Swirly-flo Pipe Arrangement (pos 5)

Run: 2kglsf40

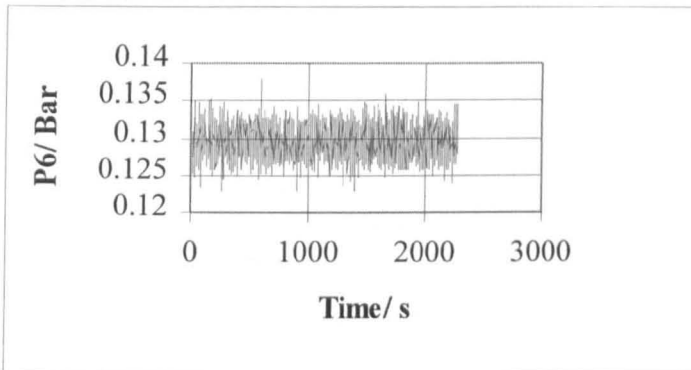
Volumetric Flow: 2.517 l/s

Mass Flow: 2.584 Kg/s

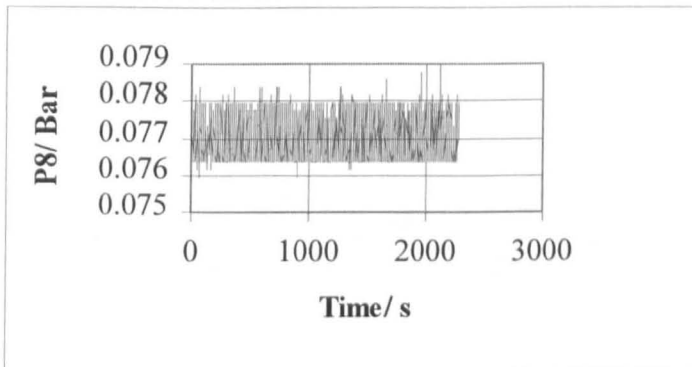
Number of Data Points:2277



CCCXVII P4 variation with time



CCCXVIII P6 variation with time



CCCXIX P8 variation with time

	p1	p2	p3	p4	p5	p6	p7	p8
mean	0.700921	0.566273	0.548291	0.519499	0.505887	0.129572	0.099927	0.076974
median	0.70059	0.56618	0.54828	0.51957	0.50598	0.12948	0.09986	0.07695
mode	0.70059	0.56618	0.54726	0.51896	0.50639	0.12968	0.10027	0.07633
standard deviation	0.002463	0.003626	0.003059	0.002766	0.002653	0.001979	0.001904	0.000592
variance	6.07E-06	1.31E-05	9.36E-06	7.65E-06	7.04E-06	3.91E-06	3.63E-06	3.51E-07
skew	-0.19164	0.053639	0.02473	-0.01494	-0.04475	0.041987	0.012415	0.458498
kurtosis	0.133531	0.036592	0.129385	0.135388	0.109134	0.074187	0.187613	-1.07018

CCCXX Pressure Readings and Statistical Data

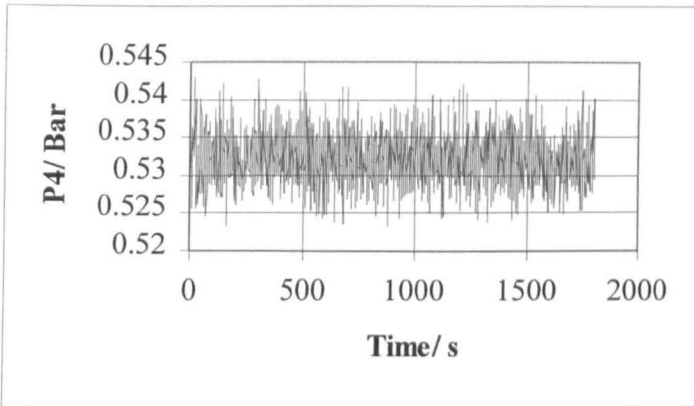
Long Swirly-flo Pipe Arrangement (pos 5)

Run: 2kglsf45

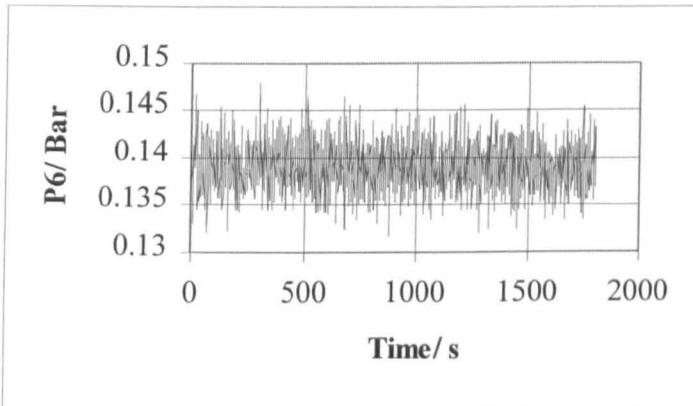
Volumetric Flow: 2.884 l/s

Mass Flow: 2.961 Kg/s

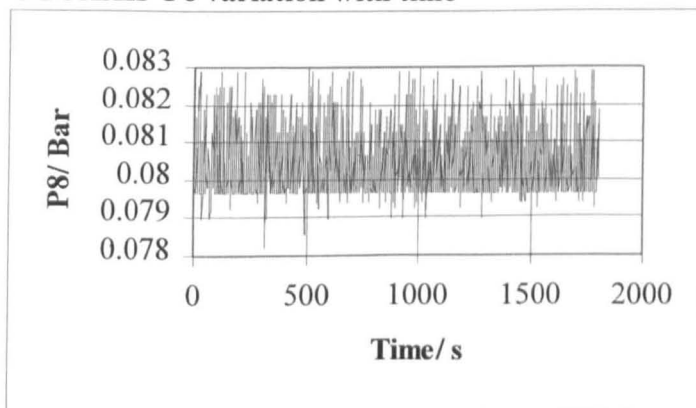
Number of Data Points:1807



CCCXXI P4 variation with time



CCCXXII P6 variation with time



CCCXXIII P8 variation with time

	p1	p2	p3	p4	p5	p6	p7	p8
mean	0.776233	0.589997	0.567336	0.532236	0.518729	0.139014	0.109032	0.080389
median	0.77628	0.58991	0.5671	0.53205	0.51867	0.13889	0.10886	0.08022
mode	0.77526	0.58623	0.56649	0.53123	0.51867	0.13889	0.10825	0.07961
standard deviation	0.002668	0.004424	0.00344	0.003204	0.003161	0.002336	0.00228	0.000831
variance	7.12E-06	1.96E-05	1.18E-05	1.03E-05	9.99E-06	5.45E-06	5.2E-06	6.91E-07
skew	0.149233	0.213469	0.190921	0.172651	0.162265	0.139297	0.125963	0.953521
kurtosis	0.068005	0.190869	0.069963	0.049792	0.028157	0.127014	0.08238	0.234133

CCCXXIV Pressure Readings and Statistical Data

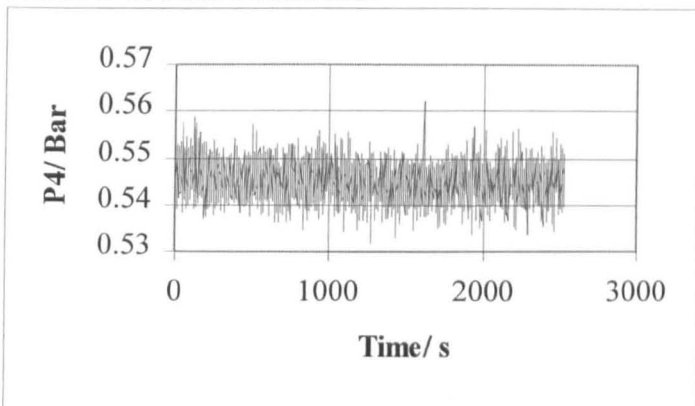
Long Swirly-flo Pipe Arrangement (pos 5)

Run: 2kglsf50

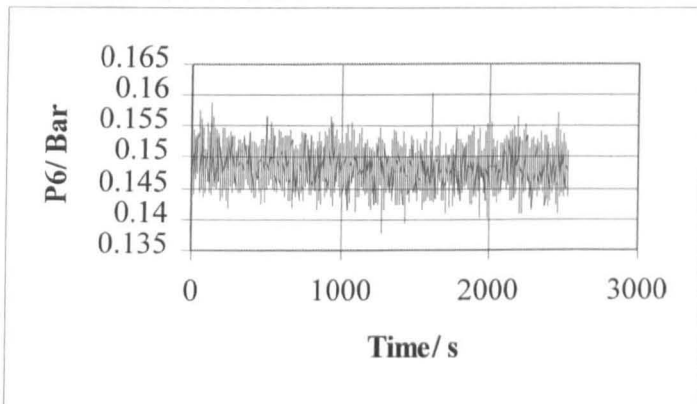
Volumetric Flow: 3.215 l/s

Mass Flow: 3.289 Kg/s

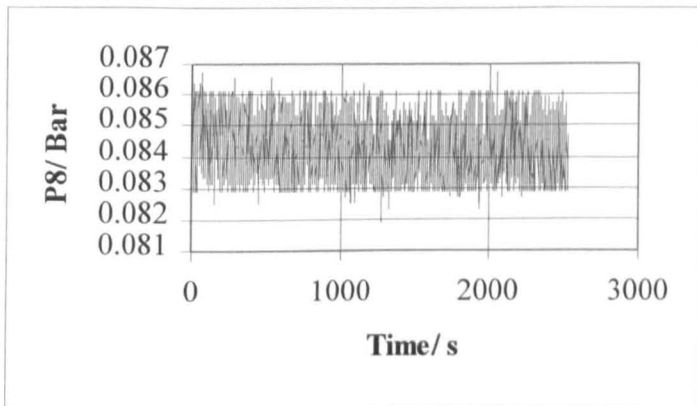
Number of Data Points:2527



CCCXXV P4 variation with time



CCCXXVI P6 variation with time



CCCXXVII P8 variation with time

	p1	p2	p3	p4	p5	p6	p7	p8
mean	0.856905	0.613568	0.586023	0.54501	0.53176	0.148481	0.118269	0.084257
median	0.85709	0.61344	0.58593	0.54494	0.53156	0.1483	0.11807	0.08411
mode	0.85709	0.61508	0.58572	0.54515	0.53053	0.14789	0.11786	0.08452
standard deviation	0.004417	0.005374	0.00413	0.003795	0.003709	0.00272	0.002665	0.000916
variance	1.95E-05	2.89E-05	1.71E-05	1.44E-05	1.38E-05	7.4E-06	7.1E-06	8.39E-07
skew	0.030907	0.144754	0.129036	0.12897	0.105376	0.083709	0.129163	0.279582
kurtosis	0.226765	0.114717	0.275242	0.24352	0.229264	0.226907	0.240445	-0.74081

CCCXXVIII Pressure Readings and Statistical Data

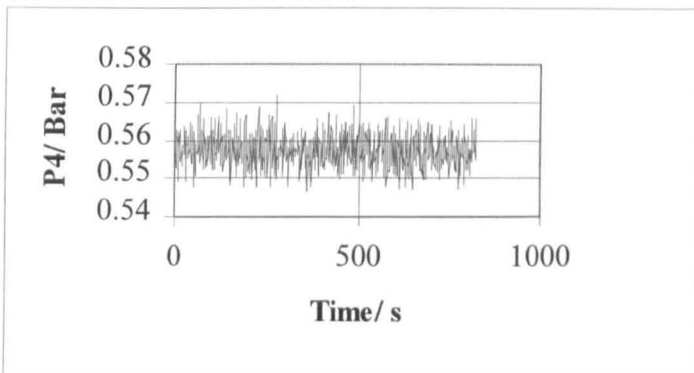
Long Swirly-flo Pipe Arrangement (pos 5)

Run: 2kgl55

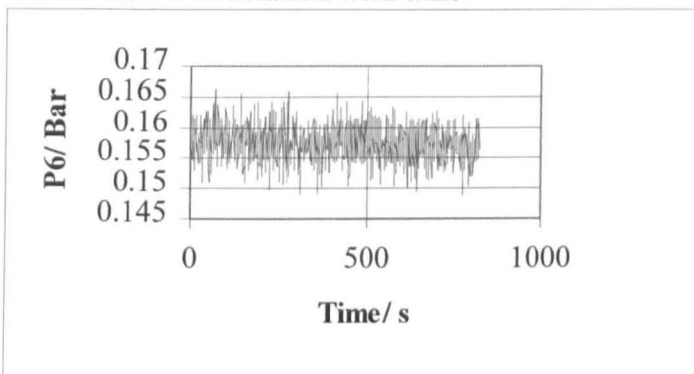
Volumetric Flow: 3.508 l/s

Mass Flow: 3.596 Kg/s

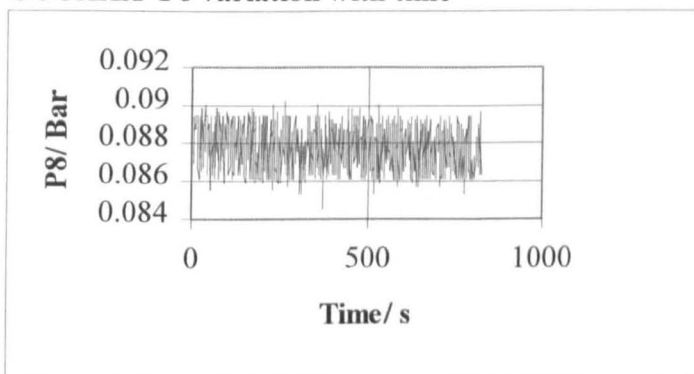
Number of Data Points:824



CCCXXIX P4 variation with time



CCCXXX P6 variation with time



CCCXXXI P8 variation with time

	p1	p2	p3	p4	p5	p6	p7	p8
mean	0.933097	0.635925	0.603576	0.557398	0.544098	0.157329	0.127171	0.087733
median	0.93279	0.63553	0.60332	0.55722	0.54404	0.1573	0.12727	0.08759
mode	0.93177	0.63533	0.60332	0.55701	0.54281	0.15935	0.12523	0.08615
standard deviation	0.005194	0.00588	0.004585	0.00421	0.004004	0.002971	0.002921	0.001144
variance	2.67E-05	3.47E-05	2.11E-05	1.77E-05	1.61E-05	8.86E-06	8.57E-06	1.31E-06
skew	-0.07565	0.128521	0.085095	0.074847	0.024187	0.003888	-0.03945	0.025718
kurtosis	-0.36339	-0.03444	-0.02808	-0.18411	-0.10488	-0.11002	-0.12929	-1.14572

CCCXXXII Pressure Readings and Statistical Data

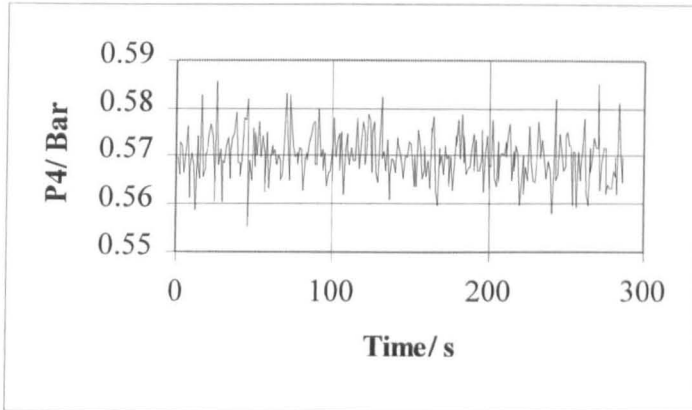
Long Swirly-flo Pipe Arrangement (pos 5)

Run: 2kglsf60

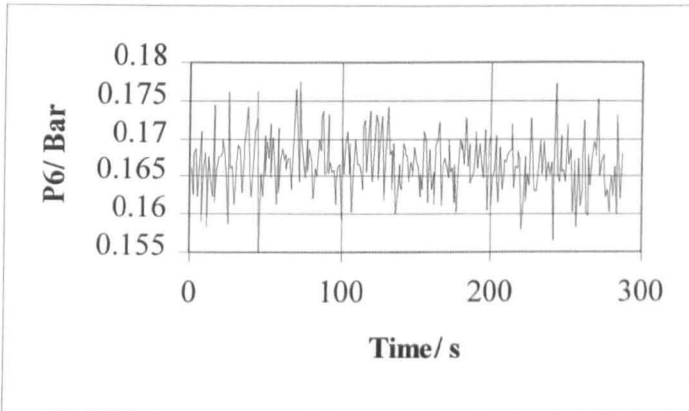
Volumetric Flow: 3.78 l/s

Mass Flow: 3.846 Kg/s

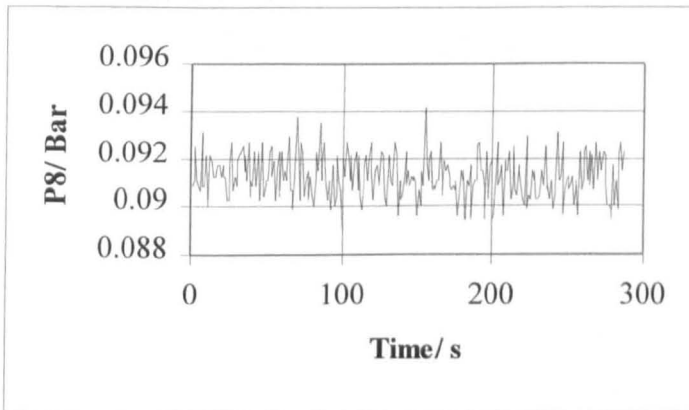
Number of Data Points:289



CCCXXXIII P4 variation with time



CCCXXXIV P6 variation with time



CCCXXXV P8 variation with time

	p1	p2	p3	p4	p5	p6	p7	p8
mean	1.010408	0.658871	0.621952	0.569933	0.55641	0.16654	0.1361	0.091211
median	1.01053	0.65865	0.62193	0.5699	0.55631	0.16631	0.13607	0.09106
mode	1.01053	0.65906	0.62357	0.5701	0.55713	0.16528	0.13607	0.09106
standard deviation	0.005616	0.007093	0.005776	0.005144	0.005126	0.003828	0.00363	0.000892
variance	3.15E-05	5.03E-05	3.34E-05	2.65E-05	2.63E-05	1.47E-05	1.32E-05	7.96E-07
skew	-0.011	0.200582	0.212016	0.19909	0.17279	0.08417	0.077802	0.254383
kurtosis	0.09795	-0.18589	0.07544	0.204548	0.183108	0.403052	0.267925	-0.15031

CCCXXXVI Pressure Readings and Statistical Data

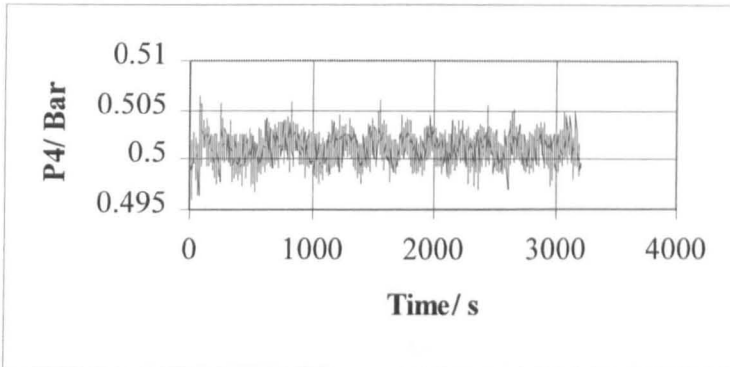
Long Swirly-flo Pipe Arrangement (pos 6)

Run: 2kglsf20

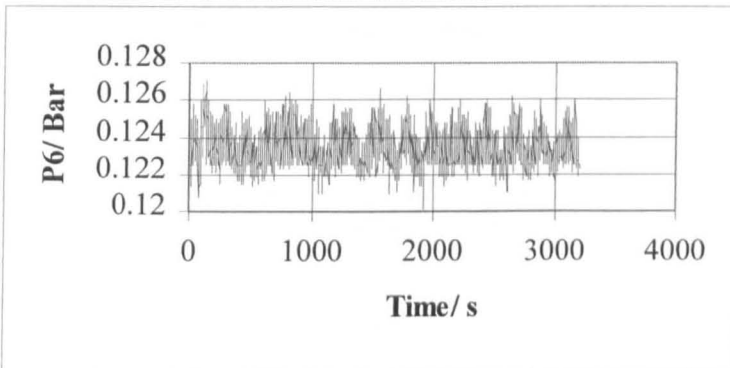
Volumetric Flow: 0.952 l/s

Mass Volumetric: 0.935 Kg/s

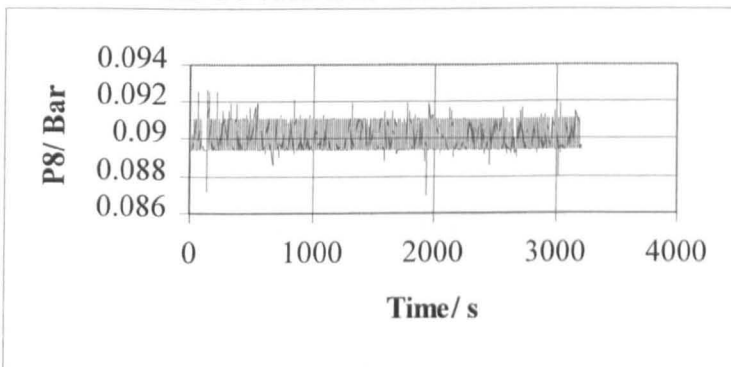
Number of Data Points:3207



CCCXXXVII P4 variation with time



CCCXXXVIII P6 variation with time



CCCXXXIX P8 variation with time

	p1	p2	p3	p4	p5	p6	p7	p8
mean	0.4991	0.51364	0.509312	0.501155	0.487818	0.123413	0.095378	0.090035
median	0.49907	0.5136	0.50941	0.50116	0.48778	0.12334	0.09515	0.08984
mode	0.49907	0.5136	0.50778	0.50259	0.48778	0.12252	0.09515	0.08943
standard deviation	0.000331	0.001648	0.001519	0.001354	0.001412	0.000935	0.000982	0.000681
variance	1.09E-07	2.71E-06	2.31E-06	1.83E-06	1.99E-06	8.74E-07	9.63E-07	4.64E-07
skew	17.72326	-0.12277	-0.08692	-0.12571	-0.06512	0.550897	0.37158	0.584287
kurtosis	372.7812	0.725589	0.245741	0.033333	0.099088	-0.01424	0.597714	-0.71538

CCCXXX Pressure Readings and Statistical Data

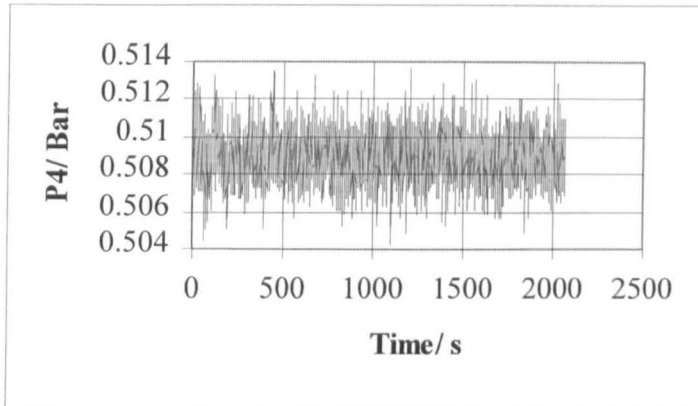
Long Swirly-flo Pipe Arrangement (pos 6)

Run: 2kglsf25

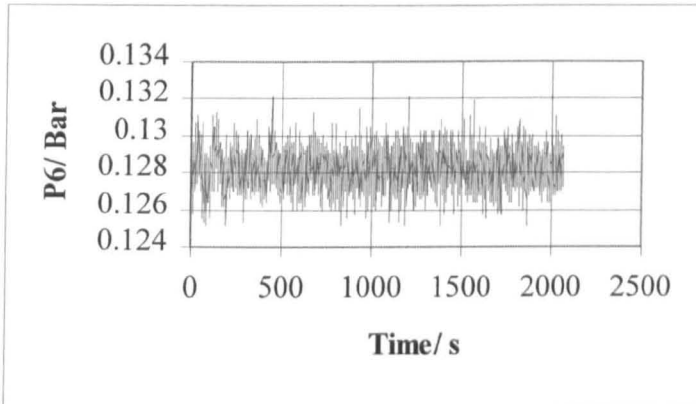
Volumetric Flow: 1.327 l/s

Mass Flow: 1.368 Kg/s

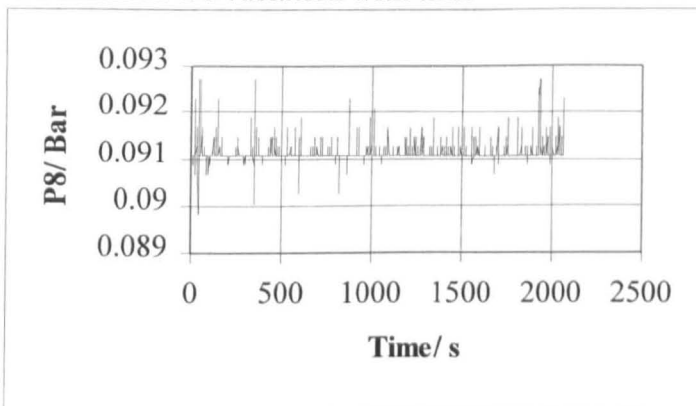
Number of Data Points:2066



CCCXXXXI P4 variation with time



CCCXXXXII P6 variation with time



CCCXXXXIII P8 variation with time

	p1	p2	p3	p4	p5	p6	p7	p8
mean	0.539515	0.52802	0.521071	0.508918	0.495524	0.128317	0.100096	0.091095
median	0.53999	0.52813	0.52107	0.50893	0.49555	0.12846	0.10006	0.09106
mode	0.53999	0.52833	0.52087	0.5075	0.49616	0.12907	0.10006	0.09106
standard deviation	0.000928	0.001595	0.001465	0.001443	0.00133	0.001041	0.000971	0.00017
variance	8.62E-07	2.55E-06	2.15E-06	2.08E-06	1.77E-06	1.08E-06	9.42E-07	2.89E-08
skew	-2.45376	0.049707	-0.05459	0.082871	-0.02397	-0.11701	0.063178	4.391384
kurtosis	7.619493	-0.40025	-0.07932	-0.25162	0.12539	0.088558	0.201633	34.92233

CCCXXXXIV Pressure Readings and Statistical Data

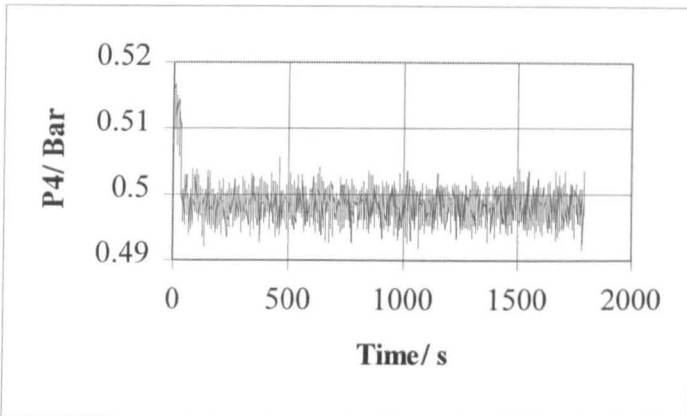
Long Swirly-flo Pipe Arrangement (pos 6)

Run: 2kglf30

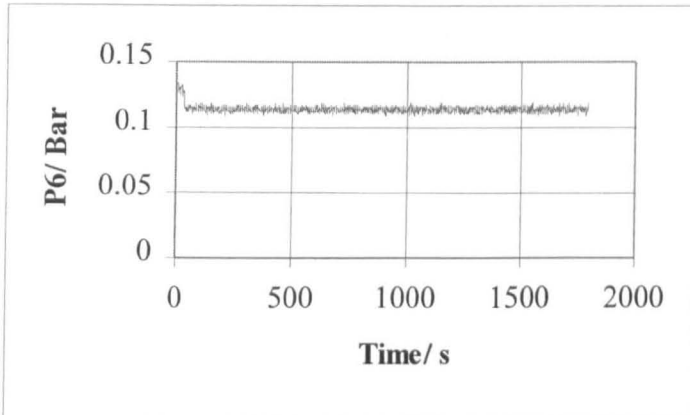
Volumetric Flow: 1.762 l/s

Mass Flow: 1.809 Kg/s

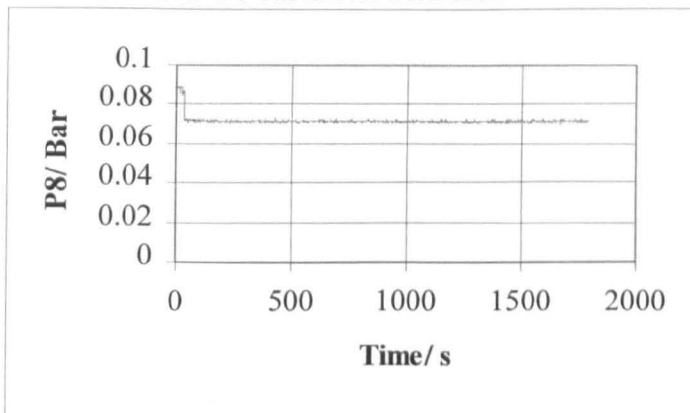
Number of Data Points:1795



CCCXXXV P4 variation with time



CCCXXXVI P6 variation with time



CCCXXXVII P8 variation with time

	p1	p2	p3	p4	p5	p6	p7	p8
mean	0.580381	0.527812	0.516684	0.498586	0.484777	0.114288	0.085441	0.07172
median	0.57988	0.52751	0.51657	0.4983	0.4845	0.11414	0.08533	0.07142
mode	0.58091	0.5271	0.51535	0.49809	0.48491	0.11434	0.08636	0.07142
standard deviation	0.002499	0.002689	0.002749	0.002869	0.002941	0.002808	0.002743	0.002172
variance	6.24E-06	7.23E-06	7.56E-06	8.23E-06	8.65E-06	7.88E-06	7.52E-06	4.72E-06
skew	0.115855	1.40892	1.712819	1.976303	1.935358	2.529726	2.766406	7.08074
kurtosis	0.403936	5.294541	7.381285	9.180336	8.732416	12.80945	14.43072	50.55687

CCCXXXVIII Pressure Readings and Statistical Data

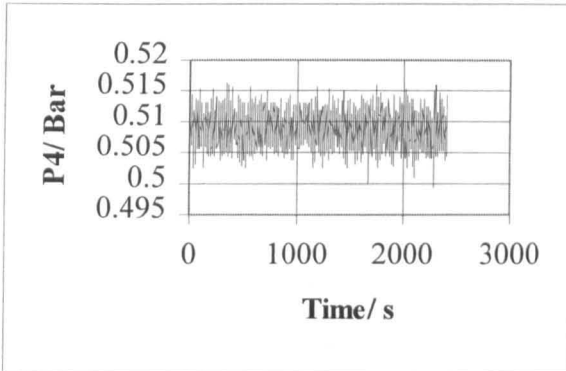
Long Swirly-flo Pipe Arrangement (pos 6)

Run: 2kglsf35

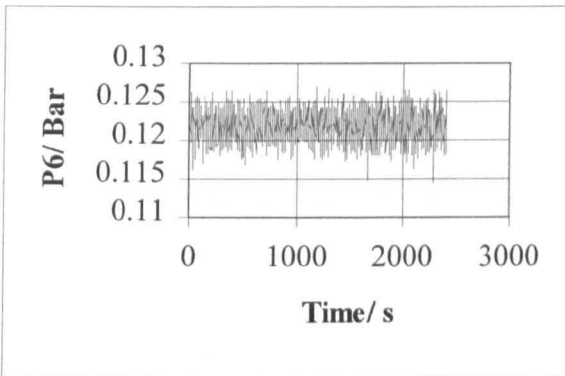
Volumetric Flow:2.155 l/s

Mass Flow: 2.197 Kg/s

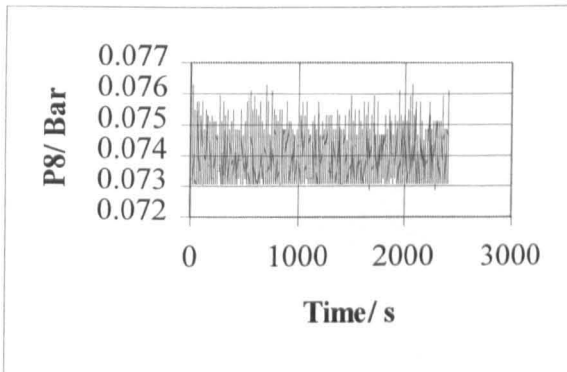
Number of Data Points:2416



CCCXLIX P4 variation with time



CCCL P6 variation with time



CCCLI P8 variation with time

	p1	p2	p3	p4	p5	p6	p7	p8
mean	0.639128	0.546744	0.531968	0.508848	0.495184	0.121844	0.092454	0.073946
median	0.63921	0.54674	0.53192	0.50893	0.49514	0.12191	0.09249	0.07388
mode	0.63819	0.54674	0.53151	0.50893	0.49473	0.12252	0.0927	0.07306
standard deviation	0.00204	0.003034	0.002485	0.002363	0.002242	0.001715	0.001693	0.000679
variance	4.16E-06	9.2E-06	6.17E-06	5.58E-06	5.03E-06	2.94E-06	2.86E-06	4.61E-07
skew	0.242569	0.021691	0.072406	0.007339	-0.03602	-0.0785	-0.01161	0.5728
kurtosis	0.658421	-0.00324	0.016014	-0.01528	0.042747	0.081781	0.004625	-0.25749

CCCLII Pressure Readings and Statistical Data

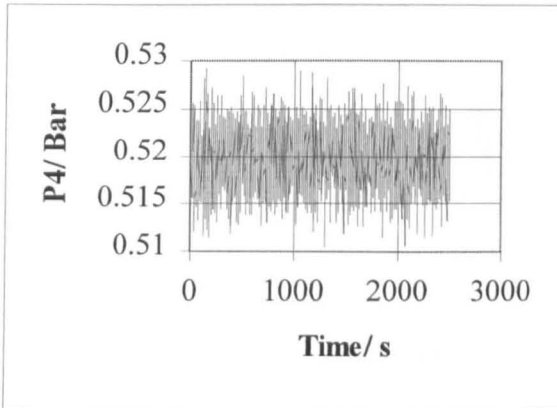
Long Swirly-flo Pipe Arrangement (pos 6)

Run: 2kglsf40

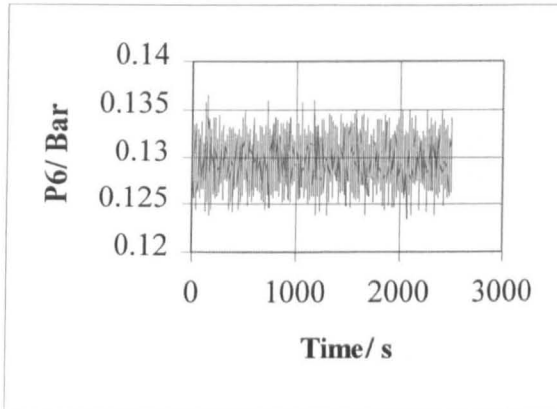
Volumetric Flow: 2.499 l/s

Mass Flow: 2.58 Kg/s

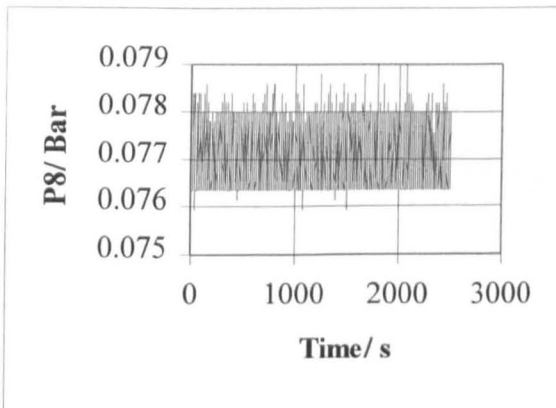
Number of Data Points:2505



CLIII P4 variation with time



CLIV P6 variation with time



CLV P8 variation with time

	p1	p2	p3	p4	p5	p6	p7	p8
mean	0.7012	0.565768	0.547828	0.519604	0.505804	0.129506	0.099921	0.077097
median	0.70161	0.56577	0.54787	0.51957	0.50578	0.12948	0.09986	0.07695
mode	0.70161	0.56475	0.54706	0.51896	0.50496	0.12887	0.09986	0.07633
standard deviation	0.002424	0.00375	0.003166	0.002854	0.002753	0.002049	0.001972	0.000608
variance	5.88E-06	1.41E-05	1E-05	8.15E-06	7.58E-06	4.2E-06	3.89E-06	3.7E-07
skew	-0.23584	0.063163	0.026589	0.017566	-0.01058	0.068239	0.035462	0.259659
kurtosis	0.226404	-0.00794	-0.09278	-0.03901	-0.10388	-0.05614	0.000896	-1.09444

CLVI Pressure Readings and Statistical Data

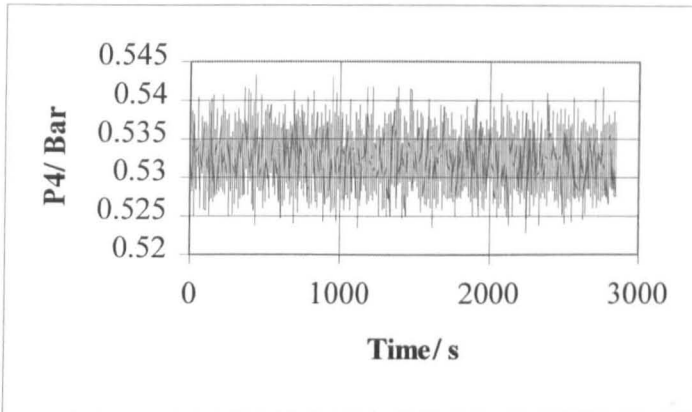
Long Swirly-flo Pipe Arrangement (pos 6)

Run: 2kglsf45

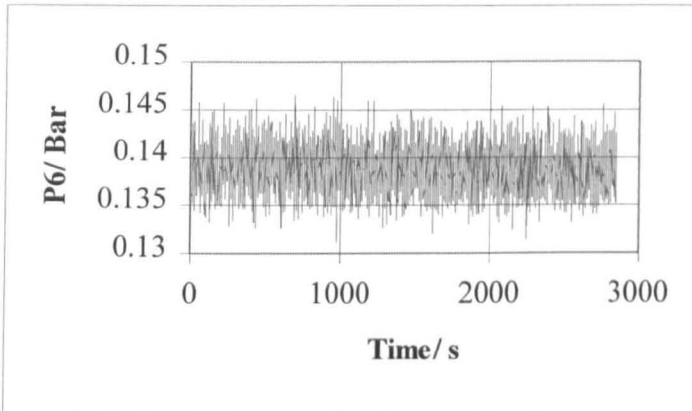
Volumetric Flow:2.892 l/s

Mass Flow: 2.971 Kg/s

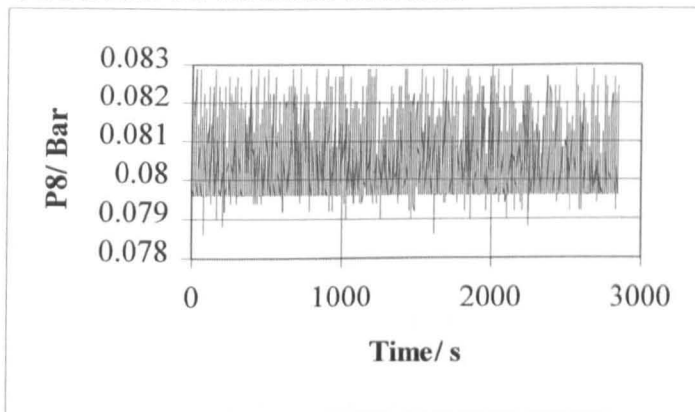
Number of Data Points:2844



CCCLVII P4 variation in time



CCCLVIII P6 variation with time



CCCLIX P8 variation with time

	p1	p2	p3	p4	p5	p6	p7	p8
mean	0.776894	0.589427	0.566842	0.532426	0.518606	0.138876	0.108982	0.080385
median	0.77731	0.5893	0.5669	0.53246	0.51867	0.13889	0.10907	0.08022
mode	0.77731	0.58868	0.56649	0.53205	0.51805	0.13889	0.10948	0.07961
standard deviation	0.002764	0.004447	0.003444	0.003177	0.00318	0.002342	0.0023	0.000846
variance	7.64E-06	1.98E-05	1.19E-05	1.01E-05	1.01E-05	5.49E-06	5.29E-06	7.16E-07
skew	0.095582	0.003389	0.047016	0.065364	0.069173	0.094831	0.070073	1.000662
kurtosis	0.102723	-0.09572	-0.12698	-0.07965	-0.11519	-0.06558	-0.13107	0.241897

CCCLX Pressure Readings and Statistical Data

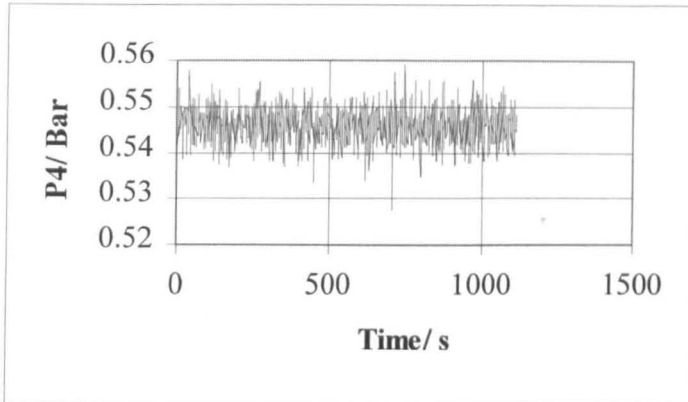
Long Swirly-flo Pipe Arrangement (pos 6)

Run: 2kglsf50

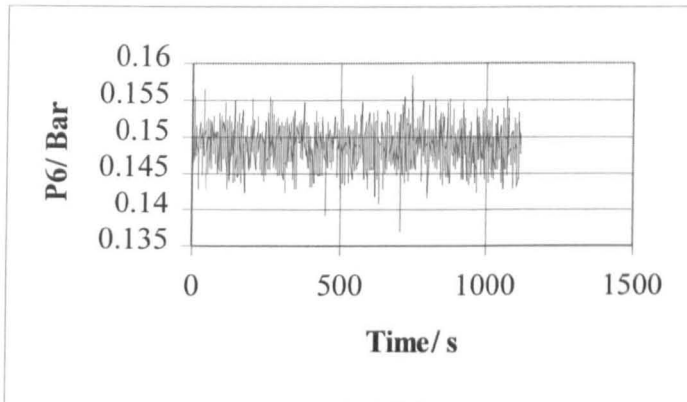
Volumetric Flow: 3.211 l/s

Mass Flow: 3.311 Kg/s

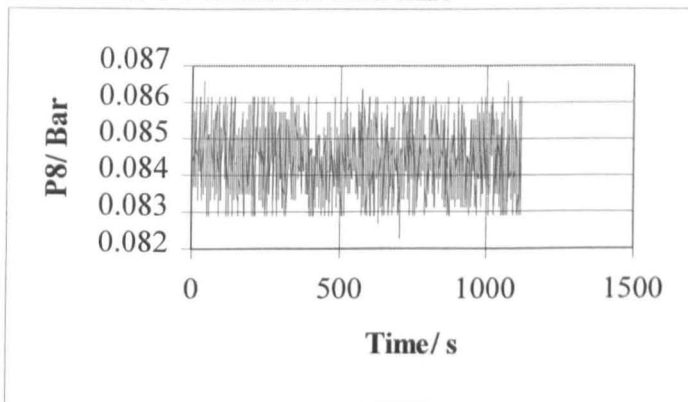
Number of Data Points:1115



CCCLXI P4 variation with time



CCCLXII P6 variation with time



CCCLXIII P8 variation with time

	p1	p2	p3	p4	p5	p6	p7	p8
mean	0.858637	0.61391	0.586173	0.545851	0.532187	0.148755	0.118564	0.084446
median	0.85812	0.61385	0.58634	0.54576	0.53237	0.14871	0.11868	0.08452
mode	0.85812	0.61405	0.58961	0.54801	0.53422	0.14932	0.11827	0.08452
standard deviation	0.003706	0.005274	0.004	0.003731	0.00364	0.002664	0.00262	0.000893
variance	1.37E-05	2.78E-05	1.6E-05	1.39E-05	1.32E-05	7.1E-06	6.86E-06	7.97E-07
skew	-0.09309	-0.09064	-0.14294	-0.0633	-0.10489	-0.08945	-0.04079	0.084534
kurtosis	0.443547	0.647691	0.559972	0.495267	0.30936	0.240194	0.2416	-0.78771

CCCLXIV Pressure Readings and Statistical Data

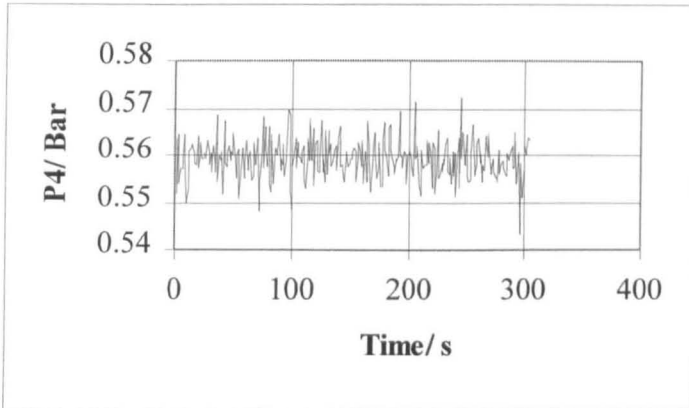
Long Swirly-flo Pipe Arrangement (pos 6)

Run: 2kglsf55

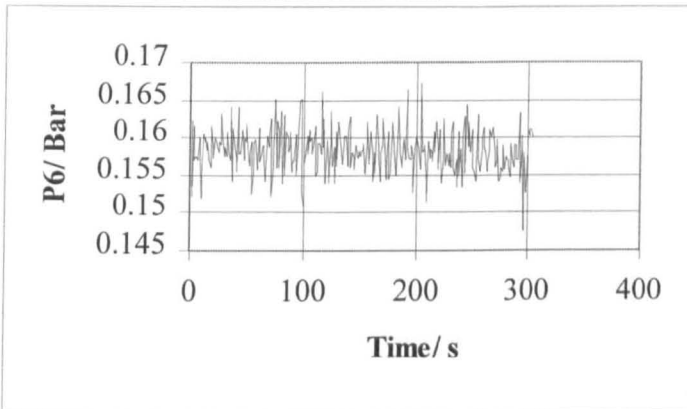
Volumetric Flow: 3.48 l/s

Mass Flow: 3.59 Kg/s

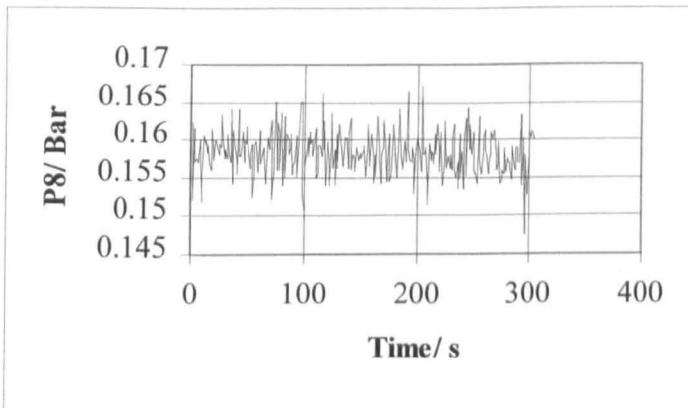
Number of Data Points:305



CCCLXV P4 variation with time



CCCLXVI P6 variation with time



CCCLXVII P8 variation with time

	p1	p2	p3	p4	p5	p6	p7	p8
mean	0.935986	0.637873	0.604931	0.559293	0.545414	0.158301	0.128048	0.088141
median	0.93586	0.63799	0.60495	0.55926	0.54547	0.15812	0.12809	0.0882
mode	0.93586	0.64126	0.60536	0.55926	0.54485	0.15812	0.12809	0.08943
standard deviation	0.00394	0.005828	0.004406	0.004071	0.003881	0.002869	0.002817	0.001098
variance	1.55E-05	3.4E-05	1.94E-05	1.66E-05	1.51E-05	8.23E-06	7.93E-06	1.21E-06
skew	0.0888	0.075658	0.115825	-0.00811	-0.02736	0.030749	-0.00662	-0.26294
kurtosis	0.205034	0.289006	0.585507	0.862625	0.597756	0.617441	0.489585	-1.1446

CCCLXVIII Pressure Readings and Statistical Data

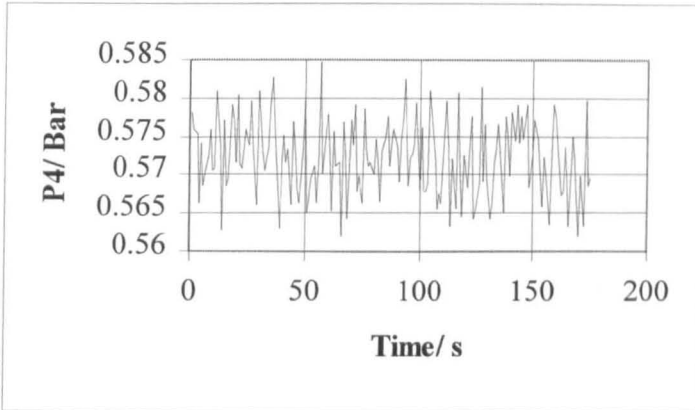
Long Swirly-flo Pipe Arrangement (pos 6)

Run: 2kglsf60

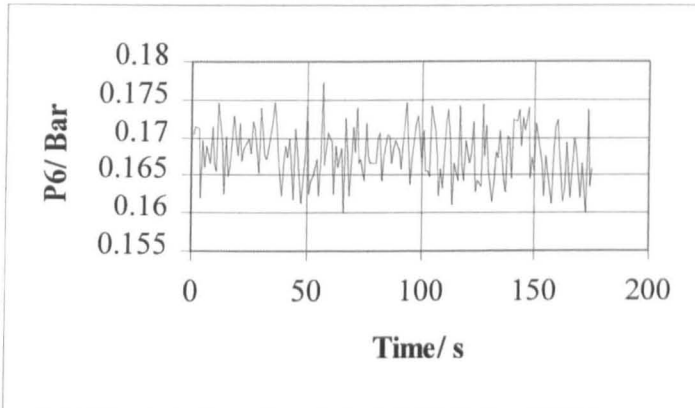
Volumetric Flow: 3.805 l/s

Mass Flow: 3.894 Kg/s

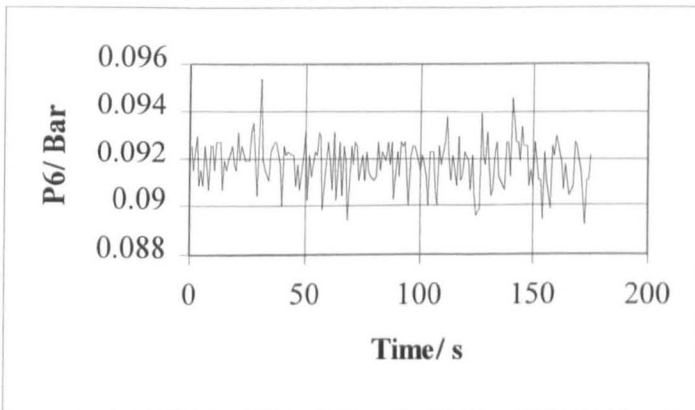
Number of Data Points:175



CCCLXIX P4 variation with time



CCCLXX P6 variation with time



CCCLXXI P8 variation with time

	p1	p2	p3	p4	p5	p6	p7	p8
mean	1.017329	0.66159	0.624029	0.572324	0.558466	0.167951	0.137289	0.091806
median	1.01769	0.66213	0.62418	0.57236	0.55856	0.16794	0.13709	0.09188
mode	1.01974	0.66459	0.62562	0.57215	0.56265	0.16671	0.13709	0.0927
standard deviation	0.004842	0.006826	0.005556	0.00491	0.004814	0.003629	0.003526	0.000995
variance	2.34E-05	4.66E-05	3.09E-05	2.41E-05	2.32E-05	1.32E-05	1.24E-05	9.9E-07
skew	-0.11593	0.05951	-0.00337	0.011928	-0.03029	-0.03463	-0.07322	-0.0966
kurtosis	-0.01425	-0.40145	-0.59047	-0.6185	-0.58068	-0.64818	-0.61025	0.476369

CCCLXXII Pressure Readings and Statistical Data

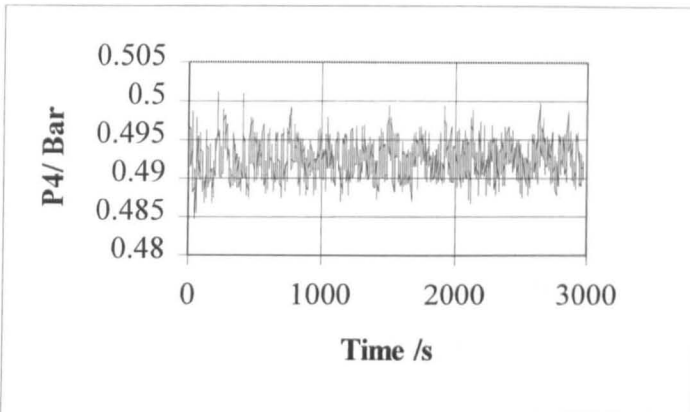
Long Swirly-flo Pipe Arrangement (optimum position)

Run: 4kglsf20

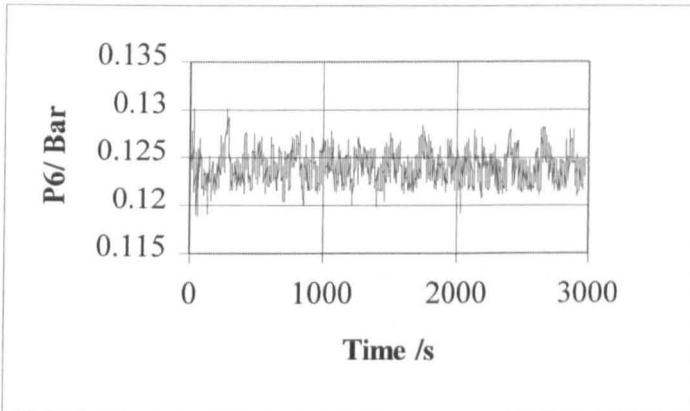
Volumetric Flow: 0.861 l/s

Mass Flow: 0.887 Kg/s

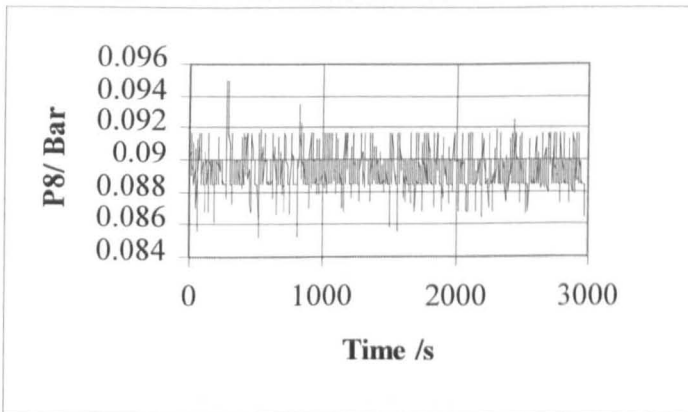
Number of Data Points:2975



CCCLXXIII P4 variation with time



CCCLXXIV P6 variation with time



CCCLXXV P8 variation with time

	p1	p2	p3	p4	p5	p6	p7	p8
mean	0.499559	0.515816	0.510353	0.492419	0.489663	0.123963	0.09786	0.089411
median	0.49907	0.51565	0.51044	0.49236	0.48962	0.12398	0.09802	0.08945
mode	0.49907	0.51851	0.51105	0.4895	0.49105	0.1248	0.09843	0.08843
standard deviation	0.001085	0.002015	0.002431	0.002343	0.002332	0.001587	0.001586	0.001037
variance	1.18E-06	4.06E-06	5.91E-06	5.49E-06	5.44E-06	2.52E-06	2.52E-06	1.07E-06
skew	2.898688	0.052215	0.115948	0.337312	0.348322	0.253481	-0.13922	0.339903
kurtosis	9.785076	-0.29548	-0.0729	-0.26935	0.170105	-0.16714	-0.19347	0.880937

CCCLXXVI Pressure Readings and Statistical Data

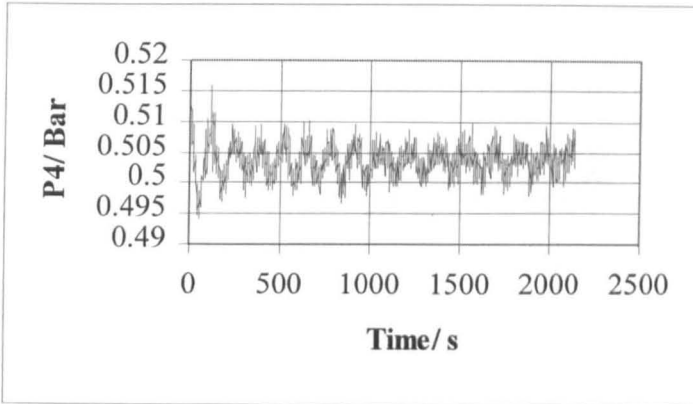
Long Swirly-flo Pipe Arrangement (optimum position)

Run: 4kglf25

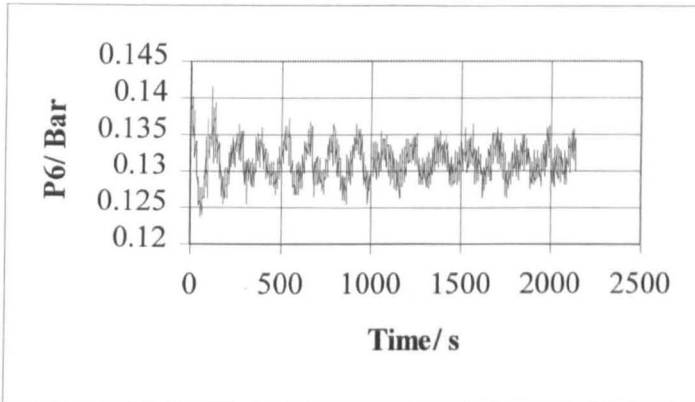
Volumetric Flow: 1.267 l/s

Mass Flow: 1.314 Kg/s

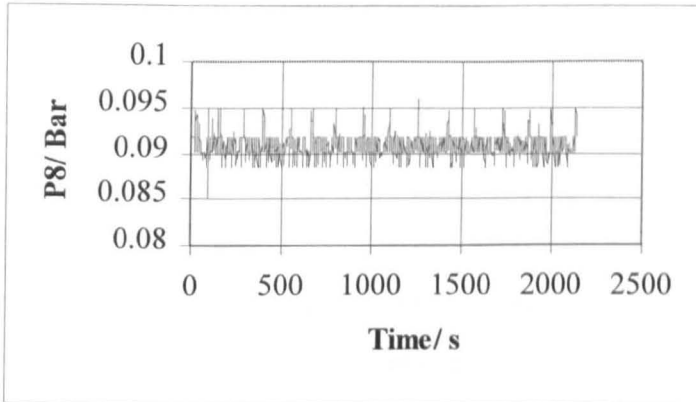
Number of Data Points:2141



CCCLXXVII P4 variation with time



CCCLXXVIII P6 variation with time



CCCLXXIX P8 variation with time

	p1	p2	p3	p4	p5	p6	p7	p8
mean	0.540267	0.534611	0.524676	0.50366	0.500501	0.13132	0.105075	0.090752
median	0.53999	0.53467	0.52476	0.50361	0.50046	0.13134	0.10497	0.09027
mode	0.53999	0.53488	0.52414	0.50259	0.50087	0.13134	0.10497	0.09006
standard deviation	0.00068	0.002133	0.002597	0.002552	0.0026	0.00234	0.002335	0.001126
variance	4.64E-07	4.56E-06	6.75E-06	6.51E-06	6.77E-06	5.49E-06	5.46E-06	1.27E-06
skew	2.397232	-0.16493	-0.05551	0.039056	0.034074	0.132949	0.150449	0.932674
kurtosis	8.848163	-0.29042	0.337766	0.567883	0.374706	0.100292	0.217733	2.682212

CCCLXXIX Pressure Readings and Statistical Data

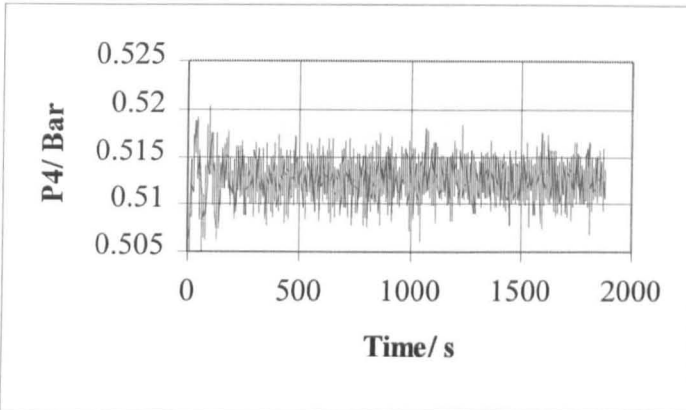
Long Swirly-flo Pipe Arrangement (optimum position)

Run: 4kglsf30

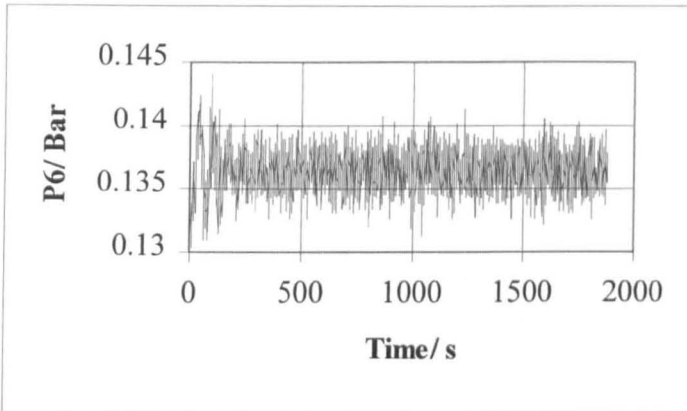
Volumetric Flow: 1.711 l/s

Mass Flow: 1.773 kg/s

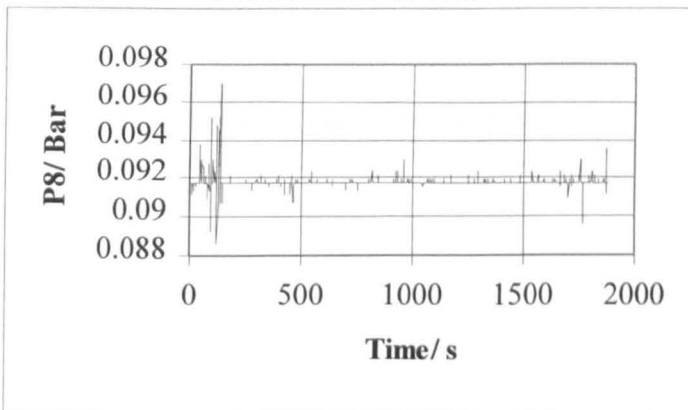
Number of Data Points:1878



CCCLXXX P4 variation with time



CCCLXXXI P6 variation with time



CCCLXXXII P8 variation with time

	p1	p2	p3	p4	p5	p6	p7	p8
mean	0.589332	0.550734	0.538145	0.512578	0.50883	0.13644	0.109778	0.091726
median	0.58909	0.55084	0.53826	0.51262	0.50885	0.13646	0.10988	0.0917
mode	0.58909	0.55125	0.53826	0.51262	0.50905	0.13666	0.10988	0.0917
standard deviation	0.000645	0.002055	0.00199	0.002051	0.001963	0.001742	0.001725	0.000284
variance	4.16E-07	4.22E-06	3.96E-06	4.21E-06	3.85E-06	3.03E-06	2.98E-06	8.09E-08
skew	1.626016	0.132241	-0.00829	-0.01022	0.045722	0.015783	0.002654	6.180596
kurtosis	5.801693	0.772081	0.386542	0.353489	0.443535	0.218961	0.223975	115.0685

CCCLXXXIII Pressure Readings and Statistical Data

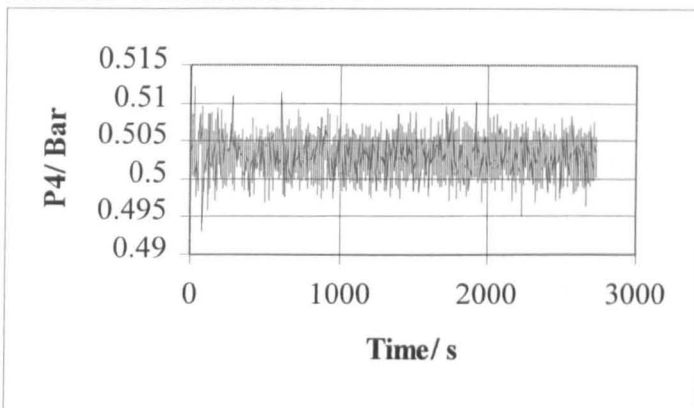
Long Swirly-flo Pipe Arrangement (optimum position)

Run: 4kglsf35

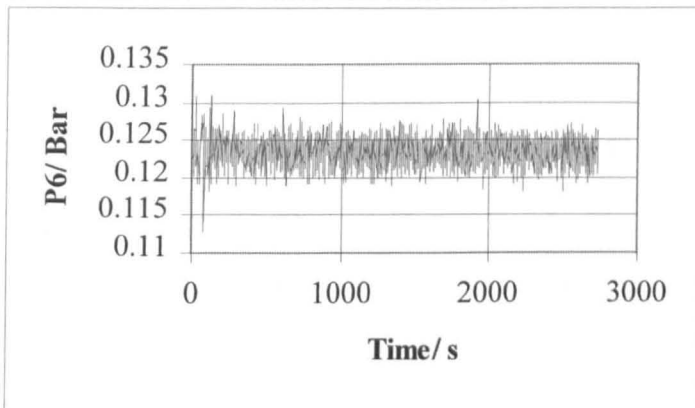
Volumetric Flow: 2.137 l/s

Mass Flow: 2.208 Kg/s

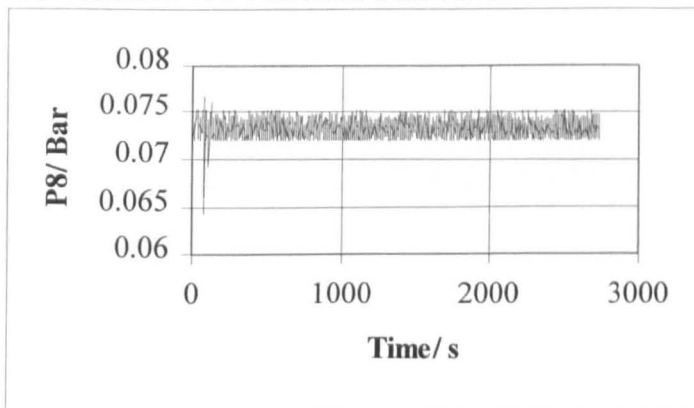
Number of Data Points:2734



CCCLXXXIV P4 variation with time



CCCLXXXV P6 variation with time



CCCLXXXVI P8 variation with time

	p1	p2	p3	p4	p5	p6	p7	p8
mean	0.641169	0.551835	0.535343	0.502981	0.499246	0.123414	0.095961	0.073374
median	0.64126	0.55165	0.53539	0.503	0.49923	0.12337	0.09597	0.07349
mode	0.64023	0.55165	0.53539	0.5028	0.49903	0.12316	0.09618	0.0737
standard deviation	0.002364	0.00294	0.002481	0.002259	0.002247	0.001709	0.001699	0.000839
variance	5.59E-06	8.65E-06	6.15E-06	5.1E-06	5.05E-06	2.92E-06	2.89E-06	7.04E-07
skew	0.284205	0.085788	0.041417	-0.00023	-0.01117	-0.04222	-0.05227	-0.2216
kurtosis	0.134303	0.076015	-0.03099	0.235241	0.152752	0.847674	0.848609	4.626805

CCCLXXXVII Pressure Readings and Statistical Data

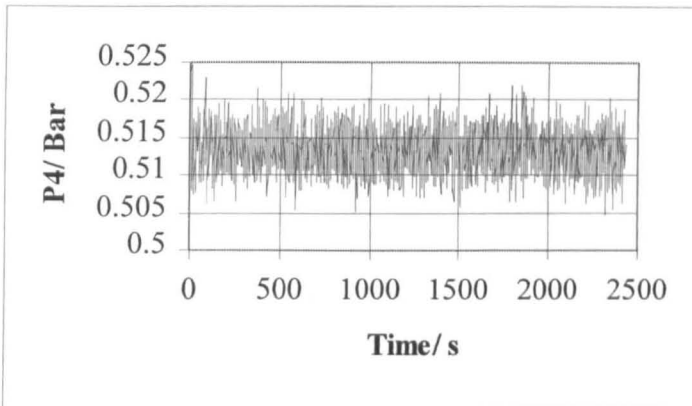
Long Swirly-flo Pipe Arrangement (optimum position)

Run: 4kglsf40

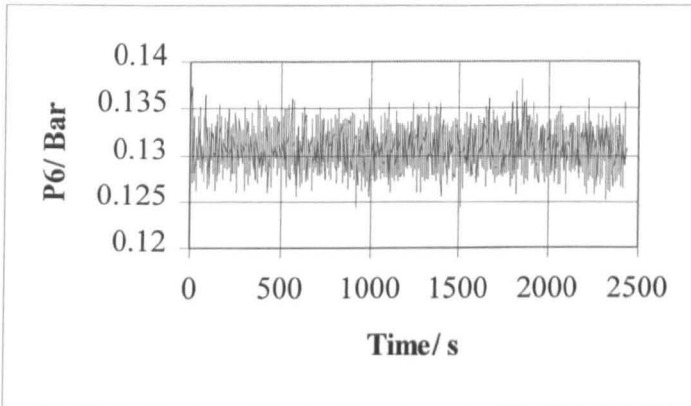
Volumetric Flow: 2.479 l/s

Mass Flow: 2.58 Kg/s

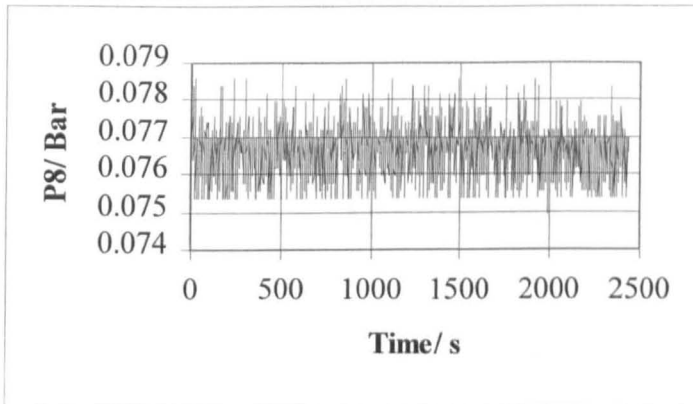
Number of Data Points:2433



CCCLXXXVIII P4 variation with time



CCCLXXXIX P6 variation with time



CCCXC P8 variation with time

	p1	p2	p3	p4	p5	p6	p7	p8
mean	0.702888	0.570311	0.551092	0.513423	0.509431	0.130752	0.103176	0.07668
median	0.70263	0.57027	0.55094	0.51344	0.50946	0.13073	0.10313	0.07697
mode	0.70263	0.57109	0.55033	0.51303	0.50844	0.13032	0.10293	0.07697
standard deviation	0.002448	0.003611	0.002987	0.002748	0.002558	0.00194	0.001865	0.000589
variance	5.99E-06	1.3E-05	8.92E-06	7.55E-06	6.55E-06	3.77E-06	3.48E-06	3.47E-07
skew	-0.10967	0.161157	0.098414	0.082076	0.131762	0.111315	0.134364	-0.32363
kurtosis	0.239991	0.051279	-0.00337	0.048734	0.160446	-0.07918	-0.02266	0.547161

CCCXCI Pressure Readings and Statistical Data

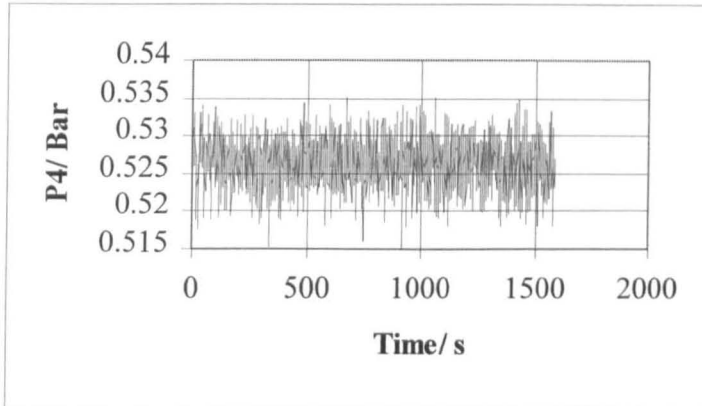
Long Swirly-flo Pipe Arrangement (optimum position)

Run: 4kglsf45

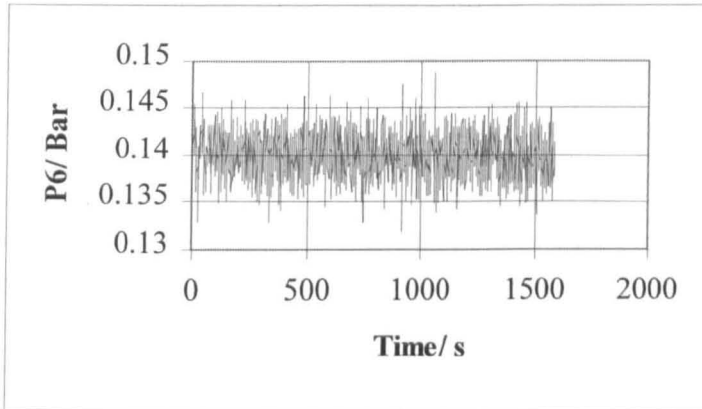
Volumetric Flow: 2.865 l/s

Mass Flow: 2.97 Kg/s

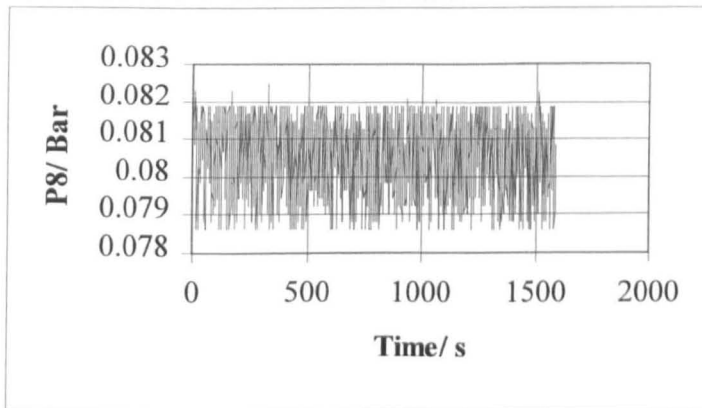
Number of Data Points:1590



CCCXCII P4 variation with time



CCCXCIII P4 variation with time



CCCXCIV P8 variation with time

	p1	p2	p3	p4	p5	p6	p7	p8
mean	0.778963	0.593577	0.569993	0.526244	0.522268	0.14002	0.112066	0.080573
median	0.77833	0.59359	0.56997	0.52632	0.52215	0.13994	0.11213	0.08065
mode	0.77731	0.59155	0.5712	0.52714	0.52337	0.14035	0.11111	0.08188
standard deviation	0.003035	0.004338	0.003405	0.003161	0.003105	0.002286	0.002223	0.000969
variance	9.21E-06	1.88E-05	1.16E-05	9.99E-06	9.64E-06	5.22E-06	4.94E-06	9.38E-07
skew	0.141268	0.05494	0.002236	-0.08898	-0.05186	-0.01611	-0.04644	-0.335
kurtosis	0.144498	-0.06234	-0.03573	-0.00385	0.005984	0.101894	0.08694	-0.95455

CCCXCIV Pressure Readings and Statistical Data

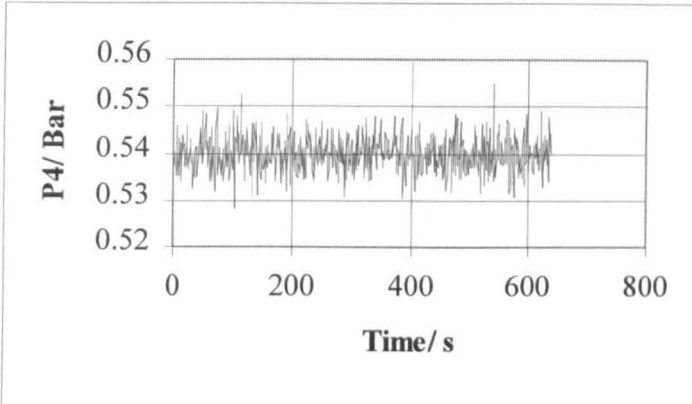
Long Swirly-flo Pipe Arrangement (optimum position)

Run: 4kglsf50

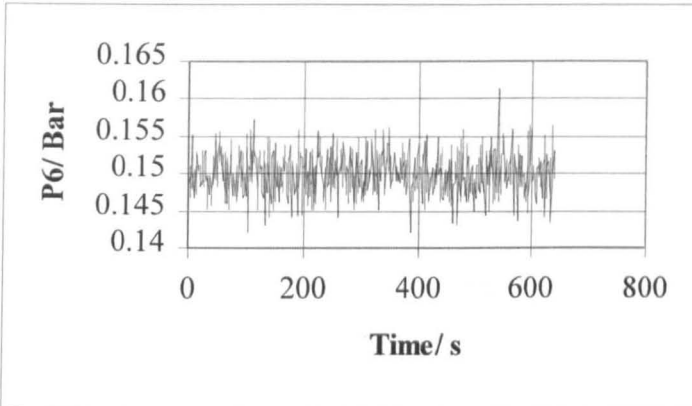
Volumetric Flow:3.196 l/s

Mass Flow: 3.326 Kg/s

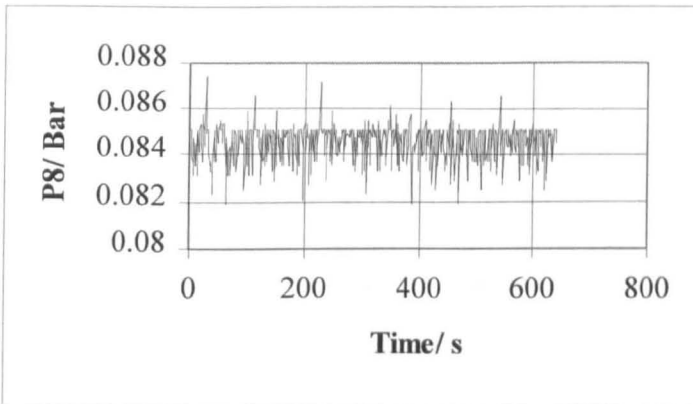
Number of Data Points:640



CCCXCIV P4 variation with time



CCCXCVI P6 variation with time



CCCXCVII P8 variation with time

	p1	p2	p3	p4	p5	p6	p7	p8
mean	0.865859	0.61901	0.590254	0.539876	0.536238	0.149946	0.121609	0.084551
median	0.8663	0.61876	0.59002	0.539725	0.53606	0.14996	0.12155	0.08475
mode	0.8663	0.61855	0.58777	0.53921	0.53463	0.15098	0.12216	0.08515
standard deviation	0.002968	0.005183	0.003996	0.003789	0.003723	0.002728	0.002722	0.000768
variance	8.81E-06	2.69E-05	1.6E-05	1.44E-05	1.39E-05	7.44E-06	7.41E-06	5.9E-07
skew	-0.26545	0.245364	0.207464	0.21248	0.143152	0.12556	0.208617	-0.66228
kurtosis	0.093544	0.360675	0.201614	0.168114	0.102621	0.168261	0.314038	0.725554

CCCXCVIII Pressure Readings and Statistical Data

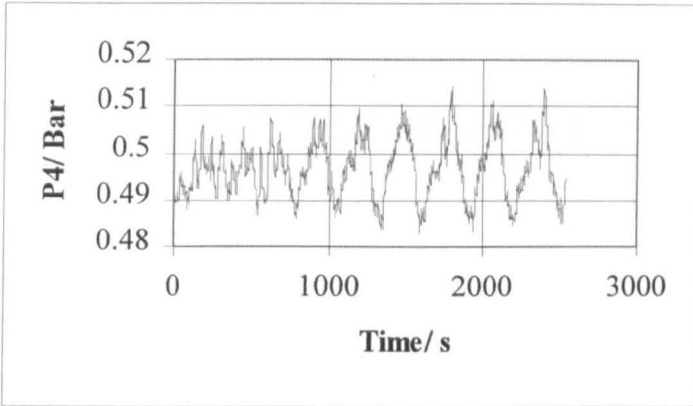
Long Swirly-flo Pipe Arrangement (optimum position)

Run: 6kglsf20

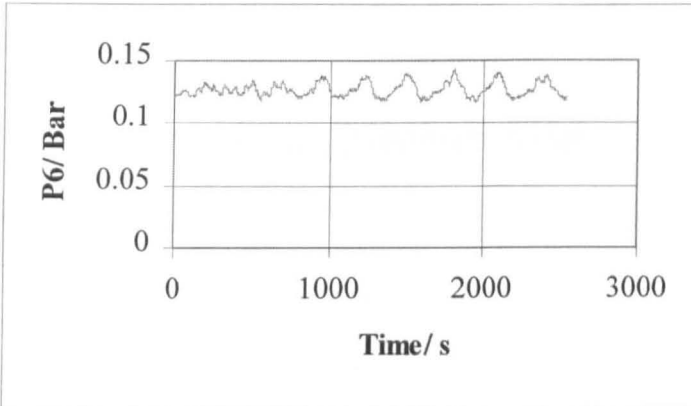
Volumetric Flow: 0.789 l/s

Mass Flow: 0.816 Kg/s

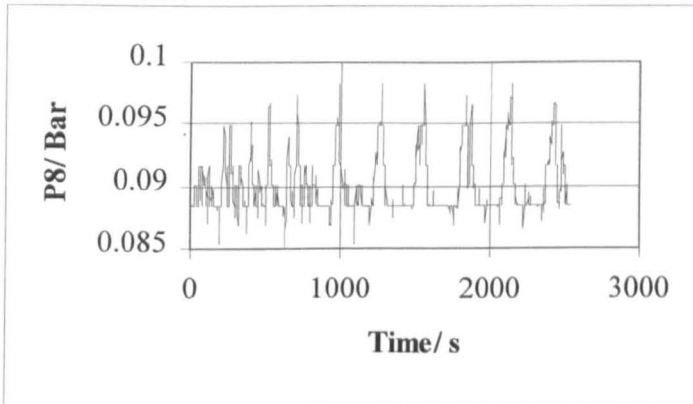
Number of Data Points:2537



CCCXCIX P4 variation with time



CD P6 variation with time



CDI P8 variation with time

	p1	p2	p3	p4	p5	p6	p7	p8
mean	0.503687	0.520588	0.513338	0.496542	0.492063	0.126767	0.100679	0.089972
median	0.50419	0.52097	0.51309	0.49625	0.49166	0.12562	0.09945	0.08843
mode	0.50726	0.52506	0.51432	0.49605	0.49105	0.12152	0.09843	0.08843
standard deviation	0.003025	0.004484	0.006489	0.006277	0.006356	0.005679	0.005759	0.002296
variance	9.15E-06	2.01E-05	4.21E-05	3.94E-05	4.04E-05	3.23E-05	3.32E-05	5.27E-06
skew	-0.25828	-0.42447	0.131228	0.147107	0.152777	0.562143	0.602981	1.411485
kurtosis	-1.35202	-0.06739	-0.68104	-0.66195	-0.7152	-0.56022	-0.50222	1.18565

CDII Pressure Readings and Statistical Data

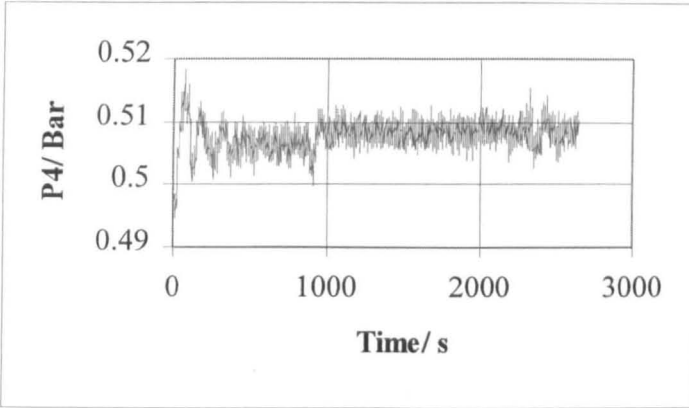
Long Swirly-flo Pipe Arrangement (optimum position)

Run: 6kglsf25

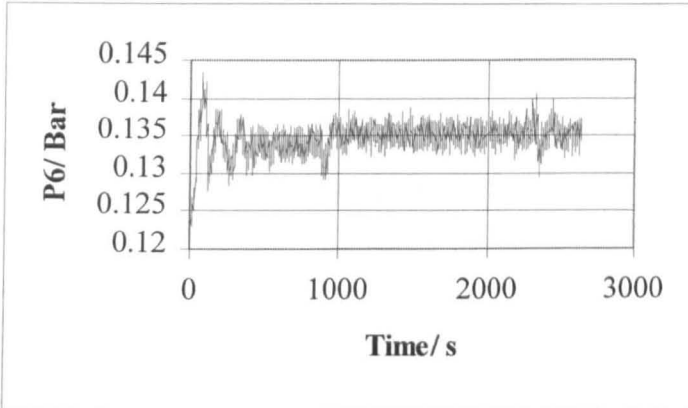
Volumetric Flow: 1.199 l/s

Mass Flow: 1.236 Kg/s

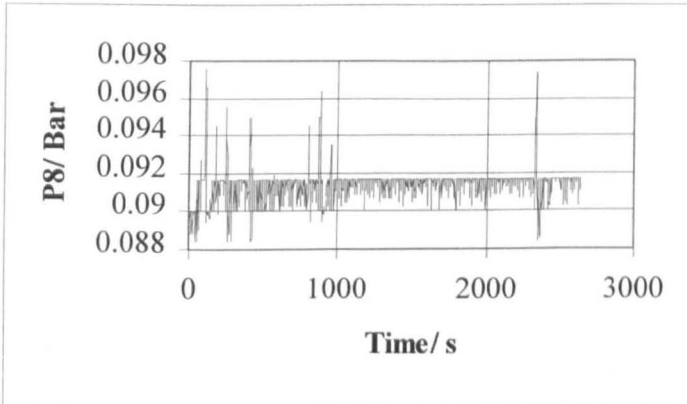
Number of Data Points:2644



CDIII P4 variation with time



CDIV P6 variation with time



CDV P8 variation with time

	p1	p2	p3	p4	p5	p6	p7	p8
mean	0.542863	0.53969	0.527358	0.507797	0.503582	0.13472	0.108438	0.091465
mode	0.54203	0.53815	0.52742	0.5075	0.50414	0.13462	0.10825	0.0917
median	0.54203	0.53958	0.52762	0.50791	0.50373	0.13482	0.10845	0.0917
standard deviation	0.002213	0.002333	0.0023	0.002424	0.002372	0.002033	0.002081	0.000788
variance	4.9E-06	5.44E-06	5.29E-06	5.88E-06	5.63E-06	4.13E-06	4.33E-06	6.21E-07
skew	0.71132	-0.30309	-1.03802	-0.83827	-1.00106	-1.17984	-1.03786	1.559747
kurtosis	0.085571	1.143347	4.816242	3.961077	4.424213	5.906252	5.135776	14.07751

CDVI Pressure Readings and Statistical Data

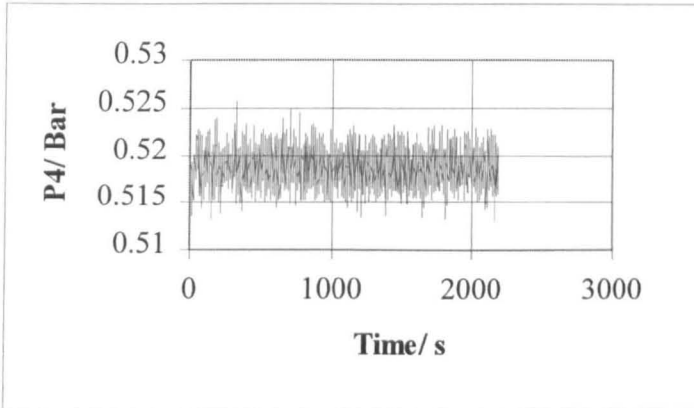
Long Swirly-flo Pipe Arrangement (optimum position)

Run: 6kglsf30

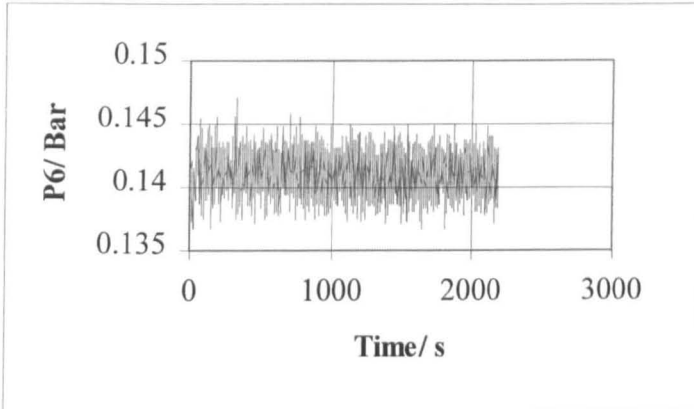
Volumetric Flow: 1.685 l/s

Mass Flow: 1.755 Kg/s

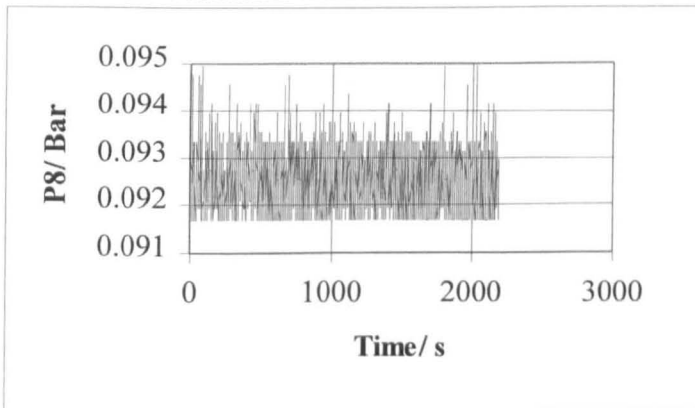
Number of Data Points:2190



CDVII P4 variation with time



CDVIII P6 variation with time



CDIX P8 variation with time

	p1	p2	p3	p4	p5	p6	p7	p8
mean	0.591134	0.558462	0.542852	0.518714	0.514117	0.141045	0.114335	0.092532
mode	0.59113	0.55779	0.54276	0.51855	0.51417	0.14116	0.11377	0.0917
median	0.59113	0.55841	0.54276	0.51875	0.51417	0.14096	0.11439	0.09252
standard deviation	0.001664	0.001841	0.001788	0.001786	0.00182	0.001591	0.001553	0.000622
variance	2.77E-06	3.39E-06	3.2E-06	3.19E-06	3.31E-06	2.53E-06	2.41E-06	3.87E-07
skew	0.926829	-0.02711	0.038517	0.016329	0.054403	0.060775	0.021693	0.553771
kurtosis	1.087655	0.297083	-0.04731	-0.05732	-0.13985	-0.23927	-0.27713	0.083633

CDX Pressure Readings and Statistical Data

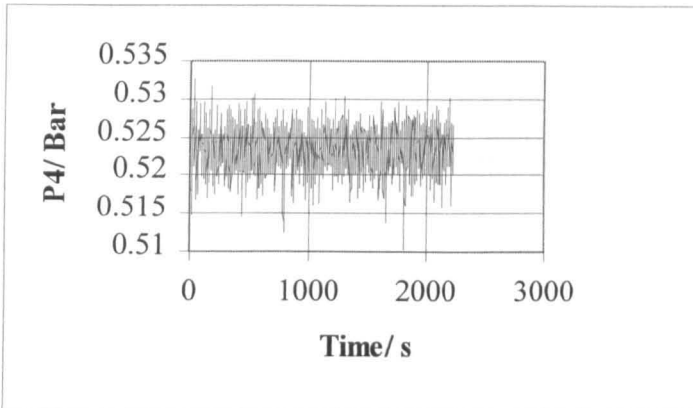
Long Swirly-*flo* Pipe Arrangement (optimum position)

Run: 6kglsf35

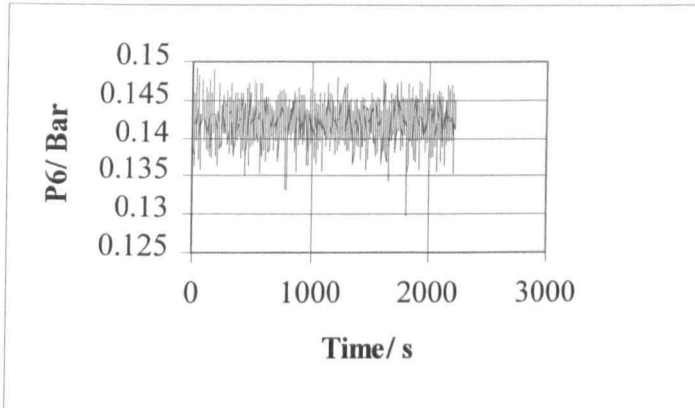
Volumetric Flow: 2.104 l/s

Mass Flow: 2.2 Kg/s

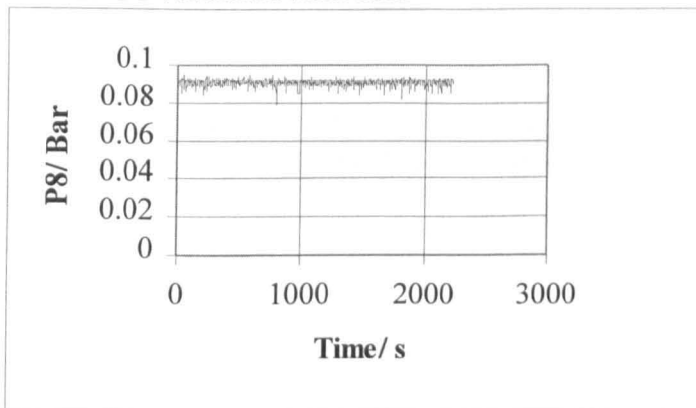
Number of Data Points:2226



CDXI P4 variation with time



CDXII P6 variation with time



CDXIII P8 variation with time

	p1	p2	p3	p4	p5	p6	p7	p8
mean	0.651575	0.571643	0.553937	0.523434	0.518909	0.142092	0.114825	0.090493
median	0.65149	0.5717	0.55401	0.52366	0.51908	0.14219	0.115	0.09088
mode	0.65251	0.57314	0.55401	0.52428	0.5199	0.14239	0.1152	0.0917
standard deviation	0.00227	0.003027	0.002718	0.002586	0.002575	0.002183	0.00217	0.001574
variance	5.15E-06	9.16E-06	7.39E-06	6.69E-06	6.63E-06	4.77E-06	4.71E-06	2.48E-06
skew	-0.80583	-0.06362	-0.24569	-0.30511	-0.32551	-0.3329	-0.39946	-1.60376
kurtosis	0.693827	0.078504	0.398662	0.662644	0.673357	1.010083	1.140298	4.832527

CDXIV Pressure Readings and Statistical Data

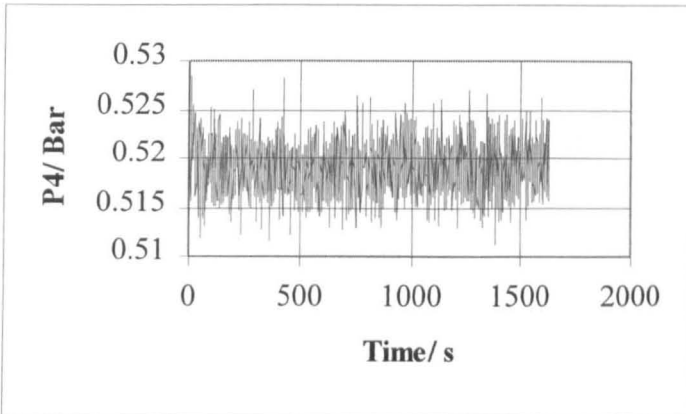
Long Swirly-flo Pipe Arrangement (optimum position)

Run: 6kglsf40

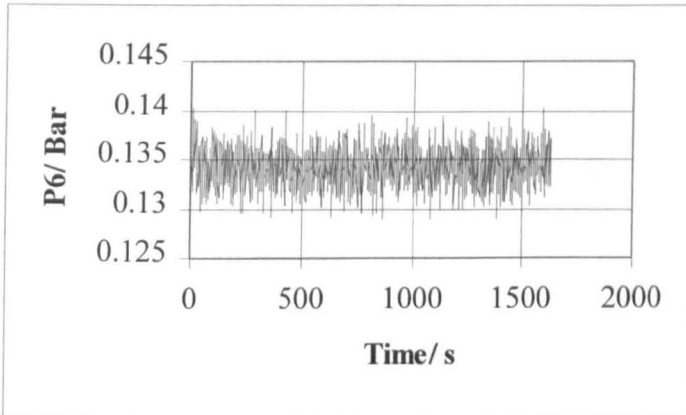
Volumetric Flow: 2.45 l/s

Mass Flow: 2.547 Kg/s

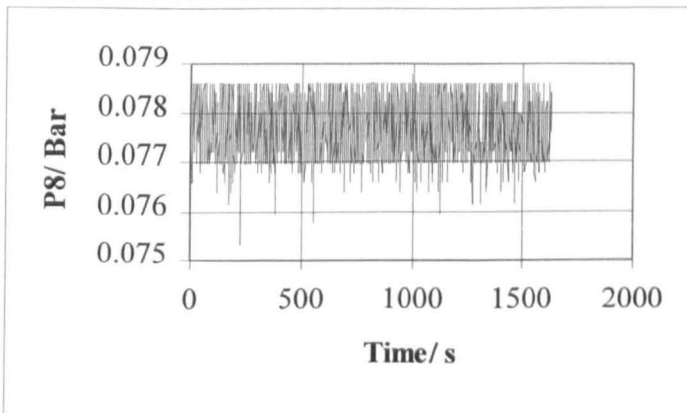
Number of Data Points:1626



CDXV P4 variation with time



CDXVI P6 variation with time



CDXVII P8 variation with time

	p1	p2	p3	p4	p5	p6	p7	p8
mean	0.704634	0.577384	0.556121	0.519014	0.51446	0.134202	0.106245	0.077643
median	0.70468	0.57743	0.55606	0.51896	0.51437	0.13421	0.1062	0.07758
mode	0.70468	0.57764	0.55688	0.51794	0.51396	0.13339	0.10661	0.07697
standard deviation	0.002409	0.003436	0.002811	0.002558	0.002523	0.001855	0.001833	0.00063
variance	5.8E-06	1.18E-05	7.9E-06	6.54E-06	6.36E-06	3.44E-06	3.36E-06	3.97E-07
skew	0.082806	0.193689	0.099453	0.115504	0.1279	0.052105	0.062562	0.112903
kurtosis	0.425235	0.20024	-0.08877	-0.03361	-0.02623	-0.02593	-0.02984	-1.04933

CDXVIII Pressure Readings and Statistical Data

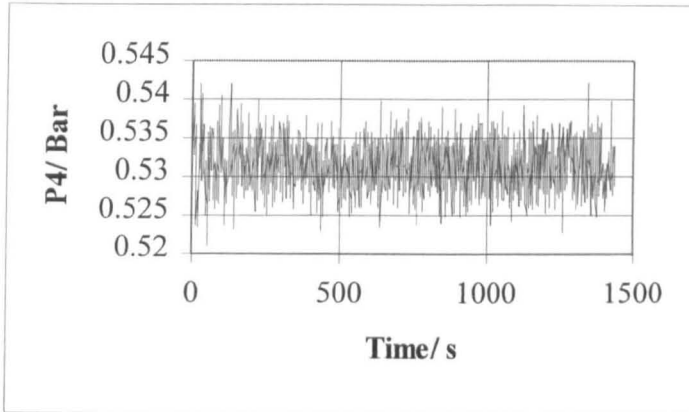
Long Swirly-*flo* Pipe Arrangement (optimum position)

Run: 6kglsf45

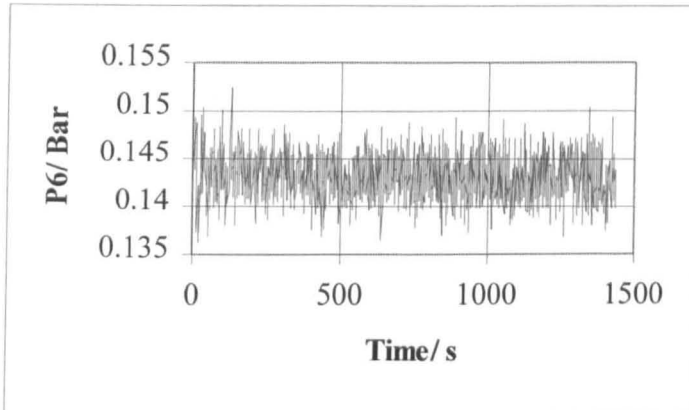
Volumetric Flow: 2.857 l/s

Mass Flow: 2.97 Kg/s

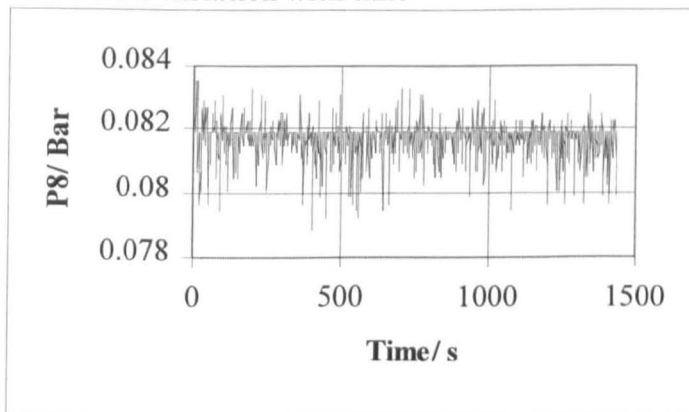
Number of Data Points:1438



CDXIX P4 variation with time



CDXX P6 variation with time



CDXXI P8 variation with time

	p1	p2	p3	p4	p5	p6	p7	p8
mean	0.780118	0.600375	0.574893	0.531445	0.527143	0.14312	0.11484	0.08171
median	0.78037	0.60014	0.57467	0.53144	0.52706	0.14301	0.11479	0.08188
mode	0.78037	0.59932	0.57365	0.53082	0.52603	0.14219	0.11582	0.08188
standard deviation	0.002946	0.004184	0.003353	0.003124	0.003145	0.00236	0.002269	0.000516
variance	8.68E-06	1.75E-05	1.12E-05	9.76E-06	9.89E-06	5.57E-06	5.15E-06	2.66E-07
skew	0.163472	0.153767	0.154046	0.111488	0.097385	0.108856	0.104529	-1.45739
kurtosis	-0.10873	0.14828	0.055842	0.016088	-0.03612	-0.07786	-0.0491	5.585466

CDXXII Pressure Readings and Statistical Data

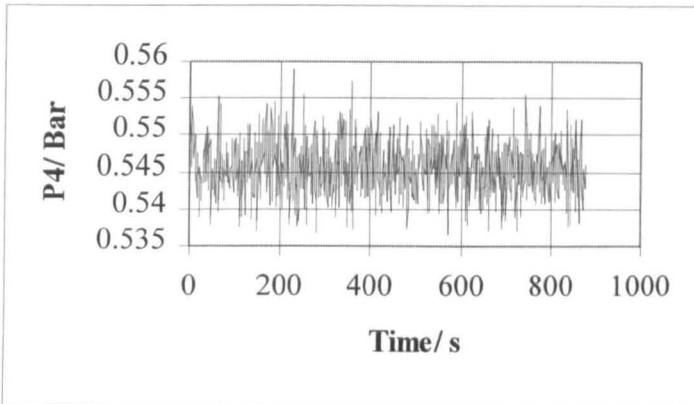
Long Swirly-flo Pipe Arrangement (optimum position)

Run: 6kglsf50

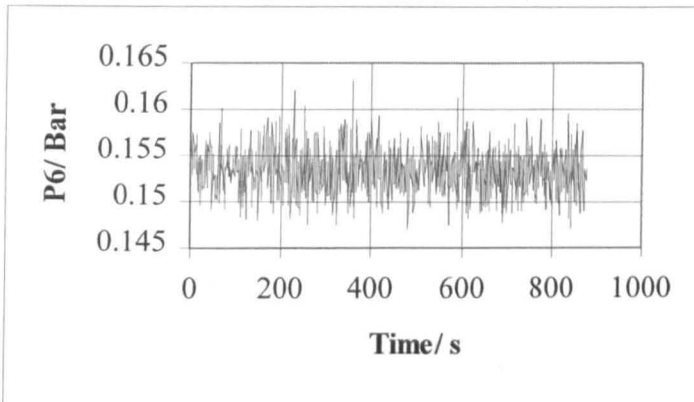
Volumetric Flow: 3.213 Kg/s

Mass Flow: 3.36 Kg/s

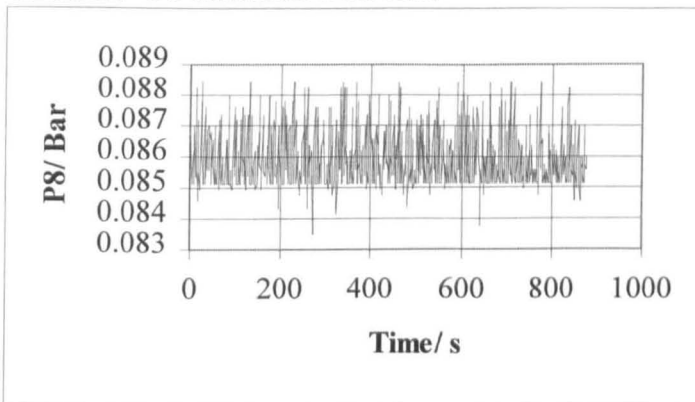
Number of Data Points:877



CDXXIII P4 variation with time



CDXXIV P6 variation with time



CDXXV P8 variation with time

	p1	p2	p3	p4	p5	p6	p7	p8
mean	0.866777	0.626208	0.595813	0.545557	0.541521	0.153431	0.124871	0.085897
median	0.86732	0.62592	0.59554	0.54535	0.54138	0.15323	0.12482	0.08556
mode	0.8663	0.62531	0.59554	0.54371	0.54199	0.15303	0.12421	0.08515
standard deviation	0.002915	0.004958	0.003873	0.00365	0.003467	0.002586	0.002608	0.000874
variance	8.5E-06	2.46E-05	1.5E-05	1.33E-05	1.2E-05	6.69E-06	6.8E-06	7.64E-07
skew	-0.0668	0.185614	0.198537	0.209092	0.185494	0.180216	0.166097	1.005661
kurtosis	0.485762	0.439202	-0.00352	-0.10875	-0.07391	-0.20889	-0.23607	0.396844

CDXXVI Pressure Readings and Statistical Data

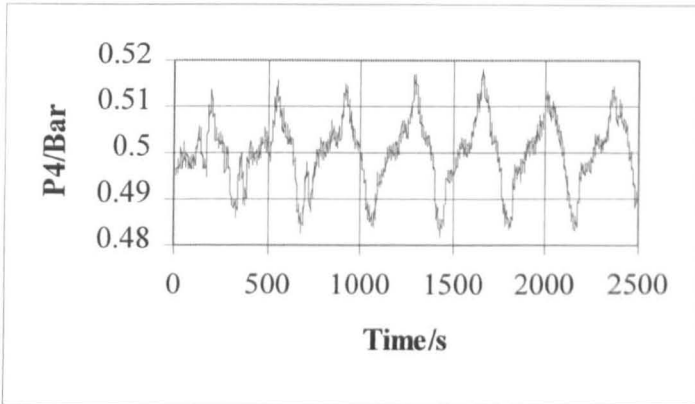
Long Swirly-flo Pipe Arrangement (optimum position)

Run: 8kglsf20

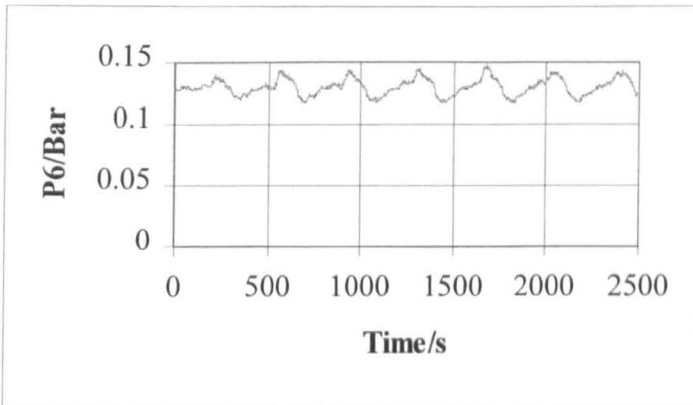
Volumetric Flow:0.731 l/s

Mass Flow: 0.759 Kg/s

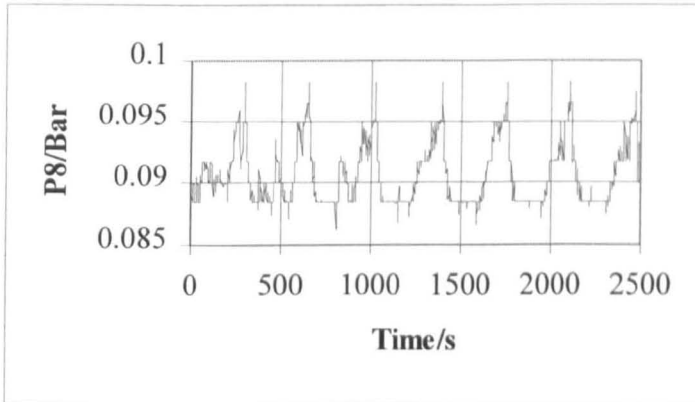
Number of Data Points:2490



CDXXVII P4 variation with time



CDXXVIII P6 variation with time



CDXXIX P8 variation with time

	p1	p2	p3	p4	p5	p6	p7	p8
mean	0.5059	0.526042	0.51726	0.50002	0.497122	0.130155	0.103231	0.090653
median	0.50726	0.5269	0.5176	0.50075	0.4976	0.13012	0.10293	0.09006
mode	0.50726	0.52506	0.5176	0.50259	0.4976	0.12807	0.1017	0.08843
standard deviation	0.002764	0.004812	0.007409	0.00725	0.007301	0.006772	0.006896	0.002493
variance	7.64E-06	2.32E-05	5.49E-05	5.26E-05	5.33E-05	4.59E-05	4.76E-05	6.22E-06
skew	-1.07877	-0.56772	-0.26509	-0.26515	-0.25409	0.082368	0.163134	0.865885
kurtosis	0.69647	-0.39071	-0.22922	-0.22679	-0.32306	-0.71851	-0.75268	-0.25489

CDXXX Pressure Readings and Statistical Data

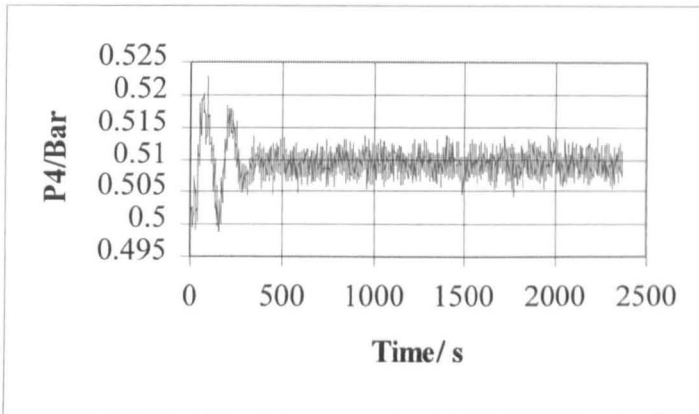
Long Swirly-flo Pipe Arrangement (optimum position)

Run: 8kglsf25

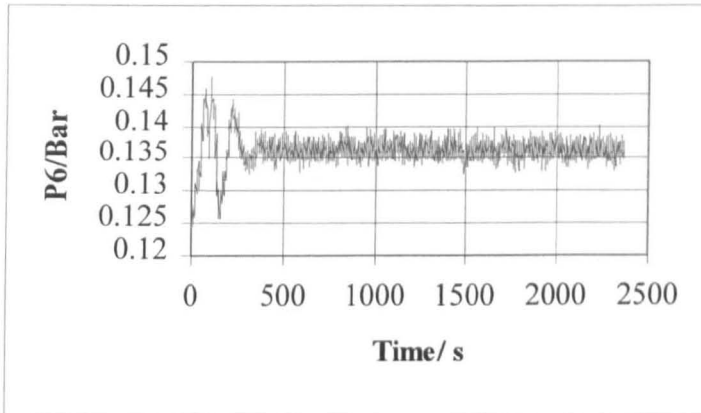
Volumetric Flow: 1.169 l/s

Mass Flow: 1.22 Kg/s

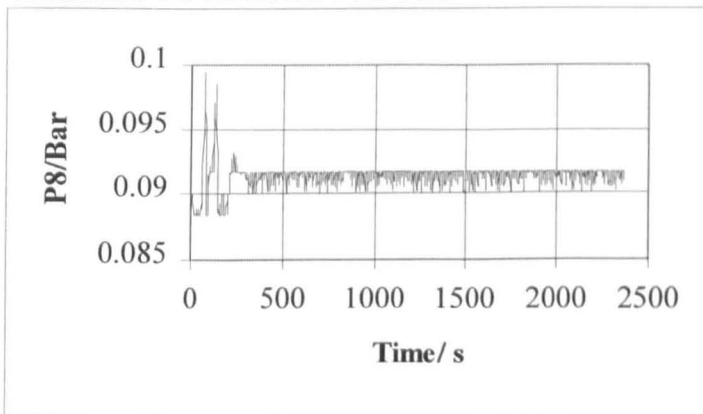
Number of Data Points:2368



CDXXXI P4 variation with time



CDXXXII P6 variation with time



CDXXXIII P8 variation with time

	p1	p2	p3	p4	p5	p6	p7	p8
mean	0.54039	0.54297	0.52875	0.509438	0.506306	0.136294	0.109955	0.091432
mode	0.53999	0.5447	0.52844	0.50975	0.50742	0.13687	0.10968	0.0917
median	0.53999	0.54306	0.52864	0.50934	0.50639	0.13625	0.11009	0.0917
standard deviation	0.001045	0.002246	0.002409	0.002538	0.002445	0.002317	0.002368	0.000907
variance	1.09E-06	5.04E-06	5.8E-06	6.44E-06	5.98E-06	5.37E-06	5.61E-06	8.22E-07
skew	2.770705	0.217704	0.037311	0.172807	0.071521	-0.50617	-0.65516	0.968206
kurtosis	16.51932	2.280049	4.457452	3.8336	4.014921	6.160357	6.112365	16.03082

CDXXXIV Pressure Readings and Statistical Data

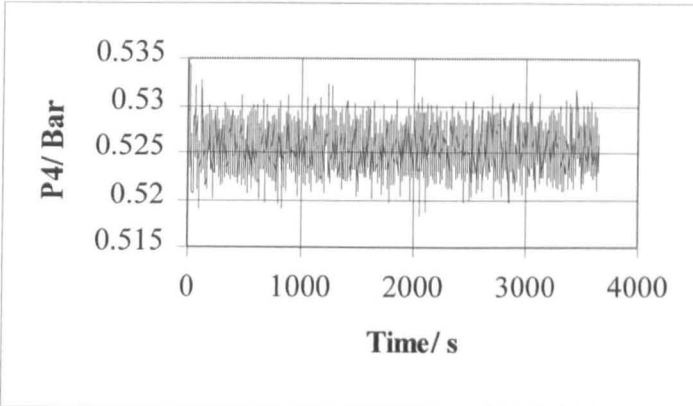
Long Swirly-flo Pipe Arrangement (optimum position)

Run: 8kglsf30

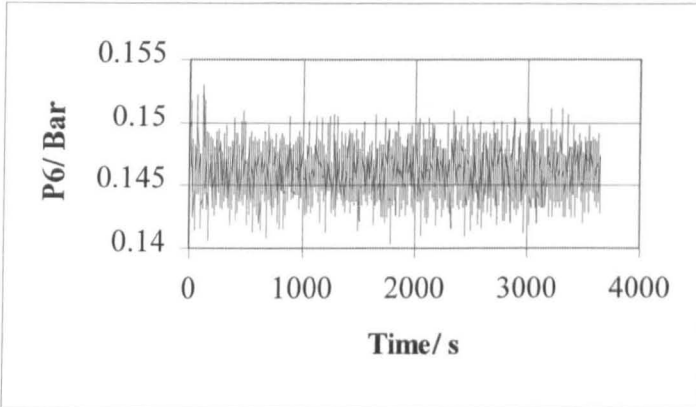
Volumetric Flow:1.629 l/s

Mass Flow:1.711 Kg/s

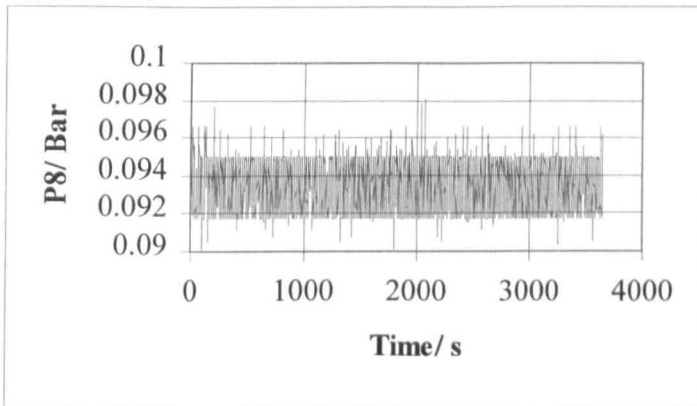
Number of Data Points:3650



CDXXXV P4 variation with time



CDXXXVI P6 variation with time



CDXXXVII P8 variation with time

	p1	p2	p3	p4	p5	p6	p7	p8
mean	0.596126	0.568637	0.549518	0.525458	0.521525	0.146058	0.119113	0.093591
median	0.59625	0.56864	0.54951	0.52551	0.52153	0.14607	0.11909	0.09354
mode	0.59727	0.56864	0.55033	0.5253	0.52112	0.1471	0.11868	0.09497
standard devaitio	0.002586	0.002046	0.002082	0.002041	0.002036	0.001755	0.001742	0.001257
variance	6.69E-06	4.19E-06	4.34E-06	4.17E-06	4.15E-06	3.08E-06	3.03E-06	1.58E-06
skew	-0.02888	0.070088	0.076155	0.102408	0.115237	0.023621	0.057759	-0.13489
kurtosis	-0.2276	0.383991	0.177299	0.054197	0.136755	-0.1223	-0.1232	-1.08893

CDXXXVIII Pressure Readings and Statistical Data

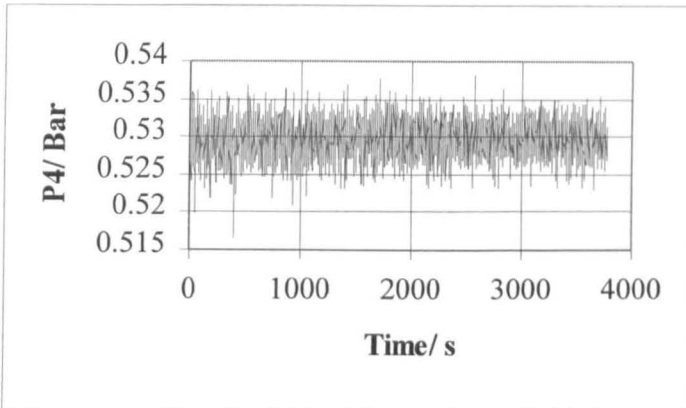
Long Swirly-flo Pipe Arrangement (optimum position)

Run: 8kglsf35

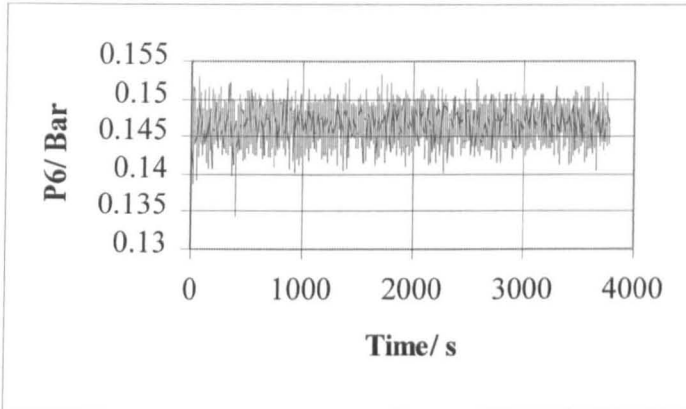
Volumetric Flow: 2.05 l/s

Mass Flow: 2.159 Kg/s

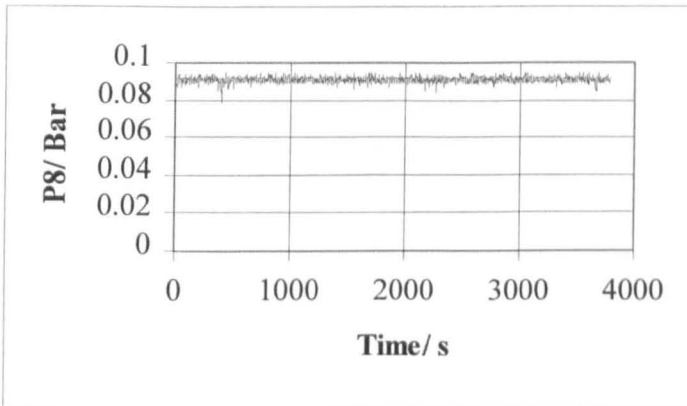
Number of Data Points:3782



CDXXXIX P4 variation with time



CDXL P6 variation with time



CDXLI P6 variation with time

	p1	p2	p3	p4	p5	p6	p7	p8
mean	0.653775	0.581228	0.560158	0.529769	0.525781	0.146752	0.119389	0.090959
median	0.65456	0.58132	0.56015	0.5298	0.52583	0.14689	0.1195	0.0915
mode	0.65456	0.58152	0.55892	0.53042	0.52603	0.14771	0.12011	0.0917
standard deviation	0.001365	0.002893	0.002517	0.00239	0.002437	0.002068	0.002072	0.001386
variance	1.86E-06	8.37E-06	6.33E-06	5.71E-06	5.94E-06	4.28E-06	4.29E-06	1.92E-06
skew	-1.36721	-0.08273	-0.17447	-0.29963	-0.2167	-0.54352	-0.50587	-1.72868
kurtosis	3.538943	0.196697	0.449167	0.862343	0.706787	1.664608	1.804773	11.37942

CDXLII Pressure Readings and Statistical Data

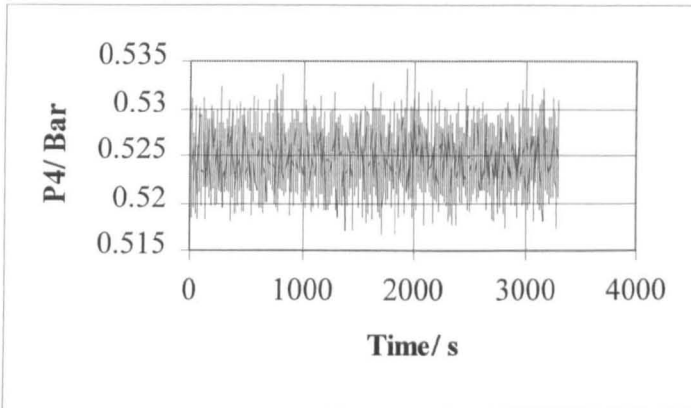
Long Swirly-flo Pipe Arrangement (optimum position)

Run: 8kglsf40

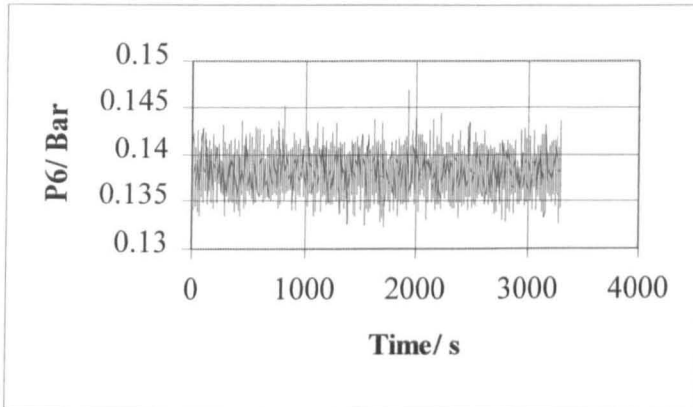
Volumetric Flow:2.428 l/s

Mass Flow: 2.58 Kg/s

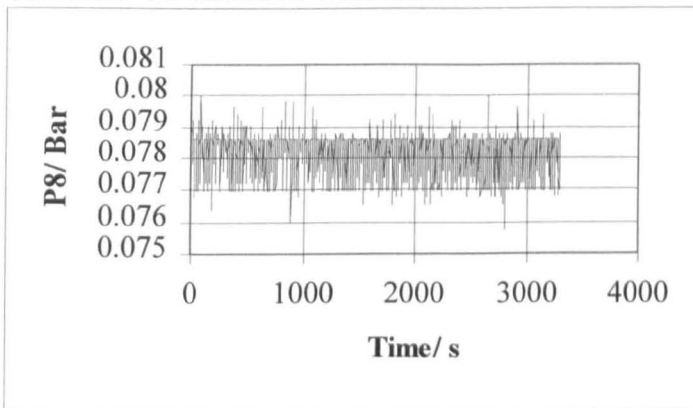
Number of Data Points:3306



CDXLIII P4 variation with time



CDXLIV P6 variation with time



CDXLV P8 variation with time

	p1	p2	p3	p4	p5	p6	p7	p8
mean	0.706978	0.585763	0.561807	0.524743	0.520632	0.138137	0.110226	0.078273
median	0.70672	0.58582	0.56179	0.52469	0.52071	0.1381	0.11029	0.07861
mode	0.70672	0.58602	0.56179	0.52387	0.52051	0.13891	0.11029	0.07861
standard deviation	0.00253	0.003369	0.002702	0.002553	0.002506	0.001876	0.001857	0.000528
variance	6.4E-06	1.13E-05	7.3E-06	6.52E-06	6.28E-06	3.52E-06	3.45E-06	2.78E-07
skew	0.172331	0.038746	-0.03942	0.000982	0.008935	0.022733	-0.00738	-1.21116
kurtosis	0.15368	-0.07218	0.013785	-0.02507	0.024914	0.026865	0.010165	0.962438

CDXLVI Pressure Readings and Statistical Data

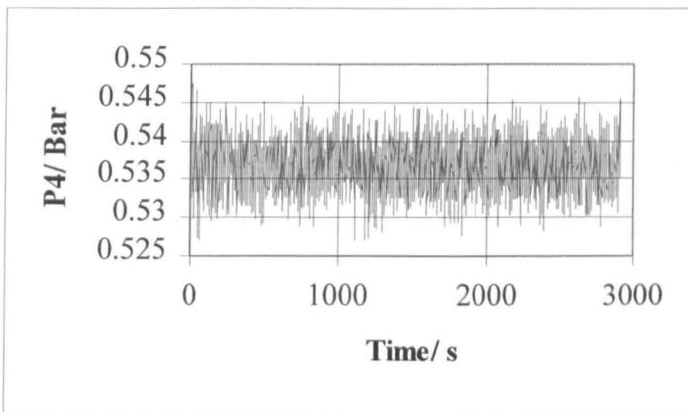
Long Swirly-flo Pipe Arrangement (optimum position)

Run: 8kglf45

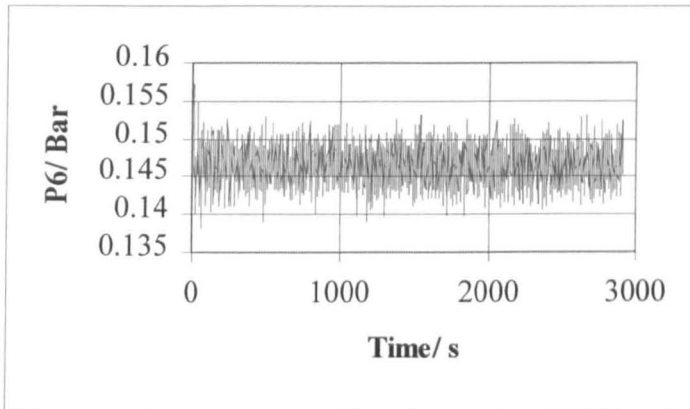
Volumetric Flow: 2.865 l/s

Mass Flow: 3 Kg/s

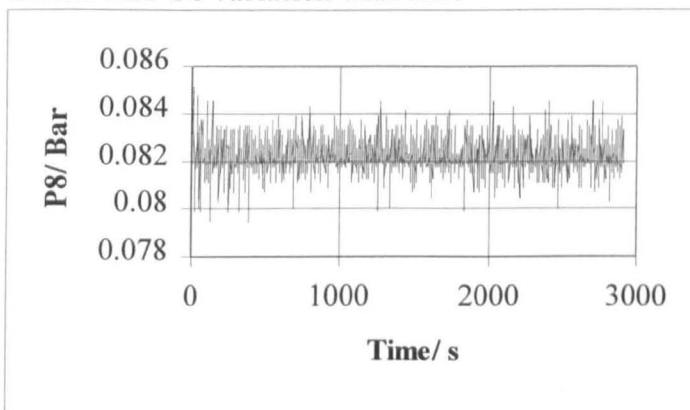
Number of Data Points:2907



CDXLVII P4 variation with time



CDXLVIII P6 variation with time



CDXLIX P8 variation with time

	p1	p2	p3	p4	p5	p6	p7	p8
mean	0.781986	0.607943	0.580244	0.536689	0.532918	0.146582	0.118246	0.082094
mode	0.78242	0.60771	0.5804	0.53717	0.53319	0.1473	0.11868	0.08188
median	0.78242	0.60792	0.5802	0.53655	0.53299	0.14648	0.11827	0.08188
standard deviation	0.003032	0.004154	0.003367	0.003111	0.003104	0.002327	0.002294	0.00057
variance	9.19E-06	1.73E-05	1.13E-05	9.68E-06	9.63E-06	5.42E-06	5.26E-06	3.25E-07
skew	0.084154	0.092075	0.096433	0.076952	0.071988	0.019479	0.074576	0.980575
kurtosis	-0.26472	0.027114	-0.11274	-0.03262	-0.04593	0.15451	0.174916	3.870935

CDL Pressure Readings and Statistical Data

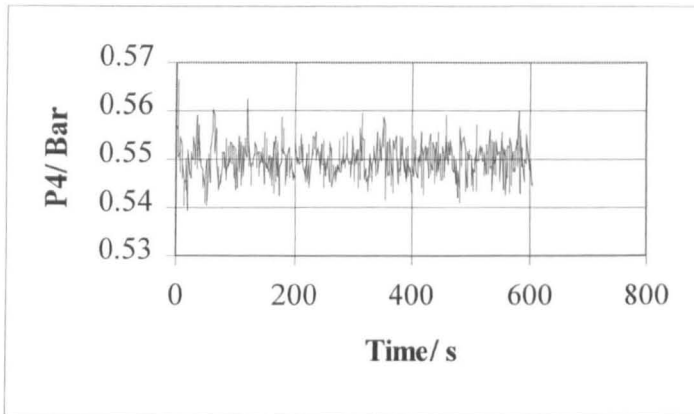
Long Swirly-flo Pipe Arrangement (optimum position)

Run: 8kglsf50

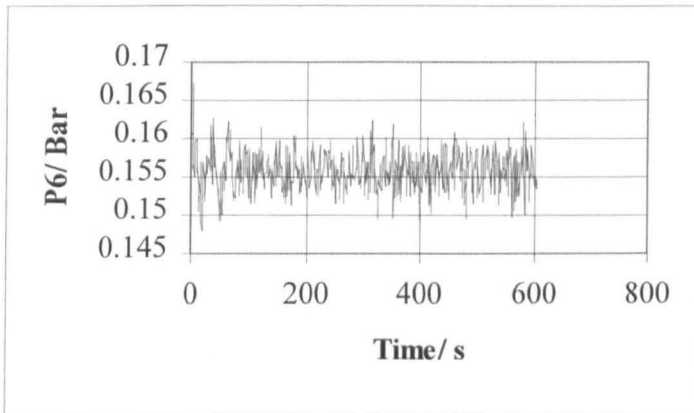
Volumetric Flow: 3.213 l/s

Mass Flow: 3.39 Kg/s

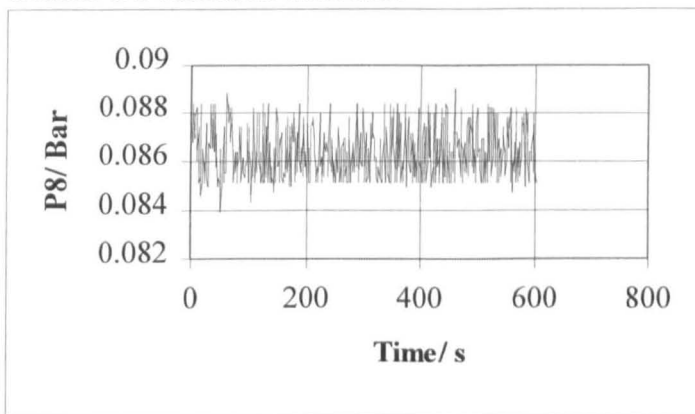
Number of Data Points:606



CDLI P4 variation with time



CDLII P6 variation with time



CDLIII P8 variation with time

	p1	p2	p3	p4	p5	p6	p7	p8
mean	0.86734	0.631881	0.600018	0.549768	0.545816	0.155784	0.127286	0.086329
median	0.86732	0.63175	0.60004	0.54985	0.54567	0.15579	0.12727	0.08618
mode	0.8663	0.63022	0.59738	0.55108	0.54567	0.15692	0.12789	0.08515
standard deviation	0.002908	0.00464	0.003705	0.003587	0.003396	0.002494	0.002495	0.001033
variance	8.46E-06	2.15E-05	1.37E-05	1.29E-05	1.15E-05	6.22E-06	6.23E-06	1.07E-06
skew	-0.06996	0.364895	0.226002	0.226195	0.133163	0.120952	0.041562	0.507298
kurtosis	0.729064	1.168906	1.113476	0.823139	0.8318	0.555963	0.354805	-0.79942

CDLIV Pressure Readings and Statistical Data